ADVANCES IN INORGANIC CHEMISTRY

Volume 49

A. G. Sykes

Advances in

INORGANIC CHEMISTRY

Including Bioinorganic Studies

Volume 49

ADVISORY BOARD

I. Bertini
Universitá degli Studi di Firenze
Florence, Italy

A. H. Cowley, FRS
University of Texas
Austin, Texas, USA

H. B. Gray
California Institute of Technology
Pasadena, California, USA

M. L. H. Green, FRS
University of Oxford
Oxford, United Kingdom

O. Kahn
Institut de Chimie de la Matière Condensée de Bordeaux
Pessac, France

André E. Merbach
Institut de Chimie Minérale et Analytique
Université de Lausanne
Lausanne, Switzerland

D. M. P. Mingos, FRS
Imperial College of Science, Technology, and Medicine
London, United Kingdom

J. Reedijk
Leiden University
Leiden, The Netherlands

A. M. Sargeson, FRS
The Australian National University
Canberrs, Australia

Y. Sasaki
Hokkaido University
Sapporo, Japan

D. F. Shriver
Northwestern University
Evanston, Illinois, USA

R. van Eldik
Universität Erlangen-Nümberg
Erlangen, Germany

K. Wieghardt
Max-Planck Institut
Mülheim, Germany

Advances in
INORGANIC CHEMISTRY

EDITED BY

A. G. Sykes

Department of Chemistry
The University of Newcastle
Newcastle upon Tyne
United Kingdom

VOLUME 49

ACADEMIC PRESS

San Diego London Boston
New York Sydney Tokyo Toronto

This book is printed on acid-free paper. ♾

Copyright □ 2000 by ACADEMIC PRESS

All Rights Reserved.
No part of this publication may be reproduced or transmitted in any form or by any means, electronic or mechanical, including photocopy, recording, or any information storage and retrieval system, without permission in writing from the Publisher.
The appearance of the code at the bottom of the first page of a chapter in this book indicates the Publisher's consent that copies of the chapter may be made for personal or internal use of specific clients. This consent is given on the condition, however, that the copier pay the stated per copy fee through the Copyright Clearance Center, Inc. (222 Rosewood Drive, Danvers, Massachusetts 01923), for copying beyond that permitted by Sections 107 or 108 of the U.S. Copyright Law. This consent does not extend to other kinds of copying, such as copying for general distribution, for advertising or promotional purposes, for creating new collective works, or for resale. Copy fees for pre-1998 chapters are as shown on the title pages. If no fee code appears on the title page, the copy fee is the same as for current chapters.
0898-8838/00 $30.00

Academic Press
a division of Harcourt Brace & Company
525 B Street, Suite 1900, San Diego, California 92101-4495, USA
http://www.apnet.com

Academic Press Limited
24-28 Oval Road, London NW1 7DX, UK
http://www.hbuk.co.uk/ap/

International Standard Book Number: 0-12-023649-4

PRINTED IN THE UNITED STATES OF AMERICA
00 01 02 03 04 05 QW 9 8 7 6 5 4 3 2 1

CONTENTS

Medicinal Inorganic Chemistry

ZIJIAN GUO AND PETER J. SADLER

The Cobalt(III)-Promoted Synthesis of Small Peptides

REBECCA J. BROWNE, DAVID A. BUCKINGHAM, CHARLES R. CLARK, AND PAUL A. SUTTON

Structures and Reactivities of Platinum-Blues and the Related Amidate-Bridged Platinum^{III} Compounds

KAZUKO MATSUMOTO AND KEN SAKAI

This Page Intentionally Left Blank

INORGANIC AND BIOINORGANIC REACTION MECHANISMS: APPLICATION OF HIGH-PRESSURE TECHNIQUES

RUDI VAN ELDIK, CARLOS DÜCKER-BENFER, and FLORIAN THALER

Institute for Inorganic Chemistry, University of Erlangen-Nürnberg, 91058, Erlangen, Germany

I. Introduction

The aim of this chapter is to review advances made in elucidating inorganic and bioinorganic reaction mechanisms through the application of high-pressure kinetic and thermodynamic techniques to a wide range of reactions in solution. This topic has been addressed in a number of reviews that have appeared in recent years (*15*), and readers are advised to consult these references for further background information. The area has been of interest to many groups and more than 1500 data sets were published for inorganic systems studied over the period of 1987 to 1996 (*4*).

Copyright □ 2000 by Academic Press.
All rights of reproduction in any form reserved.
0898-8838/00 $30.00

The approach adopted involves first a short outline of the basic principles and experimental techniques involved in the work in an effort to answer the questions of why and how do we make these measurements. An account of the mechanisms of ligand substitution reactions of metal complexes and the mechanistic insight gained through the application of high-pressure kinetic techniques is presented. This section forms the basis for many chemical processes in inorganic and bioinorganic systems and then allows a treatment of the activation of small molecules by metal complexes in a subsequent section. Such activation processes usually involve a direct interaction between the small molecule and the metal center, which in many cases is a substitution-controlled process. Thus once the small molecule is bound to the metal complex, the actual activation involves in many cases an electron-transfer process. This section of the chapter addresses a treatment of the effect of pressure on electron-transfer processes of inorganic and bioinorganic interest. Subsequently, a number of miscellaneous reactions are also considered. Numerous examples are used to demonstrate the kind of mechanistic information that can be obtained through the application of high-pressure techniques in the study of these reactions.

It has been our philosophy to obtain as much mechanistic insight from detailed kinetic investigations as a function of as many experimental variables as possible. These include the concentrations of the reactants and products, the composition of the solvent, pH, buffer composition, and ionic strength, which all form part of the chemical variables in mechanistic studies. In addition, there are two physical variables that can be applied in such studies, i.e., temperature and pressure, and we have made use of these where possible. Such detailed kinetic data can provide, along with all other known chemical and structural properties of the system and possible intermediates, detailed insight into the nature of the underlying reaction mechanism. In many cases our insight is restricted by the number of variables covered during such investigations. The suggested mechanism based on this information only then approaches the "real" mechanism when it is in line with all available experimental as well as theoretical information.

In this chapter we focus on the role of the pressure variable in such mechanistic studies. Almost all chemical reactions in solution exhibit a characteristic pressure dependence over a moderate pressure range of a few hundred megapascals. The pressure dependence of an equilibrium (K) or a rate constant (k) results in the reaction volume, ΔV, or the volume of activation, $\Delta V^{\#}$, via the relationships $(\delta \ln K/\delta P)_T =$

$-\Delta V/RT$ or $(\delta \ln k/\delta P)_T = -\Delta V^{\#}/RT$, respectively. This information combined with partial molar volume data for reactant and product species can now be used to construct a volume profile for the studied reaction, which represents the partial molar volume changes associated with the process along the reaction coordinate in a kinetic and thermodynamic sense. Such volume profiles, of which many have been reported (*3*, *6*) and which are discussed in this chapter, greatly assist in determining the core mechanism on the basis of the location of the transition state in reference to that of the reactant and product species on a volume basis. Thus the reaction mechanism is interpreted in terms of specific volume changes along the reaction coordinate, which consist mainly of intrinsic and solvational contributions that result from changes in bond lengths and angles and from changes in electrostriction or dipole moment, respectively.

Much of the achieved advances result from the development and availability of instrumentation to study slow and fast reactions at pressures up to 300 MPa, including stopped-flow, T-jump, P-jump, NMR, ESR, flash-photolysis, and pulse-radiolysis instrumentation (*1*, *2*, *4*, *6*, *7*). Readers are advised to consult the quoted references for more detailed information, since these present a detailed account of the present instrumentation and commercial availability of such equipment.

II. Ligand Substitution Reactions

The general understanding of ligand-substitution mechanisms of square planar and octahedral complexes since the earlier concepts were developed benefited greatly from the numerous high-pressure kinetic studies performed during the past 2 decades. In this respect Merbach and coworkers have contributed in an impressive way toward resolving mechanisms of symmetrical solvent-and-ligand exchange processes on transition-metal complexes (*2*, *8–10*).

A. Solvent and Ligand Exchange Reactions

Solvent exchange processes are the most fundamental substitution reactions that characterize the lability and reaction mechanism of a metal center within a coordination geometry. For these reactions the interpretation of the volume of activation becomes rather straightforward since these reactions do not involve major changes in solvation due to changes in dipole moments and electrostriction, which can in

the case of nonsymmetrical reactions significantly complicate the interpretation. The results and mechanistic information obtained from these studies are presently well accepted by the mechanistic community, but have in the past resulted in discrepancies in the literature, especially with theoretical chemists.

One example involves the activation volumes for solvent exchange on the divalent cations of the first row of transition metals, which exhibit clear evidence for a mechanistic changeover along the series, i.e., from more associative for the earlier, larger cations to a more dissociative one for the later, smaller cations (*8*). It was claimed on the basis of theoretical calculations (*11*, *12*) that the interpretation of such activation volume data is incorrect, and theoretical arguments were presented against a mechanistic changeover along the series. Additional calculations were needed in order to investigate the validity of the mechanistic proposals that were based on calculations in an effort to resolve the disparate conclusions.

The original studies (*11*, *12*) involved *ab initio* self-consistent field (SCF) calculations of the binding energies, ligand–field effects, water exchange reactions, and exchange of hexahydrated divalent first-row transition-metal cations. In subsequent work, Rotzinger (*13*, *14*) succeeded in computing the structures of the transition states and the intermediates formed during the water exchange reactions of the first-row transition metals with *ab initio* methods at the Hartree–Fock or CAS- (complete active space)–SCF level. It was now possible to generate A, I_a, I_d, and D pathways and to optimize the structures of the transition and intermediate states. Furthermore, the calculated bond length changes that occurred during the activation process were entirely consistent with the activation volume data and indicated that an associative interchange mechanism can operate for some metal ions, in contrast to the previous theoretical prediction (*12*). In general, *ab initio* calculations as well as molecular dynamics simulations have contributed significantly toward the validation of mechanistic assignments reached on the basis of activation volume data (*15–17*).

Density functional theory has also been applied successfully to describe the solvent exchange mechanism for aquated Pd(II), Pt(II), and Zn(II) cations (*18–19*). Our own work on aquated Zn(II) (*19*) was stimulated by our interest in the catalytic activity of such metal ions and by the absence of any solvent (water) exchange data for this cation. The optimized transition state structure clearly demonstrated the dissociative nature of the process; in no way could a seventh water molecule be forced to enter the coordination sphere without the simultaneous dissociation of one of the six coordinated water molecules. More

recently, the same techniques were applied to solvent exchange on aquated Ti(III) for which a stable seven-coordinate intermediate, in line with a limiting associative mechanism, could be computed (*20*). The deprotonation of this species to form $[Ti(H_2O)_5OH]^{2+}$ resulted in a changeover in mechanism to a more dissociative substitution mode, something that has been observed experimentally for a number of water exchange reactions (*21*), (see below). Other groups have also in recent years concentrated on the theoretical analysis of hydration and solvent exchange reactions of metal cations (*22–26*).

Solvent exchange mechanisms are not only of fundamental interest in coordination chemistry, their understanding is of direct interest to the application of certain metal complexes as contrast agents for magnetic resonance imaging. For instance, in the case of $[Gd(DOTA)]^-$ (DOTA = 1,4,7,10-tetraaza-1,4,7,10-tetrakis(carboxymethyl)cyclododecane), a ninth coordination site at a capping position above the plane of the four oxygen donors is occupied by a water molecule. The water molecule exchanges rapidly with the bulk solvent, which results in a remarkable increase in the relaxation rate of the solvent water protons. For this reason the solvent exchange reactions of a series of DOTA complexes of different trivalent cations (Sc, Y, La, and Ce to Lu) were studied in detail, including their pressure dependence (*27*). In the case of Gd(III), volumes of activation were reported for water exchange on complexes with DTPA and different modifications of DTPA (DTPA = diethylenetriamine-*N*,*N*,*N*′,*N*″,*N*″-pentaacetate) as a chelating ligand (*28–30*). The reported volumes of activation clearly support the operation of a dissociative exchange process in cases where a nine-coordinate complex exists in solution compared to an associative mechanism where eight-coordinate complexes exist in solution. Such a mechanistic changeover could also be modeled using molecular dynamics simulations (*15*).

A series of ligand exchange reactions were investigated by Funahashi and co-workers (*31–34*). The exchange of ethylenediamine, 1,3-propanediamine, and n-propylamine on Ni(II), Fe(II), and Mn(II) was studied as a function of pressure using ^{14}N-NMR line-broadening. The reported activation volumes exhibit a trend from slightly negative values for ethylenediamine exchange on Mn(II) and Fe(II) to significantly positive values for Co(II) and Ni(II), again demonstrating a change in mechanism along the series of complexes. For exchange of the bulkier 1,3-propanediamine, the reported activation volume is practically zero for Mn(II) but significantly positive for the other three metal ions. The influence of the steric size of the solvent on the solvent exchange mechanism was investigated for the exchange of a se-

ries of nitriles on Mn(II) (*35*). In general the reported data favor a less associative mechanism with increasing bulkiness of the solvent molecule.

B. Solvent and Ligand Displacement Reactions

The level of understanding reached for solvent exchange reactions on solvated metal ions has encouraged investigations of nonsymmetrical complex formation and ligand substitution reactions. Complex formation of the divalent first-row transition elements exhibited volumes of activation that are very similar to those observed for the water exchange reactions, from which it followed that very similar mechanisms must be operating (*4*, *8*). The same was observed for an extended series of aquation reactions for complexes of the type $[M(NH_3)_5L]^{3+}$, M = Co(III), Cr(III) and L = neutral nucleophile (*4*); the results once again agree very well with the solvent exchange data. Along these lines, a volume profile was recently constructed for the reaction

$$[Fe^{II}(CN)_5NH_3]^{3-} + H_2O \leftrightarrow [Fe^{II}(NH_3)_5H_2O]^{3-} + NH_3.$$

The pressure dependence of the forward and reverse reactions resulted in significantly positive volumes of activation (*36*), and the volume profile reported in Fig. 1 clearly demonstrates the dissociative nature of the substitution process. Such conclusions can more easily

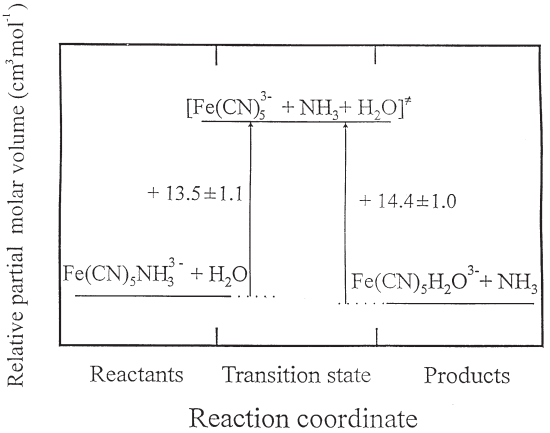

FIG. 1. Volume profile for the reaction $[Fe^{II}(CN)_5NH_3]^{3-} + H_2O \leftrightarrow [Fe^{II}(NH_3)_5H_2O]^{3-} + NH_3$.

be reached when we are dealing with the displacement of neutral molecules such that no major changes in solvation due to changes in electrostriction accompany the overall reaction. In reality, many ligand displacement processes are accompanied by charge creation or charge neutralization, and the resulting volume of activation is a composite of intrinsic and solvational volume contributions. Recently, activation and reaction volume data were reported for a series of ligand substitution reactions of $[Pd(H_2O)_4]^{2+}$ (*37*). A few typical volume profiles for such reactions are shown in Fig. 2, from which the compact nature of the transition state is seen. A good linear correlation between $\Delta V^{\#}$ for the complex-formation reaction and the overall reaction volume ΔV was found (see Fig. 3), demonstrating that the location of the transition state is controlled by the overall reaction volume. No clear correlation between $\Delta V^{\#}$ and the partial molar volume of the entering ligand could be observed (*37*).

Contrary to many of the examples quoted so far, the observed volumes of activation may differ significantly from the expected and could lead to the suggestion of an unexpected mechanism. Basallote and co-workers (*38*) investigated the substitution of coordinated H_2 by MeCN in THF in *trans*-$[FeH(H_2)(DPPE)_2]^+$ (DPPE = 1,2-bis(diphenylphosphino)ethane. The volumes of activation were measured under limiting conditions, i.e., where the observed rate constant is indepen-

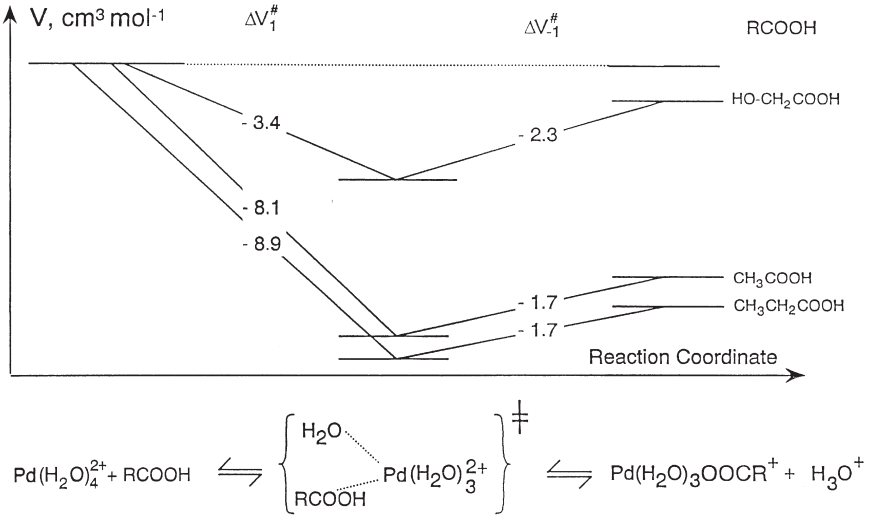

FIG. 2. Volume profiles for the reaction $[Pd(H_2O)_4]^{2+} + RCOOH \leftrightarrow [Pd(H_2O)_3OOCR]^+ + H_3O^+$.

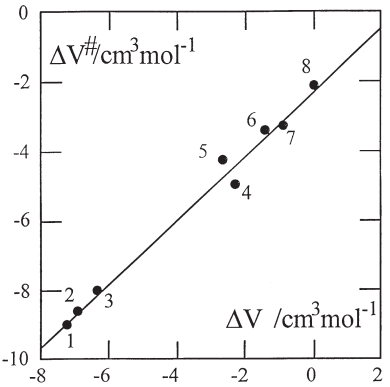

FIG. 3. Linear correlation between $\Delta V^{\#}$ and ΔV for substitution reactions of $[Pd(H_2O)_4]^{2+}$; (1) Me_2SO; (2) propionic acid; (3) acetic acid; (4) malonic acid; (5) MeCN; (6) citric acid; (7) glycolic acid; (8) water.

dent of the MeCN concentration. In contrast to the expected dissociative reaction mechanism, the $\Delta V^{\#}$ values of -18, -23, and -35 cm^3 mol^{-1} in acetone, THF, and MeCN, respectively, support the opposite. The authors therefore suggest a mechanism in which the initial opening of the DPPE chelate ring leads to an intermediate that contains monodentate DPPE and a weakly bound solvent molecule. The rate-determining step is suggested to involve associative attack of the entering ligand L on this intermediate to produce a species that contains both coordinated L and H_2.

Substitution reactions of metal carbonyl complexes also exhibit characteristic pressure dependences that assist in the elucidation of the underlying reaction mechanism (*1*, *4*, *39*). In many cases such substitution reactions are induced photochemically, and a detailed account on the effect of pressure on such reactions has appeared recently (*3*). Intermediate species are usually short-lived solvento complexes and can only be observed using fast kinetic techniques. Recently, intermediate complexes of the type $Cr(CO)_5L$–L could be isolated, and it was possible to study the subsequent thermal ring-closure reaction directly (*40*). The activation volumes found are all large and positive, between 12.5 and 17.9 cm^3 mol^{-1}, and strongly support the operation of a dissociative mechanism, i.e., dissociation of one carbonyl ligand prior to ring closure.

Nonsymmetrical ligand substitution reactions also play an important role in a number of biological processes. One of these concerns the antitumor activity of platinum metal complexes, for which substitution processes involving DNA moieties are generally accepted to

play a key role. Application of high-pressure kinetic techniques has assisted the elucidation of the underlying reaction mechanisms. Substitution reactions of square planar d^8 metal complexes in general follow an associative mechanism and are characterized by negative volumes of activation (*4*). Substitution reactions of the type

$$[PtX_2(N_2)] + H_2O \leftrightarrow [PtX(N_2)(H_2O)]^+ + X^- \qquad k_1, k_{-1}$$

$$[PtX(N_2)(H_2O)]^+ + H_2O \leftrightarrow [Pt(N_2)(H_2O)_2]^{2+} + X^- \qquad k_2, k_{-2},$$

where (N_2) = *cis*-$(NH_3)_2$, *trans*-$(NH_3)_2$, $NH_2(CH_2)_2NH_2$, $NH_2(CH_2)_3NH_2$, and X = Cl, Br exhibit activation volumes of between -5.1 and -10.4 $cm^3\ mol^{-1}$ for k_1 and k_2, which clearly underline the associative nature of the substitution process (*41*). On average the volumes of activation for the anation of the diaqua complexes are *ca.* 5 $cm^3\ mol^{-1}$ less negative than for the corresponding monoaqua complexes. This difference can be accounted for in terms of the larger charge neutralization effect accompanied by a larger decrease in electrostriction in the case of the diaqua complexes. Reactions of model Pd(II) complexes of the type $[Pd(dien)H_2O]^{2+}$ and $[Pd(R_4en)(H_2O)_2]^{2+}$, where dien = $NH_2(CH_2)_2NH(CH_2)_2NH_2$ and R_4en = $NR_2(CH_2)_2NR_2$ (R = H, Me, Et) with DNA moieties such as inosine, adenosine, cytidine, thymidine, uridine, and a d(GpG) sequence, are all characterized by negative volumes of activation for either the complex-formation or reverse aquation reactions (*4244*). Similar results were also reported for the reactions of the corresponding L-methionine complex with inosine and inosine monophosphate (*45*). The data support the general concept of associative substitution processes in these systems. Recently, the reaction of $[Pd(pic)(H_2O)_2]^{2+}$ (pic = 2-picolylamine) with $CBDCAH^-$ (1,1-cyclobutanedicarboxylate) to produce [Pd(pic)(CBDCA-*O*)(H_2O)] was found to be practically independent of pressure (*46*), demonstrating that intrinsic and solvational volume contributions cancel out in this particular case. A complete volume profile (see Fig. 4) was reported for the aquation of a bicycloalkyl-substituted ethylenediamine dichloro Pt(II) complex in an effort to resolve the different *in vivo* antitumor activities of a series of such complexes (*47*). The volume profile underlines the associative nature of the aquation and reverse anation reactions and rules out the possible participation of a dissociative mechanism.

A further example concerns the substitution reactions of the cobalamins (vitamin B_{12}). Here the usually inert Co(III) center is labilized by the corrin ring, which induces a dissociative substitution behavior. A series of detailed studies of the effect of pressure on com-

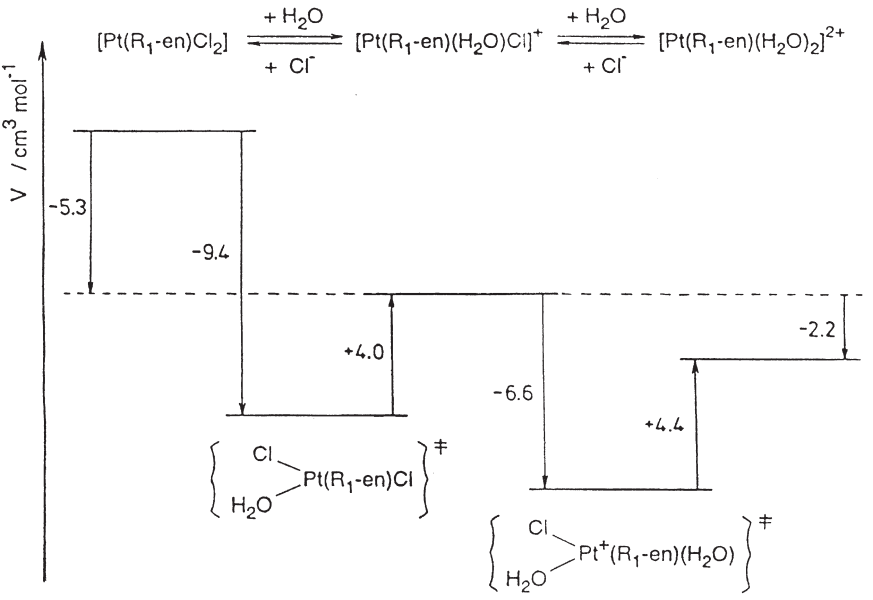

FIG. 4. Volume profile for the two-step reversible aquation of $[Pt(R_1\text{-en})Cl_2]$, where R_1-en = (1R,2R,4S)-*exo*-2-(aminomethyl)-2-amino-7-oxabicyclo[2.2.1]heptane.

plex-formation and reverse aquation reactions of the type

$$[B_{12}\text{–}H_2O]^+ + L^{n-} \leftrightarrow [B_{12}\text{–}L]^{(1-n)+} + H_2O$$

indicated that the overall substitution process can at its best be described by a dissociative interchange (I_d) mechanism (*48*, *51*). A typical volume profile for the reaction of aquacobalamin with 3-acetylpyridine is shown in Fig. 5 (*50*). From the nonlinear dependence of the observed pseudo-first-order rate constant on the entering ligand concentration, the precursor formation constant and rate-determining interchange rate constant could be determined and so also their pressure dependences. The volume profile clearly demonstrates the dissociative nature of the transition state and supports the operation of an I_d mechanism. Recent work in our laboratories on the subsequent substitution reactions of B_{12}–L to produce the 1:2 complex, in which the α-dimethylbenzimidazole chelate is displaced by a further ligand L for L = imidazole and histidine, revealed evidence for a dissociative substitution mechanism. The substitution process is characterized by large positive volumes of activation (*52*).

The substitution behavior of coenzyme B_{12}, in which a cobalt–carbon bond is present between the Co(III) center and the 5′-desoxy-

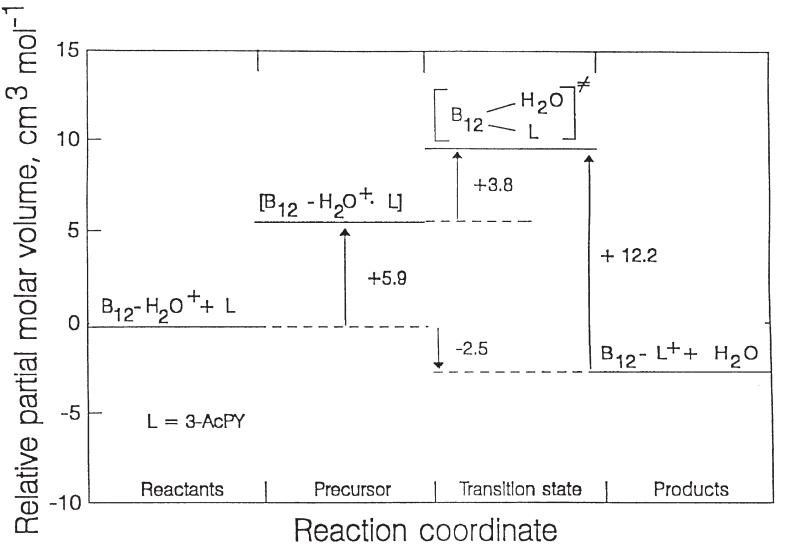

FIG. 5. Volume profile for the reaction of aquacobalamine with 3-acetylpyridine.

adenosyl moiety in the β-position, was studied in more detail recently (*53*). Surprisingly, we found that the presence of a metal–carbon bond does not induce a dissociative substitution mode. All available kinetic evidence for the reaction with cyanide, including a volume of activation of -10 cm^3 mol^{-1}, point to an associative mechanism.

C. Mechanistic Tuning of Substitution Reactions

On the basis of the available mechanistic information, a challenging question is to what extent can the substitution mechanism of metal complexes be adjusted by structural modifications of the systems. These usually involve the tuning of steric and electronic effects. A number of such examples are treated in the following sections.

The mechanistic understanding of solvent exchange reactions has reached the point where specific labilization effects can be studied in a systematic way. In this respect it is appropriate to refer to the significant translabilization caused by the deprotonation of a coordinated water molecule. In the case of the hexaaqua complexes of Fe(III), Rh(III), and Ir(III), such deprotonation can cause an increase in the water exchange rate of between 700 and 20,000 times at 298 K (*21*). This labilization is also accompanied by a changeover in mechanism from a more associative interchange for the hexaaqua-complex ions to a more dissociative interchange mechanism for the pentaaquamono-

TABLE I

RATE CONSTANTS AND ACTIVATION PARAMETERS FOR WATER EXCHANGE ON HEXAAQUA AND MONOHYDROXY PENTAAQUA TRIVALENT METAL IONS[a]

Species	Parameter	Ga(III)	Ti(III)	Fe(III)	Cr(III)	Ru(III)	Rh(III)	Ir(III)
$[M(H_2O)_6]^{3+}$	$k_1^{298}(s^{-1})$	4.0×10^2	1.8×10^5	1.6×10^2	2.4×10^{-6}	3.5×10^{-6}	2.2×10^{-9}	1.1×10^{-10}
	$\Delta H_1^{\#}$(kJ mol^{-1})	67.1	43.4	64.6	108.6	89.8	131.2	130.5
	$\Delta S_1^{\#}$(J mol^{-1} K^{-1})	+30.1	+1.2	+12.1	+11.6	−48.2	+29.3	+2.1
	$\Delta V_1^{\#}$(cm^3 mol^{-1})	+5.0	−12.1	−5.4	−9.6	−8.3	−4.1	−5.7
	Mechanism	I_d	A, I_a	I_a	I_a	I_a	I_a	I_a
$[M(OH)(H_2O)_5]^{2+}$	k_{OH}^{298} (s^{-1})	1.1×10^5		1.2×10^5	1.8×10^{-4}	5.9×10^{-4}	4.2×10^{-5}	5.6×10^{-7}
	k_{OH}/k_1	275		750	75	170	19100	5100
	$\Delta V_{OH}^{\#}$ (cm^3 mol^{-1})	+6.2		+7.0	+2.7	+0.9	+1.5	+1.3
	Mechanism	I_d		I_d	I	I	I	I

[a] From Ref. *21*.

hydroxo-complex ions. A summary of the available data is given in Table I (*21*). As a result of rapid proton exchange, labilization by coordinated hydroxide is not site specific, with the result that all five coordinated water molecules are labilized to the same extent.

Recently, the effect of pressure on the water exchange reaction of a di-μ-hydroxo Rh(III) dimer, in which the hydroxo labilization must now be site specific, was studied (*54*). The ^{17}O NMR experiments clearly demonstrated that the coordinated water molecules located cis and trans to the hydroxo bridging ligands exhibit different chemical shifts and exchange significantly faster with the bulk solvent than the bridging hydroxo groups. Surprisingly, however, was the finding that these water molecules exchange at a rather similar rate (*ca.* 5×10^{-7} s^{-1} at 298.2 K), which is *ca.* 10^2 faster than water exchange on the hexaaquarhodium(III) monomer, but *ca.* 10^2 slower than exchange on the pentaaquamonohydroxo monomer. The estimated volumes of activation were found to be between +9 and +10 cm^3 mol^{-1}, which is a clear indication for a dissociative exchange mechanism. The surprising similarity in the exchange rates of the cis and trans water molecules becomes quite understandable in terms of a dissociative mechanism. Dissociation of the more labile trans water molecules will result in the formation of a trigonal bipyramidal five-coordinate intermediate, which can via a Berry pseudo-rotation convert to a tetragonal pyramidal species with the consequence that the entering solvent molecule will take the cis position. Thus dissociative solvent exchange in such complexes results in an almost equal labilization of both the cis and trans bound water molecules.

Other examples of large labilization effects include the introduction of metal–carbon bonds on traditionally inert metal centers such as Rh(III) and Ir(III). For instance, the presence of Cp* (Cp* = Me_5Cp, Cp = cyclopentadienyl) in the complexes $M(Cp^*)(H_2O)_3^{2+}$ (M = Rh(III) and Ir(III)) causes an increase in the solvent exchange rate constant of 10^{14} as compared to the hexaaqua species (*55*). Similar reactions were also studied for the exchange of MeCN and Me_2SO on these complexes (*56*). The data in Table II demonstrate the acceleration of the solvent exchange process induced by Cp*, which, according to the volumes of activation, involves a mechanistic changeover to a dissociative interchange mechanism. In the case of water exchange on $[Ru(H_2O)_6]^{2+}$, introduction of $H_2C{=}CH_2$ into the coordination sphere increases the solvent exchange rate constant in the axial position from 1.5×10^{-3} to 0.26 s^{-1} at 279 K (*57*). In comparison, the equatorial water molecules exchange *ca.* 10^3 times slower in the substituted complex. The associated volumes of activation for the exchange of the

TABLE II

RATE CONSTANTS AND ACTIVATION PARAMETERS FOR SOLVENT EXCHANGE ON RHODIUM(III) AND IRIDIUM(III) SOLVATES[a]

Solvate	k_{ex}^{298} (s^{-1})	$\Delta H^{\#}$ (kJ mol^{-1})	$\Delta S^{\#}$ (J mol^{-1} K^{-1})	$\Delta V^{\#}$ (cm^3 mol^{-1})	Mechanism
$[Rh(H_2O)_6]^{3+}$	$(2.2 \pm 2.7) \times 10^{-9}$	131 ± 23	+29 ± 69	−4.2 ± 0.6	I_a
$[Ir(H_2O)_6]^{3+}$	$(1.1 \pm 0.1) \times 10^{-10}$	130.5 ± 0.6	+2.1 ± 1.7	−5.7 ± 0.5	I_a
$[(\eta^5\text{-}C_5Me_5)Rh(H_2O)_3]^{2+}$	$(1.6 \pm 0.3) \times 10^{5}$	65.6 ± 7.0	+75 ± 24	+0.6 ± 0.6	D
$[(\eta^5\text{-}C_5Me_5)Ir(H_2O)_3]^{2+}$	$(2.5 \pm 0.1) \times 10^{4}$	54.9 ± 3.0	+24 ± 8	+2.4 ± 0.5	D
$[(\eta^5\text{-}C_5Me_5)Rh(MeCN)_3]^{2+}$	$(3.7 \pm 0.1) \times 10^{1}$	76.7 ± 1.8	+42 ± 6	+0.8 ± 0.5	D
$[(\eta^5\text{-}C_5Me_5)Ir(MeCn)_3]^{2+}$	$(8.8 \pm 0.9) \times 10^{-2}$	85.9 ± 2.6	+23 ± 7	+1.5 ± 0.8	D
$[(\eta^5\text{-}C_5Me_5)Rh(Me_2SO)_3]^{2+}$	$(3.6 \pm 0.1) \times 10^{3}$	54.6 ± 0.3	+6.4 ± 1.1	+3.3 ± 0.1	D
$[(\eta^5\text{-}C_5Me_5)Ir(Me_2SO)_3]^{2+}$	$(2.5 \pm 0.1) \times 10^{3}$	60.3 ± 1.4	+22 ± 5	+2.8 ± 0.4	D

[a] From Ref. *55*.

axial and equatorial water molecules in $[Ru(H_2O)_5(CH_2{=}CH_2)]^{2+}$ are +6.5 and +6.1 $cm^3\ mol^{-1}$, respectively, as compared to almost zero for water exchange on $[Ru(H_2O)_6]^{2+}$, which demonstrates that a dissociative solvent exchange process is induced by $H_2C{=}CH_2$.

In a similar way, the substitution behavior of square planar complexes can be controlled systematically through appropriate ligand design and the introduction of labilizing donor ligands such as Sb, P, C, and Si. In many cases labilization is controlled by the trans effect, which in turn often results from a trans influence. There are two conceivable ways to account for the trans effect: one is the lowering of the ground state energy which results in the weakening of the bond trans to the selected ligand, i.e., increasing the bondlength (σ-donor); the other is the lowering of the transition state energy (π-acceptor). Such effects in square planar d^8 complexes were the first where detailed kinetic studies were performed in order to investigate the kinetic trans effect (*58*, *59*).

It is generally accepted that Pt(II) and Pd(II) complexes react via an associative transition state (*58*, *59*). Therefore, a large number of complexes were synthesized in efforts to induce a changeover in reaction mechanism. It could be shown that steric effects only cause a decrease in the substitution rate, but do not affect the substitution mechanism. This could be demonstrated impressively using activation volume data (*60*). In other complexes the introduction of a C atom as a strong σ-donor ligand increases the reactivity of Pt(II) by 6 orders of magnitude compared to $[Pt(H_2O)_4]^{2+}$, but does not induce a changeover in mechanism. Surprisingly, there is only one example in the literature where the authors report a changeover in the substitution mechanism, i.e., from the usual associative to the unusual dissociative mechanism. The authors point out that at least two strong σ-donors are needed to change the reaction mechanism (*61*). Various efforts followed to increase the donor capacity of the nonlabile ligand in order to weaken the trans position.

In the case of NCN donor complexes of Pt(II), where NCN represents $2,6\text{-}C_6H_3(CH_2NMe_2)_2$, van Koten and collaborators were able to compare the ligand substitution kinetics in water directly with the data for water exchange on $[Pt(NCN)H_2O]^+$ (*62*, *63*). The $\Delta V^{\#}$ values for ligand substitution and water exchange are between −9 and −12 $cm^3\ mol^{-1}$ and clearly support the associative character of the reactions. A typical volume profile for a closely related system also involving NCN donor ligands is presented in Fig. 6, from which the compact and associative nature of the transition state can be seen (*64*). This mechanistic suggestion is also supported by the discrimination ability

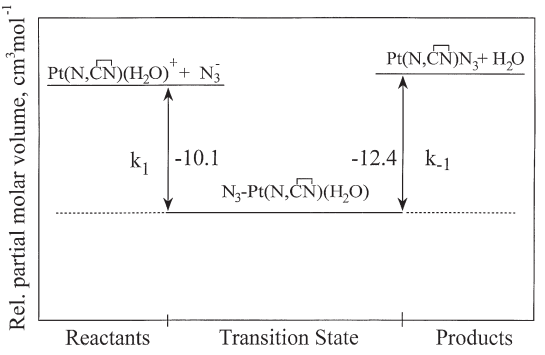

FIG. 6. Volume profile for anation of $[Pt(N,C\text{-}N)(H_2O)]^+$ by azide.

of the Pt(II) center toward various entering ligands, $SCN^- >$ thiourea $> Br^- > Cl^- > H_2O$. In addition, steric effects on the incoming ligand are important in the associative reaction mode, and for that reason tetramethylthiourea reacted slower than dimethylthiourea, which in turn reacted slower than the unsubstituted ligand. Independent of the entering ligand, the $\Delta V^{\#}$ values are all strongly negative and support the five-coordinate transition state for the substitution process.

The use of π-acceptors can also achieve a higher rate of substitution. In our group we were able to compare the substitution behavior of the Pt(II) aqua complexes of ethylenediamine and 1,10-phenanthroline, and although the reactivity of the phenanthroline complex is $\sim 10^2$ higher than the ethylenediamine complex, the activation parameters strongly indicate that an associative mechanism is operative (*65*).

Elding and co-workers synthesized a series of Pt(II) complexes with nonlabile carbon, silyl, and stilbine donor ligands to increase the σ-donor and/or the π-acceptor ability and so the rate of substitution in the trans position and the possibility of a changeover in mechanism (*66–69*). The ligands introduced into the Pt(II) coordination sphere exhibit a tremendous trans influence in the crystal structures, where the bond trans to the nonlabile ligand is lengthened by *ca.* 10 pm as compared to ligands with a weaker trans influence such as NH_3. The activation volumes and entropies for the direct and the solvolytic paths for the substitution of chloride by iodide in a series of aryl complexes, *trans*-$[Pt(Ph)Cl(SMe_2)_2]$, *trans*-$[Pt(Ph)Cl(SEt_2)_2]$, *trans*-$[Pt(mesityl)Cl(SMe_2)_2]$, and *trans*-$[Pt(p\text{-anisyl})Cl(SMe_2)_2]$, are all very negative (between -7 and -15 cm^3 mol^{-1}) and support an associative

behavior (*68*). Substitution of the chloride in the trans position in Pt(II) silyl complexes by bromide and iodide in acetonitrile and the reaction of the corresponding acetonitrile complex with iodide were studied in detail (*67*). *Trans*-[$Pt(SiPh_3)Cl(PMe_2Ph)_2$] and *trans*-[$Pt(SiPh_3)(MeCN)(PMe_2Ph)_2$] were used because they show an unusually high trans influence. The solvento complex especially is one of the most reactive complexes known. The high reactivity is ascribed to the very high trans effect of the R_3Si group and a possible π-acceptor role of the triphenylsilyl group in the five-coordinate transition state. Although the activation parameters $\Delta S^{\#}$ and $\Delta V^{\#}$ are all negative, the authors prefer an I_d type of mechanism on the basis of the low discrimination found between iodide and bromide and the effect of the leaving ligand on the activation process. The activation volume is only slightly negative and may indicate that some change in the reaction mechanism is starting to occur. Definite proof for a mechanistic changeover in these systems is still outstanding.

Solvent exchange and ligand substitution reactions can be largely affected by the influence of chelating ligands. For instance, solvent exchange on $[Fe(H_2O)_6]^{3+}$ occurs at a rate of 2×10^2 s^{-1} at 298 K and is characterized by an activation volume of -5.4 cm^3 mol^{-1}, typical for an associative interchange mechanism (*70*). The introduction of hexadentate chelating ligands such as ethylenediaminetetraacetate, cyclohexyldiaminetetraacetate, and phenylenediaminetetraacetate to produce seven-coordinate complexes of the type $[Fe^{III}(L)H_2O]^-$ result in solvent exchange rates of *ca.* 10^7 s^{-1} at 298 K (i.e., an acceleration of 10^5) and volumes of activation of between $+3.2$ and $+4.6$ cm^3 mol^{-1}, which are typical for a dissociative interchange process (*71*, *72*). Thus the increase in lability is once again accompanied by a changeover in the nature of the ligand substitution mechanism from more associative to more dissociative.

In comparison to other divalent first-row transition-metal aqua ions, the $[Cu(H_2O)_6]^{2+}$ ion is extremely labile (*73*–*76*): k_{ex} equals 4.4×10^9 s^{-1} at 298 K, which is *ca.* 5 or 3 orders of magnitude higher than in the case of the hexaqua complexes of Ni^{2+} and Co^{2+}, respectively. It is generally accepted that this effect is a consequence of Jahn–Teller distortion (*77*). As a result of the d^9 electronic configuration, an elongation of the axial-bound solvent molecules can be observed. This tetragonal distorted geometry was also found in the solid state by employing X-ray (*78*–*80*) and neutron diffraction (*81*) techniques. Due to this distortion the axial water molecules are weaker bound to the central atom and therefore can be more easily substituted. The temperature and pressure dependence of the water exchange process of the

hexaqua copper ion yields $\Delta H^{\#}$, $\Delta S^{\#}$, and $\Delta V^{\#}$ values of 11.5 ± 0.3 kJ mol^{-1}, −21.8 ± 0.9 J K^{-1} mol^{-1}, and +2.0 ± 1.5 cm^3 mol^{-1}, respectively (*75*, *76*). The activation volume indicates an interchange mechanism with a dissociative character, but it is smaller than those found for water exchange on Co^{2+} and Ni^{2+} (viz. +6.1 and +7.2 cm^3 mol^{-1}, respectively). This is also assumed to be a consequence of the Jahn–Teller distortion. The water exchange occurs mainly at the more distant axial position, and due to the Jahn–Teller inversion the coordinated water molecules invert several times before they are substituted by a bulk water molecule. The lifetime of this inversion is about 5×10^{-12} s, within the time of a single vibration (*75*). The elongated bond therefore requires a smaller increase in bondlength (and volume) to reach the dissociative transition state. More positive values for the activation volumes were found in the case of methanol and DMF exchange on Cu^{2+}, viz. +8.3 (methanol) and +8.5 cm^3 mol^{-1} (DMF), clearly indicating a dissociative character of the exchange process (*76*). The bulkiness of the coordinated solvent molecules also contributes to the more positive observed volume of activation.

The influence of the Jahn–Teller effect on the lability of six-coordinate copper ions was further illustrated by studying the reactivity of trigonal bipyramidal copper(II) complexes. One example of a trigonal bipyramidal coordinated complex is $[Cu(tren)(H_2O)]^{2+}$ (with tren = 2,2′,2″-triaminotriethylamine) with the water molecule in the fifth, axial position (*82, 83*). By employing ^{17}O-NMR measurements, a k_{ex} value of 2.4×10^6 s^{-1} at 298 K was obtained. This means that the reactivity is reduced by a factor of *ca.* 2000. In addition, a mechanistic changeover is found. The activation entropy of −34 ± 5 J K^{-1} mol^{-1} and the activation volume of −4.7 ± 0.2 cm^3 mol^{-1} indicate that the water exchange occurs via an associative interchange (I_a) mechanism with a six-coordinate transition state. The substitution of the coordinated water on $[Cu(tren)(H_2O)]^{2+}$ by pyridine and substituted pyridines also follows an I_a mechanism (*83*). The activation volumes for the forward and reverse reactions were between −5 and −10 cm^3 mol^{-1}. A second example of a trigonal bipyramidal complex is $[Cu(Me_6tren)(H_2O)]^{2+}$ (with Me_6tren = 2,2′,2″-tris(dimethylamino)triethylamine), where the terminal amino groups are fully methylated. The six methyl groups have a dramatic influence on the lability of the coordinated molecule in the fifth position. Compared to $[Cu(tren)(H_2O)]^{2+}$, the lability is reduced by factor of *ca.* 10^5 (*84*). An activation volume of +6.5 ± 0.2 cm^3 mol^{-1} for DMF exchange on $[Cu(Me_6tren)(DMF)]^{2+}$ (*85*) shows that a mechanistic changeover toward an I_d process is occurring. Even though no data for the water exchange pro-

cess is reported in the literature and DMF exchange processes usually show a more dissociative character (*86*), the reactivity pattern and the activation parameters for ligand substitution indicate that an associative process is no longer possible due to the steric hindrance on Me_6tren.

In a recent publication from our laboratory (*87*), the substitution behavior of the Cu(II) complex of the trimethylated tren (Me_3tren, each amino-terminal nitrogen is monomethylated) was studied. The substitution of the coordinated water molecule by pyridine was only slightly slower than in the tren case. The activation volumes of -8.7 ± 4.7 cm^3 mol^{-1} for the forward reaction and -6.2 ± 1.1 cm^3 mol^{-1} for the reverse aquation reaction (see the volume profile in Fig. 7) indicate that substitution occurs via an associative pathway and that the steric influence is not as significant as in the case of Me_6tren.

An associative character was also found in the study of the water exchange on $[Cu(tmpa)(H_2O)]^{2+}$ (with tmpa = tris(2-pyridylmethyl) amine) (*88*). The exchange rate constant of 8.6×10^6 s^{-1} at 298 K is only three times larger than in the tren case; a $\Delta V^{\#}$ of -3.0 ± 0.1 cm^3 mol^{-1} shows that the process is associatively activated.

Although only four examples of trigonal bipyramidal copper(II) complexes have been studied in the literature so far, these investigations have shown that substitution generally occurs via an I_a mechanism with a six-coordinate transition state. In the case of the Me_6tren complex, the steric hindrance prevents the formation of a six-coordinate transition state. The consequence is a dramatic reduction in lability and a mechanistic changeover toward an I_d mechanism. It

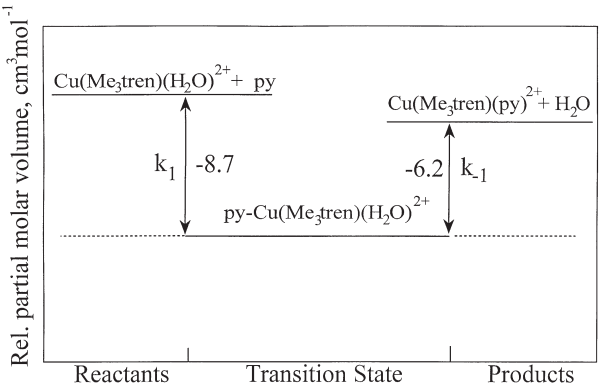

FIG. 7. Volume profile for the reaction $[Cu(Me_3tren)(H_2O)]^{2+} + py \leftrightarrow [Cu(Me_3tren)(py)]^{2+} + H_2O$.

should be noticed, however, that in some cases additional effects have to be taken into account. The substitution of the coordinated water in $[Cu(tmpa)(H_2O)]^{2+}$ by pyridine was found to be much faster than the water exchange process. This acceleration may be attributed to a $\pi-\pi$-stacking effect between the coordinated pyridine groups of tmpa and the entering aromatic amine (*89*).

D. Substitution-Induced Isomerization Reactions

A number of systems have been studied where a formal ligand displacement reaction is followed by an isomerization process. One recently described example involves the cleavage of a Pt-C(alkyl) σ-bond in complexes of the type *cis*-$[Pt(R)(R')(PEt_3)_2]$ to produce *cis*-$[Pt(R)(PEt_3)_2(MeOH)]^+$ and R′H, which subsequently isomerizes to *trans*-$[Pt(R)(PEt_3)_2(MeOH)]^+$ (*90*). The first protonolysis reaction is characterized by significantly negative volumes of activation between -8 and -16 cm^3 mol^{-1} for different combinations of R and R′. These data are discussed in terms of an electrophilic, S_E2, mechanism. In contrast, the subsequent isomerization reactions are characterized by significantly positive volumes of activation, between $+16$ and $+20$ cm^3 mol^{-1}. These values clearly underline the dissociative nature of the isomerization process involving release of coordinated MeOH to produce a three-coordinate T-shaped intermediate (*90*). Another example concerns the lability of a mononuclear tris-chelated Co(II) complex $[Co(L)_3]^{2+}$ (L = 5-methyl-2-(1′-methylbenzimidazol-2-yl)-pyridine), which undergoes rapid isomerization between the *mer* and *fac* forms (*91*). The *mer*$\rightarrow$*fac* isomerization is characterized by a volume of activation of $+6.3 \pm 0.4$ cm^3 mol^{-1} and the *fac*$\rightarrow$*mer* isomerization by a value of $+5.4 \pm 0.2$ cm^3 mol^{-1}. These values suggest a dissociatively activated isomerization process for which a volume profile is presented in Fig. 8.

In another study the kinetics and mechanism of an unprecedented η^2-vinyl isomerization of a highly fluorinated tungsten(II) metallacyclopropene complex was studied (*92*). Photolysis of a tungsten(II) tetrafluoroaryl metallacycle **1** and perfluoro-2-butyne results in the formation of the kinetic η^2-vinyl complex **2** in which the fluoride is *trans* to the inserted acetylene and *cis* to both carbonyl ligands. Upon heating **2** is converted to the thermodynamic η^2-vinyl complex **3** in which the fluoride ligand is now *cis* to the inserted alkyne and *trans* to one CO and *cis* to the second CO ligand as shown in Scheme 1.

In the absence of added CO or a phosphite ligand, the spontaneous

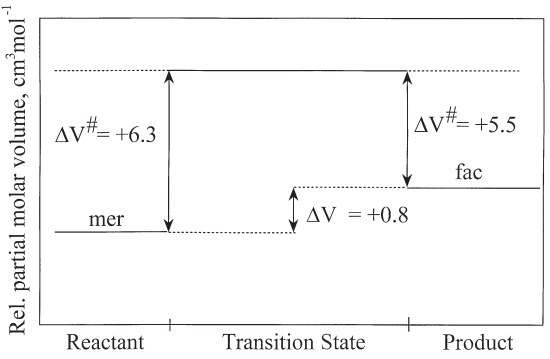

FIG. 8. Volume profile for the *mer*→*fac* intramolecular isomerization.

isomerization reaction is characterized by the activation parameters $\Delta H^{\#} = 124 \pm 2$ kJ mol^{-1}, $\Delta S^{\#} = +48 \pm 5$ J K^{-1} mol^{-1}, and $\Delta V^{\#} = +15.6 \pm 0.4$ cm^3 mol^{-1}. These data support the operation of a limiting dissociative mechanism that involves the release of CO. In the presence of added CO, the isomerization reaction is accelerated, and the mechanism in the lower part of Scheme 2 was suggested to account for this effect (*92*).

A final example concerns the question to what extent a multiple series of ligand substitution reactions can lead to the irreversible exchange of two metal centers. The system studied in our laboratories involved the exchange of Mn and Cr in the series of reactions shown in Scheme 3 (*93*).

A detailed kinetic study indicated that the overall reactions follow first-order behavior, do not exhibit a meaningful dependence on the polarity of the solvent, are independent of the concentration of the complex, do not undergo exchange with ^{13}CO during the reaction, and exhibit activation entropies and activation volumes close to zero. These findings underline the operation of an intramolecular metal exchange process, for which the mechanism in Scheme 4 was suggested (*93*).

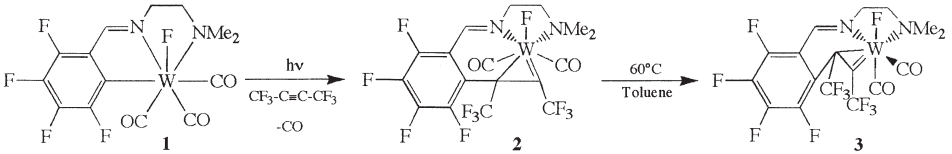

SCHEME 1.

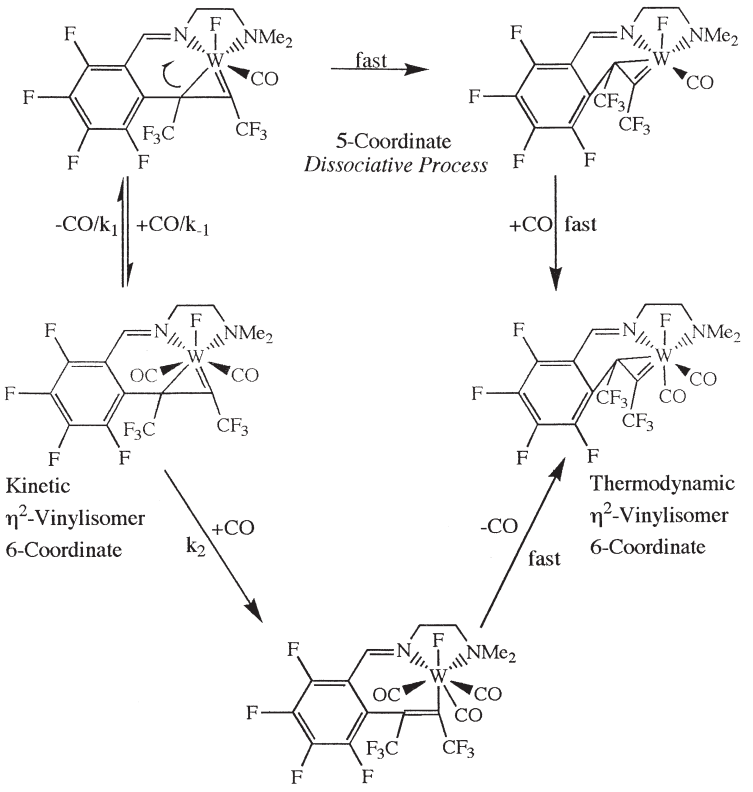

SCHEME 2.

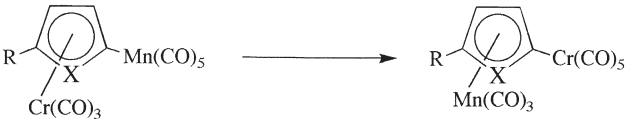

1 X = S, R = H
2 X = S, R = Me
3 X = Se, R = H

4 X = S, R = H
5 X = S, R = Me
6 X = Se, R = H

SCHEME 3.

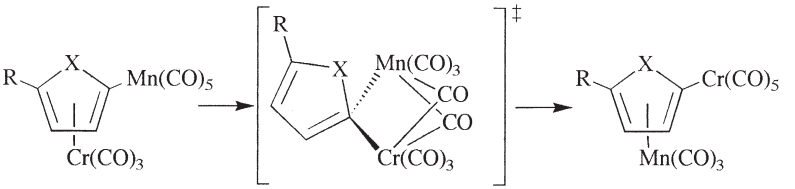

1 X = S, R = H
2 X = S, R = Me
3 X = Se, R = H

4 X = S, R = H
5 X = S, R = Me
6 X = Se, R = H

SCHEME 4.

III. Reactions with Small Molecules

This section addresses a wide variety of systems that all, in a direct or indirect way, involve the activation of small molecules. The treated systems are of biological, environmental, or industrial interest and form the basis of homogeneously catalyzed processes.

A. DIOXYGEN

Reviews on the activation of dioxygen by transition-metal complexes have appeared recently (*94*–*97*). Details of the underlying reaction mechanisms could in some cases be resolved from kinetic studies employing rapid-scan and low-temperature kinetic techniques in order to detect possible reaction intermediates and to analyze complex reaction sequences. In many cases, however, detailed mechanistic insight was not available, and high-pressure experiments coupled to the construction of volume profiles were performed in efforts to fulfill this need.

Following earlier work on the binding of dioxygen to myoglobin (*98*, *99*), a volume profile for the binding of dioxygen to hemerythrin was constructed (see Fig. 9, *100*). For the oxygenation of the iron proteins, positive activation volumes of $+13.3 \pm 1.1$ and $+5.2 \pm 0.5$ cm^3 mol^{-1} for hemerythrin and myoglobin, respectively, were found. Since bond formation processes are usually characterized by a decrease in volume (see *15*), the positive values were assigned to desolvation of oxygen during its entrance into the protein and to conformational changes on the protein itself. The release of oxygen is characterized by very positive activation volumes, $+52 \pm 1$ and $+23.3 \pm 1.8$ cm^3 mol^{-1}, for hemerythrin and myoglobin, respectively, such that the overall reaction

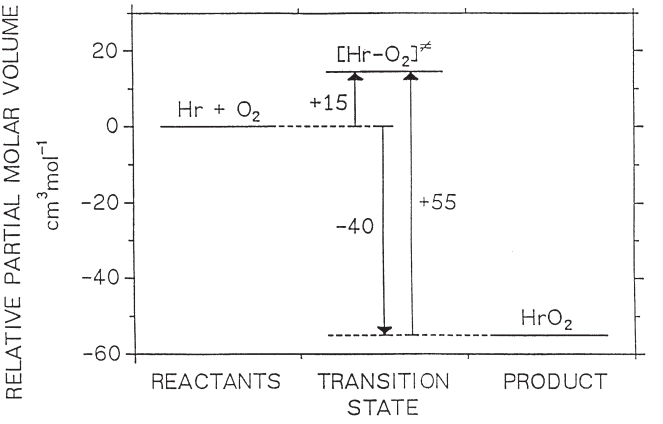

FIG. 9. Volume profile for the reaction of hemerythrin with dioxygen.

volume for the oxygenation process is strongly negative in both cases. The activation and reaction volumes for mononuclear myoglobin are about half of those found for binuclear hemerythrin. In the hemerythrin system, two Fe(II) centers are oxidized to Fe(III) during which dioxygen is reduced and bound as hydroperoxide to one Fe(III) center. The significant volume decrease that occurs following the formation of the transition state can be ascribed to the oxidation of the Fe(II) centers and the reduction of O_2 to O_2^{2-}. The fact that the overall volume collapse is almost double that observed for the oxygenation of myoglobin may indicate similar structural features in oxyhemerythrin and oxymyoglobin. This suggests that a description of the bonding mode as $Fe^{III}–O_2^-$ or $Fe^{III}–O_2H$ (H from histidine E7) instead of $Fe^{II}–O_2$ is more appropriate for oxymyoglobin.

A suitable model for the oxygen carrier protein hemerythrin is $[Fe_2(Et\text{-}HPTB)(OBz)](BF_4)_2$ (Et-HPTB = *N*,*N*,*N*′,*N*′-tetrakis[(N-ethyl-2-benzimidazolyl)methyl]-2-hydroxy-1,3-diaminopropane, OBz = benzoate). It can mimic the formation of a binuclear peroxo iron complex in the natural system (*101*). The measured value of -12.8 cm^3 mol^{-1} for the activation volume of the oxidation reaction together with the negative value of the activation entropy confirm the highly structured nature of the transition state.

One of the most fundamental questions when dealing with the activation of dioxygen by transition metal complexes is whether the process is controlled kinetically by ligand substitution or by electron transfer. A model system that involved the binding of dioxygen to a macrocyclic hexamethylcyclam Co(II) complex to form the correspond-

ing Co(III) superoxo species, thus modeling the first redox activation step of dioxygen, was studied in detail (*102*):

$$Co^{II}(L)(H_2O)_2^{2+} + O_2 \leftrightarrow Co^{III}(L)(H_2O)(O_2^-)^{2+} + H_2O$$

(L = Me_6cyclam).

The overall reaction involves ligand substitution and electron transfer, the question being which occurs first. From the pressure dependence of the overall equilibrium constant a reaction volume of -22 $cm^3\ mol^{-1}$ was determined, which demonstrated that the displacement of a water molecule on the Co(II) complex by dioxygen is accompanied by a significant volume collapse, probably mainly due to the oxidation of Co(II) to Co(III) during the overall reaction. The kinetics of the reaction could be studied by flash-photolysis, since the dioxygen complex can be photo-dissociated by irradiation into the CT band, and the subsequent reequilibration could be followed on the microsecond time scale. From the effect of pressure on the binding and release of dioxygen, the activation volumes for both processes could be determined. A combination of these activation volumes resulted in a reaction volume that is in excellent agreement with the value determined directly from the equilibrium measurements as a function of pressure. The volume profile for this reaction is given in Fig 10. The small volume of activation associated with the binding of dioxygen is clear evidence for a rate-limiting interchange of ligands, dioxygen for water, which is followed by an intramolecular electron-transfer reaction between

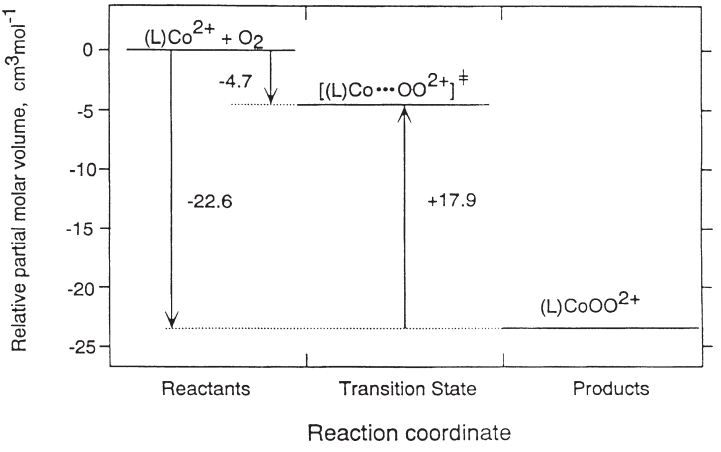

FIG. 10. Volume profile for the reaction of $[Co^{II}(Me_6cyclam)(H_2O)_2]^{2+}$ with dioxygen.

Co(II) and O_2 to form $Co^{III}–O_2^-$, the superoxo species. It is the latter process that accounts for the large volume reduction en route to the reaction products. Thus during flash-photolysis, electron transfer in the reverse direction occurs due to irradiation into the CT band, which is followed by the rapid release of dioxygen.

Oxygenation reactions of chelated Fe(II) model complexes are all markedly accelerated by pressure and accompanied by significantly negative volumes of activation (*103–105*). In these studies it was possible to resolve the different reaction steps that form part of the overall oxygenation reaction; depending on the nature of the polyamine-carboxylate chelate employed, up to four kinetically distinguishable steps could be observed. These involved coordination of dioxygen to the Fe(II) complex, intramolecular electron transfer to produce the Fe(III) superoxo complex, formation of a mixed valence superoxo-bridged complex, and electron transfer to form a peroxo-bridged dimeric Fe(III) complex. The negative volumes of activation could be accounted for in terms of the oxidation of Fe(II) to Fe(III) accompanied by the reduction of dioxygen to superoxide and peroxide.

The reaction of binuclear copper complexes with oxygen as models for tyrosinase activity was also markedly accelerated by applying pressure (*106–108*). Tyrosinase is a dinuclear copper protein which catalyses the hydroxylation of phenols. This reaction was first successfully modeled by Karlin and co-workers (*109*), who found that an intramolecular hydroxylation occurred when the binuclear Cu(I) complex of XYL–H was treated with oxygen (Scheme 5).

In a recent paper a detailed mechanistic study of this reaction was presented (*108*). The first step is the reversible binding of oxygen by forming a μ-peroxo species. This intermediate reacts further via an irreversible step to the hydroxylated product. The kinetic measurements at high pressure were performed at $-20°C$, since at room temperature no peroxo intermediate can be observed. The forward reaction of the Cu(I) complex with oxygen is characterized by a strongly

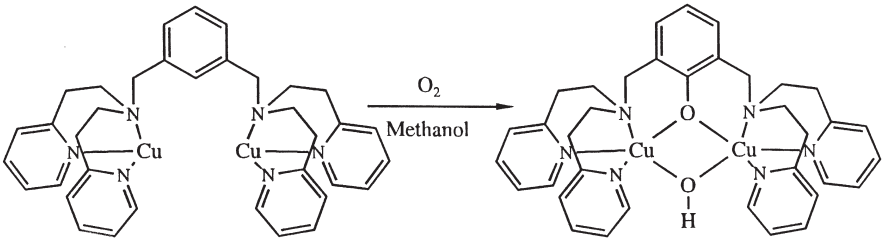

SCHEME 5.

negative activation volume of -15.0 ± 2.5 cm^3 mol^{-1}, whereas the release of oxygen from the peroxo species occurs via a dissociative interchange mechanism with a $\Delta V^{\#}$ of $+4.4 \pm 0.5$ cm^3 mol^{-1}. The latter is a consequence of bond breakage. The negative volume of activation for the forward reaction is caused by Cu–O_2 bond formation and the accompanied electron transfer process, whereby Cu(I) is oxidized to Cu(II) and O_2 is reduced to O_2^{2-}. This leads to the collapse in the partial molar volume. The volume profile for this reaction is presented in Fig. 11. The profile clearly shows a more "productlike" transition state. The second step, the formation of the hydroxylated product, is again modestly accelerated by pressure and a $\Delta V^{\#}$ of -4.1 ± 0.7 cm^3 mol^{-1} was found. This rather small value is ascribed to the combination of bond breakage and geometrical rearrangement processes. This was the first study where activation volumes for different steps involved in such reactions could be obtained. It has to be considered, however, that also these parameters are in part combinations of those of more complicated step processes.

In two earlier studies (*106*, *107*), the oxidation of two Schiff base complexes were studied at room temperature, but in these cases only activation parameters for the overall process could be obtained since it was not possible to detect the formation of an intermediate species which could be attributed to a peroxo species. Nevertheless, the kinetic measurements provided indirect evidence for the existence of this intermediate. In both studies negative values for the activation entropies and the activation volumes were obtained. The oxidation of $[Cu_2(H\text{-}BPB\text{-}H)(CH_3CN)_2](PF_6)_2$ (H-BPB-H = 1,3-bis[*N*-(2-pyridylethyl)-formidoyl]benzene) is accompanied by an activation entropy of -53 ± 11 J K^{-1} mol^{-1} and an activation volume of -9.5 ± 0.5 cm^3 mol^{-1}. In

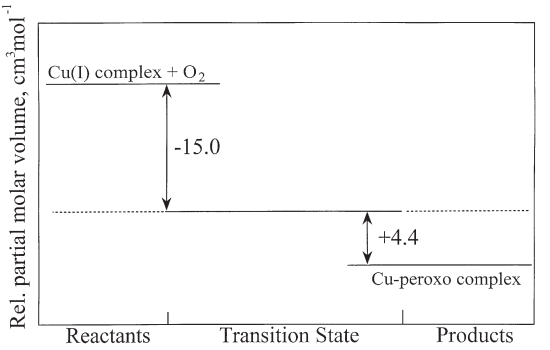

FIG. 11. Volume profile for the reaction of the Cu(I) complex with dioxygen.

the case of the oxidation of $[Cu_2(mac)(CH_3CN)_2](PF_6)_2$ (mac = 3,6,9,17,20,23-hexatricyclo-[23.3.1.1]tiacontal(29),2,9,11-(30),12(13),14,16,23,25,27-decaene), a $\Delta S^{\#}$ of -146 ± 8 J K^{-1} mol^{-1} and a $\Delta V^{\#}$ of -21 ± 1 cm^3 mol^{-1} are even more negative than in the previous example. These negative values are indicative of a highly ordered transition state, including a strong copper–oxygen bond formation and a volume collapse caused by the electron-transfer process. The even more negative values in the latter case were attributed to an additional occurrence of geometrical rearrangements for the macrocyclic complex which are not observed in the open complex.

In one case pulse-radiolysis techniques were employed to study the effect of pressure on such reactions. The oxidation of $[Cu^{I}(phen)_2]$ by dioxygen proceeds via a Cu^{I}–O_2 transient in which a copper–oxygen bond is formed, followed by the rapid formation of $[Cu^{II}(phen)_2]$ and O_2^- (*110*). This process is characterized by a $\Delta V^{\#}$ of -22 cm^3 mol^{-1}, which is close to the reaction volume expected for the binding of dioxygen.

B. Carbon Monoxide

The binding of CO has in many studies been used as a model for the activation of dioxygen, since this molecule does not undergo any real activation in the systems studied; it merely binds to the metal center. The absence of subsequent electron transfer reactions simplifies the kinetic analysis and reveals more mechanistic insight on the actual binding process.

A typical example concerns the comparative binding of O_2 and CO to deoxymyoglobin (*111*). The volume profile for the binding of O_2, as described above, is characterized by a substantial increase in volume in going from the reactant to the transition state, followed by a significant volume reduction on going to the product state. The volume profile for the binding of CO (see Fig. 12), however, shows a considerable volume decrease on going from the reactant state to the transition state, which was ascribed to rate-determining bond formation. The reverse bond cleavage reaction is accompanied by a volume decrease, which may be related to the different bonding mode of CO compared with O_2. The difference in bonding mode must also account for the much smaller absolute reaction volume observed in this case.

In another study the binding of CO to lacunar Fe(II) complexes was studied in detail as a function of temperature and pressure (*112*, *113*). In these systems the high-spin Fe(II) center is five coordinate and has a vacant pocket available for the binding of CO. These systems can

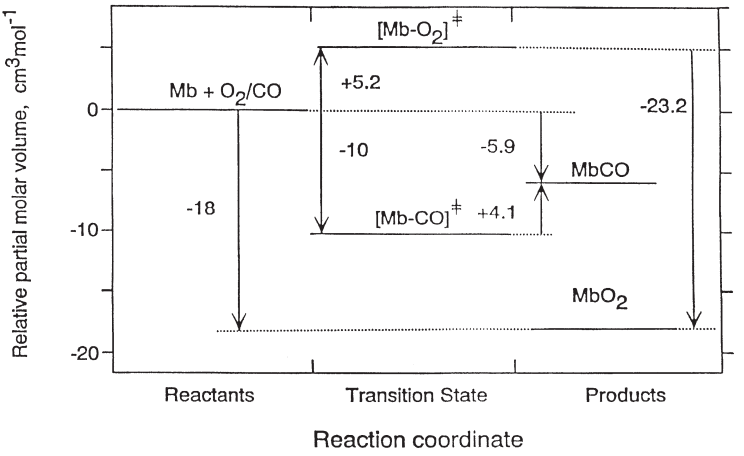

FIG. 12. Volume profile for the reaction of CO and O_2 with myoglobin.

therefore be considered as ideal for the modeling of biological processes. A detailed kinetic analysis of the "on" and "off" reactions, as well as a thermodynamic analysis of the overall equilibrium, enabled the construction of the energy and volume profiles for the binding of CO to $[Fe^{II}(PhBzXy)](PF_6)_2$, of which the latter is shown in Fig. 13 (*113*). The free energy profile demonstrates the favorable thermodynamic driving force for the overall reaction as well as the relatively low activation energy for the binding process. The entropy profile demonstrates the high degree of order in the transition state on the binding of CO. The large volume collapse associated with the forward reaction is very close to the partial molar volume of CO, which suggests that CO completely disappears within the ligand pocket cavity of the complex in the transition state during partial Fe–CO bond formation. It is also known (*112*) that Fe^{II}–CO bond formation is accompanied by a high-spin to low-spin conversion of the Fe(II) center. In forming the six-coordinate, low-spin Fe(II) complex, the metal moves into the plane of the equatorial nitrogen donors. Thus following the transition state for the binding of CO, there is a high-spin to low-spin change during which bond formation is completed and the metal center moves into the ligand plane. These processes account for the subsequent volume decrease observed from the transition to the product state. The overall reaction volume of -49 cm^3 mol^{-1} therefore consists of a volume decrease of *ca.* -37 cm^3 mol^{-1} associated with the disappearance of CO into the ligand cavity and *ca.* -12 cm^3 mol^{-1} for the high-spin to low-spin transition.

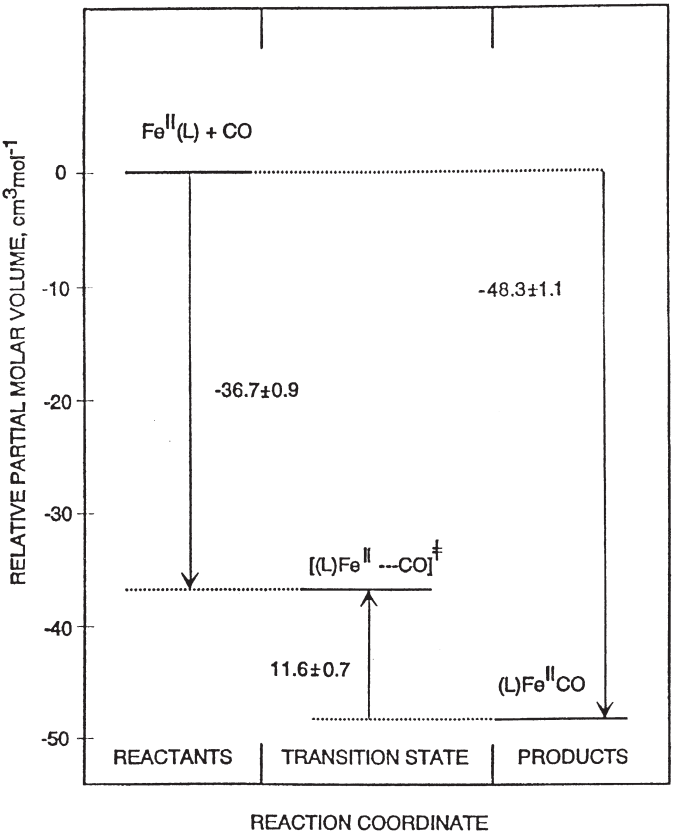

FIG. 13. Volume profile for the reaction of $[Fe^{II}(PhBzXy)](PF_6)_2$ with CO.

C. Carbon Dioxide

The most fundamental process dealing with the activation of CO_2 involves the hydration of CO_2 to produce bicarbonate and the reverse dehydration of bicarbonate to produce CO_2. These processes are of biological and environmental significance since they control the transport and equilibrium behavior of CO_2. The spontaneous hydration of CO_2 and dehydration of HCO_3^- are processes that are too slow and must therefore be catalyzed by metal complexes in order to expedite the overall conversion rate. In biological systems, a series of enzymes, the carbonic anhydrases, are the efficient catalysts and can accelerate the reactions by up to 7 orders of magnitude. The mechanism of this

catalytic process has been the subject of many experimental and theoretical studies.

The active center of the zinc-containing metalloenzyme carbonic anhydrase (CA) consists of three histidine residues and one water molecule coordinated to zinc in a slightly distorted tetrahedral geometry. Catalytic activity is integrally related to the ionization (pK_a value *ca.* 7) of the coordinated water molecule, which is significantly more acidic than in the case of octahedrally coordinated $[Zn(H_2O)_6]^{2+}$ (pK_a value *ca.* 9) (*114-115*). In the case of human CA II, the mechanism is referred to as the zinc hydroxide mechanism, which has been described and modeled theoretically in considerable detail (*116*). According to this mechanism it is the hydroxo form of the enzyme that can bind CO_2 to produce a bicarbonato complex, which subsequently undergoes a ligand exchange reaction with water to rapidly release HCO_3^-. During the reverse dehydration reaction, it is the aqua form of the enzyme that is the reactive species, which rapidly binds HCO_3^- via a substitution of coordinated water, followed by decarboxylation to release CO_2, with the result that the hydration and dehydration reactions exhibit very characteristic pH dependences. Two mechanisms are discussed in the literature to account for the formation of the bicarbonato complex: the formation may involve a proton transfer process, the so-called Lipscomb mechanism (*117*), or it may proceed via a bidentate carbonato intermediate, the so-called Lindskog mechanism (*118*). The mechanisms are outlined in Scheme 6.

From a recent study in our laboratories, a high-pressure kinetic investigation was performed in order to gain further insight into the mechanism of this process (*119*). In the first step of the reaction the OH moiety of the enzyme attacks the entering carbon dioxide and a bicarbonato intermediate is formed. In the consecutive step the bicarbonato ligand is substituted by a water molecule and the aqua species is produced. The active hydroxo species is reproduced via deprotonation of the coordinated water molecule through a two-water-molecule bridge to the neighboring His-64 group. The activation volume of -9 ± 1 cm^3 mol^{-1} for the nucleophic attack of the hydroxo group on carbon dioxide indicates an associative bond formation process. The formation of the bicarbonato species is accompanied by an overall volume collapse of -18 cm^3 mol^{-1}. The dehydration of HCO_3^- by the Zn–H_2O moiety is slowed down by increasing pressure and an activation volume of $+14.0 \pm 1.2$ cm^3 mol^{-1} was reported. This value supports a limiting dissociative displacement of coordinated water by bicarbonate. The activation volume for the reverse substitution of coordinated bicarbonate by water could be estimated from this value and the over-

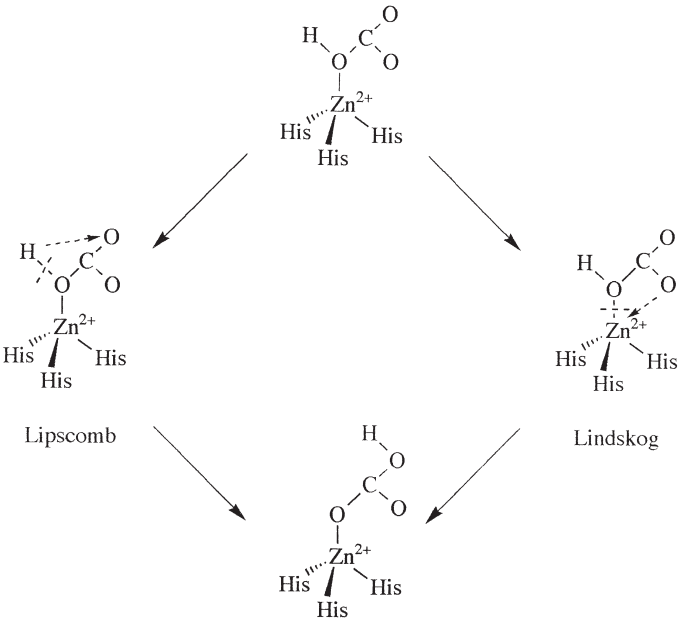

SCHEME 6.

all reaction volume of -26.0 cm^3 mol^{-1}. The resulting $\Delta V^{\#}$ of $+6.0 \pm 0.6$ cm^3 mol^{-1} also indicates a dissociative character for the substitution reaction of the bicarbonato species. The smaller absolute value can be accounted for in terms of an increase in electrostriction due to partial charge creation during the dissociation of bicarbonate. The resulting, first complete volume profile for an enzymatic process is shown in Fig. 14 (*119*). In general, a close agreement exists between the volume profile for the uncatalyzed reaction obtained earlier (*120*) and that reported in Fig. 14 (see left side) for the binding of CO_2 to the metal hydroxo species. Both transition states lie approximately halfway between the reactant and product states on a volume basis along the reaction coordinate. Since these reactions involve a CO_2 addition process, the associated volume profiles differ completely from that observed for the ligand substitution of bicarbonate by water (see right side of Fig. 14).

Model complexes should on the one hand mimic the active site of the enzyme and on the other hand exhibit the characteristic pH dependence observed in the catalytic activity of the enzyme. The first model complex that could adhere to both these requirements was the

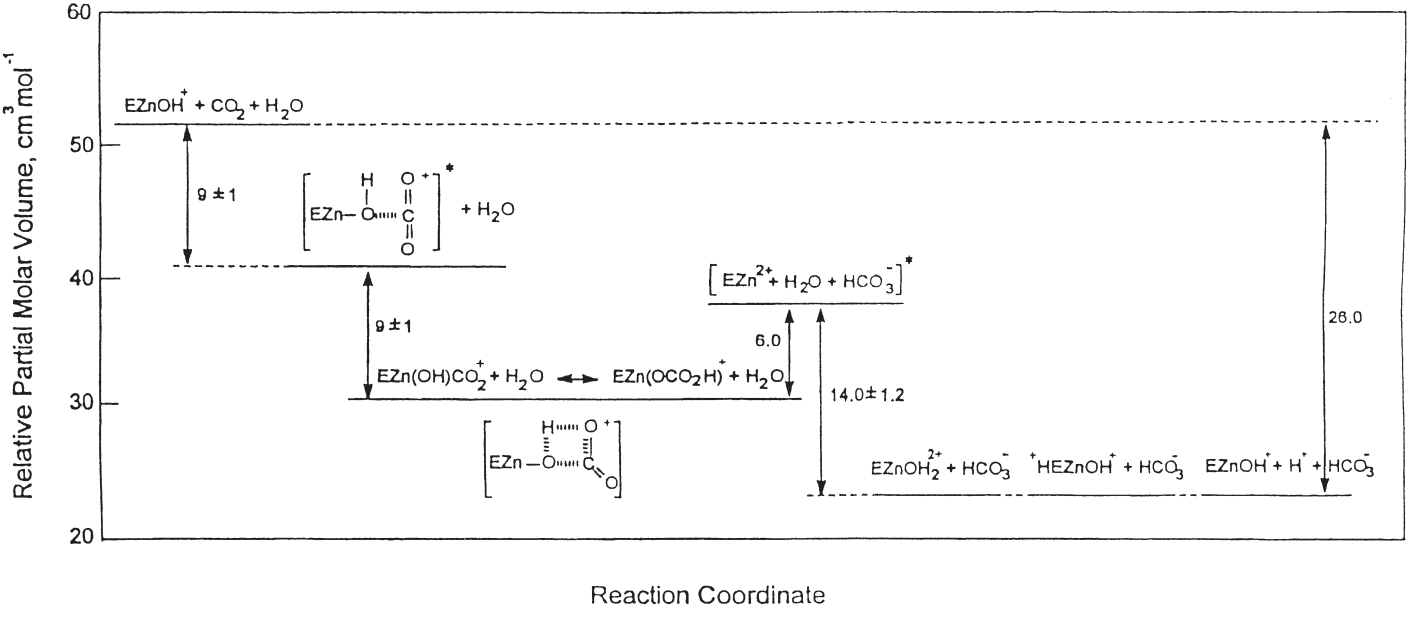

FIG. 14. Volume profile for the carbonic anhydrase catalyzed hydration of CO_2 and dehydration of HCO_3^-.

triazacyclododecane complex of Zn(II), i.e., $Zn([12]aneN_3)H_2O^{2+}$, which has a pK_a value of 7.3 (*121*). From the pH dependence of both the hydration and dehydration reactions, it followed that only the hydroxo complex catalyzes the hydration of CO_2 and only the aqua complex catalyzes the dehydration of HCO_3^-. A significantly higher catalytic activity was found for the five-coordinate tetraazacyclododecane complex, i.e., $Zn([12]aneN_4)H_2O^{2+}$, which has a pK_a value of 8.0 (*122*). Both the hydration and dehydration rate constants of this model catalyst were between five and six times higher than for the four-coordinate triazacyclododecane complex. This is associated with the possibility that the four-coordinate complex can stabilize the bicarbonate intermediate through ring closure, something that is less likely for the five-coordinate complex and thus its higher catalytic activity (*122*). The ability of these simple coordination compounds to mimic the catalytic activity of CA is impressive, but their actual reactivity is still orders of magnitude below that of CA.

Fujita *et al.* (*123*) and others have used a wide range of methods to study cobalt(I) complexes with tetraazamacrocyclic ligands as potential catalysts for the reduction of CO_2. The interaction of the low-spin $[Co^{I}HMD]^+$ species (HMD = 5,7,7,12,14,14-hexamethyl-1,4,8,11-tetraazacyclotetradecane-4,11-diene) with CO_2 in CH_3CN leads to a five-coordinate species, $[CoHMD(CO_2)]^+$, which is in equilibrium with a six-coordinate complex ion, $[CoHMD(CO_2)(CH_3CN)]^+$, formed through addition of CH_3CN. Results from an XANES study together with other information provide a clear indication that in the six-coordinate complex cobalt is in the +3 oxidation state, meaning that the complex ion is $Co^{III}–CO_2^{2-}$ (i.e., CO_2 is coordinated as carboxylate). Hence the initial cobalt(I) complex has reduced the bound CO_2 to carboxylate. The change in coordination number equilibrium can be studied readily by UV-vis spectrophotometry; a decrease in temperature or an increase in pressure favor the formation of the $Co^{III}–CO_2^2-$ species. The thermodynamic parameters for this equilibrium are $\Delta H^\circ = -29$ kJ mol^{-1}, $\Delta S^\circ = -113$ J mol^{-1} K^{-1}, and $\Delta V^\circ = -17.7$ cm^3 mol^{-1}. The latter two are mutually compatible and consistent with a highly ordered and compact six-coordinate complex ion. It has been proposed that a major part of the volume decrease arises from the intramolecular electron-transfer process accompanied by a shortening of the Co–CO_2 bond (as supported by XANES and EXAFS studies) and an increase in electrostriction. Only a relatively minor contribution to the large negative reaction volume is suggested to result from the intrinsic effect of CH_3CN addition (*123*).

IV. Electron-Transfer Reactions

In the following sections the effect of pressure on different types of electron-transfer processes is discussed systematically. Some of our work in this area was reviewed as part of a special symposium devoted to the complementarity of various experimental techniques in the study of electron-transfer reactions (*124*). Swaddle and Tregloan recently reviewed electrode reactions of metal complexes in solution at high pressure (*125*). The main emphasis in this section is on some of the most recent work that we have been involved in, dealing with "long-distance" electron-transfer processes involving cytochrome *c*. However, by way of introduction, a short discussion on the effect of pressure on self-exchange (symmetrical) and nonsymmetrical electron-transfer reactions between transition metal complexes that have been reported in the literature, is presented.

A. Self-Exchange Reactions

Self-exchange reactions are the most simple type of electron-transfer reaction; they are symmetrical processes for which both the reaction free energy and reaction volume are zero and thus are ideal for theoretical modeling. They form the basis for much of the discussion and interpretation of nonsymmetrical reactions in a similar way as solvent exchange reactions form a basis for the understanding of ligand substitution reactions. Swaddle and co-workers have made a significant contribution in this area. They have studied the effect of pressure on the self-exchange reactions (volumes of activation are quoted in brackets in cubic centimeters per mole): $[Fe(H_2O)_6]^{3+/2+}$ (-11.1) (*126*), $[Fe(phen)_3]^{3+/2+}$ (-2.2) (*127*), $[Fe(CN)_6]^{3-/4-}$ ($+22$) (*128*), $[MnO_4]^{2-/-}$ (-23) (*129*), $[Co(sep)]^{3+/2+}$ (-6.4) (*130*), $[Co([9]aneS_3)]^{3+/2+}$ (-4.8) (*130*), $[Co(diamsarH_2)]^{5+/4+}$ (-9.6) (*131*), $[Co(diamsar)]^{3+/2+}$ (-10.4) (*131*), $[Co(en)_3]^{3+/2+}$ (-15.5) (*132*), and $[Co(phen)_3]^{3+/2+}$ (-17.6) (*133*). In the majority of cases the self-exchange reaction is significantly accelerated by pressure, with the exception of the $[Fe(CN)_6]^{3-/4-}$ system, which goes in exactly the opposite way, and the observed volume of activation is in agreement with the significantly negative entropy of activation reported for such systems. In addition, they have also gone through impressive efforts to calculate the volumes of activation theoretically based on the Marcus-Hush-Stranks treatment and their own modifications and additions (*134*, *135*). For a large number of systems a good agreement between the experimental and

theoretically calculated volumes of activation were found, as shown in Fig. 15. In most cases solvent reorganization accounts for the largest contribution toward the observed volume of activation. Large deviations were found only for the $[Co(en)_3]^{3+/2+}$ and $[Co(phen)_3]^{3+/2+}$ systems where the theoretical volume of activation is between 10 and 15 cm^3 mol^{-1} more positive than the experimental value (*132*, *133*). This deviation is most probably related to the participation of a high-spin to low-spin changeover associated with the electron-transfer process, which can account for an additional volume collapse of *ca.* 10 to 15 cm^3 mol^{-1} (*131*).

More recently, Swaddle and co-workers (*136-138*) have demonstrated that a good correlation exists between the volume of activation for a homogeneous self-exchange reaction and the activation volume for the heterogeneous self-exchange reaction at an electrode. The slope of the line in Fig. 16 for 10 sets of data is 0.50 and in precise agreement with an extension of the Marcus theory. This led the authors to suggest a "fifty-percent rule" with which volume of activation data can be predicted for self-exchange reactions, which cannot be measured directly for technical reasons, on the basis of electrochemical data recorded as a function of pressure.

The above-quoted reactions all proceed via an outer-sphere electron-transfer mechanism. By way of comparison, the volume of activa-

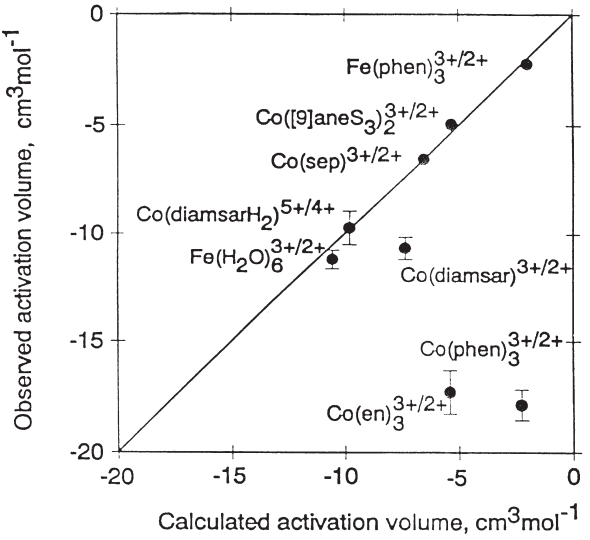

FIG. 15. Plot of $\Delta V^{\#}$ (observed) versus $\Delta V^{\#}$ (calculated) for a series of self-exchange electron-transfer reactions.

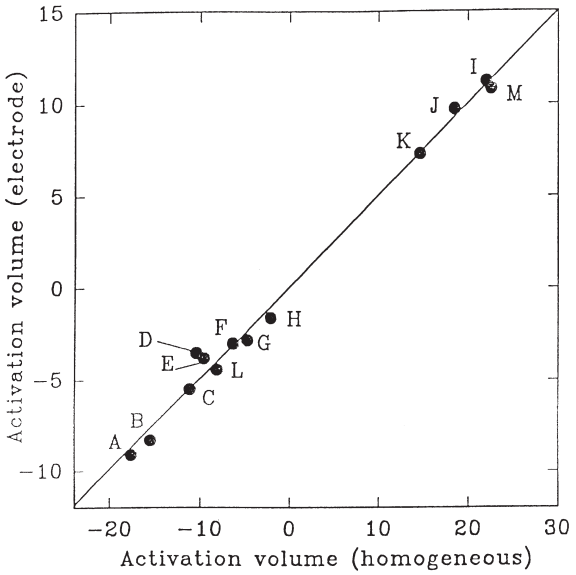

FIG. 16. Plot of $\Delta V^{\#}$ (electrode) versus $\Delta V^{\#}$ (homogeneous) for a series of self-exchange couples: (A) $Co(phen)_3^{3+/2+}$; (B) $Co(en)_3^{3+/2+}$; (C) $Fe(H_2O)_6^{3+/2+}$; (D) $Co(diamsar)^{3+/2+}$; (E) $Co(diamsarH_2)^{5+/4+}$; (F) $Co(sep)^{3+/2+}$; (G) $Co(ttcn)_2^{3+/2+}$; (H) $Fe(phen)_3^{3+/2+}$; (I) $Fe(CN)_6^{3-/4-}$; (J) $Os(CN)_6^{3-/4-}$; (K) $Mo(CN)_8^{3-/4-}$; (L) $Mo(CN)_8^{3-/4-}$; (M) $W(CN)_8^{3-/4-}$.

tion for the exchange reaction in $[Fe(H_2O)_5OH]^{2+}/[Fe(H_2O)_6]^{2+}$ was reported to be $+0.8$ cm^3 mol^{-1}, i.e., significantly more positive than found for $[Fe(H_2O)_6]^{3+/2+}$ (*126*). This difference was ascribed to the release of a solvent molecule associated with the formation of an hydroxo-bridged intermediate in terms of an inner-sphere mechanism.

B. Nonsymmetrical Reactions

For the mechanistic interpretation of activation volume data for nonsymmetrical electron-transfer reactions, it is essential to have information on the overall volume change that can occur during such a process. This can be calculated from the partial molar volumes of reactant and product species, when these are available, or can be determined from density measurements. Efforts have in recent years focused on the electrochemical determination of reaction volume data from the pressure dependence of the redox potential. Tregloan and coworkers (*139*, *140*) have demonstrated how such techniques can reveal information on the magnitude of intrinsic and solvational volume changes associated with electron-transfer reactions of transition

metal complexes. The measured reaction volumes have to be corrected for the effect of pressure on the reference electrode, and they conducted a well-designed set of experiments on a series of $Fe^{II/III}$ couples in which the ligands were systematically varied in order to adjust the overall charge of the complex and therefore the solvational contribution toward the overall reaction volume. A good correlation was found between the reaction volume and the difference in the square of the charge on the oxidized and reduced forms of the complex as shown in Fig. 17 (*139*). By interpolation to $\Delta z^2 = 0$, the reaction volume for the Ag/AgCl reference electrode was determined to be -11.9 ± 0.5 cm^3 mol^{-1}. Measurements on a series of Cr, Co, and Ru complexes (*140*) enabled a systematic differentiation to be made between intrinsic and solvational volume contributions associated with the redox process.

It has in general been the objective of many mechanistic studies dealing with inorganic electron-transfer reactions to distinguish between outer- and inner-sphere mechanisms. Along these lines high-pressure kinetic methods and the construction of reaction volume profiles have also been employed to contribute toward a better understanding of the intimate mechanisms involved in such processes. The differentiation between outer- and inner-sphere mechanisms depends

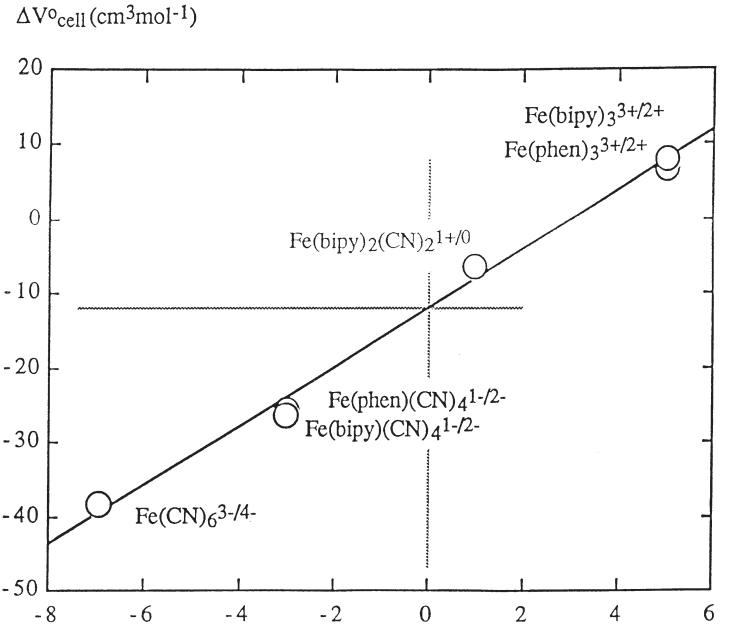

FIG. 17. Plot of ΔV^{o}_{cell} versus $Z^2_{ox} - Z^2_{red}$ for a series of Fe(II)/Fe(III) redox systems.

on the nature of the precursor species (Ox//Red in the following scheme), which can be an ion pair, an encounter complex, or a bridged intermediate, respectively:

$$\mathrm{Ox} + \mathrm{Red} \leftrightarrow \mathrm{Ox//Red} \quad ,K$$

$$\mathrm{Ox//Red} \rightarrow \mathrm{Ox^{-}//Red^{+}} \quad ,k_{\mathrm{ET}}$$

$$\mathrm{Ox^{-}//Red^{+}} \leftrightarrow \mathrm{Ox^{-}} + \mathrm{Red^{+}}.$$

The coordination sphere of the reactants remains intact in the former case and is modified by ligand substitution in the latter, which will naturally affect the associated volume changes.

A general difficulty encountered in kinetic studies of outer-sphere electron-transfer processes concerns the separation of the precursor formation constant (K) and the electron-transfer rate constant (k_{ET}) in the reactions outlined above. In the majority of cases, precursor formation is a diffusion controlled step, followed by rate-determining electron transfer. In the presence of an excess of Red, the rate expression is given by

$$k_{\mathrm{obs}} = k_{\mathrm{ET}}K[\mathrm{Red}]/(1 + K[\mathrm{Red}]).$$

In many cases K is small, such that this equation simplifies to $k_{\mathrm{obs}} = k_{\mathrm{ET}}K[\mathrm{Red}]$, which means that the observed second-order rate constant and the associated activation parameters are composite quantities, viz. $\Delta V^{\#} = \Delta V^{\#}(k_{\mathrm{ET}}) + \Delta V(K)$. When K is large enough such that $1 + K[\mathrm{Red}] > 1$, it is possible to separate k_{ET} and K kinetically and also the associated activation parameters, viz. $\Delta V^{\#}(k_{\mathrm{ET}})$ and $\Delta V(K)$ (*141*). A series of reactions were studied where it was possible to resolve K and k_{ET}, i.e., $\Delta V(K)$ and $\Delta V^{\#}(k_{\mathrm{ET}})$. In this case oppositely charged reaction partners were selected as indicated in the following reactions (*142-144*):

$$[\mathrm{Co(NH_3)_5X}]^{(3-n)+} + [\mathrm{Fe(CN)_6}]^{4-} \leftrightarrow \{\mathrm{Co(NH_3)_5X^{(3-n)+}, Fe(CN)_6^{4-}}\} \quad ,K$$

$$\{\mathrm{Co(NH_3)_5X^{(3-n)+}, Fe(CN)_6^{4-}}\} \rightarrow \mathrm{Co^{2+}} + 5\mathrm{NH_3} + \mathrm{X^{n-}} + [\mathrm{Fe(CN)_6}]^{3-} \quad ,k_{\mathrm{ET}}$$

$$\mathrm{X^{n-}} = \mathrm{H_2O, Me_2SO, py, Cl^{-}, N_3^{-}}.$$

Throughout the series, ion-pair formation is accompanied by significantly negative ΔS° values and close-to-zero ΔV values. The latter is rather surprising, since it is generally accepted that ion-pair formation should involve considerable charge neutralization accompanied

by strong desolvation due to a decrease in electrostriction. The values of ΔV therefore indicate that the reaction partners most probably exist as solvent-separated ion pairs, i.e., with no significant charge neutralization accompanied by desolvation. The activation parameters demonstrate that the electron-transfer steps exhibit a strong pressure deceleration, most systems have a $\Delta V^{\#}$ value of between +25 and +34 $cm^3\ mol^{-1}$. These values indicate that electron transfer is accompanied by extensive desolvation, most probably related to charge neutralization associated with the electron-transfer process (*144*). A simplified model based on partial molar volume data, in which electron transfer occurs from the precursor ion pair $\{Co(NH_3)_5X^{(3-n)+},Fe(CN)_6^{4-}\}$ to the successor ion pair $\{Co(NH_3)_5X^{(2-n)+},Fe(CN)_6^{3-}\}$, predicts an overall volume increase of *ca.* 65 $cm^3\ mol^{-1}$. This means that according to the reported $\Delta V^{\#}$ values the transition state for the electron-transfer process lies approximately halfway between the reactant and product states on a volume basis for the precursor and successor ion pairs. The largest volume contribution arises from the oxidation of $[Fe(CN)_6]^{4-}$ to $[Fe(CN)_6]^{3-}$, which is accompanied by a large decrease in electrostriction and an increase in partial molar volume. Theoretical calculations also confirmed that the transition state for these reactions lies approximately halfway along the reaction coordinate on a volume basis (*144*). This first information on the nature of the volume profile for an outer-sphere electron-transfer reaction proved to be in good agreement with subsequently reported results for systems with low driving forces in which it was possible to construct a complete volume profile by studying the effect of pressure on both the forward and reverse reactions as well as on the overall equilibrium constant (see below). Data have also been reported for a series of related complexes containing phosphoroxo ligands (*145*–*147*), and the results can be interpreted in terms of major solvational changes associated with the oxidation of $[Fe(CN)_6]^{4-}$.

C. Bioinorganic Reactions

A number of electron-transfer reactions of biological interest have been studied using high-pressure techniques (*4*, *5*). These include the oxidation of L-ascorbic acid by $[Fe(CN)_6]^{3-}$ (*148*), $[Fe(CN)_5NO_2]^{3-}$ (*149*), and $Fe(phen)_2(CN)_2]^{-}$ (*150*). The first two reactions are characterized by volumes of activation of −16 and −10 $cm^3\ mol^{-1}$, respectively, which indicate that solvent rearrangement as a result of an increase in electrostriction must account for the volume collapse on going to

the transition state. In comparison, the third reaction exhibited almost no pressure dependence, in line with significantly less charge formation than in the case of the 3− charged complexes. The oxidation of deoxy- and oxymyoglobin by $[Fe(CN)_6]^{3-}$ was also studied as a function of pressure (*151*). The oxidation of deoxymyoglobin is approximately seven times faster than the oxidation of oxymyoglobin at 298 K, and the corresponding volume of activation, determined under limiting kinetic conditions, is -20 cm^3 mol^{-1}. This value is in good agreement with that reported above for the reduction of $[Fe(CN)_6]^{3-}$ to $[Fe(CN)_6]^{4-}$. The oxidation of oxymyoglobin is characterized by an activation volume of -3 cm^3 mol^{-1}, which must be corrected for the reaction volume of -19 cm^3 mol^{-1} associated with the binding of dioxygen to myoglobin (*98*). The resulting -22 cm^3 mol^{-1} is once again in good agreement with that expected for the reduction of $[Fe(CN)_6]^{3-}$.

A challenging question concerns the feasibility of the application of high-pressure kinetic and thermodynamic techniques in the study of such reactions. Do "long-distance" electron-transfer processes exhibit a characteristic pressure dependence and to what extent can a volume profile analysis reveal information on the intimate mechanism?

The systems that we investigated in collaboration with others involved intermolecular and intramolecular electron-transfer reactions between ruthenium complexes and cytochrome *c*. We also studied a series of intermolecular reactions between chelated cobalt complexes and cytochrome *c*. A variety of high-pressure experimental techniques, including stopped-flow, flash-photolysis, pulse-radiolysis, and voltammetry, were employed in these investigations. As the following presentation shows, a remarkably good agreement was found between the volume data obtained with the aid of these different techniques, which clearly demonstrates the complementarity of these methods for the study of electron-transfer processes.

Application of pulse-radiolysis techniques revealed that the following intramolecular and intermolecular electron-transfer reactions all exhibit a significant acceleration with increasing pressure. The reported volumes of activation are -17.7 ± 0.9, -18.3 ± 0.7, and -15.6 ± 0.6 cm^3 mol^{-1}, respectively, and clearly demonstrate a significant volume collapse on going from the reactant to the transition state (*152*):

$$(NH_3)_5Ru^{II}\text{-(His33)cyt } c^{III} \rightarrow (NH_3)_5Ru^{III}\text{-(His33)cyt } c^{II}$$

$$(NH_3)_5Ru^{II}\text{-(His39)cyt } c^{III} \rightarrow (NH_3)_5Ru^{III}\text{-(His39)cyt } c^{II}$$

$$[Ru^{II}(NH_3)_6]^{2+} + \text{cyt } c^{III} \rightarrow [Ru^{III}(NH_3)_6]^{3+} + \text{cyt } c^{II}.$$

At this stage it was uncertain what the negative volumes of activation really meant since overall reaction volumes were not available. There was, however, data, now in the literature (*140*), that suggested that the oxidation of $[Ru(NH_3)_6]^{2+}$ to $[Ru(NH_3)_6]^{3+}$ is accompanied by a volume decrease of *ca.* 30 cm^3 mol^{-1}, which would mean that the activation volumes quoted above could mainly arise from volume changes associated with the oxidation of the ruthenium redox partner.

In order to obtain further information on the magnitude of the overall reaction volume and the location of the transition state along the reaction coordinate, a series of intermolecular electron-transfer reactions of cytochrome *c* with pentaammineruthenium complexes were studied, where the sixth ligand on the ruthenium complex was selected in such a way that the overall driving force was low enough so that the reaction kinetics could be studied in both directions (*153*, *154*). The selected substituents were isonicotinamide (isn), 4-ethylpyridine (etpy), pyridine (py), and 3,5-lutidine (lut). The overall reaction can be formulated as

$$[Ru^{III}(NH_3)_5L]^{3+} + \text{cyt } c^{II} \leftrightarrow [Ru^{II}(NH_3)_5L]^{2+} + \text{cyt } c^{III}.$$

For all the investigated systems, the forward reaction was significantly decelerated by pressure, whereas the reverse reaction was significantly accelerated by pressure. The absolute values of the volumes of activation for the forward and reverse processes were indeed very similar, demonstrating that a similar rearrangement occurs in order to reach the transition state. In addition, the overall reaction volume for these systems could be determined spectrophotometrically by recording the spectrum of an equilibrium mixture as a function of pressure and electrochemically by recording cyclic and differential pulse voltammograms as a function of pressure (*155*). A comparison of the ΔV data demonstrates the generally good agreement between the values obtained from the difference in the volumes of activation for the forward and reverse reactions and those obtained thermodynamically. Furthermore, the values also clearly demonstrate that $|\Delta V^{\#}| \approx 0.5 |\Delta V|$, i.e., the transition state lies approximately halfway between the reactant and product states on a volume basis independent of the direction of electron transfer. The typical volume profile in Fig. 18 presents the overall picture, from which the location of the transition state can clearly be seen.

Similar results were obtained for the redox reactions of a series of cobalt diimine complexes with cytochrome *c* (*156*, *157*). In general a good agreement exists between the kinetically and thermodynami-

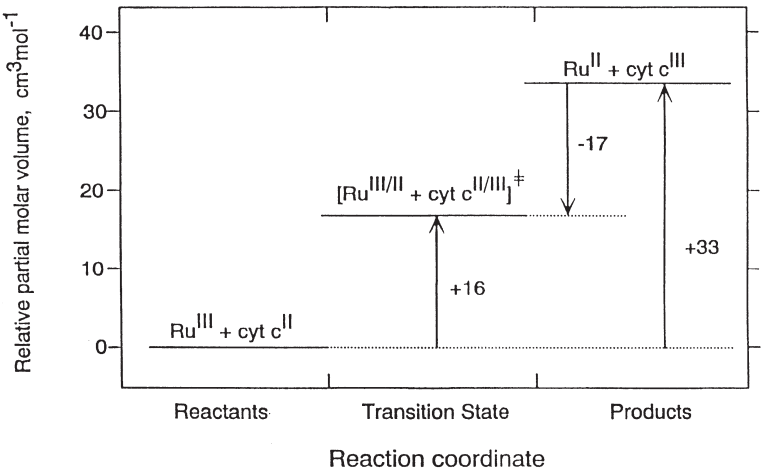

FIG. 18. Volume profile for the reaction $Ru(NH_3)_5isn^{3+}$ + Cyt c^{II} ↔ $Ru(NH_3)_5isn^{2+}$ + Cyt c^{III}.

cally determined parameters, and the typical volume profile in Fig. 19 once again demonstrates the symmetrical location of the transition state with respect to the reactant and product states.

At this point it is important to ask the question where these volume changes really come from. We have always argued that the major

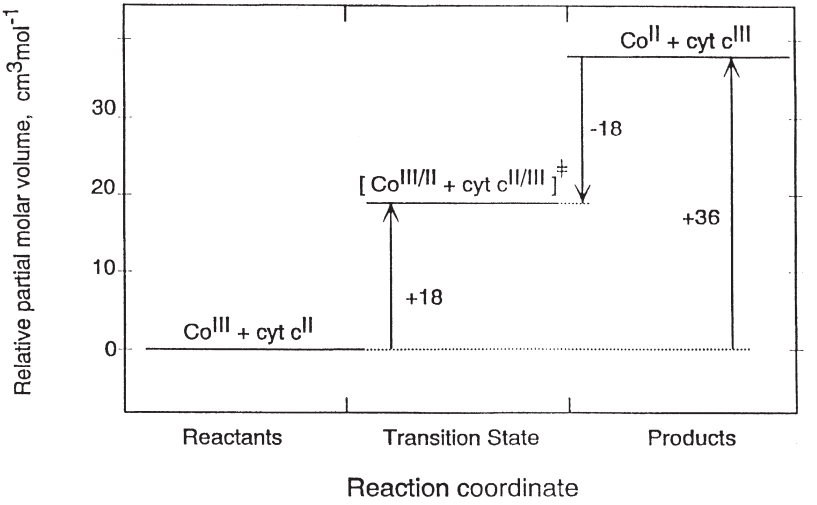

FIG. 19. Volume profile for the reaction $Co(terpy)_2^{3+}$ + Cyt c^{II} ↔ $Co(terpy)_2^{2+}$ + Cyt c^{III}.

volume change arises from changes on the redox partner and not on cytochrome *c* itself. This was suggested by the fact that the change in partial molar volume associated with the oxidation of the investigated Ru(II) and Co(II) complexes as obtained from electrochemical and density measurements almost fully accounted for the observed overall reaction volume. Thus the reduction of cytochrome *c* can only make a minor contribution toward the overall volume change.

These arguments were apparently in contradiction with electrochemical results reported by Cruanes *et al.* (*158*), according to which the reduction of cytochrome *c* is accompanied by a volume collapse of 24 $cm^3\ mol^{-1}$. This value is so large that it almost represents all of the reaction volume found for the investigated reactions discussed above. A reinvestigation of the electrochemistry of cytochrome *c* as a function of pressure, using cyclic and differential pulse voltammetric techniques (*155*), revealed a reaction volume of $-14.0 \pm 0.5\ cm^3\ mol^{-1}$ for the reaction

$$\text{Cyt } c^{III} + \text{Ag(s)} + \text{Cl}^- \rightarrow \text{Cyt } c^{II} + \text{AgCl(s)}.$$

A correction for the contribution from the reference electrode can be made on the basis of the data published by Tregloan *et al.* (139), and a series of measurements of the potential of the Ag/AgCl(KCl saturated) electrode relative to the Ag/Ag^+ electrode as a function of pressure. The contribution of the reference electrode turned out to be $-9.0 \pm 0.6\ cm^3\ mol^{-1}$, from which it then followed that the reduction of cytochrome c^{III} is accompanied by a volume decrease of $5.0 \pm 0.8\ cm^3\ mol^{-1}$. This contribution is significantly smaller than concluded by Cruanes *et al.* (*158*) and is also in line with the other arguments referred to above. Thus we conclude that the observed activation and reaction volumes mainly arise from volume changes on the Ru and Co complexes, which in turn will largely be associated with changes in electrostriction in the case of the ammine complexes. The oxidation of the Ru(II) ammine complexes will be accompanied by a large increase in electrostriction and almost no change in the metal–ligand bond length, whereas in the case of the Co complexes a significant contribution from intrinsic volume changes associated with the oxidation of Co(II) will partially account for the observed effects (*140*).

The available results nicely demonstrate the complementarity of the kinetic and thermodynamic data obtained from stopped-flow, UV-vis, electrochemical, and density measurements. The resulting picture is very consistent and allows a further detailed analysis of the data. The overall reaction volumes determined in four different ways

are surprisingly similar and underline the validity of the different methods employed. The volume profiles in Figs. 18 and 19 demonstrate the symmetric nature of the intrinsic and solvational reorganization in order to reach the transition state of the electron-transfer process. In these systems the volume profile is controlled by effects on the redox partner of cytochrome *c*, but this does not necessarily always have to be the case. The location of the transition state on a volume basis will reveal information concerning the "early" or "late" nature of the transition state and reveal details of the actual electron-transfer route followed.

Recent investigations on a series of intramolecular electron transfer reactions, closely related to the series of intermolecular reactions described above, revealed nonsymmetrical volume profiles (*159*). Reactions of the type

$$(NH_3)_4(L)Ru^{III}\text{-(His33)-Cyt } c^{II} \leftrightarrow (NH_3)_4(L)Ru^{II}\text{-(His33)-Cyt } c^{III},$$

where L = isonicotinamide, 4-ethylpyridine, 3,5-lutidine, and pyridine, all exhibited volumes of activation for the forward reaction of between +3 and +7 $cm^3\ mol^{-1}$ compared to overall reaction volumes of between +19 and +26 $cm^3\ mol^{-1}$. This indicates that electron transfer from Fe to Ru is characterized by an "early" transition state in terms of volume changes along the reaction coordinate (see Fig. 20).

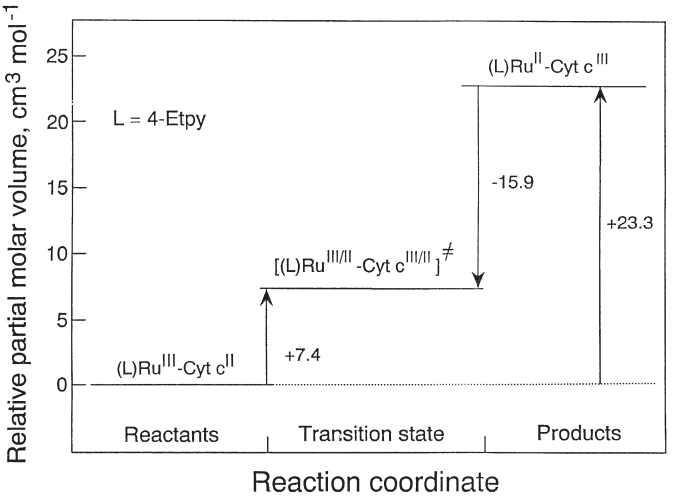

FIG. 20. Volume profile for the reaction $(NH_3)_4$(4-Etpy)Ru^{III}-Cyt $c^{II} \leftrightarrow$ $(NH_3)_4$(4-Etpy)Ru^{II}-Cyt c^{III}.

The overall volume changes could be accounted for in terms of electrostriction effects centered around the ammine ligands on the ruthenium center. A number of possible explanations in terms of the effect of pressure on electronic and nuclear factors were offered to account for the asymmetrical nature of the volume profile (*159*).

One system has been investigated where the effect of pressure on the electron-transfer rate constant revealed information on the actual electron-transfer route. In this study the effect of pressure on distant electronic coupling in $Ru(bpy)_2(im)$-modified His-33 and His-72 cytochrome *c* derivatives, for which the electron transfer from Fe(II) to Ru(III) is activationless (*160*). In the case of the His-33-modified system the electron-transfer rate constant exhibited no dependence on pressure within experimental error limits. However, the rate constant for the His72-modified protein increased significantly with increasing pressure, corresponding to a $\Delta V^{\#}$ value of -6 ± 2 cm^3 mol^{-1}. Since this value is exactly opposite to that expected for the reduction of Ru(III), the result was interpreted as an increase in electronic coupling at elevated pressure. The application of moderate pressures will cause a slight compression of the protein that in turn shrinks the through-space gaps that are key units in the electron-tunneling pathway between the heme and His-72. A decrease of 0.46 Å in the tunneling path length at a pressure of 150 MPa can account for the observed increase in rate constant. This in turn means that there is an average decrease in the space-gap of 0.1 Å. The absence of an effect for the His-33-modified species is understandable since electronic coupling through covalent and hydrogen bonds will be less pressure sensitive than coupling via van der Waals gaps (*160*).

Recently, Morishima and co-workers (*161*) investigated the effect of pressure on electron transfer rates in zinc/ruthenium-modified myoglobins. The rate constant for electron transfer from photoexcited ^{3}ZnP* to a covalently attached $[Ru(NH_3)_5]^{3+}$ moiety on the surface of the protein decreased from 5×10^7 to 55 s^{-1} upon increasing the distance from 9.5 to 19.3 Å when the Ru complex is attached to His-70 and His-83, respectively. This decrease in the rate constant was accompanied by an increase in $\Delta V^{\#}$ from $+4$ to $+17$ cm^3 mol^{-1}. Within the context of the results reported above and the volume changes associated with the reduction of the Ru(III) ammine complexes, the gradual increase in $\Delta V^{\#}$ with increasing donor–acceptor distance and with decreasing rate constant could be a clear demonstration of "early" (for the fast reactions) and "late" (for the slow reactions) transition states. Volume changes mainly associated with changes in electrostriction on the Ru ammine center will control the

solvent reorganization and so account for the "early" (reactantlike) and "late" (productlike) transition states.

V. Miscellaneous Reactions

In this section a number of different reaction types are presented, for which the application of high-pressure techniques has resulted in important mechanistic information.

In some cases pulse-radiolysis techniques were employed to study the effect of pressure on inorganic reactions. For instance the oxidation of $[Cu^{I}(phen)_2]$ by dioxygen via the formation of a $Cu^{I}–O_2$ transient species was studied using this technique (see Section III,A). Other examples include the formation and cleavage of metal–carbon σ-bonds, which formally involve a change in the oxidation state of the metal. A typical example of a volume profile for the formation and cleavage of a Co–CH_3 bond is reported in Fig. 21 for the reaction (*162*)

$$[Co^{II}(nta)(H_2O)_2]^- + {}^{\cdot}CH_3 \rightarrow [Co^{III}(nta)(CH_3)(H_2O)]^- + H_2O.$$

The volume profile indicates an increase in partial molar volume in going to the transition state, which is interpreted in terms of an I_d

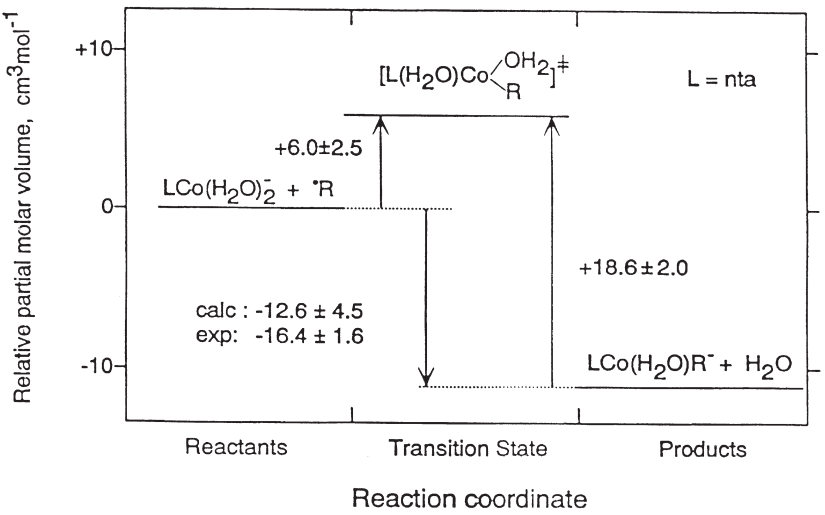

FIG. 21. Volume profile for the reaction of methyl radicals with the nitrilotriacetate complex of Co(II).

substitution controlled binding of the methyl radical to the Co(II) complex. The large volume collapse following the transition state is ascribed to metal–carbon bond formation that is accompanied by oxidation of Co(II) to Co(III) and accompanied by a large volume contraction (*162*).

The reaction of aquated Cr(II) with 10 different aliphatic radicals, R, showed a decrease in rate constants with increasing pressure and volumes of activation between +3.4 and +6.3 $cm^3\ mol^{-1}$ (*163*). These data could be interpreted in terms of a water-exchange-controlled formation of the Cr–R bond, from which it followed that water exchange on Cr(II) must proceed according to an I_d mechanism. The volume profile in Fig. 22 demonstrates this point; the large volume collapse following the transition state was assigned to Cr–R bond formation accompanied by the conversion of Cr^{II}–R to Cr^{III}–R^-. In general it was found that in reactions of metal complexes with free radicals, based on the observed pressure effects, the radicals can be treated as normal nucleophiles in ligand substitution processes, which are often controlled by solvent exchange on the metal complex (*164*).

Another reaction type to be mentioned in this section deals with oxidative addition/reductive elimination. Such reactions not only involve significant bond formation/bond breakage, but also a change in the oxidation state and coordination number of the metal complex. These effects cause significant volume changes such that large

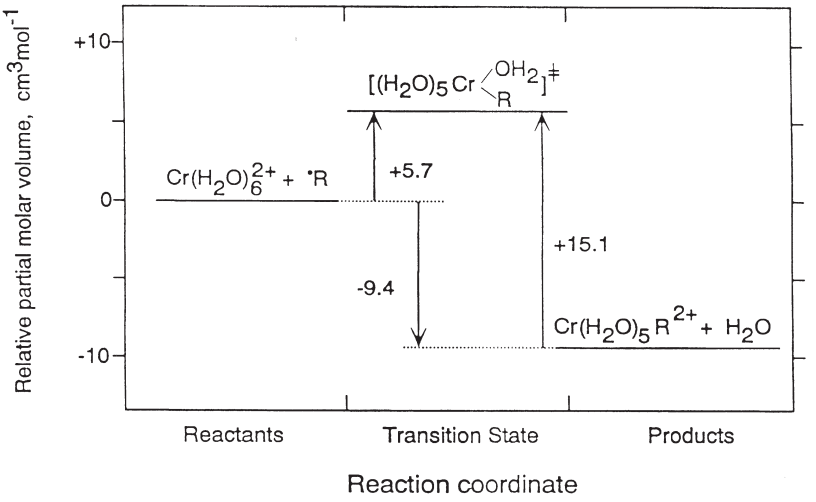

FIG. 22. Volume profile for the reaction of an aliphatic radical with aqua Cr(II) species R = $C(CH_3)_2OH$.

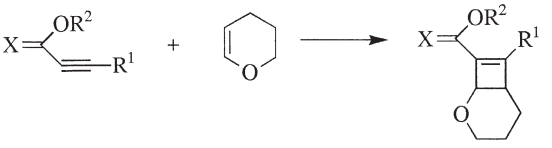

X = $Cr(CO)_5$, R^1 = Me, R^2 = Me
X = $W(CO)_5$, R^1 = Me, R^2 = Me
X = $W(CO)_5$, R^1 = Ph, R^2 = Et

SCHEME 7.

negative/large positive volumes of activation are expected. By way of comparison, addition reactions on their own already result in significant volume changes. For instance [2 + 2] cyclo-addition reactions of the type shown in Scheme 7 revealed a significant acceleration by pressure and almost no dependence on the polarity of the solvent (*165*). The average $\Delta V^{\#}$ of -16 ± 1 cm^3 mol^{-1} and the solvent independence of the process suggested that the reaction follows a nonpolar, concerted, synchronous one-step mechanism. The observe pressure acceleration is very similar to that found for the insertion of dipropylcyanamide and 1-(diethylamino)propene into the metal–carbene bond of pentacarbonyl-(methoxyphenylcarbene)chromium and −tungsten for which $\Delta V^{\#}$ varies between −17 and −25 cm^3 mol^{-1} (*166*). Addition reactions of α,β-unsaturated Fischer carbene complexes as shown in Scheme 8 all exhibit $\Delta V^{\#}$ values between −15 and −17 cm^3 mol^{-1} in acetonitrile. On decreasing the solvent polarity, $\Delta V^{\#}$ becomes significantly more negative and exhibits a good correlation with the solvent parameter q_p (*167*). From the solvent dependence an intrinsic contribution of −14 cm^3 mol^{-1} could be estimated. It was concluded that the

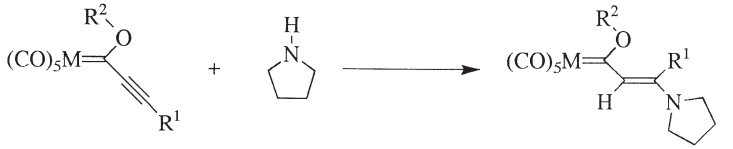

M	R^1	R^2
Cr	Ph	Et
Mo	Ph	Et
W	Ph	Et
W	Me	Me

SCHEME 8.

addition of pyrrolidine follows a two-step process with a polar transition state leading to a zwitterionic intermediate. The addition of a series of p-substituted anilines to a Fischer carbene complex shown in Scheme 9 is characterized by $\Delta V^{\#}$ values between -21 and -27 cm^3 mol^{-1} (*168*), i.e., significantly more negative than for the reaction with pyrrolidine mentioned above. The second-order rate constant for the addition reactions exhibited an excellent correlation with the basicity of the selected aniline. The observed trend in the activation volumes could be correlated with an "early" or "late" transition state for the fast and slow addition reactions, respectively. On the basis of these results it is not surprising that oxidative addition/reductive elimination reactions can be characterized by even larger volumes of activation, i.e., they show a high pressure sensitivity.

One interesting example involves the addition of MeI to the Pd(II) complex [$PdMe_2$(bpy)] to form [$PdMe_3$(I)(bpy)], which is accompanied by a $\Delta V^{\#}$ value of -11.9 cm^3 mol^{-1} (*169*). A similar value was reported for the corresponding reaction with the Pt(II) complex (*170*). This value confirms the operation of an S_N2 mechanism. The reductive elimination of C_2H_6 from the Pd(IV) complex forming [PdMe(I)(bpy)] as product yielded a $\Delta V^{\#}$ value of $+17$ cm^3 mol^{-1}, which is in line with the formal change in oxidation state and bond breakage. On the assumption that the transition states for the oxidative addition and reductive elimination processes have a similar partial molar volume, then an overall reaction volume of 29 cm^3 mol^{-1} can be calculated for such reactions (see volume profile in Fig. 23).

Reactions that involve significant bond formation in the rate-determining step are in general expected to exhibit large and negative volumes of activation. This was for instance found for a series of cyclometallation reactions of benzylidenebenzylamines, -anilines, and -propylamine with palladium acetate in toluene and acetic acid solution (*171*, *172*). The cyclometallated compounds are formed via C–H electrophilic bond activation to produce different types of metalla-

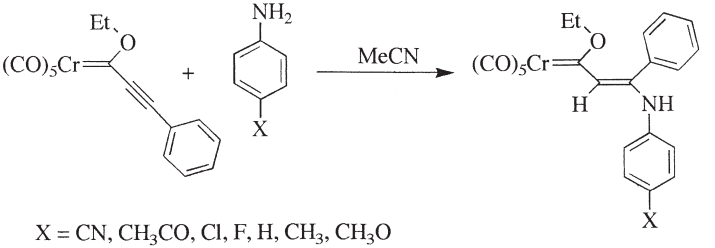

X = CN, CH_3CO, Cl, F, H, CH_3, CH_3O

SCHEME 9.

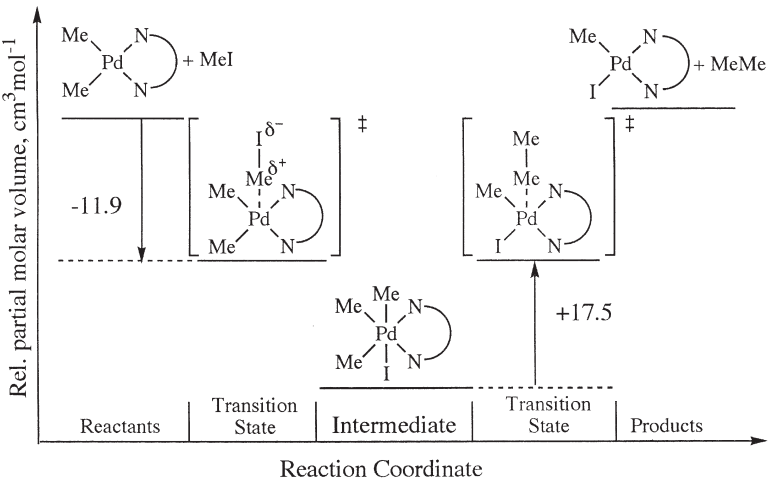

FIG. 23. Volume profile for the combined oxidative addition and reductive elimination reaction $[PdMe_2(bpy)] + MeI \rightarrow [Pd(I)Me_3(bpy)] \rightarrow [Pd(I)Me(bpy)] + C_2H_6$.

cycles. The cyclometallation reactions are characterized by negative activation entropies and activation volumes, and the latter vary between -11 and -25 cm^3 mol^{-1}. These values are very similar for the spontaneous and acid-catalyzed reactions, although the reaction can be accelerated by up to 2 orders of magnitude in acidic solution. The results are interpreted in terms of a highly ordered four-centered transition state, involving C–H and Pd–O(acetato) bounds. Recently, activation volumes were also determined for the intramolecular oxidative C–X (X = H, F, Cl, or Br) addition to Pt(II) imine complexes (*173*). The values varied between -9 and -31 cm^3 mol^{-1}, with the smaller absolute values found for the C–F activation process. An "early" transition state was suggested to account for this particular effect. The absence of any significant solvent dependence and the very negative activation volumes suggested that no polar transition state is formed during the reaction and that a common highly ordered three-centered C–Pt–X interaction is present for all the imines used.

VI. Concluding Remarks/Future Perspectives

The aim of this chapter was to demonstrate how the application of high-pressure thermodynamic and kinetic techniques can contribute to the elucidation of inorganic and bioinorganic reaction mechanisms.

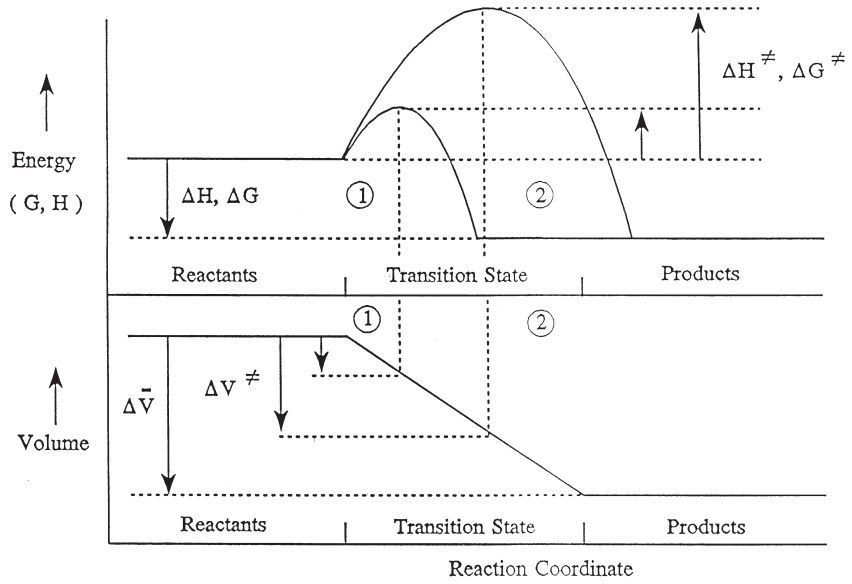

FIG. 24. Schematic comparison of energy and volume profiles; (1) "early" transition state and (2) "late" transition state.

In many cases the insight gained with these techniques is rather unique and has added a further dimension to the study of reaction mechanisms in solution. The construction of volume profiles can be very helpful in resolving finer details of the nature of the transition state. In some of the simplest cases (viz., solvent exchange and self-exchange reactions), the experimental data could be supported by theoretical calculations. Significant developments are expected to occur in the area, such that theoretical optimization of transition state structures will become standard practice in mechanistic studies. Here again the volume of activation data is expected to play a crucial role, since it presents an experimental measure of the intrinsic and solvational volume changes in the transition state and forms a basis for comparison of theoretical predictions. An ideal situation is one in which volume profiles can be constructed for the more complex reaction sequences; for instance, for catalytic cycles in enzymatic processes. This will, as in the case of simple reactions, enhance our understanding of more complex chemical processes and improve our ability to tune them.

The correlation of rate constant data with activation volume data for a series of closely related reactions in terms of an "early" or "late"

transition state has been reported in a number of cases. The ultimate goal will be to correlate energy and volume profiles for series of related reactions, where a low activation barrier (fast reaction) will correspond to an "early" transition state and a high activation barrier (slow reaction) will correspond to a "late" transition state. A schematic presentation of such a correlation between the location of "early" and "late" transition states on energy and volume profiles is shown in Fig. 24. A three-dimensional presentation of free energy and partial molar volume changes along the reaction coordinate should represent the ultimate way to combine energy and volume profile information.

References

1. "Chemistry under Extreme or Non-Classical Conditions"; van Eldik, R.; Hubbard, C. D., Eds.; Wiley: New York, 1997; Chapter 2.
2. Frey, U.; Helm, L.; Merbach, A. E. In "Dynamics of Solutions and Fluid Mixtures by NMR"; Delpuech, J.-J.; Ed.; Wiley: Chichester, 1995; p. 263.
3. van Eldik, R.; Ford, P. C. In "Advances in Photochemistry"; Neckers, D. C.; Volman, D. H.; von Brünau, G., Eds.; Wiley: New York, 1998; Vol. 24; p. 61.
4. Drljaca, A.; Hubbard, C. D.; van Eldik, R.; Asano, T.; Basilevsky, M. V.; le Noble, W. J. *Chem. Rev.* **1998,** *98,* 2167–2289.
5. Stochel, G.; van Eldik, R. *Coord. Chem. Rev.,* in press.
6. Hubbard, C. D.; van Eldik, R. *Instrum. Sci. Technol.* **1995,** *22,* 1.
7. Magde, D.; van Eldik, R. In "High Pressure Techniques in Chemistry and Physics: A Practical Approach"; Holzapfel, W.; Isaacs, N., Eds.; Oxford Univ. Press: Oxford, 1997; Chapter 6.
8. van Eldik, R.; Merbach, A. E. *Comments Inorg. Chem.* **1992,** *12,* 341.
9. Lincoln, S. F.; Merbach, A. E. *Adv. Inorg. Chem.* **1995,** *42,* 1.
10. Frey, U.; Helm, L.; Merbach, A. E.; Roulet, R. In "Advanced Applications of NMR to Organometallic Chemistry"; Gielen, M.; Willem, R.; Wrackmeyer, B., Eds.; Wiley: Chichester, 1996, p. 193.
11. Akesson, R.; Petterson, L. G. M.; Sandström, M.; Wahlgren, U. *J. Am. Chem. Soc.* **1994,** *116,* 8691.
12. Akesson, R.; Petterson, L. G. M.; Sandström, M.; Wahlgren, U. *J. Am. Chem. Soc.* **1994,** *116,* 8705.
13. Rotzinger, F. P. *J. Am. Chem. Soc.* **1996,** *118,* 6760.
14. Rotzinger, F. P. *J. Am. Chem. Soc.* **1997,** *119,* 5230.
15. Kowall, T.; Foglia, F.; Helm, L.; Merbach, A. E. *Chem. Eur. J.* **1996,** *2,* 285.
16. Bleuzen, A.; Foglia, F.; Furet, E.; Helm, L.; Merbach, A. E.; Weber, J. *J. Am. Chem. Soc.* **1996,** *118,* 12777.
17. Kowall, T.; Caravan, P.; Bourgeois, H.; Helm, L.; Rotzinger, F. P.; Merbach, A. E. *J. Am. Chem. Soc.* **1998,** *120,* 6569.
18. Deeth, R. J.; Elding, L. I. *Inorg. Chem.* **1996,** *35,* 5019.
19. Hartmann, M.; Clark, T.; van Eldik, R. *J. Am. Chem. Soc.* **1997,** *119,* 5867.
20. Hartmann, M.; van Eldik, R.; Clark, T. submitted for publication.

21. Cusanelli, A.; Frey, U.; Richens, D. T.; Merbach, A. E. *J. Am. Chem. Soc.* **1996,** *118,* 5265.
22. Tsutsui, Y.; Wasada, H.; Funahashi, S. *Bull. Chem. Soc. Jpn.* **1997,** *70,* 1813.
23. Tsutsui, Y.; Wasada, H.; Funahashi, S. *Bull. Chem. Soc. Jpn.* **1998,** *71,* 73.
24. Li, J.; Fisher, C. L.; Chen, J. L.; Bashford, D.; Noodleman, L. *Inorg. Chem.* **1996,** *35,* 4694.
25. Martin, R. L.; Hay, P. J.; Pratt, L. R. *J. Phys. Chem. A* **1998,** *102,* 3565.
26. Hermansson, K.; Wojcik, M. *J. Phys. Chem. B* **1998,** *102,* 6089.
27. Aime, S.; Botta, M.; Fasano, M.; Marques, M. P. M.; Geraldes, C. F. G. C.; Pubanz, D.; Merbach, A. E. *Inorg. Chem.* **1997,** *36,* 2059.
28. Lammers, H.; Maton, F.; Pubanz, D.; van Laren, M. W.; van Bekkum, H.; Merbach, A. E.; Muller, R. N.; Peters, J. A. *Inorg. Chem.* **1997,** *36,* 2527.
29. Aime, S.; Barge, A.; Borel, A.; Botta, M.; Chemerisov, S.; Merbach, A. E.; Müller, U.; Pubanz, D. *Inorg. Chem.* **1997,** *36,* 5104.
30. Toth, E.; Burai, L.; Brücher, E.; Merbach, A. E. *J. Chem. Soc. Dalton Trans.* **1997,** 1587.
31. Soyama, S.; Ishii, M.; Funahashi, S.; Tanaka, M. *Inorg. Chem.* **1992,** *31,* 536.
32. Aizawa, S.; Matsuda, K.; Tajima, T.; Maeda, M.; Sugata, T.; Funahashi, S. *Inorg. Chem.* **1995,** *34,* 2042.
33. Aizawa, S.; Iida, S.; Matsuda, K.; Funahashi, S. *Inorg. Chem.* **1996,** *35,* 1338.
34. Aizawa, S.; Iida, S.; Matsuda, K.; Funahashi, S. *Bull. Chem. Soc. Jpn.* **1997,** *70,* 1593.
35. Inada, Y.; Sugata, T.; Ozutsumi, K.; Funahashi, S. *Inorg. Chem.* **1998,** *37,* 1886.
36. Maciejowska, I.; van Eldik, R.; Stochel, G.; Stasicka, Z. *Inorg. Chem.* **1997,** *36,* 5409.
37. Shi, T.; Elding, L. I. *Inorg. Chem.* **1997,** *36,* 528.
38. Basallote, M. G.; Durán, J.; Fernández-Trujillo, M. J.; González, G.; Máñez, M. A.; Martinez, M. *Inorg. Chem.* **1998,** *37,* 1623.
39. van Eldik, R. *Org. Synth. Organometall.* **1993,** *4,* 27.
40. Dücker-Benfer, C.; Grevels, F.-W.; van Eldik, R. *Organometallics* **1998,** *17,* 1669.
41. Hindmarsh, K.; House, D. A., van Eldik, R. *Inorg. React. Mechn.* in press.
42. Breet, E. L. J.; van Eldik, R. *Inorg. Chem.* **1987,** *26,* 2517.
43. Hohmann, H.; Hellquist, B.; van Eldik, R. *Inorg. Chem.* **1992,** *31,* 345.
44. Suvachittanont, S.; Hohmann, H.; van Eldik, R.; Reedijk, J. *Inorg. Chem.* **1993,** *32,* 4544.
45. Prinsloo, F. F.; Pienaar, J. J.; van Eldik, R. *J. Chem. Soc. Dalton Trans.* **1995,** 3581.
46. Rau, T.; Shoukry, M.; van Eldik, R. *Inorg. Chem.* **1997,** *36,* 1454.
47. Jestin, J.-L.; Chottard, J.-C.; Frey, U.; Laurenczy, G.; Merbach, A. E. *Inorg. Chem.* **1994,** *33,* 4277.
48. Stochel, G.; van Eldik, R. *Inorg. Chem.* **1990,** *29,* 2075.
49. Meier, M.; van Eldik, R. *Inorg. Chem.* **1993,** *32,* 2635.
50. Prinsloo, F. F.; Meier, M.; van Eldik, R. *Inorg. Chem.* **1994,** *33,* 900.
51. Prinsloo, F. F.; Breet, E. L. J.; van Eldik, R. *J. Chem. Soc. Dalton Trans.* **1995,** 685.
52. Brasch, N. E.; Choroba, O. W.; van Eldik, R. unpublished results.
53. Brasch, N. E.; Hamza, M. S. A.; van Eldik, R. *Inorg. Chem.* **1997,** *36,* 3216.
54. Drljaca, A.; Zahl, A.; van Eldik, R. *Inorg. Chem.* **1998,** *37,* 3948.
55. Dadci, L.; Elias, H.; Frey, U.; Hörnig, A.; Koelle, U.; Merbach, A. E.; Paulus, H.; Schneider, J. S. *Inorg. Chem.* **1995,** *34,* 306.

56. Cusanelli, A.; Nicula-Dadci, L.; Frey, U.; Merbach, A. E. *Inorg. Chem.* **1997,** *36,* 2211.
57. Aebischer, N.; Sidorenkova, E.; Ravera, M.; Laurenczy, G.; Osella, D.; Weber, J.; Merbach, A. E. *Inorg. Chem.* **1997,** *36,* 6009.
58. "Mechanisms of Inorganic Reactions"; Basolo, F.; Pearson, R. G.; Wiley: New York/London/Sydney, 1967; 2nd Edition.
59. "Kinetics and Mechanism of Reactions of Transition Metal Complexes"; Wilkins, R. G.; Au:, Ed.; Verlag-Chemie: Weinheim, 1991; 2nd Edition.
60. "Inorganic High Pressure Chemistry. Kinetics and Mechanisms"; van Eldik, R., Ed.; Elsevier: Amsterdam, 1986.
61. Frey, U.; Helm, L.; Merbach, A. E.; Romeo, R. *J. Am. Chem. Soc.* **1989,** *111,* 8161.
62. Frey, U.; Grove, D. M.; van Koten, G. *Inorg. Chim. Acta* **1998,** *269,* 322.
63. Schmülling, M.; Grove, D. M.; van Koten, G.; van Eldik, R.; Veldman, N.; Spek, A. L. *Organometallics* **1996,** *15,* 1384.
64. Schmülling, M.; Ryabov, A. D.; van Eldik, R. *J. Chem. Soc. Dalton Trans.* **1994,** 1257.
65. Fekl, U.; van Eldik, R. *Eur. J. Inorg. Chem.* **1998,** 389.
66. Wendt, O. F.; Elding, L. I. *J. Chem. Soc. Dalton Trans.* **1997,** 4725.
67. Wendt, O. F.; Elding, L. I. *Inorg. Chem.* **1997,** *36,* 6028.
68. Wendt, O. F.; Oskarsson, Å.; Leipoldt, G. J.; Elding, L. I. *Inorg. Chem.* **1997,** *36,* 4514.
69. Wendt, O. F.; Scodinu, A.; Elding, L. I. *Inorg. Chim. Acta* **1998,** *277,* 237.
70. Laurenczy, G.; Rapaport, I.; Zbinden, D.; Merbach, A. E. *Magn. Res. Chem.* **1991,** *29,* 545.
71. Mizuno, M.; Funahashi, S.; Nakasuka, N.; Tanaka, M. *Inorg. Chem.* **1991,** *30,* 1550.
72. Tregloan, P. A.; Seibig, S.; Zahl, A.; van Eldik, R. unpublished results.
73. Sokol, L. S. W. L.; Fink, T. D.; Rorenbacher, D. B. *Inorg. Chem.* **1980,** *19,* 1263.
74. Laurenczy, G.; Ducommun, Y.; Merbach, A. E. *Inorg. Chem.* **1989,** *28,* 3024.
75. Powell, D. H.; Helm, L.; Merbach, A. E. *J. Chem. Phys.* **1991,** *95,* 9258.
76. Powell, D. H.; Furrer, P.; Pittet, P. A.; Merbach, A. E. *J. Phys. Chem.* **1995,** *99,* 16622.
77. West, R. J.; Lincoln, S. F. *J. Chem. Soc. Dalton Trans.* **1974,** 281.
78. Licheri, G.; Musinu, A.; Paschinga, G.; Piccaluga, G.; Pinna, G.; Sedda, A. F. *J. Chem. Phys.* **1984,** *80,* 5308.
79. Sham, T. K.; Hastings, J. B.; Perlman, L. *Chem. Phys. Lett.* **1982,** *83,* 391.
80. Magini, M. *Inorg. Chem.* **1982,** *21,* 1535.
81. Salmon, P. S.; Neilson, G. W. *J. Phys. Condens. Matt.* **1989,** *1,* 5291.
82. Cayley, G.; Cross, D.; Knowles, P. F. *J. Chem. Soc. Chem. Commun.* **1976,** 837.
83. Powell, D. H.; Merbach, A. E.; Fábián, I.; Schindler, S; van Eldik, R. *Inorg. Chem.* **1994,** *33,* 4468.
84. Coates, J. H.; Collins, P. R.; Lincoln, S. F. *J. Chem. Soc. Faraday Trans.* **1979,** *75,* 1236.
85. Lincoln, S. F.; Hounslow, A. M.; Pisaniello, D. L.; Doddridge, B. G.; Coates, J. H.; Merbach, A. E.; Zbinden, D. *Inorg. Chem.* **1984,** *23,* 1090.
86. "Reaction Mechanisms of Inorganic and Organometallic Systems"; Jordan, R. B.; Oxford Univ. Press: New York, 1991.
87. Thaler, F.; Hubbard, C. D.; Heinemann, F. W.; van Eldik, R.; Schindler, S.; Fabian, I.; Dittler-Klingemann, A. M.; Hahn, F. E.; Orvig, C. *Inorg. Chem.* **1998,** *37,* 4022.

88. Neubrand, A.; Thaler, F.; Hubbard, C. D.; Zahl, A.; van Eldik, R. prepared for publication.
89. Thaler, F.; PhD Thesis, University of Erlangen-Nürnberg, Erlangen, Germany, 1998.
90. Romeo, R.; Plutino, M. R.; Elding, L. I. *Inorg. Chem.* **1997,** *36,* 5909.
91. Charbonniere, L. J.; Williams, A. F.; Frey, U.; Merbach, A. E.; Kamalaprija, P.; Schaad, O. *J. Am. Chem. Soc.* **1997,** *119,* 2488.
92. Kiplinger, J. L.; Richmond, T. G.; Arif, A. M.; Dücker-Benfer, C.; van Eldik, R. *Organometallics* **1996,** *15,* 1545.
93. Waldbach, T. A.; van Eldik, R.; van Rooyen, P. H.; Lotz, S. *Organometallics* **1997,** *16,* 4056.
94. Valentine, A. M.; Lippard, S. J. *J. Chem. Soc. Dalton Trans.* **1997,** 3925.
95. Que, L. *J. Chem. Soc. Dalton Trans.* **1997,** 3933.
96. Tolman, W. B. *Acc. Chem. Res.* **1997,** *30,* 227.
97. Karlin, K. D.; Kaderli, S.; Zuberbühler, A. D. *Acc. Chem. Res.* **1997,** *30,* 139.
98. Projahn, H.-D.; Dreher, C.; van Eldik, R. *J. Am. Chem. Soc.* **1990,** *112,* 17.
99. Taube, D. J.; Projahn, H.-D.; van Eldik, R.; Magde, D.; Traylor, T. G. *J. Am. Chem. Soc.* **1990,** *112,* 6880.
100. Projahn, H.-D.; Schindler, S.; van Eldik, R.; Fortier, D. G.; Andrew, C. R.; Sykes, A. G. *Inorg. Chem.* **1995,** *34,* 5935.
101. Feig, A. L.; Becker, M.; Schindler, S.; van Eldik, R.; Lippard, S. J. *Inorg. Chem.* **1996,** *35,* 2590.
102. Zhang, M.; van Eldik, R.; Espenson, J. H.; Bakac, A. *Inorg. Chem.* **1994,** *33,* 130.
103. Seibig, S.; van Eldik, R. *Inorg. Chem.* **1997,** *36,* 4115.
104. Seibig, S.; van Eldik, R. *Eur. J. Inorg. Chem.,* **1999,** 447.
105. Seibig, S.; van Eldik, R. *Inorg. React. Mechn.,* in press.
106. Becker, M.; Schindler, S.; van Eldik, R. *Inorg. Chem.* **1994,** *33,* 5370.
107. Ryan, S.; Adams, H.; Fenton, D. E.; Becker, M.; Schindler, S. *Inorg. Chem.* **1998,** *37,* 2134.
108. Becker, M.; Schindler, S.; Karlin, K. D.; Kaden, T. D.; Kaderli, S.; Palanché, T. *Inorg. Chem.,* **1999,** *38,* 1989.
109. Karlin, K. D.; Hayes, J. C.; Gultneh, Y.; Cruse, R. W.; McKnown, J. W.; Hutchinson, J. P.; Zubieta, J. *J. Am. Chem. Soc.* **1984,** *106,* 2121.
110. Goldstein, S.; Czapski, G.; van Eldik, R.; Cohen, H.; Meyerstein, D. *J. Phys. Chem.* **1991,** *95,* 1282.
111. Projahn, H. D.; van Eldik, R. *Inorg. Chem.* **1992,** *30,* 3288.
112. Buchalova, M.; Warburton, P. R.; van Eldik, R.; Busch, D. H. *J. Am. Chem. Soc.* **1997,** *119,* 5867.
113. Buchalova, M.; Busch, D. H.; van Eldik, R. *Inorg. Chem.* **1998,** *37,* 1116.
114. "Bioanorganische Chemie"; Kaim, W.; Schwederski, B.; B. G. Teubner: Stuttgart, 1995; 2nd Edition.
115. Eriksson, A. E.; Jones, A. T.; Liljas, A. *Proteins* **1988,** *4,* 274.
116. Silverman, D. N.; Lindskog, S. *Acc. Chem. Res.* **1988,** *21,* 30, and the literature survey in ref. 119.
117. Lipscomb, W. N. *Ann. Rev. Biochem.* **1983,** *52,* 17.
118. "Zinc Enzyme"; Lindskog, S.; Wiley: New York, 1983.
119. Zhang, X.; Hubbard, C. D.; van Eldik, R. *J. Phys. Chem.* **1996,** *100,* 9161.
120. van Eldik, R.; Palmer, D. A. *J. Sol. Chem.* **1982,** *11,* 239.
121. Zhang, X.; van Eldik, R., Koike, T.; Kimura, E. *Inorg. Chem.* **1993,** *32,* 5749.
122. Zhang, X.; van Eldik, R. *Inorg. Chem.* **1995,** *34,* 5606.

123. Fujita, E.; van Eldik, R. *Inorg. Chem.* **1998,** *37,* 360 and literature cited therein.
124. van Eldik, R. In "Photochemistry and Radiation Chemistry: Complementary Methods in the Study of Electron Transfer"; Nocera, D.; Wishart, J. F., Eds.; American Chemical Society: Washington, DC, 1998; Vol. 254; Chapter 19.
125. Swaddle, T. W.; Tregloan, P. A. *Coord. Chem. Rev.* in press.
126. Jolley, W. H.; Stranks, D. R.; Swaddle, T. W. *Inorg. Chem.* **1990,** *29,* 1948.
127. Dione, H.; Swaddle, T. W. *Can. J. Chem.* **1988,** *66,* 2763.
128. Takagi, H.; Swaddle, T. W. *Inorg. Chem.* **1992,** *31,* 4669.
129. Spiccia, L.; Swaddle, T. W. *Inorg. Chem.* **1987,** *26,* 2265.
130. Doine, H.; Swaddle, T. W. *Inorg. Chem.* **1991,** *30,* 1858.
131. Shalders, R. D.; Swaddle, T. W. *Inorg. Chem.* **1995,** *34,* 4815.
132. Jolley, W. H.; Stranks, D. R.; Swaddle, T. W. *Inorg. Chem.* **1990,** *29,* 385.
133. Grace, M. R.; Swaddle, T. W. *Inorg. Chem.* **1993,** *32,* 5597.
134. Swaddle, T. W. *Inorg. Chem.* **1990,** *29,* 5017.
135. Grace, M. R.; Takagi, H.; Swaddle, T. W. *Inorg. Chem.* **1994,** *33,* 1915.
136. Fu, Y.; Swaddle, T. W. *Chem. Commun.* **1996,** 1171.
137. Swaddle, T. W. *Can. J. Chem.* **1996,** *74,* 631.
138. Fu, Y.; Swaddle, T. W. *J. Am. Chem. Soc.* **1997,** *119,* 7137.
139. Sachinidis, J. J.; Shalders, R. D.; Tregloan, P. A. *Inorg. Chem.* **1994,** *33,* 6180.
140. Sachinidis, J. J.; Shalders, R. D.; Tregloan, P. A. *Inorg. Chem.* **1996,** *35,* 2497.
141. van Eldik, R. *High Press. Res.* **1991,** *6,* 251.
142. Krack, I.; van Eldik, R. *Inorg. Chem.* **1986,** *25,* 1743.
143. Krack, I.; van Eldik, R. *Inorg. Chem.* **1989,** *28,* 851.
144. Krack, I.; van Eldik, R. *Inorg. Chem.* **1990,** *29,* 1700.
145. Martinez, M.; Pitarque, M.-A.; van Eldik, R. *J. Chem. Soc. Dalton Trans.* **1996,** 2665.
146. Martinez, M.; Pitarque, M.-A. *J. Chem. Soc. Dalton Trans.* **1995,** 4107.
147. Martinez, M.; Pitarque, M.-A.; van Eldik, R. *Inorg. Chim. Acta* **1997,** *256,* 51.
148. Bänsch, B.; Martinez, P.; Zuluaga, J.; Uribe, D.; van Eldik, R. *Z. Phys. Chem.* **1991,** *170,* 59.
149. Wanat, A.; van Eldik, R.; Stochel, G. *J. Chem. Soc. Dalton Trans.* **1998,** 2497.
150. Matsumoto, M.; Tarumi, T.; Sugimoto, K.-I.; Kagayama, N.; Funahashi, S.; Takagi, H. D. *Inorg. Chim. Acta* **1997,** *255,* 81.
151. Ilkowska, I.; van Eldik, R.; Stochel, G. *J. Biol. Inorg. Chem.* **1997,** *2,* 603.
152. Wishart, J. F.; van Eldik, R.; Sun, J.; Su, C.; Isied, S. S. *Inorg. Chem.* **1992,** *31,* 3986.
153. Bänsch, B.; Meier, M.; Martinez, M.; van Eldik, R.; Su, C.; Sun, J.; Isied, S. S.; Wishart, J. F. *Inorg. Chem.* **1994,** *33,* 4744.
154. Meier, M.; Sun, J.; Wishart, J. F.; van Eldik, R. *Inorg. Chem.* **1996,** *35,* 1564.
155. Sun, J.; Wishart, J. F.; van Eldik, R.; Shalders, R. D.; Swaddle, T. W. *J. Am. Chem. Soc.* **1995,** *117,* 2600.
156. Meier, M.; van Eldik, R. *Inorg. Chim. Acta* **1994,** *225,* 95.
157. Meier, M.; van Eldik, R. *Chem. Eur. J.* **1997,** *3,* 33.
158. Cruanes, M. T.; Rodgers, K. K.; Sligar, S. G. *J. Am. Chem. Soc.* **1992,** *114,* 9660.
159. Sun, J.; Su, C.; Meier, M.; Isied, S. S.; Wishart, J. F.; van Eldik, R. *Inorg. Chem.* **1998,** *37,* 6129.
160. Meier, M.; van Eldik, R.; Chang, I.-J.; Mines, G. A.; Wuttke, D. S.; Winkler, J. R.; Gray, H. B. *J. Am. Chem. Soc.* **1994,** *116,* 1577.
161. Sugiyama, Y.; Takahashi, S.; Ishimori, K.; Morishima, I. *J. Am. Chem. Soc.* **1997,** *119,* 8592.

162. van Eldik, R.; Cohen H.; Meyerstein, D. *Angew. Chem. Int. Ed. Engl.* **1991,** *30,* 1158.
163. van Eldik, R.; Gaede, W.; Cohen, H.; Meyerstein, D. *Inorg. Chem.* **1992,** *31,* 3695.
164. van Eldik, R.; Cohen, H.; Meyerstein D. *Inorg. Chem.* **1994,** *33,* 1566.
165. Pipoh, R.; van Eldik, R.; Wang, S. L. B.; Wulff, W. D. *Organometallics* **1992,** *11,* 490.
166. Schneider, K. J.; Neubrand, A.; van Eldik, R.; Fischer, H. *Organometallics* **1992,** *11,* 267.
167. Pipoh, R.; van Eldik, R.; Henkel, G. *Organometallics* **1993,** *12,* 2236.
168. Pipoh, R.; van Eldik, R. *Organometallics* **1993,** *12,* 2668.
169. Dücker-Benfer, C.; van Eldik, R.; Canty, A. J. *Organometallics* **1994,** *13,* 2412.
170. Skauge, A. R. L.; Shalders, R. D.; Swaddle, T. W. *Can. J. Chem.* **1996,** *74,* 1998.
171. Gómez, M.; Granell, J.; Martinez, M. *Organometallics* **1997,** *16,* 2539.
172. Gómez, M.; Granell, J.; Martinez, M. *J. Chem. Soc. Dalton Trans.* **1998,** 37.
173. Crespo, M.; Martinez, M.; de Pablo, E. *J. Chem. Soc. Dalton Trans.* **1997,** 1231.

ADVANCES IN INORGANIC CHEMISTRY, VOL. 49

SUBSTITUTION STUDIES OF SECOND- AND THIRD-ROW TRANSITION METAL OXO COMPLEXES

ANDREAS ROODT,* AMIRA ABOU-HAMDAN,†
HENDRIK P. ENGELBRECHT,* and ANDRÉ E. MERBACH†

*Department of Chemistry, University of the Free State, Bloemfontein 9300, South Africa and
†Institut de Chimie Minérale et Analytique, Université de Lausanne, Bâtiment de Chimie (BCH), Lausanne CH-1015, Switzerland

Copyright © 2000 by Academic Press.
All rights of reproduction in any form reserved.
0898-8838/00 $30.00

I. Introduction

The substitution and protonation behavior of the *trans*-dioxotetracyanometalate complexes of Re(V), Tc(V), W(IV), Mo(IV), and Os(VI) have been extensively investigated in the past decade and selected aspects have been reviewed (*1*, *2*). Previous studies demonstrated the use of oxygen-17 NMR in different metal systems (*3*), including the complex oligomeric Mo(IV) aqueous systems (*4*), and therefore, since these oxocyano complexes contain an even wider range of nuclei such as ^{13}C, ^{15}N, ^{17}O, ^{99}Tc, and ^{183}W, they are attractive model complexes to study by multinuclear NMR. Thus, detailed studies on the dynamics therein have been investigated in the past few years (*5–8*).

The equilibria governing the complex formation and oxygen and proton exchange in these systems are given by Scheme 1, where CN denotes the total free cyanide, i.e., HCN/CN^-, and is used as such throughout this chapter. In the complex formation in Eq. (2) X represents different entering nucleophiles such as NCS^-, F^-, CN^-, and pyridine (py).

The relative dynamics of the different exchange processes taking place on the selected second- and third-row transition metal oxo com-

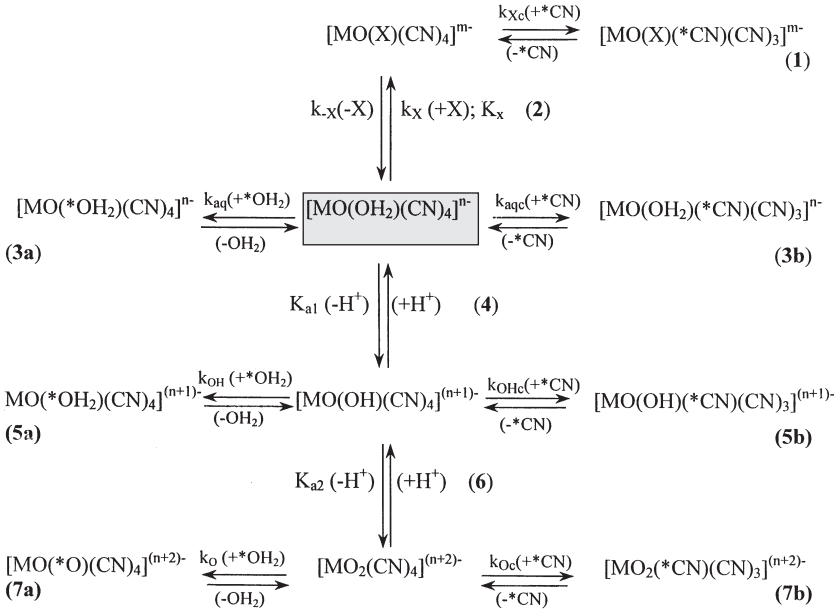

SCHEME 1.

plexes are thus compared and reviewed in this chapter, focusing on the proton, oxygen, and cyanide exchange. Reactivity manipulation by selective ligand variation is also discussed, while emphasis is given to a comparison of recent reactivity studies of analogous technetium and rhenium complexes as models to radiopharmaceuticals having important applications in diagnostic and therapeutic nuclear medicine (*9–12*). The kinetic behavior is especially an important aspect determining the preparation, uptake, and clearance of such radiopharmaceutical agents (*13–15*).

II. Characterization of $[MO(L)(CN)_4]^{m-}$ Complexes

A. Solid State X-Ray Studies

Many of the complexes described in this chapter have been characterized by X-ray studies and selected aspects of their structures have been reviewed previously (*1*, *2*). Some new aspects of significance in terms of mechanistic conclusions and other correlations are presented below.

Examples of selected species listed in Scheme 1, which have been characterized by solid-state structures, are shown in Figs. 1–4. The structures of $[ReO_2(CN)_4]^{3-}$ (*16*) and $[ReO(OH)(CN)_4]^{2-}$ (*17*) (Figs. 1a and 1b respectively), $[ReO(H_2O)(CN)_4]^{-}$ (*18*), and $[MoO(H_2O)(CN)_4]^{2-}$ (*19*) (Figs. 2a and 2b respectively) as well as the dinuclear species, $[Re_2O_3(CN)_8]^{4-}$ (*20*) (Fig. 3) are shown. Examples of $[MO(X)(CN)_4]^{m-}$ complexes include the $[WO(CN)_5]^{3-}$ (*21*), $[MoO(HCN)(CN)_4]^{2-}$ (*22*),

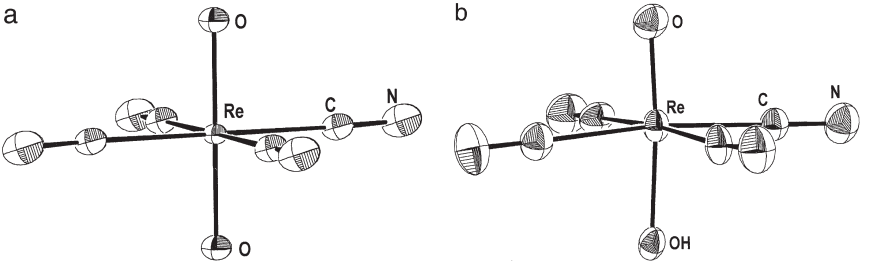

Fig. 1. Crystal structures of (a) $[ReO_2(CN)_4]^{3-}$ (*16*). (Adapted with permission from Murmann, R. K.; Schlemper, E. O. *Inorg. Chem.* **1971,** *10,* 2352–2354. Copyright 1971 American Chemical Society); (b) $[ReO(OH)(CN)_4]^{2-}$ (*17*) (Adapted with permission from Purcell, W.; Roodt, A.; Basson, S. S.; Leipoldt, J. G. *Transition Met. Chem.* **1989,** *14,* 5–6. Copyright 1989 Kluwer Academic Publishers.)

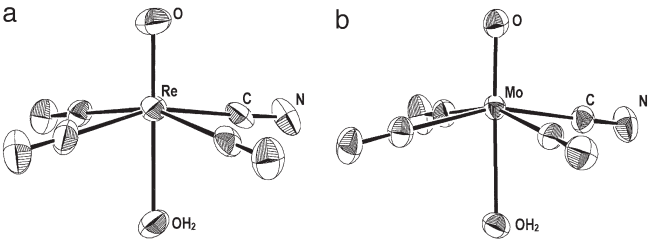

FIG. 2. Crystal structure of (a) $[ReO(H_2O)(CN)_4]^-$ (*18*). (Adapted with permission from Purcell, W.; Roodt, A.; Basson, S. S.; Leipoldt, J. G. *Transition Met. Chem.* **1990,** *15,* 239–241. Copyright 1990 Kluwer Academic Publishers); (b) $[MoO(H_2O)(CN)_4]^{2-}$ (*19*) (Adapted with permission from Robinson, P. R.; Schlemper, E. O.; Murmann, R. K. *Inorg. Chem.* **1975,** *14,* 2035–2041. Copyright 1975 American Chemical Society.)

$[TcO(NCS)(CN)_4]^{2-}$ (*13*) and $[MoO(dimap)(CN)_4]^{2-}$ (*23*) species (Figs. 4b and 4c respectively).

Of special importance is the fact that upon protonation, the M=O bonds along the apical O=M–OH and O=M–OH_2 axes are shortened significantly, coinciding with a weakening of the protonated M–O bond. This further results in an increase in distortion as observed from the displacement (Δ) of the metal center from the equatorial plane formed by the four cyano carbon atoms (see Table I).

This distortion results in changes in the overlap of the ligand–metal orbitals and variations in the corresponding bond strengths and

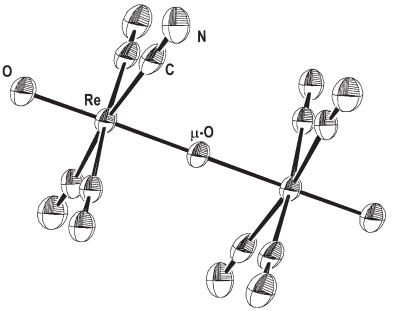

FIG. 3. Crystal structure of $[Re_2O_3(CN)_8]^{4-}$ (*20*). (Adapted with permission from Basson, S. S.; Leipoldt, J. G.; Roodt, A.; Purcell, W. *Transition Met. Chem.* **1987,** *12,* 82–84. Copyright 1987 Kluwer Academic Publishers.)

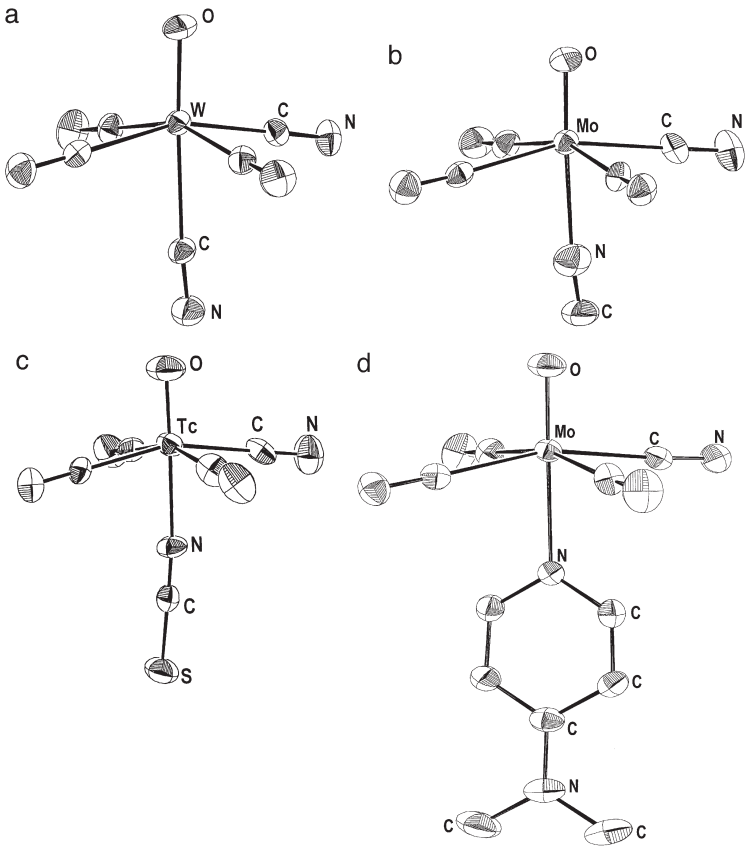

FIG. 4. Crystal structure of (a) $[WO(CN)_5]^{3-}$ (*21*); (b) $[TcO(NCS)(CN)_4]^{2-}$ (*13*). (Adapted with permission from Roodt, A.; Leipoldt, J. G.; Deutsch, E. A.; Sullivan, J. C. *Inorg. Chem.* **1992,** *31,* 1080–1085. Copyright 1992 American Chemical Society); (c) $[MoO(HCN)(CN)_4]^{2-}$ (*22*) (Adapted with permission from Smit, J. P.; Purcell, W.; Roodt, A.; Leipoldt, J. G. *J. Chem. Soc. Chem. Commun.* **1993,** *18,* 1388–1389. Copyright 1993 Royal Society of Chemistry); (d) $[MoO(dimap)(CN)_4]^{2-}$ (*23*).

has definite effects on the proton, water, and cyanide exchange processes, as is illustrated below. This distortion is also dependent on the strength of the M–L bond trans to the oxo ligand and is further manifested in the O=M–CN and L–M–CN bond angles shown in Table I; a good example being the $[MoO(H_2O)(CN)_4]^{2-}$ complex (Fig. 2b), with an average O=Mo–CN angle of 100(1)° (L–Mo–CN = 80(1)°)

TABLE I

SUMMARY OF CRYSTALLOGRAPHIC DATA FOR $[MO(L)(CN)_4]^{m-}$ AND RELATED COMPLEXES

Complex	Bond distance (Å)			Angles (°)			
	M=O/N	M−C/S (*cis* to O/N)	M−L (*trans* to O/N)	O=M−C	L−M−C	Δ (Å)[a]	Reference
$[MoO_2(CN)_4]^{4-}$	1.834(9)	2.20(1)	1.834(9)	90.0(5)	90.0(5)	0	*24*
$[WO_2(CN)_4]^{4-}$	1.841(5)	2.177(7)	1.841(5)	90.0(2)	90.0(2)	0	*25*
$[ReO_2(CN)_4]^{3-}$	1.781(3)	2.135(6)	1.781(3)	90.8(1)	90.8(1)	0	*16*
$[OsO_2(CN)_4]^{2-}$	1.75(1)	2.09(1)	1.75(1)	89.8(3)	89.8(3)	0	*26*
$[MoO(OH)(CN)_4]^{3-}$	1.698(7)	2.11(1)	2.077(7)	97.4(3)	83.5(3)	0.19	*19*
$[ReO(OH)(CN)_4]^{2-}$	1.70(1)	2.12(1)	1.90(1)	92.3(7)	87.7(7)	0.08	*17*
$[MoO(H_2O)(CN)_4]^{2-}$	1.668(5)	2.16(1)	2.271(4)	100(1)	80.1(3)	0.34	*19*
$[ReO(H_2O)(CN)_4]^{-}$	1.667(8)	2.11(1)	2.142(7)	98.4(3)	81.7(3)	0.30	*18*
$[MoO(pipe)(CN)_4]^{2-}$ [b]	1.676(3)	2.16(1)	2.528(4)	100.1(2)	79.9(2)	0.38	*21*
$[MoO(dimap)(CN)_4]^{2-}$ [c]	1.664(3)	2.171(4)	2.387(3)	98.3(1)	81.7(1)	0.36	*23*
$[MoO(N_3)(CN)_4]^{3-}$	1.70(1)	2.17(1)	2.29(2)	98.6(5)	81.4(4)	0.28	*27*
$[MoO(CN)_5]^{3-}$	1.705(4)	2.18(1)	2.373(6)	100.2(2)	79.9(2)	0.38	*28*
$[MoO(HCN)(CN)_4]^{2-}$	1.655(9)	2.14(2)	2.44(1)	99.9(5)	80.3(5)	0.37	*22*
$[MoO(en)(CN)_4]^{2-}$ [d]	1.666(4)	2.160(8)	2.491(5)	101.6(3)	78.4(3)	0.44	*29*
$[MoO(NCMe)(CN)_4]^{2-}$	1.658(7)	2.16(1)	2.500(7)	102.3(1)	77.8(1)	0.46	*30*
$[WO(F)(CN)_4]^{3-}$	1.77(1)	2.14(2)	2.017(8)	94.8(5)	85.1(5)	0.18	*31*
$[WO(CN)_5]^{3-}$	1.730(3)	2.154(6)	2.362(5)	100.0(2)	80.0(2)	0.37	*21*
$[WO(N_3)(CN)_4]^{3-}$	1.82(8)	2.02(4)	2.4(1)	98(2)	82(2)	0.27	*32*
$[WO(NCS)(CN)_4]^{3-}$	1.61(2)	2.14(3)	2.23(2)	98.9(9)	80.7(9)	0.35	*33*
$[TcO(NCS)(CN)_4]^{2-}$	1.61(1)	2.11(1)	2.16(1)	99.1(5)	80.9(4)	0.33	*13*
$[ReO(NCS)(CN)_4]^{2-}$	1.67(1)	2.11(1)	2.12(1)	98.3(3)	81.8(3)	0.30	*34*
$[Re_2O_3(CN)_8]^{4-}$	1.69(1)	2.12(2)	1.921(1)	92.9(6)	87.1(4)	0.11	*20*
$[ReN(N_3)(CN)_4]^{3-}$	1.65(2)	2.11(1)	2.36(2)	98.0(5)	82.0(5)	0.34	*35*
$[ReN(H_2O)(CN)_4]^{2-}$	1.64(1)	2.11(1)	2.496(7)	99.5(4)	80.6(4)	0.35	*36*
$[ReN(CN)_5]^{3-}$	1.68(1)	2.12(1)	2.39(1)	98.6(5)	81.5(5)	0.31	*37*
$[OsN(OH)(CN)_4]^{2-}$	1.606(5)	2.068(8)	2.123(5)	97.2(3)	82.8(3)	0.26	*38*
$[Re(NO)(H_2O)(CN)_4]^{2-}$ [e]	1.732(7)	2.09(1)	2.165(5)	94.6(4)	85.4(3)	0.17	*39*
$[Re(NO)(tu)(CN)_4]^{2-}$ [f]	1.74(1)	2.12(1)	2.23(1)	97.3(5)	82.5(4)	0.17	*40*
$[ReO(H_2O)(tu)_4]^{3+}$	1.62(1)	2.35(1)	2.47(1)	100.6(1)	79.60(5)	0.425	*15*
$[ReO(H_2O)(mtu)_4]^{3+}$	1.662(5)	2.382(2)	2.326(5)	99.2(2)	81.2(2)	0.332	*41*
$[ReO(H_2O)(dmtu)_4]^{3+}$	1.645(4)	2.386(1)	2.300(5)	99.2(1)	80.9(1)	0.380	*42*

[a] Central metal displacement from plane formed by four cyano ligand carbon atoms.
[b] pipe = piperidine.
[c] dimap = *N*,*N*-dimethylaminopyridine.
[d] en = ethylenediamine.
[e] Uncertainty in I+/III+ oxidation state for rhenium.
[f] tu *cis* to NO atom.

compared to the 90° angle in the dioxo complexes. Furthermore, the distortion in the $[ReO(H_2O)(CN)_4]^-$ complex is less than the Mo(IV) analog, coinciding with the M–L bond strength (Table I). The weakening of the M–OH and M–OH_2 bonds in the M(IV) and M(V) systems has definite effects on the reactivity toward oxygen exchange, see Section IV.

Good correlations with other parameters in the coordination polyhedron, such as in the chemical shifts of the different donor atoms, also exist and are further discussed below. It will be further illustrated

that valuable information concerning different aspects of the mechanisms applicable in the exchange processes could be obtained from the structural data as presented above.

B. Solution NMR Studies

The NMR investigation is presented in two parts; the first covers ^{13}C, ^{99}Tc, and ^{15}N studies where protonations of the dioxo complexes induce chemical shift changes but where line-broadening effects due to exchange are not observed. The second part covers ^{17}O studies which produce more complicated spectra due to protonation and simultaneous exchange with bulk water.

1. Carbon-13, Technetium-99, and Nitrogen-15 NMR

Carbon-13 NMR was utilized to study different aspects of the reactivity of the metal complexes as a function of certain structural features in the selected oxocyano complexes of Mo(IV), W(IV), Tc(V), Re(V), and Os(VI) as depicted in Scheme 1 and illustrated in Figs. 1–4. The NMR spectral properties were similar to those obtained from ^{13}C NMR in general, i.e., very sharp lines indicative of fairly long relaxation times in the order of a few seconds. The large quadrupolar moment of Tc-99 (I = 9/2, 100% abundance) led to a very broad bound ^{13}C signal (Fig. 5), thus excluding the quantitative study of the cyanide exchange by ^{13}C NMR. However, ^{15}N NMR was successfully used instead.

a. Equilibrium Studies

i. Rhenium(V) The complexes were studied by carbon-13 NMR in order to investigate the species behavior in solution since ^{13}C spectra were expected to be much simpler than those of ^{17}O NMR.

The two protonation steps of the $[MO_2(CN)_4]^{3-}$ complexes (M=Tc(V), Re(V); equilibria (4) and (6) in Scheme 1) occur in acidic medium while the two protonation steps for the $[MO_2(CN)_4]^{4-}$ (M=Mo(IV), W(IV)) occur in basic aqueous solutions. The pK_a values which demonstrate the acid/base behavior of the complexes are given in Table II. Other aspects of these complexes are also presented therein but are discussed in later sections.

The pH dependence of the ^{13}C spectra for the rhenium(V) system was studied in the pH range 0–8, and showed only one signal, resulting from the fast proton exchange between the dioxo, hydroxo oxo and aqua oxo species. Thus ^{13}C NMR provides an excellent means for

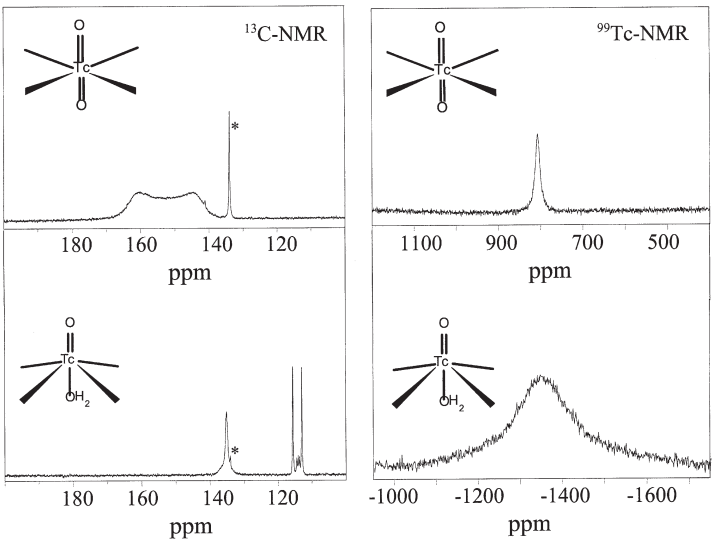

FIG. 5. The ^{13}C and ^{99}Tc NMR spectra at 25°C of $[TcO_2(^{13}CN)_4]^{3-}$ (total complex concentration [Tc] = 0.12 *m*; pH = 8.0) and $[TcO(H_2O)(CN)_4]^-$ (total complex concentration [Tc] = 0.12 *m*; total cyanide concentration [^{13}CN] = 0.83 *m*; pH = 1.0; note the signal structure of the free HCN due to proton–carbon and deuterium–carbon couplings), illustrating the quadrupolar effect introduced by ^{99}Tc (I = 9/2, 100%) and the effect of reduced symmetry upon protonation, i.e., formation of the oxo aqua complex. The asterisked signal refers to the $[Re_2O_3(CN)_8]^{4-}$ internal reference (*8*). (Adapted with permission from Abou-Hamdan, A.; Roodt, A.; Merbach, A. E. *Inorg. Chem.* **1998,** *37,* 1278–1288. Copyright 1998 American Chemical Society.)

the accurate determination of the acid dissociation constants (Fig. 6 and Table II).

In fact, it is not always possible to determine acid dissociation constants for such complexes spectrophotometrically (or even by potentiometric titration, see Section II,B,2) as a result of the presence of other reactions. In this present case, the formation of the dinuclear species $[Re_2O_3(CN)_8]^{4-}$, having a large molar absorptivity, can easily complicate the UV/visible absorption measurements in spectrophotometric studies. However, the formation of the $[Re_2O_3(CN)_8]^{4-}$ ion (Fig. 3) is easily observed in the ^{13}C spectrum, showing, as expected, only one signal since all eight carbon atoms of the cyano ligands are equivalent (*20*). The chemical shift of this species is pH independent, δ = 134.0 ppm, confirming that the dinuclear complex is unreactive toward protonation in the pH range studied and subsequently providing a good internal standard for chemical shift calibration.

The ^{13}C spectrum characteristics of the dioxo-, hydroxo oxo, and

TABLE II

COMPARISON BETWEEN NMR, X-RAY, ACID/BASE AND KINETIC DATA (298 K, μ = 1.5 *m*) FOR $[MO_2(CN)_4]^{(n+1)-}$ COMPLEXES, M = Mo(IV), W(IV), Tc(V), Re(V) AND Os(VI)

Metal center	pK_{a1}	pK_{a2}	δ (ppm) ^{17}O	δ (ppm) ^{13}C	Bond distance (Å)[b] (M=O)	Bond distance (Å)[b] (M−CN)	ν(M=O) [Ref. (*26*)] (cm^{-1})	k_{NCS} (M^{-1} s^{-1})[c]	k_{aq} (s^{-1})[d]	k_{Oc} (s^{-1})[e]
Mo(IV)	9.88 ± 0.05	⩾14	460	170	1.834(9)	2.20(1)	730	116[f]	4.1×10^4	$>4 \times 10^{-1}$
W(IV)	7.89 ± 0.05	14.5	390	166	1.841(5)	2.177(7)	730	2.9	137 ± 5	$(4.4 \pm 0.4) \times 10^{-3}$
Tc(V)	2.90 ± 0.08	4–5	578	153	—	—	785	23	500	$(4.8 \pm 0.4) \times 10^{-3}$[g]
Re(V)	1.31 ± 0.07	3.72 ± 0.05	462	142	1.781(3)	2.135(6)	785	0.0035	$(9.1 \pm 0.1) \times 10^{-2}$	$(3.6 \pm 0.3) \times 10^{-6}$
Os(VI)	≤−3[h]	≤−1[h]	568	120[i]	1.75(1)	2.09(1)	840	≪10^{-3}[j]	$<10^{-8}$	$<4 \times 10^{-9}$[k]

[a] Acid dissociation constants of $[Mo(OH_2)(CN)_4]^{n-}$ complexes as defined in Scheme 1 (*8*).

[b] Average M=O and M−CN distances; Table I.

[c] Substitution of aqua ligand in the $[MO(OH_2)(CN)_4]^{n-}$ complexes; esd's less than 5% (*1*), μ = 1 *m* KNO_3.

[d] Water exchange rate in the $[MO(OH_2)(CN)_4]^{n-}$ complexes (*7*); μ = 1.5 *m* KNO_3.

[e] Cyanide exchange rate in the $[MO_2(CN)_4]^{(n+2)-}$ complexes (*8*), μ = 1 *m* KNO_3.

[f] Cyanide ion as entering ligand, 293 K (*43*).

[g] At 279 K.

[h] Estimated from the pK_{a1} value difference of at least 5 pH units observed in $[ReN(H_2O)(CN)_4]^{2-}$ and $[OsN(H_2O)(CN)_4]^{-}$ (*38*); coupled with the fact that no UV/vis spectrum or chemical shift change is observed even in $[H^+]$ = 5 *m*.

[i] Observed $|^1J(^{187}Os-^{13}C)|$ = 92 Hz, a tripletlike structure where the two satellites correspond to the spin ½ osmium-187 (1.64%).

[j] Estimated (*8*).

[k] At 348 K.

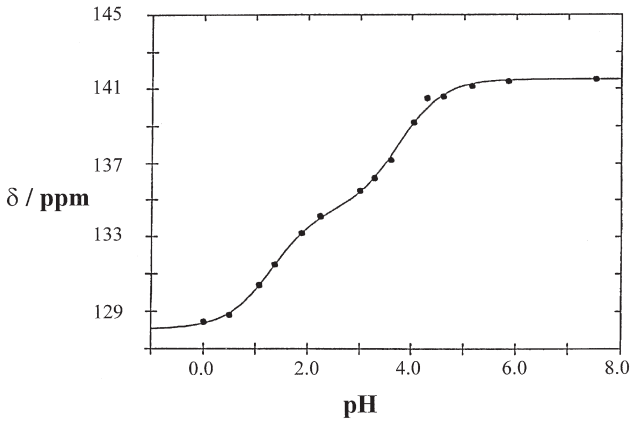

FIG. 6. Influence of pH on ^{13}C chemical shift for the protonation of $[ReO_2(CN)_4]^{3-}$ at 25°C. The total complex concentration [Re] = 0.2 *m*, μ = 1−1.4 *m* (KNO_3), NMR chemical shift reference = 3-(trimethylsilyl)tetradeuteriopropionate (*5*). (Adapted with permission from Roodt, A.; Leipoldt, J. G.; Helm, L.; Merbach, A. E. *Inorg. Chem.* **1992,** *31,* 2864–2868. Copyright 1992 American Chemical Society).

aqua oxo tetracyano complexes of Re(V) as well as the dinuclear species $[Re_2O_3(CN)_8]^{4-}$ are further addressed below.

ii. Molybdenum(IV) and tungsten(IV) As in the case of the abovementioned Re(V) (*20*), the Mo(IV) and W(IV) systems were also investigated by carbon-13 NMR to verify previously observed protonation behavior prior to the evaluation of the more complex ^{17}O spectra.

The ^{13}C chemical shift pH dependence for both the Mo(IV) and W(IV) systems is similar to that observed in Fig. 6 for the Re(V), with the exception that only one protonation step is observed in weak to mild basic solutions (there is a large difference in the pK_{a1} and pK_{a2} values for both the Mo(IV) and W(IV) systems, see Table II). The corresponding acid dissociation constants were similarly determined as in the case of Re(V) complexes.

iii. Technetium(V) The significant quadrupolar moment of the technetium-99 nucleus (I = 9/2, 100% abundance) (*44–46*) led to a very broad observed bound ^{13}C signal (Fig. 5, partially quadrupole collapsed decet in the $[TcO_2(CN)_4]^{3-}$ complex, having a line width of 2.5 kHz, estimated $1/T_{2Q}$ *ca.* 1500 s^{-1} and $|^1J(^{13}C-^{99}Tc)|$ of ~200 Hz) at 153 ppm overlapping that of the free ^{13}C cyanide signal and excluding the quantitative study of the cyanide exchange by ^{13}C NMR (see discussion below). However, it is being relaxed significantly upon protonation, forming the $[TcO(H_2O)(CN)_4]^-$ complex as shown in Fig. 5. The exchange was, however, conveniently studied by ^{15}N (I = 1/2) NMR

using ^{15}N enriched cyanide, since the indirect scalar coupling constant $|^{2}J(^{15}N–^{99}Tc)|$ is smaller than $|^{1}J(^{13}C–^{99}Tc)|$. The ^{15}N chemical shift data obtained for some of the Re(V) and Tc(V) complexes show a similar general trend as were obtained from the ^{13}C and ^{17}O NMR (*8*).

Even though the ^{13}C spectra for the Tc(V) system span a large range of chemical shift there was a rapid formation of the dinuclear $[Tc_2O_3(CN)_8]^{4-}$ species whenever there were appreciable amounts of the $[TcO(OH)(CN)_4]^{2-}$ ion present (*13*). This excluded the determination of the pK_a values for the Tc(V) system by ^{13}C NMR.

Of significance is the fact that the chemical shift of the $[^{99}TcO(H_2O)(CN)_4]^{-}$ ($\delta = -1350$ ppm) is the most shielded reported for a Tc(V) complex to date, the previous lowest shift being for the $[^{99}TcO_2(CN)_4]^{3-}$ ($\delta = +806$ ppm), shown in Fig. 5. This observation underlined the fact that the oxidation state of a Tc center cannot be directly estimated (other than maybe for the identification of Tc(I) complexes) from ^{99}Tc chemical shift, as has been suggested previously (*45, 46*).

iv. Osmium(VI) The investigation of the chemical shifts for the Os(VI) system was limited to the dioxotetracyano complex. A first-order coupling constant of 92 Hz was observed between the ^{192}Os ($I = 1/2$, 1.64% natural abundance) and ^{13}C. No acid dissociation constants' values were determined since these are estimated to be substantially less than -1, see Table II. In summary it can be noted that for all the above complexes, the acid/base characteristics could in general be studied using carbon-13 NMR (see below).

b. Correlation between Structural Results and $|^{1}J(^{13}C–^{183}W)|$ In the case of the W(IV) additional valuable information could be obtained from the first-order coupling between ^{183}W ($I = 1/2$, 14.4% natural abundance) and the ^{13}C of the bound cyanide. These first-order couplings were studied for a range of different L ligands in the $[WO(L)(CN)_4]^{m-}$ complexes and are illustrated in Fig. 7 for $[WO(CN)_5]^{3-}$, $[WO(H_2O)(CN)_4]^{2-}$, and $[WO(F)(CN)_4]^{3-}$. The data for a range of $[WO(L)(CN)_4]^{m-}$ complexes are reported in Table III. These coupling constants are correlated with the observed bond distances in selected complexes of this type and also with stability constants obtained from complex formation studies (*13*, *43*, *47*, *48*).

The correlation between the X-ray crystallographic data of the W–CN bond lengths and the first-order coupling constants between the ^{183}W and ^{13}C in the equatorial cyano ligands, as predicted by the Fermi-contact term (*51*), is fairly good (see Table III). This illustrates the increase in cis W–CN bond length induced by increased donor

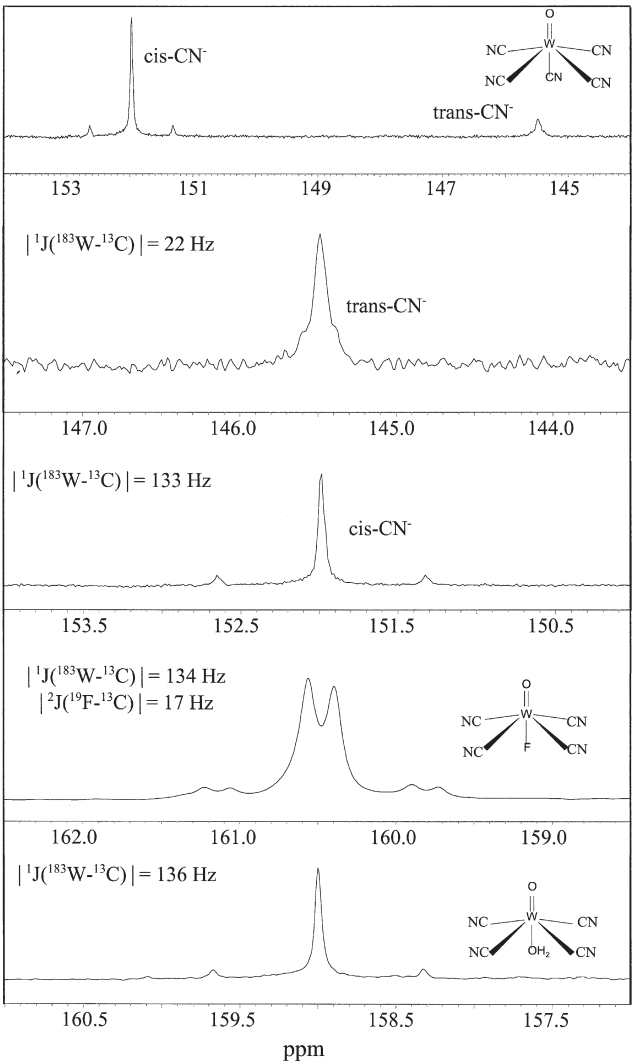

FIG. 7. The ^{13}C NMR spectra for $[WO(X)(^{13}CN)_4]^{m-}$ illustrating the variation in chemical shift and $|\ ^1J(^{183}W-^{13}C)\ |$ coupling constants. For $[WO(^{13}CN)_5]^{3-}$: the total complex concentration [W(IV)] = 0.2 *m*, the total cyanide concentration [^{13}CN] = 0.3 *m*, pH = 8.8; for $[WO(F)(^{13}CN)_4]^{3-}$: the total complex concentration [W(IV)] = 0.2 *m*, the total cyanide concentration [^{13}CN] = 0.3 *m*, the total fluoride concentration [KF] = 0.33 *m*, pH = 5.2 and for $[WO(H_2O)(^{13}CN)_4]^{2-}$: the total complex concentration [W(IV)] = 0.2 *m*, the total cyanide concentration [^{13}CN] = 0.3 *m*, pH = 3.1 (*8*). (Adapted with permission from Abou-Hamdan, A.; Roodt, A.; Merbach, A. E. *Inorg. Chem.* **1998,** *37,* 1278–1288. Copyright 1998 American Chemical Society).

TABLE III

CORRELATION BETWEEN EQUATORIAL CYANIDE ^{13}C NMR, X-RAY AND INFRARED DATA FOR *Trans*-$[WO(L)(CN)_4]^{m-}$ COMPLEXES (ANALOGOUS Mo(IV) DATA IN PARENTHESES)

Trans ligand L	$\delta^{13}C$ (ppm)	$^1J(^{183}W-^{13}C)$ (Hz)	K_x $(M^{-1})^a$	W—CN bond distance (Å)[b]	L—W—CN angle (°)	Δ (Å)[c]	$\delta^{17}O$ of M=O signal (ppm)	ν(W=O) $(cm^{-1})^d$	Reference
O^{2-}	166	128	—	2.177(7)	90	0	390	728	*25*
	—	—	—	(2.20(1))	90	0	(460)	(730)	*24*
CN^{-e}	145	22	—	2.362(5)	—	—	—	—	*21*
	(154)	—	—	2.373(6)	—	—	—	—	*28*
OH^-	162	132	—	—	84.8	0.19	649	915	*25*
	—	—	—	(2.11(1))	—	—	—	(915)	*19*
CN^-	151.9	133	1000	2.154(6)	79.9	0.37	—	924	*21*
	(160)	—	(100)	(2.18(1))	(79.9)	(0.38)	—	(925)	*28*
F^-	160.5	134	150	2.14(2)	84.1	0.18	—	946	*31*
	—	—	(12)	—	—	—	(869)	—	*49*
N_3^-	157	135	48	2.02(4)	82(2)	0.27	—	952	*32*
	—	—	(2)	(2.17(2))	(82.4)	(0.28)	—	(953)	*27*
NCS^-	158.7	135	2.0	2.14(3)	80.6	0.35	734	954	*33*
	—	—	—	—	—	—	(889)	—	*25*
py[f]	159	136	0.27	—	—	—	—	964	*25*
	—	—	—	(2.171(4))	(80.5)	(0.36)	—	(966)	*21*
OH_2	159	136	—	—	—	—	751	980	*25*
	—	—	—	(2.16(1))	(81.9)	(0.34)	(904)	(990)	*19*

[a] Stability constant for *trans*-$[WO(X)(CN)_4]^{m-}$ complexes (*50*) as defined in Scheme 1.
[b] Average equatorial W—CN distances from crystal structures, see Table I.
[c] Distance of metal center from equatorial plane formed by the four cyano carbons.
[d] Ref. (*1*).
[e] *Trans* to oxo.
[f] For Mo(IV), py = *N*,*N*-dimethylaminopyridine.

strength of the trans ligand. Furthermore, the increase in stability constants ($pK_x = -\log K_x$, K_x = stability constant) of the relevant $[WO(X)(CN)_4]^{m-}$ complexes, as a function of ligand strength, is also in good agreement with this effect.

The equatorial M–CN bond length decreases from the M(IV) dioxo complex to the hydroxo- and aqua-related complexes from 2.18 to *ca.* 2.14 Å respectively (see Table III) which corresponds to an increase of about 10 Hz in the coupling constant, i.e., an increase in M–CN bond length induced by the two oxo ligands forming the trans O=M=O moiety. The introduction of the two double bonds trans to each other introduces substantial electron density to the metal center, resulting in lengthening of the equatorial M–CN bonds. This weakening of the cyano bonds is well illustrated in the *ca.* 2- to 3-order increase which was observed in the cyanide exchange rate constants for all the systems, which is also in good agreement with a dissociative mechanism for the cyanide exchange for these metal centers (see further discussion in Section V).

The chemical shift of the equatorial ^{13}CN ligands in the $[WO(L)(CN)_4]^{m-}$ complexes does not show a systematic correlation with the crystallographic data (Table III). This is to be expected considering the significant differences in the electronic environment introduced to the metal center and therefore on the ^{13}C cyano nuclei due to the different trans L ligands such as F^-, py (pyridine), NCS^-, CN^-, H_2O, OH^-, and O^{2-}. It is, however, interesting to note that the equatorial ^{13}C chemical shift in the $[WO(CN)_5]^{3-}$ complex (Fig. 4a) is 152 ppm compared to the other $[MO(L)(CN)_4]^{m-}$ complexes with chemical shifts of 162, 161, 157, 159, 159, and 159 ppm for L = OH^-, F^-, N_3^-, NCS^-, py, and H_2O, respectively. The significant down-frequency shift for the pentacyano complex relative to the others is worth noting and might be related to the enhanced exchange rate of the pentacyano complexes compared to the other $[MO(L)(CN)_4]^{m-}$ complexes (see further discussion below).

In Table III is also given the distortion of the W(IV) complexes as demonstrated by the displacement from the plane as well as the change in bite angle of the equatorial cyano ligand with the M=O moiety as well as the ν(W=O) as obtained from IR studies and the oxygen-17 NMR data. It is clear that a reasonable correlation between all these parameters, excluding the chemical shift for the $[WO(CN)_5]^{3-}$ complex (Fig. 4a), exists.

2. Oxygen-17 NMR

a. Rhenium(V) Figure 8 illustrates the ^{17}O spectra observed at a pH of *ca.* 1.30, where $[ReO(H_2O)(CN)_4]^-$ is the main Re(V) species in solution. The first spectrum (Fig. 8a) was recorded after 3 min, showing a substantial signal at *ca.* 440 ppm in contrast with the fact that coordinated water is expected to display a signal close to 0 ppm (*52*). This signal showed a slow decrease with time, accompanied by the simultaneous formation of two signals at 765 and 229 ppm respectively (Figs. 8b and 8c). Analysis of these spectra (*5*) led to the assignment of the signals to the corresponding terminal and μ-oxo sites in $[Re_2O_3(CN)_8]^{4-}$ ion (Fig. 3), respectively, and it was noted that the μ-O exhibited a very slow relaxation rate.

It was concluded that the signal at *ca.* 440 ppm represents the average signal of the oxo and aqua sites and that once exchange of the coordinated water molecule by a H_2O from the bulk has taken place, as a result of the rapid proton exchange, the signal of the enriched metal oxo site is observed (see also further discussion below). It is, however, not the oxo as such that undergoes the actual exchange with the bulk water. Thus the rapid oxo exchange reported in the literature should be interpreted with care since it might be attributed to

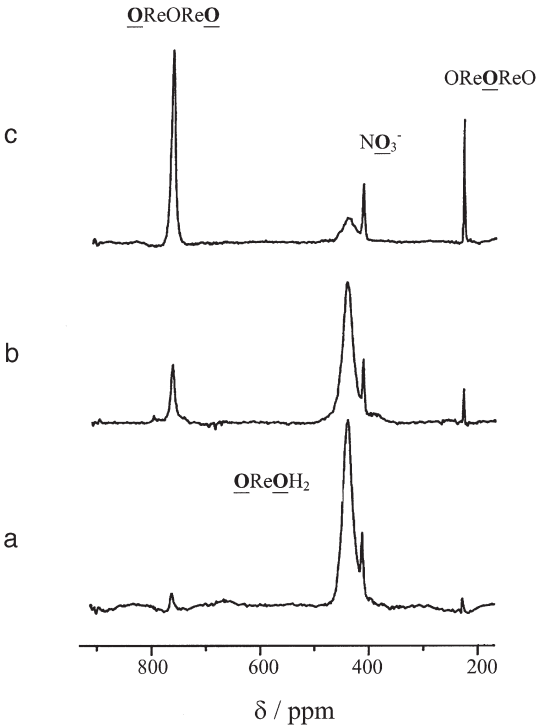

FIG. 8. Oxygen-17 NMR spectra at pH = 1.3, illustrating the formation of the dinuclear complex at 25°C after (a) 3 min, (b) 1 h and (c) 6 h of mixing $[ReO_2(CN)_4]^{3-}$ and $H_2{}^{17}O$. The total complex concentration [Re] = 0.2 *m*, μ = 1.0 *m* (KNO_3), NMR chemical shift reference is the nitrate ion ($\delta(NO_3)$ = 413 ppm) (*5*). (Adapted with permission from Roodt, A.; Leipoldt, J. G.; Helm, L.; Merbach, A. E. *Inorg. Chem.* **1992,** *31,* 2864–2868. Copyright 1992 American Chemical Society).

fast proton exchange. This was the case in, for example, the Ti(IV) aqueous system (*53*).

Figure 9 illustrates the effect of excess monodentate ligand, e.g., thiocyanate, on the $[ReO(H_2O)(CN)_4]^-$ complex. In fact the addition of solid KNCS to a solution (pH = 1.10) caused the ^{17}O signal at *ca.* 440 ppm to disappear, which in turn corresponded to the simultaneous formation of a new signal at *ca.* 884 ppm, attributed to the formation of the $[Re^*O(NCS)(CN)_4]^{2-}$ complex. Furthermore, the formation of this thiocyanato complex can be monitored with ease in the presence of the dinuclear species. The rate increase of this signal at *ca.* 884 ppm corresponds to the previously observed formation rate of $[Re^*O(NCS)(CN)_4]^{2-}$ (*48*). However, the integral of the newly formed signal at 884 ppm was only half that of the original signal at approxi-

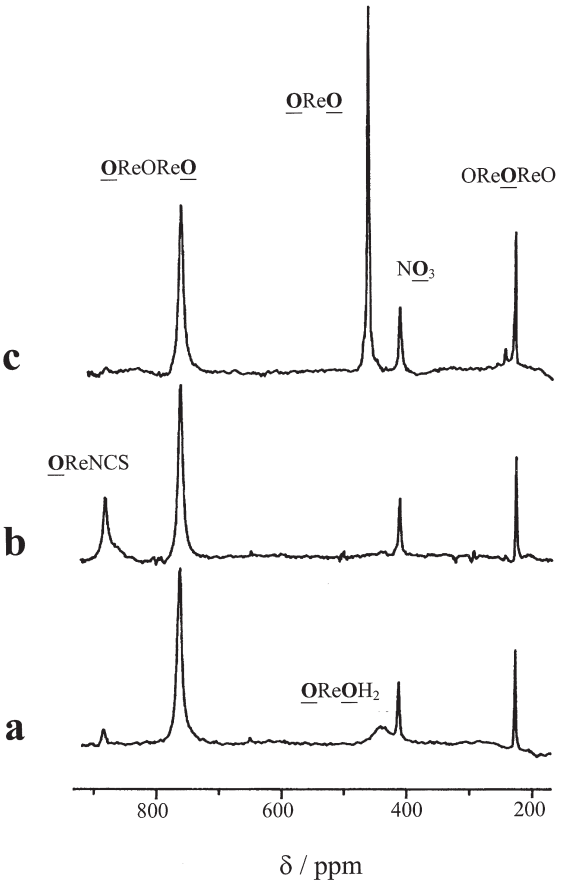

FIG. 9. Qualitative oxygen-17 NMR spectra of a Re(V) solution at (a) pH = 1.10, showing the effect of added (b) NCS^- and (c) OH^- (pH = 8) at 25°C. The total complex concentration [Re] = 0.2 *m*, μ = 1.0–1.4 *m* (KNO_3), NMR chemical shift reference is the nitrate ion ($\delta(NO_3)$ = 413 ppm) (*5*). (Adapted with permission from Roodt, A.; Leipoldt, J. G.; Helm, L.; Merbach, A. E. *Inorg. Chem.* **1992,** *31,* 2864–2868. Copyright 1992 American Chemical Society).

mately 440 ppm, which is consistent with an expected Re : O molar ratio of 1 : 1 in the $[Re^*O(NCS)(CN)_4]^{2-}$ ion. Upon addition of base to this solution containing the thiocyanato complex (pH = 8), the 884 ppm signal disappeared rapidly (hydrolysis of the coordinated NCS-ligand), forming a signal at 463 ppm (Fig. 9b) with a Re : O ratio again 1 : 2, similar to that described above for the dioxo species. This substitution/hydrolysis process is reversible by simple pH manipulation.

Acidity manipulation in the pH range 0–8 led to the observation of only one ^{17}O signal over the whole pH range investigated. Analysis of the chemical shift variation yielded a reliable value for the first protonation constant (*5*). In the case of the $[Re^*O(^*OH)(CN)_4]^{2-}$ complex, as was found for the aqua species, only the weighted *average* oxygen-17 signal of the oxo and the hydroxo sites is observed due to the rapid proton exchange. However, a significant broadening of the signal as a result of the proton exchange was also observed, which is further discussed in Section III.

This hypothesis was tested using DMSO (*5*) to limit both proton and water exchange whereupon the ^{17}O signals of the four oxygen sites in the $[ReO(H_2O)(CN)_4]^-$ and $[ReO(OH)(CN)_4]^{2-}$ ions were clearly identified (Fig. 10).

An additional interesting observation (Scheme 2) in this study spe-

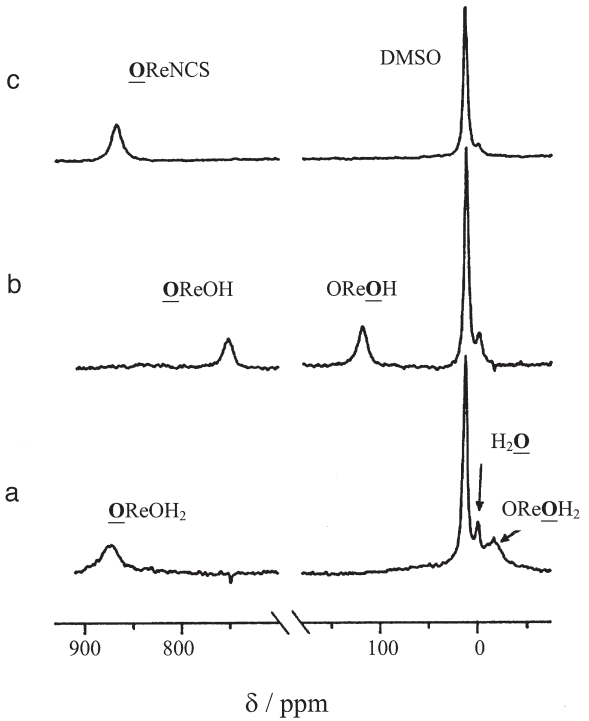

FIG. 10. Oxygen-17 NMR spectra of ^{17}O-enriched oxo cyano complexes in DMSO at 25°C: (a) $[Re^*O(H_2^*O)(CN)_4]^-$; (b) $[Re^*O(^*OH)(CN)_4]^{2-}$; (c) $[Re^*O(NCS)(CN)_4]^{2-}$ (*5*). (Adapted with permission from Roodt, A.; Leipoldt, J. G.; Helm, L.; Merbach, A. E. *Inorg. Chem.* **1992,** *31,* 2864–2868. Copyright 1992 American Chemical Society.)

cifically concerned the formation of this dinuclear species (Fig. 3). It is known that the presence of the $[ReO(OH)(CN)_4]^{2-}$ plays an important role in the formation of the $[Re_2O_3(CN)_8]^{4-}$ complex, and pH changes are expected upon formation of significant concentrations (monitored with ease by both ^{13}C and ^{17}O NMR) thereof. This has indeed been observed (*5*), i.e., a significant decrease in solution pH at pH values around 1.3 and the opposite at pH values around the pK_{a2} value (= 3.72) of the aqua species, in agreement with the equilibria in Scheme 2. The chemical shift data for the Re(V) complexes are summarized in Fig. 11, and several important conclusions can be made from this ^{17}O NMR study.

For both the $[ReO(H_2O)(CN)_4]^-$ and $[ReO(OH)(CN)_4]^{2-}$ complexes, only one signal was observed over the whole pH range in the above study, which represents the average signal of the enriched oxo and hydroxo/aqua sites. The integrals of the ^{17}O signal obtained at pH values of 1.8, 3.2, and 5.5 were the same within experimental error, in all three cases, and consistent with a Re : O molar ratio of 1 : 2. This implies that the signal observed at pH values around 5 represents the true position of the ^{17}O signal of the dioxo complex $[ReO_2(CN)_4]^{3-}$ (Fig. 9c), both Re=O sites being observed and equivalent. As soon as the pH is, however, lowered to below pK_{a2}, only average signals are observed (Figs. 8 and 9). The fact that *both* oxygen sites are enriched, hence the O : Re molar ratio of 2 : 1, can therefore be explained by a rapid proton exchange according to Scheme 3.

(pH *ca.* 1.3)

$$[ReO(H_2O)(CN)_4]^- + [ReO(OH)(CN)_4]^{2-} \rightleftharpoons [Re_2O_3(CN)_8]^{4-} + H_3O^+$$

(pH *ca.* 3.7)

$$[ReO(OH)(CN)_4]^{2-} + [ReO_2(CN)_4]^{3-} + H_2O \rightleftharpoons [Re_2O_3(CN)_8]^{4-} + OH^-$$

SCHEME 2.

The full analysis of this proton exchange is presented in Section III, wherein further evidence for the assignment of the different species for the Re(V) as obtained from the study of the other metal centers, and specifically the W(IV), is also discussed.

The data obtained from this ^{17}O study on the Re(V), also that obtained in DMSO solutions, can be correlated with results from previous X-ray crystallographic and infrared solid-state studies on these oxocyanorhenate(V) complexes and are summarized in Fig. 12.

An excellent correlation is obtained with rhenium–oxygen bond

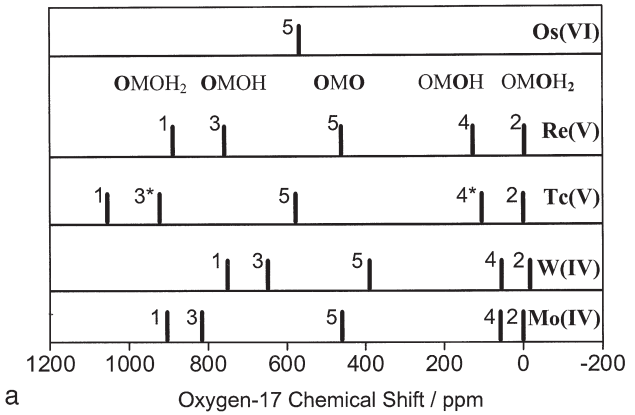

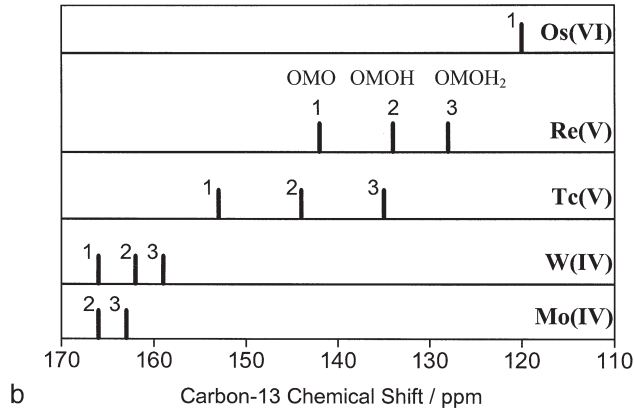

FIG. 11. Chemical shifts of the different sites in the Os(VI), Tc(V), Re(V), W(IV) and Mo(IV) systems (asterisked bars refer to expected values (*6*) at 25.0°C and μ = 1.0–1.4 *m* (KNO_3): (a) oxygen-17 and (b) carbon-13.

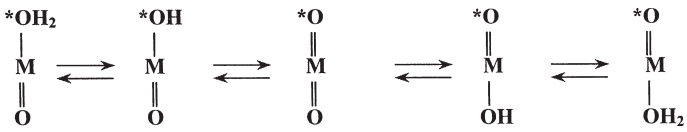

SCHEME 3.

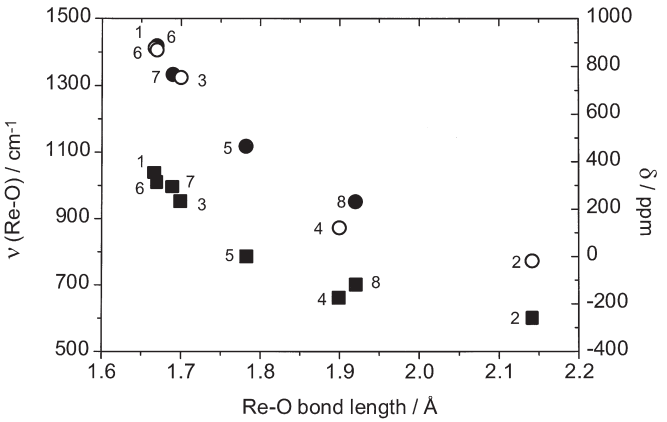

FIG. 12. Comparison of structural, infrared (■) and ^{17}O NMR data (● in DMSO and O in H_2O) for the Re(V) system where 1, 2, 3, 4, and 5 refer to the sites described in Fig. 11, whereas sites 6, 7, and 8 refer to Re=O in $[ReO(NCS)(CN)_4]^{2-}$, Re=O and Re-μ-O in $[Re_2O_3(CN)_8]^{4-}$ respectively (*5*).

distances as determined from crystallographic studies (see Table I). The Re–O bond strength decreases systematically from the strongest Re=O bond in $[ReO(H_2O)(CN)_4]^-$ (bond distance = 1.667(8) Å to 2.147(8) Å of the Re–OH_2 bond. The other Re–O bonds in the $[ReO(OH)(CN)_4]^{2-}$, $[ReO(NCS)(CN)_4]^{2-}$, and the $[ReO_2(CN)_4]^{3-}$ complexes are all intermediate between these two extreme values. It is also clear that the electronic environments of the hydroxo in the $[ReO(OH)(CN)_4]^{2-}$ complex and the μ-oxo in the dimeric species are quite similar, the same being true for the respective terminal oxo groups. This Re–O bond strength decrease, and therefore the electron density increase on the oxygen atom, are in direct correlation, as was found in other systems (*1*). Furthermore, it is also of interest to note that the observed infrared stretching frequencies, ν(Re–O), for all five of the Re=O bonds as well as the Re–O bonds (in the dinuclear, hydroxo oxo, and aqua oxo complexes respectively) in the above-mentioned five Re(V) complexes (*5*), correlate with the increase in bond strength and therefore with the decrease in electron density on the oxo ligand.

Finally, a good correlation also exists between the distortion induced by protonation, as evident from both the apical displacement of the Re(V) center from the equatorial cyano-carbon plane as well as the bond angle (O–Re–CN), deviating significantly from the ideal 90° as in the symmetrical dioxo complex, see Table I.

b. Tungsten(IV) The pH dependence of the W(IV) system was carefully studied over the pH range 6–14 and the effects of the pH on the linewidth, chemical shift, and species distribution are shown in Fig. 13 (*6*). A significant change in signal shift from *ca.* 750 to 650 ppm is observed upon a pH increase from 6 to 8, followed by a signal broadening and eventual disappearance of the signal if the pH is increased from 9 to 10. A further increase in pH above 10 results in the appearance of a new signal at *ca.* 360 ppm. At pH = 6, where only the aqua oxo complex of W(IV) is present, the signal at 751 ppm represents the oxo site in the $[WO(OH_2)(CN)_4]^{2-}$ complex since a W : O molar ratio of approximately 1 : 1 is obtained, taking into account the integral (with reference to the bulk water) of the specific oxo signal and the concentration of the W(IV) used. At pH values of *ca.* 9 a W : O ratio of 1 : 1 is still observed for this signal, as expected for the oxo signal of the hydroxo oxo complex. The chemical shifts for the aqua

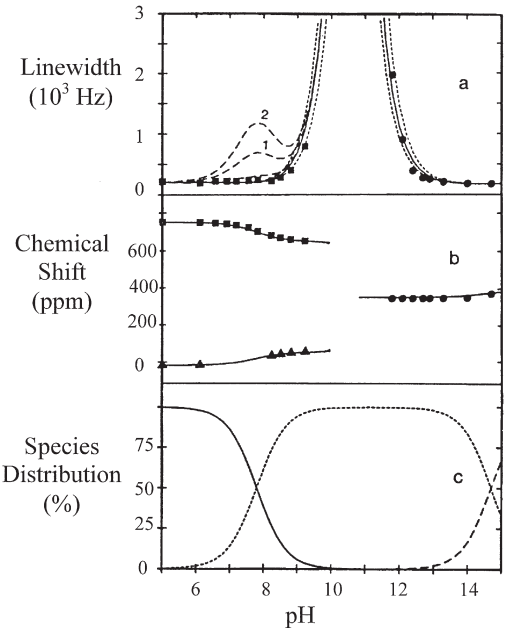

FIG. 13. Observed and calculated pH dependence of 54.227 MHz ^{17}O signal for the W(IV) complex (a) linewidth (oxo: ■; fast exchange: ●). Dashed lines 1 and 2 illustrate how the limiting value of k_{lb} was determined (*6*). (b) Chemical shift (oxo: ■; aqua/hydroxo: ▲; fast exchange: ●) and (c) species distribution ($OWOH_2$—; OWOH-----; OWO — — —) at 25.0°C with total complex concentration [W] = 0.2 *m* and μ = 1.0–1.4 *m* (KNO_3). (Adapted with permission from Roodt, A.; Leipoldt, J. G.; Helm, L.; Merbach, A. E. *Inorg. Chem.* **1994,** *33,* 140–147. Copyright 1994 American Chemical Society.)

and hydroxo signals of the aqua oxo and hydroxo oxo complexes in the slow exchange regime (pH < 9) are only just observed (on the side of the strong bulk water signal) at *ca.* −15 and 55 ppm respectively. The signal of the bound water signal was successfully detected using a selective pulse sequence (*7*).

However, at pH > 10, the system enters the fast exchange regime and produces an average signal at *ca.* 360 ppm (Figs. 13 and 14) for the two oxygen sites of the $[WO(OH)(CN)_4]^{3-}$ complex (W : O ratio = 1 : 2 under these conditions). In contrast, for the Re(V) system, only an average signal resulting from the oxo and aqua sites in the $[ReO(OH_2)(CN)_4]^-$ ion (Re : O molar ratio = 1 : 2) could be observed over the whole accessible pH range in aqueous medium (*5*).

The ^{17}O chemical shift data obtained for the W(IV) are summarized in Fig. 11, while further kinetic information from lineshape analysis of the above study is described in Section III.

c. Molybdenum(IV) Similar signal behavior to the W(IV) was obtained for the Mo(IV), showing similar chemical shift dependence of the oxo signal upon increasing the pH above the pK_{a1} value (9.9),

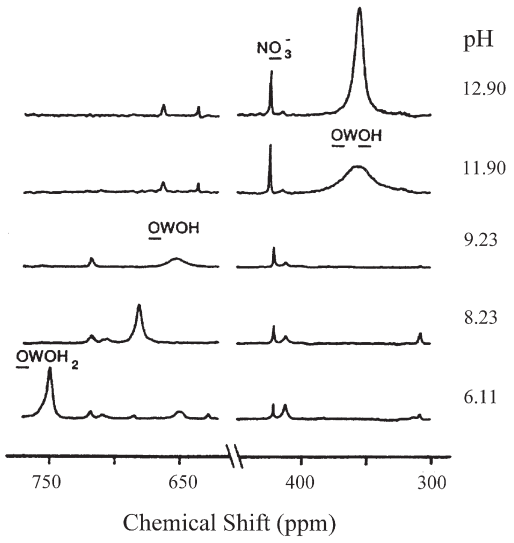

FIG. 14. The pH dependence of ^{17}O spectra for the W(IV) system at 25.0°C with total complex concentration [W] = 0.2 *m* and μ = 1.0–1.4 *m* (KNO_3), NMR chemical shift reference is the nitrate ion ($\delta(NO_3)$ = 413 ppm). The spurious signals have not been identified but are partially due to the dimeric species (*6*). (Adapted with permission from Roodt, A.; Leipoldt, J. G.; Helm, L.; Merbach, A. E. *Inorg. Chem.* **1994,** *33,* 140–147. Copyright 1994 American Chemical Society.)

allowing (as for the W(IV) system) to accurately measure the chemical shifts and linewidths of both the oxo sites in the aqua oxo and hydroxo oxo complexes. The chemical shifts for the hydroxo and aqua signals of the Mo(IV) system could not be measured due to the small differences with respect to the bulk aqua peak and due to rapid exchange and were consequently calculated from the average observed peak for the hydroxo oxo complex and the chemical shifts of the oxo sites measured for the aqua oxo and hydroxo oxo complexes. The data are reported in Fig. 11.

d. Technetium(V) The Tc(V) system was chemically less feasible to study as a result of the rapid formation of a dinuclear species (*13*) as soon as the $[TcO(OH)(CN)_4]^{2-}$ complex is present in appreciable amounts. Some data points for the Tc(V) system were thus analyzed by means of information obtained from the other systems (*6*). The chemical shifts are reported in Fig. 11.

e. Osmium(VI) The data are limited to the dioxo complex and are reported in Fig. 11.

C. Conclusions

1. Correlation between Chemical Shift and Acid Base Behavior

The chemical shift data of the five metal systems in the absence of exchange, as schematically summarized in Fig. 11, show the relative effect that mono and diprotonation have on these metal centers. The oxo signals are at high frequency (*ca.* 700–1050 ppm), the dioxo signals at intermediate values (400–600 ppm), while the hydroxo and the aqua signals are close to the bulk water signal. The high chemical shift value for the oxo in the $[TcO(H_2O)(CN)_4]^-$ suggests significant interaction with the Tc(V) center, in agreement with the reactivity observed of the labilized coordinated water molecule (Table II).

The ^{13}C and ^{17}O (Fig. 11) chemical shift data for the signals of the individual sites included in Tables II and III are determined by the electronic environment of the coordinated cyano and oxygen ligands and can in turn be correlated with the Lewis acidity of the metal centers. The ^{17}O chemical shifts for the signals of the oxo ligands in both the $[MO(OH)(CN)_4]^{(n+1)-}$ and $[MO(OH_2)(CN)_4]^{n-}$ complexes suggest that the ability of the metal center to accept electron density from the oxo ligand is in the order Os(VI) > Tc(V) > Mo(IV) > Re(V) > W(IV). This results in M=O "cores" for which the Lewis acidity of the sites trans to the oxo follow the sequence: (Os=O) >

(Re=O) > (Tc=O) > (W=O) > (Mo=O) (see pK_{a1} and pK_{a2} values in Table II). However, it is clear that the effect of the metal center on the cyano ligands cis to the oxo ligand, as obtained from the ^{13}C data, shows a different order: Mo(IV) > W(IV) > Tc(V) > Re(V) > Os(VI). This suggests that the carbon atoms of the cyano ligands coordinated to the Re(V) center are more electron-rich than those coordinated to the Tc(V) center, which in turn are more than the W(IV) and the Mo(IV). This is in agreement (*54–55*) with proton NMR data obtained for corresponding Re(V) and Tc(V) complexes, where it was shown that ligands coordinated cis to the oxo ligand in these centers experience more interaction with the metal atom in the case of Tc(V) than Re(V). This is also in line with the above-mentioned effect of the metal center on the oxo ligand as well as the fact that the third row metals are more difficult to reduce than their corresponding second-row congeners.

Protonation of an oxo ligand in any of these four metal systems results in electron density changes on the metal centers in the protonated complexes. The decrease in electron density on any one oxo ligand upon protonation of the other oxo ligand trans thereof is clear from the ^{17}O chemical shifts for all four metal systems (see Table II and III and Fig. 11). On the other hand, protonation in these systems results in an increase in the trans M=O bond strength as was shown crystallographically (see Table I), which in turn also results in an increase in electron density on the cyano carbon atoms as observed from the ^{13}C chemical shifts.

Furthermore, protonation results in a significant distortion of the coordination polyhedron, i.e., the metal ion is displaced from the plane formed by the four cyano ligand carbon atoms toward the oxo along the M=O axis by as much as 0.34 Å, which represents about 20% of the total metal–oxo bond length. In spite of this distortion stronger metal–cyano bonds are observed crystallographically, suggesting a better π back-donation by the metal center to the cyano carbons since d–π^* overlap is increased. This observation is in line with both the ^{13}C and ^{15}N chemical shift and kinetic data (Section V) for the protonated complexes (*8*).

2. General

This study demonstrated the power of NMR spectroscopy whereby the use of carbon-13, nitrogen-15, and, more specifically, oxygen-17 in these oxo systems proved that the different species in the protonation, complex formation, ligand exchange, and condensation of the Re(V) system can be exceptionally well characterized in solution. The re-

sults were in direct agreement with those derived from crystallographic and infrared studies. It was also demonstrated, however, that care needs to be taken before assigning observed signals to specific coordinated sites without having a knowledge of the complete system.

Next, the quantitative analysis of the protonation equilibria is discussed.

III. Proton Exchange Kinetics

This section deals with the quantitative description of the proton transfer processes (denoted by Eqs. (4) and (6) in Scheme 1), identified by the qualitative NMR experiments on the acid/base behavior of the Mo(IV), W(IV), Re(V), Tc(V), and Os(VI) systems as described in Section II. The data obtained on the signal behavior from these similar complexes were used to simulate spectra and model the proton exchange processes to finally obtain rate constants associated therewith.

Earlier pioneering work by Eigen (*56*) showed that the exchange process of a proton in aqueous acidic/basic medium between species MOH and MO^{*-} can in general be represented by Scheme 4 (which can also be adapted to include the proton transfer between a $[MOH_2]$ and a [MOH] species). This mechanism, involving protolysis and hydrolysis (acid and base catalysis) and direct proton transfer, can be

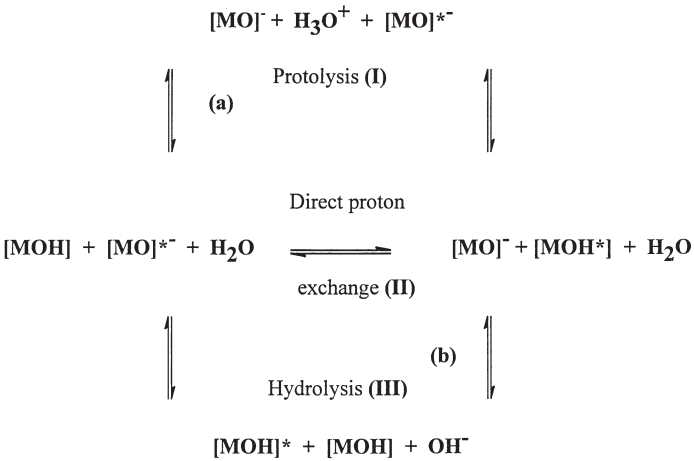

SCHEME 4.

used as a model for the interpretation of the H^+ transfer in these oxocyano systems.

If only the acid/base proton dissociation of complex MOH is considered, Scheme 4 is simplified to include only steps (a) and (b) therein. According to this model, (**I**) is the primary deprotonation pathway in acidic medium, while (**III**) is of importance in basic media. On the other hand, direct proton transfer (**II**) can occur around neutral pH values.

A. Mechanisms of Proton Exchange

The complicated signal characteristics (as for example illustrated in Section II for the Re(V)) can be rationalized using the Eigen (*56*) exchange model given in Scheme 4. Based on this model, the following reactions are visualized to potentially contribute to the proton exchange in these oxocyano complexes, with the five exchange sites shown in Eqs. (8–10) (for the $[MO(OH_2)(CN)_4]^{n-}$ complex) and Eqs. (13–15) (for the $[MO(OH)(CN)_4]^{(n+1)-}$) referring to Eqs. (4) and (6) in Scheme 1 respectively.

1. Exchange on the $[MO(OH_2)(CN)_4]^{n-}$ Complexes

Proton transfer reactions on the aqua oxo complex are described by Eq. (8) (acid catalysis or protolysis), Eq. (9) (base catalysis or hydrolysis), and Eq. (10) (direct proton exchange).

$$[(\overset{(1)}{O}{=}M{-}\overset{(2)}{O}H_2)(CN)_4]^{n-} \underset{k_{-1a}}{\overset{k_{1a}}{\rightleftharpoons}} [(\overset{(3)}{O}{=}M{-}\overset{(4)}{O}H)(CN)_4]^{(n+1)-} + H^+ \tag{8}$$

$$[(\overset{(1)}{O}{=}M{-}\overset{(2)}{O}H_2)(CN)_4]^{n-} + OH^- \underset{k_{1b}}{\overset{k_{-1b}}{\rightleftharpoons}} [(\overset{(3)}{O}{=}M{-}\overset{(4)}{O}H)(CN)_4]^{(n+1)-} + H_2O \tag{9}$$

$$[(\overset{(1)}{O}{=}M{-}\overset{(2)}{O}H_2)(CN)_4]^{n-} + [(\overset{(3)}{O}{=}\overset{*}{M}{-}\overset{(4)}{O}H)(CN)_4]^{(n+1)-} \overset{k_{1ex}}{\rightleftharpoons}$$

$$[(\overset{(3)}{O}{=}M{-}\overset{(4)}{O}H)(CN)_4]^{(n+1)-} + [(\overset{(1)}{O}{=}\overset{*}{M}{-}\overset{(2)}{O}H_2)(CN)_4]^{n-}. \tag{10}$$

The rate of protonation/deprotonation at the aqua oxo complex, which in principle can proceed via any of the above three pathways, is then given by Eq. (11)

$$-d[MOH_2]/dt = k_{1a}[MOH_2] + k_{-1b}[MOH_2][OH^-] + k_{1ex}[MOH_2][MOH]. \tag{11}$$

The observed protonation constant describing the proton transfer on the aqua oxo complexes as a function of the total metal complex concentration, $[M]\{(k_{obs})_{aq} = d[MOH_2]/[M]dt\}$, is therefore given by Eq. (12)

$$(k_{obs})_{aq} = \{k_{1a}[H^+]^2 + k_{1b}K_{a1}[H^+] + k_{1ex}[MOH_2]K_{a1}[H^+]\}/([H^+]^2 + K_{a1}[H^+] + K_{a1}K_{a2}). \quad (12)$$

2. Exchange on the $[MO(OH)(CN)_4]^{(n+1)-}$ Complexes

Similarly, the proton transfer on the hydroxo oxo complex is illustrated by Eqs. (13)–(15), based on the Eigen model (Scheme 4), and can again be due to protolysis, hydrolysis, or direct proton exchange

$$[(\overset{(3)}{O}{=}M{-}\overset{(4)}{O}H)(CN)_4]^{(n+1)-} \underset{k_{-2a}}{\overset{k_{2a}}{\rightleftharpoons}} [(\overset{(5)}{O}{=}M{-}\overset{(5)}{O})(CN)_4]^{(n+2)-} + H^+ \quad (13)$$

$$[(\overset{(3)}{O}{=}M{-}\overset{(4)}{O}H)(CN)_4]^{(n+1)-} + OH^- \underset{k_{2b}}{\overset{k_{-2b}}{\rightleftharpoons}} [(\overset{(5)}{O}{=}M{-}\overset{(5)}{O})(CN)_4]^{(n+2)-} + H_2O \quad (14)$$

$$[(\overset{(3)}{O}{=}M{-}\overset{(4)}{O}H)(CN)_4]^{(n+1)-} + [(\overset{(5)}{O}{=}\overset{*}{M}{=}\overset{(5)}{O})(CN)_4]^{(n+2)-} \overset{k_{2ex}}{\rightleftharpoons}$$

$$[(\overset{(5)}{O}{=}M{=}\overset{(5)}{O})(CN)_4]^{(n+2)-} + [(\overset{(3)}{O}{=}\overset{*}{M}{-}\overset{(4)}{O}H)(CN)_4]^{(n+1)-}. \quad (15)$$

The overall rate of protonation transfer on the hydroxo oxo is given by Eq. (16)

$$-d[MOH]/dt = k_{2a}[MOH] + k_{-2b}[MOH][OH^-] + k_{1ex}[MO_2][MOH]. \quad (16)$$

The observed protonation constant describing the proton transfer on the hydroxo oxo complex, is a function of the total metal complex concentration, $[M]\{(k_{obs})_{OH} = d[MOH]/[M]dt\}$, therefore given by Eq. (17)

$$(k_{obs})_{OH} = \{k_{2a}K_{a1}[H^+] + k_{2b}K_{a2}K_{a1} + k_{1ex}K_{a1}K_{a2}[MOH]\}/([H^+]^2 + K_{a1}[H^+] + K_{a1}K_{a2}). \quad (17)$$

The line-broadening data as a function of pH, typically shown for the W(IV) in Figs. 13 and 14, incorporating the known pK_a values (Table II), were fitted in 5 × 5 Kubo-Sack matrices describing the exchange based on the above schemes (*6*, *57*). The experimentally determined chemical shift and linewidth data in the absence of exchange for the aqua oxo, hydroxo oxo, and dioxo species and the pH-dependent species distribution as calculated from the acid dissociation constants for the four systems were all introduced in the different matrices and the spectra were computer simulated. For each set of chosen rate con-

TABLE IV

PROTON EXCHANGE RATE CONSTANTS (298 K, μ = 1.2 − 2.4 m (KNO_3)), FOR $[MO(OH_2)(CN)_4]^{n-}$, $[MO(OH)(CN)_4]^{(n+1)-}$, AND $[MO_2(CN)_4]^{(n+2)-}$ [a]

Rate constants [b]	Value [c]	
	Mo(IV)	W(IV)
k_{-1b} (M^{-1} s^{-1})	Not defined	Not defined
k_{-2b} (M^{-1} s^{-1})	$(2 \pm 1) \times 10^7$	$(4 \pm 2) \times 10^8$
k_{2b} (s^{-1})	$(1.3 \pm 0.2) \times 10^9$	$(7 \pm 2) \times 10^8$
k_{1ex} (M^{-1} s^{-1})	$\geq 1 \times 10^7$	$\geq 1 \times 10^7$
	Tc(V)	Re(V)
k_{1a} (s^{-1})	$\geq 1 \times 10^7$	$\geq 1 \times 10^8$
k_{-1a} (M^{-1} s^{-1})	$\geq 8 \times 10^9$	$\geq 2 \times 10^9$
k_{2a} (s^{-1})	$(1.1 \pm 0.5) \times 10^7$	$(1.1 \pm 0.2) \times 10^7$
k_{-2a} (M^{-1} s^{-1})	$(1.0 \pm 0.4) \times 10^{11}$	$(6 \pm 1) \times 10^{10}$
k_{2ex} (M^{-1} s^{-1})	$\geq 5 \times 10^8$	$\leq 5 \times 10^7$

[a] Ref. (*6*).

[b] Eqs. (8)–(17).

[c] For values reported with (≥) and (≤) only limits could be estimated.

stants (two or three) the pH dependence of the shifts and linewidths (one or two signals) were determined graphically and visually compared to the experimental data.

From these fits, the data for the rate constants given in Eqs. (12) and (17) were obtained for all four metal centers (see Table IV). However, it is clear that due to the complexity and the behavior of these systems, only limiting values for some of the constants could be obtained. These results, see discussion below, nevertheless illustrate how the above exchange scheme could be analyzed using NMR. For a detailed description of the procedure followed to determine these rate constants, the reader is referred to the original paper (6).

B. COMPARISON OF METAL CENTERS

The exchange mechanism of proton transfer in these systems is explained in terms of the Eigen model (Scheme 4) as discussed above by either hydrolysis (Mo(IV) and W(IV)) or protolysis (Tc(V) and Re(V)) pathways, coupled with direct proton transfer in the intermediate pH

range. The reverse rate constants are calculated from the pK_a values (Table II) and are summarized in Table IV for comparative purposes.

a. Molybdenum(IV) and Tungsten(IV) The results obtained from the evaluation of the systems by both the hydrolysis (**III** in Scheme 4) and hydrolysis/direct proton transfer (**III** and **II** in Scheme 4) pathways indicate that the proton exchange can be explained most convincingly by the second alternative. The overall process can therefore be summarized to proceed via hydrolysis (Eq. (14)) in strong basic medium and via direct proton transfer (Eq. (10)) in weak basic solution. The deprotonation of the O=M−OH moiety to form the O=M=O core is *ca.* 1 order of magnitude more rapid for the W(IV) than for the Mo(IV) (Table IV), which is in agreement with the acidity of the −OH function (in the $[MO(OH)(CN)_4]^{3-}$ complexes) of the W(IV) and Mo(IV) systems. The limiting values determined for the direct proton exchange rate constant, k_{1ex}, for the two systems are largely reflecting the fact that this pathway is quite important.

b. Rhenium(V) The results obtained for the proton transfer reactions for the Re(V) system as described in Scheme 4 show that these reactions proceed in strong acid via protolysis (Eq. (8)) and in weak acid medium via both protolysis (Eq. (13)) and direct proton transfer (Eq. (15)). The value for k_{2a} of 1.1×10^7 s^{-1} is well defined, resulting in an accurate calculation for the k_{-2a} value of 6×10^{10} M^{-1} s^{-1}, since the pK_{a2} value for the Re(V) system is accurately known, see Table IV. This k_{-2a} value is very high but in principle possible. Limiting values for both the k_{-1a} and k_{2ex} were also obtained.

c. Technetium(V) The results for the proton transfer reactions for the Tc(V) system are similar to those of the Re(V) in the sense that the transfer proceeds via protolysis and direct proton transfer (Eqs. (8), (13), and (15)). The value of k_{2a} of 1.1×10^7 s^{-1} is equally well defined. Since the pK_{a2} value for the Tc(V) system is not accurately known (as a result of the rapid (*13*) formation of the dinuclear species $[Tc_2O_3(CN)_8]^{4-}$) and was estimated to be *ca.* 4–5, a similar uncertainty is reflected in the k_{-2a} value. Using a value for the pK_{a2} of 4, a value for $k_{-2a} = 1 \times 10^{11}$ M^{-1} s^{-1} is calculated, which is very high, but acceptable if the few data points for the Tc(V) system as well as the uncertainty in the pK_{a2} are considered. Limiting values for the k_{-1a} and k_{2ex} were again obtained as in the case of the Re(V). Of significance is the fact that a lower limit for the direct exchange constant for the Tc(V) is obtained, whereas in the case of the Re(V) an upper limit could be calculated. This is fortunate and allows, because a large difference in

behavior for the Tc(V) and Re(V) complexes is not expected, to obtain good estimations of the limiting values of k_{2ex} of 5×10^8 and 5×10^7 M^{-1} s^{-1}, respectively.

C. Related Features

The above-mentioned proposed direct proton exchange pathways, given by Eqs. (10) and (15), are likely considering the existence of dimeric species with the linear O=M−O−M=O orientation for all four metal systems investigated in this study. The formation of such species necessitates the association of two of the metal centers in a required way for direct proton transfer. Furthermore, different literature examples of metal complexes, e.g., $[-Rh(en)_2(H_3O_2)(en)_2Rh-]$ (*58*) and $\{[M_3O_2(O_2CC_2H_5)_6(H_2O)_2]_2(H_3O_2)\}^{3+}$ (M = Mo, W) (*59–61*), are known, which confirms the existence of metal centers bridged by the $-(H_3O_2)-$ moiety. Consequently, it is also considered likely for such an intermediate (i.e., in Eqs. (10) and (15)) to exist in aqueous solutions of the aqua oxo tetracyano systems of the four metals investigated in this study, allowing for a direct proton transfer process.

The values obtained for the proton transfer in these four systems (Table IV) are typically as expected for these rapid processes. Examples from the literature where similar reactions were studied in metal complexes include the $[Cr(OH)(OH_2)]^{2+}$ (*62*) and $[VO(OH_2)_5]^{2+}$ (*63*) systems. In the proton exchange study of the hexaaqua aluminate(III) system a bimolecular process, similar to that proposed for the systems in this study, for the exchange between the $[Al(OH_2)_6]^{3+}$ and $[Al(OH_2)_5(OH)]^{2+}$ (*64*) complexes was postulated.

The results from the Mo(IV) and W(IV) systems showed a dramatic ^{17}O signal dependence on pH, changing from a fast exchange regime at high pH (increased concentrations of the $[MO_2(CN)_4]^{4-}$ ion present), with only a coalescent signal (average of oxo and hydroxo) observed, to a slow exchange regime where two signals (the oxo on both the oxo aqua and the oxo hydroxo complexes) are observed, see e.g., Figs. 13 and 14 (W(IV)). For the Re(V) system, however, only the fast exchange region is observed (*6*) as a result of the strong acid character of the $[ReO(OH_2)(CN)_4]^-$ complex (Table IV). Of significance is the fact that in the case of the Tc(V), the slow exchange regime was just accessible at $[H^+] = 1–10$ *M,* since the $[TcO(OH_2)(CN)_4]^-$ ion is a weaker acid (Table IV) than the corresponding Re(V) complex. In fact, it was calculated by simulation of the Re(V) system that the slow exchange regime should be observed at pH of *ca.* −2, i.e., $[H^+] = 100$ *M,* and therefore only theoretically accessible. Analysis and study of the Tc(V)

system (*6*) has, however, confirmed that the signal behavior observed in the rhenium system was in fact correct, but is difficult to explain based on the available results of the Re(V) system.

This proton transfer study showed that the oxo sites in these types of complexes are enriched as a result of H_2O/OH^- exchange followed by deprotonation/protonation. A significant observation is the fact that enrichment of the oxo site of the oxo aqua complexes has to proceed via the dioxo complex, which was also the case in other studies (*65, 66*). The concentration of the dioxo complex, coupled with the proton exchange thereof, therefore acts as a "bottleneck" and determines primarily the pH dependence of the systems entering the fast/slow exchange regimes. It is interesting to note that all the systems exit from the fast exchange regime at approximately 2 pH units below the pK_{a2} value.

It has been shown previously by crystal structure determinations and kinetic studies that protonation of the hydroxo oxo complex results in the formation of the aqua oxo complex rather than the dihydroxo species (*1*). The existence of a symmetrical dihydroxo species in solution, even as an intermediate, is also ruled out by this work since the observed exchange scheme would be altered significantly. No coalescent signals would in such a case be observed since the system will always be in fast exchange with regard to proton exchange. The dioxo complex acting as "bottleneck" would not have shown the pronounced effect as was observed in this study (Scheme 3).

In conclusion, oxygen-17 NMR line-broadening provides the unique opportunity to study very fast proton transfer reactions on these metal oxocyano complexes by lowering the concentration of the reacting species through pH manipulation.

D. Inversion of the Coordination Polyhedron Along the O–M–O Axis

The proton transfer processes described above induce interesting effects on the geometry of these metal complexes upon protonation (see also Section II). If it is assumed that the equatorial cyano ligands form a reference plane and are stationary for any of these distorted octahedral cyano oxo complexes, the protonation/deprotonation process as illustrated in Scheme 3 is responsible for the oxygen exchange at the oxo sites. This process effectively induces a dynamic oscillation of the metal center along the O–M–O axis at a rate defined by k_{INV}, illustrated in Fig. 15. This rate of inversion is determined by the rate at which the proton is transferred via the bulk water from the one

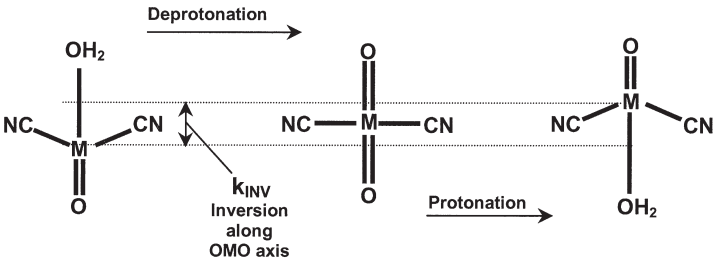

FIG. 15. Illustration of the inversion of the metal complex $[MO(H_2O)(CN)_4]^{n-}$ along the O–M–O axis.

trans site to the other and can be quantitatively expressed using the rate laws derived for the proton exchange processes described in Section III,A. Additionally, the statistical probability of protonation occuring at either of the two oxo sites in the dioxo complex as the rate-determining process must be taken into account.

The dioxo complexes of W(IV) and Mo(IV), having high pK_a values (Table II), are formed via hydrolysis as the rate-determining step (Scheme 4) and the observed rate constants for the inversion along the O–M–O axis for the W(IV) and the Mo(IV) complexes are therefore defined by Eq. (18). These were calculated as a function of pH, using the proton exchange rate constants (Table IV) and the acid dissociation constants (Table II)

$$k_{INV} = (k_{2b}K_{a2}K_{a1})/2[H^+]^2/(1 + K_{a1}/[H^+] + K_{a1}K_{a2}/[H^+]^2). \quad (18)$$

The formation of the dioxo complexes for the Re(V) and Tc(V) takes place via protolysis as given in Scheme 4. Similarly, the observed rate constant for the inversion along the O–M–O axis for these two metal centers is therefore given by Eq. (19). Again, the inversion rate constants as a function of pH were calculated using the proton exchange rate constants (Table IV) and the acid dissociation constants (Table II)

$$k_{INV} = (k_{2a}K_{a1}/2[H^+])/[(1 + K_{a1}/[H^+] + K_{a1}K_{a2}/[H^+]^2)]. \quad (19)$$

Under selected conditions, the observed rate of oxygen exchange in these complexes can primarily be a function of the protonation rate, i.e., the inversion of the metal center, since the exchange on an oxo at any M=O site must proceed though the "bottleneck" of the dioxo species which is further discussed in Section V.

IV. Oxygen Exchange Kinetics

In this section the kinetics of the oxygen exchange as shown in Scheme 1, Eqs. (3a), (5a), and (7a), is described. In Section I the ^{17}O signal characteristics as observed for these complexes have been discussed, and it was shown that in absence of proton exchange, the different oxygen sites in the $[MO(OH_2)(CN)_4]^{n-}$, $[MO(OH)(CN)_4]^{(n+1)-}$, and the $[MO_2(CN)_4]^{(n+2)-}$ complexes span a range from *ca.* 1055 ppm (for the oxo signal of the Tc(V) aqua oxo complex) to −15 ppm (for the aqua signal of the W(IV) aqua oxo complex) (see Fig. 11). It was also shown that the observed exchange at the oxo sites was a result of the fast proton exchange as shown in Scheme 3, where the dioxo complex acts as a "bottleneck" for the proton exchange process. At lower pH values the oxo and the aqua/hydroxo signals are observed separately (slow exchange region with regard to proton exchange), but give a coalesced signal at higher pH, representing the average of the two specific sites (fast exchange region with regard to proton transfer). In the slow exchange regime, the oxygen exchange at each individual site with the bulk water can in principle be monitored. Similarly, in the fast exchange proton region, the isotopic oxygen exchange of the coalesced signal with the bulk can be monitored to give the rate of oxygen exchange. An example of such a kinetic run is illustrated in Fig. 16, upon mixing a sample of the Re(V) complex with oxygen-17 water.

A. Exchange Between the Bound (Average Aqua/Hydroxo/Oxo) Oxygen and Bulk Water

The exchange equations of relevance for these metal complexes can in general be represented by Eq. (20), where $OMOH_2$, OMOH, and OMO are the $[MO(OH_2)(CN)_4]^{n-}$, $[MO(OH)(CN)_4]^{(n+1)-}$, and the $[MO_2(CN)_4]^{(n+2)-}$ complexes respectively

$$\left.\begin{matrix} OMOH_2 \\ OMOH \\ OMO \end{matrix}\right] - 2H_2O^* \overset{k_{obs}}{\rightleftharpoons} \left.\begin{matrix} *OM*OH_2 \\ *OM*OH \\ *OM*O \end{matrix}\right] - + 2H_2O. \qquad (20)$$

The pseudo first-order rate constants, k_{obs}, are obtained by least-squares fits of the measured peak height increase of the relevant coalesced oxygen-17 signal as a function of time to the modified McKay equation (*7*, *67*, *68*). The kinetics can be studied by manipulation of

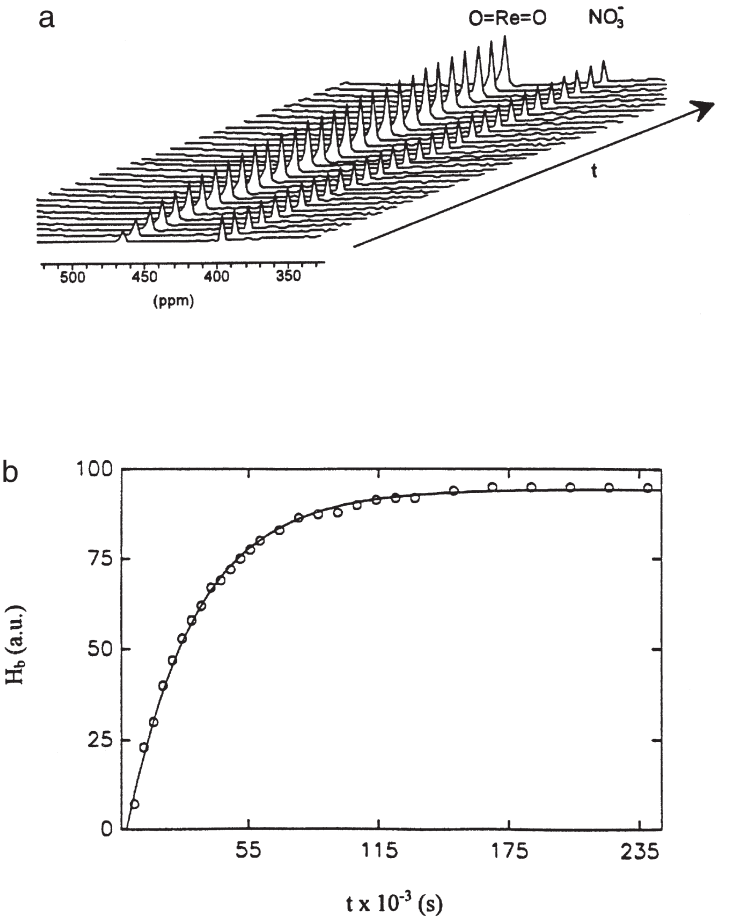

FIG. 16. Slow isotopic exchange at 35.0°C on Re(V) center. (a) Oxygen-17 spectra showing signal growth vs time for $[ReO_2(CN)_4]^{3-}$. (b) Least-squares fit of the data to the modified exponential McKay equation (7). The total complex concentration [Re] = 0.2 *m*, pH = 6.6, and μ = 1.2 *m* (KNO_3). (Adapted with permission from Roodt, A.; Leipoldt, J. G.; Helm, L.; Abou-Hamdan, A.; Merbach, A. E. *Inorg. Chem.* **1995,** *34,* 560–568. Copyright 1995 American Chemical Society.)

$[H^+]$ in selected pH ranges, displaying strictly first-order kinetics (see, for example, Fig. 16).

The three different complexes in Eq. (20) can in principle all undergo exchange, for which the overall rate law is then given by Eq. (21) for any complex M, and k_{aq}, k_{OH} and k_O represent the oxygen ex-

change rate constants according to Eqs. (3a), (5a), and (7a) in Scheme 1, respectively

$$-d[\mathrm{M}]/dt = k_{\mathrm{aq}}[\mathrm{OMOH_2}] + k_{\mathrm{OH}}[\mathrm{OMOH}] + k_{\mathrm{o}}[\mathrm{OMO}]. \tag{21}$$

By relating the concentrations of the different species in solution through the acid dissociation constants as a function of the total metal complex concentration [M], the observed rate constant (d[M]/[M]$dt = 2k_{\mathrm{obs}}$) can be obtained, and if the dioxo complex does not undergo observable oxygen exchange, it reduces to Eq. (22) (see also discussion for Re(V) and Tc(V)).

$$k_{\mathrm{obs}} = \frac{k_{\mathrm{aq}} + k_{\mathrm{OH}}(K_{a1}/[\mathrm{H^+}])}{2(1 + K_{a1}/[\mathrm{H^+}] + K_{a1}K_{a2}/[\mathrm{H^+}]^2)} \tag{22}$$

Three distinct pH regions for the observed oxygen exchange rate constant, k_{obs}, can be identified at (a) low pH values where $[\mathrm{H^+}] \gg K_{a1}$, Eq. (22) simplifies to Eq. (23); (b) intermediate pH values, where $K_{a1} \gg [\mathrm{H^+} \gg K_{a2}$, Eq. (22) simplifies to Eq. (24); and, (c) high pH values, where $K_{a2} \gg [\mathrm{H^+}]$, Eq. (22) simplifies to Eq. (25).

$$k_{\mathrm{obs}} = k_{\mathrm{aq}}/2 \tag{23}$$

$$k_{\mathrm{obs}} = k_{\mathrm{aq}}([\mathrm{H^+}]/2K_{a1}) + k_{\mathrm{OH}}/2 \tag{24}$$

$$k_{\mathrm{obs}} = k_{\mathrm{OH}}([\mathrm{H^+}]/2K_{a2}). \tag{25}$$

The oxygen exchange on the different oxo complexes for the W(IV), Mo(IV), Tc(V), Re(V), and Os(VI) metal centers were studied as described below in more detail. A summary of the rate constants thus obtained are given in Table V.

1. Rhenium(V)

The results from the ligand substitution studies show that the $[\mathrm{ReO(OH_2)(CN)_4}]^-$ complex is the least reactive oxo aqua complex of the four metal centers with regard to complex formation (*8*). However, the half-life for the water exchange of the Re(V) oxo aqua complex at 298 K, as calculated from these ligand substitution data is too rapid to study by the slow isotopic exchange. The concentration of the reactive aqua oxo can, however, be changed by simple pH manipulation to slow down the oxygen exchange process (e.g., Fig. 16). The temperature and $[\mathrm{H^+}]$ dependence of the oxygen exchange process for the

TABLE V

OXYGEN EXCHANGE RATE CONSTANTS (298 K, μ = 1.2 − 2.4 *m* (KNO_3)), AND ACTIVATION PARAMETERS FOR $[MO(OH_2)(CN)_4]^{n-}$ AND $[MO(OH)(CN)_4]^{(n+1)-}$

Parameter	Re(V)	Tc(V)	W(IV)	Mo(IV)
k_{aq} (s^{-1})	(9.1 ± 0.1) × 10^{-2}	(500)[a]	137 ± 5	(4.1 × 10^4)[a]
$\Delta H^{\#}_{k_{aq}}$ (kJ mol^{-1})	84.0 ± 0.1	—	80 ± 2	—
$\Delta S^{\#}_{k_{aq}}$ (J K^{-1} mol^{-1})	+16.9 ± 0.3	—	+64 ± 7	—
k_{OH} (s^{-1})	(2.6 ± 0.3) × 10^{-3}	13 ± 1	(6.5 ± 0.1) × 10^{-4}	(0.2)[a]
$\Delta H^{\#}_{k_{OH}}$ (kJ mol^{-1})	86 ± 6	76.0 ± 4	79.5 ± 0.3	—
$\Delta S^{\#}_{k_{OH}}$ (J K^{-1} mol^{-1})	−3 ± 20	+31 ± 15	−39 ± 1	—

[a] Estimated values, Ref. (*7*).

Re(V) under these conditions are illustrated in Fig. 17. The curve represents the least-squares fit (K_a values in Table II were used without compensation for possible temperature variation on values) of Eq. (22) to the data points. In Fig. 17, it is further illustrated (dashed line) that Eq. (24) holds for the data when $K_{a1} \gg [H^+] \gg K_{a2}$ and Eq. (25) (insert (a)) when $K_{a2} \gg [H^+]$. Note that the insert (a) shows a drawn line through the data points at higher pH values, indicating a negligible k_O. Finally, at low pH values ($[H^+] \gg K_{a1}$) the exchange rate becomes independent of proton concentration according to Eq. (23). The

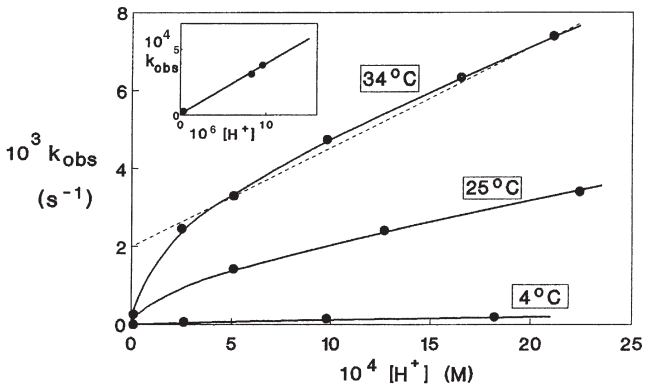

FIG. 17. Temperature and pH dependence of oxygen exchange on the Re(V) center; μ = 1.2–1.5 *m* (KNO_3). The insert shows a line drawn through the three points at high pH at 34.2°C which indicates a negligible k_o (*7*). (Adapted with permission from Roodt, A.; Leipoldt, J. G.; Helm, L.; Abou-Hamdan, A.; Merbach, A. E. *Inorg. Chem.* **1995,** *34,* 560–568. Copyright 1995 American Chemical Society.)

cyanide exchange rate constants for both the aqua oxo and hydroxo oxo complexes are reported in Table V, including the activation parameters as determined from the Eyring equation, and are also correlated in terms of the oxidation states, complex formation rate constants, and on of the metal centers in Table II.

The above observations are in agreement with oxygen-18 (*69*, *70*) isotopic exchange results reported for the Re(V) system, where a direct relationship between the observed exchange rate and the $[H^+]$ was found at pH values larger than pK_{a2}. In this specific study, only the k_{OH} value was determined but no explanation could be given for the results obtained at lower pH values, i.e., the change to linearity of the k_{obs} vs $[H^+]$ function at pH values lower than the pK_{a2} of the oxo aqua complex. The ^{17}O NMR study, however, successfully accounts for all the observed behavior, allowing the oxygen exchange constants for both the oxo aqua and the oxo hydroxo species (k_{aq} and k_{OH}, respectively) to be determined (see Table V). It is worth noting that the k_{OH} value of 0.0342(5) s^{-1} at 308 K determined by the above-mentioned oxygen-18 (*69*) isotope study for Re(V) is in reasonable agreement with that obtained by ^{17}O NMR.

2. Tungsten(IV) and Technetium(V)

The effect of temperature and $[H^+]$ on the oxygen exchange was studied for the W(IV) system by simple pH manipulation as was the case for the Re(V) mentioned above. However, here the pH had to be varied around high values (12–14) to attain the slow isotopic exchange conditions. The kinetic results were treated similarly to those of the Re(V) and are listed, together with the activation parameters, in Table V.

The $[TcO(OH_2)(CN)_4]^-$ complex is, as shown by the complex formation constants in Table II, more reactive than the corresponding complexes of either the Re(V) or W(IV). This, coupled with the fact that the dinuclear species $[Tc_2O_3(CN)_8]^{4-}$ is formed rapidly whenever there are appreciable amounts of the $[TcO(OH)(CN)_4]^{2-}$ complex present (*71*), i.e., below pH *ca.* 5.5, prohibits any experiment around these acidic conditions. A marked difference in the $[H^+]$ dependence for the Tc(V) compared to the above-mentioned Re(V) and W(IV) systems originates from the fact that the Tc(V) is much more reactive and had to be studied at pH values significantly higher than the pK_{a2} value of *ca.* 4. This yielded results similar to the insert (a) in Fig. 16 for the rhenium(V) and only the exchange rate constants and the activation parameters for the hydroxo oxo complex for Tc(V) could thus be obtained (Table V).

3. Molybdenum(IV)

The results from the complex formation reactions for the Mo(IV) oxo aqua complex compared to those of the other three metal centers indicate its very high reactivity (Table II). Similar pH manipulations to those of the W(IV) system proved to be *just* adequate to obtain one data point for the exchange reaction of the Mo(IV) system at a very high basicity. The oxygen exchange study on the coalesced signal for Mo(IV) was done by the fast-injection technique (*7*, *72*). A prethermostated aliquot of enriched oxygen-17 water was injected into the thermostated buffered metal complex solution in the NMR tube, followed by immediate commencement of data acquisition. A rate constant of 0.0167(7) s^{-1} at 1.2°C was obtained at $[OH^-] = 5$ *m* and an attempt at 25°C gave an approximate value of *ca.* 0.14 s^{-1}.

The complex-formation results in Table II showed that the Mo(IV) aqua oxo complex is 2 orders of magnitude more reactive than the W(IV) complex, in line with the oxygen exchange discussed here and in agreement with those obtained in a previous oxygen-18 isotopic exchange study (*70*), wherein the authors reported the exchange rate constant for the $[MoO(OH)(CN)_4]^{3-}$ complex as >0.07 s^{-1} at 0°C. The authors were not able to determine the exchange rate since the system is too reactive. The factor of *ca.* 300 difference between the complex-formation results for the $[MoO(OH_2)(CN)_4]^{2-}$ compared to the W(IV) complex together with all experimental results to date, suggests the substitution reactions of the oxo aqua complex proceed via a dissociative mode of activation. An estimate of both values of the oxygen exchange rate constants for the aqua oxo and hydroxo oxo complexes of Mo(IV) was made, assuming similar relative reactivities, yielding estimated values for k_{aq} and k_{OH} for the Mo(IV) center in Table V.

4. Osmium(VI)

It has previously been concluded that even in strong acidic solution, the dioxotetracyanoosmate(VI) complex cannot be protonated to form the oxo aqua complex or even the corresponding hydroxo oxo complex. The pK_{a1} and pK_{a2} values have been estimated to be substantially less than -1, which is also supported by the relationship between pK_a values and ^{17}O and ^{13}C chemical shifts (Table II). Extreme slow kinetic behavior, as expected in the case of a $+6$ charged metal center for a dissociative activation exchange process, has been observed, with only an upper limit for the oxygen exchange determined (Table II).

B. Exchange Between the Oxo and Aqua Sites in $[MO(H_2O)(CN)_4]^{2-}$ [M = W(IV) and Mo(IV)] and Bulk Water

The oxygen exchange at specific sites, i.e., oxo or aqua ligand in the $[MO(OH_2)(CN)_4]^{2-}$ complexes, can also in principle be monitored provided the technique used is adequate for this purpose. The exchange of the aqua oxygen in the $[MO(OH_2)(CN)_4]^{2-}$ complexes for Mo(IV) and W(IV) is expected to be a rapid process and it indeed required a more rapid measuring technique than conventional isotopic exchange. For the W(IV) aqua oxo complex, it was achieved by a variable temperature line-broadening study (*7*). The Mo(IV) could not be studied this way since the coordinated aqua signal could not be observed (very reactive metal center, see anation results in Table II, in fast exchange with the bulk water signal).

The exchange of the coordinated aqua ligand of the W(IV) aqua oxo species was qualitatively studied by NMR line-broadening as a function of temperature based on Eq. (26), where the transverse relaxation time of the bound oxygen-17 nucleus is given by $1/T_{2b}$. The $1/T_{2Qb}$ represents the quadrupolar relaxation rate and k_{aq} the chemical exchange rate constant

$$1/T_{2b} = 1/T_{2Qb} + k_{aq}. \tag{26}$$

The ^{17}O signal of the bound water in the aqua oxo complex of W(IV) is observed at −15 ppm at pH values 5–6, where the $[WO(OH_2)(CN)_4]^{2-}$ complex is the only W(IV) species in solution. The oxygen exchange was studied by suppressing the bulk water signal with a selective pulse sequence (*7*, *72*). Although the quadrupolar contribution to the observed signal was *ca.* 80–95%, with the water exchange (k_{aq}) contributing only 5–20% at the highest accessible temperature (at *ca.* 35°C since these complexes are very prone to decomposition at elevated temperature), an estimate of the exchange constant of 50–200 s^{-1} was obtained.

The exchange at the oxo site in the aqua oxo complex is a result of the proton exchange and consequent inversion processes shown in Scheme 3 and is controlled by the concentration of the dioxo species. At low concentrations of this dioxo species (i.e., well below pK_{a2} values for any of these metal centers) the oxygen exchange at the oxo site is a slow process and was successfully determined for both the W(IV) and Mo(IV) aqua oxo complexes at 2–10°C (*7*) by conventional isotopic exchange employing the fast-injection technique (*73*). It must be noted at this point that the oxygen exchange observed on the oxo sig-

nal basically gives the rate of inversion along the O–M–O axis (see Sections III,D and VI).

C. Mechanisms of Oxygen Exchange

The oxygen exchange processes on the aqua oxo and hydroxo oxo species of these complexes proceed by different intimate mechanisms as described below.

1. Aqua Oxo Complexes $[MO(OH_2)(CN)_4]^{n-}$ [(M = Mo(IV), W(IV), Re(V), and Tc(V)]

The aqua oxo complexes exchange by a dissociative activation mode. The evidence in support of this conclusion is given below.

In the Re(V) and W(IV) aqua oxo complexes, comparison of both the complex formation of the $[MO(OH_2)(CN)_4]^{n-}$ by NCS^- ions and the water exchange (k_{aq}) shows a relative increase in reactivity of approximately 3 orders of magnitude (Table II), which is in direct agreement with the previously (*1*, *2*, *50*) concluded dissociative mechanism. The increase in Lewis acidity of the Re(V) center compared to that of W(IV) is expected to result in a much less reactive system in a dissociative activated mode.

The ground-state distortion (Table I) from the normal octahedral geometry, i.e., the displacement of the central metal atom by up to 0.34 Å toward the oxo from the plane formed by the four cyano carbon atoms, is in further agreement with this reasoning, indicative of more reactive complex with an increased metal–oxygen bond length.

The activation entropies determined for both these systems are large and positive, which is in general agreement with a *d*-activation (see Table V). Furthermore, the determination of the volume of activation of $+10.6$ cm^3 mol^{-1} for the anation of the $[WO(OH_2)(CN)_4]^{2-}$ complex by N_3^- ions (*74*) provides strong evidence in favor of a dissociative mode of activation for the substitution reactions in the aqua oxo complexes.

2. *Hydroxo Oxo Complexes $[MO(OH)(CN)_4]^{(n+1)-}$ [M = Mo(IV), W(IV), Re(V), Tc(V), and Os(VI)]*

The evidence in favor of a process wherein associative activation is more likely for the oxygen exchange on the hydroxo oxo complexes is presented below.

Evaluation of the relative reactivity of the $[MO(OH)(CN)_4]^{(n+1)-}$ complexes for the Re(V) and W(IV) metal centers reveals that the oxygen exchange on the Re(V) hydroxo oxo complex, when compared to that of the W(IV), shows a fivefold *increase* in reaction rate compared to the 3-order-of-magnitude *decrease* for the corresponding aqua complexes (described above). Furthermore, the activation entropy values for k_{OH} in the case of both complexes (Table V) show a tendency toward negative values and might be interpreted as evidence in favor of a less dissociative or even of an associative type of mechanism being operative for the oxygen exchange in the hydroxo oxo complexes.

This reasoning is in line with the ground state properties that are available (Table I). For example, the distortion in the $[ReO(OH)(CN)_4]^{2-}$ and the $[MoO(OH)(CN)_4]^{3-}$ complexes as manifested in the displacement of the central metal atom toward the oxo from the plane formed by the four cyano carbon atoms is only *ca.* 0.08–0.19 Å compared to 0.30–0.34 Å for the aqua oxo complexes as mentioned above. The NC–M–OH bond angles are around 85–87°, whereas those of the $NC–M–OH_2$ are only *ca.* 80°. This decrease of the steric repulsion exerted by the cyano ligands in the hydroxo oxo complex implies less interaction with both the leaving and entering ligand in the probable region of attack. Furthermore, the M–OH bond in the $[MoO(OH)(CN)_4]^{3-}$ and $[ReO(OH)(CN)_4]^{2-}$ complexes are *ca.* 0.20–0.24 Å *shorter* than the corresponding $M–OH_2$ bonds in the aqua oxo complexes and are therefore obviously much stronger. This clearly suggests that the hydroxo ligand in these complexes will dissociate with more difficulty and suggests that association might even be favored.

The difference between the oxygen exchange rate in the aqua oxo complex compared to that of the hydroxo oxo (k_{aq} and k_{OH} in Table V) for the W(IV) center is *ca.* 5 orders of magnitude, but only 27 times in the case of the Re(V). This large relative increase in the reactivity of the W(IV) hydroxo complex is further evidence pointing to the importance of association in the oxygen exchange on the hydroxo complexes.

Upon comparison of the k_{OH} exchange rate of the Tc(V) system with that of the Re(V), the significant increase in reactivity (*ca.* 3 orders of magnitude) is very prominent and not necessarily indicative of an associative activation. It is, however, possible that the Tc(V) hydroxo complex might be very reactive via an associative pathway, since it is known that the Tc(V) center much more readily accepts electron density than does the corresponding Re(V) complexes (*55*). The greater ease by which coordination sphere expansion can occur in third-row d-series transition elements such as W(IV) and Re(V) (not very easily

accomplished in the second row, i.e., for Tc) furthermore favors an oxygen exchange process via a more associative pathway for the hydroxo oxo complexes.

If associative activation is assumed to apply for the hydroxo oxo complexes, it should also hold for the $[OsO(OH)(CN)_4]^-$ complex, which in turn implies that the k_{OH} for the Os(VI) should be larger than that of the Re(V). This furthermore implies that, using Eq. (25) and the limiting value obtained for the oxygen exchange (see above), the pK_{a2} value for the $[OsO(H_2O)(CN)_4]$ complex of significantly less than -1 can be estimated. This is also in general agreement with both the ^{13}C and ^{17}O chemical shift correlation for the W(IV), Re(V), and Os(VI) vs the pK_{a2} values (Table II).

Based on the above discussion it is concluded that the aqua oxo complexes undergo oxygen exchange via dissociative activation, whereas the hydroxo oxo complexes undergo oxygen exchange via an interchange or even an associative activation mode.

V. Cyanide Exchange Kinetics

In this paragraph the cyanide exchange on the complexes as described by Eqs. (1), (3b), (5b), and (7b) in Scheme 1 is discussed, where CN denotes the total free cyanide, i.e., HCN/CN^-. For the complex formation (Scheme 1, Eq. (2)) X represents different entering nucleophiles such as NCS^-, F^-, CN^-, and py.

A. Exchange Kinetics

The general rate law given in Eq. (27) describes cyanide exchange presented in Eqs. (1), (3b), (5b) and (7b) in Scheme 1

$$d[M^*CN]/dt = (k_{Xc}[MX] + k_{aqc}[MOH_2] + k_{OHc}[MOH] + k_{Oc}[MO_2])[CN]. \quad (27)$$

In Eq. (27), [MX], $[MOH_2]$, [MOH], and $[MO_2]$ represent the concentrations of the $[MO(X)(CN)_4]^{m-}$, $[MO(H_2O)(CN)_4]^{n-}$, $[MO(OH)(CN)_4]^{(n+1)-}$, and $[MO_2(CN)_4]^{(n+2)-}$ complexes, respectively. Zero-order kinetics with respect to $[CN^-]$ has been observed for cyanide and hydrogen cyanide exchange on $[ReO_2(CN)_4]^{3-}$ as well as for the cyanide exchange on $[TcO_2(CN)_4]^{3-}$ and $[WO(OH)(CN)_4]^{3-}$ and for hydrogen cyanide exchange on $[WO(OH_2)(CN)_4]^{2-}$(discussion below). This implies that the observed rate constant, k_{obs}, is independent of the free cyanide concentration.

Upon inclusion of the relative acid/base (K_{a1} and K_{a2}, reactions (4) and (6) in Scheme 1) and stability constants (K_x, reaction (2), Scheme 1), the expression for the pseudo-first-order rate constant, k_{obs} (where $(d[M^*CN]/[M]dt)] = 4\ k_{obs}$, [M] = total metal concentration), as given in Eq. (28), is obtained from Eq. (27)

$$k_{obs} = \frac{k_{CN}}{4} = \frac{k_{Xc}K_x[X][H^+]^2 + k_{aqc}[H^+]^2 + k_{OHc}K_{a1}[H^+] + k_{Oc}K_{a1}K_{a2}}{4(K_x[X][H^+]^2 + [H^+]^2 + K_{a1}[H^+] + K_{a1}K_{a2})}. \quad (28)$$

1. Cyanide Exchange on $[MO_2(CN)_4]^{(n+2)-}$ and $[MO(X)(CN)_4]^{m-}$ Complexes

As in the case of the oxygen exchange described above in Section IV (see also Fig. 16), well-behaved first-order kinetics were observed for all the cyanide exchange reactions for which the modified exponential form of the McKay equation (*8*) was used to determine the observed rate constants.

a. Tungsten(IV) The $[WO(X)(CN)_4]^{m-}$ complexes were investigated under conditions where these species were the main complexes in solution (Scheme 1), i.e., where $[H^+] > K_{a1}$ and $K_x[X] \gg 1$, with the exception being the pentacyano complex, which, since $K_x[X] \ggg 1$ and even though a pH was used where $[H^+] \approx K_{a1}$, $[WO(CN)_5]^{3-}$ was still by far the main complex in solution. Under these selected conditions, Eq. (28) simplifies to $k_{obs} = k_{Xc}/4$, which allows study of the exchange rates on the $[WO(X)(CN)_4]^{m-}$ complexes (Eq. (1) in Scheme 1). The rate constants for the cyanide exchange on the $[WO(X)(CN)_4]^{m-}$ complexes are given in Table VI.

Upon addition of the ^{13}C-labeled cyanide to the $[WO(OH_2)(CN)_4]^{2-}$ complex, there is a rapid trans substitution, ($k_X = 1\ M^{-1}\ s^{-1}$) (*50*), followed by the exchange at the equatorial cyano sites as shown in Eq. (29) (also see final spectrum in Fig. 7)

$$[WO(OH_2)(CN)_4]^{2-} \xrightarrow{k_X(+\ ^*CN)} [WO(^*CN)_{trans}(CN)_4]^{3-} \xrightarrow{k_{Xc}(+\ ^*CN)} N3$$
$$[WO(^*CN)_{trans}(^*CN)(CN)_3]^{3-}. \quad (29)$$

b. Molybdenum(IV) The cyanide exchange for the pentacyano complex of Mo(IV) showed similar behavior to that observed for the W(IV) described above, i.e., the fast formation of the $[MoO(^{13}CN)(CN)_4]^{3-}$ complex followed by the slower formation of the $[MoO(^{13}CN)_5]^{3-}$ moiety. The obtained results are reported in Table VI.

TABLE VI

EQUATORIAL CYANIDE EXCHANGE RATE CONSTANTS FOR THE *Trans*-$[MO(L)(CN)_4]^{n-}$ COMPLEXES; M = Mo(IV), W(IV), Tc(V), Re(V) AND Os(VI) AT DIFFERENT pH VALUES (GIVEN IN PARENTHESES); 298 K

Complex	k_{Oc} (s^{-1})	k_{OHc} (s^{-1})	k_{aqc} (s^{-1})	k_{Xc} (s^{-1})
$[MoO_2(CN)_4]^{4-}$	$>4 \times 10^{-1}$	$1.7(1) \times 10^{-2}$	$1.5(1) \times 10^{-2}$	—
	(14.5)[d]	(13)[d]	(4.5)[d]	—
$[MoO(CN)_5]^{3-}$	—	—	—	$9.6(8) \times 10^{-3}$
	—	—	—	(8.9)[c]
$[WO_2(CN)_4]^{4-}$	$4.4(4) \times 10^{-3}$	$9.6(9) \times 10^{-5}$	$1.1(1) \times 10^{-4}$	—
	(14.5)[d]	(11.8)[d]	(3.1)[d]	—
$[WO(CN)_5]^{3-}$	—	—	—	$1.1(1) \times 10^{-2}$
	—	—	—	>4[a]
	—	—	—	(8.8)[c]
$[WO(N_3)(CN)_4]^{3-}$	—	—	—	$3.1(2) \times 10^{-4}$
	—	—	—	(5.5)[d]
$[WO(F)(CN)_4]^{3-}$	—	—	—	$4.8(1) \times 10^{-5}$
	—	—	—	(5.2)[d]
$[TcO_2(CN)_4]^{3-}$	$4.8(4) \times 10^{-3}$	$4.00(14) \times 10^{-3}$	$<4 \times 10^{-5}$	—
	(10.6)[c]	(2.0)[c]	(*ca.* 1)[d]	—
$[TcO(NCS)(CN)_4]^{2-}$	—	—	—	$<4 \times 10^{-5}$
	—	—	—	(*ca.* 0.5)[d]
$[ReO_2(CN)_4]^{3-}$	$3.6(3) \times 10^{-6}$	$1.6(4) \times 10^{-6}$	$<4 \times 10^{-8}$	—
	(11)[d]	(2.5)[d]	(<1)[d]	—
$[OsO_2(CN)_4]^{2-}$	$<4 \times 10^{-9}$	—	—	—
	(13)[e]	—	—	—

[a] Substitution of cyanide *trans* to oxo.

[b] Equatorial cyanide exchange on the dinuclear complex ($[Re_2O_3(CN)_8]^{4-}$ (Fig. 3) or $[Tc_2O_3(CN)_8]^{4-}$).

[c] At 279 K.

[d] At 298 K.

[e] At 348 K.

c. Technetium(V) The cyanide exchange on the dioxotetracyanotechnetate(V) complex was studied by slow isotopic exchange upon introduction of $C^{15}N^-$ rather than $^{13}CN^-$ (see Section III). Two- to threefold variations in both the total cyanide as well as the [^{99}Tc] showed no significant change in the exchange rate in the dioxo species. The rate of exchange on the $[TcO(NCS)(CN)_4]^{2-}$ and $[TcO(H_2O)(CN)_4]^-$ complexes could only be estimated due to decomposition observed after 24 h (see Table VI).

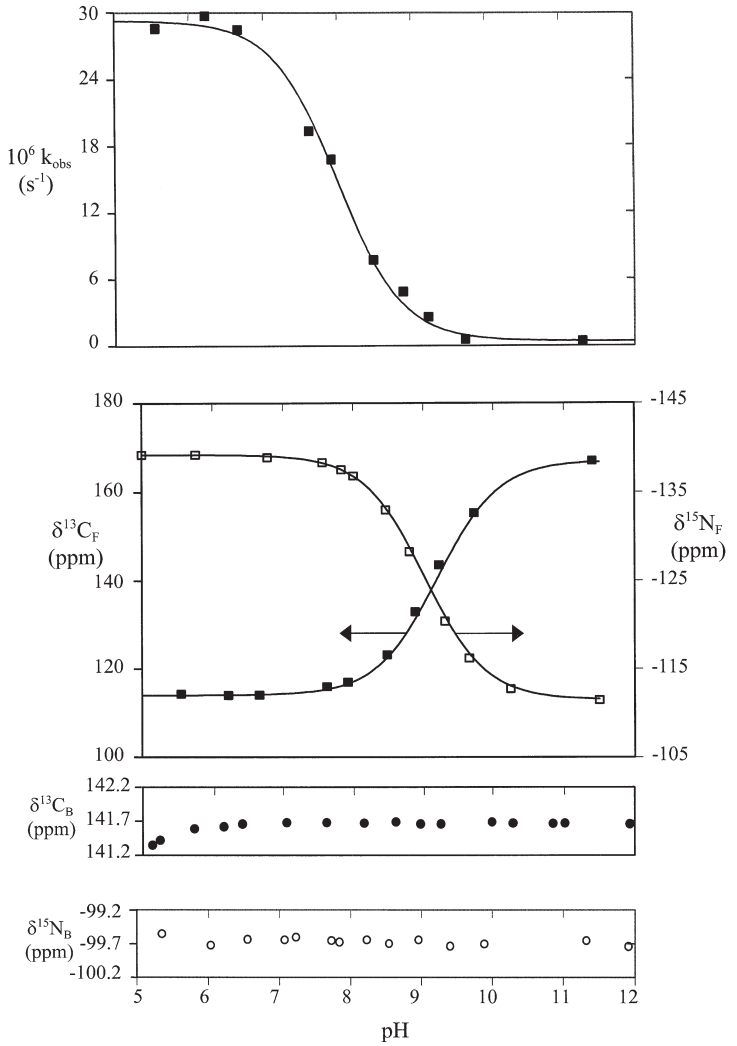

FIG. 18. The pH dependence of the cyanide exchange rate at 25°C on $[ReO_2(CN)_4]^{3-}$; δ $^{13}C_F$ and δ $^{15}N_F$ are the ^{13}C and ^{15}N chemical shifts of the free HCN/CN^- and δ $^{13}C_B$ and δ $^{15}N_B$ the chemical shifts of the bound CN^-. The total complex concentration [Re] = 0.2 *m*; the total cyanide concentration [CN] = 0.3 *m* and μ = 1.5–2.8 *m* KNO_3 (8). (Adapted with permission from Abou-Hamdan, A.; Roodt, A.; Merbach, A. E. *Inorg. Chem.* **1998,** *37,* 1278–1288. Copyright 1998 American Chemical Society.)

d. Rhenium(V) The Re(V) complexes were studied by slow isotopic exchange utilizing enriched $K^{13}CN$ and monitoring the signal growth vs time. The Brønsted acid/base properties of the tetracyano-aquaoxorhenate (V) complex (Table II) are well defined and allowed the study of the exchange between the dioxo complex and both cyanide and hydrogen cyanide, as illustrated in Fig. 18 (note a pK_a (HCN) = 9.2 determined from ^{13}C and ^{15}N free cyanide chemical shift pH dependence). The exchange reaction on $[ReO_2(CN)_4]^{3-}$, however, shows a pH dependence that does not correlate directly with the pK_a value of the HCN *or* with the protonation of either an oxo or cyano site on the complex (^{13}C-, ^{15}N-, and ^{17}O-bound chemical shifts as a function of pH in Fig. 18). Therefore, it could not be attributed to the protonation of either an oxo or cyano ligand or the pK_a value of HCN.

To accommodate this phenomenon (see discussion below), a new acid dependence (Scheme 5), possibly resulting from a protonation

$$[ReO_2(CN)_4]_A^{3-} \underset{(-\,*CN)}{\overset{k_{OcH}\,(+\,*CN)}{\rightleftharpoons}} [ReO_2(*CN)(CN)_3]_A^{3-} \qquad (30)$$

$$K_{a3}\ (-H^+) \Big\Updownarrow (+H^+) \qquad (31)$$

$$[ReO_2(CN)_4]^{3-} \underset{(-\,*CN)}{\overset{k_{Oc}\,(+\,*CN)}{\rightleftharpoons}} [ReO_2(*CN)(CN)_3]^{3-} \qquad (32)$$

SCHEME 5.

(*75*) of a cyano ligand in the $[ReO_2(CN)_4]^{3-}$ complex or an outer-sphere interaction of a cyano moiety, $[ReO_2(CN)_4]_A^{3-}$, was defined. The rate law given in Eq. (33) was then derived and upon fitting the data points (Fig. 18) yielded a k_{OcH} of $(1.2 \pm 0.4) \times 10^{-3}$ s^{-1} compared to a k_{Oc} of $(3.6 \pm 0.3) \times 10^{-6}$ s^{-1} (Table VI) and an acid dissociation constant pK_{a3} of 8.03 ± 0.07

$$d[M{*}CN]/([M]dt) = \frac{k_{OcH}[H^+] + k_{Oc}K_{a3}}{[H^+] + K_{a3}}. \qquad (33)$$

The exchange rate was independent of [CN] at pH 11 and of [HCN] at pH 6 for free ligand concentration between 0.3 and 1.6 *m*. The activation parameters determined from variable temperature studies at pH 11 and at pH 6 are $\Delta H^{\#}$: 139 ± 3 and 101 ± 1 kJ $mole^{-1}$; and $\Delta S^{\#}$: +104 ± 8 and +6 ± 3 J K^{-1} $mole^{-1}$, respectively.

e. Osmium(VI) It has previously been concluded that even in strong acid solution, the dioxotetracyanoosmate(VI) complex cannot

be protonated to form the oxo aqua complex or even the corresponding hydroxo oxo complex, and the pK_{a1} and pK_{a2} values have been estimated to be substantially less than -1 (Table II). Very slow cyanide exchange, similar to the oxygen exchange yielded at 347 K, a k_{CN} of $< 4 \times 10^{-6}$ s^{-1} at pH 13 and of $(1.2 \pm 0.1) \times 10^{-4}$ s^{-1} at pH 2.5.

B. Mechanisms of Cyanide Exchange

1. Dioxo Complexes

The cyanide exchange rate constants, k_{Oc} (Table VI, Eq. 7b, Scheme I), for the range of dioxotetracyanometalate complexes of Mo(IV), W(IV), Tc(V), Re(V), and Os(VI) show the following trend: M(IV) > M(V) > M(VI). This is in direct agreement with the acid/base behavior of these oxidation states as well as with the M–CN bond length of the corresponding oxidation states, as illustrated in Table II. The *ca.* 2–3 orders of magnitude difference observed for the cyanide exchange between the different oxidation states of the metal center is significant to note, i.e., around 10^{-1}–10^{-3} s^{-1} for the M(IV) complexes to *ca.* 10^{-3}–10^{-6} s^{-1} for the M(V) and $<10^{-9}$ s^{-1} for the M(VI). This observation is in direct agreement with a dissociative activation for the cyanide exchange on these dioxo complexes. (The same trend was observed upon comparison of the water exchange rate constants for the $[MO(OH_2)(CN)_4]^{n-}$ complexes, see Section IV.)

This conclusion of a dissociative activation mode for the cyanide exchange is further manifested by the results obtained for the Re(V) center whereby a fivefold variation in free cyanide concentration showed no effect on the exchange rate of the dioxo complex. This, together with the results obtained from a fourfold variation of cyanide concentration for the $[TcO_2(CN)_4]^{3-}$ complex (zero-order dependence on total cyanide concentration), further confirms the assignment of a D-mechanism for the cyanide exchange on these d^2 metal centers when containing two oxo ligands (classic 18-electron complexes). The positive value of the entropy of activation of $+104 \pm 8$ J K^{-1} $mole^{-1}$ determined in the case of the $[ReO_2(CN)_4]^{3-}$ complex is further evidence of a D-mechanism for the cyanide exchange in these complexes.

The significant reactivity difference for cyanide exchange on the Tc(V) and Re(V) of >4000 is in general agreement with that found in previous complex-formation and oxygen-exchange studies (*1*, *2*, *76*,

also see Table II). Since a D-mechanism is concluded for the equatorial exchange, we can imply that a dissociative activation also holds for strong π-ligands such as cyano complexes and isocyanide moieties, the latter being currently employed for heart imaging in ^{99m}Tc-sestamibi, i.e., $[^{99m}Tc(MIBI)_6]^+$ (MIBI = methoxyisobutylisocyanide) (*77*). On the other hand, the extreme slow exchange (half-life >20 h) for the equatorial cyano ligands observed, especially when the dioxo moiety is eliminated to yield only the mono oxo M=O core, indicates that for cerebral agents such as [^{99m}TcO(d,l-HMPAO)] (HMPAO = hexamethyl propylene amine oximate) (*77*), absorption in the brain might not be due to dissociation of the ligand but rather to outer-sphere ligand–biological host interactions or trans oxo addition/substitution of coordinated H_2O. Further aspects of radiopharmaceutical behavior are discussed in Section VII.

The significant variation in exchange rate observed for the Re(V) center as a function of pH around 8 (Fig. 18), which is presented in Scheme 5, cannot be explained unambiguously at this point in time. A similar situation existed in a study of the aquation of $[Cr(CN)_6]^{3-}$, wherein an intermediate of the form $[Cr(HCN)(CN)_5]^{2-}$ was postulated as a reactive species undergoing the hydrolysis process (*75*). Similar to this mentioned study, the increase in exchange rate observed for the $[ReO_2(CN)_4]^{3-}$ cannot be without doubt linked to the protonation of either an oxo or a cyano ligand, since protonation of the oxo site is well established (*1*, *2*). However, since no change in the ^{13}C chemical shift of the coordinated cyano ligands could be detected (see Fig. 18) protonation of a coordinated cyano ligand can in principle be excluded, provided that a chemical shift change can indeed be detected. Furthermore, the results obtained from the ^{15}N NMR measurements do not indicate a tendency of a chemical shift vs pH dependence around pH = 8, while ^{17}O NMR chemical shift measurements also did not reveal any pH dependence between pH 6 and 11. However, there does not necessarily have to be an observed change in the chemical shifts since in the case of the Mo(IV) center, although both the $[MoO(CN)_5]^{3-}$ and the $[MoO(HCN)(CN)_4]^{2-}$ species have been crystallographically (*22, 28*) and kinetically (*48, 50*) verified, no NMR evidence in terms of chemical shift differences in the ^{13}C spectra could be detected. It is also of interest to note a reduction of the pK_a of the bound HCN to 7.6 for this Mo(IV) complex. A similar effect, i.e., a decrease in the pK_a of the bound HCN, was observed in both $[WO(HCN)(CN)_4]^{2-}$ (*50*) and $[ReN(HCN)(CN)_4]^{2-}$ (*78*) complexes.

A further, more unlikely process occurring to account for this observed accelerated exchange can in principle be attributed to the for-

mation of an outer-sphere complex between the $[ReO_2(CN)_4]^{3-}$ and the neutral HCN. In the reactions of cyanide with Ni(II) complexes (*79–82*), HCN was postulated to be a reactant as well as CN^- but no spectral or kinetic evidence was observed. In the present study of the Re(V) complex, although no NMR evidence could be gathered to suggest this, the different activation parameters determined at pH 11 and 6 indicate different operating mechanistic pathways. However, it is worthwhile to note that, although the exchange of the HCN compared to the CN^- is not directly related to the pK_a value of HCN, the 30-fold increase in the exchange on the Re(V) center at pH = 6 compared to pH = 11 is indeed significant. A neutral entity like HCN will exhibit much better outer-sphere interaction with the trivalent $[ReO_2(CN)_4]^{3-}$ anionic complex than the negatively charged CN^- ion. It is also anticipated that the cyano ligands coordinated to the Re(V) center in the dioxo complex will be much more basic (weaker M–CN bonds, see Table I) than in the protonated oxo hydroxo or oxo aqua complexes, suggesting that this M—CN · · · H interaction might be unfavorable upon protonation of an oxo ligand.

2. Cyanide Exchange in Protonated and Substituted Complexes

The exchange on the protonated $[MO(H_2O)(CN)_4]^{n-}$ and $[MO(OH)(CN)_4]^{(n+1)-}$ as well as the monosubstituted $[MO(X)(CN)_4]^{m-}$ complexes compared to the dioxo complexes described above shows a similar cyanide exchange pattern [M(IV) > M(V)] in contrast to that described above (Table VI). However, the substantial variation of the X ligands (also resulting from protonation of one of the oxo sites), does not result in any significant change in exchange rate constants for a specific metal center (the exception is when X is an oxo ligand). There is, for example, only a sixfold variation in the exchange rate constants for the range of X ligands in the W(IV) complexes, suggesting that the cis activation of the equatorial cyano ligands only shows a significant effect when a second oxo ligand is generated on the metal center via deprotonation.

This "activation" of the cyano ligands upon formation of the dioxo core is further manifested upon comparison of the coupling constants/bond strengths of the $[MO_2(CN)_4]^{4-}$ and the $[MO(X)(CN)_4]^{m-}$ complexes in Table III for the W(IV) and Mo(IV). The trans dioxo core causes an elongation of the equatorial M–CN bonds, resulting in an increase in dissociating ability for the cyano ligands, which is in turn directly reflected in the *ca.* 2-order-of-magnitude increase in exchange for all the dioxo complexes compared to $[MO(X)(CN)_4]^{m-}$ complexes, with $X \neq O^{2-}$ (see Table VI).

The above, together with the fact that a fourfold variation of [CN^-] for the $[WO(OH)(CN)_4]^{3-}$ complex showed zero-order dependence on free cyanide concentration further points to a dissociative activation for the cyanide exchange process, also in the case of the mono oxo (classic 16-electron) $[MO(X)(CN)_4]^{m-}$ species.

C. Related Features

Of interest to note is that in previous studies, the kinetics of the substitution reactions with bidentate ligands as shown in Eqs. (34) and (35) have been reported, with Pic^- = pyridine-2-carboxylate (*83*) and phen = 1,10-phenanthroline (*84*)

$$[WO(OH_2)(CN)_4]^{2-} + Pic^- \xrightarrow{k_1} [WO(\eta^1\text{-Pic})(CN)_4]^{3-} \xrightarrow{k_2} [WO(\eta^2\text{-Pic})(CN)_3]^{2-} \quad (34)$$

$$[MoO(OH_2)(CN)_4]^{2-} + phen \xrightarrow{k_1} [MoO(\eta^1\text{-phen})(CN)_4]^{2-} \xrightarrow{k_2} [MoO(\eta^2\text{-phen})(CN)_3]^{-}. \quad (35)$$

The cyanide exchange study showed that rate constants for a range of $[WO(X)(CN)_4]^{m-}$ complexes are 10^{-4}–10^{-5} s^{-1}. In the bidentate reaction illustrated in Eq. (34), the ring closure (second step) was found to be 5×10^{-4} s^{-1} under normalized conditions (same ligand concentration as in the cyanide exchange study), which is exactly the same as the equatorial cyanide exchange rate. This confirms that the second step in Eq. (34) indeed represents the ring closure (i.e., substitution of a cyano ligand), which is *ca.* 3 orders of magnitude slower than the initial aqua substitution. The rate constant k_1 in Eq. (34) is comparable to the substitution rates obtained for monodentate ligands of *ca.* 1–10 s^{-1}, i.e., formation of the $[WO(X)(CN)_4]^{m-}$ complexes.

Similarly, the reaction rate obtained in the complex formation study on the Mo(IV) center (phen as entering bidentate ligand) illustrated in Eq. (35), i.e., 4×10^{-2} s^{-1}, for the ring closure process is in excellent agreement with the equatorial cyanide exchange rates of *ca.* 10^{-3} s^{-1} determined for the Mo(IV) center in the cyanide exchange study. This ring closure (and equatorial cyanide substitution) is again much slower than the aqua substitution of *ca.* 100 s^{-1} found for formation of the pentacyano complex of Mo(IV).

A further interesting observation from the cyanide exchange study relates to the fact that the exchange rate constants for the equatorial cyanide in the pentacyano complexes compared to the protonated spe-

cies are *ca.* 2–3 orders of magnitude faster for the W(IV) and (although less pronounced) for the Mo(IV) (only *ca.* 4 times faster) (see Table VI). This still cannot be explained at this point but it might be linked to an intramolecular rearrangement of the $^{13}CN^-$ (trans to the oxo) already coordinated to the metal center. Instead of the exchange process proceeding via complete dissociation and then recoordination, an intramolecular rearrangement is possible without the $^{13}CN^-$ leaving the primary coordination sphere. As mentioned above (Section II,B), the significant difference in chemical shift observed for the cis-CN in the pentacyano complexes relative to the other species might be an indication of different electron density distributions as a result of significant π-interactions by the five cyano ligands on the metal center, favoring this postulated intramolecular rearrangement. This rearrangement/isomerization however, has to be associated with a process involving the equatorial cyano bond reorganization/breaking/rearrangement as a rate-determining step and is not determined by the breaking of the trans M–CN bond, since the hydrolysis rate constants for the decomposition of the oxo pentacyano complex to the corresponding aqua oxo tetracyano moieties are 200 (*43*) and 8 (*50*) s^{-1} for the Mo(IV) and W(IV) respectively. This is *ca.* 2–3 orders of magnitude larger than the equatorial exchange observed in the current study and implies that the exchange process should have been much faster if the rate-determining step was directly related to the cleavage of the M–C bond in the trans O=M–CN moiety.

The data on the $[MO(X)(CN)_4]^{m-}$ complexes for Re(V) (X = OH^-, OH_2) and Tc(V) (X = OH_2, NCS^-), unfortunately limited, show that the Re(V) center is much less reactive (by about 3 orders of magnitude) than the corresponding Tc(V) complexes, thus confirming the general trends observed for the M(IV) metal centers.

The data discussed in this paragraph is further correlated in Section VI with the proton and the oxygen exchange rate constants.

VI. Comparison of the Rates of Inversion and Oxygen and Cyanide Exchange

The different exchange processes described in Sections III–V can be combined to illustrate the reactivity of the different sites in these oxo cyano complexes as a function of pH and the possible interdependence thereof. The three processes that are compared are the inversion along the O–M–O axis (illustrated in Fig. 15; related to proton exchange), the oxygen exchange, and the cyanide exchange.

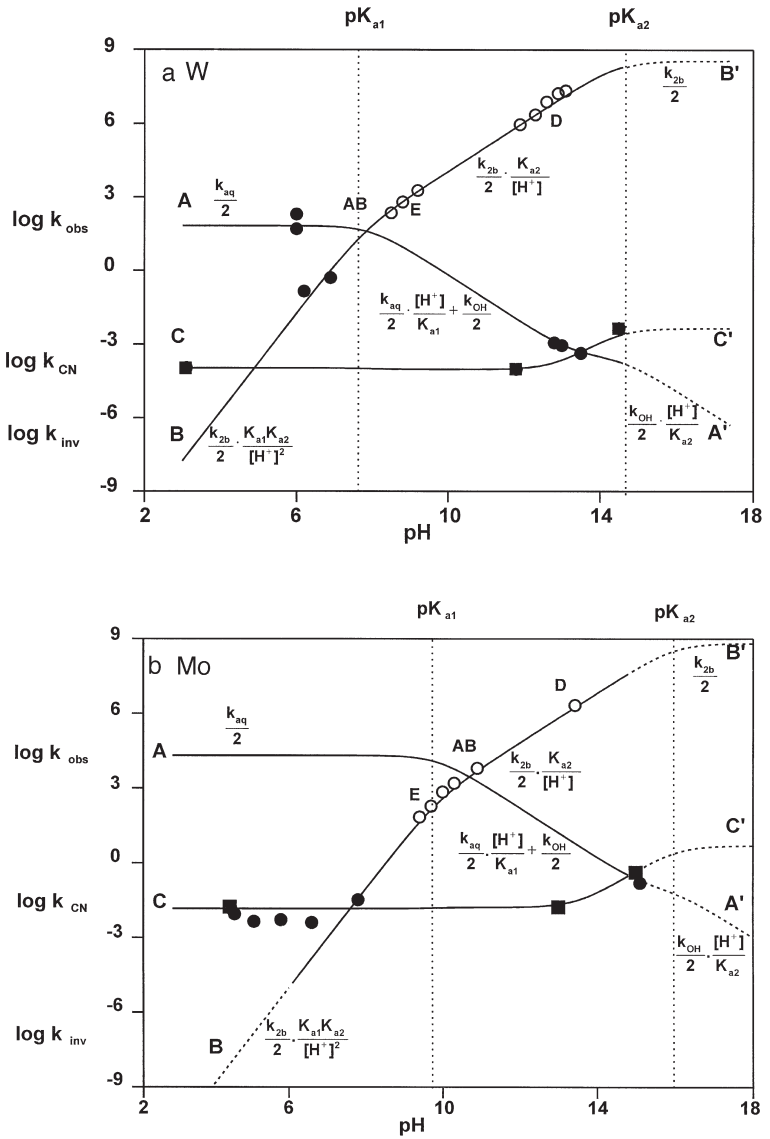

FIG. 19. Correlation between the rates of inversion of the metal center along the M=O axis and oxygen and cyanide exchange as a function of pH for (a) W(IV) and (b) Mo(IV) at 25°C. Line AA′, calculated from Eq. (22), gives the observed oxygen exchange rate. Line BB′, calculated from Eq. (18), gives the observed inversion rate. Line CC′, calculated from Eq. (28), gives the observed *cis*-cyanide exchange rate. Open and solid circles represent the ^{17}O line-broadening and isotopic exchange data points respectively whereas the solid squares represent the ^{13}C isotopic exchange data points (*8*). (Adapted with permission from Abou-Hamdan, A.; Roodt, A.; Merbach, A. E. *Inorg. Chem.* **1998,** *37,* 1278–1288. Copyright 1998 American Chemical Society.)

A. Reactivity vs pH Relationships

1. Inversion of the Metal Coordination Polyhedron along the O–M–O Axis

It was shown in Section III,D that the proton exchange processes, which can take place via two different pathways, induce oscillation of the metal center along the O–M–O axis. The inversion rate constants, k_{INV}, were calculated over a selected pH range using Eq. (18) [W(IV) and Mo(IV)] and Eq. (19) [Re(V) and Tc(V)], the appropriate proton exchange rate constants (Table IV), and the acid dissociation constants (Table II). The resulting values are presented by curves BB′ in Figs. 19 and 20 respectively (*6*).

2. Oxygen Exchange

It was shown in Section IV that oxygen exchange proceeds via acid-catalyzed pathways for all the metal centers, with the aqua oxo species being the most reactive. Furthermore, the oxygen exchange on the hydroxo oxo complexes were found to be a few orders of magnitude slower, while no exchange on the dioxo complex was detected other than that resulting from micro amounts of protonated species present. Consequently, Eq. (22) as discussed under Section IV, can be used to calculate the observed oxygen exchange over a selected pH range, using the rate constants as reported in Table V. The results are thus presented as lines AA′ in Fig. 19 for W(IV) and Mo(IV) and in Fig. 20 for Re(V) and Tc(V), respectively (*7*). In these figures, three different range-intervals, for which simplification with respect to Eq. (22) were possible (e.g., Eqs. (23)–(25)), are thus indicated.

3. Cyanide Exchange

The cyanide exchange (*8*) on the oxo cyano complexes of Mo(IV), W(IV), and Tc(V) is described by Eq. (28) and for Re(V) by additionally including Eq. (33), as discussed in Section V. The observed cyanide exchange rate constants as a function of pH were calculated using these equations and the rate constants listed in Table VI and are illustrated by lines CC′ in Fig. 19 for W(IV) and Mo(IV) and in Fig. 20 for Re(V) and Tc(V), respectively.

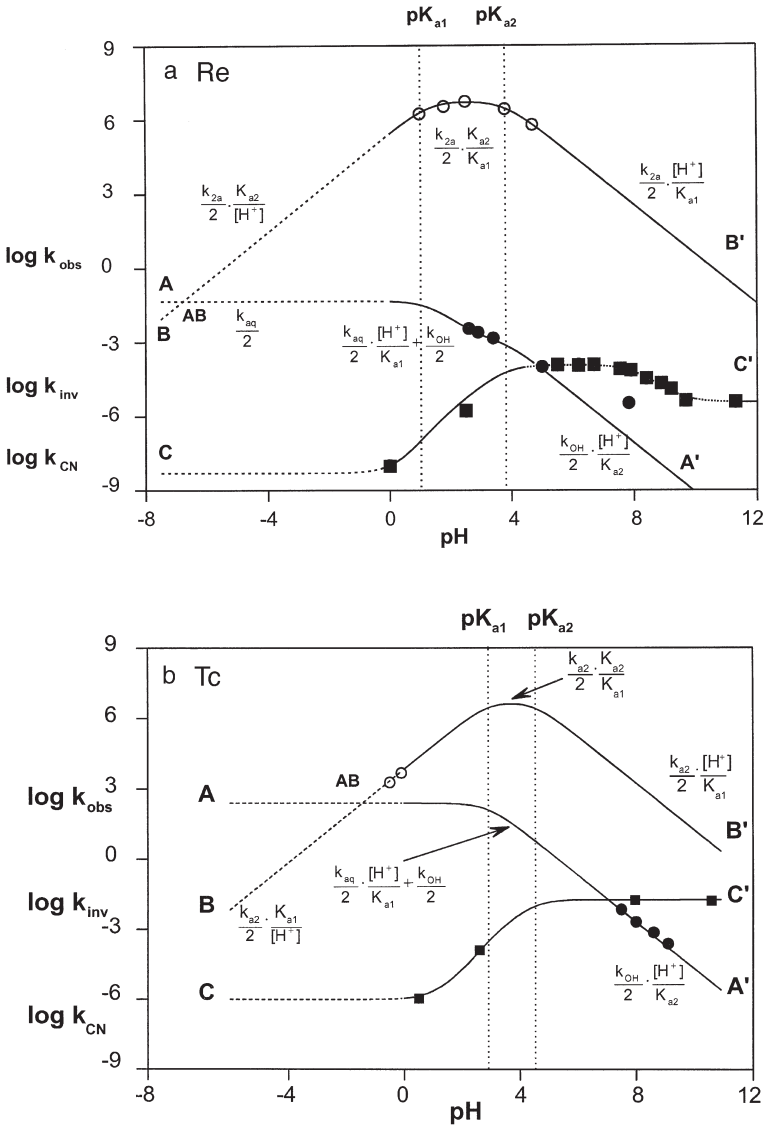

FIG. 20. Correlation between the rates of inversion of the metal center along M=O axis and oxygen and cyanide exchange as a function of pH for (a) Re(V) and (b) Tc(V) at 25°C. Line AA′, calculated from Eq. (22), gives the observed oxygen exchange rate. Line BB′, calculated from Eq. (19), gives the observed inversion rate. Line CC′, calculated from Eq. (28) for Tc(V) and from Eqs. (28) and (33) for Re(V), gives the observed *cis*-cyanide exchange rate. Open and solid circles represent the ^{17}O line-broadening and isotopic exchange data points respectively, whereas the solid squares represent the ^{15}N and ^{13}C isotopic exchange data points (*8*). (Adapted with permission from Abou-Hamdan, A.; Roodt, A.; Merbach, A. E. *Inorg. Chem.* **1998,** *37,* 1278–1288. Copyright 1998 American Chemical Society.)

B. Comparison of the Three Processes

The different processes in the four metal centers cover a 16-order-of-magnitude reactivity range and are shown in Figs. 19 and 20. Although these are beyond practical pH ranges they illustrate a wider interpretation of all the data and are just of theoretical interest, specifically at the extreme pH values.

1. Cyanide vs Oxygen Exchange / O–M–O Inversion

The cyanide exchange processes are in most cases the slowest. However, it is interesting to note that in the case of the Mo(IV) center, previously unexplained more-rapid-than-expected oxygen exchange at pH values lower than 6 (Fig. 19b) might be associated with the cyanide exchange (which was found to be of comparable rate). It is quite possible that the rapid decomposition observed for the aqua oxo complex of Mo(IV) at these pH values is due to hydrolysis stimulated by the relative rapid cyanide exchange at this acidity.

Another interesting observation stems from the slight deviation observed for the Re(V) system at pH >6 (7), as illustrated in Fig. 20a, for the oxygen exchange and the seemingly unexplained pH dependence for the CN^- exchange around pH 6–9. Around these pH values, the oxygen exchange and the cyanide exchange rates are quite similar. Therefore, it is reasonably assumed that the two exchange processes may be linked to similar intermediates.

2. Oxygen Exchange vs Inversion along the O–M–O Axis

Based on the discussion above, the question of a possible interdependence of oxygen and proton exchange (see Section III) reactions based on ^{17}O NMR observations can be raised.

a. Tungsten(IV) and Molybdenum(IV) The data points at D in Fig. 19a were calculated from the line-broadening of the coalesced signal as the system exits the fast-exchange regime with respect to proton exchange, while those at E were obtained from the line-broadening of the oxo signal in the $[WO(OH_2)(CN)_4]^{2-}$ complex. Below pH *ca.* 10 both the oxo and aqua/hydroxo signals were observed (Section III), indicative of the slow exchange with regard to the proton transfer.

The two functions for the inversion and the oxygen exchange intersect at AB in Fig 19a, leading to an interesting observation. From AB to A′ and AB to B′ it is clear that the exchange process in this domain is indicative of conventional isotopic exchange. However, once AB is reached, when moving to a lower pH, the oxygen exchange at the aqua ligand of the $[WO(OH_2)(CN)_4]^{2-}$ complex becomes *more rapid* than the proton exchange, while the *proton*-transfer process, which defines k_{INV} (Eq. (18)), can be determined from the oxo site. This was confirmed experimentally by an isotopic exchange study on the oxo site (*7*).

This reasoning also holds for the reactivity on the Mo(IV) center as illustrated in Fig. 19b and confirmed experimentally (*7*). A deviation of the experimental points for the inversion of the coordination polyhedron was obtained from the oxygen exchange on the oxo site in the $[MoO(OH_2)(CN)_4]^{2-}$ complex at pH <6 (Fig. 19b was observed and was interpreted in Section VI,B).

b. Rhenium(V) and Technetium(V) The difference in the inversion rates (line BB′) for the Re(V) and Tc(V) compared to the W(IV) and Mo(IV) stems from the fact that different mechanisms hold for the proton exchange in these systems (Eqs. (18) and (19)). It is clear from Fig. 20 that, as in the case of the W(IV) and Mo(IV) systems, points AB (theoretically at pH *ca.* -6 for the Re(V)) are reached where the increase in the observed exchange on the oxo site in the $[MO(OH_2)(CN)_4]^{-}$ complexes (M = Re(V) and Tc(V)) is determined by the proton transfer. In this case it is, however, only of theoretical relevance since such an acid concentration is not accessible.

C. Conclusions

In summary, it is clear from the above-discussed aspects that it was possible by multinuclear NMR (oxygen-17, nitrogen-15, carbon-13, and technetium-99) to successfully study the very slow cyanide exchange and the slow intermolecular oxygen exchange in these oxocyano complexes and correlate them both with the proton-transfer kinetics. Furthermore, the interdependence between the proton transfer and the actual dynamic inversion of the metal center was clearly demonstrated.

Of special significance is the fact that different kinetic aspects of these complexes were studied from the very slow exchange processes to the very fast proton transfer, spanning up to 16 orders of magnitude—indeed a wide range. An important result specifically concerns the oxygen exchange in the oxo complexes in general. It has to be underlined that observed oxygen exchange must be interpreted with care since there might be preceding protonation rate-determining steps governing the actual oxygen exchange.

To conclude, we have in this chapter combined previously studied subjects of these metal centers to construct corresponding relationships as illustrated Figs. 19 and 20. Using such a range of metal centers, reactivity and structural and general spectroscopic characteristics could be studied in even greater detail.

Some aspects related to the reactivity of the Tc(V) and Re(V) complexes, where the former is widely applied as an imaging nuclide in the radiopharmaceutical industry, are discussed below.

VII. *In Vitro* and *In Vivo* Reactivity of Technetium and Rhenium Complexes

In this section the *in vitro* reactivity of various octahedral complexes of technetium and rhenium are discussed and correlated with the *in vivo* pharmacokinetic data as observed for currently used radiopharmaceutical agents, which in most cases are indeed octahedral complexes of these metal centers.

A. Representative Literature Data

Representative literature data for *in vitro* and *in vivo* processes for a range of rhenium and technetium complexes are given in the Appendix in Section VII,C. Tables VII and VIII give the chemical rate constants for substitution and related reactions at 25°C as reported in the chemical literature as well as the calculated half-life (normalized to 1 *M* entering ligand concentration where applicable) at physiological temperature (37°C), using the corresponding activation parameters. Table IX lists representative reactivity (uptake (U), clearance (C), or airway permeability (AP)) of recent literature data as obtained from *in vivo* studies on a range of currently employed radiopharmaceuticals.

The data sets in Tables VII, VIII, and IX are divided into different categories in terms of reactivity of the two metal centers and pharmacokinetic behavior, while the data points included in Fig. 21 are chronologically indicated by the abbreviations shown below.

1. Ligand substitution in complexes of the type $[M^{V}O(L)(X)_4]^m$ (M = Re(V) and Tc(V)), wherein the equatorial ligand X (amine analogs, py, CN^-, etc.) cis to the oxo is substituted by other entering nucleophiles. The trans ligand L can be an oxo, protonated forms thereof, or other monodentate ligands and the complexes are denoted by ReOL(*X*)$_4$ and TcOL(*X*)$_4$ in Fig. 21, respectively.

2. Bridge-splitting and slow oxygen exchange in the $[Re_2O_3(CN)_8]^{4-}$ and $[MO(OH)(CN)_4]^{2-}$, denoted by ReO(*OY*)CN and TcO(*OY*)CN, respectively.

3. Substitution of the coordinated aqua trans to nitrosyl (NO) in complexes of the form *trans*-$[Re(NO)(H_2O)(CN)_4]^{2-}$, denoted by Re(NO)(*H$_2$O*)CN.

4. Oxygen exchange in $[MO(DADS)]^-$ and $[MO(DBDS)]^-$ complexes, denoted by Re*O*(DDS) and Tc*O*(DDS), respectively.

5. Substitution of the coordinated aqua ligand trans to the oxo in complexes of the form $[M^{V}O(H_2O)(CN)_4]^-$ (M = Re(V) and Tc(V), with CN^- ligands in the equatorial cis plane, denoted by ReO(*H$_2$O*)CN and TcO(*H$_2$O*)CN, respectively.

6. Substitution of the coordinated aqua ligand trans to the oxo in complexes of the form $[Re^{V}O(H_2O)(SR)_4]^{3+}$ with sulfur donor ligands (mainly thiourea type) in the equatorial cis plane, denoted by ReO(*H$_2$O*)SR.

7. The racemization of the oxo penicilinato complexes, $[MO(D/L\text{-}pen)_2]^-$, denoted by ReO-*Rac* and TcO-*Rac*, respectively.

8. The quite reactive Re(III) heptacoordinated complex, $[Re(terpy)_2(H_2O)]^{3+}$, denoted by Re(*H$_2$O*)TER, is also included.

9. Substitution of the coordinated aqua trans to the nitrido (N^{3-}) ligand in complexes of the form $[ReN(H_2O)(CN)_4]^{2-}$ with CN^- ligands in the equatorial cis plane, denoted by ReN(*H$_2$O*)CN.

10. Inversion of the metal center along the O–M–O axis in complexes of the form $[M^{V}O(OH)(CN)_4]^{2-}$ (M = Re(V) and Tc(V)) with CN^- ligands in the equatorial cis plane, indicated by ReO-*INV* and TcO-*INV*, respectively.

11. *In vivo* reactions of current radiopharmaceuticals which are denoted by Tc-*IN VIVO* and Re-*IN VIVO*, respectively.

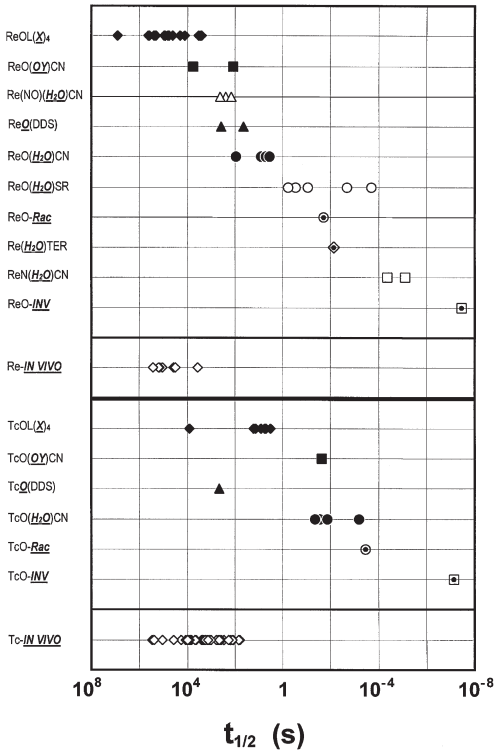

FIG. 21. Comparison of half-lives. [Data from Table VII (equatorial ligand substitution, Table VIII (aqua substitution and related reactions) and Table IX (*in vivo* reactions of technetium and rhenium radiopharmaceuticals) of the complexes described in Section VII,A. Similar symbols denote similar technetium and rhenium complexes.]

B. COMPARISON OF *IN VITRO* AND *IN VIVO* REACTIVITY

By considering the data illustrated in Fig. 21, several interesting comparisons can be made. The *in vitro* reactions for the rhenium complexes range from half-lives as long as 3–4 months for the cyanide exchange in the $[Re^{V}O(H_2O)(CN)_4]^-$ complexes to microseconds for the aqua substitution in the $[Re^{V}N(H_2O)(CN)_4]^{2-}$ complex and even the nanosecond range (inversion rate of the metal center along the O–M–O axis), i.e., ReOL($\underline{X}$)$_4$ (X = CN) vs ReN($\underline{H_2O}$)CN vs ReO-$\underline{INV}$.

On the other hand, the half-lives for the *in vitro* reactions for the technetium complexes range from around 3 h for the cyanide ex-

change in the $[Tc^{V}O(H_2O)(CN)_4]^-$ complex, to a few milliseconds for the aqua substitution therein, and again to the nanosecond range (inversion rate of the metal center along the O–M–O axis ($TcOL(\underline{X})_4$ (X = CN) vs TcO($\underline{H_2O}$)CN vs TcO-*INV*).

Furthermore, it is clear that upon substitution of cyanide in the equatorial plane by thiourea as sulfur donor ligands (i.e., $[M^{V}O(H_2O)(CN)_4]^-$ vs $[Re^{V}O(H_2O)(SR)_4]^{3+}$), the rate of aqua substitution trans to the oxo is increased by 2–4 orders of magnitude (ReO($\underline{H_2O}$)CN vs ReO($\underline{H_2O}$)SR in Fig. 21). The introduction of sulfur donor ligands cis to the oxo, however, does not have the dramatic effect that a nitrido (vs an oxo) trans to the aqua ligand (as in $[ReN(H_2O)(CN)_4]^{2-}$) has, i.e., which results in a *ca.* 6-order-of-magnitude increase in reactivity (ReO($\underline{H_2O}$)CN vs ReN($\underline{H_2O}$)CN).

Comparison of the Re(V) and Tc(V) metal centers for most reactions indicate that the Tc(V) is in general *ca.* 3–4 orders of magnitude more reactive [$ReOL(\underline{X})_4$ (X = CN) and ReO($\underline{H_2O}$)CN) vs ($TcOL(\underline{X})_4$ (X = CN) and TcO($\underline{H_2O}$)CN)].

Turning to the *in vivo* reactivities of the technetium and rhenium radiopharmaceuticals, it seems that for the phosphonate complexes, used for bone imaging and bone cancer therapy respectively (i.e., $[^{99m}TcO(OH)(HEDP)_2]^{n-}$ vs the $[^{186}ReO(OH)(HEDP)_2]^{n-}$), the technetium complex clears *slower* from the bone than does the Re-analog. This is surprising considering the relative reactivities of Tc(V) vs Re(V) in general as summarized above. However, there is one example where the Tc(V) complex also reacts 1 order of magnitude slower than the corresponding Re(V) analog, i.e., the oxygen exchange on the $[MO(DBDS)]^-$ complexes (see Table VIII), which was interpreted in terms of an associative mechanism (*66*).

A further interesting point comes from the comparison of the *in vivo* data with the other ligand substitution results in general. The *in vivo* half-lives listed are comparable with the rate data of the equatorial substitution and might suggest that the mechanisms responsible for the uptake/clearance of the radiopharmaceuticals, be they protein, peptide, or DNA interactions or innersphere redox reactions, might indeed be associated therewith. This is, however, just an observation and surely requires much more research to be well understood.

C. Appendix: Tables of *in Vitro* and *in Vivo* Rate Data

TABLE VII

Kinetic Data for Equatorial Ligand Substitution in Oxo Cyano and Related Complexes of Re(V) and Tc(V)

Complex			Re(V)[b]			Tc(V)[b]		
Code[a]	Type	Entering ligand	Rate constant (M^{-1} s^{-1}; 25°C)	$t_{1/2}$ (37°C)[c]	Ref.	Rate constant (M^{-1} s^{-1}; 25°C)	$t_{1/2}$ (37°C)[c]	Ref.
	$[MO(OH)(en)_2]^{2+}$	tu	$1.16(2) \times 10^{-4}$	45 min	*15*	0.098(1)	3.2 s	*15*
	$[MO(OH)(en)_2]^{2+}$	mtu	$9.7(1) \times 10^{-5}$	54 min	*41*	—	—	—
	$[MO(OH)(en)_2]^{2+}$	dmtu	$1.32(5) \times 10^{-4}$	40 min	*41*	—	—	—
	$[MO(OH)(eten)_2]^{2+}$	dmtu	$4.78(3) \times 10^{-6}$	18 h	*15*	—	—	—
	$[MO(OH)(deten)_2]^{2+}$	dmtu	$<1.6 \times 10^{-6}$	>2.3 d	*15*	—	—	—
	$[MO(OH)(HEDP)_2]^{n-}$	dmtu	$<4 \times 10^{-6}$	>22 h	*15*	—	—	—
$MOL(\underline{X})_4$	$[MO_2(en)_2]^{+}$	Cl^-	$<1.27 \times 10^{-6}$	>2.9 d	*85*	—	—	—
	$[MO(OH)(en)_2]^{2+}$	Cl^-	1.57×10^{-5}[d]	5.6 h	*85*	—	—	—
	$[MO(OH)(en)Cl_2]$	Cl^-	7.42×10^{-7}[d]	4.9 d	*85*	—	—	—
	$[MO(OH)(py)_4]^{2+}$	dmtu	$<8.0 \times 10^{-6}$	>10.9 h	*42*	—	—	—
	$[MO_2(py)_4]^{+}$	py	$5.5(1) \times 10^{-6}$	15.9 h	*54*	0.04(2)	7.9 s	*54*
	$[MO_2(py)_4]^{+}$	apy	—	—	—	0.065(1)	4.9 s	*86*
	$[MO_2(en)_2]^{+}$	en	8.5×10^{-7}[d]	4.3 d	*87*	—	—	—
	$[MO_2(py)_4]^{+}$	dimap	—	—	—	0.060(4)	5.3 s	*86*
	$[MO_2(en)_2]^{+}$	en	2.6×10^{-5}[d]	3.4 h	*87*	—	—	—
	$[MO_2(CN)_4]^{3-}$	CN^-	$3.6(3) \times 10^{-6}$	24.3 h	*8*	0.023(2)	13.6 s	*8*
	$[MO(OH)(CN)_4]^{2-}$	CN^-	$1.6(4) \times 10^{-6}$	2.3 d	*8*	0.019(5)	16.3 s	*8*
	$[MO(NCS)(CN)_4]^{2-}$	CN^-	—	—	—	$<4 \times 10^{-5}$	>2.2 h	*8*
	$[MO(OH_2)(CN)_4]^{-}$	CN^-	$<4 \times 10^{-8}$	>91.2 d	*8*	$<4 \times 10^{-5}$	>2.2 h	*8*

[a] See Fig. 21.
[b] Selected rate constants (e.g., cyanide exchange) are first-order rate constants, see original Refs.
[c] Normalised to entering ligand concentrations of unity where applicable.
[d] No esd's reported.

TABLE VIII

Kinetic Data for Aqua Substitution and Oxygen Exchange in Oxo Cyano and Related Complexes of Re(V) and Tc(V)

Complex		Entering ligand	Re(V)[b]			Tc(V)[b]		
Code[a]	Type		Rate constant (M^{-1} s^{-1}; 25°C)	$t_{1/2}$ (37°C)[c]	Ref.	Rate constant (M^{-1} s^{-1}; 25°C)	$t_{1/2}$ (37°C)[c]	Ref.
MO(*OY*)CN	$[M_2O_3(CN)_8]^{4-}$ [d]	CN^-	$1.3(8) \times 10^{-4}$	90 min	*88*	—	—	—
	$[MO(OH)(CN)_4]^{2-}$	(e)	0.0026(3)	121 s	*7*	13(1)	24 ms	*7*
M(NO)(*H*$_2$*O*)CN	$[M(NO)(H_2O)(CN)_4]^{2-}$ [f]	NCS^-	$7.1(2) \times 10^{-4}$	4 min	*40*	—	—	—
	$[M(NO)(H_2O)(CN)_4]^{2-}$ [f]	N_3^-	$1.1(6) \times 10^{-3}$	2.3 min	*40*	—	—	—
	$[M(NO)(H_2O)(CN)_4]^{2-}$ [f]	tu	$8(2) \times 10^{-4}$	7 min	*40*	—	—	—
M*O*(DDS)	$[MO(DBDS)]^-$	(e)	$7.5(1) \times 10^{-3}$	42 s	*66*	$7(1) \times 10^{-4}$	7.2 min	*66*
	$[MO(DADS)]^-$	(e)	$1.6(1) \times 10^{-5}$	6 min	*66*	—	—	—
MO(*H*$_2$*O*)CN	$[MO(OH_2)(CN)_4]^-$	dmtu	0.059(2)	5.3 s	*89*	11.5(1)	27 ms	*15*
	$[MO(OH_2)(CN)_4]^-$	mtu	0.067(2)	4.7 s	*89*	11.4(1)	28 ms	*15*
	$[MO(OH_2)(CN)_4]^-$	tu	0.0399(9)	7.9 s	*89*	7.4(1)	43 ms	*15*
	$[MO(OH_2)(CN)_4]^-$	NCS^-	0.00348(4)	90 s	*48*	22.2(3)	14 ms	*13*
	$[MO(OH_2)(CN)_4]^-$	HN_3	0.064(2)	4.9 s	*89*	—	—	—
	$[MO(OH_2)(CN)_4]^-$	(e)	0.091(1)	3.5 s	*7*	500	630 μs	*7*
MO(*H*$_2$*O*)SR	$[MO(OH_2)(tu)_4]^{3+}$	NCS^-	$1.6(4) \times 10^3$	197 μs	*15*	—	—	—
	$[MO(OH_2)(tu)_4]^{3+}$	HN_3	1.1(1)	286 ms	*15*	—	—	—
	$[MO(OH_2)(tu)_4]^{3+}$	HCN	0.56(4)	563 ms	*41*	—	—	—
	$[MO(OH_2)(tu)_4]^{3+}$	SNO^-	153(4)	2.1 ms	*41*	—	—	—
	$[MO(OH_2)(dmtu)_4]^{3+}$	dmtu	3.4(2)	91 ms	*15*	—	—	—
MO-*Rac*	$[MO(D/L\text{-}pen)_2]^-$	(g)	16.5(4)	19 ms	*90*	940(40)	349 μs	*90*
M(*H*$_2$*O*)TER	$[M(OH_2)(terpy)_2]^{3+}$	NCS^-	45(4)	7 ms	*91*	—	—	—
MN(*H*$_2$*O*)CN	$[MN(OH_2)(CN)_4]^{2-}$	HCN	$3.9(7) \times 10^4$	8 μs	*78*	—	—	—
	$[MN(OH_2)(CN)_4]^{2-}$	CN^-	$7.2(4) \times 10^3$	43 μs	*78*	—	—	—
MO-*INV*	$[MO(OH)(CN)_4]^{2-}$	Inversion	$<2 \times 10^7$	>35 ns	(h)	$<10^7$	>70 ns	(h)

[a] See Fig. 21.
[b] Normalized to entering ligand concentrations of unity where applicable.
[c] Selected rate constants (e.g., cyanide exchange, are first-order rate constants, see original Refs.).
[d] Bridge splitting.
[e] Oxygen exchange.
[f] Uncertainty in I+/III+ oxidation state of rhenium atom.
[g] Racemization.
[h] Section VI, Fig. 20.

TABLE IX

Half-Lives (37°C) of *IN VIVO* Reactions for Different Technetium and Rhenium Radiopharmaceuticals

Chemical formula	Commercial/general name	Organ: disease	Reaction[a]	$t_{1/2}$	Ref.
$[^{99m}TcO(DTPA)]^+$ [b]	^{99m}Tc-DTPA	Lungs: *bronc. mucosa*	C	1.2 h	*92*
		Lungs: normal	AP	5 h	*93*
		Lungs: asthmatics	AP	2 h	*93*
		Lungs[c]	C	40 min	*94*
		Blood	C	3.3 h	*95*
$[^{99m}TcO(HMPAO)]$-B[d]	Ceretec labeled WBC	Lungs	C	8 min	*96*
$[^{99m}TcO(MAG_3)]^-$ [e]	^{99m}Tc-MAG_3; Technescan	Kidney: normal	C	≤10 min	*97*
$[^{99m}Tc\{(ac)_2en\}P_2]^+$ [f]	—	Blood	C	5 min	*98*
$[^{99m}Tc(MIBI)_6]^+$ [g]	^{99m}Tc-MIBI	Tumor cells[h]	U	41 min	*99*
	Sestamibi	Tumor cells[h]	C	23 min	*99*
	Cardiolite	Heart/myocardium	U	6 min	*100*
		Blood	C	2.13 min	*101*
		Thyroid	U	2.5 min	*102*

TABLE IX (*Continued*)

Chemical formula	Commercial/general name	Organ: disease	Reaction[a]	$t_{1/2}$	Ref.
$[^{99m}TcO_2(tetfos)_2]^{+}$[j]	^{99m}Tc-Tetrofosmin	Heart/myocardium	C	2 min	*100*
	Myoview	Tumor cells[h]	U	37 min	*99*
		Tumor cells[h]	C	36 min	*99*
$^{201}Tl^{+}$	^{201}Tl/Thallous	Tumor cells[h]	U	18 min	*99*
	Chloride/Tl 201	Thyroid	U	2.5 min	*102*
		Tumor cells[h]	C	36 min	*102*
$[^{96}TcO(OH)(HEDP)_2]^{n-}$	^{96}Tc-(Sn)-HEDP[k]	Normal bone[l]	C	>80 h	*103*
$[^{99m}TcO(Ab\text{-}1)]$[m]	^{99m}Tc-LL1	Blood (1st step)	C	24 min	*104*
		(2nd step)	C	30 h	*104*
		Whole-body	C	66 h	*104*
$[^{99m}TcO(Ab\text{-}2)]$[o]	^{99m}Tc-MT-B72.3	Blood[e]	C	10.4 h	*105*
$[^{99m}TcCl(tcdmb)]$[q]	^{99m}Tc-Teboroxime/	Heart/myocardium	C	<1 min	*100*
	Cardiotec				
$[^{99m}TcO(Ab\text{-}3)]$[r]	^{99m}Tc 7E11C5.3-CYT-395	Plasma (2nd step)	C	31 h	*106*
$[^{99m}TcO_2]$	^{99m}Tc-sulfur colloid	Spleen: normal	U	29 min	*107*
		Spleen: hypersplenic	U	7.7 min	*107*
		Spleen: hyposplenic	U	1.9 h	*107*
$[^{99m}TcO(DTPA)]^{+}$-G[s]	^{99m}Tc-GSA	Liver: endocytosis	U	1.1 min	*108*
		Liver: exocytosis	C	17 min	*108*
		Liver: cytoplasma	U	23 min	*108*
$[^{99m}TcO(NPAO)]$[t]	^{99m}Tc-Nitroimidazole/	Heart/myocardium[u]			
	BMS-181321	1st step (Nonischemic)	C	2.1 min	*109*
		1st step (Ischemic)	C	3 min	*109*
		2nd step (Nonischemic)	C	77 min	*109*
		2nd step (Ischemic)	C	137 min	*109*
$[^{99m}TcO(Ab\text{-}4)]$[v]	^{99m}Tc-OVAREX	Serum	U	2.6 h	*110*
		Serum	C	31.3 h	*110*
$[^{186}ReO(OH)(HEDP)_2]^{n-}$	^{186}Re-(Sn)-HEDP[k]	Whole blood	C	40 h	*111*
		Plasma	C	41 h	*111*
		Plasma water	C	30 h	*111*
		Normal bone[l]	C	>40 h	*103*
		Soft tissue[w]	C	10 h	*112*
		Bone[w]	U[x]	1 h	*112*
		Bone[w]	C[x]	>45 h	*112*
$[^{188}ReO(Ab\text{-}5)]$[y]	^{188}Re-MN-14	Blood (1st step)	C	8.2 h	*113*
		Whole body	C	73.8 h	*113*
$[^{186}Re(DMPE)_2Cl_2]^{+}$[z]		Blood	C	1 min	*114*

[a] *In vivo* reaction; U, Uptake; C, Clearance; AP, Airway Permeability.

[b] DTPA = diethylenetriamine pentaacetate.

[c] Dogs.

[d] HMPAO = hexamethyl propylene amine oximate; −B = white blood cells (WBC).

[e] MAG_3 = mercaptoacetylglyclyglycylglycinate.

[f] $(ac)_2$en = *N*,*N*′-ethylenebis(acetylacetone iminate); P = trimethylphosphine.

[g] MIBI = (hexakis-2-methoxy-1,2-methylpropyl) isonitrile.

[h] RPMI-1640 cell line.

[i] Estimated from total washout time.

[j] Tetfos = 1,2-bis[bis(2-ethoxyethyl)phosphino] ethane.

[k] HEDP = hydroxyethylenediphosphonate (*115*, *116*).

[l] Rats.

[m] Ab-1 = LL1 antibody.

[o] Ab-2 = metallothionein (MT) −B72.3 antibody.

[p] CD1 mice.

[q] tcdmb = tri(cyclohexanedionedioxime)methylborate (*117*).

[r] Ab-3 = 7E11C5.3-CYT-395.

[s] −G = Galactosyl Human Serum Albumin.

[t] PAO-N = 1-(2-Nitroimidazole)propylene amine oxime.

[u] Swine.

[v] Ab-4 = B43.13 antibody.

[w] Chacma Baboons.

[x] Based on 30% of total uptake of agent on bone.

[y] Ab-5 = Anti-arcinoembryonic antigen antibody.

[z] DMPE = Dimethylphosphino ethane.

References

1. Leipoldt, J. G.; Basson, S. S.; Roodt, A. In "Advances in Inorganic Chemistry"; Sykes, A. G., Ed.; Academic Press; San Diego, 1993; Vol. 40; pp. 241–322.
2. Leipoldt, J. G.; Basson, S. S.; Roodt, A.; Purcell, W. *Polyhedr. Rep.* **1992,** *11,* 2277–2284.
3. Klemperer, W. G. *Angew. Chem. Int. Ed. Engl.* **1978,** *17,* 246–254.
4. Richens, D.; Helm, L.; Pittet, P.-A.; Merbach, A. E. *Inorg. Chim. Acta* **1987,** *132,* 85–89.
5. Roodt, A.; Leipoldt, J. G.; Helm, L.; Merbach, A. E. *Inorg. Chem.* **1992,** *31,* 2864–2868.
6. Roodt, A.; Leipoldt, J. G.; Helm, L.; Merbach, A. E. *Inorg. Chem.* **1994,** *33,* 140–147.
7. Roodt, A.; Leipoldt, J. G.; Helm, L.; Abou-Hamdan, A.; Merbach, A. E. *Inorg. Chem.* **1995,** *34,* 560–568.
8. Abou-Hamdan, A.; Roodt, A.; Merbach, A. E. *Inorg. Chem.* **1998,** *37,* 1278–1288.
9. Marmion, M.; Deutsch, E. A. *J. Nucl. Biol. Med.* **1996,** *40,* 121–131.
10. Maxon, H. R.; Deutsch, E. A.; Thomas, S. R.; Libson, K. F.; Lukes, S. J.; Williams, C. C.; Ali, S. *Radiology* **1988,** *166,* 501–507.
11. Deutsch, E. A.; Libson, K. F.; Vanderheyden, J. L. In "Technetium and Rhenium in Chemistry and Nuclear Medicine"; Nicolini, M.; Bandoli, G.; Mazzi, U., Eds.; Cortina International: Verona, 1993; Vol. 3; pp. 13–22.
12. Kemp, G.; Van Aswegen, A.; Roodt, A.; Marais, J.; Jansen, S. E.; Goedhals, L.; Otto, A. C.; Louw, W. In "Modern Trends in Radiopharmaceuticals for Diagnosis and Therapy"; International Atomic Energy Agency: Vienna, 1998; TecDoc-1029; pp. 626–633.
13. Roodt, A.; Leipoldt, J. G.; Deutsch, E. A.; Sullivan, J. C. *Inorg. Chem.* **1992,** *31,* 1080–1085.
14. Libson, K. F.; Helm, L.; Roodt, A.; Cutler, C.; Merbach, A. E.; Sullivan, J. C.; Deutsch, E. A. In "Technetium and Rhenium in Chemistry and Nuclear Medicine"; Nicolini, M.; Bandoli, G.; Mazzi, U., Eds.; Cortina International: Verona, 1993; Vol. 3; pp. 31–33.
15. Roodt, A.; Engelbrecht, H. P.; Botha, J. M.; Otto, S. In "Technetium, Rhenium and Other Metals in Chemistry and Nuclear Medicine"; Nicolini, M.; Mazzi, U., Eds.; Cortina International: Verona, 1999; Vol. 5; pp. 161–166.
16. Murmann, R. K.; Schlemper, E. O. *Inorg. Chem.* **1971,** *10,* 2352–2354.
17. Purcell, W.; Roodt, A.; Basson, S. S.; Leipoldt, J. G. *Transition Met. Chem.* **1989,** *14,* 5–6.
18. Purcell, W.; Roodt, A.; Basson, S. S.; Leipoldt, J. G. *Transition Met. Chem.* **1990,** *15,* 239–241.
19. Robinson, P. R.; Schlemper, E. O.; Murmann, R. K. *Inorg. Chem.* **1975,** *14,* 2035–2041.
20. Basson, S. S.; Leipoldt, J. G.; Roodt, A.; Purcell, W. *Transition Met. Chem.* **1987,** *12,* 82–84.
21. Smit, J. P.; Ph. D. thesis, University of the Free State, Bloemfontein, South Africa, 1995.
22. Smit, J. P.; Purcell, W.; Roodt, A.; Leipoldt, J. G. *J. Chem. Soc. Chem. Commun.* **1993,** *18,* 1388–1389.
23. Smit, J. P.; Roodt, A.; Purcell, W. *S. Afr. J. Chem.* Unpublished results.
24. Day, V. W.; Hoard, J. L. *J. Am. Chem. Soc.* **1968,** *90,* 3374–3379.

25. Engelbrecht, H. P.; Roodt, A. Unpublished results.
26. Purcell, W.; Roodt, A.; Basson, S. S.; Leipoldt, J. G. *Transition Met. Chem.* **1991,** *16,* 60–61.
27. Basson, S. S.; Leipoldt, J. G.; Potgieter, I. M.; Roodt, A. *Inorg. Chim. Acta* **1985,** *103,* 121–125.
28. Wieghardt, K.; Backes-Dahmann, G.; Holzbach, W. J.; Swiridoff, W. J.; Weiss, J. *Z. Anorg. Allg. Chem.* **1983,** *499,* 44–58.
29. Arzoumanian, H.; Bouraoui, A.; Lazzeri, V.; Rajzmann, M.; Teruel, H.; Krentzien, H. *New J. Chem.* **1992,** *16,* 965–972.
30. Arzoumanian, H.; Pierrot, M.; Ridouane, F.; Sanchez, J. *Transition Met. Chem.* **1991,** *16,* 422–426.
31. Leipoldt, J. G.; Basson, S. S.; Roodt, A.; Potgieter, I. M. *S. Afr. J. Chem.* **1986,** *39,* 179–183.
32. Roodt, A.; Ph. D. thesis, University of the Free State, Bloemfontein, South Africa, 1987.
33. Roodt, A.; Leipoldt, J. G.; Basson, S. S.; Potgieter, I. M. *Transition Met. Chem.* **1990,** *15,* 439–442.
34. Purcell, W.; Roodt, A.; Basson, S. S.; Leipoldt, J. G. *Transition Met. Chem.* **1989,** *14,* 369–370.
35. Purcell, W.; Damoense, L. J.; Leipoldt, J. G. *Inorg. Chim. Acta* **1992,** *195,* 217–219.
36. Purcell, W.; Potgieter, I. M.; Damoense, L. J.; Leipoldt, J. G. *Transition Met. Chem.* **1992,** *17,* 387–389.
37. Purcell, W.; Potgieter, I. M.; Damoense, L. J.; Leipoldt, J. G. *Transition Met. Chem.* **1991,** *16,* 473–475.
38. Purcell, W.; Van der Westhuizen, H. J.; Leipoldt, J. G.; Basson, S. S. *Transition Met. Chem.* **1994,** *19,* 582–584.
39. Smith, J.; Purcell, W.; Lamprecht, G. J.; Leipoldt, J. G. *Polyhedron* **1995,** *14,* 1795–1797.
40. Smith, J.; Purcell, W.; Lamprecht, G. J.; Roodt, A. *Polyhedron* **1996,** *15,* 1389–1395.
41. Botha, J. M.; Ph. D. thesis, University of the Free State, Bloemfontein, South Africa, 1995.
42. Engelbrecht, H. P.; M.Sc. thesis, University of the Free State, Bloemfontein, South Africa, 1998.
43. Smit, J. P.; Purcell, W.; Roodt, A.; Leipoldt, J. G. *Polyhedron* **1993,** *12,* 2271–2277.
44. Franklin, K. J.; Lock, C. J.; Sayer, B. G.; Schröbilgen, G. J. *J. Am. Chem. Soc.* **1982,** *104,* 5303–5306.
45. O'Connell, L. A.; Pearlstein, R. M.; Davison, A.; Thornback, J. R.; Kronauge, J. F.; Jones, A. *Inorg. Chim. Acta* **1989,** *161,* 39–43.
46. Nicholson, T.; Mahmood, A.; Jones, A.; Davison, A. *Inorg. Chim. Acta* **1991,** *179,* 53–57.
47. Roodt, A.; Leipoldt, J. G.; Basson, S. S.; Potgieter, I. M. *Transition Met. Chem.* **1988,** *13,* 336–339.
48. Purcell, W.; Roodt, A.; Basson, S. S.; Leipoldt, J. G. *Transition Met. Chem.* **1989,** *14,* 224–227.
49. Potgieter, I. M.; Basson, S. S.; Roodt, A.; Leipoldt, J. G. *Transition Met. Chem.* **1988,** *13,* 209–211.
50. Smit, J. P.; Purcell, W.; Roodt, A.; Leipoldt, J. G. *J. Chem. Soc. Dalton Trans.* **1995,** 1201–1206.

51. Steyn, G. J. J.; Roodt, A.; Poletaeva, I.; Varshavsky, Y. S. *J. Organomet. Chem.* **1997,** *536/357,* 197–205.
52. Richens, D. R.; Helm, L.; Pittet, P.-A.; Merbach, A. E.; Nicolo, F.; Chapuis, G. *Inorg. Chem.* **1989,** *28,* 1394–1402.
53. Comba, P.; Merbach, A. E. *Inorg. Chem.* **1987,** *26,* 1315–1323.
54. Helm, L.; Deutsch, K.; Deutsch, E. A.; Merbach, A. E. *Helv. Chim. Acta* **1992,** *75,* 210–217.
55. Tisato, F.; Mazzi, U.; Bandoli, G.; Cros, G.; Dardieu, M.-H.; Coulais, Y.; Guiraud, R. *J. Chem. Soc. Dalton Trans.* **1991,** 1301–1307.
56. Eigen, M. *Angew. Chem.* **1963,** *75,* 489–508.
57. Johnson, C. S.; Moreland, C. S. *J. Chem. Educ.* **1973,** *50,* 477–483.
58. Van Eldik, R.; Roodt, A.; Leipoldt, J. G. *Inorg. Chim. Acta* **1987,** *129,* L41–L43.
59. Ardon, M.; Bino, A. *Inorg. Chem.* **1985,** *24,* 1343–1347.
60. Durham, B.; Wilson, S. R.; Hodgson, D. J.; Meyer, T. J. *J. Am. Chem. Soc.* **1980,** *102,* 600–607.
61. Bino, A.; Gibson, D. *J. Am. Chem. Soc.* **1981,** *103,* 6741–6742.
62. Melton, B. F.; Pollack, V. L. *J. Phys. Chem.* **1969,** *73,* 3669–3673.
63. Copenhafer, W. C.; Rieger, P. H. *Inorg. Chem.* **1977,** *16,* 2431–2437.
64. Fong, D.-W.; Grunwald, E. *J. Am. Chem. Soc.* **1969,** *91,* 2413–2422.
65. Wong, E.; Fauconnier, T.; Bennet, S.; Valliant, J.; Nguyen, T.; Lau, F.; Lu, L. F. L.; Pollak, A.; Bell, R. A.; Thornback, J. R. *Inorg. Chem.* **1997,** *36,* 5799–5808.
66. Chen, B.; Heeg, M. J.; Deutsch, E. *Inorg. Chem.* **1992,** *31,* 4683–4690.
67. Lincoln, S. F.; Merbach, A. E. In "Advances in Inorganic Chemistry"; Sykes, A. G., Ed.; Academic Press: San Diego, 1995; Vol. 45; pp. 15–87.
68. Swaddle, T. W. *Adv. Inorg. Bioinorg. Mech.* **1983,** *2,* 95–138.
69. Toppen, D. L.; Murmann, R. K. *Inorg. Chem.* **1973,** *12,* 1611–1618.
70. Murmann, R. K.; Robinson, P. R. *Inorg. Chem.* **1975,** *14,* 2035–2041.
71. Roodt, A.; Leipoldt, J. G.; Deutsch, E. A.; Sullivan, J. C. *Inorg. Chem.* **1992,** *31,* 1080–1085.
72. Hore, P. J. *J. Magn. Reson.* **1983,** *55,* 283–288.
73. Bernhard, P.; Helm, L.; Ludi, A.; Merbach, A. E. *J. Am. Chem. Soc.* **1985,** *107,* 312–317.
74. Leipoldt, J. G.; van Eldik, R.; Basson, S. S.; Roodt, A. *Inorg. Chem.* **1986,** *25,* 4639–4642.
75. Sotomayor, J.; Parola, A. J.; Pina, F.; Zinato, E.; Riccieri, P.; Manfrin, M. F.; Moggi, L. *Inorg. Chem.* **1995,** *34,* 6532–6537.
76. Botha, J. M.; Roodt, A. Unpublished results.
77. Jurisson, S.; Berning, D.; Jia, W.; Ma, D. *Chem. Rev.* **1993,** *93,* 1137–1156 and references within.
78. Damoense, L. J.; Purcell, W.; Leipoldt, J. G. *Transition Met. Chem.* **1994,** *19,* 619–622.
79. Kolski, G. B.; Margerum, D. W. *Inorg. Chem.* **1968,** *7,* 2239–2243.
80. Kolski, G. B.; Margerum, D. W. *Inorg. Chem.* **1969,** *8,* 1125–1131.
81. Pearson, R. G.; Sweigart, D. A. *Inorg. Chem.* **1970,** *9,* 1167–1175.
82. Billo, E. G. *Inorg. Chem.* **1973,** *12,* 2783–2787.
83. Roodt, A.; Basson, S. S.; Leipoldt, J. G. *Polyhedron* **1994,** *13,* 599–607.
84. Leipoldt, J. G.; Basson, S. S.; Potgieter, I. M.; Roodt, A. *Inorg. Chem.* **1987,** *26,* 57–59.
85. Beard, J. H.; Casey, J.; Murmann, R. K. *Inorg. Chem.* **1965,** *4,* 797–803.
86. Lu, J.; Clarke, M. J. *Inorg. Chem.* **1989,** *28,* 2315–2319.

87. Beard, J. H.; Calhoun, C.; Casey, J.; Murmann, R. K. *J. Am. Chem. Soc.* **1968,** *90,* 3389–3394.
88. Purcell, W.; Basson, S. S.; Roodt, A.; van der Westhuizen, H. J. *Transition Met. Chem.* **1998,** *23,* 473–476.
89. Purcell, W.; Roodt, A.; Leipoldt, J. G. *Transition Met. Chem.* **1991,** *16,* 339–343.
90. Johnson, D. L.; Fritzberg, A. R.; Hawkins, B. L.; Kasina, S.; Eshima, D. *Inorg. Chem.* **1984,** *23,* 4204–4207.
91. Rall, J.; Weingart, F.; Ho, D. M.; Heeg, M. J.; Tisato, F.; Deutsch, E. A. *Inorg. Chem.* **1994,** *33,* 3442–3451.
92. Bennett, W. D.; Ilowite, J. S. *Am. Rev. Respir. Dis.* **1989,** *139,* 1132–1138.
93. Ilowite, J. S.; Bennett, W. D.; Sheetz, M. S.; Groth, M. L.; Nierman, D. M. *Am. Rev. Respir. Dis.* **1989,** *139,* 1139–1143.
94. Oberdörster, G.; Utell, M. J.; Morrow, P. E.; Hyde, R. W.; Weber, D. A. *Am. Rev. Respir. Dis.* **1986,** *134,* 944–950.
95. Rabito, C. A.; Moore, R. H.; Bougas, C.; Dragotakes, S. C. *J. Nucl. Med.* **1993,** *34,* 199–207.
96. Costa, D. C.; Lui, D.; Ell, P. J. *Nucl. Med. Commun.* **1988,** *9,* 725–731.
97. Saunders, C. A.; Choong, K. K.; Larcos, G.; Farlow, D.; Gruenewald, S. M. *J. Nucl. Med.* **1997,** *38,* 1483–1486.
98. Deutsch, E. A.; Vanderheyden, J. L.; Gerundini, P.; Libson, K.; Hirth, W.; Colombo, F.; Zecca, L.; Savi, A.; Fazio, F. *J. Nucl. Med.* **1987,** *28,* 1870–1880.
99. Arbab, A. S.; Koizumi, K.; Toyama, K.; Arai, T.; Araki, T. *Nucl. Med. Commun.* **1997,** *18,* 235–240.
100. Jones, S.; Hendel, R. C. *J. Nucl. Med. Technol.* **1993,** *21,* 191–195.
101. Wackers, F. J. Th.; Berman, D. S.; Maddahi, J.; Watson, D. D.; Beller, G. A.; Strauss, H. W.; Boucher, C. A.; Picard, M.; Holman, B. L.; Fridrich, R.; Inglese, E.; Delaloye, B.; Bischof-Delaloye, A.; Camin, L.; McKusick, K. *J. Nucl. Med.* **1989,** *30,* 301–311.
102. O'Doherty, M. J.; Kettle, A. G.; Wells, P.; Collins, R. E. C.; Coakley, A. J. *J. Nucl. Med.* **1992,** *33,* 313–318.
103. Cutler, C.; Roodt, A.; Deutsch, E. A. *J. Nucl. Med.* Unpublished results.
104. Juweid, M.; Dunn, R. M.; Sharkey, R. M.; Rubin, A. D.; Hansen, H. J.; Goldenberg, D. M. *Nucl. Med. Commun.* **1997,** *18,* 142–148.
105. Brown, B. A.; Dearborn, C. B.; Drozynski, C. A.; Sands, H. *Cancer Res.* (Suppl). **1990,** *50,* 835s–839s.
106. Stalteri, M. A.; Mather, S. J.; Belinka, B. A.; Coughlin, D. J.; Chengazi, V. U.; Britton, K. E. *Eur. J. Nucl. Med.* **1997,** *24,* 651–654.
107. Rutland, M. D. *Nucl. Med. Commun.* **1992,** *13,* 843–847.
108. Miki, K.; Kubota, K.; Kokudo, N.; Inoue, Y.; Bandai, Y.; Makuuchi, M. *J. Nucl. Med.* **1997,** *38,* 1798–1807.
109. Stone, C. K.; Mulnix, T.; Nickles, R. J.; Renstrom, B.; Nellis, S. H.; Liedtke, A. J.; Nunn, A. D. *Circulation* **1995,** *92,* 1246–1253.
110. Mcquarrie, S. A.; Baum, R. P.; Niesen, A.; Madiyalakan, R.; Korz, W.; Sykes, T. R.; Sykes, C. J.; Hör, G.; Mcewan, A. J. B.; Noujaim, A. A. *Nucl. Med. Commun.* **1997,** *18,* 878–886.
111. de Klerk, J. M.; van Dijk, A.; van het Schip, A. D.; Zonnenberg, B. A.; van Rijk, P. P. *J. Nucl. Med.* **1992,** *33,* 646–651.
112. Van Aswegen, A.; Roodt, A.; Marais, J.; Botha, J. M.; Naudé, H.; Lötter, M. J.; Goedhals, L. G.; Doman, M. J.; Otto, A. C. *Nucl. Med. Commun.* **1997,** *18,* 582–588.

113. Juweid, M.; Sharkey, R. M.; Swayne, L. C.; Griffiths, G. L.; Dunn, R.; Goldenberg, D. M. *J. Nucl. Med.* **1998,** *39,* 34–42.
114. Vanderheyden, J.-L.; Heeg, M. J.; Deutsch, E. *Inorg. Chem.* **1985,** *24,* 1666–1673.
115. Elder, R. C.; Yuan, J.; Helmer, B.; Pipes, D.; Deutsch, K.; Deutsch, E. A. *Inorg. Chem.* **1997,** *36,* 3055–3063.
116. Libson, K.; Deutsch, E. A.; Barnett, B. L. *J. Am. Chem. Soc.* **1980,** *102,* 2476–2478.
117. Treher, E. N.; Francesconi, L. C.; Gougoutas, J. Z.; Malley, M. F.; Nunn, A. D. *Inorg. Chem.* **1989,** *28,* 3411–3416.

PROTONATION, OLIGOMERIZATION, AND CONDENSATION REACTIONS OF VANADATE(V), MOLYBDATE(VI), AND TUNGSTATE(VI)

J. J. CRUYWAGEN

Department of Chemistry, University of Stellenbosch, Stellenbosch 7600, South Africa

I. Introduction

The elements vanadium, molybdenum, and tungsten in their highest oxidation states form the stable oxyanions $[VO_4]^{3-}$, $[MoO_4]^{2-}$, and $[WO_4]^{2-}$. In aqueous solution these ions are easily protonated and then show a strong tendency to form polyoxoanions by oxygen bridging and the release of water molecules. Depending on pH and concentration, a great variety of ions can form in each case, giving rise to complex systems of simultaneous equilibria which have proved difficult to characterize with certainty. A number of polyoxoanions that

Copyright © 2000 by Academic Press.
All rights of reproduction in any form reserved.
0898-8838/00 $30.00

occur in solution had been isolated in the solid state and were structurally characterized by X-ray analysis.

The vanadate (*1*, *2*), molybdate (*1–5*), and tungstate (*1–3*) systems have been described in previous reviews. Although the focus in this chapter is on more recent developments, earlier well-established knowledge is included where needed for perspective and also to present a coherent picture of the hydrolysis behavior of these oxyanions. Equilibria of mono- and polynuclear species are described and information about known structures are given. Some recent work about mixed polyoxoanions is briefly reviewed.

II. Vanadate(V)

A. Mononuclear Species

The orthovanadate ion $[VO_4]^{3-}$ occurs only at very high pH. It is such a strong base that the first step in its protonation, forming $[HVO_4]^{2-}$, is already complete at pH ~12. When the pH is gradually lowered to ~1 successive protonation ultimately leads to the formation of the pale yellow cationic species, usually formulated as VO_2^+

$$[VO_4]^{3-} + H^+ \overset{K_1}{\rightleftharpoons} [HVO_4]^{2-} \quad (1)$$

$$[HVO_4]^{2-} + H^+ \overset{K_2}{\rightleftharpoons} [H_2VO_4]^- \quad (2)$$

$$[H_2VO_4]^- + H^+ \overset{K_3}{\rightleftharpoons} H_3VO_4 \quad (3)$$

$$H_3VO_4 + H^+ \overset{K_4}{\rightleftharpoons} VO_2^+ + 2H_2O. \quad (4)$$

Due to the great tendency of vanadate to oligomerize, the protonated monomers $[HVO_4]^{2-}$, $[H_2VO_4]^-$, and VO_2^+ (except at very low pH) are predominant only in highly diluted solution ($\lesssim 5 \times 10^{-5}\,M$). The above protonation equilibria have been studied by different methods under various conditions (*2*, *6–19*). Spectrophotometry and also ^{51}V NMR spectroscopy have proved to be particular useful methods for the characterization of the mononuclear species. Vanadate absorbs strongly in the UV range and the $[VO_4]^{3-}$ ion, for example, has two prominent absorption peaks at wavelengths 224 and 271 nm (*17*). The ^{51}V NMR spectra of $[HVO_4]^{2-}$, $[H_2VO_4]^-$, and VO_2^+ show well-defined

chemical shifts (relative to $VOCl_3$) of −537, −561, and −543 ppm respectively (*16*). Remarkable broadening of oxygen resonances of $[HVO_4]^{2-}$ at low temperature (0°C) has been explained in terms of a significantly slowed rate ($\sim 2 \times 10^5$ s^{-1}) at which the proton jumps between the four oxygens (*20*).

Selected equilibrium constants and thermodynamic quantities of the mononuclear species are listed in Table I and the distribution of mononuclear ions as a function of pH is shown in Fig. 1. Values have also been reported which show the variation of the protonation constant of $[HVO_4]^{2-}$ with variation of added KCl from 0 to 2 *M* (*15*).

The neutral acid H_3VO_4, with an estimated value for pK_3 of 2–3, occurs in such a low percentage concentration in aqueous solution (probably less than 5%) that it can not be characterized with certainty (*9*, *16*, *17*). The two successive protonation steps of $[H_2VO_4]^-$ to form

TABLE I

SELECTED EQUILIBRIUM CONSTANTS AND THERMODYNAMIC QUANTITIES FOR THE PROTONATION OF VANADATE(V) AT 25°C[a]

	log *K*	ΔH° (kJ mol^{-1})	ΔS° (J mol^{-1} K^{-1})	Medium	Reference
VO_4^{3-}/HVO_4^{2-}	13.27 ± 0.002	−24	174	1.0 *M* NaCl	(*12*, *13*)
	13.21	—	—	3.0 *M* $NaClO_4$	(*6*)
$HVO_4^{2-}/H_2VO_4^-$	8.75 ± 0.05	−7 ± 2	145 ± 5	*I* = 0	(*16*)
	8.3	−4 ± 1.8	144 ± 3	0.1 *M* NaCl	(*15*)
	8.17	—	—	0.15 *M* NaCl	(*18*)
	8.2	−5.6 ± 1	141 ± 4	0.4 *M* KCl	(*19*)
	7.95	—	—	0.6 *M* NaCl	(*14*)
	7.92 ± 0.02	−9 ± 2	122 ± 9	1.0 *M* NaCl	(*17*)
	7.91 ± 0.05	—	—	2 *M* NaCl	(*11*)
	7.62 ± 0.07	—	—	3.0 *M* $NaClO_4$	(*7*)
$H_2VO_4^-/VO_2^+$	6.80 ± 0.10	−47 ± 5	−29 ± 15	*I* = 0	(*16*)
	7.00	—	—	0.15 *M* NaCl	(*18*)
	6.92	—	—	0.6 *M* NaCl	(*14*)
	6.76 ± 0.02	−33 ± 2	20 ± 7	1.0 *M* $NaClO_4$	(*17*)
$H_2VO_4^-/H_3VO_4$	≤3.08	—	—	0.6 *M* NaCl	(*9*)
	[2.6]	[6]	[71]	1.0 *M* $NaClO_4$	(*17*)
H_3VO_4/VO_2^+	≤3.88			0.6 *M* NaCl	(*9*)
	[4.2]	[−39]	[−51]	0.1 *M* $NaClO_4$	(*17*)

[a] Values in brackets are estimated by extrapolation (cf. text).

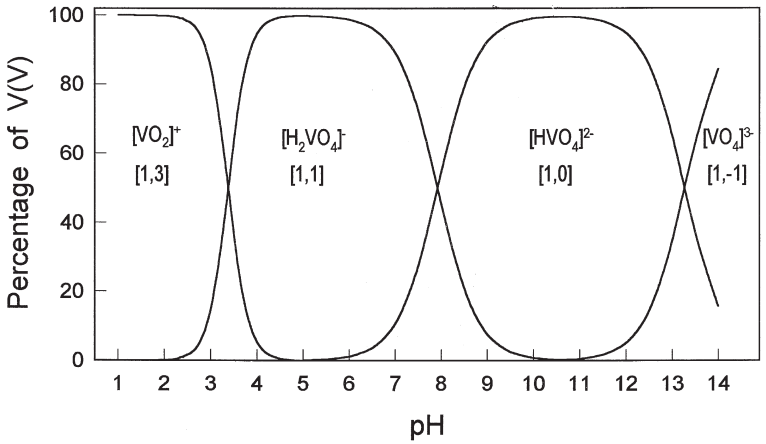

FIG. 1. Distribution of mononuclear species as a function of pH calculated from equilibrium constants (pertaining to ionic strength 1.0) given in Table I.

VO_2^+ are therefore best described by a single reaction

$$[H_2VO_4]^- + 2\,H^+ \overset{K_3K_4}{\rightleftharpoons} VO_2^+ + 2\,H_2O \tag{5}$$

for which the equilibrium constant and thermodynamic parameters can be determined with sufficient accuracy. The reason for the "absence" of H_3VO_4 is the relatively great stability of VO_2^+, which is explained (*17*) in terms of an increase in the coordination number of vanadium from 4 to 6 in the fourth protonation step as represented by

$$H_3VO_4 + H^+ + 2\,H_2O \overset{K_4}{\rightleftharpoons} [VO_2(H_2O)_4]^+. \tag{6}$$

It has been suggested that an increase in the coordination number of vanadium from 4 to 5 already takes place in the second protonation step, i.e. when $[H_2VO_4]^-$ is formed (*21*). For reactions (1) and (2), however, the protonation constants and thermodynamic parameters are comparable with those reported for PO_4^{3-} and AsO_4^{3-}, providing firm evidence that reaction (2) is not accompanied by incorporation of water in the vanadate ion (*15*, *17*). Further, the estimated thermodynamic quantities for reaction (6), $\Delta H^\circ = -39$ kJ/mol and $\Delta S^\circ = -51$ J/(mol K), obtained by extrapolation from the experimental values for reactions (1) and (2) and those for the three protonation steps of PO_4^{3-} and AsO_4^{3-}, are not typical of a simple protonation reaction (*17*). For such a reaction the entropy change is normally a positive quantity often amounting to 100 ± 50 J/(mol K) and the enthalpy

change either a small positive or negative quantity. The very favorable enthalpy change is accounted for by the extra bond energy in the six-coordinated cation and the unfavorable entropy change by the uptake of two molecules of water. The cation $[VO_2(H_2O_4]^+$ most likely has a *cis* arrangement of the oxo groups as in the case of the complexes $[VO_2(C_2O_4)_2]^{3-}$ and $[VO_2(edta)]^{3-}$ (*22*). In the case of molybdate, expansion of the coordination sphere takes place in the second protonation step when the neutral acid is formed (cf. Section III,A).

The cation forms a red dimer with a central $V_2O_3^{4+}$ group in concentrated $HClO_4$ and H_2SO_4 (*23*). A possible representation of the dimerization reaction in $HClO_4$ is given in

$$2\,[VO_2(H_2O)_4]^+ + 2\,H^+ \leftrightharpoons [V_2O_3(H_2O)_8]^{4+} + H_2O. \qquad (7)$$

The value of the dimerization constant has been determined as 1.54 in 11.8 *M* $HClO_4$ (*23*).

B. Polyoxoanions

Despite the complexity of a plethora of overlapping equilibria the system can now be regarded as fairly well characterized. Depending on the concentration, oligomers of nuclearity 2, 3, 4, 5, and 6 as well as condensed decavanadate polyanions can coexist with the protonated mononuclear species in the pH range 0–12. Even very minor species have been identified and for species occurring in sufficiently high concentration reliable formation constants have been determined in different ionic media (Table II). For practical reasons the formation constants are usually defined in terms of the monoprotonated monomer

$$p\,[HVO_4]^{2-} + q\,H^+ \overset{\beta_{p,q}}{\rightleftharpoons} [(HVO_4)_pH_q]^{(2p-q)-}$$

and the reaction products are often described by the stoichiometric coefficients of the reactants, e.g., [1,1] refers to $[H_2VO_4]^-$ and [4,4] to $[V_4O_{12}]^{4-}$.

These equilibria have been studied by various methods of which potentiometry and ^{51}V NMR spectroscopy proved to be particularly useful for the identification of species and the determination of stability constants (*8–10*, *13–16*, *18*, *20*, *22*, *24*). Values obtained for stability constants by different research groups under the same conditions usually show good agreement, e.g., for 0.60 *M* NaCl medium (Table II). In some cases so-called Brönsted (or mixed) constants (*25*) are

TABLE II

FORMATION CONSTANTS log $\beta_{p,q}$ REPORTED FOR DIFFERENT IONIC MEDIA AT 25°C FOR THE REACTIONS $p\mathrm{HVO_4^{2-}} + q\mathrm{H^+} \leftrightharpoons [(\mathrm{HVO_4^{2-}})p(\mathrm{H^+})q]$

Formula	$[p, q]$	3 *M* $NaClO_4$	0.6 *M* NaCl	0.6 *M* NaCl	0.15 *M* NaCl	0 *M*
$[VO_4]^{3-}$	[1, −1]	−13.1	−13.36	—	—	—
$[HVO_4]^{2-}$	[1, 0]	0	0	0	0	0
$[H_2VO_4]^-$	[1, 1]	8.00	7.95	7.98	8.17	8.75
$[VO_2]^+$	[1, 3]	15.16	14.87	—	15.17	—
$[V_2O_7]^{4-}$	[2, 0]	1.44	0.66	0.69	0.15	−1.1
$[HV_2O_7]^{3-}$	[2, 1]	11.12	10.45	10.67	10.49	10.2
$[H_2V_2O_7]^{2-}$	[2, 2]	18.8	18.68	19.14	18.99	19.8
$[V_3O_{10}]^{5-}$	[3, 1]	12.13[a]	—	—	—	—
$[V_4O_{13}]^{6-}$	[4, 2]	24.73	23.18	23.08	22.70	—
$[HV_4O_{13}]^{5-}$	[4, 3]	33.0	31.92	31.96	32.05	—
$[V_4O_{12}]^{4-}$	[4, 4]	43.24	41.67	41.68	41.92	42.6
$[V_5O_{15}]^{5-}$	[5, 5]	54.14	51.89	51.98	52.02	—
$[V_6O_{18}]^{6-}$	[6, 6]	64	61.58	—	—	—
$[V_{10}O_{28}]^{6-}$	[10, 14]	137.1	131.22	—	131.98	—
$[HV_{10}O_{28}]^{5-}$	[10, 15]	142.8	137.29	—	138.60	141.5
$[H_2V_{10}O_{28}]^{4-}$	[10, 16]	146.4	140.89	—	142.77	145.7
$[H_3V_{10}O_{28}]^{3-}$	[10, 17]	147.9	142.10	—	144.63	—
Reference		(*10*)	(*14*)	(*33*)	(*18*)	(*16*)

[a] Ionic medium 3 *M* NaCl (*20*).

determined, i.e. when electrodes are standardized with buffer solutions instead of their calibration in terms of hydrogen ion concentration (*8*, *15*). Values reported for equilibrium constants by different researchers at the same ionic strength are therefore not always strictly comparable and the original papers should be consulted for the exact conditions.

The application of ^{51}V and ^{17}O NMR spectroscopy played a crucial role in the successful unraveling of the system. In the so-called metavanadate region (average charge per vanadium, −1), for example, potentiometric data alone were not decisive enough to find four species having different nuclearities (1, 2, 4, and 5) but the same charge and the same number of protons per vanadium (*26*). A recent development in data treatment is the use of a computer program, LAKE (*27*), which can treat combined potentiometric and NMR equilibrium data; finding a unique "best" reaction model which is in accordance with both sets of data seems to be possible.

The distribution of the species as a function of pH are shown in

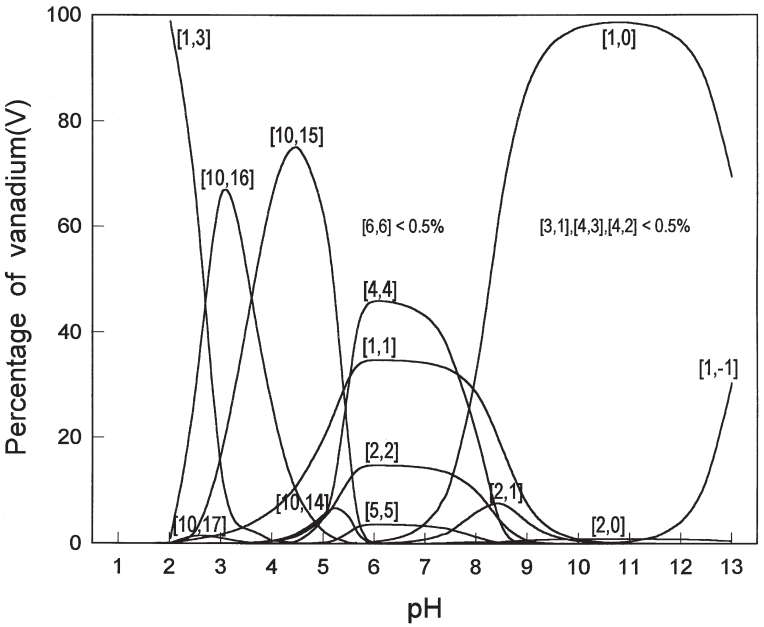

FIG. 2. Distribution of vanadium(V) species as a function of pH, calculated from constants in Table II. Vanadium(V) concentration 0.001 *M* and ionic medium 0.6 *M* NaCl.

Figs. 2 and 3 for two concentrations in 0.60 *M* NaCl medium. The relative concentrations of the species are strongly affected by the ionic medium presumably due to their interaction with the medium ions (*26*). In NaCl medium, at a vanadium concentration of 1.25 m*M,* for example, the relative concentration of $[V_4O_{12}]^{4-}$ changes from ~50 to 18% when the sodium ion concentration is decreased from 0.60 to 0.10 *M*. Other highly charged ions are affected in the same way, in particular $[V_4O_{13}]^{6-}$, $[V_5O_{15}]^{5-}$, and $[V_{10}O_{28}]^{6-}$, which occur in reasonable amounts (>20%) at vanadium concentration of 0.02 *M* in 3.0 *M* $NaClO_4$ medium, but are very minor species at low ionic strength (0.15 *M*) (*26*, *28*). Also for KCl medium an increase in the formation constants of $[V_4O_{13}]^{6-}$ and $[V_5O_{15}]^{5-}$ of 2 to 3 orders of magnitude has been reported for an increase in concentration from 0 to 2.0 *M* (*15*). Predominance diagrams for the major species, showing the effect of different ionic media on their stability, have been constructed for 0.6 *M* NaCl and 3.0 *M* $NaClO_4$ (*26*).

Enthalpy and entropy changes for the formation of the major species have been determined (*16*, *29*) and are given in Table III. Oligomerization is enthalpy driven as seen, for example, from the thermo-

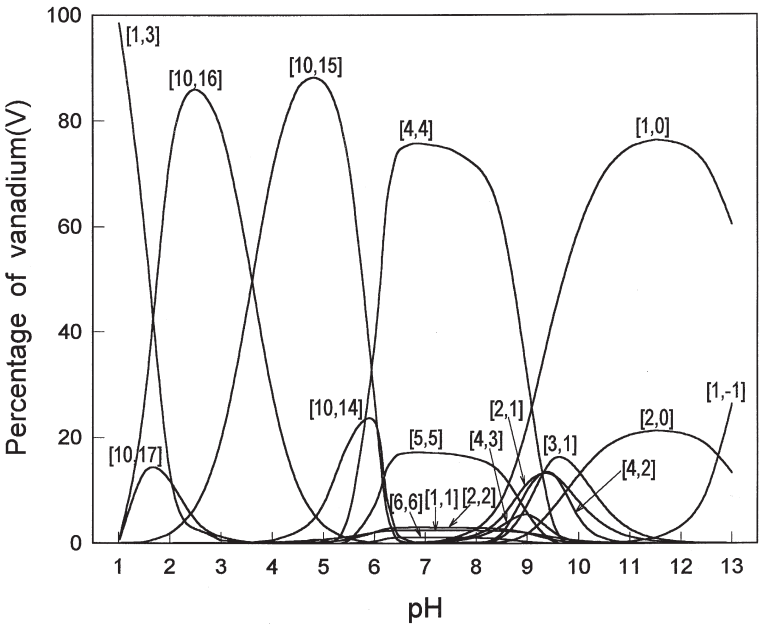

FIG. 3. Distribution of vanadium(V) species as a function of pH, calculated from constants in Table II. Vanadium(V) concentration 0.04 *M* and ionic medium 0.6 *M* NaCl.

TABLE III

THERMODYNAMIC QUANTITIES ΔH^o (kJ/mol) AND ΔS^o (J/mol K) AT 25°C FOR THE FORMATION OF SOME VANADIUM(V) POLYNUCLEAR SPECIES FROM $[HVO_4]^{2-}$

	I = 1.0 *M* NaCl (*29*)		I = 0 (*16*)	
Species	ΔH^o	ΔS^o	ΔH^o	ΔS^o
$[HVO_4]^{2-}$	0	0	0	0
$[V_2O_7]^{4-}$	−28	−77	−47	−178
$[HV_2O_7]^{3-}$	−35	87	−47.5	37
$[H_2V_2O_7]^{2-}$	—	—	−44	232
$[V_3O_{10}]^{5-}$	−55	50	—	—
$[V_4O_{13}]^{6-}$	−82	178	—	—
$[HV_4O_{13}]^{5-}$	—	—	—	—
$[V_4O_{12}]^{4-}$	−122	392	−123	410
$[V_5O_{15}]^{5-}$	−156	517	—	—
$[HV_{10}O_{28}]^{5-}$	—	—	−412	1329

dynamic quantities (kJ/mol) at 25°C for the formation of either the linear trimer or the cyclic tetramer (*29*)

$$\Delta H^{o} \quad T\Delta S^{o}$$

$$[HV_2O_7]^{3-} + [HVO_4]^{2-} \leftrightharpoons [V_3O_{10}]^{5-} + H_2O \quad -20 \quad -11 \tag{8}$$

$$4\,[H_2VO_4]^{-} \leftrightharpoons [V_4O_{12}]^{4-} + 4\,H_2O \quad -86 \quad -27. \tag{9}$$

Since vanadium is tetrahedral in all these ions the number of bonds in the oligomerization process remain the same. The favorable enthalpy therefore emanates mainly from the stronger bonds in the stable water molecules that are condensed out. The net gain in enthalpy, for each linkage of two vanadates accompanied by the formation of a molecule of water is about 20 kJ/mol.

The characteristics of the individual species are best discussed by grouping them according to nuclearity and structure in a systematic way as they occur with change in pH from alkaline to acid solution.

1. Dimers

The singly protonated monomer $[HVO_4]^{2-}$ can dimerize, forming $[V_2O_7]^{4-}$ by elimination of a water molecule. Two protonated forms of the dimer have been found to exist

$$2\,[HVO_4]^{2-} \leftrightharpoons [V_2O_7]^{4-} + H_2O \tag{10}$$

$$[V_2O_7]^{4-} + H^{+} \leftrightharpoons [HV_2O_7]^{3-} \tag{11}$$

$$[HV_2O_7]^{3-} + H^{+} \leftrightharpoons [H_2V_2O_7]^{2-}. \tag{12}$$

Since hydrogen ions do not take part in reaction (10) the unprotonated dimer occurs in the same pH region as $[HVO_4]^{2-}$ (Fig. 3). In the solid state the dimer consists of two VO_4 tetrahedra sharing a vertex (Fig. 4) and in solution it is assumed to have the same structure (*30*,

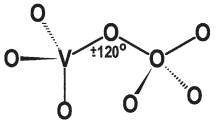

FIG. 4. Representation of the structure of $[V_2O_7]^{4-}$.

31). The changes observed in the UV spectrum on dimerization of $[HVO_4]^{2-}$ are similar to those taking place when $[HCrO_4]^-$ dimerizes to form $[Cr_2O_7]^{2-}$ (*13*). The tendency to dimerize is smaller than in the case of $[HCrO_4]^-$, but increases with increase in ionic strength (*15*, *28*). The reaction is enthalpy driven (−28 kJ/mol), but due to the unfavorable entropy change (−80 J/mol *K*) the equilibrium constant is rather small, log $\beta_{2,0} = 0.83$ in 1.0 *M* NaCl medium (*13*). Other values showing the effect of the ionic medium are log $\beta_{2,0} = 0.67$ (0.6 *M* NaCl) (*32, 33*) and log $\beta_{2,0} = 1.44$ (3.0 *M* $NaClO_4$) (*10*). The effect is interpreted in terms of interaction of Na^+ with the dimer (*26*). In fact, computer treatment with the program LAKE (*27*) of NMR and pH data in alkaline solutions where monomeric and dimeric species are predominant (average charge of −2 per vanadium) has shown that the data are best explained in terms of the formation of two Na^+ complexes, $[NaHVO_4]^-$ and $[NaV_2O_7]^{3-}$ (*28*). The results show that the $[NaV_2O_7]^{3-}$ complex is the predominating dimer at sodium ion concentration greater than ∼0.1 *M*. The values of the formation constants of the noncomplexed species $[HV_2O_7]^{3-}$ and $[V_2O_7]^{4-}$ should therefore approach the "true" formation constants rather than conditional constants (Table IV). The value log $\beta_{2,0} = -0.2$ for the formation of $[V_2O_7]^{4-}$ (Eq. 10) therefore does not differ much from that obtained in 0.05 *M* $(C_4H_9)_4NCl$ medium, log $\beta_{2,0} = -0.35$. Sodium ion complexation seems to afford a better explanation of the data at different ionic strengths than what is obtained when ionic strength parameters are introduced (*28*). A negative value for this constant, albeit significantly smaller (−1.1), has also been obtained at zero ionic strength (*16*).

The p*K* values of $[HV_2O_7]^{3-}$ and $[H_2V_2O_7]^{2-}$ are relatively high and of the same order of magnitude as those of the mononuclear species (Table II). For $[HV_2O_7]^{3-}$ in 3.0 *M* NaCl at 0° and 25°C the p*K* values are 10.21 and 9.84 respectively (*20*). At $I = 0$ the p*K* of $[H_2V_2O_7]^{2-}$ was

TABLE IV

VALUES DETERMINED FOR FORMATION CONSTANTS OF VANADIUM(V) SPECIES AT pH∼11 ASSUMING Na^+ COMPLEXATION (*28*)

Species	log $\beta \pm 3\sigma$
$[HVO_4]^{2-}$	0
$[NaHVO_4]^-$	−1.1 ± 0.2
$[V_2O_7]^{4-}$	−0.2 ± 0.3
$[NaV_2O_7]^{3-}$	0.89 ± 0.8
$[HV_2O_7]^{3-}$	10.8 ± 0.3

found to have the value (9.6 ± 0.2) at 25°C with a ΔH^{o} of ionization of −3.5 ± 5 kJ/mol and $\Delta S^{o} = -195 \pm 15$ J/mol K (*16*).

2. Linear Trimeric and Tetrameric Species

The formation of these species can be described by the following equilibria

$$3\,[HVO_4]^{2-} + H^+ \leftrightharpoons [V_3O_{10}]^{5-} + 2\,H_2O \quad (13)$$

$$4\,[HVO_4]^{2-} + 2\,H^+ \leftrightharpoons [V_4O_{13}]^{6-} + 3\,H_2O \quad (14)$$

$$4\,[HVO_4]^{2-} + 3\,H^+ \leftrightharpoons [HV_4O_{13}]^{5-} + 3\,H_2O. \quad (15)$$

As additional protons are involved in the oligomerization of $[HVO_4]^{2-}$ these species occur at a somewhat lower pH than $[V_2O_7]^{4-}$, i.e. at pH <10.

The linear $[V_3O_{10}]^{5-}$ and $[V_4O_{13}]^{6-}$ oligomers were first proposed in 1981, on the basis of limited ^{51}V and ^{17}O NMR evidence (*8*). The existence of these ions, which had not been universally acknowledged (*10*, *32*), was recently confirmed by ^{51}V and ^{17}O NMR and potentiometry (*20*). The resonances of these species are mostly broadened by an exchange process which has been shown to be independent of the monomeric or dimeric ions also present and also of the solvent oxygens. The broadenings are not consistent with a simple exchange process and an intra- rather than an interionic exchange involving a protonated intermediate has been suggested (*20*). A kinetic scheme has been proposed (Fig. 5) where the intermediate can either revert to the starting ion or break at the other equivalent V–O bond to form the same chemical species, but one of the terminal vanadiums V_t now exchanged with the central vanadium V_c.

The linear tetramer $[V_4O_{13}]^{6-}$, a relatively minor species, becomes more important with increase in the ionic strength of the solution, presumably as a result of interaction with Na^+ ions. The distributions

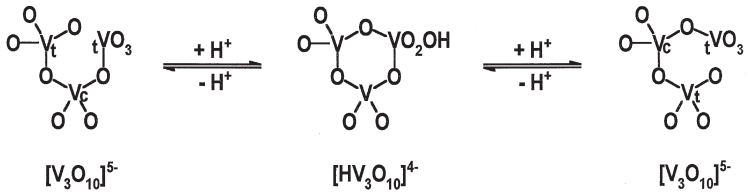

FIG. 5. Reaction scheme proposed for intramolecular exchange process in $[V_3O_{10}]^{5-}$. Local anionic charges are ignored. Subscripts t and c refer to terminal and central vanadium atoms. (Reprinted with permission from Andersson, I., Petterson, L., Hastings, J. J., Howarth, O. W., *J. Chem. Soc. Dalton Trans.* **1996,** 3357.)

of the two linear species, $[V_4O_{13}]^{6-}$ and $[V_3O_{10}]^{5-}$, as a function of pH (Fig. 3) show a strong correlation. The protonated form of the linear tetramer $[HV_4O_{13}]^{5-}$ occurs at a slightly lower pH and in very low concentrations, with a maximum share of only small percentages of the total vanadate.

3. Cyclic Tetramer, Pentamer, and Hexamer

These species coexist with $[H_2VO_4]^-$ and $[H_2V_2O_7]^{2-}$ in the pH region where the charge per vanadium is -1 (metavanadate region). The formation equilibria can be represented by the reaction equations

$$4\,[HVO_4]^{2-} + 4\,H^+ \leftrightharpoons [V_4O_{12}]^{4-} + 4\,H_2O \tag{16}$$

$$5\,[HVO_4]^{2-} + 5\,H^+ \leftrightharpoons [V_5O_{15}]^{5-} + 5\,H_2O \tag{17}$$

$$6\,[HVO_4]^{2-} + 6\,H^+ \leftrightharpoons [V_6O_{18}]^{6-} + 6\,H_2O. \tag{18}$$

In aqueous solution both the tetramer and the pentamer have cyclical structures (Fig. 6) as shown by the narrow ^{51}V NMR linewidths indicating high symmetry around vanadium (*29*). The relative amounts of the species are concentration dependent but under moderate concentrations the tetramer is the most important (Figs. 2 and 3). The hexamer $[V_6O_{18}]^{6-}$ is a very minor species under most conditions, but it becomes somewhat more prominent at high concentrations and high ionic strength (*8*, *10*, *15*, *32*). Indications are that it has a cyclic structure in aqueous solution (*10*).

The enthalpy change for reaction (16) has been determined as -123 and -122 kJ/mol for zero ionic strength (*16*) and 1.0 *M* NaCl medium (*29*) respectively. When the quantities $\Delta H^o = -122$ kJ/mol and $\Delta H^o = -156$ kJ/mol for the formation of $[V_4O_{12}]^{4-}$ and $[V_5O_{15}]^{5-}$ according to reactions (16) and (17) are compared, it is seen that the enthalpy change per vanadium atom is about the same, -30 and -31 kJ/mol

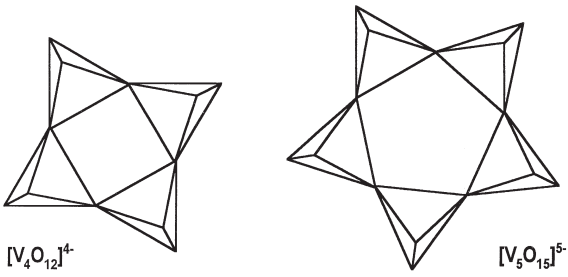

FIG. 6. Idealized representation of tetrameric and pentameric cyclic species.

respectively; the ΔS^{o} values per vanadium atom are also similar, namely 97 J/mol *K*.

No evidence has been found for the existence in aqueous solution of protonated forms of these cyclic oligomers. A protonated cyclic tetrameric anion, $[HV_4O_{12}]^{3-}$, was structurally characterized in the compound $[n\text{-}(C_4H_9)_4N]_3[HV_4O_{12}]$, which was prepared by dissolving V_2O_5 in alcoholic $n\text{-}(C_4H_9)_4NOH$ solution (*34*).

The tetrameric ion $[V_4O_{12}]^{4-}$ has been isolated in the solid state from aqueous solution as the salt of *tert*-butylammonium, $[(CH_3)_3CNH_3]_4[V_4O_{12}]$ (*35*). The X-ray analysis shows that the tetrameric ion has a cyclical structure consisting of corner-shared VO_4 tetrahedra. The bond length of the V–O bridging groups are longer (1.78 Å) than the terminal bonds (1.65 Å). The complex anions $[(\eta\text{-}C_8H_{12})Ir(V_4O_{12})]^{3-}$ and $\{[(\eta\text{-}C_8H_{12})Ir]_2(V_4O_{12})]\}^{2-}$ have been obtained from acetonitrile solution by precipitation as tetra-*n*-butylammonium salts (*36*). The $[V_4O_{12}]^{4-}$ unit is stabilized by coordinating of the oxygen atoms to $(\eta\text{-}C_8H_{12})Ir$ moieties and does not occur as a discrete polyanion.

4. Decavanadates

The decavanadate ion $[V_{10}O_{28}]^{6-}$ and its three protonated forms have a yellow-orange color and occur at pH <6.5. The formation reactions are represented by the equations

$$10\,[HVO_4]^{2-} + 14\,H^+ \leftrightharpoons [V_{10}O_{28}]^{6-} \tag{19}$$

$$10\,[HVO_4]^{2-} + 15\,H^+ \leftrightharpoons [HV_{10}O_{28}]^{5-} \tag{20}$$

$$10\,[HVO_4]^{2-} + 16\,H^+ \leftrightharpoons [H_2V_{10}O_{28}]^{4-} \tag{21}$$

$$10\,[HVO_4]^{2-} + 17\,H^+ \leftrightharpoons [H_3V_{10}O_{28}]^{3-}. \tag{22}$$

The singly and doubly protonated decamers predominate under most conditions (*10*, *32*). The percentage concentration of the unprotonated decavanadate ion is strongly dependent on the ionic strength. For instance, calculations show that its maximum concentration in ionic medium 0.15 *M* NaCl is less then 10% of the total vanadium concentration (0.02 *M*), but in 3.0 *M* $NaClO_4$ medium it amounts to about 50% (*28*).

The triply protonated decavanadate, $[H_3V_{10}O_{28}]^{3-}$, reaches its highest concentration at pH ~2, but with a decrease in the pH it is rapidly converted to the relatively more stable $[VO_2(H_2O)_4]^+$ ion, which begins to dominate from pH <1.5 (Figs. 2 and 3). Protonation and deprotonation of the decavanadates are fast, but equilibria between decavana-

dates and other species are established very slowly; depending on the pH and concentration at least 24 h are needed to attain equilibrium.

The structure of the decavanadate ion $[V_{10}O_{28}]^{6-}$ is well established. Vanadium-51 NMR spectroscopic studies have shown that the structure in solution corresponds to that in the solid state (2). Numerous X-ray studies have shown that it consists of an arrangement of 10 edge-shared VO_6 octahedra with approximate D_{2h} symmetry (Fig. 7). All vanadium atoms have distorted octahedral geometry and the oxygen atoms fall into seven categories, ranging from terminal to six coordinate.

It has been shown by ^{17}O NMR measurements that on protonation of $[V_{10}O_{28}]^{6-}$ a triply bridging type oxygen (O_B in Fig. 7) predominantly accepts the first proton (*37*, *38*). All three protonated decavanadates, $[HV_{10}O_{28}]^{5-}$, $[H_2V_{10}O_{28}]^{4-}$, and $[H_3V_{10}O_{28}]^{3-}$, have been isolated in the solid state by crystallization with large singly charged cations (*38–45*). The monoprotonated decavanadate was obtained as the compound $(acridineH)_5[HV_{10}O_{28}] \cdot 4H_2O$ (*38*, *39*). The crystal structure of

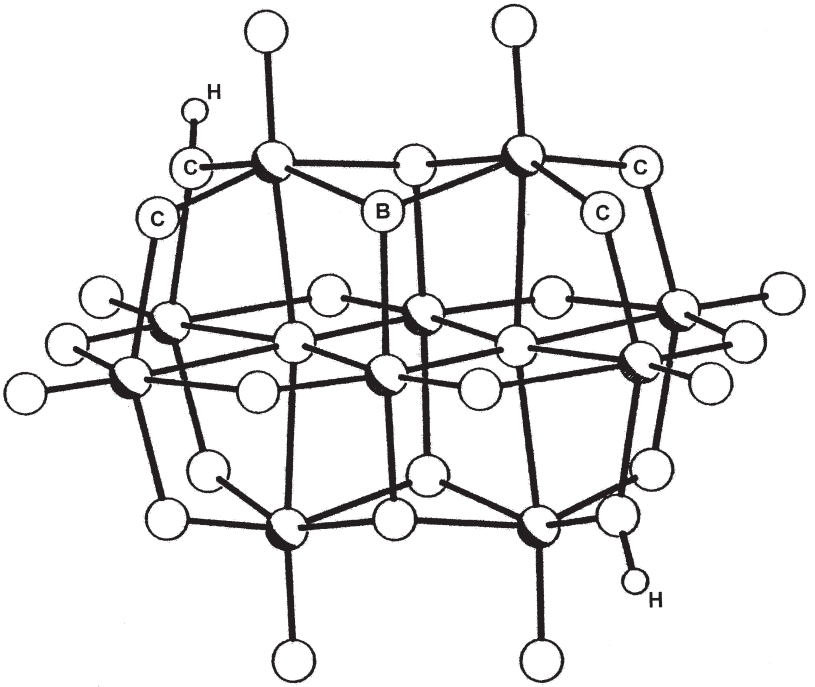

FIG. 7. Structure of $[V_{10}O_{28}]^{6-}$. A triply-bridged oxygen is indicated by B and some double-bridged oxygens by C. (Adapted with permission from Capparelli, M. V., Goodgame, D. M. L., Hayman, P. B., Skapski, A. C. *J. Chem. Soc. Chem. Commun.* **1986,** 776.)

an orange-red compound of formula (adenosinium)$_4[H_2V_{10}O_{28}] \cdot 11H_2O$ was determined. The hydrogen atoms were found to be attached to the doubly bridging C-type oxygens as shown in Fig. 7 (*43*). The hydrogen atoms are located in the same positions in the compound $[(CH_3)_3CNH_3]_4[H_2V_{10}O_{28}]$; the influence of protonation on the crystal packing has also been discussed (*46*). The crystal structure of the compound tetrakis(*n*-hexylammonium) dihydrodecavanadate(V), $[(C_6H_{13})NH_3]_4[H_2V_{10}O_{28}]$, has been determined. In this case empirical bond length/bond number calculations have located the protonation sites at two triply linked oxygen atoms (*44*).

The $[H_3V_{10}O_{28}]^{3-}$ ion has been isolated in the solid state from aqueous solution as a tetraphenylphosphonium salt (*40*) and from nonaqueous solutions as tetrabutylammonium salts (*42*). In the solid state and in solution, the $[H_3V_{10}O_{28}]^{3-}$ ion is protonated at one of the four O_B-type OV_3 oxygens and two of the eight O_C-type OV_2 oxygens (*40*). A theoretical analysis of the *ab initio*-determined distributions of the electrostatic potential and of the Laplacian of charge density provided information about the relative basicities of external oxygen sites in $[V_{10}O_{28}]^{6-}$; the most favorable site for protonation would be, first, an O_B site and, second, an O_C site (*45*). Calculations indicated that the protons in $[H_3V_{10}O_{28}]^{3-}$ would be attached to one O_B and two O_C sites.

The first tetrahydrogen decavanadate has been isolated from a methanol solution as the compound $[(n\text{-}(C_4H_9)_4N]_2[H_4V_{10}O_{28}]$. In this case the hydrogen atoms are attached to two double-linked oxygen atoms and to two triple-linked oxygen atoms (*47*).

5. Less Common Polyvanadates

a. Tridecavanadates All the aqueous isopolyvanadates described above are based on either corner-sharing VO_4 tetrahedra or on arrays of cubically packed edge-sharing VO_6 octahedra as in decavanadate. Evidence for the existence of a transient vanadium(V) polyanion having 12 vanadium atoms, arranged in a Keggin structure (four internally edge-sharing V_3O_{13} triads tetrahedrally disposed and corner-sharing) around a central, tetrahedrally coordinated vanadium (cf. Fig. 8), has been obtained by ^{51}V and ^{17}O NMR measurements (*48*). This ion, a tridecavanadate, formulated as $[H_{12}V_{13}O_{40}]^{3-}$, has a half-life of 80 min at 25°C. It is obtained by rapid acidification of a neutral aqueous solution, optimally to pH 1.5.

A tridecavanadate, $[V_{13}O_{34}]^{3-}$, was obtained in acetonitrile as the salt of the tetrabutyl ammonium cation $[(n\text{-}C_4H_9)_4N]_3[V_{13}O_{34}]$. It is a highly condensed polyanion with a structure similar to that of

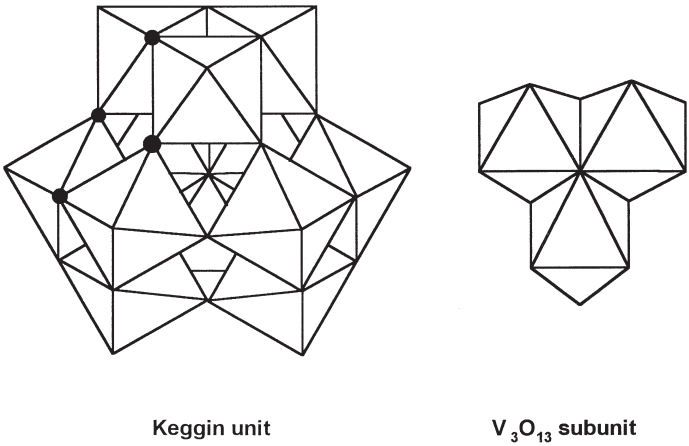

FIG. 8. Polyhedral representation of the Keggin structure (central tetrahedral atom not shown). The lines seen in the center are the edges of the V_3O_{13} subunit at the back (cf. also Fig. 21). Black dots indicate where one of the two five-coordinate capping units are attached in $[V_{15}O_{42}]^{9-}$.

$[V_{10}O_{28}]^{6-}$ from which it can be built by adding three more octahedra in the most compact way (*49*).

b. Pentadecavanadate A pentadecavanadate, $[V_{15}O_{42}]^{9-}$, the largest isopolyvanadate(V) to date, was isolated from a vanadate(V) solution but prepared by the reaction of H_2O_2 with $VOSO_4 \cdot 4H_2O$ and crystallized as the tetramethyl ammonium salt $[(CH_3)_4N]_3[H_6V_{15}O_{42}] \cdot 2.5H_2O$. It represents the first polyvanadate with the metal ion exhibiting three different coordination numbers (*50*). The structure is that of the well-known Keggin unit with two additional five-coordinate terminal VO units capping the pits on either side of the Keggin unit that lie on the C_2 axis (cf. Fig. 8). The "heteroatom" is a four-coordinate VO_4 unit. It is kinetically quite stable in water at pH ~3.5 but decomposes on boiling, forming $[V_{10}O_{28}]^{6-}$. The pentadecavanadate is compatible with water unlike either the compact tridecavanadate, $[V_{13}O_{34}]^{3-}$, described above or the $[V_{12}O_{32}]^{4-}$ polyvanadate, which had been obtained as an inclusion complex $[CH_3CN \subset (V_{12}O_{32}^{4-})]$ by precipitation with diethyl ether in acetonitrile solution (*51*).

c. Pentavanadate This $[V_5O_{14}]^{3-}$ ion has been obtained as a tetrabutylammonium salt in CH_3CN (*52*). X-ray analysis of the crystalline compound revealed the presence of discrete $[V_5O_{14}]^{3-}$ anions which each contain five tetrahedral vanadium(V) centers in a nearly trigonal–bipyramidal arrangement.

An empirical correlation has been developed for relating Raman stretching frequencies of vanadium–oxygen bonds to their bond lengths in a number of reference compounds. Together with bond strength and bond length relationships the empirical correlation provides a method for determining the coordination and bond lengths for vanadates (*53*).

III. Molybdate(VI)

A. Mononuclear Species

The molybdate ion, $[MoO_4]^{2-}$, is a weaker base than $[VO_4]^{3-}$ and protonation starts at pH $\gtrsim$7. Acidification of molybdate leads to protonation and condensation reactions. At very low molybdate concentration ($<10^{-4}\,M$) mononuclear species predominate. The protonation equilibria of the mononuclear species can be represented by the equations

$$[MoO_4]^{2-} + H^+ \overset{K_1}{\rightleftharpoons} [HMoO_4]^- \tag{23}$$

$$[HMoO_4]^- + H^+ + 2\,H_2O \overset{K_2}{\rightleftharpoons} MoO_3(H_2O)_3 \tag{24}$$

$$MoO_3(H_2O)_3 + H^+ \overset{K_3}{\rightleftharpoons} [MoO_2(OH)(H_2O)_3]^+ \tag{25}$$

$$[MoO_2(OH)(H_2O)_3]^+ + H^+ \overset{K_4}{\rightleftharpoons} [MoO_2(H_2O)_4]^{2+}. \tag{26}$$

An increase in the coordination number of molybdenum takes place in the second protonation step, which has a dramatic effect on the value of K_2. Instead of the typical decrease of 3 to 5 log units from the first to the second protonation constant, K_2 has in this case about the same value as K_1. In fact, these unusual values for the protonation constants compared to those of other oxyanions, along with the thermodynamic parameters ΔH° and ΔS°, were the basis on which the change in coordination number in the second protonation step was first proposed (*54*). Previously the small difference between the first and second pK value was interpreted in terms of an anomalously high first protonation constant, assumed to be caused by an increase in the coordination number in the first step (*2*, *3*, *54–57*).

The entropy and enthalpy changes for the first protonation are typical for protonation reactions, but in the second protonation step both

TABLE V

EQUILIBRIUM CONSTANTS AND THERMODYNAMIC QUANTITIES FOR THE PROTONATION OF $[MoO_4]^{2-}$ AT 25°C (*54*, *63*)

Reaction	I	log K	ΔH (kJ/mol)	ΔS (J/mol K)
$MoO_4^{2-}/HMoO_4^-$	1.0[a]	3.47	22 ± 2	143 ± 6
$HMoO_4^-/MoO_3(H_2O)_3$	1.0[a]	3.74	−47 ± 3	−85 ± 9
$MoO_3(H_2O)_3/MoO_2(OH)(H_2O)_3^+$	3.0[b]	1.05	6 ± 1	40 ± 8

[a] Medium 1.0 *M* NaCl.
[b] Medium 3.0 *M* $NaClO_4$.

the relatively large favorable enthalpy and unfavorable entropy changes are unusual (Table V). The favorable enthalpy change is due to the extra bond energy emanating from the increase in coordination number of molybdenum while the decrease in entropy is seen as the result of the uptake of the two water molecules (*54*, *58*). The almost similar values of K_1 and K_2 has the effect that $[HMoO_4]^-$ never reaches a higher percentage concentration than ~30% as shown in Fig. 9.

To indicate six-coordination the neutral monomeric molybdic acid is sometimes formulated as $Mo(OH)_6$, but the alternative formulations $MoO_2(OH)_2(H_2O)_2$ or $MoO_3(H_2O)_3$ are most likely closer to the truth (*58–60*); the latter formulation is used in this chapter. An interesting linear relationship has been found (*61*) between values of the known first protonation constants of the oxoanions of groups 5, 6, and 7 and

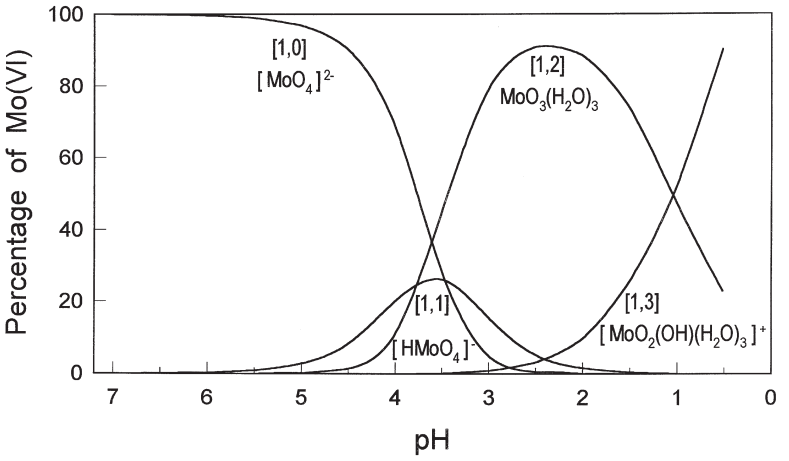

FIG. 9. Distribution of mononuclear molybdenum(VI) species as a function of the pH calculated from constants given in Table V.

the charge function z^2/r^2 (z is the charge of the oxoanion and r is the ionic radius of the metal). A similar plot for the second protonation constants shows a marked departure from linearity in the case of molybdenum and tungsten, an observation that would be in accordance with an expansion of tetrahedral to octahedral coordination of these elements in the second protonation step.

Information about the possible structures of molybdate and its protonated forms in solution has been obtained from molecular orbital calculations (*62*). By considering bond orders obtained from a Mulliken population analysis and the agreement between experimental and theoretical UV spectra it was concluded that $[MoO_4]^{2-}$ and $[HMoO_4]^-$ are tetrahedral and that the neutral acid is octahedral. For the latter a somewhat distorted octahedral structure based on the formula $MoO_2(OH)_2(H_2O)_2$ was proposed (*62*). The alternative structure $MoO_3(H_2O)_3$ was not taken into account in the calculations.

Further protonation of the neutral acid to form the cation $[(MoO_2(OH)(H_2O)_3]^+$ starts at pH ~2.5, a reaction which is completed at an acid concentration of about 1 *M* (*63–65*). Thermodynamic quantities determined for this reaction in 3.0 *M* $NaClO_4$ are typical of a normal protonation reaction (Table V). At higher acid concentration the doubly charged cation begins to form but evaluation of the protonation constant at constant ionic strength is hardly possible. By accounting for the effect on activity coefficients under conditions of varying ionic strength (using a computer program SPECA) a p$K = -2.82$ for $[MoO_2(H_2O)_4]^{2+}$ was calculated from spectrophotometric data; the corresponding pK value for the singly charged cation $[MoO_2(OH)(H_2O)_3]^+$ was found to be equal to -1.16 (*66*). The presence of $[MoO_2(H_2O)_4]^{2+}$ in a strong acid solution has also been indicated by X-ray absorption spectra (*67*).

B. Dinuclear Cationic Species

At high acid concentration, particularly in perchloric acid medium, molybdenum(VI) shows a strong tendency to dimerize (*68–71*). The value for the dimerization constant of the cation $[MoO_2(OH)(H_2O)_3]^+$ in 3.0 *M* $Na(H)ClO_4$ medium has been determined, $K = 97 \pm 15$ (*71*).

$$2\,[MoO_2(OH)(H_2O)_3]^+ \rightleftharpoons [Mo_2O_5(H_2O)_6]^{2+} + H_2O. \qquad (27)$$

The dimerization reaction is fast and has been studied by the temperature-jump method (*70*). At 25°C and ionic medium 3.0 *M* $LiClO_4$ the

rate constants have been determined as $k_f = 1.71 \times 10^5\, M^{-1}s^{-1}$ and $k_b = 3.2 \times 10^3\ s^{-1}$.

Values for a conditional dimerization constant in 1 *M* $LiClO_4$ at acid concentrations 0.1, 0.5, and 1.0 *M* $HClO_4$ have been determined at three different temperatures (*72*). The conditional constant which represents the equilibrium between all mononuclear and all dinuclear species at a particular hydrogen ion concentration increases with decrease in temperature. Dimerization is also strongly promoted by an increase in ionic strength. The value of the conditional constant, pertaining to 1.0 *M* acid, almost doubles (64 to 114) when the ionic strength is increased from 1.0 to 3.0 *M* (*71*, *72*). In 2.0 *M* CF_3SO_3H values for the dimerization constant at 25 and 50°C were determined as 400 and 270 respectively (*59*).

The ionization and protonation equilibria for the doubly charged dimer have been determined in 3.0 *M* $NaClO_4$ medium but the values for these equilibrium constants can be expected to be affected by the great changes in ionic medium required (*71*)

$$[Mo_2O_5(H_2O)_6]^{2+} \leftrightharpoons [Mo_2O_5(OH)(H_2O)_5]^{+} + H^{+} \tag{28}$$

$$[Mo_2O_5(H_2O)_6]^{2+} + H^{+} \leftrightharpoons [Mo_2O_4(OH)(H_2O)_6]^{3+}. \tag{29}$$

The values for the ionization and protonation constants (0.21 and 0.24 respectively) indicate that $[Mo_2O_5(OH_2)_6]^{2+}$ is the major dimeric species in 1.0 *M* acid with about equal concentrations of the other two dimers. The dimeric cationic species show a characteristic absorption band in the UV at ~245 nm.

The $Mo_2O_5^{2+}$ moiety is not uncommon in molybdenum(VI) chemisty. Several dinuclear complexes having this unit have been identified in solution (*73*) and isolated in the solid state, e.g., oxalate $[Mo_2O_5(C_2O_4)_2(H_2O)]^{2-}$ (*74*), nitrilotriacetate $[Mo_2O_5(Hnta)_2]^{2-}$ (*75*), and citrate $[Mo_2O_5(cit)_2]^{6-}$ (*76*) complex ions. Structure determinations show two *cis* oxygen atoms for each molybdenum and a single oxygen bridge (*74–76*). Raman spectroscopy supports this structure for the dimeric cations in solution, the bands at ~950 and 920 cm^{-1} being assigned to the asymmetric and symmetric stretching vibrations of the *cis*-MoO_2 group. Broad bands near 820 and 840 cm^{-1} were assigned to the asymmetric and symmetric stretching vibrations of the oxobridge (*77*). Further confirmation of the structure in solution has been obtained from the analysis of extended X-ray absorption fine structure; the Mo–O–Mo bond angle is ~125° (*78*).

Dimeric anions such as $[Mo_2O_7]^{2-}$ does not occur in aqueous solution

but has been found to exist in the solid state (*79*), e.g., as the tetrabutyl ammonium salt $[n\text{-}(C_4H_9)_4N]_2[Mo_2O_7]$, and in nonaqueous solution from which $[Mo_7O_{24}]^{6-}$ is immediately precipitated by the addition of small amounts of aqueous solutions containing smaller cations such as Na^+, K^+, NH_4^+, and $[N(CH_3)_4]^+$. The anion consists of two MoO_4 tetrahedra sharing a vertex. The surprisingly stability of this anion relative to heptamolybdate in nonaqueous solution has been ascribed to the presence of specific (large) counter ions.

In an equilibrium study of the adsorption of molybdenum(VI) from aqueous solution onto activated carbon it has been found that the data are best explained in terms of an absorption model comprising the three species $[HMo_2O_7]^-$, $MoO_3(H_2O)_3$, and $[HMoO_4]^-$ of which the dimer predominates by far (*80*). Computer treatment of potentiometric (*81*) and spectrophotometric data (*82*) also indicated the possible existence of $[HMo_2O_7]^-$ as a minor species in aqueous solution at low molybdenum concentration ($\sim 2 \times 10^{4-} M$). However, as its assumed stability region overlaps with several other polynuclear ions more direct evidence is needed before its existence can be accepted with certainty.

C. Polyoxoanions

Although the mechanism for the formation of polyanions is not clear it is generally accepted that the process is governed by the ability of $[MoO_4]^{2-}$ to expand its coordination sphere from four to six. The polyanions normally consist of MoO_6 octahedra, which are assembled by sharing edges and vertices. The metal ions then do not lie at the center of the octahedra but are displaced toward a corner or an edge due to Mo–O π-bonding. The resulting shorter Mo–O bonds are directed to the exterior of the polyanion (*2*).

Numerous investigations have shown the existence of the heptamolybdate, $[Mo_7O_{24}]^{6-}$, and octamolybdate, $[Mo_8O_{26}]^{4-}$, ions in aqueous solution. Potentiometric measurements with computer treatment of the data proved to be one of the best methods to obtain information about these equilibria. Stability constants are calculated for all species in a particular reaction model, which is supposed to give the best fit between calculated and experimental points. In the calculations the species are identified in terms of their stoichiometric coefficients as described by the following general equation for the various equilibria

$$p[MoO_4]^{2-} + qH^+ \leftrightharpoons [(MoO_4^{2-})_p(H^+)_q]^{(q-2p)-}.$$

For convenience these species are often represented by $[p, q]$ and the overall formation constants denoted by β_{pq}. The degree of protonation of a particular species is given by the ratio q/p. The average degree of protonation of all species in solution, Z, is defined as

$$Z = (C_H - [H^+])/C_{Mo},$$

where C_H and C_{Mo} are the analytical concentrations of acid and molybdate respectively.

Reaction models and values for stability constants obtained by different research groups, under the same conditions, generally do not differ too much from one another (Table VI). In fact, the equilibrium constants mostly agree remarkably well, e.g., the values obtained for $\log \beta_{7,8}$ in 3.0 $NaClO_4$ are 57.74 (*83*) and 57.70 (*84*) and in 1.0 *M* NaCl 52.80 (*85*) and 52.77 (*86*). Such results clearly show that the proposed models are based on reliable and reproducible data. The heptamolybdate ion $[Mo_7O_{24}]^{6-}$ and its protonated forms as well as the octamolybdate ion $[Mo_8O_{26}]^{4-}$ are included in most models (*5*, *81–89*). Whereas in some models $[H_3Mo_7O_{24}]^{3-}$ is preferred to $[Mo_8O_{26}]^{4-}$ (*83*, *89*) both these polyanions are included in some other models (*81*, *87*), but it is an open question whether the potentiometric method can discriminate unambiguously between species with an almost similar degree of protonation and comparable p and q values. Because of the limitations of potentiometry at low pH, measurements are usually restricted to pH $\lesssim$2 for which the degree of protonation Z $\lesssim$1.5. Also, inevitable overlap with the next equilibrium at the cutoff point could result in a less conclusive characterization of the species occurring at the lowest pH. Acidification to Z $\gtrsim$1.5 leads to the formation of larger polyanions of which the Mo_{36} ion is the most probable at high concentration (cf. discussion below). At lower molybdenum concentration there is evidence for the existence of an Mo_{18} ion. At still higher acid concentration these ions become unstable and the dimeric cations described above are formed.

The ionic medium has a considerable effect on the stability of polyanions, e.g., the stability constant of the heptamolybdate ion, $\log \beta_{7,8}$, increases from 52.8 to 57.7 when the ionic medium is changed from 1 *M* NaCl to 3 *M* $NaClO_4$ (Table VI). At lower ionic strength larger polyanions appear to be less stable, an effect which is similar to lowering the total molybdate concentration, and competing smaller polyanions, e.g., dimers, trimers, and so on, could therefore have a better chance to coexist in small quantities (*81*). Depending on how the stability of particular ions are affected by the chosen ionic medium some

TABLE VI

FORMATION CONSTANTS OF SPECIES IN SOME REACTION MODELS AS DETERMINED BY POTENTIOMETRY IN DIFFERENT IONIC MEDIA AT 25°C

[*p*, *q*]	Formula	3 *M* $NaClO_4$	3 *M* $NaClO_4$	1 *M* NaCl				1 *M* KNO_3	0.6 *M* $NaClO_4$
[1, 1]	$[HMoO_4]^-$	4.00	3.89	3.51	3.53	3.55	3.55	3.92	3.39
[1, 2]	$MoO_3(H_2O)_3$	7.50	7.50	7.40	7.26	7.30	7.22	8.09	7.35
[7, 8]	$[Mo_7O_{24}]^{6-}$	57.70	57.74	53.01	52.80	52.77	52.81	52.49	52.42
[7, 9]	$[HMo_7O_{24}]^{5-}$	62.14	62.14	57.53	57.42	57.52	57.40	57.57	57.23
[7, 10]	$[H_2Mo_7O_{24}]^{4-}$	65.60	65.68	61.09	60.84	60.84	60.97	61.33	60.78
[7, 11]	$[H_3Mo_7O_{24}]^{3-}$	68.34	68.21	63.47	—	—	63.03	64.96	—
[8, 12]	$[Mo_8O_{26}]^{4-}$	76.49	—	—	71.56	71.70	71.19	73.18	71.62
[8, 13]	$[HMo_8O_{26}]^{3-}$	—	—	—	—	—	73.07	—	73.38
[8, 15]	$[H_3Mo_8O_{26}]^-$	—	—	—	—	—	—	—	76.34
[10, 12]	$[Mo_{10}O_{34}]^{8-}$	—	—	—	—	—	—	79.15	—
[19, 34]	—	—	196.3	—	—	—	—	—	—
[2, 5]	$[Mo_2O_5(OH)(H_2O)_5]^+$		~19	—	—	—	—	—	—
[36, 34]	$[Mo_{36}O_{112}(H_2O_{16}]^{8-}$	—	—	—	—	—	346.5	—	—
		$Z \leq 1.5$	$Z \leq 1.8$	—	$Z \leq 1.6$	$Z \leq 1.5$	$Z \leq 1.6$	$Z < 1.5$	$Z \leq 1.7$
C_{Mo} in m*M*		2.5–160	0.3–160	—	1.25–80.0	0.5–100	1.25–80.0	0.8–33.6	1.25–80.0
Reference		*84*	*83*	*89*	*85*	*86*	*87*	*61*	*88*

variation in the proposed reaction models is to be expected. In the model proposed for 0.6 *M* NaCl medium the octamolybdate and two of its protonated forms are preferred to the triply protonated heptamolybdate, $[H_3Mo_7O_{24}]^{3-}$, found in 3.0 *M* $NaClO_4$ (Table VI) (*88*).

Although these reaction models give excellent descriptions of the system under particular conditions and are therefore quite satisfactory to account for free molybdenum(VI) in studies of complex formation, for example (*73*, *84*, *88*), some uncertainties still prevail. There is often little to choose between alternative models because the addition of a new species to a model, or the replacement of a particular species by one or two others, can have only a marginal improvement of the fit as has been shown by the authors themselves (*61*, *85*, *86*, *90*) or by others in subsequent recalculations (*81*, *87*, *90*, *91*).

Various other methods have therefore been employed in an attempt to identify species more directly. An equilibrium study based on the change in the UV spectra of acidified molybdate solutions in 1.0 *M* NaCl medium showed that the data can be satisfactorily explained in terms of a reaction model including $[Mo_7O_{24}]^{6-}$, $[HMo_7O_{24}]^{5-}$, $[H_2Mo_7O_{24}]^{4-}$, and $[Mo_8O_{26}]^{4-}$ (*82*). However, due to the many unknown parameters (equilibrium constants and spectra) to be calculated a totally independent evaluation of the data was not possible.

Raman spectroscopy has been used by several authors as an indentification method by comparing spectra of solutions with spectra of solid phases of known structure (*85*, *92–95*). The heptamolybdate could be clearly identified (cf. below) and its spectrum in the solid state and aqueous solution is well characterized (*93*, *94*). Other polyanions seem to be more difficult to identify because overlapping equilibria tend to conceal small changes in the spectrum upon acidification.

Results of X-ray scattering measurements on series of 2.0 *M* Li_2MoO_4 solutions acidified in the range Z = 0 to 1.5 are consistent with $[Mo_7O_{24}]^{6-}$ being the dominant polymolybdate species in solutions with Z = 1.14. Changes in the radial distribution curves with further acidification to Z = 1.5 indicated the formation of a polymolybdate with a different structure most likely $[Mo_8O_{26}]^{4-}$ with the β-structure (*90*). Raman spectra strongly supported the results of the scattering measurements that the predominant complex at Z = 1.14 is the heptamolybdate ion with the structure as determined from single crystal investigations (*96*). Replacement of Li^+ ions by Na^+ ions did not make a significant change to the spectrum of a solution containing $[Mo_7O_{24}]^{6-}$. This result was confirmed in another Raman spectroscopical investigation of solutions in the range Z <1.14 for molybdate con-

centrations 0.02 to 2 *M* in various ionic media (up to 3.0 *M*) with different cations, i.e. Li^+, Na^+, K^+, NH_4^+, and Mg^{2+}. Spectra showed the formation of only $[Mo_7O_{24}]^{6-}$ under these conditions and also indicated that these cations do not have a special stabilizing effect on other possible species (*92b*).

The existence of the large polyanion $[Mo_{36}O_{112}(H_2O)_{16}]^{8-}$ at low pH (*ca.* 1) in addition to $[Mo_7O_{24}]^{6-}$ has been indicated by Raman measurements (*92a*, *92c*, *95*) and confirmed by light and X-ray scattering results (*95*).

Factor analysis (*97*) of Raman spectra of molybdate solutions in the pH range of 7.2–2.1 in 3.0 *M* $LiClO_4$ revealed four factors, three of which could be identified (by comparison with the solids $Na_2[MoO_4] \cdot 2H_2O$, $(NH_4)_6[Mo_7O_{24}] \cdot 5H_2O$, and $(NH_4)_4[Mo_8O_{26}] \cdot 5H_2O$) as being the spectra of $[MoO_4]^{2-}$, $[Mo_7O_{24}]^{6-}$, and $[Mo_8O_{26}]^{4-}$. The fourth factor has been interpreted as originating from the protonated heptamolybdate $[HMo_7O_{24}]^{5-}$. Values for the formation constants could be calculated from these data, $\log \beta_{78} = 53.18 \pm 0.25$ (56.04), $\log \beta_{79} = 56.0 \pm 0.14$ (60.70), and $\log \beta_{8,12} = 69.73 \pm 0.23$ (75.31), but these values do not agree particularly well with those reported previously for the same ionic medium (given in parentheses, from Table VI). The deviations possibly indicate that an important species has been neglected in the data treatment.

In a recent investigation (*98*) seven different polyoxomolybdate compounds (cf. next section) had been prepared, their Raman spectra measured and compared with those of molybdate solutions (0.1 *M*) over the pH range 8.4 to 0.50. The following sequence of polyanions were proposed: $[MoO_4]^{2-}$, $[Mo_7O_{24}]^{6-}$ (pH = 6–4), $(Mo_3O_{10}^{2-})_\infty$ (pH = 5–3.5), α-$[Mo_8O_{26}]^{4-}$ (pH = 5–2), β-$[Mo_8O_{26}]^{4-}$ (pH = 4–1.5), and $[Mo_{36}O_{112}(H_2O)_{16}]^{8-}$ (pH = 0.5–1.5). Although the identification of $(Mo_3O_{10}^{2-})_\infty$ and α-$[Mo_8O_{26}]^{4-}$ could be questioned (the latter on the grounds of infrared spectroscopic data (*37*)) the results indicate the existence of two intermediates between the well-characterized $[Mo_7O_{24}]^{6-}$ and β-$[Mo_8O_{26}]^{4-}$. The occurrence in solution of appreciable amounts of $[Mo_6O_{19}]^{2-}$ and γ-$[Mo_8O_{26}]^{4-}$ was ruled out.

The application of ^{17}O NMR spectroscopy to obtain structural information about polyoxoanions, mainly in nonaqueous solution, had been examined and discussed in detail (*99*). A very useful finding was that chemical shifts are determined largely by metal–oxygen bond strengths. An inverse correlation exists between the ^{17}O shift and the shortest bond length to a given metal. In aqueous solution the existence of $[Mo_7O_{24}]^{6-}$ could be confirmed by the use of ^{17}O and ^{99}Mo NMR spectroscopy (*100–104*). Evidence for the existence of the three

anions, $[Mo_7O_{24}]^{6-}$, $[Mo_8O_{26}]^{4-}$, and $[Mo_{36}O_{112}(H_2O)_{16}]^{8-}$, was also obtained by using ^{95}Mo and ^{17}O and Raman spectroscopy conjointly (*103*). A ^{99}Mo and ^{17}O NMR study of aqueous molybdate solutions between pH 6 and 1.2 in 2.0 *M* $LiClO_4$ medium led to the identification of $[Mo_7O_{24}]^{6-}$, its monoprotonated form $[HMo_7O_{24}]^{5-}$, and β-$[Mo_8O_{26}]^{4-}$ (*104*). Possible sites for protonation of $[Mo_7O_{24}]^{6-}$ were identified (Fig. 10) as the triply bridged oxygens shared by octahedra D, A, and B or D, F, and G (*104*). The existence of $[H_2Mo_7O_{24}]^{4-}$ seems improbable, but strong evidence was found for the presence of another species occurring between $[HMo_7O_{24}]^{5-}$ and $[Mo_8O_{26}]^{4-}$, probably another octamolybdate, namely $[H_3Mo_8O_{28}]^{5-}$. This species is the most ready to undergo oxygen exchange. The structure is likely to be that of the $[H_2Mo_8O_{28}]^{6-}$ anion (*105*). A scheme proposed for the transformation

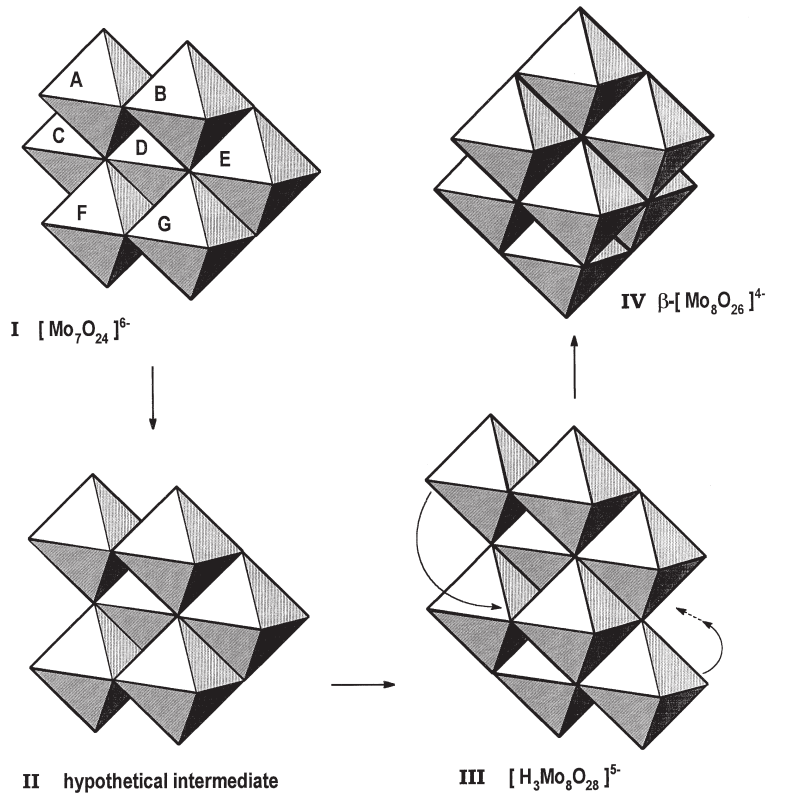

FIG. 10. Proposed scheme for the conversion of $[Mo_7O_{24}]^{6-}$ and $[HMo_7O_{24}]^{5-}$ via a hypothetical intermediate first to $[H_3Mo_8O_{28}]^{5-}$ and finally to $[Mo_8O_{26}]^{4-}$. (Adapted with permission from Howarth, O. W., Kelly, P. *J. Chem. Soc. Dalton Trans.* **1990,** 81–84.)

of heptamolydate to β-octamolybdate is shown in Fig. 10. One of the seven octahedra in $[Mo_7O_{24}]^{6-}$ (structure (**I**)), namely C or E, becomes labile on acidification (*106*). Three long Mo–O bonds are broken and the resulting MoO_4 tetrahedron detaches on further acidification, giving structure (**II**) in an unknown state of protonation. Structure (**II**) is not known in the solid state and it may exist only as a putative intermediate on the way to structure (**III**). By folding in of two labile octahedra (indicated by arrows) structure (**III**) can become structure (**IV**), i.e. β-$[Mo_8O_{26}]^{4-}$. The ^{17}O NMR results at pH ~1 were found to be roughly consistent with the $[Mo_{36}O_{112}(H_2O)_{16}]^{8-}$ ion and also with one half of this virtually dimeric structure, presumably $[Mo_{18}O_{56}(H_2O)_8]^{4-}$. It seems as if these new results cast doubt on some of the species in "well-accepted" reaction models described above, in particular the protonated heptamers $[H_2Mo_7O_{24}]^{4-}$ and $[H_3Mo_7O_{24}]^{4-}$.

The stability of the hexamolydate ion $[Mo_6O_{19}]^{2-}$ in nonaqueous media was exploited in a solvent extraction study (*107*) to obtain information about the nature of polyanions occurring at low pH. The distribution data was compatible with the presence in the aqueous phase (pH 1.0 and 1.34) of $[Mo_{36}O_{112}(H_2O)_{16}]^{8-}$ and of another large polyanion (pH 1.34–2.0) assumed to be $[Mo_{18}O_{56}]^{4-}$. The values obtained for the formation constants of these ions in 1 *M* $NaClO_4$, $\log \beta_{18,32} = 172.0 \pm 0.5$ and $\log \beta_{36,64} = 345.5 \pm 1.0$ (*107c*), agree well with those determined by potentiometry in 1.0 *M* NaCl (*81*).

Thermochemical investigations of molybdate solutions have been carried out and reaction heats were measured (*108*, *109*). As the interpretation of calorimetric data depends heavily on the correct reaction model, progress in determining reliable enthalpy and entropy changes for condensation reactions have been hampered. However, since there is little doubt that $[Mo_7O_{24}]^{6-}$ is the first polyanion which forms on acidification, the enthalpy and entropy changes obtained for its formation should be meaningful. The values for Eq. (30) are $\Delta H^\circ = -234.3 \pm 0.8$ kJ/mol and $\Delta S^\circ = 318 \pm 4$ J/mol K in 3.0 *M* $NaClO_4$ (*108*)

$$7\,[MoO_4]^{2-} + 8\,H^+ \leftrightharpoons [Mo_7O_{24}]^{6-} + 4\,H_2O. \qquad (30)$$

Other values for the enthalpy change of this reaction in different ionic media, obtained directly from titration curves, are −230.5 kJ/mol (3.0 *M* $NaClO_4$) and −237.2 kJ/mol (2.0 *M* NaCl) (*109*). All these values show good agreement and indicate that the enthalpy change for this reaction is little affected by the change in ionic medium. Judged from these values the considerable difference between the values for

the formation constant of heptamolybdate in 1.0 *M* NaCl (log $\beta_{7,8}$ = 52.8) and 3.0 *M* $NaClO_4$ (log $\beta_{7,8}$ = 57.7) must to some extent be entropy related. It is also clear that the enthalpy change is the major driving force for the condensation reaction ($\Delta H^o = -234.3$ and $T\Delta S^o$ = 94.8 kJ/mol at 25°C). A substantial amount of this favorable enthalpy change can be expected to arise from additional bond energy due to the expansion of the coordination spheres from four to six of the seven molybdenums.

From the above it can be concluded that in aqueous solution the existence of only $[Mo_7O_{24}]^{6-}$, $[HMo_7O_{24}]^{5-}$, $[Mo_8O_{26}]^{4-}$, and $[Mo_{36}O_{112}(H_2O)_{16}]^{8-}$ (at high concentrations) has been proved with sufficient certainty. The current state of knowledge is summarized in the diagram in Fig. 11.

1. Structures of Polyoxoanions Obtained in the Solid State

Counter ions play a decisive role in the isolation of polyoxoanions. Ions occurring in negligible amounts in solution such as $[Mo_6O_{19}]^{2-}$ can be precipitated from aqueous solution with the cation $[(C_4H_9)_4N]^+$ while major species remain in solution. Different ions can be isolated at the same pH by using different cations. Conditions favorable for the precipitation of some polymolybdates from aqueous solution with the cations NH_4^+, $[(NH_2)_3C]^+$, $[(CH_3)_4N]^+$, and $[(n\text{-}C_4H_9)_4N)]^+$ have been determined (*98*). The polyions isolated with these and some other cations are listed in Table VII. Most of these polyions have been structurally characterized.

The structure of the heptamolybdate ion is well established (*96*). The structure in aqueous solution is the same as in the solid state (*93, 94*) (Fig. 10).

Depending on the counter ion and conditions three different structural types of the octamolydate $[Mo_8O_{26}]^{4-}$ can be isolated from aqueous solution, namely α- (*110*, *111*), β- (*112*), and γ-structures (*113*). Raman and infrared spectra of the three isomers have been reported (*98*). As described in the previous section, only the β-octamolybdate has been shown with certainty to be a major species in aqueous solution. It is built up of eight octahedra and can be viewed as two layers of four octahedra (Fig. 10) or in an upright position (Fig. 12) as a sequence of two, four, and two octahedral building blocks. It cannot be obtained by just adding another octahedron to the heptamolydate structure. The β-structure has been isolated with a variety of cations. It has been shown that the degree of distortion of the octahedra increases with the size of the cation, which ultimately could lead to the formation of the α-structure (*114*). The α-structure has been obtained

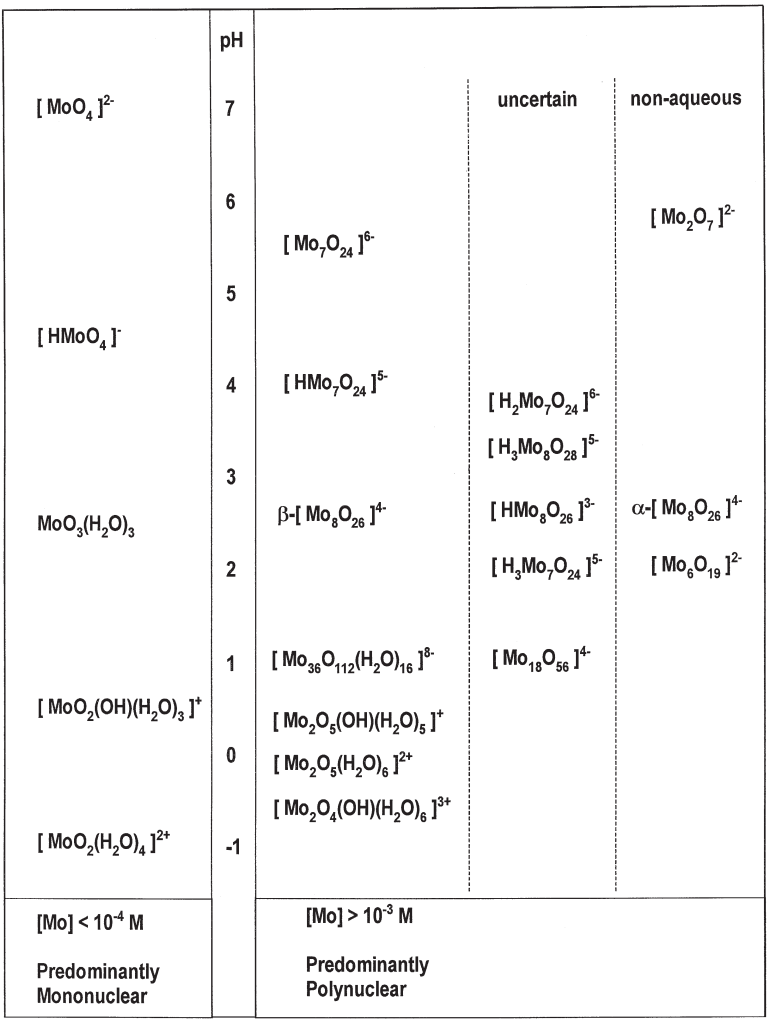

FIG. 11. Diagrammatical representation of mono- and polynuclear species. Species that might exist only under special conditions or those of doubtful existence are given in the "uncertain" column.

with only a couple of large cations, tetrabutylammonium, $[(C_4H_9)_4N]^+$, and propyl triphenylphosphonium, $[P(C_3H_7)Ph_3]^+$ (*110*, *111*).

The α- and γ-structures differ from the β-structure in that the former do not consist only of octahedra; the α-structure has two four-coordinate and the γ-structure two five-coordinate molybdenums. The α-octamolybdate consists of a planar ring of six edge-shared MoO_6

TABLE VII

POLYOXOANIONS ISOLATED IN THE SOLID STATE FROM AQUEOUS SOLUTION WITH VARIOUS COUNTERIONS

Polyoxoanion	Counterion[a]	~pH	References
$[Mo_7O_{24}]^{6-}$	NH_4^+, K^+, Na^+, $[(NH_2)_3C]^+$, $[(CH_3)_4N]^+$, $(H_3dien)^{3+}$[b]	5–6	(*96*, *98*, *112j*)
α-$[Mo_8O_{26}]^{4-}$	$[n\text{-}(C_4H_9)_4N]^+$, $[n\text{-}(C_3H_7)(C_6H_5)_3P]^+$,	2–6	(*98*, *110*, *111*)
β-$[Mo_8O_{26}]^4$	NH_4^+, $[(CH_3)_4N]^+$, $[n\text{-}(C_4H_9)_4N]^+$, $[NH_2(CH_3)_2]^+$, $[C_5H_9N_2]^+$	2–5 —	(*98*, *112*, *115*)
γ-$[Mo_8O_{26}]^{4-}$	$[(CH_3)_3N(CH_2)_6N(CH_3)_3]^{2+}$	6	(*113*)
$[Mo_6O_{19}]^{2-}$	$[(n\text{-}C_4H_9)_4N]^+$ $[HN_3P_3\{N(CH_3)_2\}_6]^+$ $[(C_6H_5)_4As]^+$	1.0	(*122*, *123*) (*130*)
$[Mo_{10}O_{34}]^{8-}$	NH_4^+	—	(*117*)
$([Mo_3O_{10}]^{2-})_\infty$	K^+ Rb^+	4.0	(*119*, *120*)
$[Mo_{36}O_{112}(H_2O_{16})]^{8-}$	$[(CH_3)_4N]^+$, NH_4^+, K^+ Na^+	1.0	(*98*, *116*)
$([Mo_8O_{27}]^{6-})_\infty$	NH_4^+	—	(*118*)
$[H_2Mo_8O_{28}]^{6-}$	$C_3H_{10}N^+$	—	(*105*)
$[HMo_5O_{17}]^{3-}$[c]	$[(n\text{-}C_4H_9)_4N]^+$	—	(*127*)
$HMo_5O_{16}(H_2O)]_\infty^-$	Na^+, K^+, NH_4^+	—	(*129*)
$[Mo_2O_7]^{2-}$[c]	$[n\text{-}(C_4H_9)_4N]^+$	—	(*79*)

[a] For a more extensive list of counterions for $[Mo_7O_{24}]^{6-}$, β-$[Mo_8O_{26}]^{4-}$, and $[Mo_6O_{19}]^{2-}$; see (*4*).

[b] $(H_3dien)^{3+} \equiv$ diethylenetriammonium.

[c] Obtained in acetonitrile solution.

octahedra capped above and below by two MoO_4 tetrahedra (Fig. 12). The γ-structure is composed of six MoO_6 octahedra interlinked along edges and two MoO_5 trigonal bipyramids each sharing two edges with the octahedra. The γ-$[Mo_8O_{26}]^{4-}$ is of interest because it has been postulated as an intermediate (~15 years before its isolation) to explain the rapid isomerization of the α- and β-structures in acetonitrile (*115*). The γ-octamolybdate does not occur in measurable amounts in aqueous solution but it can be obtained by acidification of molybdate in the presence of the hexamethonium cation $[(CH_3)_3N(CH_2)_6N(CH_3)_3]^{2+}$. It crystallizes at pH ~6, where the heptamolybdate is the predominating polynuclear species. The α- and β-forms are usually crystallized from an aqueous solution acidified to pH 3–4, the product obtained depending on the cation employed (*115*).

The very large Mo_{36} polyanion is crystallized at very low pH (Z ~1.8 to 2) (*116*). The structure of the potassium salt $K_8[Mo_{36}O_{112}(H_2O)_{16}] \cdot 36H_2O$ has been determined by X-ray crystallography. It actually consists of two 18-molybdate subunits which combine via four common oxygen atoms (*116b*).

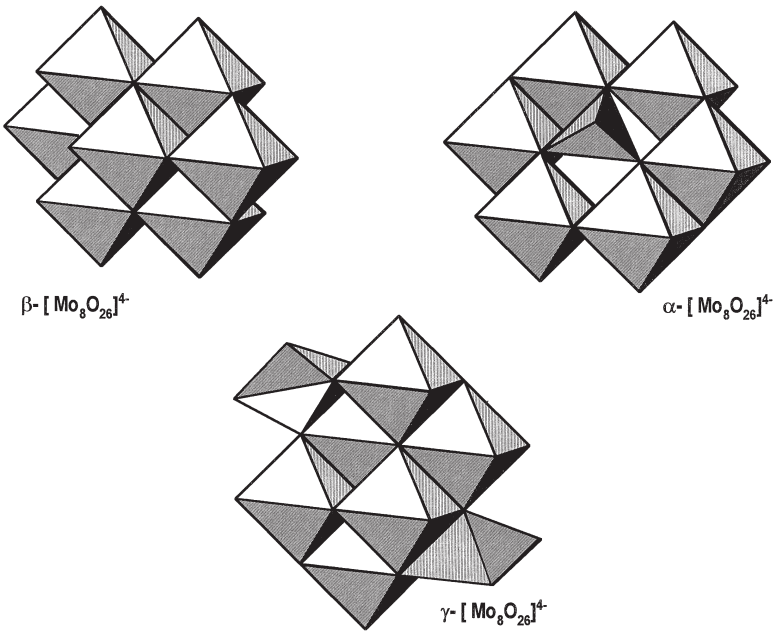

FIG. 12. Polyhedral representation of structures of octamolybdates.

The decamolybdate anion $[Mo_{10}O_{34}]^{8-}$ is obtained in the solid state as the ammonium salt $(NH_4)_8[Mo_{10}O_{34}]$ by thermal decomposition of ammonium heptamolybdate or by crystallization at 80°C from aqueous molybdate solution, but it decomposes on dissolution. It consists of a Mo_8O_{28} unit of MoO_6 octahedra with an additional tetrahedron MoO_4 connected at a vertex at both ends (Fig. 13) (*117*). It was the first discrete isopolyanion known that contained both octahedral and tetrahedral units. This Mo_8O_{28} group has the same arrangement of octahedra as in the $[H_2Mo_8O_{28})]^{6-}$ anion, which was crystallized from aqueous solution with isopropylammonium as cation (*105*). This Mo_8O_{28} structure is also the same as the fundamental unit of the polymeric octamolybdate $(NH_4)_6[Mo_8O_{27}] \cdot 4H_2O$ (*118*). The octameric units are linked through a common oxygen atom, sharing a vertex, to give chains (Fig. 13).

The trimolybdates in the solid state are polymeric in nature (*119*, *120*). Two different structure types are obtained as the potassium and rubidium salts $K_2[Mo_3O_{10}]$ and $Rb_2[Mo_3O_{10}] \cdot H_2O$ shown in Fig. 14. The rubidium compound consists of a chain of MoO_6 octahedra, whereas the potassium compound comprises edge-shared distorted MoO_5 polyhedra and MoO_6 octahedra (*121*).

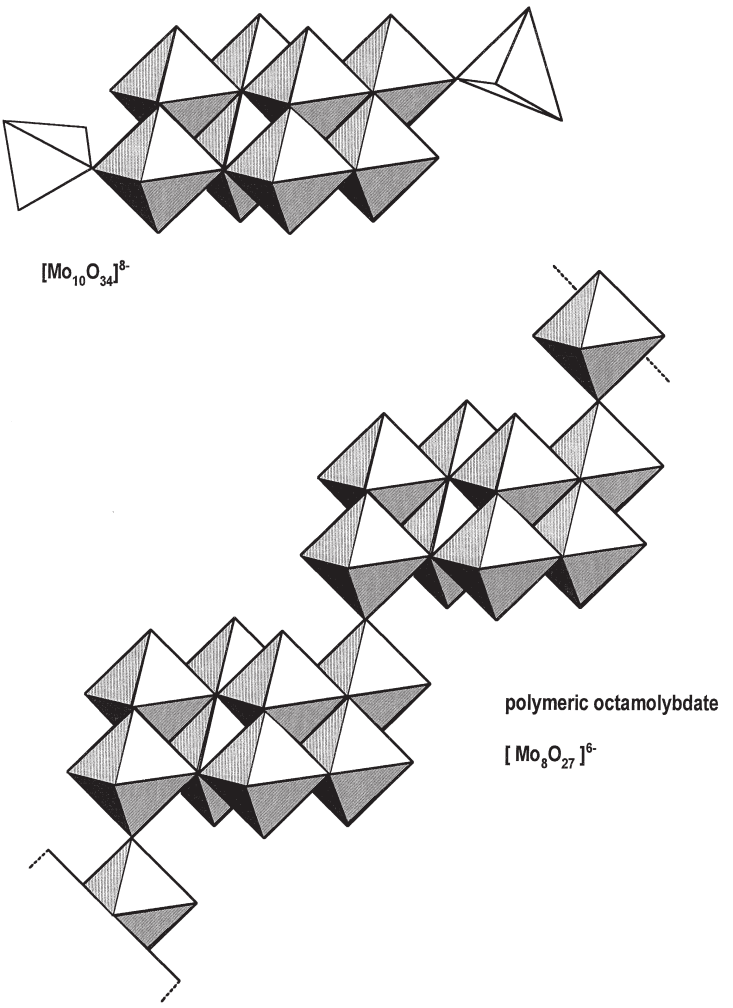

FIG. 13. Polyhedral representation of structures of $[Mo_{10}O_{34}]^{8-}$ and $[Mo_8O_{27}]^{6-}$.

An interesting polyanion is the yellow hexamolybdate ion $[Mo_6O_{19}]^{2-}$. Although it does not appear to exist in significant amounts in aqueous solution it was prepared for the first time by precipitation from aqueous solution as the tetrabutyl ammonium compound $[(C_4H_9)_4N]_2[Mo_6O_{19}]$ (*122*). The structure of the polyanion can be visualized as formed from six MoO_6 octahedra sharing a common vertex (*123*). The structure is very compact and can be seen as a fragment of the structure of the decavanadate ion $[V_{10}O_{28}]^{6-}$ from which it can be

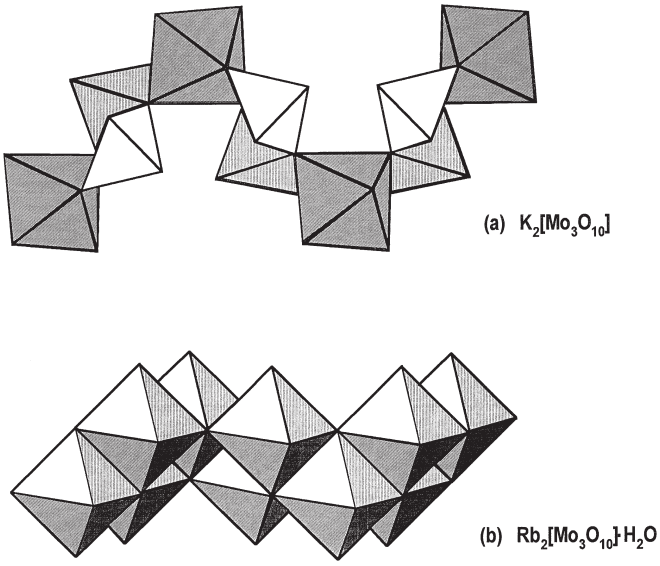

FIG. 14. Polyhedral representation of the different chain structures of the trimolybdates (a) $K_2[Mo_3O_{10}]$ and (b) $Rb_2[Mo_3O_{10}]\cdot H_2O$.

obtained by removing four octahedra (Fig. 15). The $[Mo_6O_{19}]^{2-}$ ion is quite stable in tri-*n*-butyl phosphate (TBP) into which it can be extracted from aqueous solution (*107*) and also in some other solvents, e.g. acetonitrile (*111*), propylene carbonate, and cyclohexanone (*124*, *125*). It can be stabilized in aqueous solution by the addition of large amounts of certain water-miscible solvents such as acetonitrile, acetone and ethanol (*126*). It is easily identified by three charateristic absorption bands in the UV at 222, 257, and 325 nm (*107a*). Due to the compact structure it has kinetic stability like decavanadate and

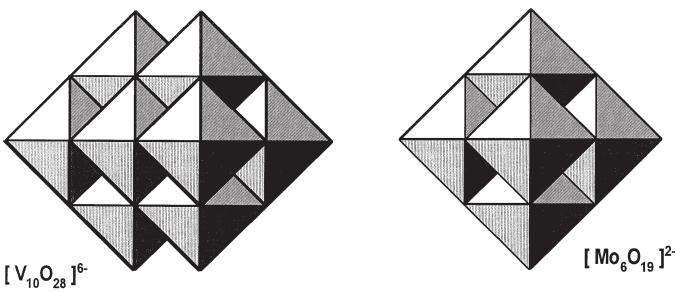

FIG. 15. Structure of $[Mo_6O_{19}]^{2-}$ viewed as a part of the $[V_{10}O_{28}]^{6-}$ structure.

needs several hours to decompose into molybdate after addition of alkali.

The pentamolybdate ion $[HMo_5O_{17}]^{3-}$, precipitated as an amorphous compound in acetonitrile with $[(n\text{-}C_4H_9)_4N]^+$ as the counter ion, is unstable in solution (*127*). It has not been structurally characterized but its IR spectrum is nearly identical with that of the methoxypentamolybdate $[Mo_3O_8(OMe)(MoO_4)_2]^{3-}$, which has two tetrahedral MoO_4 groups attached to a trigonal group of three edge-shared MoO_6 octahedra (*128*). The polymeric pentamolybdate $[HMo_5O_{16}(H_2O)]^-_\infty$, which can be obtained as a Na^+, K^+, or NH_4^+ salt by slow crystallization, has a complex three-dimensional structure (*129*).

IV. Tungstate(VI)

A. Mononuclear Species

As in the case of molybdate the first and second protonation constants of tungstate have about the same values. It can therefore be assumed, after the analogy of molybdate, that an increase in the coordination number of tungsten also occurs in the second protonation step (*54*, *58*, *61*). The equilibria are therefore formulated in the same way

$$[WO_4]^{2-} + H^+ \leftrightharpoons [HWO_4]^- \tag{31}$$

$$[HWO_4]^- + H^+ + 2\,H_2O \leftrightharpoons WO_3(H_2O)_3. \tag{32}$$

The small difference between the successive pK values (cf. values below) of tungstic acid was previously explained in terms of an anomalously high value for the first protonation constant, assumed to be effected by an increase in the coordination number of tungsten in the *first* protonation step (*2*, *3*, *55*). As shown by the values of the thermodynamic parameters for the protonation of molybdate it is actually the *second* protonation constant which has an abnormally high value (*54*, *58*). An equilibrium constant and thermodynamic quantities calculated for the first protonation of $[WO_4]^{2-}$ pertaining to 25°C and zero ionic strength (based on measurements from 95° to 300°C), namely $\log K = 3.62 \pm 0.53$, $\Delta H = 6 \pm 13$ kJ/mol, and $\Delta S = 90 \pm 33$ J, are also consistent with a normal first protonation (*131*) (cf. values for molydate, Table V).

It has proved difficult to characterize these monomeric equilibria by the usual methodology because of the presence of polynuclear ions even at very high dilution. By using a streaming apparatus which allowed the mixing of large volumes of dilute solutions (tungstate and acid in this case) and measuring the pH of the fresh mixture a value of 8.1 for (pK_1 + pK_2) at 20°C and 0.1 *M* $NaClO_4$ could be determined (*55*). The individual protonation constants were estimated to have the values log K_1 ~3.5 and log K_2 ~4.6, indicating that a maximum percentage concentration of only about 12% of $[HWO_4]^-$ exists at pH = 4 (if polynuclear ions are absent, Fig. 16). A value for (pK_1 + pK_2) = 8.2 ± 0.2 at 25°C in 1.0 *M* NaCl was obtained from adsorption data of tungstate on activated carbon (*132*).

The values estimated for the individual protonation constants of tungstate can be compared with the constants for molybdate at the same temperature and ionic strength, log K_1 = 3.7 and log K_2 = 3.8 (*54*). The significantly greater value for the second protonation constant in the case of tungsten indicates its greater tendency to increase its coordination sphere from four to six (*133*). Part of a UV spectrum (accessible for measurement), obtained by stopped-flow measurements of acidified tungstate solutions and assumed to be that of $WO_3(H_2O)_3$, has been reported. It appears to be similar to that of the molybdenum (VI) analog, but an absorption maximum cannot be observed because of the expected shift to shorter wavelengths (*134*).

Except for indirect evidence for the existence of a singly charged

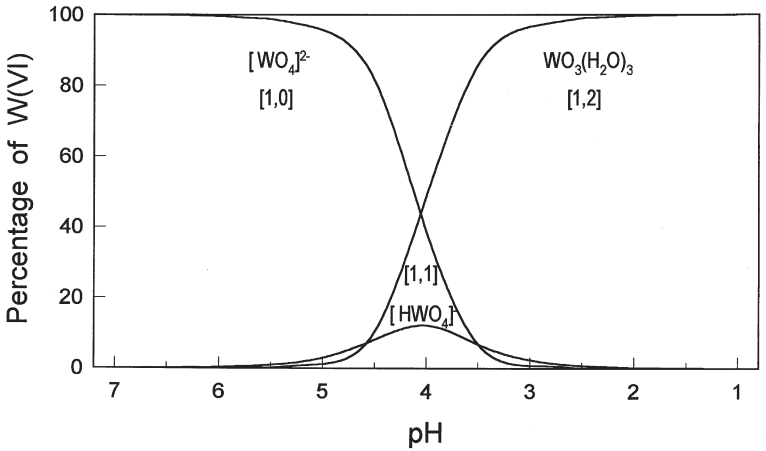

FIG. 16. Distribution of mononuclear species as a function of pH, calculated from protonation constants log K_1 = 3.5 and log K_2 = 4.6.

dimeric cation, analogous to the molybdenum dimer, with a formation constant log $\beta_{2,5} = 23 \pm 1$ at 25°C in 1.0 *M* NaCl medium, obtained from the adsorption of tungstate on activated carbon, no other information about the possible further protonation of $WO_3(H_2O)_3$ seems to be available (*132*).

B. Polyoxoanions

The aqueous chemistry of tungstate (VI) is more difficult to investigate than that of molybdenum (VI) and vanadium (V), the main reason being the slow reactions which occur on acidification and the formation of kinetic intermediates (*1–3*). Formulae of polyanions and the trivial names often used in the literature to distinguish between unidentified species in solution are given in Table VIII. Paratungstates **A** and **B**, which coexist in the pH region 5–8, are the first polyions that form upon acidification of $[WO_4]^{2-}$. At lower pH slow reactions occur when $Z \gtrsim 1.2$. Equilibrium analysis of data can therefore be attempted only in a limited pH range, although wider ranges have been studied at elevated temperatures. The results of these investigations have been interpreted mainly in terms of the formation of hexameric and dodecameric polyanions in addition to mononuclear tungstic acid

TABLE VIII

Polyoxoanions Likely to Occur in Aqueous Solution in the pH Range 9–1[a]

	Trivial name	pH	[*p*, *q*]	Z	References
$[H_2W_6O_{22}]^{6-}$		7–8	(6, 6)	1.0	(*133*, *137*)
$[W_7O_{24}]^{6-}$	Paratungstate A	8–5	(7, 8)	1.143	(*133*, *102a*, *140*, *141*)
$[HW_7O_{24}]^{6-}$			(7, 9)	1.286	(*133*)
$[H_2W_{12}O_{42}]^{10-}$	Paratungstate B	9–5	(12, 14)	1.167	(*3*, *133*, *137*, *141*, *145*)
$[H_3W_{12}O_{42}]^{9-}$		~4	(12, 15)	1.250	(*141*)
α-$[(H)W_{12}O_{40}]^{7-}$	Ψ' Metatungstate	~4	(12, 17)	1.417	(*141*, *154*, *161*)
β-$[HW_{12}O_{40}]^{7-}$		4	(12, 17)	1.417	(*141*)
α-$[(H_2)W_{12}O_{40}]^{6-}$	Metatungstate	3	(12, 18)	1.50	(*2*, *131*, *141*)
α-$[H(H)W_{12}O_{40}]^{6-}$		2	(12, 18)	1.50	(*141*)
β-$[(H_2)W_{12}O_{40}]^{6-}$	Tungstate X	~3	(12, 18)	1.50	(*141*, *145*, *151–153*)
α-$[H(H_2)W_{12}O_{40}]^{5-}$		2–1	(12, 19)	1.583	(*141*)
[b] $[H_7W_{11}O_{40}]^{7-}$		3	(11, 15)	1.364	(*141*)
[b] $[H_8W_{11}O_{40}]^{6-}$	ψ Metatungstate	2–1	(11, 16)	1.455	(*141*)
$[W_{10}O_{32}]^{4-}$	Tungstate Y	Metastable	(10, 16)	1.600	(*3*, *147–149*, *153*)
$[W_6O_{19}]^{2-}$			(6, 10)	1.67	(*155*)

[a] Some are metastable (cf. text and scheme in Fig. 18).
[b] Formula uncertain.

(*135–138*). The hexameric anion $[HW_6O_{21}]^{5-}$, first proposed by Jander (*139*), had been included in virtually all the best-fit models, but more recent work has shown that a heptatungstate, $[W_7O_{24}]^{6-}$, analogous to the well-characterized heptamolybdate, actually occurs in solution (*133*, *102a*, *140*, *141*). The correct formula for paratungstate **A** is therefore $[W_7O_{24}]^{6-}$. The formula of paratungstate **B** is $[H_2W_{12}O_{42}]^{10-}$.

An extensive potentiometric investigation of tungsten (VI) equilibria was carried out involving measurements at various temperatures and ionic strengths in the ranges 95–290°C and 0.10–5.1 *M* NaCl over the pH range *2–8* and varying the tungsten concentration from 5×10^{-4} to 10^{-2} *M* (*131*). Monomers have been found to become increasingly stable at low tungstate concentrations; high temperatures and high ionic strengths and are the only form of tungstate detected above 200°C at 5.1 *M* NaCl. Three reaction schemes, two including $[W_7O_{24}]^{6-}$, were proposed but slight preference was given to the scheme comprising the two hexamers $[HW_6O_{21}]^{5-}$ and $[W_6O_{19}]^{2-}$ in addition to monomers and the dodecamer $[H_2W_{12}O_{40}]^{6-}$. Apparently the high-temperature data can be explained in terms of fewer species (*131*).

For the purpose of equilibrium analysis measurements at normal temperatures have to be restricted to a degree of protonation, $Z \lesssim 1.2$, to exclude slow reactions. In such a potentiometric study at 25°C in 1.0 *M* NaCl medium a reaction model comprising the ions $[WO_4]^{2-}$, $[W_6O_{20}(OH)_2]^{6-}$, $[W_7O_{24}]^{6-}$, $[HW_7O_{24}]^{5-}$, and $[H_2W_{12}O_{42}]^{10-}$ unequivocally gave the best fit in the computer treatment of the data (*133*). Substitution of the heptatungstate $[W_7O_{24}]^{6-}$ for $[HW_6O_{21}]^{5-}$ significantly improved the fit, whereas calculations with models containing both $[HW_6O_{21}]^{5-}$ and $[W_7O_{24}]^{6-}$ always resulted in the rejection of the former species in the various reaction models that had been examined with the program SUPERQUAD (*142*). The stability constants are given in Table IX.

TABLE IX

FORMATION CONSTANTS AND THERMODYNAMIC QUANTITIES (kJ/mol) OF SOME POLYTUNGSTATE IONS IN 1.0 *M* NaCl MEDIUM AT 298 K (*133*)

Species	log β	ΔH°	$T\Delta S^\circ$	$\Delta H/p$
$[H_2W_6O_{22}]^{6-}$	49.01 ± 0.12	−231 ± 3	49	−38.5
$[W_7O_{24}]^{6-}$	65.19 ± 0.04	−333 ± 2	39	−47.6
$[HW_7O_{24}]^{5-}$	69.96 ± 0.06	−328 ± 3	71	−46.9
$[H_2W_{12}O_{42}]^{10-}$	115.38 ± 0.08	−542 ± 4	117	−45.2

Although the hexamolybdate $[W_6O_{20}(OH)_2]^{6-}$ was found to be a minor species (Fig. 17), as in a previous investigation (*137*), its stability constant was calculated with a rather low standard deviation (10%), making it quite acceptable on statistical grounds. It was formulated as above and not as $[W_6O_{21}]^{6-}$ to correspond to a structure consisting of edge-sharing WO_6 octahedra that would have two protonated terminal oxygen atoms, thus satisfying Lipscomb's principle (*143*) that no octahedron should have more than two unshared vertices. This struc-

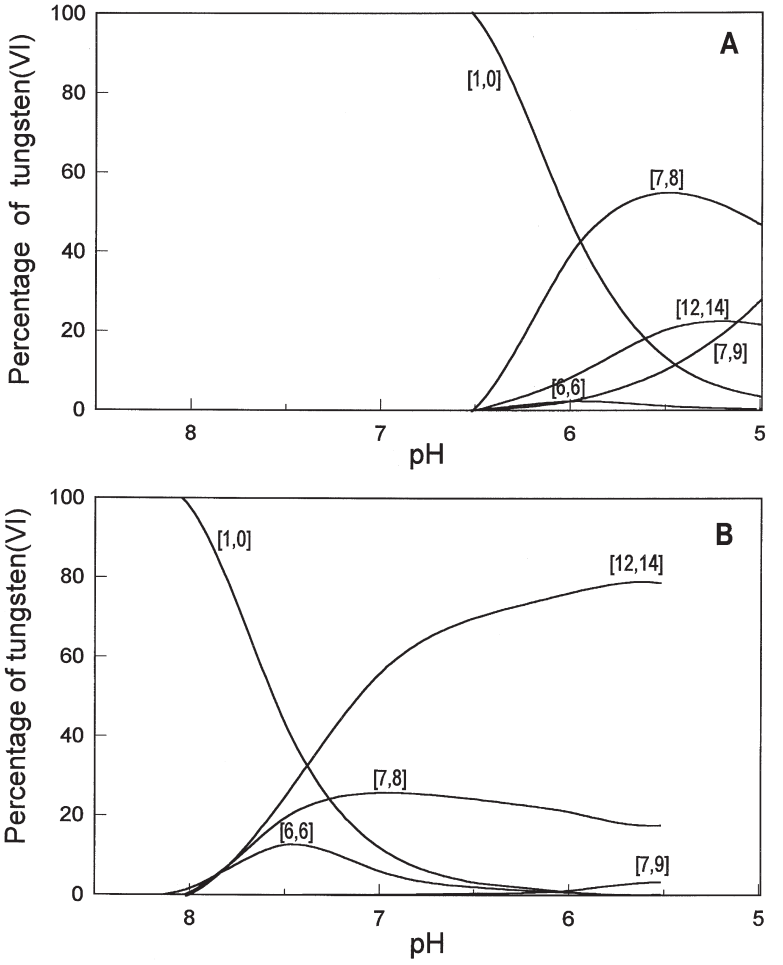

FIG. 17. Distribution of species as a function of pH, calculated from constants in Table IX. Tungsten(VI) concentration 0.001 *M* (A) and 0.20 *M* (B).

ture can be considered as a fragment of the $[W_7O_{24}]^{6-}$ structure from which it can be obtained by removing any octahedron except the central one which has no terminal oxygens. A protonated form of this structure has been isolated in the solid state as the sodium salt $Na_5[H_3W_6O_{22}] \cdot 18H_2O$ (*144*). The position of the third proton is uncertain. The degree of protonation Z = 7/6 = 1.167 corresponds to the formula $[HW_6O_{21}]^{5-}$, which is that of the species previously thought to be paratungstate **A**.

A comparison of the values of the stability constants of the heptamolybdate (log $\beta_{7,8}$ = 52.79) and heptatungstate (log $\beta_{7,8}$ = 65.19) shows the much greater stability of the latter and reflects the greater tendency of tungstate toward condensation; the protonation constants of these two ions are comparable, log K = 4.64 and 4.77 respectively (*133*). However, $[HW_7O_{24}]^{5-}$, unlike $[HMo_7O_{24}]^{5-}$, occurs in significant amounts only at rather low total concentration because of competition with $[H_2W_{12}O_{42}]^{10-}$ with which it coexists (Fig. 17).

Thermodynamic quantities have been determined for the four polyanions accepted in the reaction model (Table IX). The $[W_7O_{24}]^{6-}$ ion was not considered in an earlier calorimetric investigation (*137*), but the ΔH^o values obtained for the two species $[W_6O_{20}(OH)_2]^{6-}$ and $[H_2W_{12}O_{42}]^{10-}$ (pertaining to 3.0 M $NaClO_4$), $\Delta H_{6,6}$ = −239 and $\Delta H_{12,14}$ = −539 kJ/mol, are comparable to those given in Table IX. The relatively smaller enthalpy change for $[W_6O_{20}(OH)_2]^{6-}$ (cf. $\Delta H^o/p$ values) probably indicates the lesser stability of this type of structure. It has been found that the heat of the reaction is little affected by a considerable change in ionic medium (*137*). Neglecting the difference in ionic medium, a comparison of the enthalpy changes for the formation of $[W_7O_{24}]^{6-}$ ($\Delta H_{7,8}$ = −333 kJ/mol) and $[Mo_7O_{24}]^{6-}$ ($\Delta H_{7,8}$ = −234 kJ/mol) shows that the enthalpy factor is the reason for the much greater stability of the tungsten polyanion, reflecting the greater tendency of tungsten to increase its coordination number. An increase in the number of bonds would favor tungsten because it forms stronger bonds with oxygen than molybdenum (*2*). The thermodynamic data show that the condensation reactions are mainly enthalpy driven.

More direct evidence for the existence of $[W_7O_{24}]^{6-}$ has been obtained from Raman (*140*) and NMR spectroscopical investigations (*102a*, *141*). Also, a remarkable similarity has been noted between the infrared spectra of heptamolybdate salts and the spectra of paratungstate **A** in solution (*2*). A comparison of the Raman spectrum of $[W_7O_{24}]^{6-}$ in the solid state (isolated as a piperidinium salt) and a freshly acidified tungstate solution led to the identification of $[W_7O_{24}]^{6-}$ in solution (*140*). An ^{17}O and ^{183}W NMR investigation of

tungstate solutions in the region $Z \leq 1.17$ showed the presence of both $[W_7O_{24}]^{6-}$ and $[H_2W_{12}O_{42}]^{10-}$, of which the equilibrium concentrations depended on temperature and total concentration (*102a*). A comparison of ^{17}O NMR spectra of solutions of $Na_6[W_7O_{24}] \cdot 14H_2O$ and $(NH_4)_6[W_7O_{24}] \cdot nH_2O$ indicated that the polyanions in solution are of the same structural type (*102a*).

A thorough and comprehensive study of tungstate solutions in the pH range 8 to 1.5 was carried out by using ^{183}W, ^{17}O, and ^{1}H NMR spectroscopy (*141*). The results are summarized in a scheme (Fig. 18) which gives a new perspective on the formation of species in solution in relation to polyions already characterized in the solid state. A bet-

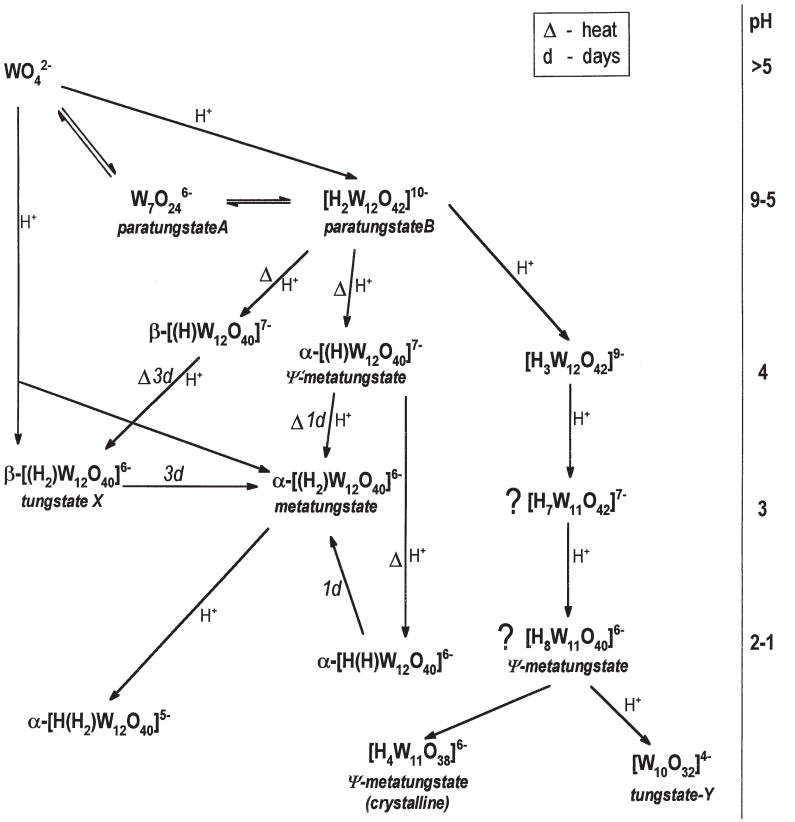

FIG. 18. Reaction scheme showing the various polyanions that can form upon acidification of $[WO_4]^{2-}$. Parentheses are used to distinguish internal H from external H where necessary. Question marks indicate tentative formulations. (Adapted with permission from Hastings, J. J., Howarth, O. W. *J. Chem. Soc. Dalton Trans.* **1992,** 209–215.)

ter understanding, especially of some complex protonation reactions and concommitant structure changes is afforded. The measurements above pH 6 confirmed the existence and identity of paratungstates **A** and **B** as $[W_7O_{24}]^{6-}$ and $[H_2W_{12}O_{42}]^{10-}$ respectively. Protonation of $[H_2W_{12}O_{42}]^{10-}$ takes place but a protonated form of $[W_7O_{24}]^{6-}$ was not observed under the conditions of these experiments, typically 2.0 *M* $Li_2[WO_4]$.

The protons in $[H_2W_{12}O_{42}]^{10-}$ are more accessible to water than in the dodecamer with Keggin structure $[(H_2)W_{12}O_{40}]^{6-}$, and a rapid exchange can be expected (*145*). Parenthesis are used in the Keggin formula to indicate the internal protons where necessary. The acceptance of a proton by paratungstate **B,** leads to the formation of three different species (*141*), its protonated form and the monoprotonated α- and β-Keggin ions

$$[H_2W_{12}O_{42}]^{10-} + H^+ \leftrightharpoons [H_3W_{12}O_{42}]^{9-} \tag{33}$$

$$[H_2W_{12}O_{42}]^{10-} + H^+ \xrightarrow{\Delta} \alpha\text{-}[(H)W_{12}O_{40}]^{7-} + H_2O \tag{34}$$

$$[H_2W_{12}O_{42}]^{10-} + H^+ \xrightarrow{\Delta} \beta\text{-}[(H)W_{12}O_{40}]^{7-} + H_2O. \tag{35}$$

The protonation constant for reaction (33) has been determined from ^{183}W chemical shifts at 20°C as $\log K = 4.59 \pm 0.03$. The protonation is complex and a rearrangement of all the protons probably takes place. A possible explanation for the observed kinetics involved is that one of the $[H_3W_{12}O_{42}]^{9-}$ isomers bears three internal protons and the other has one external and two internal protons. The exchange of a proton between the internal and external sites would then be the rate-determining step (*141*).

The presence of the protonated paratungstate **B**, $[H_3W_{12}O_{42}]^{9-}$, is essential for the formation of a W_{11} polyanion and its protonated form in solution, tentatively formulated as $[H_7W_{11}O_{40}]^{7-}$ and $[H_8W_{11}O_{40}]^{6-}$ (*141*). Some of these protons are internal. It was suggested that ψ-metatungstate $[H_4W_{11}O_{38}]^{6-}$, obtained in the solid state as a potassium salt (*146*), is formed from $[H_8W_{11}O_{40}]^{6-}$ by a process of oxygen elimination.

Further protonation of the W_{11} species leads to the formation of another polyanion, indicated to be tungstate **Y,** the decatungstate ion $[W_{10}O_{32}]^{4-}$, and which can be obtained in the solid state by the addition of a large cation such as $[(C_4H_9)_4N]^+$ (*99a, 147*) (Fig. 19). Protonation of paratungstate **B** in the presence of large cations (to disfavor Keggin structures) yields tungstate **Y**, $[W_{10}O_{32}]^{4-}$ (*147a*), but it also

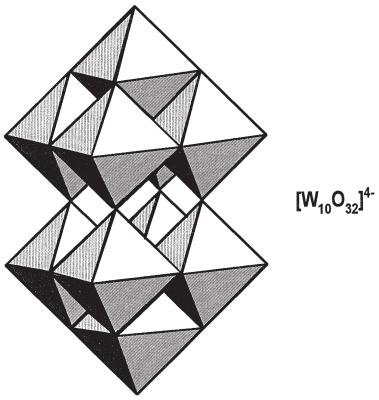

FIG. 19. Polyhedral representation of the structure of $[W_{10}O_{32}]^{4-}$.

forms immediately upon acidification of tungstate solutions to pH 0–3 and can be extracted into *n*-amyl alcohol at pH 0–1 (*148*). When dissolved in methanol $[W_{10}O_{32}]^{4-}$ slowly converts to $[W_6O_{19}]^{2-}$, but the addition of water destabilizes the hexatungstate and it transforms back to $[W_{10}O_{32}]^{4-}$ (*149*). The decatungstate ion has a pale yellow color and gives an absorption spectrum with a maximum at ~325 nm in aqueous solution and some organic solvents, e.g., acetonitrile (*150*). While indefinitely stable in nonaqueous solution the decatungstate ion is metastable in aqueous solution, forming ψ-metatungstate, β-$[(H_2)W_{12}O_{40}]^{6-}$, or $[W_7O_{24}]^{6-}$ depending on the pH and ionic strength (*153*). In fact below pH ~5.5 all species in aqueous solutions are metastable. Upon prolonged heating they yield the thermodynamically stable true metatungstate α-$[(H_2)W_{12}O_{40}]^{6-}$, which is in any case the dominant species below pH 4 (*2*, *141*). The two hydrogen atoms in the metatungstate function as the heteroatom in the well-known Keggin structure, in this case the α-Keggin isomer (cf. Figs. 20 and 21). The two protons of the α- and β-Keggin isomers are nonexchanging (2).

Polytungstate **X**, first described by Souchay *et al.* (*151*), has been identified as the β-Keggin $[(H_2)W_{12}O_{40}]^{6-}$ species (*145*, *152*). It forms spontaneously in aqueous solution as a minor transient species. The two types of structures are easily distinguishable by ^{183}W NMR: the α-structure with 12 equivalent tungsten atoms shows one singlet, whereas the β-structure shows three peaks in the ratio 1 : 2 : 1 (cf. Fig. 21). In earlier work polarography also proved to be particular useful to distinguish between some species, e.g., tungstate **X**, tungstate **Y**, ψ-metatungstate, and metatungstate, which all have different polarograms (*153*).

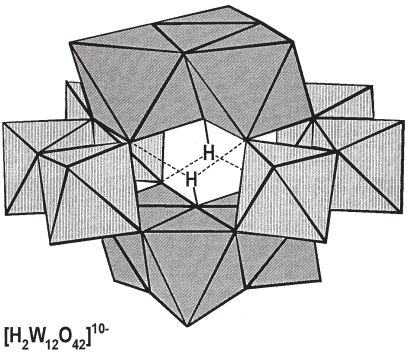

FIG. 20. Polyhedral representation of the structure of $[H_2W_{12}O_{42}]^{10-}$ (paratungstate B) showing the location of the protons in the center. The structure is built from two different types of trioctahedral subunits.

The main extra species that forms upon acidification of paratungstate was identified as α-$[(H)W_{12}O_{40}]^{7-}$, which is internally protonated and forms at higher pH than α-$[(H_2)W_{12}O_{40}]^{6-}$ (*141*). This monoprotonated species, α-$[(H)W_{12}O_{40}]^{7-}$, was previously only obtained by reduction and reoxidation (*154*). It is slowly reprotonated to α-$[(H_2)W_{12}O_{40}]^{6-}$, the half-life of the reaction being ~1 day at room tempera-

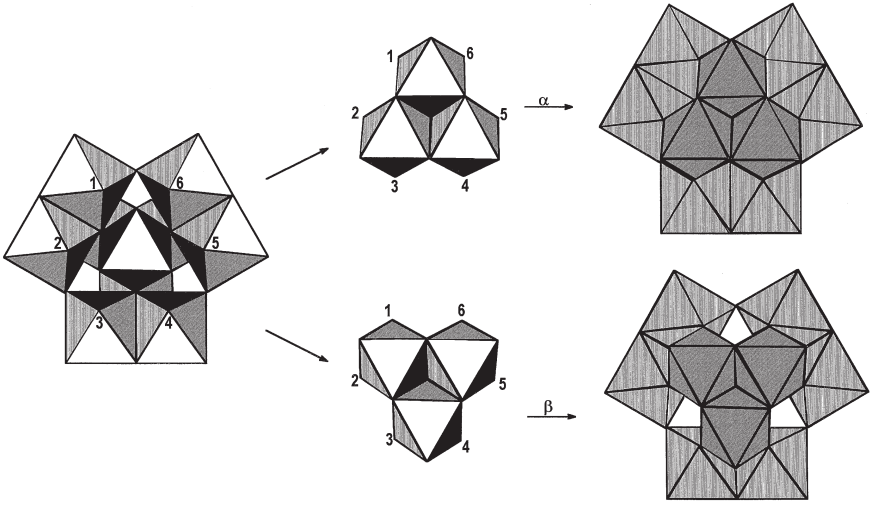

FIG. 21. Polyhedral representation of the α- and β-Keggin structures of $[(H_2)W_{12}O_{40}]^{6-}$, also known as metatungstate and tungstate X respectively. The numbers show where the W_3O_{13} unit (60° rotation involved) is attached to build the structures.

ture and at pH ~5. Evidence for the existence of another internally protonated metatungstate, a minor species β-$[(H)W_{12}O_{40}]^{7-}$, has also been presented. At very low pH α-$[H(H)_2W_{12}O_{40}]^{7-}$, which has one proton attached to the exterior of the anion, is formed (*141*). Thus there is evidence for the formation of both the internally monoprotonated and diprotonated α- and β-Keggin species and for the α-forms also accepting external protons.

Electrospray ionization mass spectroscopy have been carried out on aqueous tungstate solutions and species such as $[HWO_4]^-$, $[HW_2O_7]^{3-}$, $[W_4O_{13}]^{2-}$, $[HW_4O_{13}]^-$, $[W_6O_{19}{}^{2-}]$, $[H_2W_{10}O_{32}]^{2-}$, or $[HW_5O_{16}]^-$ have been observed in the mass spectrum (*155*).

1. Structures of Polyoxoanions Obtained in the Solid State

Several polyanions have been isolated in the solid state and their structures determined by X-ray crystallography (Table X). Unlike some structures of molybdenum (VI) and vanadium (V), where the metal ions occur in an other-than-octahedral environment of oxygen atoms, all the known structures of tungsten (VI) are built from WO_6 octahedra. With a few exceptions these octahedra share edges in such a way that structures with only single-terminal oxygens are formed. The majority of polyoxomolybdate structures, on the other hand, have *cis*-dioxo-terminal oxygens. A completely satisfying explanation for this difference has not been put forward, but the possible better overlap with oxygen orbitals of the more extended tungsten 5d orbitals could play a role (*2*).

TABLE X

EXAMPLES OF POLYOXOTUNGSTATE COMPOUNDS OBTAINED IN THE SOLID STATE

	[*p*, *q*]	*q*/*p*	References
$K_7[HW_5O_{19}]\cdot 10\ H_2O$	[5, 3]	0.60	(*162*)
$(NH_4)_2[W_2O_7]$	[2, 2]	1.0	(*140*)
$Na_6[W_7O_{24}]\cdot 14\ H_2O$, $(C_5H_{10}NH_2)_6[W_7O_{24}]$,	[7, 8]	1.143	(*102a*, *140*) (*156*)
$Na_5[H_3W_6O_{22}]\cdot 18\ H_2O$	[6, 7]	1.167	(*144*)
$Na_{10}[H_2W_{12}O_{42}]\cdot 20\ H_2O$, $(NH_4)_{10}[H_2W_{12}O_{42}]\cdot 4\ H_2O$; $K_{10}[H_2W_{12}O_{42}]\cdot 7\ H_2O$, $Mg_5[H_2W_{12}O_{42}]\cdot 38\ H_2O$	[12, 14]	1.167	(*158e*, *159*) (*158h*, *158c*)
α-$Cs_{6.5}K_{0.5}[(H)W_{12}O_{40}]\cdot 10\ H_2O$	[12, 17]	1.417	(*161*)
$K_6[H_4W_{11}O_{38}]\cdot 11\ H_2O$	[11, 16]	1.455	(*146*)
α-$Na_6[(H_2)W_{12}O_{40}]\cdot 21\ H_2O$	[12, 18]	1.500	(*145*)
α-$[(C_4H_9)_3NH]_5[H_3W_{12}O_{40}]$	[12, 19]	1.500	(*140*)
$[(C_4H_9)_3NH]_4[W_{10}O_{32}]$, $K_4[W_{10}O_{32}]\cdot 4\ H_2O$	[10, 16]	1.600	(*147*)
$[(C_6H_5)_4P]_2[W_6O_{19}]$	[6, 10]	1.667	(*157c*)

The structures of $[W_7O_{24}]^{6-}$ (paratungstate **A**) (*102a*, *140*, *156*) and $[W_6O_{19}]^{2-}$ (*157*) are the same as that of the analogous molybdenum compounds (cf. Figs. 10 and 15). If an octahedron is removed from $[W_6O_{19}]^{2-}$ and two such fragments are connected by four vertices then the structure of decatungstate $[W_{10}O_{32}]^{4-}$ (tungstate **Y**) is obtained (*147*) as shown in Fig. 19.

The structure of $[H_2W_{12}O_{42}]^{10-}$ (paratungstate **B**) has been determined in at least eight different compounds (Fig. 20). This polyanion is not very soluble and is easily crystallized from aqueous solutions at pH 6–7 with cations such as Na^+, K^+, NH_4^+, and Mg^{2+} (*158*). The role of hydrated cations in the stabilization and crystallization of this polyanion has been discussed (*159*). The position of the protons has been located by neutron diffraction as internally bound (*159, 160*) as predicted on the basis of crystallographic work (*158b*).

The two protons in the metadodecatungstate polyion $[(H_2)W_{12}O_{40}]^{6-}$ are also internally bound but stronger than in the paratungstate (*160*); $[(H_2)W_{12}O_{40}]^{6-}$ has the Keggin structure as shown by X-ray analysis of compounds isolated (*140*). The α-Keggin compound has been isolated as the tributylammonium compound $[(C_4H_9)_3NH]_5[H_3W_{12}O_{40}]$ (*140*). The less symmetrical β-Keggin structure is obtained from the α-structure by rotating one W_3O_{13} group by 60° (Fig. 21). The monoprotonated form can be made indirectly from $[(H_2)W_{12}O_{40}]^{6-}$, which is first reduced and after deprotonating reoxidized and isolated as a Cs^+ salt (*161*).

Two polytungstates, a pentatungstate and a hexatungstate, that do not satisfy the Libscomb principle (*143*) have been isolated in the solid state as the potassium and sodium salts $Na_5H_3W_6O_{22} \cdot 18H_2O$ (*144*) and $K_7HW_5O_{19} \cdot 10H_2O$ (*162*). The hexatungstate anion $[H_3W_6O_{22}]^{5-}$ can be viewed as a fragment of heptatungstate (Fig. 22). It contains two WO_6 octahedra with free faces, i.e. with three terminal oxygen atoms in *fac* configuration. According to the Libscomb principle, in a structure consisting of edge-sharing octahedra no octahedron should have more than two unshared vertices. However, in this structure two terminal oxygens are protonated. The probable positions are shown in Fig. 22 as deduced, first, from one longer W–O bond and, second, from valence sum calculations with respect to the Na^+ coordination by the terminal oxygen atoms. Thus no octahedra would have more than two terminal oxygens. The position of the third proton is uncertain (*144*).

The pentatungstate can be seen as a fragment of the hexatungstate and is obtained by removal of one octahedron (*162*). It consists of five WO_6 octahedra, two of which have free faces. According to calcula-

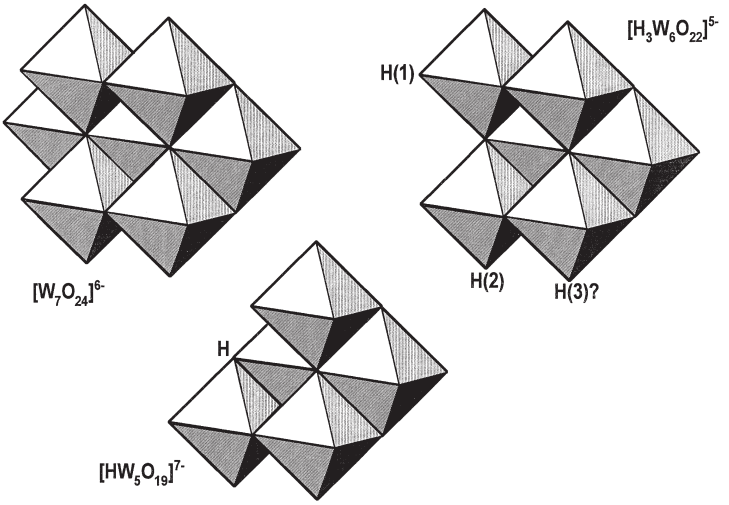

FIG. 22. Polyhedral representation of the structures of $[HW_5O_{19}]^{7-}$ and $[H_3W_6O_{22}]^{5-}$ viewed as fragments of the $[W_7O_{24}]^{6-}$ structure. The location of the third proton of $[H_3W_6O_{22}]^{5-}$ is uncertain.

tions of the valence sums the protons are not located at one of the terminal oxygens but at a bridging oxygen (Fig. 22). The two octahedra with free faces are stabilized partly by coordination with K^+ ions and by hydrogen bonding with water of crystallization.

The crystal structure of $[H_4W_{11}O_{38}]^{6-}$ has been determined by Lehman and Fuchs (*146*). The identification put forward is ψ-metatungstate. The polyion can be described as consisting of 11 octahedra assembled by connecting at vertices a tetrameric, a trimeric, and two dimeric units of edge-sharing octahedra, resulting in a rather open structure.

V. Mixed Polyoxoanions

A. Molybdovanadates

A feature of the molybdovanadates in aqueous solution is the domination of polyions whose structures are the same as those of $[V_{10}O_{28}]^{6-}$, β-$[Mo_8O_{26}]^{4-}$, and $[Mo_6O_{19}]^{2-}$. The stability of mixed hexametalates is noteworthy because of the "nonexistence" of this structure in either vanadate or molybdate aqueous solutions; $[Mo_6O_{19}]^{2-}$ is stable only in nonaqueous solution (cf. Section III,C,I).

Potentiometric data alone is not adequate to establish the specia-

tion. The consumption of protons for the formation of molybdovanadate ions is much the same as that for the formation of polymolybdate and polyvanadate ions, resulting in rather small pH changes relative to the subsystems (*163*). On the basis of a ^{51}V NMR study the existence of a monomolybdonanovanadate, $[MoV_9O_{28}]^{5-}$, having the decavanadate structure was proposed (*163*, *102b*). The molybdenum replaces a vanadium at a "capping" position (*164*).

The major part of the decavadate structure is not retained during the process of substitution by molybdenum (*163*). In a subsequent investigation of this system by potentiometry and ^{51}V, ^{17}O, and ^{99}Mo NMR spectroscopy it was shown that a second substitution of molybdenum can take place at two of the three remaining capping sites (*165*). The ion $[MoV_9O_{28}]^{5-}$ protonates primarily at the bridging oxygens furthest from Mo, with $pK_a = 2.8$ (0.6 *M* NaCl). This value can be compared with $pK_a = 3.78$, for $[HV_{10}O_{28}]^{5-}$, which has the same structure and overall charge. The dimolydate species, $[Mo_2V_8O_{28}]^{4-}$, does not protonate and exists in two forms, cis and trans, present in the ratio 9 : 11.

At a high molybdenum : vanadium ratio the system is far more complex; a greater variety of mixed polyanions are formed. At least four dominant nondecavanadate type structures have been identified: $[Mo_5VO_{19}]^{3-}$, $[Mo_4V_2O_{19}]^{4-}$ (*102b*, *165*), $[Mo_4V_5O_{27}]^{5-}$, and β-$[Mo_7VO_{26}]^{5-}$ (*165*).

The ions with six metal atoms have the same structure as the hexamolybdate ion $[Mo_6O_{19}]^{2-}$. The $[Mo_5VO_{19}]^{3-}$ ion, previously identified in acetonitrile medium (*166*) can be obtained in the solid state by precipitation from an aqueous solution with tetramethyl ammonium as cation (*165*). The vanadium atoms in both $[Mo_4V_2O_{19}]^{4-}$ and its protonated form $[HMo_4V_2O_{19}]^{3-}$ ($pK_a = 3.8$) are in *cis* positions. Protonation seems to take place at the oxygen, which bridges the two vanadium atoms.

Although no polyanions with nine metal atoms have so far been found in either vanadate(V) or molybdate(VI) solutions the $[Mo_4V_5O_{27}]^{5-}$ ion as well as its protonated form, $[HMo_4V_5O_{27}]^{4-}$ with $pK_a \sim 2.5$, have been identified in the mixed solutions (*162*, *165*).

The structure of β-$[Mo_7VO_{26}]^{5-}$ is similar to that of β-octamolydate $[Mo_8O_{26}]^{4-}$. There is tentative evidence for the existence of α-$[HMo_7VO_{26}]^{4-}$ and β-$[H_2Mo_6V_2O_{26}]^{4-}$. Less conclusive evidence has been presented for the solution species α-$[HMo_6V_2O_{26}]^{5-}$, $[Mo_4VO_{17}]^{5-}$, and $[HMo_8V_2O_{32}]^{5-}$ with a planar structure, and several α-Keggin species with central vanadium atoms, e.g. $[V(Mo_{10}V_2O_{40})]^{5-}$ and $[V(Mo_9V_3O_{40})]^{6-}$ (*165*). The vanadium atoms usually prefer central cities and mutual proximity.

Compounds isolated in the solid state and analised by x-ray crystallography, e.g. α-$[Mo_6V_2O_{26}]^{6-}$ (*167*), β-$[Mo_6V_2O_{26}]^{6-}$ (*168*), $[Mo_8V_5O_{40}]^{7-}$ (*169*), and $[Mo_4V_8O_{36}]^{8-}$ (*170*), do not correspond to any of the major species observed in solution.

Equilibrium constants for the various mixed polyions in 0.6 *M* NaCl at 25° have been calculated from combined potentiometic and ^{51}V NMR measurements over wide concentration ranges and $1.4 < pH < 7$ (*165*).

B. Tungstovanadates

In general, tungstovanadates form similar polyanions to molybdovanadates but in different proportions (*171*), and no octa-metalates appear to exist. By a combined equilibrium study involving potentiometry and ^{51}V, ^{183}W, and ^{17}O NMR spectroscopy, hexa-, deca-, and dodeca-metalate species could be identified and their formation constants determined (where relevant) in 0.6 *M* NaCl (*171*). Tungstovanadate solutions are slow to equilibrate. Above pH 3, equilibrium is reached only after 2 days at 25°. Initial warming does not help to speed up attainment of equilibrium. For solutions starting at lower pH values, changes can be detected in the ^{51}V NMR spectra after 5–10 days. These changes were not complete even after 3 months.

The hexametalates have the typical $[Mo_6O_{19}]^{2-}$ structure and are derived from $[W_6O_{19}]^{2-}$ by substitution of one, two, or three V atoms for W atoms. The ion $[W_5VO_{19}]^{3-}$ is a prominent species which appears only below pH 3 in aqueous solution (*171–173*). It has also been identified in acetonitrile (*174*). Dominant species in aqueous solution at pH >3 are *cis*-$[W_4V_2O_{19}]^{4-}$ and its protonated form *cis*-$[HW_4V_2O_{19}]^{3-}$ (*171*, *173*, *102b*, *175*). That protonation occurs at the V–O–V edge-oxygen can be deduced from the upfield shift of its ^{17}O NMR resonance, which is caused by weakening of the metal–oxygen bonds (*174*). In an *ab inito* study this oxygen was also identified as the most basic center; the terminal oxygens are by far the least basic (*176*). The protonation constant is about 1.5 log units lower than that of the corresponding molybdovanadate ion, *cis*-$[Mo_4V_2O_{19}]^{4-}$ (*171*). The trans isomers of these ions have also been identified (*171*). Owing to the tendency of tungstovanadates to protonate less readily than molybdovanadates, the trisubstituted ions *fac*-$[W_3V_3O_{19}]^{5-}$ (*171*, *172*) and *mer*-$[W_3V_3O_{19}]^{5-}$ (*171*, *178*) are also known at higher pH; the molydenum analogs are unknown.

The preference of the vanadium atoms to be mutual adjacent is confirmed by a range of α-Keggin ions with vanadium occupying the center (*172*). A metatungstate Keggin ion, α-$[H_2W_{11}VO_{40}]^{7-}$, with one

W atom replaced by a V atom, has been described (*177*, *179*). Although it does not form to any appreciable extent after 2 days it becomes a major species in an aqueous solution after several weeks at room temperature (*171*).

The decametalates are obtained by substituting a tungsten atom for a vanadium atom in a capping position in $[V_{10}O_{28}]^{6-}$ to form $[WV_9O_{28}]^{5-}$ and its protonated form $[HWV_9O_{28}]^{4-}$ (*171*, *102b*, *177*). The p*K* value is 2.15 (25°C) compared to 2.77 (20°C) for the molybdenum analog (*171*).

The tungsten complexes are all more stable than the molybdenum complexes, e.g. for *cis*-$[W_4V_2O_{19}]^{4-}$ and *cis*-$[Mo_4V_2O_{19}]^{4-}$ the log values for the formation constants are 56.67 and 44.48 respectively (*171*). This finding is consistent with the greater stability of heptatungstate with respect to heptamolybdate; the values of the formation constants pertaining to 1 *M,* NaCl are log $\beta_{7,8}$ = 65.19 (*133*) and 52.79 (*81*, *85*, *86*) respectively.

C. Molybdotungstates

Structures found with only one metal resist substitution by the other metal and in general undergo substitution at best only at a single site (*180*). The dodecatungstate $[H_2W_{12}O_{42}]^{10-}$ and more compact α-Keggin ion $[(H_2)W_{12}O_{40}]^{6-}$ have no molybdenum analogs and in each case only one tungsten can be replaced by molybdenum (*180*, *181*). Also, there is no evidence for the substitution of tungsten into $[Mo_8O_{26}]^{4-}$, a structure which does not occur in the case of tungsten.

Structures known to form with either metal also form with the entire intermediate range of mixed-metal combinations (*180*). Both molybdenum and tungsten form the heptametalate $[M_7O_{24}]^{6-}$ in aqueous solution. The existence of mixed heptametalates has been shown by the application of ^{17}O NMR (*182*) and ^{183}W NMR spectroscopy (*180*). In fact, molybdenum can replace any or all of the tungsten atoms in $[W_7O_{24}]^{6-}$ so that at least 19 mixed-metal structures can be observed (*180*). Approximate relative stability constants have been determined for the intermediate species in the series

$$[W_7O_{24}]^{6-},\ [MoW_6O_{24}]^{6-} \ldots\ldots [Mo_6WO_{24}]^{6-},\ [Mo_7O_{24}]^{6-}.$$

It has been found that W prefers a I site (relative to a III site) by a factor of 3.0 and Mo prefers a II site (relative to a III site) by a factor

of 4.3 (Fig. 23). These preferences are associated with the electron densities of the sites, which are lowest at site I and highest at site II. Owing to the stronger bonds of W(VI) with oxygen (2), it would be less disfavored than Mo(VI) by the generally lower availability of oxygen electrons at site I.

The ion $[MoW_5O_{19}]^{2-}$ has been isolated in the solid state as a tetrabutyl ammonium salt (*183*). The formation of $[Mo_3W_3O_{19}]^{2-}$ in an aqueous solution was proposed on the basis of potentiometric data (*184*).

D. Molybdotungstovanadates

Trimetallic polyanions with the $[Mo_6O_{19}]^{2-}$ structure form in aqueous solution in the pH region 2.5 to 6. The complete series of ions with two cis vanadium atoms and four other metal atoms which can be either molybdenum or tungsten or both, i.e. $[Mo_nW_{4-n}V_2O_{19}]^{4-}$, have been characterized by ^{51}V NMR spectroscopy (*185*). The bimetallic ions $[Mo_4V_2O_{19}]^{4-}$ and $[W_4V_2O_{19}]^{4-}$ have previously been shown to prefer the *cis* arrangement of the two vanadium atoms (*165*, *166*). Seven isomers of the trimetallic species have been identified. The p*K* values of the monoprotonated hexametalate ions increase with increasing substitution of molybdenum for tungsten in the range 1.85 to 3.8; protonation occurs at the edge-oxygen between the two vanadium atoms (*165*, *166*).

VII. Concluding Remarks

The complex vanadate(V), molybdate(VI), and tungstate(VI) systems have been clarified to such an extent that the identity of practi-

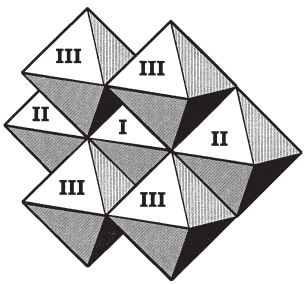

Fig. 23. Heptametalate structure. Tungsten(VI) prefers site I and molybdenum(VI) prefers site II in mixed molybdotungstate polyanions.

cally all the major species in solution are known with certainty. These species have been structurally characterized and their stability regions determined with respect to pH and concentration. It is clear that various factors can affect the formation, stability, and structure of polyoxoanions in solution. Not all the species identified in solution can be isolated in the solid state, whereas some others that are relatively unstable in solution or are present in undetectable low concentrations can be precipitated with a specific counterion.

The research also revealed new complexities and some questions are still to be answered. The molybdate(VI) system in particular needs further clarification regarding the existence of some polyions. More kinetic and thermodynamic data would also help to improve our understanding of these systems and perhaps lead to a general inclusive explanation of the mechanism of polyoxoanion formation. In this respect the new information about some structural preferences of the different metals in mixed polyoxoanions is of interest and a useful addition to known facts regarding polyoxometalate structures (*181*).

Acknowledgments

The author thanks Elisabeth Rohwer for technical assistance in the preparation of graphs and figures for this chapter.

References

1. Baes, C. F., Jr.; Mesmer, R. E. "The Hydrolysis of Cations"; Wiley-Interscience: New York, 1976.
2. Pope, M. T. "Heteropoly and Isopoly Oxometalates"; Springer-Verlag: Berlin, 1983.
3. Tytko, K. H.; Glemser, O. *Adv. Inorg. Chem. Radiochem.,* **1976,** *19,* 239.
4. Pope, M. T. *Progr. Inorg. Chem.,* **1991,** *39,* 182.
5. Tytko, K. H.; Trobisch, U. In "Gmelin Handbook of Inorganic Chemistry" Katscher, H. and Schröder, F., Eds., 8th ed. Molybdenum Suppl. Vol. B(3a); Springer-Verlag: Berlin, 1987.
6. Newman, L.; LaFleur, W. J.; Brousaides, F. J.; Ross, A. M. *J. Am. Chem. Soc.* **1958,** *80,* 4491.
7. Rieger, P. H. *Aust. J. Chem.,* **1973,** *26,* 1173.
8. Heath, E.; Howarth, O. W. *J. Chem. Soc. Dalton Trans.* **1981,** 1105.
9. Petterson, L.; Hedman, B.; Nenner, A.; Andersson, I. *Acta Chem. Scand.* **1985,** *39,* 499.
10. Pettersson, L.; Andersson, I.; Hedman, B. *Chem. Scr.* **1985,** *25,* 309.
11. Ivakin, A. A.; Kurbatova, L. D.; Kruchinina, M. V.; Medvedeva, N. I. *Russ. J. Inorg. Chem. (Eng. Transl.)* **1986,** *31,* 219.
12. Cruywagen, J. J.; Heyns, J. B. B. *Talanta* **1990,** *37,* 741.

13. Cruywagen, J. J.; Heyns; J. B. B. *Polyhedron* **1991,** *10,* 249.
14. Elvingson, K.; Fritzsche, M.; Rehder, D.; Pettersson, L. *Acta. Chem. Scand.* **1994,** *48,* 878.
15. Tracey, A. S.; Jaswal, J. S.; Angus-Dunne, S. J. *Inorg. Chem.* **1995,** *34,* 5680.
16. Larson, J. W. *J. Chem. Eng. Data* **1995,** *40,* 1276.
17. Cruywagen, J. J.; Heyns, J. B. B.; Westra, A. N. *Inorg. Chem.* **1996,** *35,* 1556.
18. Elvingson, K.; González Baró, A.; Pettersson, L. *Inorg. Chem.* **1996,** *35,* 3388.
19. Crans, D.; Boukhobza, I. *J. Am. Chem. Soc.* **1998,** *120,* 8069.
20. Andersson, I.; Pettersson, L.; Hastings, J. J.; Howarth, O. W. *J. Chem. Soc. Dalton Trans.* **1996,** 3357.
21. Harnung, S. E.; Larsen, E.; Pederson, E. *Acta Chem. Scand.* **1993,** *47,* 674.
22. O'Donnell, S.; Pope, M. T. *J. Chem. Soc. Dalton Trans.* **1976,** 2290.
23. Madic, C.; Begun, G. M.; Hahn, R. L.; Launey, J. P.; Thiessen, W. E. *Inorg. Chem.* **1984,** *23,* 469.
24. Crans, D. *Comments Inorg. Chem.* **1994,** *16,* 1.
25. Rossotti, H. "The study of Ionic Equilibria"; Longman: New York, 1978.
26. (a) Pettersson, L. *Molecular Engineering,* **1993,** *3,* 29. (b) Pettersson, L. In "Polyoxometalates: From Plantonic Solids to Anti-Retroviral Activity" Pope, M. T. and Müller, A., Eds., p. 27; Kluwer: Dordrecht, 1994.
27. Ingri, N.; Andersson, I; Petterson, L.; Yagasaki, A.; Andersson, L.; Holmström, K. *Acta Chem. Scand.* **1996,** *50,* 717.
28. (a) Petterson, L. Private communication, 1997; (b) Elvingson, K. PhD Thesis, Umeå University, 1997.
29. Cruywagen, J. J.; Heyns, J. B. B.; Westra, A. N. In "Vanadium Compounds: Chemistry, Biochemistry and Therapeutic Applications" Tracey, A. C. and Crans, D. C., Eds., ACS Symposium Series 711, p. 51; ACS: Washington DC, 1998.
30. Konnert, J. A.; Evans, H. T., Jr. *Acta Cryst.* **1975,** *B31,* 2688.
31. Björnberg. A. *Acta Chem. Scand.* **1979,** *A33,* 539.
32. Pettersson, L.; Hedman, B.; Andersson, I.; Ingri, N. *Chem. Scr.,* **1983,** *22,* 254.
33. Cruywagen, J. J.; Heyns, J. B. B.; Visagie, J. L. *Polyhedron* **1989,** *8,* 1800.
34. Fuchs, S. M.; Mahjour, S.; Pickardt, J. *Angew. Chem. Int. Ed. Eng.* **1976,** *15,* 374.
35. Román, P.; José, A. S.; Luque, A.; Gutiérrez-Zorilla, J. M. *Inorg. Chem.* **1993,** *32,* 775.
36. Day, V. W.; Klemperer, W. G.; Yagasaki, A., *Chem. Lett.* **1990,** 1267.
37. Klemperer, W. G.; Shum, W. *J. Am. Chem. Soc.* **1977,** *99,* 3544.
38. Liteanu, I.; Lukács, C.; Strusievici, C. *Analyt. Chim. Acta* **1963,** *29,* 574.
39. Corigliano, F.; Di Pasquale S. *Inorg. Chem. Acta* **1975,** *12,* 99.
40. Day, V. W.; Klemperer, W. G.; Maltbie, D. J. *J. Am. Chem. Soc.* **1987,** *109,* 2991.
41. Debaerdemaker, T.; Arrieta, J. M.; Amigó, J. M. *Acta Crystallogr. B* **1982,** *38,* 2465.
42. (a) Jahr, K.; Fuchs, J.; Oberhauser, R. *Chem. Ber.* **1968,** *101,* 482; (b) Fuchs, J.; Mahjour, S.; Palm, R. Z. *Naturforsch. B* **1976,** *31,* 544.
43. Capparelli, M. V.; Goodgame, D. M. L.; Hayman, P. B.; Skapski, A. C. *J. Chem. Soc. Commun.* **1986,** 776.
44. Roman, P.; Aranzabe, A.; Gutiérrez-Zorrilla, J. M. *J. Chem. Soc. Dalton Trans.* **1995,** 2225.
45. Kempf, J. Y.; Rohmer, M. M.; Poblet, J. M.; Bo, C.; Bénard, M. *J. Am. Chem. Soc.* **1992,** *114,* 1136.
46. Wery, A. S. J.; Gutiérrez-Zorrilla, J. M.; Luque, A.; Román, P.; Martinez-Ripoll, M. *Polyhedron* **1996,** *15,* 4555.
47. Wang, W.; Zeng, F.-L.; Wang, X.; Tan, M.-Y. *Polyhedron* **1996,** *15,* 265.
48. Petterson, L.; Andersson, I.; Howarth, O. W. *Inorg. Chem.* **1992,** *31,* 4032.

49. Hou, D.; Hagen, K. S.; Hill, C. L. *J. Am. Chem. Soc.* **1992,** *114,* 5864.
50. Hou, D.; Hagen, K. S.; Hill, C. L. *J. Chem. Soc. Chem. Commun.* **1993,** 427.
51. Day, V. W.; Klemperer, W. G.; Yaghi, O. M. *J. Am. Chem. Soc.* **1989,** *111,* 5959.
52. Day, V. W.; Klemperer, W. G.; Yaghi, O. M. *J. Am. Chem. Soc.* **1989,** *111,* 4518.
53. Hardcastle, F. D.; Wachs, I. E. *J. Phys. Chem.* **1991,** *95,* 5031.
54. Cruywagen, J. J.; Rohwer, E. F. C. H. *Inorg. Chem.* **1975,** *14,* 3136.
55. (a) Schwarzenbach, G.; Meier, J. *J. Inorg. Nucl. Chem.* **1958,** *8,* 302; (b) Schwarzenbach, G.; Meier, J; Littler, J. *Helv. Chem. Acta,* **1962,** *45,* 2601.
56. Rohwer, E. F. C. H.; Cruywagen, J. J. *J. S. Afr. Chem. Inst.* **1963,** *26,* 16.
57. (a) Cotton, F. A.; Wilkinson, G. In "Advanced Inorganic Chemistry," 3rd ed.; Interscience: New York, 1972; (b) Cotton, F. A.; Wilkinson, G. In "Advanced Inorganic Chemistry," 5th ed.; Interscience: New York, 1988.
58. Cruywagen, J. J.; Heyns, J. B. B. *J. Chem. Educ.* **1989,** *66,* 861.
59. Paffet, M. T.; Anson, F. C. *Inorg. Chem.* **1981,** *20,* 3967.
60. Tytko, K. H. *Polyhedron* **1986,** *5,* 497.
61. Brown, P. L.; Shying, M. E.; Sylva, R. N. *J. Chem. Soc.* **1987,** 2149.
62. Ozeki, T.; Adachi, H.; Ikeda, S. *Bull. Chem. Soc. Jpn.* **1996,** *69,* 619.
63. Cruywagen, J. J.; Heyns, J. B. B.; Rohwer, E. F. C. H. *J. Inorg. Nucl. Chem.* **1976,** *38,* 2033.
64. Himeno, S.; Ueda, Y.; Hasegawa, M. *Inorg. Chim. Acta* **1983,** *70,* 53.
65. Himeno, S.; Hasegawa, M. *Inorg. Chim. Acta* **1983,** *73,* 255.
66. Cazallas, R.; Citorez, M. J.; Etxebarria, N.; Fernández, L. A.; Madariaga, J. M. *Talanta* **1994,** *41,* 1637.
67. Yokoi, K.; Matsubayashi, N.; Watanabe, I.; Ikeda, S. *Polyhedron* **1993,** *12,* 911.
68. (a) Krumenacker, L. *Bull. Soc. Chim. (France)* **1971,** 362; (b) Krumenacker, L. *Bull Soc. Chim. (France)* **1971,** 368; (c) Krumenacker, L. *Bull. Soc. Chim. (France)* **1971,** 2820; (d) Krumenacker, L. *Bull. Soc. Chim. (France)* **1971,** 2824.
69. Rohwer, E. F. C. H.; Cruywagen, J. J.; Raubenheimer, H. G. *J. S. Afr. Chem. Inst.* **1972,** *25,* 338.
70. Ojo, J. F.; Taylor, R. S.; Sykes, A. G. *J. Chem. Soc. Dalton Trans.* **1975,** 500.
71. Cruywagen, J. J.; Heyns, J. B. B.; Rohwer, E. F. C. H. *J. Inorg. Nucl. Chem.* **1978,** *40,* 53.
72. Lydon, J. D.; Schwane, L. M.; Thompson, R. C. *Inorg. Chem.* **1987,** *26,* 2606.
73. (a) Cruywagen, J. J.; Heyns, J. B. B.; van de Water, R. F. *J. Chem. Soc. Dalton Trans.* **1986,** 1857; (b) Cruywagen, J. J.; Heyns, J. B. B.; Rohwer, E. A. *J. Chem. Soc. Dalton Trans.* **1994,** 45; (c) Cruywagen, J. J.; Rohwer, E. A.; Wessels, G. F. S. *Polyhedron* **1995,** *14,* 3481.
74. Cotton, F. A.; Morehouse, S. M.; Wood, J. S. *Inorg. Chem.* **1963,** *3,* 1603.
75. Matsumoto, K.; Marutani, Y.; Ooi, S. *Bull. Chem. Soc. Jpn.* **1984,** *57,* 2671.
76. Zhou, Z. H.; Wan, H. L.; Tsai, K. R. *Polyhedron* **1996,** *16,* 75.
77. Himeno, S.; Hasegawa, M. *Inorg. Chim. Acta* **1984,** *83,* L5.
78. Yokoi, K.; Matsubayashi, N.; Miyanaga, T.; Watanabe, I.; Murata, K.; Ikeda, S. *Chem. Lett.* **1987,** 1453.
79. Day, V. W.; Fredrich, M. F.; Klemperer, W. G.; Shum, W. *J. Am. Chem. Soc.* **1977,** *99,* 6146.
80. Cruywagen, J. J.; de Wet, H. F. *Polyhedron,* **1988,** *7,* 547.
81. Tytko, K. H.; Baethe, G.; Cruywagen, J. J. *Inorg. Chem.* **1985,** *24,* 3132.
82. Cruywagen, J. J.; Heyns, J. B. B. *Inorg. Chem.* **1987,** *26,* 2569.
83. (a) Sasaki, S.; Sillén, L. G. *Arkiv Kemi* **1968,** *29,* 253; (b) Sasaki, S.; Sillén, L. G. *Acta Chem. Scand.* **1964,** *18,* 104.

84. (a) Pettersson, L.; Anderson, I.; Öhman, L. O. *Acta Chem. Scand.* **1985,** *A39,* 53; (b) Pettersson, L.; Anderson, I.; Öhman, L. O. *Inorg. Chem.* **1986,** *25,* 4726; (c) Pettersson, L. Private communication, 1998.
85. Aveston, J.; Anacker, E. W.; Johnson, J. S. *Inorg. Chem.* **1964,** *3,* 735.
86. Cruywagen, J. J. *Inorg. Chem.* **1980,** *19,* 552.
87. Tytko, K. H.; Baethe, G.; Hirschfield, E. R.; Mehmke, K.; Stellhorn, D. *Z. Anorg. Allgem. Chem.* **1983,** *504,* 43.
88. Yagasaki, A.; Anderson, I.; Pettersson, L. *Inorg. Chem.* **1987,** *26,* 3926.
89. Yagasaki, A.; Sasaki, S. *Bull. Soc. Chem. Jpn.* **1987,** *60,* 763.
90. Johansson, G.; Pettersson, L.; Ingri, N. *Acta Chem. Scand.* **1979,** *A36,* 305.
91. Sillén, L. G. *Pure Appl. Chem.* **1968,** *17,* 55.
92. (a) Tytko, K. H.; Schönfeld, B. *Z. Naturforsch Teil B* **1975,** *30,* 471; (b) Tytko, K. H.; Petridis, G.; Schönfeld, B. *Z. Naturforsch Teil B* **1980,** *35,* 45; (c) Tytko, K. H.; Baethe, G. *Z. Anorg. Allg. Chem.* **1987,** *355,* 85.
93. (a) Lyham, E. L.; Cyvin, S. J. *Z. Naturforsch Teil A* **1979,** *34,* 867; (b) Lyham, L. *Acta Chem. Scand.* **1982,** *A36,* 595.
94. Lyham, E. L.; Pettersson, L. *Chem. Scr.* **1977,** *12,* 142.
95. Ng, K. Y. S.; Gulari, E. *Polyhedron* **1984,** *3,* 1001.
96. (a) Lindqvist, I. *Ark. Kemi* **1950,** *2,* 325; (b) Sjöbom, K.; Hedman, B. *Acta Chem. Scand.* **1973,** *27,* 3673; (c) Evans, H. T., Jr.; Gatehouse, B. M.; Leverett, P. *J. Chem. Soc. Dalton Trans.* **1975,** 505.
97. Ozeki, T.; Kihara, H.; Ikeda, S. *Anal. Chem.* **1988,** *60,* 2055.
98. Himeno, S.; Niija, H.; Ueda, T. *Bull. Soc. Chem. Jpn.* **1997,** *70,* 631.
99. (a) Filowitz, M.; Ho, R. C. K.; Klemperer, W. G.; Shum, W. *Inorg. Chem.* **1979,** *18,* 93; (b) Filowitz, M.; Klemperer, W. G.; Messerle, L.; Shum, W. *J. Am. Chem. Soc.* **1976,** *98,* 2345.
100. Gheller, S. F.; Sidney, M.; Masters, A. F.; Brownlee, R. T. C.; O'Connor, M. J.; Wedd, A. G. *Aust. J. Chem.* **1984,** *37,* 1825.
101. Sarrazin, P.; Mouchel, B.; Kasztelan, S. *J. Phys. Chem.* **1989,** *93,* 904.
102. (a) Maksimovskaya, R. I.; Burtseva, K. G. *Polyhedron* **1985,** *4,* 1559; (b) Maksimovskaya, R. I.; Chumachenko, N. N. *Polyhedron* **1987,** *6,* 1813.
103. Coddington, J. M.; Taylor, M. J. *J. Chem. Soc. Dalton Trans.* **1990,** 41.
104. Howarth, O. W.; Kelly, P. *J. Chem. Soc. Dalton Trans.* **1990,** 81.
105. Isobe, M.; Marumo, F.; Yamase, T.; Ikawa, T. *Acta Cryst.* **1978,** *B34,* 2728.
106. Howarth, O. W.; Kelly, P. *J. Chem. Soc. Chem. Commun.* **1988,** 1236.
107. (a) Cruywagen, J. J.; Rypstra, T. *Polyhedron* **1985,** *4,* 545; (b) Cruywagen, J. J.; Draaijer, A. G.; Rypstra, T. *J. S. Afr. J. Chem.* **1988,** *41,* 89; (c) Cruywagen, J. J.; Draaijer, A. G. *Polyhedron* **1992,** *11,* 141.
108. Arnek, R.; Szilard, I. *Acta Chem. Scand.* **1968,** *22,* 1334.
109. Kiba, N.; Takeuchi, T. *J. Inorg. Nucl. Chem.* **1974,** *36,* 847.
110. Day, V. W.; Fredrich, M. F.; Klemperer, W. G.; Shum, W. *J. Am. Chem. Soc.* **1977,** *99,* 952.
111. Fuchs, J.; Hartl, H. *Angew. Chem. Int. Ed. Engl.* **1976,** *15,* 375.
112. (a) Lindqvist, I. *Acta Crystallogr.* **1952,** *5,* 667; (b) Atovmyan, L. O.; Krasochka, O. N. *J. Struct. Chem. (USSR)* **1972,** *13,* 319; (c) Gatehouse, B. M. *J. Less-Common Met.* **1977,** *54,* 283; (d) Weakly, T. J. R. *Polyhedron* **1982,** *1,* 17; (e) Vivier, H.; Barnard, J.; Djomaa, H. *Rev. Chim. Miner.* **1977,** *14,* 584; (f) Fuchs, J.; Knöpnadel, I.; Brudgam, I. *Z. Naturforsch. Teil B* **1974,** *29,* 473; (g) Piggot, B. G.; Wong, S. F.; Hursthouse, M. B.; Short, R. L. *Polyhedron* **1988,** *7,* 2605; (h) Giter, L.; Roman, P.; Jaud, J.; Galy, J. *Z. Kristallogr.* **1981,** *154,* 59; (i) Fitzroy, M. D.; Fallon, G. D.;

Murray, K. S. *Inorg. Chim. Acta* **1989,** *157,* 187; (j) Roman, P.; Luque, A.; Aranzabe, A.; Gutierrez-Zorrilla, J. M. *Polyhedron,* **1992,** *11,* 2027.
113. Niven, M. L.; Cruywagen, J. J.; Heyns, J. B. B. *J. Chem. Soc. Dalton* **1991,** 2007.
114. Wang, X.; Xu, X. X.; Wang, Q. Y.; Zhai, Y. L. *Polyhedron* **1992,** *11,* 1423.
115. Klemperer, W. G.; Shum, W. *J. Am. Chem. Soc.* **1976,** *98,* 8291.
116. (a) Paulat-Böschen, I. *J. Chem. Soc. Chem. Comm.* **1979,** 780; (b) Tytko, K. H.; Schönfeld, B.; Buss, B.; Glemser, O. *Angew. Chem. Int. Ed. Engl.* **1973,** *12,* 330.
117. Fuchs, J.; Hartl, H.; Hunnius, W.-D.; Mahjour S. *Angew. Chem. Int. Ed. Engl.* **1975,** *14,* 644.
118. Böschen, I.; Buss, B.; Krebs, B.; Glemser, O. *Angew. Chem. Int. Ed. Engl.* **1973,** *12,* 409.
119. Kreusler, H. U.; Förster, A.; Fuchs, J. *Z. Naturforsch. Teil B* **1980,** *35,* 242.
120. Förster, A.; Kreusler, H. U.; Fuchs, J. *Z. Naturforsch Teil B* **1985,** *40,* 1139.
121. Gatehouse, B. M.; Leverett, P. *J. Chem. Soc. A* **1968,** 1398.
122. Fuchs, J.; Jahr, K. F. *Z. Naturforsch.* **1968,** *B23,* 1380.
123. Allcock, H. R.; Bissell, E. C.; Shawl, E. T. *J. Am. Chem. Soc.* **1972,** *94,* 8603.
124. Murata, K.; Yamamoto, E.; Ikeda, S. *Bull. Chem. Soc. Jpn.* **1983,** *56,* 941.
125. Murata, K.; Yamashita, S.; Yamamoto, E.; Ikeda, S. *Polyhedron* **1990,** *14,* 1717.
126. Himeno, S.; Ishii, N.; Hasegawa, M.; Saito, A.; Hori, T. *Inorg. Chim. Acta* **1987,** *131,* 11.
127. Filowitz, M.; Klemperer, W. G.; Shum, W. *J. Am. Chem. Soc.* **1978,** *100,* 2580.
128. Chen, Q.; Ma, L.; Liu, S.; Zubieta, J. *J. Am. Chem. Soc.* **1989,** *111,* 5944.
129. Krebs, B.; Paulat-Böschen, I. *Acta Cryst. Sect. B* **1976,** *B32,* 1697.
130. Clegg, W.; Sheldrick, G. M.; Garner, C. D.; Walton, I. B. *Acta Cryst.* **1982,** *B38,* 2906.
131. Wesolowski, D.; Drummond, S. E.; Mesmer, R. E.; Ohmoto, H. *Inorg. Chem.* **1984,** *23,* 1132.
132. Cruywagen, J. J.; Pienaar, A. T. *Polyhedron* **1989,** *8,* 71.
133. Cruywagen, J. J.; Van der Merwe, I. F. J. *J. Chem. Soc. Dalton Trans.* **1987,** 1701.
134. Islam, M. A.; Thompson, R. C. *Inorg. Chem.* **1989,** *28,* 4419.
135. Aveston, J. *Inorg. Chem.* **1964,** *3,* 981.
136. Sasaki, Y. *Acta. Chem. Scand.* **1961,** *15,* 175.
137. Arnek, R.; Sasaki, Y. *Acta. Chem. Scand. Ser. A* **1974,** *23,* 20.
138. Tytko, K. H.; Glemser, O. *Z. Naturforsch. Teil B* **1970,** *25,* 429.
139. Jander, G.; Mojert, D.; Aden, T. *Z. Anorg. Allg. Chem.* **1929,** *180,* 129.
140. Fuchs, J.; Flindt, E. P. *Z. Naturforsch. Teil B* **1979,** *34,* 412.
141. Hastings, J. J.; Howarth, O. W. *J. Chem. Soc. Dalton Trans.* **1992,** 209.
142. Gans, P.; Sabatini, A.; Vacca, A. *J. Chem. Soc. Dalton Trans.* **1985,** 1195.
143. Lipscomb, W. N. *Inorg. Chem.* **1965,** *4,* 132.
144. Hartl, H.; Palm, R.; Fuchs, J. *Angew. Chem. Int. Ed. Engl.* **1993,** *32,* 1492.
145. Launey, J. P.; Boyer, M.; Chauveau, F. *J. Inorg. Nucl. Chem.* **1976,** *38,* 243.
146. Lehmann, T.; Fuchs, J. *Z. Naturforsch, Teil B* **1988,** *43,* 89.
147. (a) Fuchs, J.; Hartl, H.; Schiller, W.; Gerlach, U. *Acta Crystallogr. B* **1975,** *32,* 740; (b) Nomiya, K.; Miyazaki, T.; Maeda, K.; Miwa, M. *Inorg. Chim. Acta* **1987,** *127,* 65.
148. Corsini, A.; Subramanian, K. *J. Inorg. Nucl. Chem.* **1978,** *40,* 1777.
149. Boyer, M.; LeMeur, B. *C. R. Acad. Sci. Ser. C* **1975,** *281,* 59.
150. Termes, S. C.; Pope, M. T. *Inorg. Chem.* **1978,** *17,* 500.
151. Souchay, P.; Chauveau, F.; Le Meur, B. *Compt. Rend.* **1970,** *270C,* 1401.
152. LeFebre, J.; Chauveau, F.; Doppelt, P. *J. Am. Chem. Soc.* **1981,** *103,* 4589.
153. Souchay, P.; Boyer, P.; Chauveau, F.; *K. Tek. Hoegsk. Handl. No. 259.* (Contributions to Coordination Chemistry in Solution, Stockholm 1972, p 159.)

154. Boyer, M. *J. Electroanal. Chem. Interfacial Electrochem.* **1971,** *31,* 441.
155. Deery, M. J.; Howarth, O. W.; Jennings, K. R. *J. Chem. Soc. Dalton Trans.* **1997,** 4783.
156. Burtseva, K. G.; Chernaya, T. S.; Sirota, M. I. *Dokl. Akad. Nauk SSSR* **1978,** *243,* 104.
157. (a) Fuchs, J.; Freiwald, W.; Hartl, H. *Acta Cryst.* **1978,** *B34,* 1764; (b) LaRue, W. A.; Liu, A. T.; San Filippo, J., Jr. *Inorg. Chem.* **1980,** *19,* 315; (c) Grase, R.; Fuchs, J. *Z. Naturforsch. Teil B* **1977,** *32,* 1379.
158. (a) Allman, R. *Acta Crystallogr.* **1971,** *B27,* 1393; (b) d'Amour, H.; Allman, R. *Z. Kristallogr.* **1972,** *136,* 23; (c) Tsay, Y. H.; Silverton, J. V. *Z. Kristallogr.* **1973,** *137,* 256; (d) d'Amour, H.; Allman, R. *Z. Kristallogr.* **1973,** *138,* 5; (e) Evans, H. T.; Rollins, O. W., Jr. *Acta Crystallogr.* **1976,** *B32,* 1565; (f) Averbuch-Pouchot, M. T.; Tordjman, I.; Durif, A.; Guitel, J. C., *Acta Crystallogr.* **1979,** *35B,* 1675; (g) Cruywagen, J. J.; Van der Merwe, I. F. J.; Nassimbeni, L. R.; Niven, M. L.; Symonds, E. A. *J. Crystallogr. Spectrosc. Res.* **1986,** *16,* 525; (h) Evans, H. T., Jr.; Kortz, U.; Jameson, G. B. *Acta Cryst,* **1992,** *C49,* 856.
159. Evans, H. T., Jr. In "Polyoxometalates: From Platonic Solids to Anti-Retroviral Activity" Pope, M. T. and Müller, A., Eds., p. 71; Kluwer: Dordrecht, 1994.
160. Evans, H. T., Jr.; Prince, E. *J. Am. Chem. Soc.* **1983,** *105,* 4838.
161. Launey, J. P. *J. Inorg. Nucl. Chem.* **1976,** *38,* 807.
162. Fuchs, J.; Palm, R.; Hartl, H. *Angew. Chem. Int. Ed. Engl.* **1996,** *35,* 2651.
163. Howarth, O. W.; Pettersson, L.; Andersson, I. *J. Chem. Soc. Dalton Trans.* **1989,** 1915.
164. Harrison, A. T.; Howarth, O. W. *J. Chem. Soc. Dalton Trans.* **1985,** 1953.
165. Howarth, O. W.; Pettersson, L.; Andersson, I. *J. Chem. Soc. Dalton Trans.* **1991,** 1799.
166. Klemperer, W. G.; Shum, W. *Inorg. Chem.* **1979,** *18,* 1893.
167. Björnberg, A. *Acta Crystallogr. B* **1979,** *35,* 1995.
168. Nenner, A.-M. *Acta Crystallog. C* **1985,** *41,* 1703.
169. Björnberg, A. *Acta Crystallogr. B* **1980,** *36,* 1530.
170. Björnberg, A. *Acta Crystallogr. B* **1979,** *35,* 1989.
171. Andersson, I.; Hastings, J. J.; Howarth, O. W.; Pettersson, L. *J. Chem. Soc. Dalton Trans.* **1996,** 2705.
172. Leparulo-Loftus, M. A.; Pope, M. T. *Inorg. Chem.* **1987,** *26,* 2112.
173. Flynn, C. M., Jr.; Pope, M. T. *Inorg. Chem.* **1971,** *10,* 2524.
174. Klemperer, W. G.; Shum, W. *J. Am. Chem. Soc.* **1978,** *100,* 4891.
175. Kazanskii, L. P.; Spitsyn, V. I. *Dokl. Phys. Chem.* **1975,** *223,* 721.
176. Maestra, J. M.; Sarasa, J. P.; Bo, C.; Poblet, J. M.; *Inorg. Chem.* **1998,** *37,* 3071.
177. Hastings, J. J.; Howarth, O. W. *Polyhedron* **1993,** *12,* 847.
178. Hastings, J. J.; Howarth, O. W. *Polyhedron* **1990,** *9,* 143.
179. Flynn, C. M. Jr.; Pope, M. T.; O'Donnel, S. O. *Inorg. Chem.* **1974,** *13,* 81.
180. Andersson, I.; Hastings, J. J.; Howarth, O. W.; Pettersson, L. *J. Chem. Soc. Dalton Trans.* **1994,** 1061.
181. Pope, M. T.; Müller, A. *Angew. Chem. Int. Ed. Engl.* **1991,** *30,* 34.
182. Maksimovskaya, R.; Maksimov, S. M.; Blokhin, A. A.; Taushkanov, V. P. *Russ. J. Inorg. Chem.* **1991,** *36,* 575.
183. Jeannin, Y.; Launay, J. P.; Sanchez, C.; Livage, J.; Fournier, M. *Nouv J. Chim.* **1980,** *4,* 587.
184. Bondareva, E. V.; Borisova, A. P.; Morosanova, S. A.; Evseev, A. M. *Zh. Neorg. Khim* **1989,** *34,* 3196.
185. Hastings, J. J.; Howarth, O. W. *J. Chem. Soc. Dalton Trans.* **1995,** 2891.

ADVANCES IN INORGANIC CHEMISTRY, VOL. 49

MEDICINAL INORGANIC CHEMISTRY

ZIJIAN GUO and PETER J. SADLER

Department of Chemistry, University of Edinburgh, Edinburgh EH9 3JJ, United Kingdom

Copyright □ 2000 by Academic Press.
All rights of reproduction in any form reserved.
0898-8838/00 $30.00

I. Introduction

Biomedical inorganic chemistry ("Elemental Medicine") is an important new area of chemistry. It offers potential for the design of novel therapeutic and diagnostic agents and hence for the treatment and understanding of diseases which are currently intractable (*1–3*). Moreover, it is evident that many organic compounds used in medicine do not have a purely organic mode of action; some are activated or biotransformed by metal ions, including metalloenzymes, others have a direct or indirect effect on metal ion metabolism. The involvement of nonmetallic inorganic compounds in the mechanism of action of organic drugs is also important although not directly the subject of this chapter. Here we focus on metal complexes, and especially on recent developments which are having an impact on medical practice.

Platinum complexes are now among the most widely used drugs for the treatment of cancer. Three injectable Pt(II) compounds have been approved and several other *cis*-diam(m)ine complexes are on clinical trials, including an oral Pt(IV) complex. The established structure–activity rules are being broken: active Pt complexes without coordinated NH groups and active trans complexes are emerging. With appropriate choice of ligands, it is possible to change the mode of Pt binding to DNA and to circumvent acquired resistance of cancer cells to cisplatin; a trinuclear Pt complex with two monofunctional Pt centers has recently been found to exhibit an intriguing new mode of DNA binding and has entered clinical trials.

Other metal complexes also have promising anticancer activity. Two Ti(IV) complexes are on clinical trial, an acetylacetonate derivative (budotitane) and titanocene dichloride, and the antimetastic activity of octahedral Ru(III) complexes is attracting attention, one of which is now on clinical trial. Ru(III), like several other metal ions, can be delivered to cells via the iron transport protein transferrin.

There is potential in the anti-HIV field. Polyoxometallates of the Keggin type bind to viral envelope sites on cell surfaces and interfere with virus adsorption. Metal-chelating macrocyclic bicyclam ligands are among the most potent inhibitors of HIV ever described, and there is considerable interest in the role of Zn proteins in the viral life cycle.

Metal ions are required for the activity of anti-HIV G-quartet oligonucleotides (antisense oligonucleotides) such as T30177, a potent inhibitor of the enzyme HIV-1 integrase.

Microbial resistance to established organic antibiotics is a potentially serious problem and provides an impetus for the development of novel antimicrobial metal compounds. The potency of Ag(I) ions is well known—but how does Ag(I) kill a bacterium? Much current attention is focused on Bi(III) on account of its ability to kill *Helicobacter pylori,* an organism which prevents ulcers from healing. Bismuth(III) chemistry has many unusual features: a variable coordination number, strong bonds to alkoxide ligands, the stereochemical role of its $6s^2$ lone pair, facile formation of polymers, and dual "hard" and "soft" character.

Injectable Au(I) thiolates and an oral Au(I) phosphine complex are widely used for the treatment of rheumatoid arthritis. Proteins appear to be the targets for gold therapy, including albumin in blood plasma and enzymes in joint tissues. The recent detection of $[Au(CN)_2]^-$ in the blood and urine of patients undergoing gold therapy (chrysotherapy) raises the possibility that this is an active metabolite. Cyanide could be intimately involved in the metabolic pathways for other metal ions (both natural and therapeutic) in the body since it can readily be synthesized by some cells. The recent discovery that oxidation of administered Au(I) compounds to Au(III) may be responsible for some of the side-effects of gold therapy has highlighted interests in the biological redox chemistry of gold, including possible stabilization of Au(III) by peptides and proteins. Redox-active metal ions can be used to control free radical formation and destruction: manganese superoxide dismutase mimics such as $[Mn([15]aneN_5)Cl_2]$ offer new possibilities for treating inflammation as well as myocardial ischemic and reperfusion injury, and Mn(III) and Fe(III) porphyrins can destroy damaging peroxynitrite.

Metal porphyrins as well as texaphyrin and phthalocyanin complexes are also featuring in the development of new photodynamic and sonodynamic therapeutic modes.

Design concepts are now being applied more effectively to mineral supplements. For example, by controlling the redox potential of iron, toxic effects associated with excess Fe(II) during parental supplementation can be avoided. Peroxovanadate complexes can inhibit insulin-receptor-associated phosphotyrosine phosphatase and activate insulin receptor kinase, and both V(IV) and V(V) offer promise as potential insulin mimics.

Lithium compounds are kinetically labile and are used on a large scale (*ca.* 1 in 1500 of the UK population) for the treatment of bipolar

disorders, and Li(I) inhibition of Mg(II)-dependent inositol monophosphatase enzymes leads to interference with Ca(II) metabolism.

Less labile metal ions can be used to control the levels of biologically active ligands in the body. Thus Fe(III) in sodium nitroprusside delivers NO to tissues and is used for the treatment of hypertension and control of blood pressure. The possibility arises of utilizing Ru(III) to scavenge NO in the treatment of septic shock.

The injection of gram quantities of Gd(III) complexes to provide contrast in magnetic resonance images (MRI) of the body illustrates how the toxicity of metal ions and their targeting can be finely controlled by the appropriate choice of ligands. Four Gd(III) complexes and a Mn(II) complex are currently in clinical use. Relaxation and contrast can be optimized via control of the number of metal-bound H_2O molecules, their exchange rate with bulk water, and the tumbling time of the complex. Radioactive metal ions can be used in diagnosis and therapy or for both (e.g., ^{67}Cu). Metastable ^{99m}Tc has optimum radioemission and half-life properties for diagnosis and with the appropriate choice of oxidation state and ligands can be targeted to many different organs; its chemistry is rich with oxidation states ranging from -1 to $+7$ and coordination numbers from 4 to 7. More than 20 ^{99m}Tc complexes are currently in clinical use. Metal-tagged antibodies offer promise for specific targeting to tumor cells. Exciting is the potential use of activatable radioactive or paramagnetic complexes to probe biological functions; for example, specific diastereomers of Tc complexes can be trapped in the brain via biotransformation mechanisms, and the ability of certain Gd(III) complexes to produce MRI contrast can be switched on by enzymes.

The strong relationship between metals and some organic drugs is becoming apparent. The organic anticancer drug Batimastat, for example, is a chelating agent targeted to a zinc metalloenzyme; bleomycin requires iron for activation; and complexation of anthracyclines with Ca(II) can inhibit their oral adsorption. Metalloenzyme inhibitors in particular will provide new generations of novel drugs.

Although we have attempted to review the area comprehensively, the topic is vast with a wide range of applications, and the reader is referred to reviews elsewhere to complement our treatment (*4*, *632–634*).

II. Anticancer Agents

The search for antitumor activity among metal compounds has been greatly stimulated by the success of cisplatin. Some recent advances in this field are considered here. There are useful recent books on the

use of metal compounds in cancer therapy including those of Lippert (*635*), Keppler (*5*), and Fricker (*6*) and the proceedings of a 1995 symposium (*7*).

A. Platinum Complexes: Design and Mechanism of Action

In 1965 Rosenberg *et al.* (*8*, *9*) accidentally discovered the antiproliferative effect of *cis*-diammine platinum complexes, which led to the first clinical trials of *cis*-$[PtCl_2(NH_3)_2]$ **1** in 1971 and resulted in the clinical use of cisplatin worldwide. Cisplatin and carboplatin **2** are the most widely used anticancer drugs, and two other analogs, nedaplatin **3** and oxaliplatin **4** (chiral centers indicated), have recently been approved for clinical use in Japan and France, respectively.

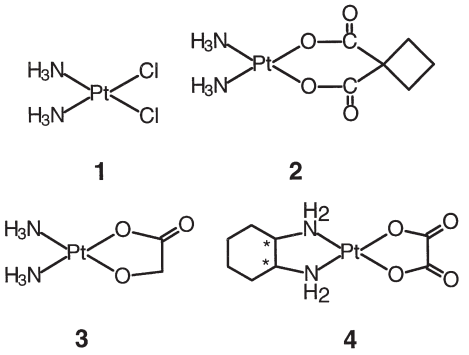

Knowledge of the mechanism of action of cisplatin has provided a rational for the design of new platinum drugs. There are excellent recent reviews on various aspects of Pt anticancer complexes including those by Lippard (DNA repair, HMG recognition) (*10–12*), Reedijk (DNA binding) (*13*, *14*), Lippert (transplatin, multistranded DNA) (*15*, *16*), Kozelka (modeling nucleic acid complexes, DNA) (*17*, *18*), Leng (catalytic activity of DNA) (*19*), Lilley (HMG recognition) (*20*), Leuba (protein recognition) (*21*), Farrell (active trans complexes) (*22*), Arpalahti (kinetics) (*23*), Wang (DNA structure) (*24*), Hambley (structure–reactivity relationship, modeling DNA adducts) (*25*), and Appleton (amino acid and peptide complexes) (*26*).

1. Mechanism of Action and Resistance to Cisplatin

It seems clear that the cytotoxic effects of cisplatin are due to the formation of a variety of stable adducts on DNA which then block

replication or inhibit transcription. Some of the important events relating to the mechanism of action of cisplatin and cellular resistance are summarized in Fig. 1. It is apparent that resistance significantly undermines the curative potential of platinum-based drugs against some cancers.

a. Cisplatin Transport The mechanism by which cisplatin enters the cell is still not fully understood (*27*). It appears that both diffusion and active transport mechanisms are involved. The latter may require a gated channel or specific transport proteins (*28*).

Reduced transport of cisplatin across the cell membrane can be related to drug resistance. A transmembrane P-glycoprotein with a molecular mass of 170 kDa, encoded by the so-called multidrug resistance (MDR1) gene, has been found in multidrug-resistant cell lines and can act as a pump to prevent the accumulation of drugs in the cell (drug efflux) (*29*). Overexpression of this glycoprotein is one of the major mechanisms by which cancer cells develop resistance. A 190 kDa membrane-bolted glycoprotein, encoded by a multidrug resistance-associated protein (MRP) gene, could also play a role in resistance by direct extrusion of platinum drugs from the cell and/or by mediating sequestration of the drugs into intracellular compartments, both leading to a reduction in effective intracellular drug concentration (*30*). However, other evidence shows that reduced drug influx rather than enhanced drug efflux is a consistent feature of acquired cisplatin resistance (*31*, *32*). Changes in cell membrane properties (*33*) can also affect cisplatin transport and result in drug resistance. Sharp *et al.* (*34*) have shown that cisplatin enters cisplatin-

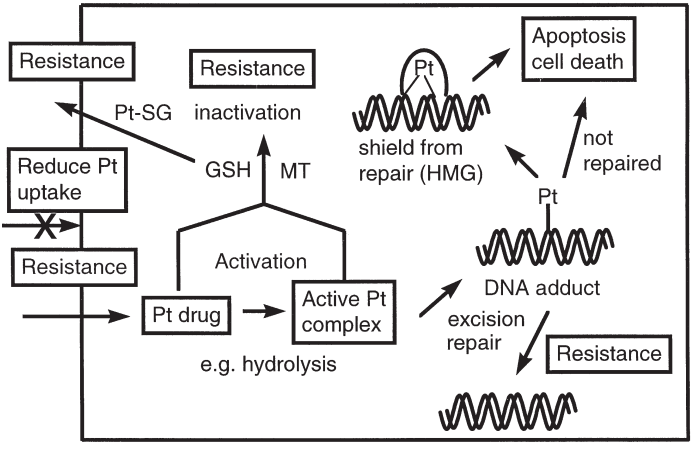

FIG. 1. Some of the factors involved in the mechanism of action and resistance of cisplatin.

resistant human ovarian carcinoma cell lines by passive diffusion only; active/facilitated transport is not observed.

Intracellular thiolate ligands such as glutathione (GSH, the tripeptide γ-L-Glu-L-Cys-Gly) are believed to inactivate cisplatin because the reactions with cisplatin tend to be irreversible (*35*). Elevated levels of GSH have been observed in cisplatin-resistant cells. Recently, it has been shown that an MRP gene, which encodes a human ATP-dependent glutathione *S*-conjugate export pump (GS-X pump), is expressed at higher levels in cisplatin-resistant (HL-60/R-CP) cells than in sensitive cells (*36*). The GS-X pump may contribute to the excretion of Pt–GS complexes from cells (*37*).

Cisplatin resistance in some cell types involves the cysteine-rich intracellular protein metallothionein (MT). High levels of MT are found in cisplatin-resistant cells (*38*). Cisplatin administration leads to the induction of MT in, e.g., the liver, and may bind and inactivate Pt, but MT may also be involved in scavenging free radicals. Reactions between MT and cisplatin lead to the displacement of the ammine ligands and $Pt_{7\text{-}10}$–MT containing PtS_4 groups (S = Cys) (*39*). Platinum binding to MT is *ca.* 10–30 times stronger than Zn(II) and Cd(II) (*40*). Transplatin reacts with MT faster than cisplatin (*41*).

b. Hydrolysis (Aquation) Intracellular aquation has long been thought to be an important process for the activation of chloro Pt anticancer diam(m)ine complexes. The Cl^- ligands are substituted by aqua ligands, which are much more reactive, e.g., toward substitution by guanine residues on DNA (Scheme 1).

The aquation rate is mainly determined by the trans effect of the ligand trans to Cl. The aquation rate constants of some platinum complexes are listed in Table I. For example, the rate of hydrolysis of Cl^- trans to c-$C_6H_{11}NH_2$ in complex **14**, a metabolite of the oral drug **11** (*42*), is about twice as fast as trans to NH_3 (*43*).

Steric hindrance is well known to slow down the rates of ligand substitution reactions in square-planar metal complexes. An example for which steric hindrance controls the aquation rate is complex **9**. The effect of 2-picoline on the rate of hydrolysis of Cl^- trans to NH_3 (cis to 2-picoline) is dramatic, being about 5 times as slow as the analogous Cl^- ligand in the nonsterically hindered 3-picoline complex (Table I) (*44*).

Cisplatin diaqua is very reactive, but the deprotonated hydroxo forms are usually considered to be relatively inert, therefore the acidity of the coordinated water molecules in aqua complexes can be directly relevant to their reactivity with target molecules. The pK_a values of some Pt–aqua complexes are listed in Table II.

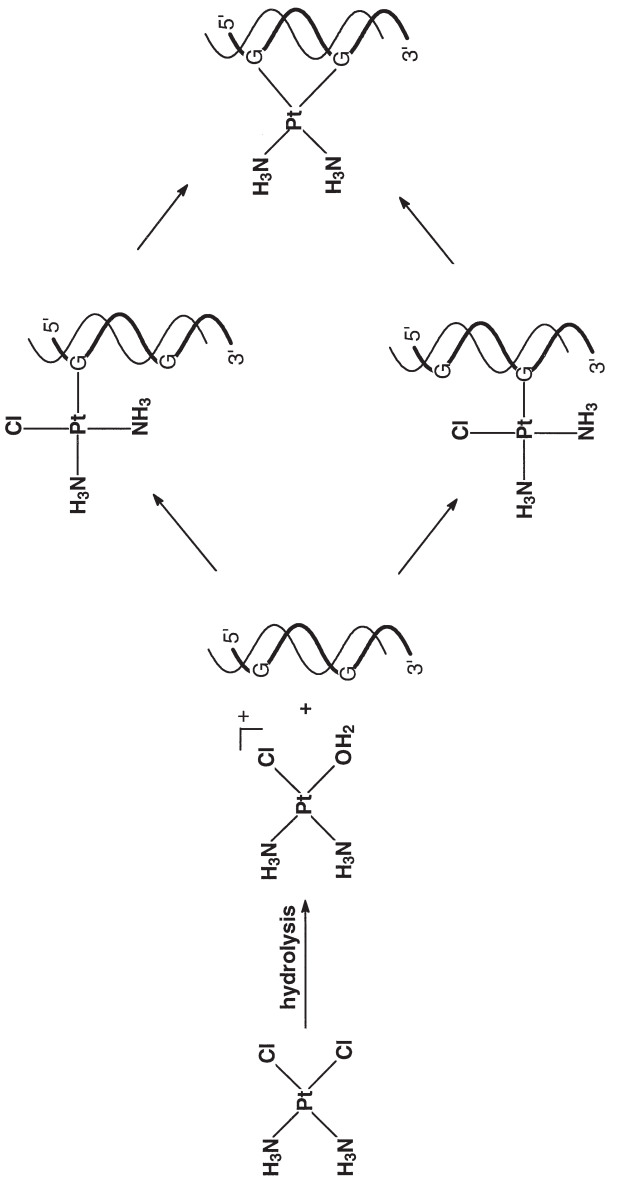

SCHEME 1.

TABLE I

RATE CONSTANTS k FOR AQUATION IN PLATINUM(II)–AM(M)INE COMPLEXES

Complex	10^5 k (s^{-1})	$t_{1/2}$ (h)	I (M)	Temp (°C)	Reference
Cisplatin	k_1: 7.66[a]	2.51	0.01	37	(*609*)
	k_2: 7.51[a]	2.56			
	k: 10.2[a]	1.9		37	(*613*)
	k_1: 7.56	2.55	0.1	25	(*612*)
	k_1: 6.32	3.04	1	25	
Transplatin	k: 9.8	1.96	0.3	25	(*612*)
$[Pt(en)Cl_2]$	k: 5.13	3.75	0.1	25	(*612*)
$[Pt(CHXN)Cl_2]$	k: 7.25	2.66	0.1	25	(*612*)
$[Pt(R\text{-}en)Cl_2]$	k_1: 3.2	6.01	0.1	25	(*611*)
	k_2: 7.8	2.47	0.1	25	
$[Pt(R'\text{-}en)Cl_2]$	k: 8.1	2.38		37	(*610*)
cis-$[Pt(NH_3)$[b]	k_{1a}: 6.10	3.14		37	(*43*)
$(c\text{-}C_6H_{12}NH_2)Cl_2]^+$[b]	k_{1b}: 3.68	5.20			
cis-$[Pt(NH_3)(2\text{-}Py)Cl_2]$[c]	k_{1a}: 3.19	6.03	0.1	37	(*44*)
	k_{1b}: 2.21	8.71			
cis-$[Pt(NH_3)(3\text{-}Py)Cl_2]$	k_{1a}: 4.47	4.31	0.1	37	(*44*)
	k_{1b}: 10.3	1.87			

[a] Rate constants determined during the reaction of cisplatin with DNA.

[b] k_{1a} corresponds to the hydrolysis of Cl^- *trans* to the $c\text{-}C_6H_{11}NH_2$, and k_{1b} to the hydrolysis of Cl^- *trans* to NH_3.

c. DNA Platination i. *Intrastrand crosslinks* The major adducts of platinum drugs with DNA are the 1,2-GpG and 1,2-ApG intrastrand cross-links, which account for *ca.* 90% of the platination adducts. The properties of these adducts have been extensively characterized and reviewed. Solution NMR and solid-state X-ray crystal structures have shown that platinum crosslinks induce bending and unwinding of DNA and cause partial destacking of purine bases. The NMR solution structure of *cis*-$\{Pt(NH_3)_2\}^{2+}$–d(CCTG*G*TCC)·d(GGACCAGG) indicates that the B-DNA backbone conformation is significantly altered to accommodate the platinated lesion (Fig. 2) (*45*). A recent X-ray crystal structure of cisplatin-bound duplex DNA d(CCTCTG*G* TCTCC)·d(GGAGACCAGAGG) shows that cisplatin bends DNA by 35°–40° in the direction of the major groove with a dihedral angle of 26° between the two guanine rings (Fig. 3) (*46*, *47*). The duplex adopts a juxtaposition of A-like and B-like helical DNA segments. Spectroscopic and calorimetric studies on the major adduct of cisplatin with a 20-mer DNA duplex containing a GG intrastrand cross-link have suggested that platination induces a conformational shift from a B-like to an A-like form (*48*). Such a feature for cisplatin-

TABLE II

pK_a VALUES OF H_2O LIGANDS IN PLATINUM(II)–AM(M)INE COMPLEXES (298 K)

Compound	pK_a	H_2O (*trans* to)	Reference
cis-$[Pt(NH_3)_2(H_2O)_2]^{2+}$	5.37	NH_3	(*614*)
cis-$[Pt(NH_3)_2(H_2O)(OH)]^{+}$	7.21	NH_3	(*614*)
	7.87		(*615*)
	7.1		(*616*)
cis-$[PtCl(NH_3)_2(H_2O)]^{+}$	6.42	NH_3	(*614*)
	6.85		(*615*)
	6.3		(*616*)
cis-$[Pt(NH_3)]$	5.81	NH_3/c-$C_6H_{11}NH_2$	(*607*)
$(c\text{-}C_6H_{11}NH_2)(H_2O)_2]^{2+}$	7.56		
cis-$[PtCl(NH_3)]$	6.73	NH_3/c-$C_6H_{11}NH_2$	(*607*)
$(c\text{-}C_6H_{11}NH_2)(H_2O)]^{+}$			
trans-$[PtCl(NH_3)]$	5.9	Cl	(*607*)
$(c\text{-}C_6H_{11}NH_2)(H_2O)]^{+}$			
trans-$[PtCl(NH_3)_2(H_2O)]^{+}$	5.63	Cl	(*612*)
cis-$[Pt(NH_3)(2\text{-Py})(H_2O)_2]^{2+}$	5.22		
	7.16		
cis-$[Pt(NH_3)(2\text{-Py})Cl(H_2O)]^{+}$	6.49	NH_3	(*44*)
cis-$[Pt(NH_3)(2\text{-Py})Cl(H_2O)]^{+}$	6.13	2-Py	(*44*)
cis-$[Pt(NH_3)(3\text{-Py})(H_2O)_2]^{2+}$	5.07		(*44*)
	6.94		
cis-$[Pt(NH_3)(3\text{-Py})Cl(H_2O)]^{+}$	6.26	NH_3	(*44*)
cis-$[Pt(NH_3)(3\text{-Py})Cl(H_2O)]^{+}$	5.98	3-Py	(*44*)
$[Pt(en)Cl(H_2O)]^{+}$	5.60	NH_2	(*612*)
$[Pt(dien)(H_2O)]^{2+}$	6.24	NH	(*617*)
	6.0	NH	(*618*)
$[Pt(NH_3)_3(H_2O)]^{2+}$	6.0	NH_3	(*49*)

modified DNA duplexes may be essential for recognition by cellular proteins such as HMG (see "Protein Recognition").

It is known that platinum forms bifunctional DNA adducts with the following order of sequence preference: -GG- > -AG- ≫ -GA and that DNA platination is kinetically controlled. Therefore there have been a number of approaches to examine the kinetics of formation of adducts with DNA of different base sequences. Chottard and colleagues have determined the rates of both platination and chelation steps for reactions of cisplatin diaqua *cis*-$[Pt(NH_3)_2(H_2O)_2]^{2+}$ with short DNA oligonucleotides (*49*, *50*). For the double-stranded oligonucleotide $d(TTGGCCAA)_2$ the formation of the 5′-G monoaqua adduct is faster than that of the 3′-G monoadduct, and macrochelate ring closure of the 5′-G monoaqua to give the bifunctional adduct (half-life 3.2 h at 293 K) is much slower than that of the 3′-G monoadduct.

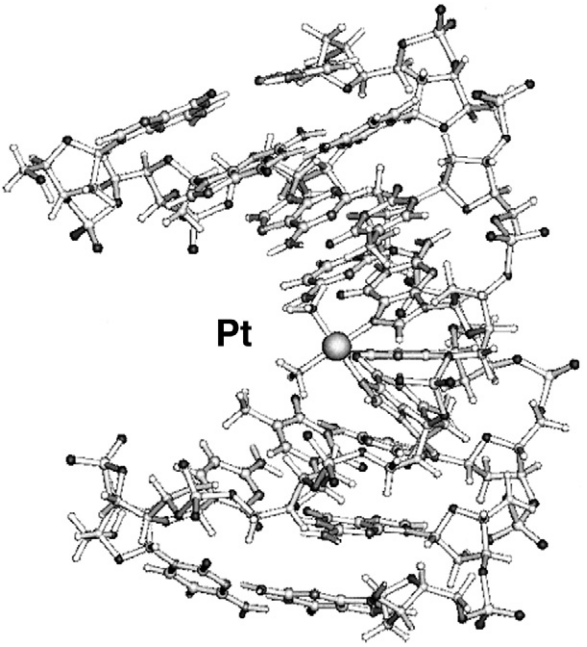

FIG. 2. The NMR-refined structure of *cis*-{$Pt(NH_3)_2$}$^{2-}$–d(CCTG*G*TCC)·d(GGAC CAGG) showing how DNA is significantly altered from the B-form to accommodate platination (structure reference: PDBID, 1AU5). Adapted from (*45*).

For the platination of two hairpin-stabilized duplexes d(TAT**GG**TAT TTTTATACCATA) and d(TAT**AG**TATTTTTATACTATA) by *cis*-$[Pt(NH_3)_2(H_2O)_2]^{2+}$, the overall rate of platination of the former is approximately 3 times larger than that of the latter (*51*).

ii. *Interstrand Cross-links* Deoxyribonucleic acid interstrand cross-linking occurs predominantly between two guanines on opposite strands, which requires a distance of *ca.* 3 Å between the two N7 atoms. One known interstrand cross-linking sequence is 5′-CG and 3′-CG (*52*). In this sequence the two guanines are separated at least by 7–9 Å, and therefore a large distortion of double-helix B-DNA is necessary to fulfill the requirement for cross-linking. A solution NMR structure of the adduct *cis*-{$Pt(NH_3)_2$}–d(CATAGCTATG)$_2$ has shown that the duplex undergoes a significant rearrangement at the lesion site so that platinum is located in the minor groove (Fig. 4) (*53*). The deoxyribose of the platinated G residue is inverted so that O4′ is pointing in the opposite direction to those of the remaining nucleotides. Moreover, the C residue which was originally base-paired to the platinated G is extruded and becomes extrahelical. Another solution

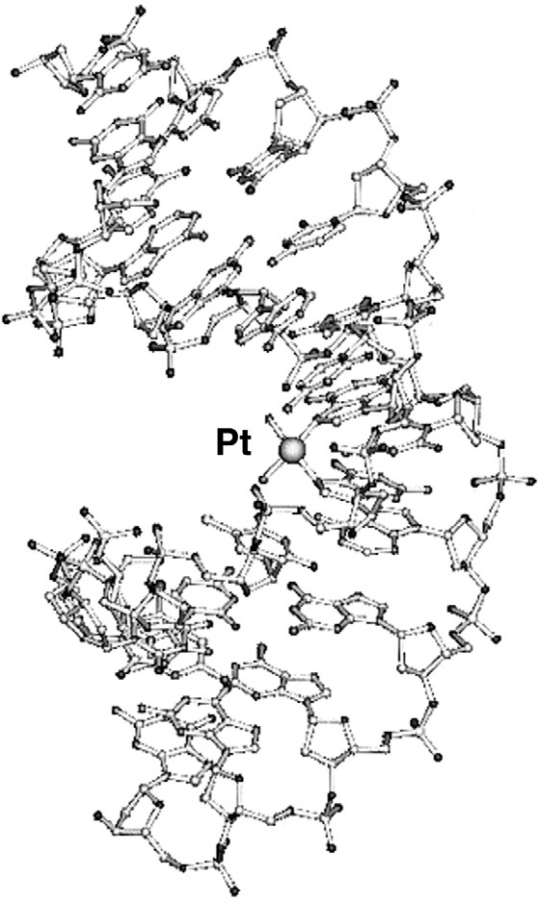

FIG. 3. X-ray crystal structure of *cis*-{$Pt(NH_3)_2$}$^{2-}$–d(CCTCTG*G*TCTCC) · d(GGA GACCAGAGG) showing that the DNA duplex is kinked by *ca.* 40° toward the major groove and has a juxtaposition of A-like and B-like helical DNA segments (structure reference: PDBID, 1AIO). Adapted from (*47*).

NMR structure (*54*) of an interstrand cross-linked duplex *cis*-{$Pt(NH_3)_2$}–5′-d(CCTCG*CTCTC) · d(GGAGCG*AGAG) has shown that *cis*-{$Pt(NH_3)_2$}$^{2+}$ is also located in the minor groove. The stacking of the two cross-linked guanines with the surrounding bases induces a bend of 40° toward the minor groove. These structural features are similar to those observed for left-handed Z-DNA. Such an unusual DNA structure is likely to be recognized differently by cellular proteins, e.g., repair enzymes or HMG proteins.

The role of interstrand cross-linking in the cytotoxicity is not clear. The antitumor-inactive transplatin forms twice as many interstrand cross-links compared with cisplatin under similar reaction conditions

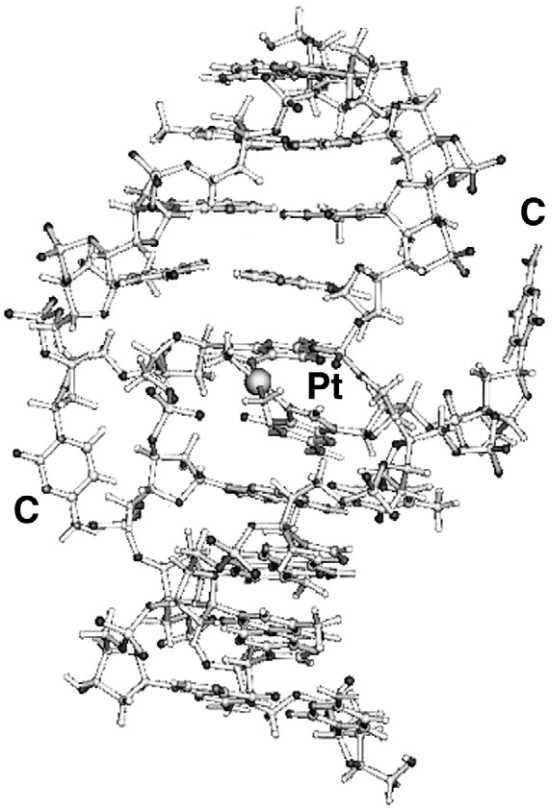

FIG. 4. The NMR-refined structure of interstrand cross-linked *cis*-$\{Pt(NH_3)_2\}^{2-}$–$d(CATAGCTATG)_2$. The deoxycytosine residues opposite to the platinated deoxyguanines have become extrahelical (structure reference: PDBID, 1DDP). Adapted from (*53*).

(48 h) (*55*). From the drug design point of view, the formation of interstrand cross-links provides a potential route for the irreversible binding of antisense oligonucleotides to their target nucleotide sequences (*4*, *56*).

iii. *Monofunctional adducts* Surprisingly, one of the two monofunctional adducts formed during the reaction of cisplatin with the 14-mer DNA duplex d(ATACATGGTACATA)·d(TATGTACCATGTAT) is very long lived with a half-life of 80 h at 298 K (*57*). The longer lived adduct has been identified as the 5′G adduct via enzymatic digestion studies (*58*). The lifetimes of the two monofunctional G adducts with the GG single strand are similar, suggesting that the 3D structure of DNA plays a role in stabilizing this adduct either by shielding the Cl ligand from aquation (compared to cisplatin) or by

constraining the position of the incoming 3′-G N7 ligand. Molecular modeling studies suggest that H-bonding between the NH_3 ligands and carbonyl groups on DNA plays a major role in determining the orientation of the Pt–Cl bonds and their accessibility. Molecular mechanics calculations show that the chloride ligand in the monofunctional adduct faces outward, away from the helix, whereas the aqua ligand which replaces it after aquation faces inward on account of its strong H-bonding properties. Modeling of transition states is now required.

There is a clear preference for the formation of monofunctional adducts of cisplatin with -AG- over -GA- sequences (*59*). Closure to form bifunctional adducts is more rapid in the former case than in the latter. These could explain, at least in part, why -AG- bifunctional adducts are preferentially formed and few platinated -GA- adducts are observed.

The biological significance of long-lived monofunctional adducts on DNA remains to be determined, but these alone may be sufficient to kill cells if they are not repaired, which seems to be the case for the active trans iminoether complex **18** (*60*). Long-lived monofunctional adducts may also promote the formation of DNA–protein cross-links.

d. Stability of Pt–DNA Adducts The stability of the Pt-N7 bond is usually considered to be high and broken only by very strong nucleophiles such as cyanide or thiourea. However, there is an increasing number of examples in which the lability of such bonds in certain platinated DNA adducts has been demonstrated. The adduct *trans*-$\{Pt(NH_3)_2\}^{2+}$–d(TCTACG*CG* TTCT) (1,3-GG cross-link) is unstable at neutral pH and rearranges to form the linkage isomer *trans*-$\{Pt(NH_3)_2\}^{2+}$–d(TCTAC*GCG* TTCT) (1,4-CG cross-link) (*61*). It was found subsequently that intra- and interstrand transplatin-DNA adducts undergo isomerization in both single- and double-stranded DNA (*62–64*). For example, interstrand cross-links between a platinated 5′-G and the complementary C can be formed (Scheme 2) (*62*).

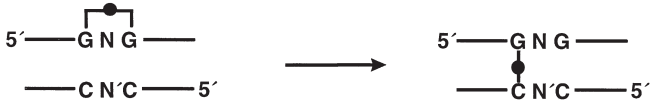

SCHEME 2.

The monofunctional adduct formed between *cis*-$[Pt(NH_3)_2(4\text{-MePy})Cl]^+$ and heptamer duplex 5′-d(CCTG*TCC)·d(GGACAGG) is unstable, and the platinum moiety is gradually released from DNA (*65*). Similarly, a slow dissociation of platinum from the single-stranded

adduct {Pt(dien)}–d(ATACATGGTACATA) is induced by chloride ions (*66*).

The isomerization of the 1,2-intrastrand cross-link *cis*-{$Pt(NH_3)_2$}-d(CCTG*G*TCC)·d(GGACCAGG) to the 1,5-interstrand cross-link d(CCTG*GTCC)·d(GGACCAGG*) is also induced by chloride ions, which shows that even Pt–N7 bonds in Pt-1,2-GpG cross-links can be destabilized (*67*).

e. Repair of Cisplatin–DNA Adducts Deoxyribonucleic acid intrastrand cross-links formed by cisplatin are removed by a combination of excision and recombination repair mechanisms (*68*). These include damage recognition, incision of DNA strands on both sides of the lesion, and removal of the damaged oligonucleotide. The repair system recognizes a variety of modified DNA structures, binds to the cisplatin-damaged site, and then excises and removes the damaged DNA. The resultant gap in the DNA duplex is then filled in via DNA polymerases and sealed by a DNA ligase. However, due to the complicated nature of the excision–repair system, which is believed to require at least 30 proteins (*69*), studies on the repair of cisplatin- and transplatin-modified DNA in eukaryotes have yielded many discrepancies (*70*). Nevertheless, the evidence gathered so far seems to show that the repair efficiency for cisplatin-modifed DNA by mammlian excinuclease (*in vitro* repair assay) follows the order 1,3-d(GTG) cross-link > AG > GG. This fits well with the notion that 1,2-d(GG) intrastrand bifunctional adducts may be responsible for the cytotoxicity of cisplatin (*12*). Increased repair of platinated DNA contributes to cisplatin resistance (*71*).

Mismatch repair is a postreplication repair system that corrects unpaired or mismatched nucleotides. Loss of mismatch repair may result in drug resistance by impairing the ability of the cell to detect DNA damage and activate apoptosis, and by increasing the mutation rate throughout the genome (*72*). Tumors that contain a significant fraction of cells deficient in mismatch repair may show reduced responses to specific drugs.

f. Protein Recognition Since the discovery of a protein that preferentially binds to cisplatin-damaged DNA (*73*), many such proteins have been identified with similar binding affinities toward cisplatin-modified DNA. These proteins may participate in the DNA repair process, but their *in vivo* function is largely unknown.

High mobility group (HMG) proteins are a family of small nonhistone chromatin-associated proteins which recognize structural distortions in DNA (*11*, *74*, *75*). Several NMR structures of HMG domains have been determined (*76–78*). High mobility group 1 (HMG1) box A

consists of three α-helical regions, joined by small loops, and folded into an L-shaped structure (Fig. 5). The N-terminal A-domain and the central B-domain are positively charged and bind to DNA, while the acidic terminal C-domain interacts with histones.

Dunham *et al.* (*79*) have shown that the binding affinity of HMG1 toward a series of cisplatin-modified 15-mer DNA duplexes, d(CCTCTCN$_1$G*G*N$_2$TCTTC) · (GAAGAN$_3$CCN$_4$ GAGAGG) (where N* denotes the Pt-bound guanosine) can be greatly affected by the variation of bases surrounding the Pt lesion. The preference of HMG1 domain A for this sequence follows the order N2 = dA > T > dC, with a difference of over 2 orders of magnitude. When N1 = N2 = dA, platinated DNA is bound 100-fold stronger to HMG1 domain A (K_d = 1.6 n*M*) than to HMG1 domain B (K_d = 134 n*M*). Binding to high mobility group proteins causes additional bending of platinated DNA by angles of up to 75° to 85° (*80*).

Deoxyribonucleic acid footprinting studies have shown that HMG domains A and B inhibit cleavage by nucleases over a 12- to 15-base-pair region centered around the platinum adduct (*81*). The HMG proteins can modulate cisplatin cytotoxicity by inhibition of the excinuclease-mediated removal of Pt–d(GpG) adducts from DNA (*82*). However, this hypothesis has been questioned because there is no evidence for cellular protein shielding of Pt–d(GpG) adducts from repair enzymes (*83*).

Nuclear magnetic resonance studies of the cisplatin GG chelate of

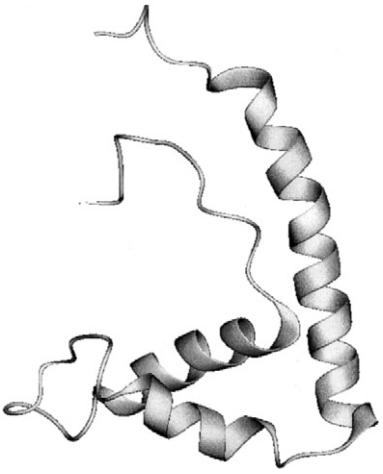

FIG. 5. The NMR-refined structure of the A-domain of high-mobility group protein 1 (PDBID: 1AAB). Adapted from (*78*).

a 14-mer suggest that the kinked duplex binds in the elbow region of HMG1 box A (*84*). Recent x-ray crystallographic studies of a 16-base-pair DNA duplex bound to HMG1 domain A (636) show that the protein inserts a Phe side-chain into the platination site.

Nuclear protein, the linker histone H1, binds much more strongly to cisplatin-modified DNA than to transplatin-modified or to unmodified DNA (*85*). Competitive binding to a cisplatin-modified 123-bp DNA fragment shows that histone H1 binding is stronger than that of HMG1. Moreover, this protein is 10-fold more abundant than the HMG proteins in the cell nucleus. Also, the promoter recognition factor TATA box-binding protein (TBP)/TFIID binds selectively to and is sequestered by cisplatin-damaged DNA. This may lure TBP/TFIID away from its normal promoter sequence, explaining the inhibition of RNA synthesis (*86*). These proteins may therefore also play important roles in the mechanism of action of platinum drugs.

g. Metabolites of Pt(II) Drugs The major binding sites for cisplatin in human blood plasma are thought to be on the protein albumin (*87*). Human serum albumin is a single-chain 66-kDa protein which contains 17 disulfide bridges and one free thiol at Cys-34 as well as six Met residues: M87, M123, M298, M329, M446, and M548. Reaction between cisplatin and HSA is thought to be the main route for platinum binding in human blood plasma. Recent data suggest that cisplatin reacts mainly with methionine residues of albumin forming Met-*S*,*N* macrochelates together with formation of a minor adduct with Cys-34 and a monodentate *S*-Met product (*88*).

The chelated square-planar metabolite [Pt(Met)$_2$)] has been detected in urine of patients treated with cisplatin (*89*). It is a relatively unreactive complex, existing in solution as a mixture of three diastereoisomers of each of the two geometrical isomers (*90*). The cis isomer predominates over the trans isomer by 87 : 13, and interconversion is slow (half-lives for conversion of cis to trans 22.4 h and of trans to cis 3.2 h at 310 K).

In rat blood and in the cell culture medium RPMI 1640 (+15% fetal calf serum) oxaliplatin (**4**) forms the major biotransformation products [Pt(dach)Cl$_2$], [Pt(dach)(H$_2$O)Cl]$^+$ (only in plasma ultrafiltrate), and [Pt(dach)(methionine)]$^+$ (*91*).

It has been postulated that carboplatin and its analogs act as prodrugs, reacting with chloride in plasma to give cisplatin. However, the rate of aquation of carboplatin is too slow to account for its *in vivo* activity (half-life 11 days in water), and the reactions of carboplatin with phosphate, chloride, or water are slower than direct reactions

with 5′-GMP (*92*). This implies that carboplatin, unlike cisplatin, may bind to DNA via direct attack or via a different activation mechanism.

It is possible that carboplatin can be activated by thioether ligands such as methionine. Reaction of carboplatin with L-Met leads to a surprisingly stable ring-opened intermediate (half-life of 28 h at 310 K) which may be stabilized by intramolecular H-bonding, and such complexes appear to exist in urine (*93*). Similar ring-opened intermediates have also been observed during reactions of carboplatin analogs and methionine-containing peptides (*94*).

Sulfur-bound L-Met, as opposed to S,N-chelated L-Met, is more reactive as a ligand on Pt(II) and can be slowly replaced by N7 of G (*95*, *96*). Transfer of Pt onto DNA via Met-containing peptides or proteins may therefore be possible. Monofunctional adducts of the type [Pt(en)(G)(L-Met-S)] appear to be very stable (*97*) and so methionine may play a role in trapping these adducts. Also, the high trans influence of S as a Pt(II) ligand can lead to the facile labilization of trans-am(m)ine ligands and this allows cisplatin to react with GMP faster in the presence of L-Met then in its absence (*98*), which introduces another route to DNA platination.

2. Pt Complexes on Clinical Trials

Although the second generation of platinum drugs is less toxic than cisplatin, many appear to be cross-resistant with cisplatin. Requirements which are influencing the search for new generations of active complexes include (1) lower toxicity to normal cells than cisplatin, (2) activity against tumors with acquired cisplatin resistance, (3) activity against a wider spectrum of types of cancer, and (4) oral activity.

Currently more than 10 platinum complexes are in different stages of clinical trials. Complexes **5** (NK 121) (*99*) and **6** (DWA 2114 R)

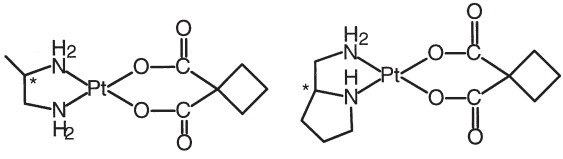

5 **6**

(*100*), which are on clinical trial in Japan, show promising features for overcoming cisplatin-induced resistance and nephrotoxicity (*101*). Interestingly, complex **6** containing the *R*-enantiomer of the chiral

amine ligand is not toxic, whereas the *S*-enantiomer is toxic (*102*). Lobaplatin **7** (D-19466) was introduced into clinical trial in 1992 (*103*) and is currently in phase II trials for cisplatin-resistant ovarian cancer (*104*), advanced head and neck cancers (*105*), and small-cell lung cancer (*106*). Complex **8** (N-DDP), *cis*-bis(neodecanoato)(*trans-R,R*-

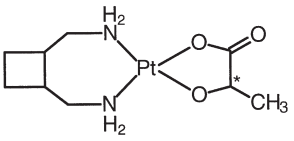

7

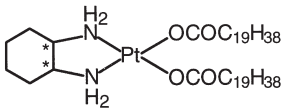

8

1,2-diaminocyclohexane) platinum(II), is a liposome-incorporated lipophilic cisplatin analog with *in vivo* activity against liver metastases and tumors resistant to cisplatin and is currently under clinical evaluation (*107*, *108*). This drug may be activated by forming intermediates in lipid bilayers, and the activity is highly dependent on the presence of liposomes (*109*). The only active intermediate identified so far is *cis*-dichloro-*trans-R,R*-1,2-diaminocyclohexaneplatinum(II) (*110*).

The sterically hindered complex **9** (AMD 473, ZD0473) is active (injection and oral) against an acquired cisplatin-resistant subline of a

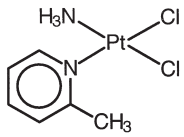

9

human ovarian carcinoma xenograph (Fig. 6) and entered clinical trial in 1997 (*111*). The steric hindrance provided by the 2-methyl group (which lies over the top of the Pt square-plane, in comparison with the 3-methyl pyridine complex in which it is rotated away) is evident (Fig. 7). Complex **9** is less reactive than cisplatin, for example, inducing DNA interstrand cross-links in cells and binding to plasma proteins more slowly. This may due to the effect of 2-picoline on the rate of hydrolysis of the two chloride ligands ($t_{1/2}$, 6 h for C1 trans to 2-picoline; 6.7 h for Cl trans to NH_3, at 310 K), which is 2 to 3 times slower than cisplatin (*112*).

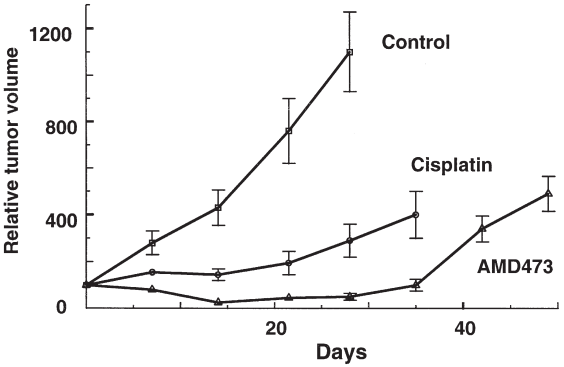

FIG. 6. *In vivo* antitumor activity of complex **9** (40 mg/kg) compared to cisplatin **1** (4 mg/kg) against CH1cisR human ovarian carcinoma xenograft. Adapted from (*111*).

A candidate for clinical trials is the trinuclear complex **10** (BBR3464) (counter anion = Cl^- or NO_3^-), in which the central Pt unit

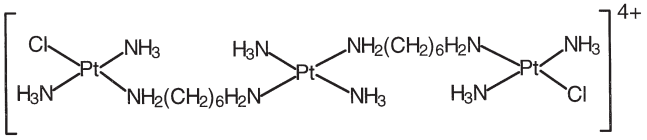

10

is capable only of H-bonding interactions with DNA (*113*). The overall charge (+4) greatly enhances DNA affinity, which is characterized by long-range interstrand cross-linking up to six basepairs apart with significant unwinding and efficient, irreversible conversion of B- to Z-DNA. BBR3464 shows potent cytotoxicity against both cisplatin-sensitive (L1210) and -resistant (LI210/CDDP) murine leukemia cell lines, and it is 30 times more cytotoxic than cisplatin (*113*).

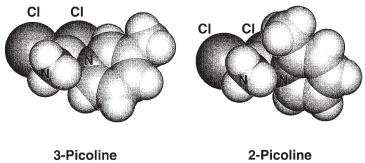

FIG. 7. X-ray crystal structure of the sterically hindered 2-picoline anticancer complex **9** in comparison with its 3-picoline analog. The 2-methyl group in **9** lies directly over the Pt-square plane ($H_3C \cdots$ Pt: 3.22 Å). The hydrogen atoms are omitted. Adapted from (*44*).

Complex **11** (JM216) is currently in phase II clinical trials as an oral drug. It is reported to have superior *in vitro* and *in vivo* activity

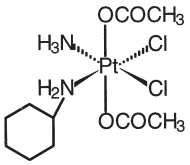

11

compared to cisplatin against human cervical, small-cell lung, and ovarian carcinoma cell lines (*114*). Incubation of JM216 in human plasma gives rise to at least six biotransformation products, which include the mono and dihydroxo Pt(IV) complexes **12** (JM383) and **13** (JM518) and the Pt(II) complex **14** (JM118) (*115*, *116*). All of these metabolites **12–14** are active complexes. The parent Pt(IV) drug is

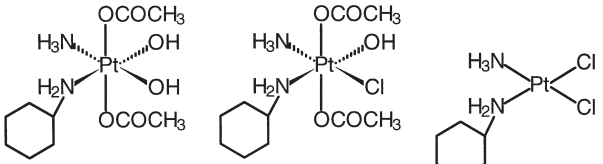

12 **13** **14**

detectable in blood plasma from mice 1 h postadministration, but not in patients. In patients, the major metabolite is complex **14**.

Orally active Pt(IV) cyclohexanediamine complexes are being developed by Kidani *et al.* (*117*, *118*). They have identified complexes such as **15** (C5-OHP) and the monohalogeno–monovalerato complexes as

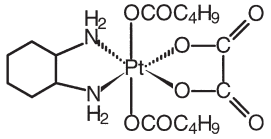

15

candidates for clinical trials. These complexes are readily reduced, e.g., by ascorbate, and oxaliplatin **4** is likely to be the active metabolite.

It is generally believed that Pt(IV) complexes are prodrugs which are transformed to Pt(II) species before binding to DNA. However, the direct reaction of Pt(IV) complexes such as *cis,trans,cis*-$[Pt(NH_3)_2(OH)_2Cl_2]$ with double-stranded oligonucleotides is reported to give Pt(IV) intra- and interstrand cross-links (*119*).

3. Design of New Drugs

The early empirical structure–activity relationships promoted discovery of second-generation anticancer drugs such as complexes **2** and **3**. However, analogs of these drugs usually display similar clinical profiles to the parent drugs. Therefore new classes of platinum complexes are required with distinct properties.

a. Active Trans Complexes Interests in the anticancer activity of Pt(II) complexes with a trans geometry has been stimulated by the observation that introduction of bulkier pyridine ligands greatly enhances cytotoxicity in comparison with transplatin (*120*). For example, complex **16** is highly active against murine and human tumor cell lines, especially against cisplatin-resistant cell lines (*121*). The pyridine ligand in the trans complex **16** reduces the rate of DNA binding and enhances DNA interstrand cross-linking (*122*). It has also been shown that adducts of **16** terminate *in vitro* RNA synthesis preferentially at guanine residues (*123*). Interestingly, the type and extent of conformational alterations induced in DNA indicate that **16** behaves in some respects like cisplatin, as indicated by the fact that **16**-modified DNA is recognized by cisplatin-specific antibodies.

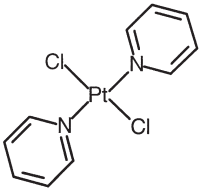

16

Kelland *et al.* (*124*, *125*) have developed a series of *trans*-platinum(IV) complexes such as **17** (JM335) with marked antitumor efficacy against both murine and human s.c. tumor models (*125*). It is

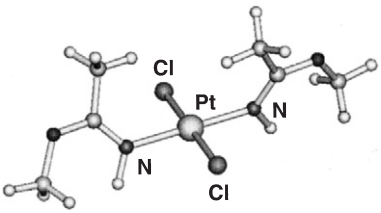

FIG. 8. X-ray crystal structure of the *trans*-Pt(II)-iminoether anticancer complex **18**. Adapted from (*129*).

notable that **17** efficiently promotes DNA interstrand cross-links and single-strand breaks (*126*). These properties may account for its un-

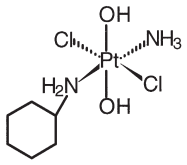

17

usual cytotoxicity profile against cisplatin-resistant tumors (*127*). Intriguingly, the corresponding *trans*-Pt(II) complexes (without the axial hydroxo groups) are inactive.

Natile *et al.* (*128*, *129*) have found that *trans*-imino ether platinum complexes (Fig. 8) have much higher antitumor activity than their cis analogs (OCH_3 and Pt are cis with respect to the C=N double bond in the Z isomer and trans in the E isomer). The mechanism of action of these agents appears to be different from that of cisplatin and may be related to the properties of the iminoether ligands (*130*). Although these trans complexes react with DNA more slowly than cisplatin, they appear to achieve the same level of DNA binding after 24 h. The *trans*-EE complex **18** is the most effective in inhibiting DNA synthesis

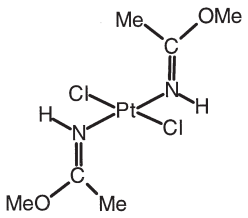

18

and cell proliferation but does not induce DNA local conformational changes (*131*). It preferentially forms monofunctional adducts at guanine residues in double-helical DNA even after long incubation times (48 h at 310 K) (*132*). The reactivity of the second chloride ligand in the monofunctional adduct is markedly reduced. The adducts formed on DNA by complex **18** are not recognized by the HMG proteins (V. Brabec, personal communication), which is probably relevant to their distinct biological efficacy (*132*).

b. Aminophosphine Complexes Under physiological conditions cisplatin does not readily attack the DNA base thymine (T), but by changing the ligands on Pt to amino phosphines it is possible to achieve such an attack. Aminophosphine ligands bind strongly to Pt(II) but in bischelated cis complexes such as **19** the Pt–N bond is

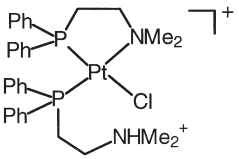

19

relatively labile on account of the high trans influence of P and steric interactions between the substituents on the N atoms. Despite the presence of four phenyl groups, these complexes are usually soluble in water. Chelate ring-opening in these complexes can be controlled by the substituents on N, by the size of the chelate ring, and by the pH (protonation of the displaced N ligand) and concentration of competing ligands such as Cl^- (*133*). Reaction between complex **19** and GMP occurs rapidly with opening of one of the chelate rings and binding to N7. However, GMP can be displaced by Cl^- at high concentrations. This complex does not bind to A, but does bind to T (and U) at N3 (*134*). Deprotonation of N3 may be assisted by the displaced amino group. Complex **19** exhibits activity against cisplatin-resistant tumor cells *in vitro* although there is as yet no evidence for activity *in vivo*. Two mechanisms may be responsible for the cytotoxicity. First, the complex may act as a positively charged lipophilic antimitondrial agent similar to $[Au(dppe)_2]^+$. Second, in the ring-opened form it can bind to DNA bases and form lesions different from cisplatin (*135*). Recent data show that the double ring-opened complex *cis*-

$[PtCl_2(Me_2N(CH_2)_3PPh_2)_2]$ terminates DNA synthesis *in vitro* more efficiently than cisplatin (*136*).

c. Photoactivation A novel approach to DNA binding by Pt complexes has been taken by Kratochwil *et al.* (*137*), who have synthesized Pt(IV) complexes containing iodide ligands which absorb visible light. Thus the toxicity of *trans,cis*-$[Pt(OAc)_2I_2(en)]$ (**20**) toward hu-

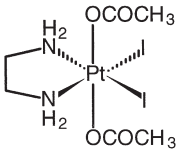

20

man bladder cancer cells is enhanced (by 35%) when the treated cells are irradiated with light of $\lambda > 375$ nm. Nuclear magnetic resonance studies show that irradiation of **20** with visible light ($\lambda = 457$ nm) in the presence of the nucleotide 5′-GMP induces photaquation followed by photoreduction to give the bis-GMP adduct of $\{Pt(en)\}^{2+}$ (*138*). Reactions of **20** with glutathione in the absence of light involve the initial attack of thiol on an iodide ligand of Pt(IV) to generate reactive intermediates (*139*). Such electron-transfer-driven trans-ligand labilization reactions may provide a useful new concept in drug design.

Ultraviolet-induced cleavage of both intra- and interstrand cross-links involving Pt–G bonds has been observed by Payet and Leng (*140*). Kane and Lippard (*141*) have reported that irradiation of DNA modified by cisplatin with UV light ($\lambda > 300$ nm) can induce specific cross-links to HMG1, thought to involve Lys6 in the B-domain, with labilization of a Pt–purine bond.

d. Stereochemical Influence Early work demonstrated that substituents on the amine ligand can have an important influence on activity for *cis*-$[PtCl_2(amine)_2]$, decreasing in the order $NH_3 > RNH_2 > R_2NH > R_3N$ for alkyl substituents (*142*).

Introduction of chiral centers in the nonleaving groups can achieve interesting binding differences for enantiomers toward DNA. For example, [Pt(*R*-DACH)Cl_2] binds to DNA twice as strong as the *S*-enantiomer (*143*). Pt(II) complexes containing the *meso* form of 1,2-bis(2-hydroxyphenyl) ethanediamine exhibit the lowest antitumor activity and reactivity because of the steric hindrance provided by the aromatic rings (*144*).

Hambley *et al.* (*145*) have also investigated the enantioselective binding of platinum complexes to DNA. When the rigid ligand 3-aminohexahydroazepine is used, a pair of enantiomeric Pt(II) complexes are formed. The *S*-enantiomer binds more readily to calf thymus DNA than the *R*-isomer. Molecular modeling data suggest the presence of more steric hindrance for the *R*-enantiomer. The *R*-enantiomer is more cytotoxic toward bladder cell lines but less cytotoxic toward lung cell lines compared to the *S*-isomer (*146*).

e. Targeting Platinum Various attempts have been made to target Pt to different tissues. For example, Keppler *et al.* (*147*) have reported that the complexes *cis*-diammine(nitrilotris(methylphosphonato-*O*, *N*))platinum(II) and *cis*-cyclohexane-1,2-diamine(nitrilotris-(methylphosphonato-*O*,*N*))platinum(II) show promising cytotoxicity against rat colorectal carcinoma and human colorectal cancer cell lines. The diamine complex is more active and more toxic in contrast to the cyclohexane 1,2-diamine complex, which is less active and also less toxic. Both complexes form GG chelates with DNA with the release of the nitrilotris(methylphosphonato) ligand (*148*). Platinum complexes containing aminophosphonate ligands show high activity against bone tumors, and the presence of Ca(II) increases the rate of binding to DNA (*149*).

B. Metallocenes

The antitumor activity of titanocene dichloride **21** was first recognized in 1979 (*150*), and since then the activity of several other metallocenes (V, Nb, Mo, Fe, Ge, and Sn) has been reported (*151*). Most interest has centered on titanocene dichloride and on vanadocene dichloride **22,** which are active against a diverse range of human carcinomas, including gastrointestinal and breast carcinomas, but not against head and neck cancers. There appears to be a lack of cross-resistance between titanocene dichloride and cisplatin.

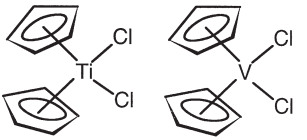

21 **22**

Phase I dose-escalation trials of titanocene dichloride, formulated in maleic acid buffer, have shown that nephrotoxicity is cumulative

and dependent on the dose. There are emetic and metallic taste side-effects. One patient (with adenocarcinoma) out of 24 had a minor response and a dose of 140 mg/m^2/week has been recommended for phase II trials (*152*).

Good antitumor activity has also been found among ionic metallocene complexes of Ti(IV), Nb(V), Mo(VI), and Re(V), such as **23–26,**

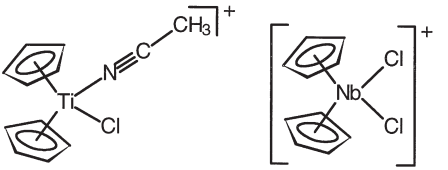

23 **24**

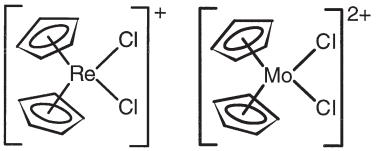

25 **26**

and ferrecinium salts (*153*). These have the advantage of improved water solubility. Dose-limiting damage from metallocenes appears to involve the liver and gastrointestinal tract. It is notable that the cyclopentadiene ligands of metallocenes are hydroxylated in the liver by the P450 system and can then form glucuronides and sulfate derivatives in a similar manner to aromatic organic drugs (*154*).

It is not clear whether DNA is the main target for metallocene complexes. The Ti and V complexes are known to hydrolyze rapidly and bind strongly to oxygen donors (DNA phosphates) as well as to N. Thus vanadium complex **22** loses the first chloride ligand within seconds and the second with a half-life of 24 min in water; the pK_a values for the two aqua ligands (4.7 and 5.2) are lower than for cisplatin (*155*). The aqua complex of **21**, $[(C_5H_5)_2Ti(H_2O)_2]^{2+}$, is even more acidic, with pK_a values of 3.51 and 4.35 (*156*). Therefore at physiological pH, the hydroxo species will predominate in solution. It has been shown that in the solid state $[(C_5H_5)_2V(OH)_2]^{2+}$ hydrogen bonds strongly to a phosphatediester oxygen of nucleotides and has little effect on base pairing (*157*). Some adducts of biscyclopentadienyl Ti(IV), V(IV), and Mo(IV) with N-bound nucleobases have been reported, but the cyclopentadienyl ligands are

readily lost in water during such reactions (*153, 158*). It is notable that $(C_5H_5)_2NbCl_2$ readily undergoes hydrolysis and undergoes oxidation to **24** in aqueous solution but does not interact with nucleobases, suggesting a different mechanism of action from other metallocence complexes (*159*). It is possible that the cytotoxicity of metallocenes originates from their inhibitory effects on DNA-processing enzymes such as topoisomerase II and protein kinase C (*155*). Vanadocene and molybdocene dichloride have been shown to act as inhibitors of these enzymes.

It is evident that the formulation of metallocene complexes for clinical use will have to be carefully controlled. New species with unknown biological properties could easily be generated during the formulation process.

C. Ruthenium Antimetastatic Agents

The pioneering work of Clarke demonstrated the excellent antitumor activity of ruthenium complexes such as *cis*-$[RuCl_2(NH_3)_4]$, and *fac*-$[RuCl_3(NH_3)_3]$, but they are too insoluble for pharmacological use (*160*). Ruthenium(III) complexes may be prodrugs which are reduced to more reactive Ru(II) species inside cells. Indeed, Mestroni *et al.* have shown that Ru(II) complexes such as $[RuCl_2(DMSO)_4]$ are active against solid tumor metastases; the antimetastatic activity of *trans*-$[RuCl_2(DMSO)_4]$ (**27**) is higher than the activity against the primary tumor, whereas for *cis*-$[RuCl_2(DMSO)_4]$ this difference is less pronounced (*161*). In water, rapid replacement of two S-bound DMSO ligands from **27** occurs to give the *cis*-diaqua complex (*162*).

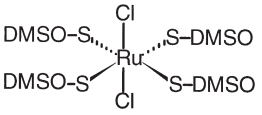

27

Keppler *et al.* have shown that the introduction of heterocyclic ligands into Ru(III) complexes such as **28** (*163*) and **29** (*164*) can improve the solubility and retain the antitumour activity, especially

against colorectal tumors (*165*). Complex **29** (indazole) is a candidate for clinical trial.

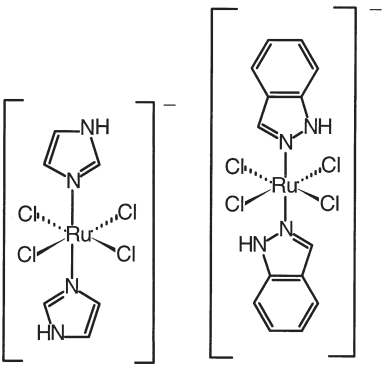

28 **29**

The first Ru(III) antimetastic complex to be introduced into clinical trials is the imidazolinium salt of *trans*-[Ru(III)Cl_4(DMSO)Im]$^-$ (**30**) (NAMI-A) (*166*), which contains both DMSO and a heterocyclic ligand.

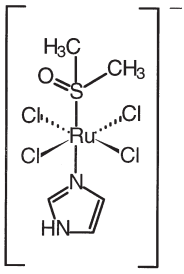

30

The crystal structure of the sodium salt of **30** (NAMI) is shown in Fig. 9, where Na(I) bridges two molecules of **30** via oxygens of S-bound DMSO and water. This complex may be readily reduced *in vivo* ($E_{1/2}$, −0.001 V) (*166*), whereas the bis-imidazole complex **28** has a lower redox potential and is more difficult to reduce. The reduction potential of **28** is strongly pH dependent ($\Delta E = -118$ mV/pH unit near pH 7), reduction being more favorable at acidic pH values (*167*). This complex hydrolyses at a similar rate to cisplatin ($t_{1/2}$ *ca.* 3 h at 310 K) and, like cisplatin, aquation appears to be necessary for DNA binding (*168*).

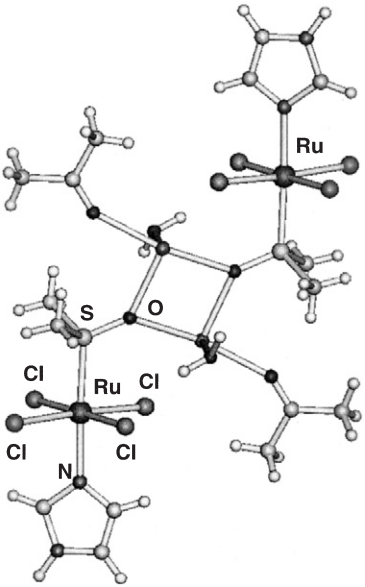

FIG. 9. X-ray crystal structure of the Ru(III) antimetastatic complex **30** (NAMI). Adapted from (*166*).

González-Vílchez *et al.* (*169*, *170*) have reported the first example of a Ru(IV) antitumor complex **31**.

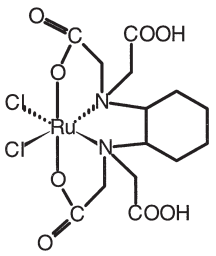

31

The Ru(IV)/Ru(III) redox potential is 0.78 V, so that Ru(III) or even Ru(II) species may be present *in vivo*. Indeed, the related Ru(III) complex **32** is also active (*171*), and the pendant arms in these octahedral polyaminocarboxylate complexes increase the rate of substitution reactions. Complex **32** binds rapidly to the blood proteins albumin and transferrin (*172*), and the ruthenium ion appears to remain in the

3(+) oxidation state with the polyaminocarboxylate ligand bound to the metal. Ruthenium(III) complexes with polypyridyl ligands such as **33** exhibit significant cytotoxicity against murine and human tumor

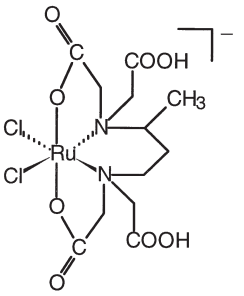

32

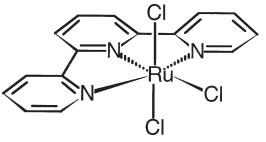

33

cell lines and are active against murine lymphosarcoma *in vivo* (*173*). This complex forms significant amounts of interstrand DNA cross-links and in ethanol solution forms a *trans*-bis(9-ethylguanine)Ru(II) adduct (*174*). There is no difference between the intracellular Ru uptake and cytotoxicity of the enantiomers of *cis*-$[Ru(bp)_2Cl_2]$ (bp = 2,2′-bipyridine).

It seems clear that complexes **28** and **29** both enter cancer cells by transferrin-mediation. Tumor cells are known to have a high density of transferrin receptors, and this provides a route for the uptake of ruthenium (*175*). In normal blood plasma, transferrin is only one-third saturated with Fe(III) and therefore vacant sites are available for Ru(III) binding. Baker *et al.* have shown by X-ray crystallography that complex **29** binds to His-253 of apolactoferrin, one of the Fe(III) ligands in the iron binding cleft of the N-lobe, with displacement of a chloride ligand (*176*). Ruthenium(III) is well known to have a high affinity for solvent-exposed His side chains of proteins (*177*). Complex **28** can be displaced from both the N- and C-lobes of transferrin at pH 4–5 in the presence of citrate or ATP (*178*). Transferrin-bound **28** and **29** exhibit high antiproliferative activity against human colon cancer cells, which appears to confirm that transferrin can deliver Ru to cells via the transferrin receptor. Similarly, complex **30** also reversibly forms a 1 : 2 complex with apotransferrin (*179*). It has been known for some time that radioisotopes of Ru (^{103}Ru, ^{97}Ru) bind to transferrin and accumulate in tumor cells; ^{97}Ru ($T_{1/2}$ 2.9 d, γ emission, 215 KeV) is useful in diagnostic nuclear medicine. Further investigations of the ability of ruthenium to interfere with the biochemistry of iron may shed light on its antimetastatic activity.

Clarke *et al.* (*180*) have reported that Ru(III) complexes with ammonia and imidazole ligands, such as **34,** are potential immunosuppressive agents. These complexes are very effective at inhibiting the antigen-independent phase of T-cell proliferation. The role of the imidazole ligands in tuning the Ru(II)/Ru(III) redox potential to the optimal range may be significant (*181*).

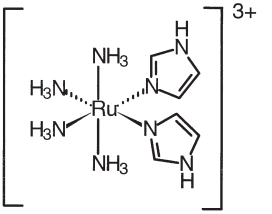

34

Both Ru(II) and Ru(III) complexes are known to bind DNA preferentially at N7 of G but also to A and C bases (*182*, *183*). Although most ruthenium antitumor agents have two reactive coordination sites, GG intrastrand cross-links on DNA do not appear to form readily. The only example appears to be the adduct of **27** with GpG, which has been structurally characterized by NMR spectroscopy (*184*). In this complex, the two N7-coordinated guanines adopt a head-to-head conformation and the two bases are strongly destacked.

Intercalative binding to DNA is often proposed as a route to enhancing selectivity of anticancer agents, and shape-selective intercalation of ruthenium-polyaromatic amines has been widely used for probing DNA structure (*185*). This approach could yield new drugs.

D. β-Diketonato Complexes

The bis(β-diketonato) Ti(IV) complex [Ti(bzac)$_2$(OEt)$_2$] **35** (budotitane, shown as the predominant cis,cis,cis isomer) entered phase I clinical trials in Germany in 1986 for the treatment of colon cancer (*186*). The complex is very susceptible to aquation, and to minimize this, the coprecipitate (Cremophor EL, 1,2-propylene glycol in ethanol and **35**) is dissolved in water prior to administration. As for titanocene dichloride, liver damage is the dose-limiting side-effect (*187*). The activity of this class of complexes shows little dependence on the nature of the leaving group (e.g., OEt, Cl), but aromatic substituents

on the β-diketonato ligands are important for activity; the acetylacetonato analog is inactive. For the benzoylacetonato metal(IV) com-

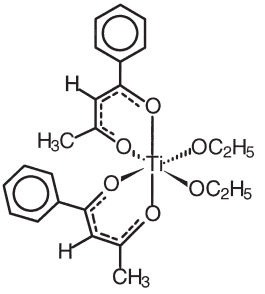

35

plexes, the activity against sarcoma 180 ascitic tumor follows the order (*188*) Ti ~ Zr > Hf > Mo > Sn > Ge (inactive). Difficulties with formulation may limit the clinical usefulness of this class of complexes.

E. Gold Antimitochondrial Complexes

The cytotoxicity of Au(I) complexes is markedly dependent on the ligands. A large number of Au(I) phosphine complexes are toxic to cells in the micromolar concentration range. For example, some linear Au(I) phosphine complexes, including the antiarthritic complex auranofin (see Section VII), are potently cytotoxic toward cancer cells in culture (*189*).

Two-coordinate Au(I) monophosphine complexes are usually not active *in vivo* because they are too reactive, e.g., toward plasma components such as albumin, and do not reach cancer cells. In contrast, diphosphine complexes such as **36, 37,** and **38** are active *in vivo*. The

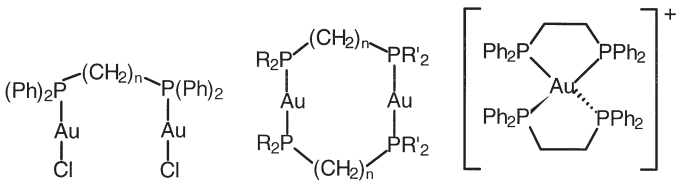

36 **37** **38**

activity is highly dependent on the substituents on P, being highest for Ph and lowest for Et. The diphosphine ligands themselves are active but less potent. They are usually readily oxidized in culture. Therefore Au(I) may protect the diphosphines from oxidation before they enter cells.

The tetrahedral bis(diphosphine) complex **38** is much less reactive, e.g., toward thiols, than linear Au(I) complexes. It exhibits activity in a range of cancer models and was a candidate for clinical trial. It has a different mechanism of action than cisplatin and targets mitochondria where it destroys membrane potentials. Complex **38** (as a lactate salt) proved to be too cardiotoxic for clinical use. Berners-Price *et al.* (*190*) have shown that the introduction of pyridyl substituents on P can increase the hydrophilicity of bischelated Au(I) diphosphine complexes and that potent and selective activity toward cisplatin-sensitive and -resistant ovarian tumor cells can be achieved. It remains to be seen whether cardiotoxicity can be reduced. Gold(I) binds only weakly to nitrogen and oxygen donors, therefore DNA binding of Au(I) is expected to be weak. Deoxyribonucleic acid–protein cross-links may be the primary lesions induced by complex **38** ($[Au(dppe)_2]^+$) in cells. Bis(diphosphine) complexes of Ag(I) and Cu(I) also exhibit anticancer activity (*191*), and $[Ag(Et_2PCH_2CH_2PPh_2)_2]^+$ is a potent antimitochondrial agent (*192*).

Linear gold(I) complexes containing aminophenylphosphines such as **39** and **40** exhibit comparable cytotoxicity to cisplatin (*193*). These

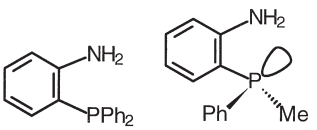

39 **40**

ligands can be derivatized to achieve the desired solubility and toxicity, and chiral ligand **40** allows the synthesis of diastereomers of metal complexes. Copper(I) and silver(I) complexes with these ligands also showed similar activities, which implies that the ligands play an important role in the activity. Some chiral Au(I) complexes with derivatives of glucose (2- or 3-diphenylphosphine) are cytotoxic to P388 leukemia cells (*194*).

Gold(III) complexes are isoelectronic and usually isostructural with those of Pt(II). Gold(III) complexes such as $[Au(en)_2]^{3+}$, $[AuCl(dien)]^{2+}$, and $[Au(cyclam)]^{3+}$ bind rapidly to DNA, with preference for GC se-

quences (*195, 196*). Their cytotoxicity against human tumor cell lines is comparable to cisplatin, and they are active against cisplatin-resistant tumor cell lines (*197*). However, they undergo rapid aquation and reduction to Au(I) in the presence of serum proteins. Little Au(III) may therefore reach DNA. Organogold(III) complexes such as **41** exhibit differential cytoxicity toward human tumor cell lines similar to cisplatin, but they have a low aqueous solubility and exhibit only limited activity against the ZR-75-12 xenograph (*198*).

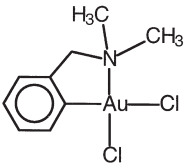

41

F. Main Group Metals

Interest in the anticancer activity of gallium salts such as gallium nitrate and chloride has been revived recently after reports that gallium salts are synergistic with cisplatin in the treatment of lung cancer (*199*). Gallium(III) maltolate has recently entered clinical trials for the treatment of bone disease and related conditions (*200*). Keppler *et al.* (*201*) have demonstrated the potential of tris(8-quinolinolato)gallium(III) (**42**, KP 46) in anticancer therapy. Although the compound has a better bioavailability after oral administration than gallium chloride, it is also more toxic. It has become apparent that the dominant mechanism of action of Ga(III) is its ability to act as a chemically irreducible Fe(III) analog in a wide range of systems (*202*).

Complex **43** (Germanium-132 or spirogermanium) is active in a number of preclinical tumor models, but was disappointing in clinical trials (*199*). It has recently been reported that **43** and related azaspirane show promising activity against psoriasis (*203*).

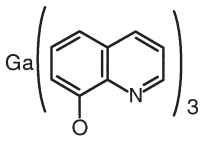

42

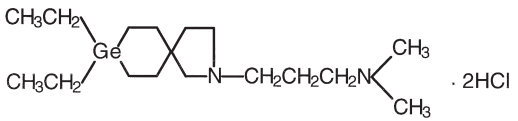

43

Arsenic compounds have been used medically for nearly 2500 years, for example, for the treatment of ulcers, syphilis, and trypanosomal diseases (*204*). Recently it has been reported that arsenic trioxide As_2O_3 can induce complete remissions in patients with acute promyelocytic leukemia (APL) (*205*, *206*). The induction of apoptosis and partial differentiation may be responsible for the activity of As_2O_3 (*207*). Acute promyelocytic leukemia is associated with a specific t(15;17) translocation that generates a fusion protein between promyelocytic leukemia protein (PML), a zinc finger protein that contains a coiled-coil domain, and a nuclear receptor for retinoic acid (*208*). Arsenic trioxide degrades the fusion protein, targets nuclear bodies at micromolar concentrations, and triggers apoptosis (*209*).

Many tin compounds (*ca.* 29% of those tested) are active against P388 leukemia, but are inactive in most other screens (*210*). Hence the search for a tin compound which might enter clinical trials goes on. In general, octahedral Sn(IV) monoorganotin trihalides $RSnX_3 \cdot L_2$ (where L_2 is a bidentate ligand) are not active against P388 leukemia and are the least toxic in the mono- to tetraorganotin series. Diorganotin complexes are more promising. For example some di(*n*-butyl) Sn(IV) complexes are highly active against a range of human tumor cell lines *in vitro* (*211*). Both di- and triorganotin compounds inhibit oxidative phosphorylation. Problems of water solubility have hampered the construction of reliable structure–activity relationships for diorganotin compounds but improvements in aqueous solubility have usually been accompanied by a loss of activity.

Dibutyltin glycylglycinate **44** (where R = butyl) is the most active organotin complex against p388 leukemia, but is inactive against L1210 leukemia, B16 melanoma, and Lewis lung carcinoma in mice (*212*).

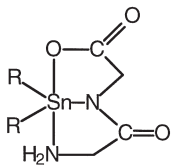

44

The mechanism of action of tin complexes is not known. Deoxyribonucleic acid may not be the target, and involvement in protein synthesis and energy metabolism is possible.

G. Rhodium Complexes

So far rhodium complexes have not exhibited the characteristics required for an antitumor drug, perhaps because they often show activity only in a very limited number of tumor models. Nevertheless, activity data for complexes in several oxidation states are encouraging for further studies.

Am(m)ine and pyridine complexes such as *mer*-[$RhCl_3(NH_3)_3$] (**45**) were the first rhodium(III) complexes to be tested because they contain *cis*-chloride ligands as does cisplatin (*213*). Complex **45** displays a positive dose–response relationship against several tumor cells such as Sarcoma 180.

Dinuclear rhodium(II) carboxylate complexes with cage-like structures **46**, in which carboxylate groups bridge the two metals and a

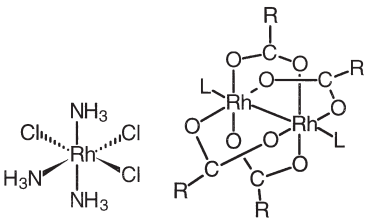

45 **46**

variety of ligands occupy the axial positions, are active against tumor cells such as Ehrlich, P388 leukemia, and Sarcoma 180 (*214*, *215*). Some complexes with bidentate N-ligands (e.g., bipyridine and 1,10-phenanthroline) in the axial positions exhibit high cytotoxicity against human oral carcinoma KB cell lines (*216*). The activity increases with the increasing chain length of the carboxylate ligands, with the pentanoate complexes being the most active species. It appears that the cytotoxicity parallels the lipophilicity of the complexes and hence their partition coefficients. *In vitro* experiments have shown that although **46** (R = pentanoate) binds to denatured DNA, it does not bind to native double-stranded calf thymus DNA (*217*, *218*). X-ray crystallographic evidence shows that dinuclear rhodium carboxylate complexes bind preferentially to guanine and adenine (e.g., 9-ethyl-guanine and 9-ethyl-adenine) via bridging and/or chelation involving N7 positions as well as the O6 position of guanine and N6 position of adenine (*219*, *220*). However, the formation of *cis*-bis-N7G or *cis*-bis-N7A adducts is not observed. Rhodium dicarboxylate

complexes also bind to proteins and may interact with enzymes such as DNA and RNA polymerase (*217*). The rhodium carboxylates tested do not appear to be active against a wide enough spectrum of cancers and are not stable enough in biological media to be candidates for clinical trial.

Square-planar Rh(I)–1,5-cyclooctadiene complexes with antitumor activity include **47–50**. In these complexes, the bidentate cycloocta-

47 **48**

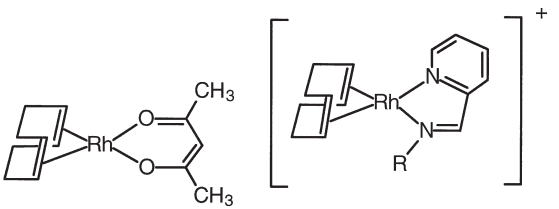

49 **50**

diene ligand acts as the nonlabile group (*221*). Complex **49** shows *in vivo* activity against Ehrlich ascites carcinoma but is less toxic than cisplatin. Such complexes are not stable and are readily oxidized to unreactive Rh(III) species. Sava *et al.* (*222, 223*) have shown that Rh(I) complexes such as **50** have high activity against primary tumors and reduce the number and the size of lung metastases.

H. Copper Phenanthrolines and Organocobalt Complexes

Copper complexes offer a rich redox chemistry which can be controlled by varying the bound ligands. Petering *et al.* reported the antitumor activity of copper(II)-bis(thiosemicarbazone) complexes such as **51** in the 1960s (*224*), and the current status of structural and biological studies of copper-thiocarbazone complexes has been summarized (*225*, *226*). Copper(II)-1,10-phenanthroline complexes are highly cytotoxic to tumor cells (*227*), and, interestingly, the Cu(I) complex of 1,10-dimethylphenanthroline (neocuproine) is also cytotoxic and dis-

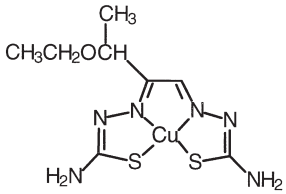

51

plays inhibitory effects toward leukemic cells in mice (*228*). Copper(II) complexes of salicylaldehyde derivatives are active against a variety of tumor cell lines (*229*, *230*).

Mixed-ligand Cu(II) complexes with salicylato and phenanthroline derivatives as ligands can also be highly cytotoxic (*231*). Mixed-ligand Cu(II) amino acid phenanthroline complexes (Casiopeinas) such as $[Cu(L\text{-Ser})(phen)(H_2O)]^+$ **52** are reported to be effective anticancer agents (*232*). It is possible that a complex in this class will soon enter clinical trials.

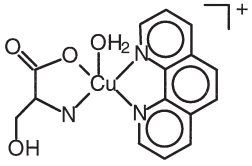

52

The pH value in a solid tumor is typically 0.2–0.5 units lower than in normal tissues. Therefore it may be possible to design pH-dependent cell-selective antitumor agents. Some free radicals are known to damage biological targets and especially to cleave nucleic acids (*233*). Alkylcobalt(III) complexes such as **53** generate alkyl radicals via ho-

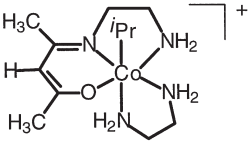

53

molytic decomposition under mild conditions (*234*). The decomposition of complex **53** at pH 6.5 is *ca.* 3 times faster than at pH 7.5, and such a source of free radicals might be expected to damage tumors selectively in view of their lower pH. Experiments with L1210 leukemia and carcinoma cell lines show that **53** possesses significant activity, provided the pH of the tumor cells is lowered by glucose infusion (*234*).

Photolysis of $[Co(cyclam)(H_2O)(CH_3)]^{2+}$ is known to produce methyl radicals via Co–C bond homolysis (*235*). The complex is stable in water and in the presence of oxygen, and it is capable of converting supercoiled plasmid DNA into a nicked circular form after 2 h in ordinary room light (*236*). Longer photolysis results in increased yields of nicked DNA. The complex is not selective in its attack on nucleotides.

I. Radiosensitizers

Radiation therapy is frequently used for the treatment of cancer. Irradiation of tumor sites with X-rays or γ-rays (^{60}Co) generates high-energy electrons and highly reactive free radicals such as HO·, which attack DNA and cause cell death. Nitroimidazoles and halogenated pyrimidines are radiosensitizers which can increase irradiation sensitivity. These ligands can be even more effective when linked to Pt(II) as in **54** (*237*). The Ru(II), Cu(II), and Ni(II) complexes of these ligands have also been studied as potential radiosensitizers (*238, 239*).

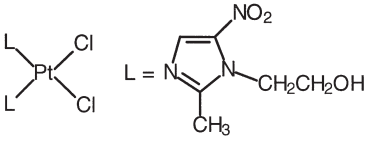

54

Metal–texaphyrin complexes such as **55** selectively accumulate in tumor cells (*240*) (see Section III). Complex **55** readily undergoes aone-electron reduction ($E_{1/2}$ = 0.08 V vs NHE), forming a free radical which is capable of damaging DNA. Because of the high electron affinity of **55,** it may prolong the lifetime of HO· radicals formed by radiolysis of water. Complex **55** is now in phase II clinical trials for the treatment of brain tumors and lung, head, neck, and pancreatic cancer.

The oral platinum compound **11** is capable of radiosensitizing a platinum-sensitive tumor line, as is cisplatin **1** (*241*).

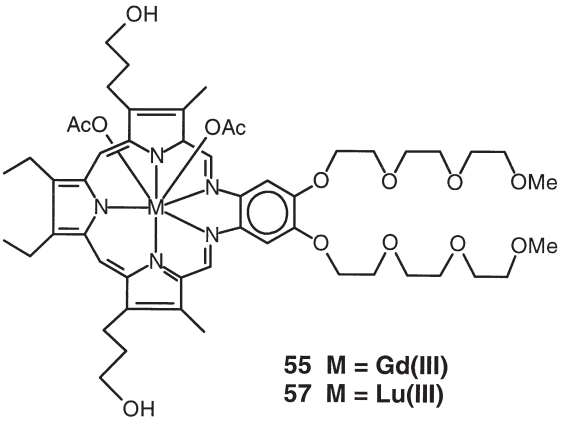

55 M = Gd(III)
57 M = Lu(III)

III. Photodynamic and Sonodynamic Therapy

Photodynamic therapy (PDT) involves the treatment of diseased tissue and cells using a photosensitizer and visible light. Most clinical interests have focused on three areas: photodynamic therapy of cancer, porphyrias and hematological diseases, and various forms of jaundice. Photodynamic therapy requires a good photosensitizer which shows some selectivity toward photodamage to tumor tissue. On exposure to light, photosensitizers generate singlet oxygen ($^1O_2$), which reacts with a variety of biological molecules. However, it has been difficult to obtain direct evidence for the involvement of $^1O_2$ because of its very short lifetime (*ca.* 6 μs in water).

Most clinically used PDT sensitizers are metal-free porphyrins and porphyrin derivatives such as **56.** Hematoporphyrin and its deriva-

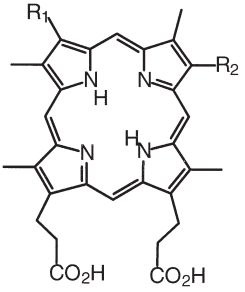

56

tives, photfrin, photsan, photogem, and photocarcinorin, have provided the first generation PDT agents. Their synthesis and detailed structures have been reviewed (*242*, *243*). The disadvantages of these compounds are that they are often mixtures of various porphyrin species, and their individual contributions to the biological effects is unclear. Also their adsorptions (λ_{max} *ca.* 630 nm) are weak in the red region of the visible spectrum (*244*). Therefore there has been much interest in the design of tumor photosensitizers with improved absorption characteristics and which are less toxic. Criteria for new PDT agents have been summarized (*242*). They should be single substances and have little or no dark toxicity, suitable photophysical parameters, appropriate hydrophobicity and hydrophilicity, and strong absorption bands at the red end of the visible spectrum (λ_{max} in the region of 700–800 nm).

Sessler *et al.* have developed the class of expanded porphyrins known as texaphyrins (*245*, *246*). Some texaphyrin complexes with Cd(II), La(III), and Lu(III) exhibit characteristics required for photosensitizers: strong absorbance in the physiologically important far-red spectral region (700–800 nm), high yields for the production of long-lived triplet states, and high efficiency for production of singlet oxygen.

The lutetium complex **57** is currently under clinical evaluation as a photosensitizer for the treatment of cancer. This complex possesses a strong broad absorption band centered at 732 nm (*247*). Upon absorption of light, **57** becomes activated to a long-lived triplet state and reacts with $^3O_2$ to generate cytotoxic $^1O_2$. Complex **57** is also on clinical trial as a photosensitizer for the treatment of atherosclerisis, a vascular disease caused by deposition of cholesterol and other fatty materials in the walls of blood vessels.

Several other metal complexes have promising photodynamic activity and are currently under development (*248*). Metalloporphyrins inhibit the enzyme heme oxygenase; for example, chromium porphyrin and mesoporphyrin are potent inhibitors of heme oxygenase both *in vitro* and *in vivo* (*249*, *250*) and are being used for the treatment of the neonatal jaundice.

Tin(IV) ethyl etiopurpurin **58** (SnET2) (*251*) is a second-generation photosensitizer currently under clinical evaluation (*242*). Once delivered to blood plasma, complex **58** interacts with lipoproteins and preferentially binds to high-density lipoproteins (*252*). The aggregation of **58** is slow and it binds to lipoproteins as a monomer (*253*).

Tin(IV)–protoporphyrin (*254*), Ga–deuteroporphyrin (*255*), and Co–mesoporphyrin (*256*) complexes are potent inhibitors of heme oxygenase. The Sn(IV) complex significantly inhibits bilirubin production

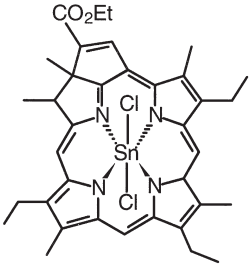

58

in vivo (*257*). Zinc-porphyrins are also promising photosensitizers (*249*, *258*).

Phthalocyanine (**59**) and naphthalocyanine (**60**) complexes appear to be highly active, and Zn-**60** adducts have attracted commercial interest (*259*, *260*). Many metal complexes of **56, 59** and **60** are very

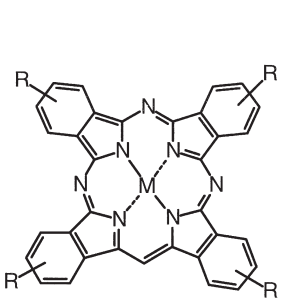

59

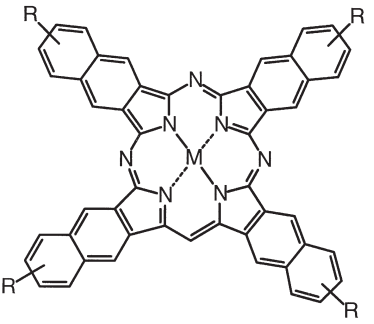

60

hydrophobic and therefore suitable delivery systems have to be devised. Liposomal vesicles can provide good tumor accumulation and photodynamic activity (*261–263*) and increased tumor uptake of the Zn complexes.

Sonodynamic therapy is a promising new method for cancer treatment and is based on the synergistic effect on tumor cell killing of a photosensitizer and ultrasound. Photoexcitation of the sensitizer by sonoluminescent light produces singlet oxygen (*264*, *265*). The gallium–porphyrin derivative ATX-70 is a highly active sonodynamic agent. For example, focused ultrasound in the range 500 kHz to 1 MHz significantly increases the cytotoxicity of ATX-70 *in vitro* (*264*)

and *in vivo* (*265*) toward colon 26 carcinoma, while ultrasound or ATX-70 alone do not cause any necrosis (*266*).

IV. Radiopharmaceuticals

A wide range of metal radionuclides is used for the diagnosis of disease. Although they are selected on the basis of favorable physical and nuclear properties, the chemical properties of these radionuclides play a vital role in the development of new and improved techniques (*267*). Some of the metal radionuclides which are suitable for use in diagnosis and/or therapy are listed in Table III.

The radiopharmaceuticals used for diagnostic imaging usually satisfy the following requirements (1) radiation from the nuclide penetrates the body and is detectable by instrumentation (requires emission of photons of energy >35 KeV, preferably >80 KeV (*268*)) and

TABLE III

METAL RADIONUCLIDES SUITABLE FOR IMAGING AND/OR THERAPY[a]

Isotope	Half-life (h)	Maximum energy	
		β (MeV)	γ (KeV)
Diagnostic			
^{64}Cu	12.7	0.58	1346
^{67}Ga	78.3		93, 184, 300
^{68}Ga	1.1	1.83	1077
^{99m}Tc	6.0		141
^{111}In	67.2		171, 245
^{186}Re	90.5	1.07	123, 137
^{188}Re	16.9	2.12	155
Therapeutic			
^{47}Sc	80.4	0.44, 0.6	159
^{67}Cu	62	0.39, 0.48	185
^{89}Sr	50.5d	1.49	909
^{90}Y	64.1	2.28	
^{109}Pd	13.5	1.03	88
^{111}Ag	7.5d	1.04	245, 342
^{153}Sm	46.3	0.64, 0.69	69, 103
^{188}Re	16.9	1.96, 2.12	155
^{201}Tl	73	0.48 (E.C.)	135, 167
^{211}At	7.2	5.87, 5.98 (α)	669, 687, 743
^{212}Pb	10.6	0.28, 0.57	239
^{212}Bi	1.0	6.05	727

[a] Data from Ref. (*619*).

(2) the half-life must be sufficiently long to allow synthesis of the radiopharmaceutical, injection into the patient, and capture of the images.

A. Clinical Agents

Diagnostic radiopharmaceuticals currently in clinic use are mainly ^{99m}Tc complexes because of the nuclear properties of ^{99m}Tc ($t_{1/2}$ of ^{99}Tc is 2.12×10^5 years), its availability, and low cost (*269*, *270*). Metastable is usually obtained from a ^{99}Mo/^{99m}Tc generator in which $^{99}MoO_4^{2-}$ is adsorbed on an acid alumina column. The ion $^{99m}TcO_4^-$ is eluted in high yield with 0.9% (0.154 *M*) saline, whereas the more highly charged $^{99}MoO_4^{2-}$ is retained on the alumina. When the generator eluate containing $^{99m}TcO_4^-$ is added to the "instant kit" (often consisting of a sterile pyrogen-free vial containing a freeze-dried mixture of stannous chloride as a reducing agent and the ligand) the ^{99m}Tc complex is produced in high yield. The main γ-emission energy of ^{99m}Tc is 141 KeV, which consists of 89% of the total emission, and the majority of it can be adsorbed by thin NaI (Tl) crystals in the gamma cameras used for imaging (*271*, *272*). The half-life of ^{99m}Tc (6 h) is long enough to allow the necessary preparation to be done and yet short enough to minimize radiation damage to the patient.

The diverse chemical properties of technetium are derived from its position in the periodic table (group 7) with oxidation states ranging from -1 to 7, coordination numbers from 4 to 9, and strong binding to a variety of types of ligands (*273*). These properties allow for specificity in targeting of radiopharmaceuticals containing ^{99m}Tc by design of the ligand system. Clinically used ^{99m}Tc agents are listed in Table IV, and examples are given below according to their application for imaging of different organs.

Complex **61** (^{99m}Tc(V)-D,L-HM-PAO, Ceretec) is an approved cerebral perfusion imaging agent for evaluation of stroke. The tetradentate

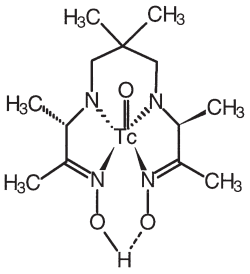

61

TABLE IV

SOME CLINICALLY USED ^{99m}Tc RADIOPHARMACEUTICALS

Drug	Commercial name	Clinical imaging
^{99m}Tc-D,L-HM-PAO	Ceretec	Cerebral perfusion
^{99m}Tc-MAG_3	TechneScan MAG_3	Renal
^{99m}Tc-Teboroxime	Cardiotec	Myocardial perfusion
^{99m}Tc-Sestamibi	Cardolite	Myocardial perfusion
^{99m}Tc-HIDA series		Hepatobiliary
^{99m}Tc-Mebrofenin	Choletec	
^{99m}Tc-Disofenin	Hepatolite	
^{99m}Tc-Lidofenin	TechneScan	
^{99m}Tc-succimer	MPI DMSA kidney reagent	Kidney
^{99m}Tc-gluceptate	Glucoscan	Renal and brain
	TechneScan-Glucepate	
^{99m}Tc-penetate	AN-DTPA	Kidney
	MPI DTP Kit	
	Techniplex	
	DTPA	
^{99m}Tc-MDP	AN-MDP	Skeletal
	Osteolite	
	TechneScan-MDP	
	MPI MDP Kit	
	MDP-Squibb	
^{99m}Tc-HMDP	Osteoscan-HDP	Skeletal
^{99m}Tc-DPD		Skeletal
^{99m}Tc-pyrophosphate	Technescan PYP	Skeletal and myocardial infarcts
	Pyrolite	
^{99m}Tc-MAA	AN-MAA	Lung perfusion
	Pulmolite	
	Technescan MAA	
	Macrotec	
^{99m}Tc-albumin colloid	Microlite	Liver imaging
^{99m}Tc-sulfur colloid	AN-Sulfur colloid	Liver
	TechneColl	
	Tc^{99m} TSC	
	Tesuloid	
^{99m}Tc-red blood cells	Ultratag	Blood pool
	^{99m}Tc-pyrophosphate	Spleen
$^{99m}TcO_4^-$		Thyroid

hexamethyl propyleneamine oxime loses two amine protons and an oxime proton when it coordinates to monooxo Tc(V), resulting in a neutral complex and a strong intramolecular hydrogen bond between oxime oxygen atoms (*274*). The molecule has a square-pyramidal geometry with the oxo group occupying the apical position. The Tc atom

lies about 0.68 Å above the plane defined by the four nitrogen atoms (Fig. 10). Complex **61** is taken up by the brain and is transformed into a more hydrophilic species which is retained in the brain. Intriguingly, the isomers containing chiral D,L-HM-PAO are retained in the brain significantly longer than those containing the meso ligand (*275*). In the crystal structure of the meso complex, there are two molecules in the unit cell and in one of these the six-membered propylene ring adopts a chair conformation, in contrast to the boat conformation observed for the D,L-isomer of **61** and other complexes of this ligand type. This may contribute to the differential retention properties of the two complexes by the brain.

The lipophilic complex ^{99m}Tc(IV)-L,L-ECD (**62**) with a deprotonated L,L-ethylcysteine dimer as ligand, is clinically used as a cerebral perfusion imaging agent. It crosses the blood–brain barrier and

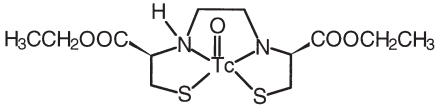

62

is retained in the brain following hydrolysis of one of the esters by intracellular esterases, giving an ionized monoester, monoacid metabolite (*276*). The presence of the two ester groups in **62** appears to be an essential structural requirement for its brain uptake and retention (*277*). The L,L-isomer is retained in the brain, and the D,D-isomer is not, although both isomers diffuse into the brain equally well (*278*). The clinical advantage of **62** compared to **61** is the greater stability after formulation.

The compound ^{99m}Tc(V)-MAG (**63**) is clinically used as a renal-im-

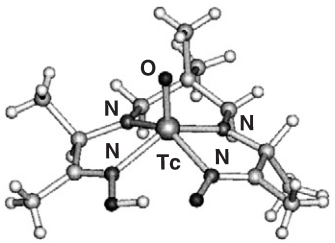

FIG. 10. X-ray crystal structure of the cerebral perfusion imaging agent **61** (Ceretec); the D,L-form of ligand HM-PAO is used. Adapted from (*275*).

aging agent. It exhibits square-pyramidal geometry with an oxo group in the apical position and Tc(V) situated above the plane defined by the sulfur and the three amide nitrogens (*279*). The free carboxylic acid group is deprotonated at physiological pH, which may contribute to the efficient renal excretion of **63.**

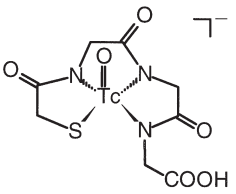

63

The complex ^{99m}Tc(V)-DMSA (**64**) has been used for a long time for the imaging of renal blood flow and morphology of the kidneys. The exact composition and structure of the agent is still unknown, as is the mechanism of retention. A structure of **64** (where R = COOH) has been proposed with three possible conformations, *syn-endo, syn-exo,* and *anti,* of the carboxylic acid groups with respect to the Tc=O core (*280*).

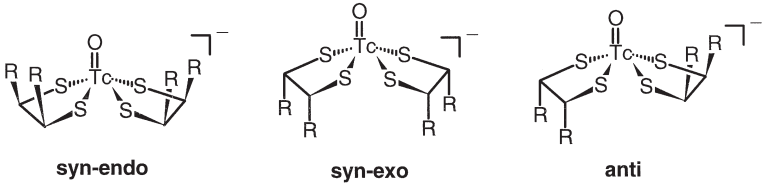

64

Complex **65** (Cardiolite), ^{99m}Tc(I)-sestamibi, is used for myocardial perfusion imaging. It was designed on the basis that lipophilic cationic complexes behave as potassium mimics and are taken up by the myocardium (*281*). The sequential metabolism of the six methoxy groups of **65** to hydroxyl groups in the liver leads to formation of ^{99m}Tc complexes with greater hydrophilicity which are not retained in myocardial tissues (*282*).

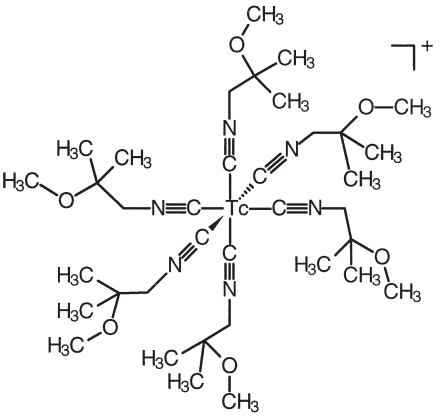

65

TechneScan (Q12), ^{99m}Tc(III)-Q12 (**66**), is a recently approved myocardial perfusion agent. The complex contains a tetradentate Schiff base ligand occupying the equatorial plane and two phosphine ligands in the axial sites (*283*). The ether linkages on the backbone of the Schiff base ligand and the phosphines serve to reduce protein binding *in vivo* by increasing the hydrophilicity. In addition the incorporation of the furanone moiety into the Schiff base backbone serves to stabilize the complex. Complex **66** has a rapid blood, lung, and liver clearance, which allows good myocardial imaging (*284*). Its myocardial activity is related to the actual myocardial flow at the time of tracer injection. It shows no myocardial redistribution as long as 4 h after intravenous injection (*285*).

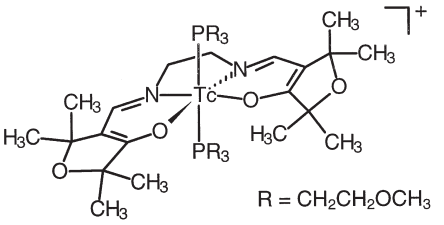

66

Myoview ^{99m}Tc-tetrofosmin (**67**) is another clinically approved, lipophilic, cationic perfusion agent (*286*). The molecule contains *trans*-

dioxotechnetium(V) with two bidentate phosphine ligands. The combination of lipophilicity and dipole moment in **67**, which is

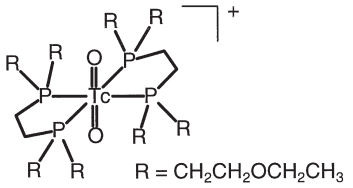

67

influenced by the eight ethoxy-ethyl groups, facilitates its solubility in serum and permeability through the cytosolic membrane of heart cells. Complex **67** has a rapid clearance from the blood stream via the liver and kidneys with excretion into the biliary and urinary systems, respectively (*287*).

Several clinically approved diagnostic pharmaceuticals are based on radionuclides other than ^{99m}Tc, such as ^{201}Tl, ^{111}In, ^{169}Yb, ^{67}Ga, ^{51}Co, and ^{51}Cr. Thallous chloride (Tl^{201}), an important radiopharmaceutical, has been used as a myocardial (heart muscle) perfusion agent since 1975 for assessing the integrity of the myocardium using stress-and-rest techniques. The less-than-optimal nuclear properties of ^{201}Tl for imaging are likely to result in its eventual replacement by suitable ^{99m}Tc agents. Indium-111–oxine (thought to be In(oxyquinoline)$_3$) is approved for the labeling of leukocytes (white blood cells) and imaging of sites of infection or inflammation. Indium-111–DTPA (where DTPA is diethylenetriaminepentaacetic acid) is used for radiographic cisternography studies. Diethylenetriaminepentaacetic acid is chelated to In(III) through three nitrogens and all five carboxylate oxygens, resulting in an eight-coordinate complex (*288*), with a very high stability (log K 29.0) at neutral pH (*289*). Ytterbium-169–DTPA is also an approved agent for such imaging studies. After injection of ^{67}Ga-citrate into the blood stream, ^{67}Ga concentrates in certain viable primary and metastatic tumors as well as focal sites of infection. Gallium(III) mimics Fe(III) and is taken up by the serum iron transport protein transferrin. However, it is not reduced *in vivo* and does not become incorporated into hemoglobin. Cobalt-57–cyanocobalamin is used for the diagnosis of pernicious anemia and as an adjunct for the evaluation of other defects of the intestinal system.

B. Design of New Radiopharmaceuticals

The use of ligands which chelate extensively and therefore give rise to highly stable metal complexes, and possess additional functionality allowing targeting is illustrated for radiopharmaceuticals in this section, and in Section V.

Radioisotopes conjugated with monoclonal antibodies (mAbs) are useful for radioimmunodetection of cancer and hold promise for radioimmunotherapy. The first mAb radiopharmaceutical, ^{111}In satumomab pendetide (anti-B 72.30), was approved for clinical use in 1992 for diagnosis of colorectal and ovarian cancer (*291*). Since then four other murine mAbs linked to ^{99m}Tc (CEA-Scan and Verluma) and to ^{111}In (Myoscint and ProstaScint) have been approved for imaging of cancer (*292*). In these conjugates, the radionuclides are held as stable chelates linked to the mAb. Although the prolonged circulation of radiolabeled mAb results in significant total body irradiation, several mAbs have shown impressive results in radiosensitive malignancies such as lymphomas (*293*). Numerous mAbs, including human and humanized immunoglobulins, have been radiolabled with ^{67}Cu, ^{90}Y, ^{99m}Tc, and ^{111}In and are currently under clinical evaluation (*292*). Most promising results for copper have been achieved with ^{64}Cu and ^{67}Cu complexes with macrocyclic polyaminocarboxylate or macrocyclic polyamines, due to their favorable kinetic and thermodynamic stabilities in the presence of serum proteins (*294*). Encapsulation in fullerenes may also provide a novel method for the delivery of radionuclides to target sites (*295*, *296*).

Metastable ^{99m}Tc-based receptor-specific radiopharmaceuticals to image organ perfusion and function are being designed (*297*). The most successful are those which target cell-surface receptors or transporters and can aid monitoring of disease states that are difficult to diagnose.

Selective ^{99m}Tc serotonin receptor imaging agents are of interest because of the involvement of this receptor in Alzheimer's disease as well as in depression. Complex **68** is a conjugate of ^{99m}Tc complex with

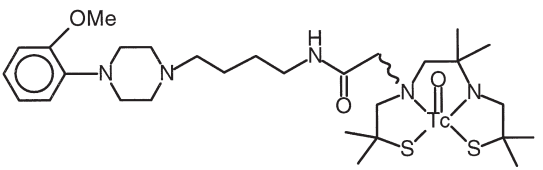

68

a high affinity for the serotonin receptor. Although **68** has good *in vitro* binding (K_i = 10.4 n*M*), the compound does not exhibit neutral tissue uptake (*297*).

The dopamine transporter provides a presynaptic dopamine binding site for which cocaine analogs are high-affinity antagonists. Changes in transporter concentration have been implicated in CNS diseases such as Parkinson's disease. ^{99m}Tc-labeled dopamine transporter-specific complexes such as **69** have been designed (*298*). The first human-tested ^{99m}Tc-based SPECT agent **69** has provided good contrast in basal ganglia images (*299*). The complex exists as a mixture of *syn*- and *anti*-diastereomers.

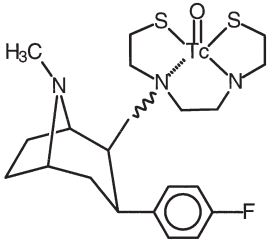

69

Technetium-labeled peptides and proteins have been investigated as potential thrombus-imaging agents. Complex **70**, which combines ^{99m}Tc with the tripeptide motif Arg-Gly-Asp, binds GP Iib/IIIa recep-

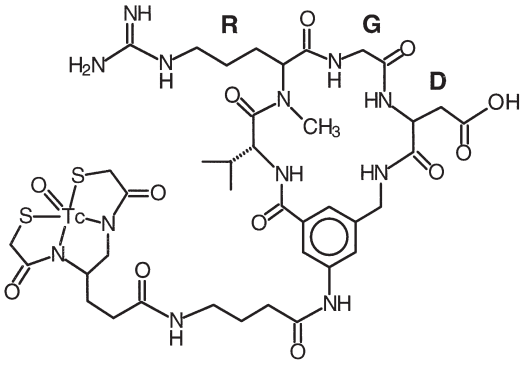

70

tor with high affinity and has provided good contrast in SPECT images of canine deep vein thrombus (*300*).

V. Magnetic Resonance Imaging Contrast Agents

Magnetic resonance imaging is now a powerful tool in clinical diagnosis (*301*). Diseases can be detected from differences in ^{1}H NMR resonances (mainly H_2O) between normal and abnormal tissues via administration of external paramagnetic contrast agents. Magnetic resonance imaging contrast agents shorten proton relaxation times and therefore provide improved tissue contrast. The effectiveness of interactions between paramagnetic metal complexes and H_2O is a function of several parameters.

$$R_i = f(T_{1e}, \tau_M, \tau_R, \tau_D),$$

where R_i is the relaxivity ($R_1 = 1/T_1, R_2 = 1/T_2$), T_{1e} is the longitudinal electron spin relaxation time, τ_M is the residence lifetime of bound H_2O, τ_R is the rotational tumbling time of the complex, and τ_D is the relative translational diffusion time (outer sphere relaxation) (*302*, *303*). These factors are illustrated in Fig. 11.

It should be possible to maximize the relaxivity by optimizing the contributions of these various factors, especially by increasing the water exchange rate, decreasing the rotational correlation time, and by incorporating features into the complex which allow targeting of paramagnetic complexes to specific tissues. Most applications are concerned with high spin Gd(III), Mn(II), and Fe(III), ions which have a

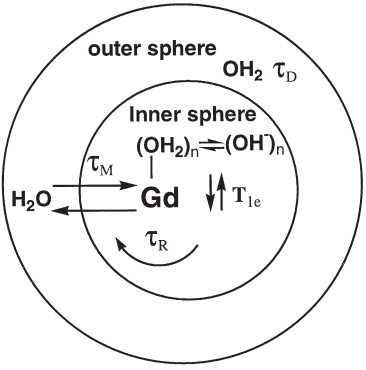

FIG. 11. Some of the factors which influence the relaxivity of Gd(III) complexes.

large number of unpaired electrons (7, 5, and 5, respectively) and long electron spin relaxation times (*304*, *305*). Contrast agents are used in about 20% of the 5 million MRI scans currently carried out each year on the 10,000 instruments now installed (1998).

A. Clinical Gd, Mn, and Fe Compounds

Four approved Gd(III) complexes are now widely used clinically. Complexes containing DTPA **71** (Magnevist) and DOTA **72** (Dotarem) are ionic, whereas those of DTPA–BMA **73** (Omniscan) and HP–DOTA **74** (Prohance) are neutral; their low osmolarity decreases the pain of the injections. All these agents are extracellular and they rapidly diffuse into the interstitial space. Doses are usually in the region of 0.1 mmol kg^{-1}, which means that total injected doses are close to 4 g.

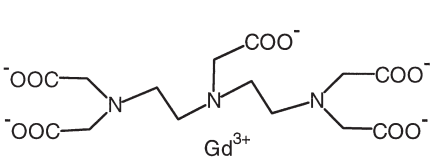

71

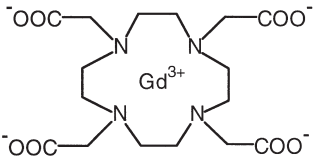

72

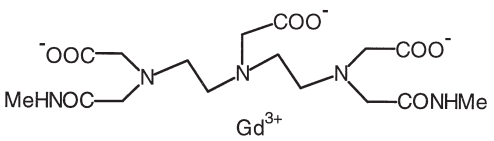

73

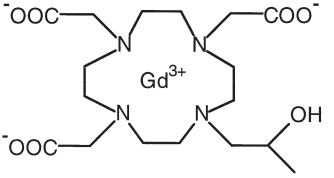

74

Gadolinium(III) is nine coordinate in each complex and contains one bound H_2O ligand. The crystal structure of **72** is shown in Fig. 12 (*306*). Water exchange on Gd(III) in these complexes (*638*) is dissociative, and steric-crowding at the H_2O site enhances the exchange rate. Thus the H_2O exchange rate for DTPA–BMA, for which Gd–amide oxygen distances (2.44 Å) are longer than for Gd–DTPA (2.40 Å), is 10 times less than for Gd–DTPA (Table V). Aime *et al.* have shown that the water residence time (τ_M) in the Eu(III) complex of 1,4,7,10-tetrakis(carbamoylmethyl)-1,4,7,10-tetraazacyclododecane (**72**-like ligand) is dependent on the conformation of the complex. Water release from the m isomer (square antiprismatic geometry) is more facile

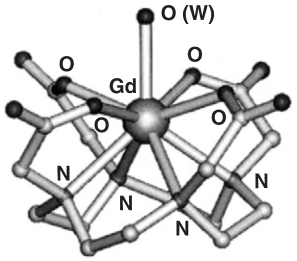

FIG. 12. X-ray crystal structure of complex **72**, Na[Gd(DOTA)(H_2O)], an MRI contrast agent used clinically for detection of blood–brain barrier abnormalities. Adapted from (*306*).

than from the M isomer (twisted antiprismatic geometry) with τ_M being 1.88×10^{-5} s for the former and 4.16×10^{-3} s for the latter (*307*).

Both the DTPA– and DOTA–Gd(III) complexes are thermodynamically very stable (Table V), but DOTA complexes have a higher kinetic stability. The stabilities are highly pH dependent. For example, log *K* for [Gd(DTPA)] falls by a factor of about 4 when the pH drops from 7.4 to 5. This could be significant in some biological compartments, e.g., lysosomes, where the pH can be as low as 5.

Dendrimer-metal chelate complexes offer the possibility of delivering high concentrations of Gd(III) effectively. Thus adducts of the

TABLE V

RELAXIVITIES (20 MHz) AND OTHER PROPERTIES OF Gd(III) CONTRAST AGENTS[a]

Agent	Structure number	τ_R (ps)[b]	k_{ex}^{298} (10^6 s^{-1})[b]	Relaxivity R_1[b] (mM^{-1} s^{-1})	log *K*	Reference
$[Gd(DTPA)]^{2-}$	**71**	58	3.3	4.5	22.5	(*619*)
$[Gd(DOTA)]^{-}$	**72**	73	4.8	3.4	25.8	(*622*)
$[Gd(BMA\text{-}DTPA)]^{2-}$	**73**	66	0.45	4.4	16.9	(*621*)
[Gd(HP-DOTA)]	**74**			3.6	23.8	(*622*)
[Gd(DO3A)]				4.8	21.1	(*622*)
$[Gd(Texaphyrin)]^{2+}$	**55**			19.0		(*623*)
[Gd(DO3MA)]				4.4	25.2	(*624*)
$[Gd(BOPTA)]^{2-}$	**Gd-76**	88		4.39	22.5	(*625*)
$[Gd_{170}(dendrimer)]$				5800		(*308*)
[Gd(DTPA-BSA)]				19.0		(*626*)
Mn(DPDP)	**75**			1.88[c]	15.1	(*627*)

[a] Data taken from Refs. (*628*, *629*).

[b] Relaxivity is the enhancement of proton relaxation rate in aqueous solution per unit of concentration (mM^{-1}).

Starburst (TM) dendrimers with DTPA can contain 170 bound Gd(III) ions and have relaxivities (per bound Gd) up to 6 times that of Gd–DTPA (*308*). Both global and local motion contribute to the overall rotational correlation time. Attempts have been made to increase the relaxivity of Gd(III) by optimizing the rotational correlation time via binding of Gd(III) to derivatized polysaccharides (*309*) and by binding lipophilic complexes to albumin in serum (*310*). The latter approach has achieved relaxivities as high as 44.2 $mM^{-1}\,s^{-1}$ for derivatized **72** (*311*).

Manganese(II)–*N*,*N*′-dipyridoxylethylenediamine-*N*,*N*′-diacetate 5,5′-bis(phosphate) **75** (DPDP) is clinically used for enhancing contrast in the liver (detection of hepatocellular carcinomas) (*312*). Some dissociation of Mn(II) appears to occur in the liver, and enhancement can also be obtained in functional adrenal tissues (*313*). Manganese(II)–tetrasulfonated phthalocyanine also shows tumor localization properties and is a more efficient relaxation agent than the analogous Gd(III) complexes (*314*).

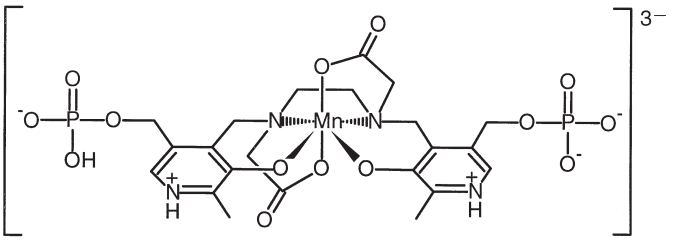

75

Paramagnetic particles are being used as MRI contrast agents for gastrointerstinal, liver, and blood pool imaging. The distribution of injected particles in the body is dependent on particle size. Nanoparticles consisting of iron oxide of diameter 150 nm coated with dextran (Endorem) (*315*) provide specific liver imaging, whereas those of diameter 30 nm (Sinerem) (*316*) can be used as blood pool agents. The larger particles of Lumirem (300 nm in diameter) (*317*) can be administered orally for gastrointestinal tract imaging as can Gadolite (*318*), a zeolite with Gd(III) trapped in its cages.

B. Targeting

The DTPA and DOTA complexes currently in clinical use act as extracellular markers which are associated with changes in blood

flow. However, the enhancement provided by these agents in internal organs is limited. Thus there is a need for developing targeted MRI contrast agents.

Meade *et al.* (*319*) have shown that it is possible to deliver Gd(III) to T cells via DTPA-modified poly-D-lysine conjugated to transferrin and that this conjugate can be used to transfer DNA. Hence this procedure may allow the noninvasive monitoring of gene delivery using MRI. They have also synthesized a family of "Smart" MRI contrast agents, 4,7,10-triaceticacid-1-(eth-2-oxy-β-galactopyranosyl)-1,4,7,10-tetraazacyclododecane-gadolinium (Egad), which can be activated by the enzyme β-galactosidase (*320*). As synthesized, an oxygen from a galactopyranose side arm occupies the ninth coordination site of Gd(III). Exposure of Egad to the enzyme β-galactosidase removes β-galactopyranose from the chelator, allowing an increase in the average number of bound H_2O molecules from 0.7 to 1.2 and giving a 20% increase in relaxivity.

Complex **71** does not enter cells and is excreted almost exclusively by the kidney. Introduction of a benzyloxymethyl substituent on a terminal acetate of DTPA as in BOPTA (**76**) produces a Gd(III) complex (Gadobenate), which enters hepatocytes and is excreted in bile.

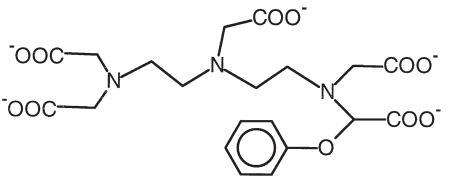

76

The coordination sphere of Gd(III) is almost identical in the complexes of DTPA and BOPTA (Fig. 13), which have similar stabilities and relaxivities (*321*). By introducing a butylbenzyl group into DTPA, hepatobiliary specificity can be achieved, giving rise to a twofold enhancement of liver tumors *in vivo* (*322*).

Glycoproteins derivatized with DTPA at surface lysine residues and labelled with Gd(III) (or In(III)) are internalized by cells and metabolized to Gd(-DTPA-lysine), which is released only slowly from cells (*323*). Some Gd(III) may dissociate from this complex since the pH in lysosomes, where the metabolism occurs, is low (pH 5).

Metal–texaphyrin complexes are readily taken up by tumor cells and have clinical potential as photosensitizers (see Section III) and

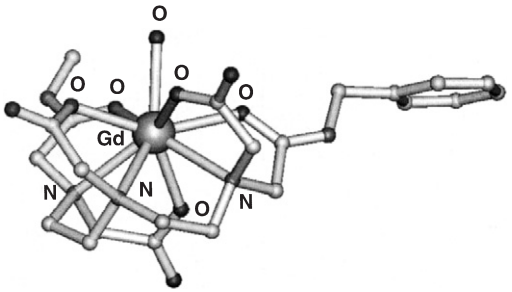

FIG. 13. X-ray crystal structure of complex Gd(III)–**76**, Na_2[Gd(BOPTA)(H_2O)], an MRI contrast agent on clinical trial for liver imaging. Adapted from (*321*).

MRI contrast agents. Therefore the possibility of combined diagnostic imaging and photodynamic therapy arises (*324*). Lanthanide texaphyrin complexes are more kinetically stable than the porphyrin analogs.

Gadolinium(III) complexes containing phosphonate groups can be targeted to bone. Examples are the DOTA derivatives (*325*, *326*) and complexes of aminophosphonate ligands (*327*).

VI. Anti-infective Agents

A. Antimicrobial

Silver and its compounds have long been used as antimicrobial agents in medicine. The mechanisms of silver toxicity as they relate to human exposure to pharmaceuticals have been reviewed (*328*). Silver is active at low concentrations and has a low toxicity. The practice of instilling the eyes of infants with 1% of $AgNO_3$ solution immediately after birth is still common in some countries, for prevention of opthalmia neonatorum (*329*). Silver sulfadiazine **77** is clinically used as a topical antimicrobial and antifungal agent and applied as a cream to prevent bacterial infections in cases of severe burns. It is an insoluble polymeric compound and releases Ag(I) ions slowly.

The mechanism of Ag(I) cytotoxicity is unknown. Cell wall damage may be important and it has been shown that Cys-150 in the enzyme phosphomannose isomerase, an essential enzyme for the biosynthesis of *Candida albicans* cell walls, is the Ag(I) target in this organism (*330*). Silver resistant bacteria are known, but only recently has significant progress been made in understanding the resistance mechanisms (*637*).

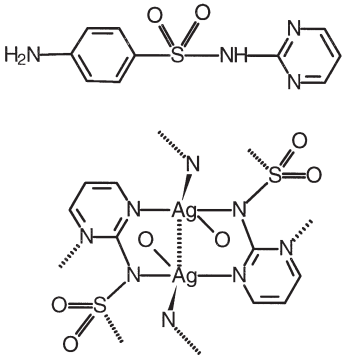

77

The silver salt of the steroid fusidic acid is reported to be more active than silver sulfadiazine against a range of microorganisms including *Candida albicans* (*331*). Tetrahedral Ag(I) bis-diphosphine complexes such as $[Ag(depe)_2]NO_3$ (depe = $Et_2P(CH_2)_2PPh_2$) are active against bacteria and fungi, but are inactivated by interactions with components of broth culture media (*332*). The neutral, sparingly soluble Ag(I)–imidazolate complex $[Ag(imd)]_n$ exhibits a wide spectrum of antimicrobial activity against bacteria, yeast, and fungi (*333*). Monomeric, cationic, water-soluble $[Ag(Himd)_2](NO_3)$ is also an effective antimicrobial agent.

Mixed-ligand zinc complexes with sulfadiazine and amine ligands are reported to exhibit higher activity than silver sulfadiazine against Gram-positive and Gram-negative bacteria as well as fungi (*334*). The zinc compounds have better aqueous solubility and skin permeability than silver sulfadiazine.

Material-based approaches to metalloantimicrobial agents are being developed. For example, $AgCl/TiO_2$ composite (e.g., 20 : 80) formulated with sulfosuccinate salts can maintain an equilibrium of ppm–ppb levels of cytotoxic Ag(I) ions when suspended in solution (*335*, *336*).

Chagas' disease is caused by a kinetoplastid trypanosoma parasite and affects millions of people in Latin America. The disease is currently incurable. Chemotherapy is based mainly on nitrofuran and nitroimidazole compounds and sterol biosynthesis inhibitors such as ketoconazole (*337*). Toxicity and high doses are the major problems for these organic drugs. Urbina *et al.* (*338*, *339*) have found that complexation of antiparasitic organic agents such as chloroquine (**78**)

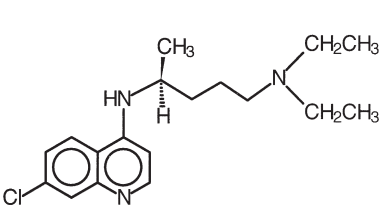

78

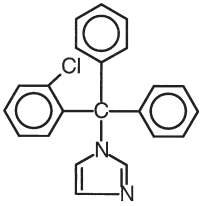

79

and chlorotrimazole (**79**) to Ru(II) or Rh(I) enhances the activity of the parental drugs. For example, the activity of Ru(II)–**78** against chloroquine-resistant strains of *Plasmodium falciparum* is 2–5 times higher than chloroquine alone (*339*), and Ru(II)–**79** causes a 90% inhibition of the proliferation of *Trypanosoma cruzi,* a causative agent of Chagas' disease, at a concentration of 10^{-5} *M* (*338*).

Antimony has been used for medicinal purposes for many centuries. Antimony(III) complexes are generally more toxic than those of Sb(V). The Sb(V) drugs *N*-methylglucamine antimonate (glucantime) and sodium stibogluconate (pentostan) are currently used clinically for the treatment of *Leishmaniasis,* a disease caused by intracellular parasites. The carbohydrate may serve to deliver Sb(V) to macrophages. The Sb(V) complexes may be prodrugs which are converted to more toxic Sb(III) at or near the site of action. Little is known about the complexation between Sb(V) and polyhydroxy ligands, but 4,6- and 2,3-dihydroxy groups of mannopyranosyl units may be involved in binding to Sb(V), and the polymeric complexes are probably based on octahedral SbO_6 cores. Proposed mechanisms of action of Sb drugs involve (a) macrophage uptake of the Sb complex via recognition by an α-mannosyl receptor and endocytosis; (b) fusion of the endocytic vesicle carrying the complex with the parasitophorous vacuole; (c) dissociation of the complex at the acidic pH of the parasitophorous vacuole; and (d) destruction of the parasites without affecting macrophage viability. Antimony(III) and Sb(V) complexes with yeast mannan appear to be promising for improving the stability and solubility of Sb drugs (*340*, *341*).

Malaria is still one of the world's most devastating infectious diseases. An estimated 270 million people are affected by the parasite every year, and close to 2 million children die. The most deadly species, *Plasmodium falciparum,* has become widely resistant to most of the available antimalarial drugs such as quinolines.

Metal complexes such as $[Ga(madd)]^+$ (**80**) (Fig. 14) where madd = 1,12-bis(2-hydroxy-3-methoxybenzyl)-1,5,8,12-tetraazadodecane exhibit high selective activity against chloroquine-resistant *Plasmodium falciparum* (*342*, *343*). The A1(III), Ga(III), and Fe(III) complexes are hydrolytically stable and posses a balance of hydrophobicity and delocalized monocationic charge, which enhances cell membrane permeability. The complexes inhibit heme polymerization directly, with IC_{50} values of *ca.* 1 μM. The tetraamine backbone and a variety of positions on the aromatic ring in the ligand can be modified for optimization of selectivity and bioavailability. Heme is released from hemoglobin in the parasite digestive vacuole, and the parasite polymerizes heme to prevent membrane lysis and inhibition of critical proteases, a process which involves a His-rich protein (*342*).

Iron chelators have been intensively studied as potential therapeutic agents for malaria, since iron is essential for parasite survival (*344, 345*). This is discussed in detail in Section XII.

Cationic cobalt(III) cage complexes such as **81**, containing lipophilic paraffin tails, have detergentlike characteristics and are able to penetrate biological membranes (*346*). Compounds with C_8 tails possess high stability in solution and can kill parasitic nematodes at micromolar concentrations (*347*). The molecules, which have a 3+ charge and a large tail, can destabilize membrane bilayers and altering the curvature and charge distribution of cells.

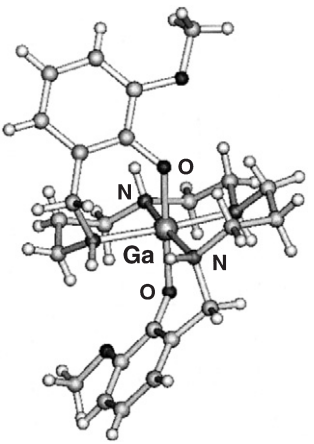

FIG. 14. X-ray crystal structure of $[Ga(madd)]^+$ **80**, a potential antimalarial agent. Adapted from (*343*).

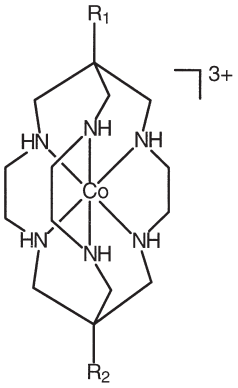

81

B. Antiviral

There is a need for more effective anti-HIV agents, especially since resistance to all the currently used agents is beginning to develop; a combination of different agents targeting different stages of the virus replicative cycle could provide a more effective therapy (*348*).

1. Polyoxometalates

Early work in 1971 showed that polyoxometalates exhibit antiviral activity (*349*). Although inhibition of HIV-1 reverse transcriptase in lymphocytes taken from patients treated with $[NaW_{21}Sb_9O_{86}](NH_4)_{17}(Na)$ (HPA-23) was demonstrated (*350*), subsequent clinical trials of HPA-23 as an anti-HIV agent showed that it was too toxic to allow sufficiently long administration of the drug, in high enough doses, to produce adequate therapeutic efficacy (*351*). Recent work has led to the discovery of less toxic and more effective agents in this class. A comprehensive review on polyoxometalates in medicine has appeared recently (*352*). The anti-HIV activities of some polyoxometallates are listed in Table VI. In general, polyoxotungstates of Keggin (Fig. 15), lacunary Keggin, trivacant Keggin, Keggin sandwich, Wells-Dawson, and Wells-Dawson sandwich structures exhibit anti-HIV activity, whereas most other structural categories do not (*353*).

It appears that polyoxometalates are active at the cell surface (*354*, *355*), and they exhibit anti-HIV activity by binding to viral envelope sites (*356*, *357*), interfering with virus adsorption (*358*). They also inhibit the binding of HIV-1-infected lymphocytes to uninfected lympho-

TABLE VI

ANTI-HIV ACTIVITY OF SOME POLYOXOMETALLATES[a]

Compound	EC_{50}[b] (μg/ml)	CC_{50}[c] (μg/ml)	Selectivity index (CC_{50}/EC_{50})
$K_5[BW_{12}O_{40}]$	1.4	654	467
$K_{13}[Ce(SiW_{11}O_{39})_2] \cdot 26H_2O$	0.7	230	328
$K_{12}H_2[P_2W_{12}O_{48}] \cdot 24H_2O$	0.3	339	1130
$K_{10}[P_2W_{18}Zn_4(H_2O)_2O_{68}] \cdot 20H_2O$	0.7	466	666
$K_8H[P_2W_{15}V_3O_{62}] \cdot 34H_2O$	1.1	293	266
$K_5[BW_{11}Ga(H_2O)O_{39}]$	2.8	>500	>178
$K_5[SiW_{11}(C_5H_5)TiO_{39}]$	1.9	>500	>263
$[Me_3NH]_8[Si_2W_{18}Nb_6O_{77}]$	3.2	>500	>156

[a] Data taken from Ref. (*630*).
[b] EC_{50}: effective concentration which suppresses virus by 50%.
[c] CC_{50}: 50% cytotoxicity.

cytes (*354*, *355*). Hill and co-workers (*359*) have shown that $K_{12}H_2[P_2W_{12}O_{48}] \cdot 24H_2O$ (JM 1591), $K_{10}[P_2W_{18}Zn_4(H_2O)_2O_{68}] \cdot 20H_2O$ (JM 1596), and $[(CH_3)_3NH]_8[Si_2W_{18}Nb_6O_{77}]$ (JM 2820) are tightly bound to plasma proteins and accumulate at high levels in the kidneys and liver. Certain polyoxometalates can also penetrate cell membranes and localize intracellularly. For example, when J774 cells are cultured in the presence of polyoxometalates such as the $K_{12}H_2[P_2W_{12}O_{48}] \cdot 24H_2O$, tungsten can be found inside the cells (*360*, *361*). Some polyoxometalates with higher negative charge densities, such as $[(O_3POPO_3)_4W_{12}O_{36}]^{16-}$ and $[(O_3PCH_2PO_3)_4W_{12}O_{36}]^{16-}$, selectively inhibit HIV-1 reverse transcriptase (*362*, *363*).

The activity of polyoxometalates depends on the structure, negative

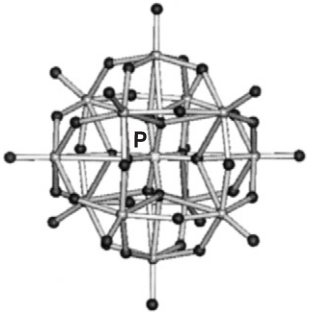

FIG. 15. Crystal structure of the Keggin-type polyoxometallate ion $[PMo_{4.27}W_{7.73}O_{40}]^{6-}$. Adapted from (*608*).

charge, and the counter ions. In one study, none of the complexes with less than eight metal ions showed activity against HIV-1, and the replacement of monoatomic cations (such as Na(I), K(I), and H^+) with NH_4^+ did not affect the anti-HIV activity but considerably reduced toxicity, e.g., bone marrow toxicity (*364*). However, it has been emphasized that considerable caution must be exercised in interpreting structure–activity relationships for polyoxometalates since many are unstable in water and degrade into a mixture of inorganic products in physiological media. For example, the Keggin phosphotungstate $[PW_{12}O_{40}]^{3-}$ readily gives rise to relatively stable isomers of $[PW_9O_{34}]^{9-}$ at pH 7. There is currently very little kinetic data available on the degradation of polyoxometalates in solution.

Polyoxometalates are poorly absorbed following oral administration, and even when they are delivered directly into the bloodstream, they may be retained by various plasma proteins before reaching their site of action. Therefore improvements in the bioavailability of polyoxometalates are required.

2. *Bicyclams*

Macrocyclic bicyclams ligands such as **82** (JM3100, AMD3100) are among the most potent inhibitors of HIV ever described, being active at nanomolar levels (*365*). Since they are nontoxic at micromolar levels, they have a high selectivity index (*ca.* 10^5). They target the early stages of the retrovirus replicative cycle and block HIV-1 entry and membrane fusion via the CXCR4 coreceptor (*366*, *367*). The linker between the two tetraazamacrocycles plays an important role in determining both the anti-HIV activity and cellular toxicity (*368*, *369*). In resistant viral strains, mutations have been found within the V3 loop of the envelope protein gp120, and bicyclams such as **82** and **83** (JM2763) may target this protein (*370*, *371*).

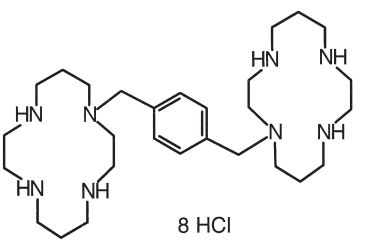

82

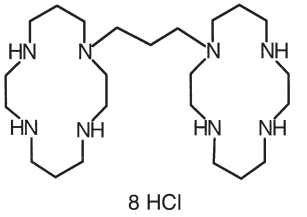

83

The effect of several metal ions on the anti-HIV activity of bicyclams has been reported (*371*). Zinc may facilitate the binding of bicyclams to the virus, and bis-Zn(II)–bicyclam complexes exhibit activity comparable to that of the parent bicyclam, but activity is reduced for other metal complexes such as Ni(II), Cu(II), Co(II), and Pd(II).

The 12-membered tetraamine cyclen and bicyclen have inferior anti-HIV activity and are more toxic compared to cyclams and bicyclams. However, Kimura *et al.* (*372*) have shown that complexation of the monomeric cyclen (**84**) to Ni(II), Cu(II), and Zn(II) reduces the toxicity and increases the anti-HIV activity. This is also true for the bicyclen (**85**), for which the combination of dimerization and metal complexation potentiates the inhibition against HIV-infected MOLT-4 cells (*373*).

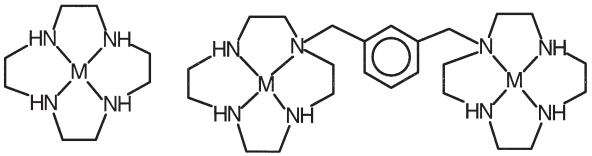

84 **85**

In general, dimeric polyamines are more active than their monomeric analogs. Since the charge on the macrocycle appears to be more important to its activity than ring size, it is possible that metal binding is not a requirement for activity (*374*). It is notable that positively charged azamacrocycles can form strong complexes with negatively charged biomolecules (*375*), although the recognition properties of metallomacrocycles are also well known (*376*).

3. Zn(II) Removal from Proteins

Zinc-finger proteins are also possible targets for bicyclams. All nucleocapsid proteins of known strains of retroviruses contain one or two copies of an invariant sequence, Cys-X_2-Cys-X_4-His-X_4-Cys. Proteins with this sequence bind zinc stoichiometrically with dissociation constants of *ca.* 10^{-12} *M* (*377*). Under physiological conditions, a 10-fold excess of EDTA removes only 50% of zinc from the zinc finger domain of HIV-1 nucleocapsid protein (*378*).

A DNA sequence of 10 base pairs, called the κB site, is present in various cell genes critical for immune or inflammatory responses. The

zinc-finger protein HIV-EP1 (HIV enhancer-binding protein) and Rel-family transcription-factor protein NF-κB bind to the κB site and become active upon binding. The two proteins cooperatively regulate κB site-directed transcription. The DNA binding of HIV-EP1 can be inhibited by extracting zinc from the protein by Zn chelators containing dimethylaminopyridine and cysteine units, e.g., **86** (*379*). Similar che-

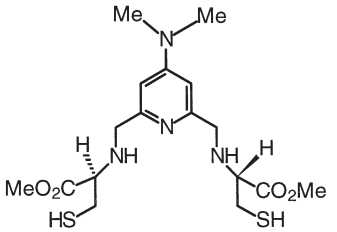

86

lators have discriminative activity in the inhibition of HIV-EP1 and NF-κB, which should allow selective control over the two signaling pathways (*380*). The introduction of sulfur-containing groups enhances the inhibitory activity of the chelators (*381*).

An alternative method for removing Zn from the active site of zinc proteins is to use aromatic nitroso compounds such as 3-nitrosobenzamide and 6-nitroso-1,2-benzopyrone (*382*). These agents can oxidize Zn-bound cysteine S and can inhibit HIV-1 infection in human lymphocytes. They also eject zinc from isolated HIV-1 nucleocapsid zinc-fingers and from intact HIV-1 virions.

The role of zinc(II) in clinical responses is complex and inconsistent. Nevertheless the idea that Zn(II) supplementation might improve the immunodeficiency in AIDS patients has prompted clinical trials of Zn(II) in humans. The results have been controversial; in one study no significant effect of zinc gluconate in patients with AIDS-related complex was observed (*383*), while in another study (*384*), the administration of Zn(II) showed promising effects. At neutral pH, Zn(II) is an effective inhibitor of HIV protease (*385*).

4. Antisense and Antigene Oligonucleotides

Antisense oligonucleotides are a class of potent inhibitors of HIV-1 integrase (*386*). Several of these oligonucleotides including T30175, T30177 (also referred as AR177 or Zintevir), T30677, T30695,

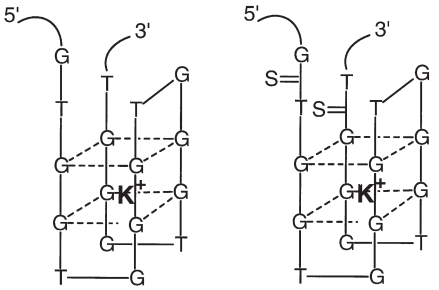

FIG. 16. The folding of anti-HIV oligonucleotides T30175 and T30177 (see Section VI,B) in the presence of potassium ions.

GEM91, and 15152922, are currently on clinical trials. Some oligonucleotides such as T30175 and T30177, 5′-G*TGGTGGGTGGGT GGG*T-3′ (* indicates phosphorothioate linkages), are composed entirely of deoxyguanosine and thymidine. These fold up in the presence of potassium to give a highly stable four-stranded DNA structure dominated by two stacked guanine-quartet motifs (Fig. 16) (*387*). The anti-HIV activity of some of these oligonucleotides is listed in Table VII.

TABLE VII

INHIBITION OF HIV-1 INTEGRASE 3′ PROCESSSING (3′-PROC), STRAND TRANSFER (ST) AND HIV-1RF CYTOPATHICITY (HIV-1_{RF}) BY SOME GUANINE QUARTETS IN CELL CULTURES

		IC_{50} (nM)[c]		IC_{50} (μM)
Oligo[a]	Sequence (5′-3′)[b]	3′-Proc	ST	HIV-1_{RF}
T30177	GTGGTGGGTGGGTGGGT	79 ± 24	49 ± 5	0.075
T30661[d]	GTGGTGGGTGGGTGGGT	111 ± 11	84 ± 41	46.6
T30526	GTGaTGGGTGGGTGGGT	159 ± 41	126 ± 4	11.7
T30679	GTGGTtGGTGGGTGGGT	159 ± 41	156 ± 28	3.46
T30678	GTGGTGGGTGGGTtGGT	98 ± 13	120 ± 50	3.95
T30677	GTGGTtGGTGGGTtGGT	725	620	>40
T30676	GTGGTGGGTG*T*GGTGGGT	148 ± 26	134 ± 16	1.0
T30675	GTGGTGGGTG*T*GGTtGGT	485	500	>30
T30674	GTGGTtGGTG*T*GGTtGGT	760	610	>50
T30673	GTGGTtGGTG*T*GGTtGGt	790	600	>35
T30659	GGTtGGTG*T*GGTtGG	870	750	>20

[a] Data taken from Ref. (*631*).

[b] Insertions (italicized and underlined) and mutations (lower case) from the parent sequence of T30177.

[c] IC_{50}: inhibitory concentration where cellular toxicity is 50%.

[d] RNA version of T30177.

T30177 is the most potent inhibitor of HIV-1 integrase identified so far, with IC_{50} values in the nanomolar range (Table VII) toward HIV-1 integrase 3′-processing, strand transfer and HIV-1RF cytopathicity. Unlike other oligonucleotides, intravenous administration of T30177 to cynomolgus monkeys does not cause hemodynamic toxicity at plasma concentrations showing anti-HIV activity *in vitro*.

T30177 binds to the N-terminal region of HIV-1 integrase (which contains a putative zinc finger) and blocks the binding of the normal viral DNA substrate to the enzyme. T30177 is a more potent inhibitor of integrase in buffers containing Mg(II) than with Mn(II), suggesting that divalent metal ion coordination along the phosphodiester backbone may play a role in the inhibitory activity. However, it is not clear whether the inhibitory effect of T30177 toward HIV integrase accounts for its anti-HIV activity. Time-of-addition experiments with T30177 indicate that the oligonucleotide inhibits HIV replication at a step which coincides with virus adsorption and/or fusion (*388*). The fact that resistant HIV strains selected under continuous pressure of T30177 reveal the presence of mutations in gp120 rather than the integrase gene further supports the view that the adsorption/fusion process is the primary target for the anti-HIV action of T30177 (*389*).

Antisense and antigene oligonucleotides labeled with manganese(III) porphyrins can selectively cleave double-stranded DNA (*390*). Meunier *et al.* (*391–393*) have used this approach to study the cleavage of the *pol* gene of HIV-1. Manganese–porphyrin–spermine oligonucleotides such as **87** form a triple helix with targeted double-stranded DNA, with T_m values for the triplex ranging from 20° to 30°C for oligonucleotides of 16–25 bases. The manganese–porphyrin 19-mer conjugate cleaves an HIV 35-mer at concentrations of 10 n*M* (*391*).

The Mn(III)–porphyrin in these agents produces oxidative DNA breaks when activated by potassium monopersulfate ($KHSO_5$). However, the mechanism of reaction is still under investigation (*394*). A high-valent metal–oxo complex is generated when Mn(III)–porphyrin is activated by $KHSO_5$. The high-valent metal–oxo complex appears to damage DNA by hydroxylation of the C–H of Cl′ or one of the two C–H bonds at C5′ of the deoxyribose on the sugar–phosphodiester backbone (*395*), which leaves a 3′-phosphate and a 5′-aldehyde at the ends (*396*). Hydroxylation at C4′ of deoxyribose is also possible. The preferred cleavage site is on the 3′-side of AT sequences. The cleavage efficiency is determined by the nature of the polyamine linker (*393*). When spermine is used, the conjugate has the highest efficiency (80% cleavage yield), while when an aliphatic diamine linker is used, the

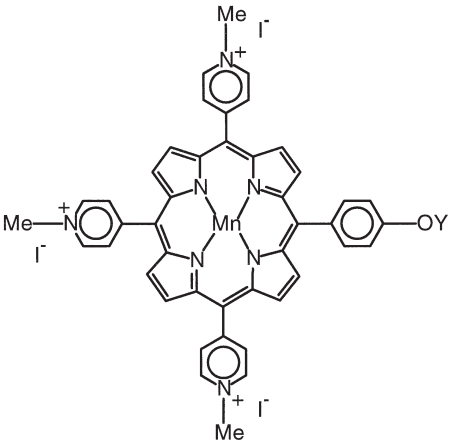

Y = $(CH_2)_4CONH(CH_2)_3NH(CH_2)_4NH(CH_2)_3NHCO_2$-$T_4CT_4G_6T$-3'OH

87

efficiency is largely reduced (*397*). Therefore the hydrophobicity of the linker, the location of the peptide bond within the linker can be tuned to achieve the maximum cleavage efficiency (*398*). The charge on the porphyrin moiety, which determines the affinity for the DNA target, also plays a key role, and cationic porphyrins are the best cleavers (*399*). This class of conjugates exhibits higher inhibition of the translation of chloramphenicol acetyltransferase mRNA than the unmodified oligonucleotides (*400*). This may not involve direct strand breaks of the RNA target, but induction of damage to RNA by base oxidation (*401*).

5. Other Metal Complexes

The protease encoded by HIV-1 is essential for processing viral polyproteins which contain the enzymes and structural proteins required for the infectious virus. Copper(II) compounds such as $CuCl_2$ can inhibit the activity of HIV-1 protease (*402*). The inhibitory activity depends on the presence of cysteine residues in the enzyme; $CuCl_2$ does not inhibit the activity of synthetic proteases lacking cysteine residues. However, the activity of proteases lacking cysteines can be inhibited by $CuCl_2$ when compounds which can act as both copper chelators and reducing agents such as dithiothreitol (DTT) and ascorbate are also present (*402*). Diethyldithiocarbamate, a potent copper

chelating agent and antioxidant, has been used in the treatment of HIV-infected patients (*403*). Davis *et al.* (*404*) have shown that Cu(I) bathocuproine disulfonate acts as a competitive inhibitor of HIV-1 protease as well as a mutant HIV-1 protease lacking cysteines and can inhibit the replication of the HIV-1 virus.

Enzyme-stabilized single-stranded DNA (known as the open complex) is the first intermediate formed in transcription initiation of RNA polymerases; its formation is the rate-limiting step. Designing molecules which bind specifically to the open complex is a strategy for generating potent transcription inhibitors. The redox-stable complex of Cu(I) with 1,2-dimethyl-1,10-phenanthroline is an example of such a strategy (*405*). The Cu(I) complex binds specifically to the single-stranded DNA of transcriptional open complexes and is an effective inhibitor of eukaryotic and prokaryotic transcription.

Divalent metal ions are essential for ribonuclease H activity. Two Mn(II) ions have been located in the catalytic site of ribonuclease H domain of HIV-1 reverse transcriptase in close proximity to the four acidic residues Asp443, Glu478, Asp498, and Asp549 after soaking crystals in 45 m*M* $MnCl_2$ (*406*).

Metal compounds showing anti-HIV activity include those of Bi(III) (*407*), Pt(II) (*408*, *409*), and Au(I). Gold(I)–thiolates such as **88** and **89**

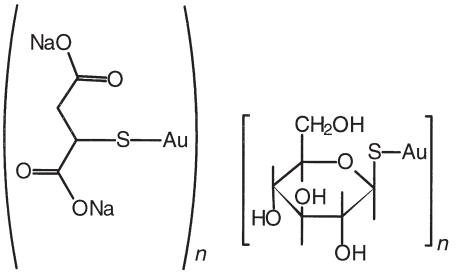

88 **89**

Section VII) have been reported to inhibit HIV-1 infectivity via Au(I) ligand exchange with a component of the virus surface (*410*). The major components of the HIV-1 surface are the external glycoproteins gp120 and gp41, both of which contribute to the infectivity of the virus. Gold(I) targets are probably the cysteine residues of the glycoproteins. A common metabolite of gold antiarthritic drugs, $[Au(CN)_2]^-$ (Section VII), is reported to inhibit the replication of HIV *in vitro* at levels of 20 ppb (**411**).

VII. Anti-inflammatory and Antiarthritic Agents

A. Gold Antiarthritic Complexes

Gold has been used in medicine for many centuries, and since the 1920s several injectable gold compounds have been widely used for the treatment of rheumatoid arthritis. Recent reviews of the medicinal uses of gold compounds have been published (*412–414*).

Injectable 1 : 1 Au(I)–thiolato complexes are used clinically for the treatment of difficult cases of rheumatoid arthritis, including sodium aurothiomalate **88** (myocrisin), aurothioglucose **89** (solganol), sodium aurothiopropanol sulfonate **90** (allochrysine), and sodium aurobisthiosulfate **91** (sanochrysin). Several grams of gold are given during the course of chrysotherapy, and gold can remain in the body for many years after treatment has stopped.

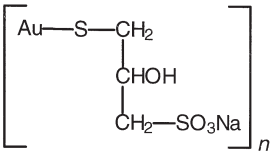

90

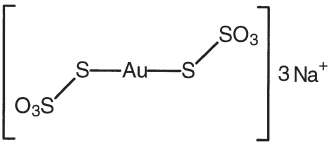

91

Most of the gold thiolate drugs have a gold-to-ligand ratio close to 1 : 1, but often contain a small molar excess of (e.g., 10%) of thiol over Au(I). Both EXAFS (*415*) and WAXS (*416*) data have suggested that they are polymeric complexes (e.g., chain or ring forms) with thiolate S bridging linear Au(I) ions. A hexameric ring structure for **88** was postulated by Isab and Sadler (*417*) and has been found for the Au(I) complex of 2,4,6-tri(isopropyl)thiophenol (Fig. 17) (*418*). Re-

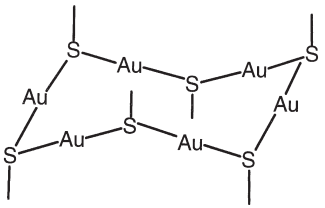

Fig. 17. Schematic drawing of a predicted hexameric ring structure for a 1 : 1 gold(I)–thiolate (*417*) and found in the crystal structure of Au(I)–2,4,6-tri(isopropyl)thiophenolate (*418*).

cently, Bau has crystallized the Au(I)–thiomalate complex **88** using techniques for crystallization of macromolecules (*419*). The linear S–Au–S units are arranged into polymeric double-helical chains (Fig. 18).

The only oral complex in clinical use is auranofin **92** (Ridaura), containing tetraacetyl-β-D-thioglucose and triethyl phosphine ligands. Auranofin is a lipophilic complex, a monomer containing linear two-coordinate Au(I).

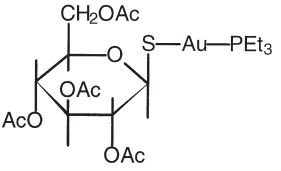

92

A common metabolite found in the urine and plasma of patients treated with gold drugs is $[Au(CN)_2]^-$, an ion which readily enters cells and can inhibit the oxidative burst of white blood cells. It may therefore be an active metabolite of gold drugs. It also exhibits anticancer and anti-HIV activity. The high Au contents of red blood cells of smokers receiving gold therapy has been attributed to the inhalation of HCN in smoke (*420*).

Under conditions mimicking red blood cell concentrations, Elder *et al.* (*421*) have observed that $[Au(CN)_2]^-$ reacts with GSH to form $[Au(SG)_2]^-$, which is also very stable. Because of the high concentration of GSH in the cells, the concentration of $[Au(SG)_2]^-$ in cells may be high.

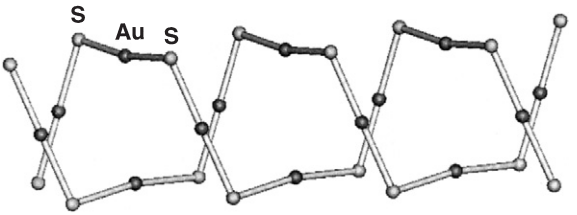

FIG. 18. X-ray crystal structure of the injectable antiarthritic complex gold(I)–aurothiomalate **88** (side-chain on S omitted) showing the double helical chains. The right-handed helix shown contains thiomalate ligands with the **R** absolute configuration. Au–S bond lengths: 2.283 and 2.286 Å: S–Au–S angles: 178.88° and 169.41°. Adapted from (*419*).

Gold(I) has a very high affinity for thiolate S, but binds only weakly to O and N ligands. Hence proteins containing thiolate groups (especially those with low pK_a values) are targets for Au(I), but DNA is not a target. Moreover, thiolate exchange reactions are usually rapid. During therapy, Au levels in the blood typically reach 20 μM, and Au is transported by albumin, bound to Cys-34. The rate of gold binding is determined by the rate of opening of the cleft containing Cys-34 (*422*, *423*), and the binding appears to induce a "flip-out" of this residue (*424*). Aurothiomalate is a potent inhibitor of neutrophil collagenase, a zinc enzyme which contains Cys ligands in the metal binding site (*425*, *426*). Gold(I) drugs can bind strongly to the thiol groups of DNA binding proteins such as Jun–Jun and Jun–Fos, which are transcription factors, giving rise to the possibility that gold can regulate transcription factor activity (*427*).

The side-effects of Au(I) drugs may be due to the production of Au(III) metabolites (*428*). Hypochlorite is synthesized from H_2O_2 and Cl^- by the enzyme myeloperoxidase in phagocytic cells and can oxidize Au(I) in aurothiomalate, aurothioglucose, and auranofin to Au(III). Patients with gold-induced dermatitis exhibit significant proliferation of their lymphocytes in response to Au(III) but not Au(I) (*429*), and $[AuCl_4]^-$ can inhibit peptide-dependent proliferation of T cells *in vitro* (*430*). Gold(III) readily oxidizes thiol, disulfide, and methionine thioether groups in peptides and proteins, but also can deprotonate amide NH groups even in highly acidic solutions. For example, the square-planar complex $[Au(Gly\text{-}Gly\text{-}His\text{-}H_{-2})]^+$ forms at pH 1.5 (*431*).

B. Metal SOD Mimics and Control of Peroxynitrite

The radical anion superoxide O_2^- is a product of activated leukocytes and endothelial cells and has been postulated to be a mediator of ischemia–reperfusion injury and inflammatory and vascular diseases. Various superoxide dismutase (SOD) enzymes are known: Cu,Zn–SOD in the cytoplasm of eukaryotic cells, Mn–SOD in mitochondria, and Fe–SOD and Mn–SOD in prokaryotic cells. They catalyze the conversion of O_2^- into H_2O_2 and O_2

$$M^{n+1} + O_2^- \rightarrow M^{n+} + O_2$$

$$M^{n+} + O_2^- + 2H^+ \rightarrow M^{n+1} + H_2O_2.$$

The use of SOD in therapy is limited by its short plasma half-life (clearance by the kidney) and inability to penetrate cell membranes

(extracellular activity only). Low molecular mass mimics of SOD are therefore of much interest as potential pharmaceuticals (*432*). A variety of Mn- and Fe-based porphyrins and macrocyclic complexes are known to have SOD mimetic activity (*433–436*), and these are potentially useful for the treatment of diseases such as ischemia–reperfusion injury.

Many copper(II) complexes, including $Cu(DIPS)_2$ (DIPS = diisopropylsalicylate), $Cu(salicylate)_2$, and Cu(Gly-His-Lys), are also active in superoxide dismutation (*437*, *438*), but their use *in vivo* is limited by dissociation of Cu(II) and binding to natural ligands such as albumin (*439*). In contrast, the activity of Fe–**93** is not affected by albumin (*439*, *440*).

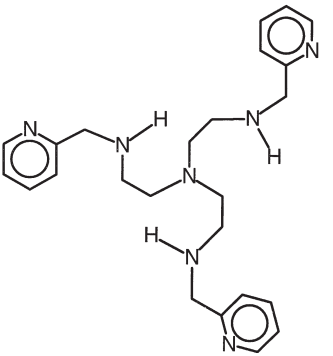

93

Unlike Cu(II), free Mn(II) ions are not active in superoxide dismutation, but some Mn(II)–macrocycle complexes catalyze the dismutation of O_2^- and are biologically active (*441*). For example, complex **94** (SC-52608) inhibits neutrophil-mediated killing of human aortic endothelial cells *in vitro*, attenuates inflammation, protects against myo-

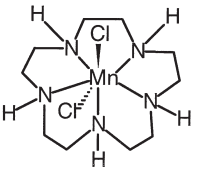

94

cardial ischemia–reperfusion injury, and inhibits coronary tissue injury and neutrophil accumulation into coronary tissue *in vivo* (*442*).

Attempts to optimize the stability and SOD activity of C-substituted (R = methyl and fused cycloalkyl) [Mn(II)[15]aneN5)Cl_2] complexes **95** have shown that increasing the number of hydrocarbon substituents greatly increases the kinetic stability of the complex toward dissociation via protonation (Fig. 19). (*443*). There is also some enhancement of thermodynamic stability. The trans-fused endohexano Mn(II) complex **96** has a faster dismutation rate constant ($9.09 \times 10^7 M^{-1}$ s^{-1}, pH 7.4) and a 10 times higher thermodynamic stability than the unsubstituted complex.

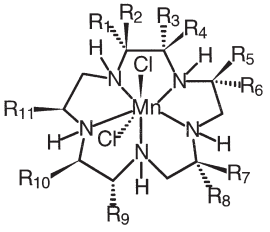

95

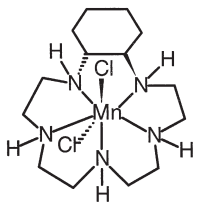

96

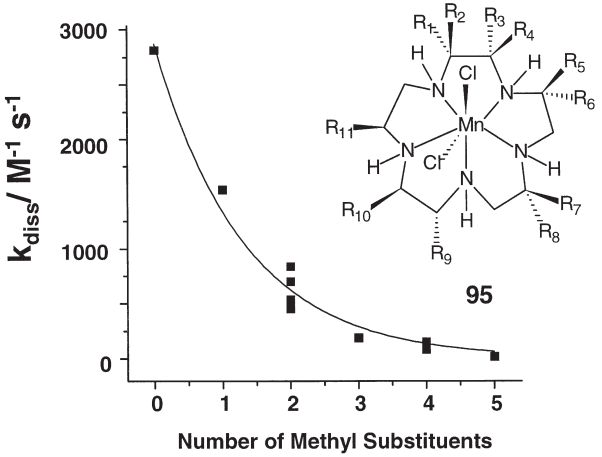

FIG. 19. Plot of the second-order rate constants for Mn(II) dissociation, k_{diss}, vs the number of methyl substituents on the chelate rings of **95**. Data taken from (*443*).

Since the Mn(II) complexes (log K 10–12) are much less stable than the analogous Cu(II)–macrocycle complexes (log K *ca.* 28), kinetic stability is important to the biological behavior of the Mn(II) complexes.

As part of the macrophage immune response, e.g., during ischemia–reperfusion, peroxynitrite can be formed

$$O^{-}_{2} + NO \rightarrow ONO^{-}_{2}.$$

Peroxynitrite, the anion of the weak acid peroxynitrous acid (pK_a of *ca.* 6.8), exists predominantly in the cis configuration and has a short half-life (1 s at pH 7.4), but can freely diffuse across membranes, with a permeability coefficient (8.0×10^{-4} cm^{-1}) close to that of water and *ca.* 400 times faster that that of the superoxide (*444*). It is highly reactive, being capable of nitrating Tyr residues in proteins and oxidizing metal ions, DNA, lipids, SH groups, and Met. It has been implicated in various diseases (e.g., arthritis, sepsis, inflammatory bowel disease, and stroke). Metal complexes capable of catalytically decomposing ONO^{-}_{2} are potential drugs. Examples include Mn(III) and Fe(III) porphyrin (TMPyP) complexes such as **97** (*445–448*). It has been shown that **97** can significantly prolong the survival of mice

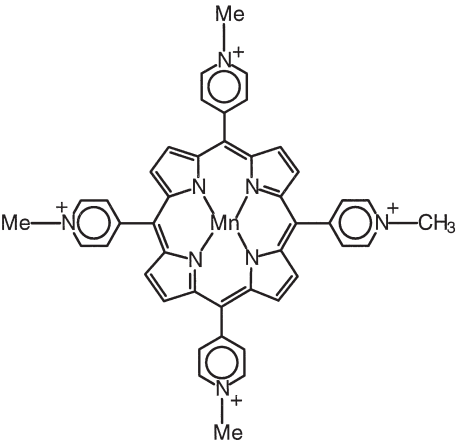

97

lacking mitochondrial Mn–SOD (*449*). In the presence of physiological antioxidants such as ascorbate or glutathione, Mn(III)TMPyP (**97**) de-

composes ONO_2^- rapidly (*450*). During the catalytic reaction, Mn(III) is oxidized to an oxoMn(IV) intermediate which is then reduced back to Mn(III) by the antioxidants to complete the catalytic circle. In the absence of the antioxidants, **97** does not catalyze the decomposition, perhaps due to the slow conversion of the oxoMn(IV) intermediate back to Mn(III) (*450*).

Iron(III)–TMPyP rapidly catalyzes the isomerization of ONO_2^- to NO_3^- (*447*) and the reaction also involves formation of an oxoFe(IV) intermediate. Iron(III)–TMPyP has been shown to have significant cytoprotective effects on cells both *in vitro* and *in vivo* and does not elevate mean arterial pressure suggesting a lack of interaction with NO (*448*).

VIII. Bismuth Antiulcer Drugs

Bismuth compounds have been used for treating gastrointestinal disorders for more than two centuries (*451*). These include bicarbonate, nitrate and salicylate salts, and colloidal bismuth subcitrate. These are all Bi(III) compounds; Bi(V) is usually a strong oxidant. Their structures are largely unknown and often contain a mixture of anionic ligands. This reflects the strong tendency of Bi(III) to hydrolyze and form stable hydroxo and oxo complexes. The first pK_a of Bi(III) in water is *ca.* 1.5. Bismuth(III) has a variable coordination number, from 3 to 10.

The best understood in structural terms are the citrate complexes for which about seven X-ray structures have been determined (*452*), none of which has exactly the same composition as the drugs themselves (*453*). The dominant feature is the dimeric $[(cit)BiBi(cit)]^{2-}$ unit, where citric acid is H_4cit, which contains bridging citrate anions (Fig. 20). The Bi–O(alkoxide) bond is very short (2.2 Å) and strong,

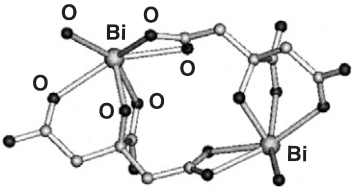

FIG. 20. X-ray crystal structure of the dimer $[Bi_2(cit)_2]^{2-}$, a possible constituent of bismuth antiulcer compounds. An additional bridging O from a neighboring unit is also shown bonded to Bi(III). Note that asymmetry in the coordination sphere due to the lone pair on the metal (cit = $C(O)(CO_2)(CH_2CO_2)_2$). Adapted from (*452*).

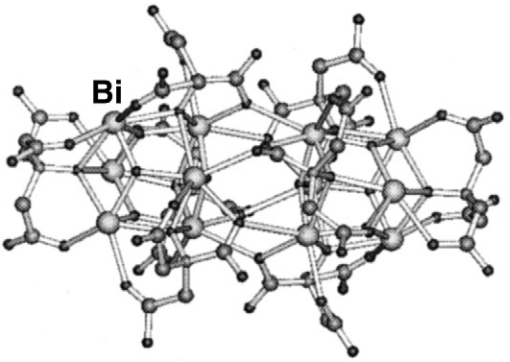

FIG. 21. The bismuth citrate cluster $(NH_4)_{12}[Bi_{12}O_8(cit)_8] \cdot 10\ H_2O$ showing citrate and oxo bridging. Adapted from (*454*).

and there is a prominent lone-pair effect in the trans position (vacant coordination site). These dimers aggregate into chains and sheets in the crystal via a network of H-bonds involving citrate, counter ions, and water. An example of a polymeric bismuth citrate structure is shown in Fig. 21 (*454*). Such polymers may be deposited on the surface of ulcers. Bismuth(III) citrate complexes appear to be stable in solution over a pH range of *ca.* 3.5 to 7.5. At lower pH, precipitates of e.g., BiOCl are obtained, and at higher pH citrate can be displaced by hydroxide and oxide. [Bi(III)(Hcit)] can be solubilized by a variety of amines (*455*), and the adduct with the organic histamine antagonist ranitidine (*456*, *457*) has recently been marketed as a new drug, ranitidine bismuth citrate.

The antimicrobial activity of Bi(III) against the bacterium *Helicobacter pylori* appears to be important for its antiulcer activity (*458*). This organism may be involved in other conditions such as cancer. The mechanism of antimicrobial activity may involve interference in Fe(III) or Zn(II) biochemical pathways. Bismuth(III) is not known to bind to DNA. Attempts to synthesize new Bi(III) complexes with activity against *H. pylori* include those of Keppler *et al.* (*459*), who have found that Bi(III)–tropolonato complexes such as **98** are highly active

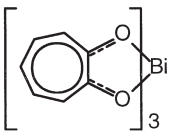

98

in vitro. The same group has reported that Bi(III) complexes with thiosemicarbazones and dithiocarbazonic acid methylesters are also active *in vitro* (*460*).

The molecular basis for the biological activity of Bi(III) is poorly understood (*453*, *461*). It can induce metallothionein (MT) synthesis (*462*) and binds strongly to cysteine sulfur forming Bi_7–MT, which is stable even at pH 1 (*463*). However, Bi(III) can also bind strongly to O- and N-ligands and binds to transferrin (2 Tyrosinate O, Asp O, His N, and carbonate as synergistic anion) only slightly less strongly than Fe(III) (log *K* 19.6 vs 20.7) (*464*). Binding constants of Bi(III) for a range ligands with oxygen and nitrogen donor ligands correlate with those of Fe(III).

The tripeptide glutathione (γ-L-Glu-L-Cys-Gly) may play a role in the transport of Bi(III) in the body. The complex $[Bi(SG)_3]$ is very stable (log *K* 29.6) over a wide pH range (2–10) with binding via the S atom only (*465*). Exchange of GSH between free and bound forms is relatively rapid at physiological pH (*ca.* 1500 s^{-1}).

Inhibition of the dinuclear Ni(II) enzyme urease by Bi(III) thiolates may be important for its antibacterial activity. *Helicobacter pylori* relies on urease for the production of ammonia which allows survival under the highly acidic conditions of the gastric lumen and mucosa. Bismuth(III) mercaptoethanol complexes are *ca.* 10^3 more active inhibitors than mercaptoethanol alone (*466*). The thiol can bind directly to Ni(II) in the active site and also form a disulfide with a Cys residue in the active site cavity (*467*).

Inorganic compounds such as aluminium hydroxide, sodium bicarbonate, and magnesium and calcium carbonates are commonly used as antacids. There is much scope for the redesign of these agents to achieve fine control of local pH values in the gastrointestinal tract via control of the rate of release of the active bases (e.g., from insoluble compounds).

IX. Neurological Agents

A. Lithium for Manic Depression

Lithium, like alcohol, can influence mood. This was discovered nearly 50 years ago by Cade (*468*), who was investigating the effects of lithium urate merely because it is a soluble urate salt. Lithium and not urate turned out to be the effective agent. Simple salts such as Li_2CO_3 are widely used (by as many as 1 in every 1000 of the popula-

tion in some countries) as a prophylatic treatment for bipolar disorders such as maniac depression (*469*). Doses are gram quantities and the level of Li(I) in the blood typically reaches 1–2 m*M* during therapy. On account of the high liability of Li(I), and weakness of its complexes, it becomes widely distributed in the body. New designs for lithium drugs which reduce the kinetic lability and allow slow release of Li(I) ions might find a place in the clinic.

Lithium(I) ions are small but strongly hydrated and could interfere with Mg(II) biochemistry. However, the favored mode of action is interference with Ca(II) metabolism via inhibition of enzymes in the inositol phosphate pathways (*470–472*). Inositol phosphates are responsible for mobilizing Ca(II) inside cells in response to external stimulii. Lithium also stimulates glutamate release presumably via activation of the *N*-methyl-D-asparate receptor and leads to Ca(II) entry (*473*). The increased influx of intracellular Ca(II) may activate phospholipase C and stimulate accumulation of inositol 1,4,5-triphosphate (*473*).

Lithium(I) acts as an uncompetitive inhibitor for inositiol monophosphatase (EC 3.1.3.25) by blocking the release of the aquation product phosphate from the active site (*474*). The enzyme catalyzes the aquation of inositol monophosphates and ribonucleoside 2-monophosphates and requires Mg(II) (or Mn(II)) ions for activity. Several crystal structures of human inositiol monophosphatase have been reported, and the active site has been described in the presence of excess of Li(I) (*475*, *476*). However, the bound lithium was not crystallographically detectable. In one structure of the enzyme at 2.6 Å resolution, three Mn(II) ions are bound per active site (*477*), one of which can be displaced by soaking crystals with inorganic phosphate. The first metal is ligated by Asp-90, Asp-93, Ile-92, Thr-95, and Glu-70, the second by Asp-90, Asp-93, and Asp-220, and the third only by the side chain of Glu-70. Kinetic studies and molecular modeling have suggested that only two metal ions are required for the catalytic mechanism (*478*). Modeling studies suggest that the first metal ion activates water for nucleophilic attack; the second metal ion, coordinated by three aspartate residues, appears to act as a Lewis acid, stabilizing the leaving inositol oxyanion (*478*). At therapeutic levels (*ca.* 1 m*M*), Li(I) binds to the second catalytic Mg(II) site (Mg(II)2), and modeling studies suggest that replacement of Mg(II)2 gives a stable complex with phosphate binding slightly closer to Mg(II)1 than in the corresponding complex containing two Mg(II) ions (Fig. 22) (*479*).

Lithium can selectively inhibit the activity of glycogen synthase kinase-3 β (GSK-3 β), an enzyme which regulates cell fate determina-

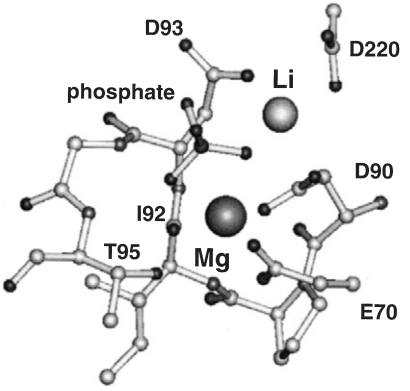

FIG. 22. A model for the interaction of Li(I) with the enzyme inositol monophosphatase. Lithium(I) occupies the second Mg(II) site in the enzyme. Adapted from (*479*).

tion in diverse organisms including *Drosophila* and *Xenopus* (*480*). However, lithium is not a general inhibitor of other protein kinases.

B. METALLOPROTEINS IN THE BRAIN

Metallothionein was first discovered in 1957 as a cadmium-binding cysteine-rich protein (*481*). Since then the metallothionein proteins (MTs) have become a superfamily characterized as low molecular weight (6–7 kDa) and cysteine rich (20 residues) polypeptides. Mammalian MTs can be divided into three subgroups, MT-I, MT-II, and MT-III (*482*, *483*, *491*). The biological functions of MTs include the sequestration and dispersal of metal ions, primarily in zinc and copper homeostasis, and regulation of the biosynthesis and activity of zinc metalloproteins.

The recently identified brain-specific isoform of metallothionein, MT-III (neuronal growth inhibitory factor, GIF), has been linked with its potential role in neurophysiological and neuromodulatory functions (*484*). The human form of MT-III contains 68 amino acids with a 70% sequence (Fig. 23) similarity to other mammalian MTs and a

```
1          10         20         30
MDPETCPCPSGGSCTCADSCKCEGCKCTSCKKSCC

    40         50         60
SCCPAECEKCAKDCVCKGGEAAEAEAEKCSCCQ
```

FIG. 23. The amino acid sequence of the brain-specific protein metallothionein III.

preserved array of 20 Cys residues (*485*). The subgroup MT-III contains two inserts, a Thr at position 5 and a Glu-rich hexapeptide in the C-terminal region, and binds 4–5 Cu(I) and 2–2.5 Zn(II) ions, probably in cluster structures similar to those of MT-I and MT-II (Zn_3 and buried Cu_4 clusters) (*486*). The Cu(I) cluster is stable to air oxidation, in contrast to MT-I and MT-II.

The levels of MT-III (GIF) are low in the brains of Alzheimer's disease patients. This appears to lead to excessive neuronal growth, neuronal degradation, and neuronal death. The subgroup MT-III is expressed preferentially in the hippocampus (*491*) where it probably controls the levels of free Zn(II) (and Cu(I)).

The roles of Na(I), K(I), and Ca(II) in neurochemistry are well known, but it is also apparent that Fe and Cu enzymes can control neurotransmitter biosynthetic pathways, and there are millimolar levels of Zn^{2+} in the hippocampus during neurotransmission (*487*, *488*). Moreover, Mn is abundant in brain enzymes such glutamine synthase and superoxide dismutase.

Elevated intracellular levels of Zn(II) are toxic to neurons and may contribute to the pathogenisis of epileptic brain damage (*489*). Brain ischemia may be mediated by the toxic trans-synaptic movement of Zn(II) from presynaptic terminals into postsynaptic neurons (*490*). Hence chelating agents which reduce Zn(II) influx may protect brain neurons. For example, intraventricular injection of CaEDTA has been shown to reduce neuronal degeneration in all brain regions. The Zn-binding protein MT-III is located in these Zn-ergic neurons (*491*).

The normal cellular form of prion protein (PrP^c) can exist as a Cu-metalloprotein *in vivo* (*492*). This PrP^c is a precursor of the pathogenic protease-resistant form PrP^{sc}, which is thought to cause scrapie, bovine spongiform encephalopathy (BSE), and Creutzfeldt–Jakob disease. Two octa-repeats of PHGGGWGQ have been proposed as Cu(II) binding sites centered on histidine (*493*). They lack secondary and tertiary structure in the absence of Cu(II). Neurons may therefore have special mechanisms to regulate the distribution of copper.

Intracellular Fe is usually tightly regulated, being bound by ferritin in an insoluble ferrihydrite core, and impaired Fe homeostasis has been linked to Parkinson's disease and Alzheimer's disease. A consistent neurochemical abnormality in Parkinson's disease is degeneration of dopaminergic neurons relating to a reduction of striatal dopamine levels. As tyrosine hydroxylase (Fig. 24) (*494*), an Fe enzyme, catalyzes the formation of L-DOPA, the rate-limiting step in the biosynthesis of dopamine, the disease can be considered as a tyrosine

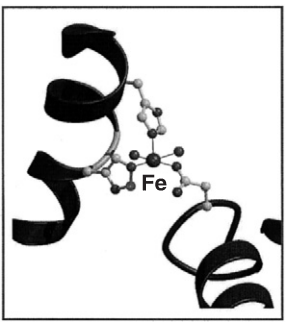

FIG. 24. X-ray crystal structure of the catalytic domain of tyrosine hydroxylase. The catalytic iron is located 10 Å below the enzyme surface and is coordinated by the conserved residues His-331, His-336, and Glu-376 (PDBID: 1TOH). Adapted from (*494*).

hydroxylase deficiency syndrome of the striatum (*495*). This enzyme may therefore be involved in the pathogenesis of Parkinson's disease and provide a basis for developing new treatments.

Glutamine synthetase, a brain Mn enzyme, is located mainly in astrocytes, and its synthesis may be modulated by nitric oxide (*496*). Inhibition of this enzyme could be relevant to aging diseases (*497*). There is evidence that human NT2-N neurons die via ionotropic glutamate receptor-mediated mechanisms when exposed to hypoxia in the presence of glutamate (*498*).

X. Cardiovascular and Hematopoietic System

Nitric oxide is a vasodilator (muscle relaxant) and neurotransmitter involved in a wide range of physiological processes, such as the regulation of cardiovascular function, signaling in the nervous systems, and mediating host defence against microorganisms and tumor cells (*499*, *500*). As a consequence, overproduction or deficiency of nitric oxide may cause or contribute to several diseases. Excess levels of NO are potentially involved in diseases such as inflammatory bowel disease (IBD), septic shock, arthritis, stroke, and psorasis. Compounds that selectively enhance or inhibit the synthesis of NO, modify its effects, or eliminate it from physiological media are potentially interesting as therapeutic agents.

Sodium nitroprusside, $Na_2[Fe(CN)_5NO] \cdot 2H_2O$ (**99**), is the only clinically used metal complex of nitric oxide (*501*). It is often used to lower

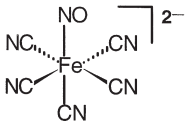

99

blood pressure in human subjects. Its hypotensive effect is evident within seconds after infusion and the desired blood pressure is usually obtained within 1–2 min. It is also useful in cases of emergency hypertension, heart attacks, and surgery.

The therapeutic effects of sodium nitroprusside depend on release of nitric oxide which relaxes vascular muscle. Sodium nitroprusside is best formulated as a nitrosonium (NO^+) complex. Its *in vivo* activation is probably achieved by reduction to $[Fe(CN)_5NO]^{3-}$, which then releases cyanide to give $[Fe(CN)_4NO]^{2-}$, which in turn releases nitric oxide and additional CN^- to yield aquated Fe(II) species and $[Fe(CN)_6]^{4-}$ (*502*). There are problems associated with its use, namely reduced activity due to photolysis (*501*) and its oxidative breakdown due to the action of an activated immune system (*503*), both of which release cyanide from the low-spin d^6 iron complex.

There is interest in the possible use of other metal nitrosyl complexes as vasodilators, but from the series $K_n[M(CN)_5NO]$ where M = V, Cr, Mn, and Co ($n = 3$) or M = Mo ($n = 4$) neither the Cr nor the Mn complexes exhibit any hypotensive action (*504*). Iron–sulfur–nitrosyl clusters such as $[Fe_4S_4(NO)_4]$ are active, and their effects can be potentiated by visible light (*505*).

Ruthenium–edta complexes such as K[Ru(Hedta)Cl] (**100**, JM1226) have been proposed as nitric oxide scavengers which might be useful in the control of NO levels in conditions of medical interest. Complex **100** in water exists in equilibrium with the aqua species [Ru(Hedta)(H_2O)] (pK_a of dangling arm carboxyl group 2.4). Complex **100** gives a pale yellow solution in phosphate buffer pH 6.5–8 but after >5 h forms a dark green mixed valence Ru(III)/Ru(IV) μ-oxo dimer (*506*). Both **100** and **101** bind to NO very rapidly (rate constant $>10^8$ M^{-1} s^{-1} at body temperature, 310 *K*) and tightly ($K > 10^8\,M^{-1}$) (*507*), forming a linear Ru(II)–NO adduct **102** (i.e., a nitrosonium NO^+ complex).

Complex **101** has been shown to reverse the poor response of the artery to vasoconstrictor drugs (*508*), which is a major clinical problem in the treatment of patients with septic shock. The excessive production of NO appears to be a major contributory factor not only in

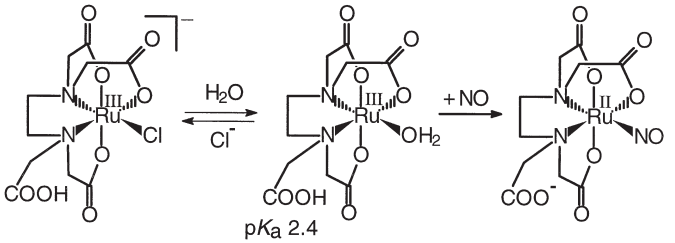

100 **101** **102**

septic shock (caused by very high levels of circulating bacteria in the body), but also in diabetes, arthritis, inflammation, and epilepsy. Iron (III) complexes such as Fe(III)–DTPA bind readily to NO upon reduction to Fe(II) at physiologically relevant potentials, and are able to protect mice against death caused by septic shock (*509*).

XI. Insulin Mimetics

Therapy for insulin-dependent diabetes mellitus is usually achieved by daily subcutaneous injections of insulin, and insulin-mimetics which can be orally administered may be useful for the treatment of type I diabetes (insulin dependent) if suitable complexes of low toxicity can be identified (*510*, *511*).

A. Vanadium Complexes

It was discovered nearly 20 years ago that V(V) as vanadate and V(IV) as vanadyl can mimic some of the effects of insulin (stimulate glucose uptake and oxidation and glycogen synthesis) (*512*, *513*). Vanadate is an effective insulin mimetic in the diabetic rat (*514*), but has proved to be too toxic for human use. Vanadyl, as $VOSO_4$, is also unsuitable because high doses are needed on account of its poor oral absorption. Vanadium complexes with organic ligands have proved to be less toxic and can have improved aqueous solubility and lipophilicity.

Sakurai *et al.* have observed that vanadyl complexes with coordination modes such as $VO(S_4)$ (**103**) can normalize blood glucose levels (*515*) and are effective for normalizing both serum glucose and free fatty acid levels in streptozotocin rats and are orally active (*516*). Bis(picolinato)oxovanadium(IV) is also orally active against the diabe-

tes of streptozotocin rats (*517*) and the bis(methylpicolinato) derivative (**104**), which has a higher partition coefficient, is more effective,

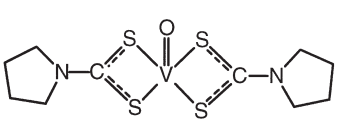

103

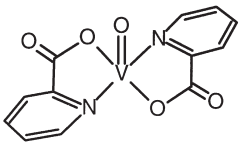

104

and is less toxic than the picolinato complex (*518*). The major accumulation of vanadium is in the bone and kidney. Vanadium accumulated in the bone may be released gradually to other organs via the bloodstream after the cessation of administration of **104**, therefore it has long-term activity.

Peroxovanadates are effective at much lower doses (*ca.* 100-fold) than vanadate itself, but readily decompose in aqueous solution and must be administered by injection. Posner *et al.* have shown that organic ligands can stabilize peroxo complexes and that peroxovanadate complexes such as **105** (with L–L = e.g., phenanthroline, picolinate,

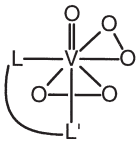

105

or oxalate) are effective insulin mimetics (*519*, *520*). This class of compounds can lower blood sugar levels in type I diabetes without insulin administration. Bisperoxovanadium(V)–imidazolium complexes are also reported to have high *in vitro* insulin-mimetic activity (*521*). However, it remains to be seen whether peroxovanadates suitable for oral administration can be designed.

Orvig *et al.* (*522*) have shown that the orally active bis(maltolato) oxovanadium(IV) complex **106** (BMOV) is 3 times more effective *in*

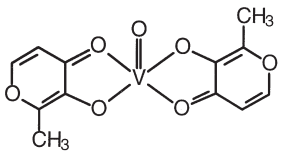

106

vivo as an insulin mimetic than uncomplexed $VOSO_4$ (*523*). In the solid state, the complex has a five-coordinate square-pyramidal geometry with the oxo ligand in the axial position and trans maltol ligands (*524*). Upon dissolution in water or methanol under anaerobic conditions, **106** binds solvent (as methoxide or hydroxide, pK_a of bound $H_2O = 2$) in a position *cis* to the oxo ligand and becomes six coordinate. Under aerobic conditions in these solvents, the complex is rapidly oxidized to dioxovanadium(V) species (*525*).

It is not clear whether V(V) or V(IV) (or both) is the active insulin-mimetic redox state of vanadium. In the body, endogenous reducing agents such as glutathione and ascorbic acid may inhibit the oxidation of V(IV). The mechanism of action of insulin mimetics is unclear. Insulin receptors are membrane-spanning tyrosine-specific protein kinases activated by insulin on the extracellular side to catalyze intracellular protein tyrosine phosphorylation. Vanadates can act as phosphate analogs, and there is evidence for potent inhibition of phosphotyrosine phosphatases (*526*). Peroxovanadate complexes, for example, can induce autophosphorylation at tyrosine residues and inhibit the insulin-receptor-associated phosphotyrosine phosphatase, and these in turn activate insulin-receptor kinase.

B. Chromium Complexes

It was once thought that glucose tolerance factor, which potentiates the action of insulin and is present in yeast, is a chromium complex, perhaps containing glutathione and nicotinic acid as ligands (*527*), but this factor is no longer thought to contain chromium (*528*). There is significant current interest in the biological activity of the lipophilic complex [Cr(III)(picolinate)$_3$], which can affect the metabolic parameters regulated by insulin (*529*). Both chromium picolinate and chromium polynicotinate are currently marketed as nutritional supplements, although they have not been fully chemically characterized (*530*, *531*). There are reports showing that, when taken over extended periods, this complex can induce chromosome damage in Chinese hamster cells (*532–534*). Therefore the long-term biological effects of this complex on humans need to be investigated. Cromate, CrO_4^{2-}, has been shown to have insulin-like action on glucose transport (*535*).

Low-molecular-weight chromium-binding substance (LMWCr), a naturally occurring oligopeptide (*ca.* 1500 Da, consisting of Cr(III), Asp, Glu, Gly, and Cys in 4 : 2 : 4 : 2 : 2 ratio), has been found to activate the insulin-dependent tyrosine protein kinase activity of insulin receptors, with the activity being proportional to the Cr content of the oligopeptide (maximal at four Cr(III) per oligopeptide) (*536*). The cry-

stal structure of the trinuclear cation $[Cr_3O(O_2CCH_2CH_3)_6(H_2O)_3]^+$ (**107**) is shown in Fig. 25 (*537*). This complex can activate insulin receptor protein tyrosine kinase activity in a fashion almost identical to that of LMWCr (*538*). When propionate in **107** is replaced by acetate, the complex does not activate but rather inhibits both the membrane phophatase and kinase activity. The trinuclear Cr complex is stable in aqueous and acidic solutions and therefore its effects on models for diabetes deserve further investigation.

Tungstate and molybdate oxyanions show similar insulin-mimicking effects as vanadate and vanadyl (*539*). High concentrations (10–30 m*M*) of tungstate and molybdate are required for insulin-like activity (*540*). However, peroxides of tungstate and molybdate are much more potent than the parent oxometallates in normalizing blood glucose levels in streptozotocin-induced diabetic rats (*540*, *541*), perhaps due to a higher level of intracellular conversion of glutathione to the oxidized form which results in higher inhibition of phosphotyrosine phosphotase and higher activation of the insulin-receptor tyrosine kinase (*541*).

XII. Chelation Therapy

Excessive iron in specific tissue sites is associated with development of infection, neoplasia, cardiomyopathy, arthropathy, and a variety of endocrine and neurological diseases. Chelators, which remove excess iron, while not depriving cells of the essential iron needed for normal metabolism and prevent iron from participating in the generation of harmful free radicals, are potential drugs. We mention a few examples only.

Desferrioxamine (**108**) is the only clinically approved iron chelator. As well as being used for the treatment of iron overload diseases it is

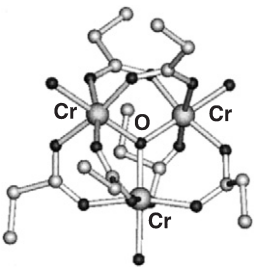

107

FIG. 25. X-ray crystal structure of trinuclear complex $[Cr_3O(O_2CCH_2CH_3)_6(H_2O)_3]^+$ **107**, a potential insulin mimetic. Adapted from (*537*).

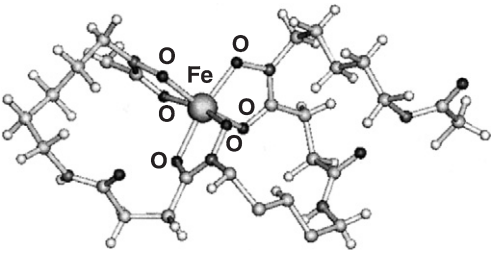

FIG. 26. X-ray crystal structure of the Fe(III) complex of the antimalarial chelator desferrioxamine **108**. Adapted from (*542*).

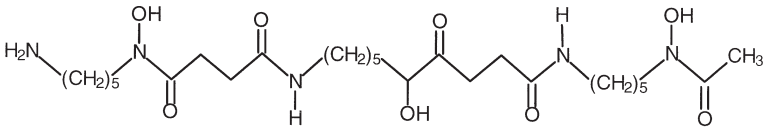

108

also used for the treatment of malaria, perhaps acting via disruption of Fe(III) metabolism within the digestive vacuole. Compound **108** binds Fe(III) over a large pH range (1–12). The crystal structure of Fe(III)–**108** is shown in Fig. 26. Fe(III) is chelated by three hydroxamate groups (*542*).

The pharmacological properties of **108** are not ideal. It removes iron only slowly and it is not well absorbed by oral administration so it has to be administered by injection. Therefore there is need for new chelators. The orally active chelator 1,2-dimethyl-3-hydroxypyridin-4-one (L1) **109** is on clinical trial for the treatment of thalassemia (*543*). Several other chelators which contain 3-hydroxy-4(H)-pyridinone such as **110–112** also possess oral availability, and have comparable activity to **109** for the removal of iron from the liver (*544*, *545*). These

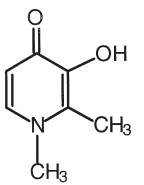

109

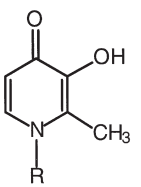

110 R = CH_2CH_3

111 R = $CH_2CH_2NH_2$

112 R = $CH_2CH_2NHCOCH_2CH_3$

chelators have potential application in diseases characterized by iron overload (*546*, *547*). The 3-hydroxy-2(H)-pyridinones are also strong iron chelators.

Compound **113** (O-TRENSOX) is a promising water-soluble iron chelator based on 3 hydroxyquinoline sub-units (*548*) which forms

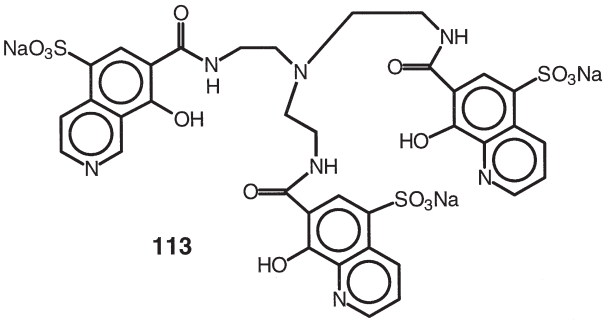

113

stable complexes with both Fe(III) (log K 29.5) and Fe(II) (log K = 17.9) at pH 7.4 (*549*). It offers more efficient protection from ferric citrate-induced iron toxicity in hepatocyte cultures than **108,** and it is also more effective than **108** in quenching hydroxyl radicals (*550*).

Radioactive actinide ions pose threats to our health and environment, and specific removal of these ions is therefore important. Raymond *et al.* have designed a variety of chelators containing groups such as **113** which show promising specific *in vivo* chelation of Pu, Am, and Np (*551*). Combination of **113** with naturally occurring ligands such as **108**, for example, gives rise to formation of a highly stable Pu complex (log K 33) (*552*).

The amino acid histidine is used for the treatment of copper overload in Wilson's disease and forms a strong 1 : 2 complex (Fig. 27) (*553*). Copper–histidine therapy is also an efficient treatment for copper deficiency in Menkes' disease (*554*).

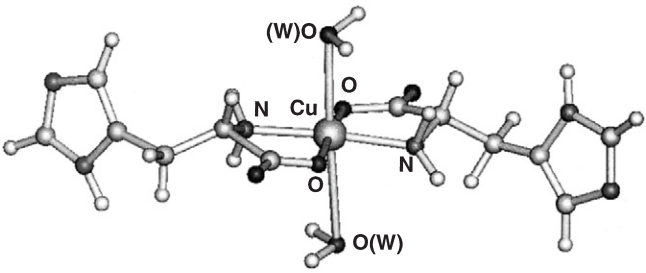

FIG. 27. X-ray crystal structure of $[Cu(His)(HHis)(H_2O)_2]^+$. Adapted from (*553*).

XIII. Metal Activation of Organic Drugs

A. Organic Drugs

Bleomycin (BLM) was first isolated as a copper complex from a culture of *Streptomyces verticillus*. Since then numerous analogs have been prepared by modifying the conditions of fermentation. Bleomycins (**114**, bleomycin A2) are used clinically in combination cancer chemotherapy for the treatment of head and neck cancer, certain lymphomas, and testicular cancer (*555*).

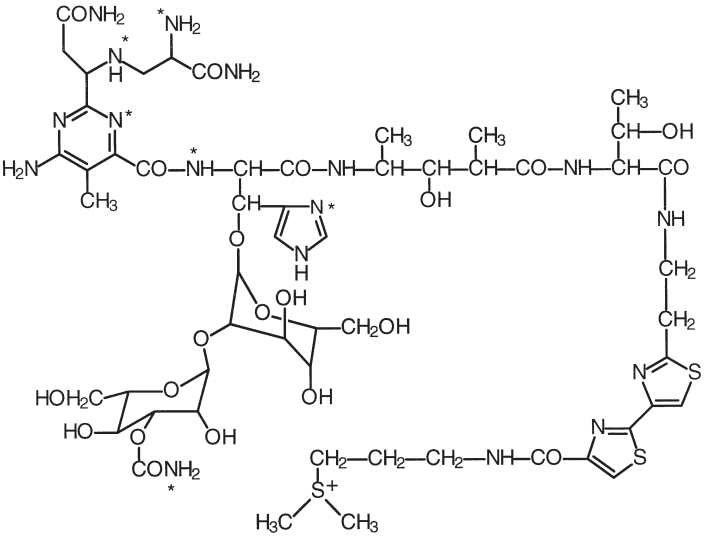

114

The cytotoxicity of BLM is believed to result from its ability to bind iron, activate oxygen, and form an "activated BLM" (Fe-114) (*556*) which cleaves DNA and possibly RNA (*557*). The ability of the Fe(II)–BLM complex to bind to oxygen and produce oxygenated BLM species such as O_2^-–Fe(III)–BLM or O_2–Fe(II)–BLM may be due to the presence of delocalized π-electrons around the iron and the strong iron–pyrimidine π-back-bonding (*558, 559*). Oxygenated BLM accepts an additional electron to form activated low-spin ferric–peroxide–BLM (O_2^{2-}–Fe(III)–BLM) (*558*, *559*). The structural features of Fe–BLM responsible for DNA (or RNA) degradation remain unclear (*560*). Bleo-

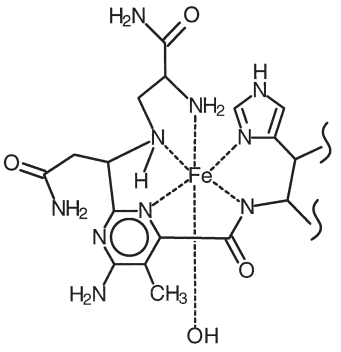

Fe-114

mycin complexes of cobalt and manganese can also mediate damage to DNA.

Anthracyclines such as doxorubicin and adriamycin are widely used antitumor agents but chemotherapy with these drugs is limited by cardiotoxicity after cumulative dosing. Doxorubicin binds strongly to metal ions such as Fe(III), and the binding stimulates the generation of the free radicals through self-reduction of the complexes, and this may be the cause of the cardotoxicity. Husken *et al.* (*561*) have shown that iron chelators such as flavonoids can inhibit doxorubicin-induced cardiotoxicity.

The antiulcer drug famotidine **115** exerts its activity by blocking the histamine H2 receptor in a similar manner to cimetidine. Famoti-

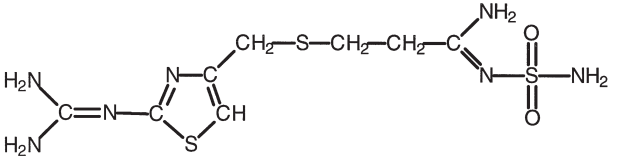

115

dine forms strong chelate complexes with metal ions such as Cu(II) (*562*). Upon Cu(II) coordination an envelopelike conformation of the six-membered S,N-chelate ring forms (Fig. 28) (*563*).

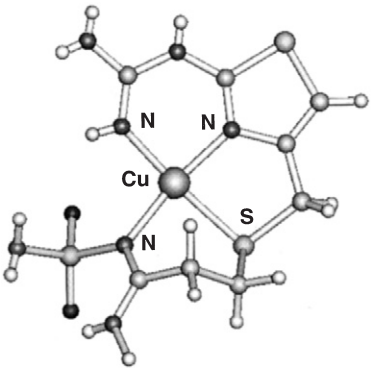

FIG. 28. X-ray crystal structure of the Cu(II) complex of the antiulcer drug famotidine **115**. Adapted from (*563*).

Quinobenzoxazine compounds such as **116** are a class of potential antineoplastic agents that are catalytic inhibitors of topoisomerase II.

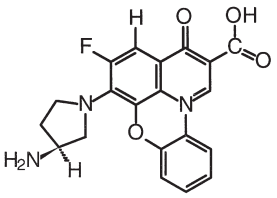

116

They are active against a wide range of human and murine cell lines. Activity is dependent on the presence of divalent ions such as Mg(II) and Mn(II), although the precise role of the metal ions in the mechanism of action is not clear. It has been proposed that quinobenzoxazines bind to duplex DNA through intercalation and that Mg(II) bridges the phosphate backbone of the DNA and the β-ketoacid unit of the intercalated quinobenzoxazine, giving rise to a 2 : 2 drug–Mg(II) dimeric structure (*564*). This has been confirmed by photochemical studies (*565*). These compounds are sensitive to visible light, especially in the presence of DNA or other electron acceptors, and therefore phototoxicity must be considered as a potential side-effect.

Metal ions such as Cu(II) (*566*) and Mn(II) (*567*) react specifically with the hormone vasopressin and vasopressin-like peptides, and this

may play a role in determining the conformation of the peptides and their biological activity.

B. Ribozymes

Ribozymes are a class of metallo-enzymes based on RNA rather than proteins. They have potential in clinical medicine, for example, as potential anti-HIV agents (*568*, *569*) and as possible new tools for the treatment of cancer (*570*). The active structures of ribozymes contain domains of stacked helices which pack together through tertiary contacts. Divalent metal ions such as Mg(II), Zn(II), and Mn(II) can tune the reactivity and shape the structures of ribozymes (*571*). Manganese(II) and Mg(II) have similar hexacoordinate ionic radii (0.86 and 0.97 Å, respectively) (*572*) and octahedral geometry (pK_a of hydrates: Ca(II), 12.7; Mg(II), 11.4; Mn(II), 10.7; Zn^{2+}, 9.6) (*571*). There are several potential oxygen donors on the ribose sugar moiety.

Ribozymes can be divided into two classes according to whether they catalyze (a) attack of an exogenous nucleophile on the scissile phosphate, resulting in release of a 3′-hydroxyl leaving group and 5′-phosphate, or (b) activation of the proximal 2′-hydroxyl group at the active site, which attacks the adjacent phosphate residue, resulting in a 5′-hydroxyl leaving group and a 2′,3′-cyclic phosphate. The former class tends to be larger than the latter. The first class of ribozymes includes: group I intron and group II intron ribozymes, spliceosomes, and ribonuclease P.

The recent X-ray crystal structure of the large ribozyme domain *Tetrahymena* group I intron p4–p6 shows that five Mg(II) ions bind in a three-helix junction at the center of the molecule to form a magnesium ion core (*573*). These five metal ions bridge noncontiguous nucleotides to form a structural core that buries parts of the RNA backbone. Any change in one of four magnesium sites at the helix junction destroys folding of the entire domain. The metal ion core may provide a scaffold in the native structure of ribozymes similar to the hydrophobic cores often found in proteins.

The hammerhead ribozyme and leadzyme belong to the second class of ribozymes. The short extra sequences of the ribozymes form the so-called catalytic loop which acts as the enzyme. There are two likely functions for metal ions in the mechanism of action of hammerhead ribozymes: formation of metal hydroxide groups or direct coordination to phosphoryl oxygens.

XIV. Metalloenzyme Inhibitors as Drugs

Matrix metalloproteinases (MMPs) are a family of zinc-dependent enzymes that degrade the major component of the extracellular matrix. Overexpression and activation of these enzymes have been linked with diseases such as cancer, arthritis, and multiple sclerosis. The MMP family members are listed in Table VIII. Based on sequence similarities and their ability to hydrolyze fibrillar collagens, MMP-1, MMP-8, and MMP-13 are considered as a subfamily. For example, human neutrophil collagenase (MMP-8) cleaves triple-helical collagens (types I, II, and III) and punches holes in the protective proteoglycan coat of cartilage collagen. Thus, cartilage loses its resilience, setting the stage for the onset of arthritis. Another subfamily is MMP-3, MMP-10, and MMP-7. For example, stromelysin 1 (MMP-3) clears the path and allows cancer cells to traverse the extracellular matrix. The third subfamily comprises the 72-kDa gelatinase (MMP-2) and 92-kDa gelatinase (MMP-9). A characteristic of this subgroup is the preference for basement membrane collagens (types IV and V). The other three enzymes, metalloelastase (MMP-12), membrane-type MMP (MMP 14), and stromelysin 3 (MMP-11), do not fit into any of the above three subfamilies.

TABLE VIII

THE MATRIX METALLOPROTEINASES (MMPs)

Enzyme		Substrates	Related disease
Fibroblast collagenase	MMP 1	Fibrillar collagens	Cancer
Neutrophil collagenase	MMP 8	Fibrillar collagens	Arthritis
Collagenase 3	MMP 13	Fibrillar collagens	Cancer
Stromelysin 1	MMP 3	Nonfibrillar collagens Laminins Fibronectins	Arthritis
Stromelysin 2	MMP 10	Nonfibrillar collagens Laminins Fibronectins	Arthritis
Matrilysin	MMP 7	Nonfibrillar collagens Laminins Fibronectins	Inflammation
72-kDa gelatinase	MMP 2	Membrane collagens	Arteriosclerosis
92-kDa gelatinase	MMP 9	Membrane collagens	Arteriosclerosis
Metalloelastase	MMP 12	Elastin	Inflammation
Membrane-type MMP	MMP 14	Membrane collagens	
Stromelysin 3	MMP 11		Cancer

The inhibitors of these enzymes possess zinc-binding groups to chelate to the active-site zinc(II) ion and a peptide backbone complementary to the enzyme cleavage site (Fig. 28) (*574*). The function of the substituents is as follows: R1 increases activity against collagenase and can be modified to provide oral bioavailability; R2 is the major determinant of activity and selectivity; R3 and R4 can be a wide range of functional groups, with aromatic and bulky groups preferred.

Batimastat (BB-94) (4-(*N*-hydroxyamino)-2(*R*)-isobutyl-3(*S*)-[2-thienylthiomethyl) succinyl]-L-phenylalanine-*N*-methylamide) is a broad-spectrum inhibitor with nanomolar activity against the MMPs and is in phase II clinical trial for treatment of breast and ovarian cancer (*575*). The crystal structure of the catalytic domain of human neutrophil collagenase with bound batimastat (Fig. 7) shows that batimastat coordinates to the catalytic zinc(II) in a bidentate manner via the hydroxyl and carbonyl oxygens of the hydroxamate group (Fig. 29) (*576*).

Inhibitors of human neutrophil collagenase and human stromelysin have been designed (*577*) which are based on previous classes of MMP inhibitors, *N*-carboxyalkyl peptides (*578*, *579*), and peptide-based hydroxamic acids (**117**) (*580*, *581*). The -CH_3 and 2-phenylethyl groups are important for inhibition of MMP-3. The X-ray crystal structure of MMP-3 with bound **117** shows that the inhibitor chelates Zn(II)

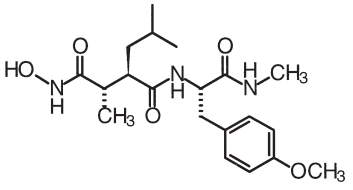

117

through the hydroxamic acid group, and other groups form hydrogen bonds to the enzyme and cause a conformational change around the active site (Fig. 30).

The vasoactive peptides angiotensin-II and atrial natriuretic peptide display opposing biological effects. The former stimulates vasoconstriction and sodium retention, while the latter produces vasodilation, diuresis, and natriuresis (*582*). Angiotensin-II is regulated by the angiotensin-converting-enzyme (ACE, EC 3.4.15.1), which plays a role in congestive heart failure and chronic hypertension. On the other hand, neutral endopeptidase (NEP, EC 3.4.24.11) appears to be

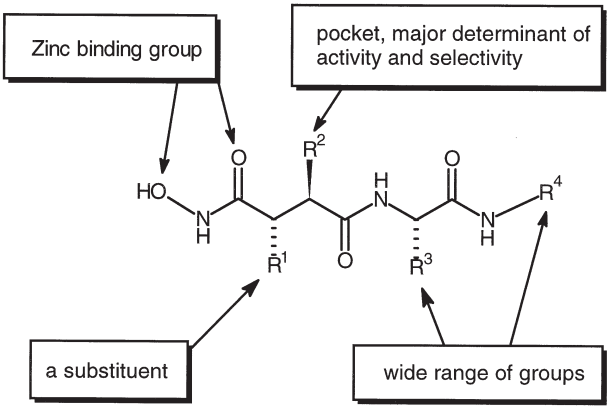

FIG. 29. Backbone structure of matrix metalloproteinase inhibitors.

responsible for the inactivation of atrial natriuretic peptide (*583*). Both ACE and ANP are zinc metalloproteases and have similar mechanisms of action and the same consensus sequence (*584*). Therefore, inhibitors of these two enzymes could be useful for the treatment of cardiovascular disorders. Several compounds are known to inhibit the activity of both enzymes (*585–587*). Inhibitors such as $HSCH_2CH(CH_3)PhCONHCH(CH_3)COOH$ reduce blood pressure in ex-

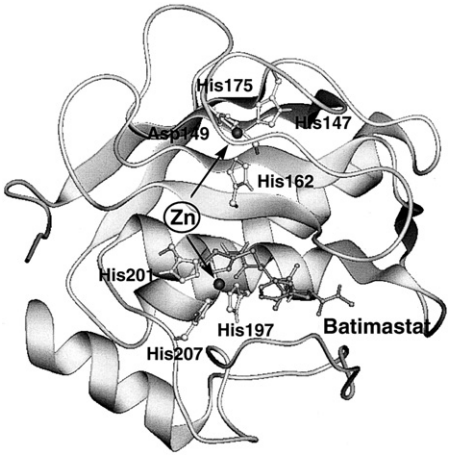

FIG. 30. X-ray crystal structure of batimastat–human neutrophil collagenase complex, showing the inhibitor coordinated to the catalytic Zn(II) (PDBID: 1JAQ). Adapted from (*576*).

perimental models of hypertension. Alpha-thiol dipeptides also have high *in vitro* and *in vivo* inhibitory effects on the enzymes (*588*, *589*). The combination of bicyclic monocyclic azepinones with mercaptoacetyl dipeptides gives compounds of high potency (*590*).

Ras proteins are mutationally activated in a variety of human cancers. Since farnesylation of Ras proteins is required for expression of their oncogenic potential, the enzyme responsible for this reaction, farnesylprotein transferase, has become a major target for anticancer drug development. Inhibitors of this enzyme are being developed as potential antitumour agents, and zinc is essential for its catalytic activity (*591*). The peptidomimetic B958 and its methyl ester B1086 are cytotoxic toward several human tumor cells and their activity has been correlated with the inhibition of farnesyl-protein transferase (*592*). The monocyclic terpene D-limonene, a major component of many citrus essential oils, has been used for many years as a flavoring agent, food additive, and fragrance. It was recently found to be a farnesyl-protein transferase inhibitor and is on phase I clinical trial for the treatment of advanced cancer (*593*).

Ribonucleotide reductase (RNR), which contains a binuclear Fe(III) active site, is the rate-limiting enzyme of DNA synthesis. Its activity is significantly increased in tumor cells corresponding to the increase in proliferation rate. Ribonucleotide reductase is also necessary for DNA replication of viruses. Inhibitors of this enzyme hold promise as potential anticancer and antiviral drugs (*594*). Hydroxyurea, a potent inhibitor of RNR, is on clinical trials for the treatment of chronic myelogenous leukemia (*595*), head and neck cancer (*596*), and HIV-infected patients (in combination with other anti-HIV drugs (*597*)). Novel peptidomimetic inhibitors such as **118** (BILD 1263) have shown very high *in vivo* antiviral activity against mice infected with Herpes simplex viruses (*598*).

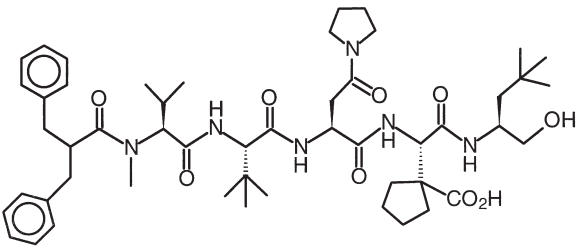

118

Protein kinase C (PKC) is a phospholipid-dependent enzyme involved in signal transduction mechanisms associated with cellular growth and differentiation. At least 11 PKC isozymes, classified as conventional (α, β_1, β_2, γ), novel (δ, ε, η, θ, μ), and atypical (ξ, λ) have been reported. Conventional PKC isozymes are Ca(II) dependent, while some others do not require Ca(II) for activation. The binding of Ca(II) translocates PKC to the membrane where it interacts with DAG and transforms into a fully active enzyme (*599*). Based on their role in signal transduction and their functional divergence and molecular heterogeneity, PKC isoenzymes are attractive targets for the development of anticancer drugs.

Calcineurin is a serine/threonine protein phosphatase widely distributed in the brain, but its role in brain function remains unknown. It is critical for several important cellular processes including T-cell activation, and recent data indicate that it may be involved in hyperphosphorylation of tau in Alzheimer's disease (*600*, *601*). The active site of native calcineurin contains zinc and iron metal ions and three metal-bound water molecules (*602*), one of which may be involved in nucleophilic attack on the substrate. Compound **119** (FK506, tacroli-

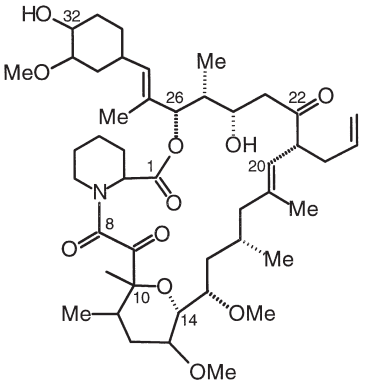

119

mus), a clinical immunosuppressant drug, binds to intracellular immunophilins resulting in a complex that inhibits specifically the activity of calcineurin (*603*). Recent data show that **119** blocks voltage-gated calcium channel-dependent long-term potentiation in the hippocampus (*604*) and exhibits neuroprotective effects (*605*). Therefore the design of selective inhibitors of calcineurin is of interest in relation to

the discovery of efficient drugs for the treatment of neurodegeneration-related diseases. Several small molecules such as **121–122**, with designs based on the dicarboxylic acid ring system **120** of endothall, a known inhibitor of calicineurin, have been shown to bind tightly to calcineurin and inhibit the enzyme (*606*).

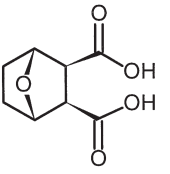

120

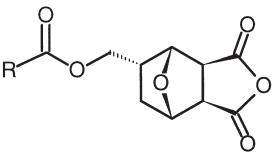

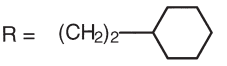

121

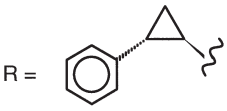

122

XV. Conclusion and Outlook

We hope that it is clear from the examples given in this chapter that inorganic chemistry is beginning to have a major impact on medicine. Metal complexes can often be designed to have specific biological activity. It is possible to control redox and ligand substitutions of metal complexes and to investigate these under conditions of physiological relevance. It is the metal and the ligands which determine the biological activity and not just the metal. Moreover, metals and in particular metals at the active sites of metalloenzymes can be target sites for organic agents. It will take some time before major success with inorganic pharmacology can be demonstrated on a large scale; however, some examples are already emerging. The best known is probably that of platinum anticancer drugs and studies of the mechanism of action of platinum not only provide the basis for the design of novel effective platinum complexes, but also provide deeper insights into fundamental biological processes. Platinum(II) attacks DNA, but

other metal ions may have different target sites, and it will be interesting to follow the progress of the newer metals in the clinical trials, notably Ti and Ru. Much more biological testing of inorganic compounds is needed, but it is important that these are highly characterized and that reactions under biological conditions, including reactions with components of the test media, are considered. The complex which enters cells may not be that which was synthesized.

The MRI contrast field has led the way recently in demonstrating that metal toxicity can be finely controlled with the appropriate choice of ligands, and skillful ligand design is probably the key to major successes in the metallopharmaceuticals field in general. We can confidently expect biomedical inorganic chemistry to make major contributions to areas of medicine which are currently lacking in new development, a notable example being that of neurological disorders. This is an exciting interdisciplinary field.

Acknowledgments

We acknowledge the generous support for our own work provided by The Biotechnology and Biological Sciences Research Council, Engineering and Physical Sciences Research Council, Medical Research Council, the Wellcome Trust, the European Commission, The Royal Society, Association for International Cancer Research, GlaxoWellcome plc, Delta Biotechnology, and our collaborators. We acknowledge also use of the Protein Data Bank (Brookhaven National Laboratory, USA) and Cambridge Structural Database (Daresbury laboratory, UK) for some of the structural data shown in this work. We thank those who provided us with preprints of their work, and acknowledge stimulating discussions with members of the EC COST Action D8 "The Chemistry of Metals in Medicine."

References

1. Sadler, P. J. *Advances Inorg. Chem.* **1991,** *36,* 1–48.
2. Sadler, P. J. "Lectures in Bioinorganic Chemistry," Nicolini, M., and Sindellari, L., Eds.; pp. 1–24; Cortina Int./Raven: Verona/New York; 1991.
3. Abrams, M. J.; Murrer, B. A. *Science,* **1993,** *261,* 725–730.
4. For example, reviews in "Topics in Biological Inorganic Chemistry," Clarke, M. J. and Sadler, P. J., Eds.; Vols. 1–2; Springer-Verlag: Berlin, 1999.
5. "Metal Complexes in Cancer Chemotherapy," Keppler, B. K., Ed.; VCH; Weinheim, 1993.
6. "Metal Compounds in Cancer Therapy," Fricker, S. P., Ed.; Chapman & Hall: London, 1994.
7. "Platinum and Other Metal Coordination Compounds in Cancer Chemotherapy 2," Pineto, H. M. and Schornagel, J. H., Eds.; Plenum: New York, 1996.

8. Rosenberg, B.; van Camp, L.; Krigas, T. *Nature* **1965,** *205,* 698.
9. Rosenberg, B.; van Camp, L.; Trosko, J. E.; Mansour, V. H. *Nature* **1969,** *222,* 385–387.
10. Zamble, D. B.; Lippard, S. J. *Trends Biochem. Sci.* **1995,** *20,* 435–439.
11. McA'Nulty, M. M.; Lippard, S. J. *Mutation Res. DNA Rep.* **1996,** *362,* 75–86.
12. Whitehead, J. P.; Lippard, S. J. *Met. Ions Biol. Sys.* **1996,** *32,* 687–725.
13. Reedijk, J. *Chem. Commun.* **1996,** 801–806.
14. Bloemink, M. J.; Reedijk, J. *Met. Ions Biol. Syst.* **1996,** *32,* 641–685.
15. Lippert, B. *Met. Ions Biol. Sys.* **1996,** *33,* 105–141.
16. Sabat, M.; Lippert, B. *Met. Ions Biol. Sys.* **1996,** *33,* 143–176.
17. Kozelka, J. *Met. Ions Biol. Sys.* **1996,** *33,* 1–28.
18. Augé, P.; Kozelka, J. *Transition Met. Chem.* **1997,** *22,* 91–96.
19. Boudvillan, M.; Dalbiés, R.; Leng, M. *Met. Ions Biol. Sys.* **1996,** *33,* 87–104.
20. Lilley, D. M. J. *J. Biol. Inorg. Chem.* **1996,** *1,* 189–191.
21. Zlatanova, J.; Yaneva, J.; Leuba, S. H. *FASEB J.* **1998,** *12,* 791–799.
22. Farrell, N. *Met Ions Biol. Sys.* **1996,** *32,* 603–639.
23. Arpalahti, J. *Met Ions Biol. Sys.* **1996,** *32,* 379–395.
24. Yang, D.; Wang, A. H.-J. *Prog. Biophys. Mol. Biol.* **1996,** *66,* 81–111.
25. Hambley, T. W. *Coord. Chem. Rev.* **1997,** *166,* 181–223.
26. Appleton, T. G. *Coord. Chem. Rev.* **1997,** *166,* 313–359.
27. Los, G.; Gately, D.; Costello, M. L.; Thiebaut, F.; Naredi, P.; Howell, S. B. "Platinum and Other Metal Coordination Compounds in Cancer Chemotherapy 2," Pineto, H. M. and Schornagel, J. H., Eds.; pp. 91–105; Plenum: New York, 1996.
28. Gately, D.; Howell, S. B. *Br. J. Cancer* **1993,** *67,* 1171–1176.
29. Gottesman, M. M. *Cancer Res.,* **1993,** *53,* 747–754.
30. Nooter, K.; Stoter, G. *Pathol. Res. Practice,* **1996,** *192,* 768–780.
31. Andrews, P. A.; Velury, S.; Mann, S. C.; Howell, S. B. *Cancer Res.* **1988,** *48,* 68–73.
32. Christen, R. D.; Jekunen, A. P.; Jones, J. A.; Tiebaut, F.; Shalinsky, D. R.; Howell, S. B. *J. Clin. Invest.* **1993,** *92,* 431–440.
33. Kawai, K.; Kamatani, N.; Georges, E.; Ling, V. *J. Biol. Chem.* **1990,** *265,* 13137–13142.
34. Sharp, S. Y.; Rogers, P. M.; Kelland, L. R. *Clin. Cancer Res.* **1995,** *1,* 981–989.
35. Berners-Price, S. J.; Kuchel, P. W. *J. Inorg. Biochem.* **1990,** *38,* 327.
36. Ishikawa, T.; Bao, J. J.; Yamane, Y.; Akimaru, K.; Frindrich, K.; Wright, C. D.; Kuo, M. T. *J. Biol. Chem.* **1996,** *271,* 14981–14988.
37. Ishikawa, T.; Wright, C. D.; Ishikawa, H. *J. Biol. Chem.* **1994,** *269,* 29085–29093.
38. Kelley, S. L.; Basu, A.; Teicher, B. A.; Hacker, M. P.; Hamer, D. H.; Lazo, J. S. *Science* **1988,** *241,* 1813–1815.
39. Lemkuil, D. C.; Nettesheim, D.; Shaw, C. F., III; Petering, D. H. *J. Biol. Chem.* **1994,** *269,* 24792–24797.
40. Zhang, B. L.; Sun, W. Y.; Tang, W. X. *J. Inorg. Biochem.,* **1997,** *65,* 295–298.
41. Zhang, B. L.; Tang, W. X. *J. Inorg. Biochem.,* **1994,** *56,* 143–153.
42. Poon, G. K.; Mistry, P.; Raynaud, F. I.; Karrap, K. P.; Murre, B. A.; Barnard, C. F. J. *J. Pharm. Biomed. Anal.* **1995,** *13,* 1493–1498.
43. Barton, S. J.; Barnham, K. J.; Habtemariam, A.; Sue, R. E.; Frey, U.; Sadler, P. J. *Aust. J. Chem.* **1999,** *52,* 173–177.
44. Chen, Y.; Guo, Z.; Parsons, S.; Sadler, P. J. *Chem. Eur. J.* **1998,** *4,* 672–676.
45. Yang, D.; van Boom, S. S. G. E.; Reedijk, J.; van Boom, J. H.; Wang, A. H.-J. *Biochemistry,* **1995,** *34,* 12912–12920.

46. Takahara, P. M.; Rosenzwig, A. C.; Frederick, C. A.; Lippard, S. J. *Nature* **1995,** *377,* 649–652.
47. Takahara, P. M.; Frederick, C. A.; Lippard, S. J. *J. Am. Chem. Soc.* **1996,** *118,* 12309–12321.
48. Poklar, N.; Pilch, D. S.; Lippard, S. J.; Redding, E. A.; Dunham, S. U.; Breslauer, K. J. *Proc. Nat. Acad. Sci. USA* **1996,** *93,* 7606–7611.
49. Gonnet, F.; Reeder, F.; Kozelka, J.; Chottard, J. C. *Inorg. Chem.,* **1996,** *35,* 1653–1658.
50. Reeder, F.; Gonnet, F.; Kozelka, J.; Chottard, J. C. *Chem. Eur. J.,* **1996,** *2,* 1068–1076.
51. Legendre, F.; Kozelka, J.; Chottard, J.-C. *Inorg. Chem.* **1998,** *37,* 3964–3967.
52. Lemaire, M. A.; Schwartz, A.; Rahmount, A. R.; Leng, M. *Proc. Natl. Acad. Sci. USA* **1991,** *88,* 1982–1985.
53. Huang, H.; Zhu, L.; Reid, B. R.; Drobny, G. P.; Hopkins, P. B. *Science* **1995,** *270,* 1842–1845.
54. Paquet, F. Perez, C.; Leng, M.; Lancelot, G.; Malinge, J.-M. *J. Biomol. Str. Dyn.* **1996,** *14,* 67–77.
55. Brabec, V.; Leng, M. *Proc. Natl. Acad. Sci. USA* **1993,** *90,* 5345–5349.
56. Dalbies, R.; Payet, D.; Leng, M. *Proc. Natl. Acad. Sci. USA* **1994,** *91,* 8147–8151.
57. Berners-Price, S. J.; Barnham, K. J.; Frey, U.; Sadler, P. J. *Chem. Eur. J.* **1996,** *2,* 1283–1291.
58. Reeder, F.; Guo, Z.; Murdoch, P. del S.; Hambley, T. W.; Berners-Price, S. J.; Sadler, P. J. *Eur. J. Biochem.* **1997,** *249,* 370–382.
59. Davies, M. S.; Berners-Price, S. J.; Hambley, T. W. *J. Am. Chem. Soc.* **1998,** *120,* 11380–11390.
60. Brabec, V.; Vrana, O.; Novakova, O.; Kleinwachter, V.; Intini, F. P.; Coluccia, M.; Natile, G. *Nucleic Acids Res.* **1996,** *24,* 336–341.
61. Comess, K. M.; Costello, C. E.; Lippard, S. J. *Biochemistry* **1990,** *29,* 2102–2110.
62. Dalbies, R.; Payet, D.; Leng, M. *Proc. Natl. Acad. Sci. USA,* **1994,** *91,* 8147–8151.
63. Dalbies, R.; Boudvillain, M.; Leng, M. *Nucleic Acids Res.* **1995,** *23,* 949–953.
64. Perez, C.; Leng, M.; Malinge, J. M. *Nucleic Acids Res.* **1997,** *25,* 896–903.
65. Bauer, C.; Peleg-Shulman, T.; Gibson, D.; Wang, A. H. J. *Eur. J. Biochem.* **1998,** *256,* 253–260.
66. Murdoch, P. D. S.; Guo, Z.; Parkinson, J. A.; Sadler, P. J. *J. Biol. Inorg. Chem.* **1999,** *4,* 32–38.
67. Yang, D.; van Boom, S. S. G. E.; Reedijk, J.; van Boom, J. H.; Wang, A. H.-J. *Biochemistry* **1995,** *34,* 12912–12920.
68. van Houten, B. *Microbiol. Rev.* **1990,** *54,* 18–51.
69. Aboussekhra, A.; Biggerstaff, M.; Shivji, M. K. K.; Vilpo, J. A.; Moncollin, V.; Podust, V. N.; Protic, M.; Hubscher, U.; Egly, J.-M.; Wood, D. *Cell* **1995,** *80,* 859–868.
70. Tanaka, K.; Wood, R. D. *Trends Biol. Sci.* **1994,** *19,* 83–86.
71. Eastman, A.; Schulte, N. *Biochemistry* **1988,** *27,* 4730–4734.
72. Fink, D.; Aebi, S; Howell, S. B. *Clin. Cancer Res.* **1998,** *4,* 1–6.
73. Toney, J. H.; Donahue, B. A.; Kellett, P. J.; Bruhn, S. L.; Essigmann, J. M.; Lippard, S. J. *Proc. Natl. Acad. Sci. USA* **1989,** *86,* 8328–8332.
74. McA'Nulty, M. M.; Lippard, S. J. *Nucleic Acids Mol. Biol.* **1995,** *9,* 264–284.
75. Whitehead, J. P.; Lippard, S. J. *Met. Ions Biol. Syst.* **1996,** *32,* 687–726.
76. Weir, H. M.; Kraulis, P. J.; Hill, C. S.; Raine, A. R. C.; Laue, E. D.; Thomas, J. O. *EMBO J.* **1993,** *12,* 1311–1319.

77. Read, C. M.; Cary, P. D.; Crane-Robinson, C.; Driscoll, P. C.; Norman, D. G. *Nucleic Acids Res.* **1993,** *21,* 3427–3436.
78. Hardman, C. H.; Broadhurst, R. W.; Raine, A. R.; Grasser, K. D.; Thomas, J. O.; Laue, E. D. *Biochemistry* **1995,** *34,* 16596–16607.
79. Dunham, S. U.; Lippard, S. J. *Biochemistry* **1997,** *36,* 11428–11436.
80. Chow, C. S.; Whitehead, J. P.; Lippard, S. J. *Biochemistry* **1994,** *33,* 15124–15130.
81. Locker, D.; Decoville, M.; Maurizot, J. C.; Bianchini, M. E.; Leng, M. *J. Mol. Biol.* **1995,** *246,* 243–247.
82. Zamble, D. B.; Mu, D.; Readon, D.; Sancar, A.; Lippard, S. J. *Biochemistry* **1996,** *35,* 10004–10013.
83. Moggs, J. G.; Szymkowski, D. E.; Yamada, M.; Karran, P.; Wood, R. D. *Nucleic Acids Res.* **1997,** *25,* 480–490.
84. Berners-Price, S. J.; Corazza, A.; Guo, Z.; Barnham, K. J.; Sadler, P. J.; Ohyama, Y.; Leng, M.; Locker, D. *Eur. J. Biochem.* **1997,** *243,* 782–791.
85. Yaneva, J.; Leuba, S. H.; van Holde, K.; Zlatanova, J. *Proc. Natl. Acad. USA* **1997,** *94,* 13448–13451.
86. Vichi, P.; Coin, F.; Renaud, J.-P.; Vermeulen, W.; Hoeijmakers, J. H. J.; Moras, D.; Egly J.-M. *EMBO J.* **1997,** *16,* 7444–7456.
87. Nagai, N.; Okuda, R.; Kinochita, M.; Ogata, H. *J. Pharm. Pharmacol.* **1996,** *48,* 918–924.
88. Ivanov, A. I.; Christodoulou, J.; Parkinson, J. A.; Barnham, K. J.; Tucker, A.; Woodrow, J.; Sadler, P. J. *J. Biol. Chem.* **1998,** *273,* 14721–14730.
89. Riley, C. M.; Sternson, L. A.; Repta, A. J.; Slyter, S. A. *Anal. Chem.* **1983,** *130,* 203–214.
90. Murdoch, P. del S.; Ranford, J. D.; Sadler, P. J.; Berners-Price, S. J. *Inorg. Chem.* **1993,** *32,* 2249–2255.
91. Woynarowski, J. M.; Chapman, W. G.; Napier, C.; Raymond, E. "Proc. 88th Annual Meeting American Association for Cancer Research," April 12–16, 1997, San Diego, CA, Vol 38, No. 2084, pp. 311.
92. Frey, U.; Ranford, J. D.; Sadler, P. J. *Inorg. Chem.* **1993,** *32,* 1333–1340.
93. Barnham, K. J.; Djuran, M. I.; Murdoch, P. del. S.; Ranford, J. D.; Sadler, P. J. *J. Am. Chem. Soc.* **1994,** *116,* 11175–11176.
94. Guo, Z.; Hambley, T. W.; Murdoch, P. del S.; Sadler, P. J.; Frey, U. *J. Chem. Soc. Dalton Trans.* **1997,** 469–478.
95. Barnham, K. J.; Djuran, M. I.; Murdoch, P. del S.; Sadler, P. J. *J. Chem. Soc. Commun.* **1994,** 721–722.
96. van Boom, S. S. G. E.; Reedijk, J. *J. Chem. Soc. Chem. Commun.* **1993,** 1397–1398.
97. Barnham, K. J.; Guo, Z.; Sadler, P. J. *J. Chem. Soc. Dalton Trans.* **1996,** 2867–2876.
98. Barnham, K. J.; Djuran, M. I.; Murdoch, P. del S.; Ranford, J. D.; Sadler, P. J. *J. Chem. Soc. Dalton Trans.* **1995,** 3721–3726.
99. Takahashi, K.; Okamoto, K.; Minamide, S.; Yamashita, T. *Proc. Am. Assoc. Cancer Res.* **1988,** *29,* 339.
100. Kobayashi, H.; Takemura, Y.; Miyachi, H.; Ogawa, T. *Invest. New Drugs* **1991,** *9,* 313–319.
101. Yang, L. Y.; Liu, Y. Z.; Li, L.; Kantarjian, H. H.; Keating, M. J. *Int. J. Oncol.* **1994,** *5,* 597–602.
102. Matsumoto, T.; Endoh, K.; Akamatsu, K.; Kamisango, K.; Mitsui, H.; Koizumi, K.; Morikawa, K.; Koizumi, M.; Matsuno, T. *Br. J. Cancer,* **1991,** *64,* 41–46.

103. Mross, K.; Meyberg, F.; Fiebig, H. H.; Hamm, K.; Hieberr, U.; Aulenbacher, P.; Hossfeld, D. K. *Onkologie* **1992,** *15,* 139–146.
104. Gietema, J. A.; Veldhuis, G. J.; Guchelaar, H. J.; Willemse, P. H. B.; Uges, D. R. A.; Cats, A.; Boonstra, H.; van der Graaf, W. T. A.; Sleijfer, D. T.; Devries, E. G. E.; Mulder, N. H. *Br. J. Cancer* **1995,** *71,* 1302–1307.
105. De Garddin, M.; Armand, J. P.; Chevallier, B.; Cappelaere, P.; Lentz, M. A.; David, M.; Roche, H. *Invest. New Drugs* **1995,** *13,* 253–255.
106. Fiebig, H. H.; Henss, H.; Vonpawel, L.; Gatzemeier, U.; Manegold, C.; Edler, L.; Berdel, W. *Onkologie,* **1996,** *19,* 328–332.
107. Perez-Soler, R.; Khokhar, A. R. *Proc. Am. Assoc. Cancer Res.* **1998,** *29,* 509.
108. Khokhar, A. R.; Albaker, S.; Brown, T.; Perez-Soler, R. *J. Med. Chem.* **1991,** *34,* 325–329.
109. Perez-Soler, R.; Khokhar, A. R. *Cancer Res.* **1992,** *52,* 6341–6347.
110. Han, I.; Khokhar, A. R.; Perez-Soler, R. *Cancer Chemother. Pharmacol.* **1996,** *39,* 17–24.
111. Raynaud, F. I.; Boxall, F. E.; Goddard, P. M.; Valenti, M.; Jones, M.; Murrer, B. A.; Abrams, M.; Kelland, L. R. *Clin. Cancer Res.* **1997,** *3,* 2063–2074.
112. Chen, Y.; Guo, Z.; Parsons, S.; Sadler, P. J. *Chem. Eur. J.,* **1998,** *4,* 672–676.
113. Di Blasi, P.; Bernareggi, A.; Beggiolin, G.; Piazzoni, L.; Menta, E.; Formento, M. L. *Anticancer Res.* **1998,** *18,* 3113–3117.
114. Kelland, L. R.; Abel, G.; McKeage, M. J.; Jones, M.; Goddard, P. M.; Valenti, M.; Murrer, B. A.; Harrap, K. R. *Cancer Res.* **1993,** *53,* 2581–2586.
115. Raynaud, F. I.; Mistry, P.; Donaghue, A.; Poon, G. K.; Kelland, L. R.; Murrer, B. A.; Harrap, K. R. *Cancer Chemother. Pharmacol.* **1996,** *38,* 155–162.
116. Raynaud, F. I.; Boxall, F. E.; Goddard, P. ; Barnard, C. F.; Murrer, B. A.; Kelland, L. R. *Anticancer Res.* **1996,** *16,* 1857–1862.
117. Kidani, Y.; Kizu, R.; Miyazaki, M.; Noji, M.; Matsuzawa, A.; Takeda, Y.; Akiyama, N.; Eriguchi, M. "Platinum and Other Metal Coordination Compounds in Cancer Chemotherapy 2," Pinedo, H. M. and Schornagel, J. H., Eds.; pp. 43–51. Plenum: New York, 1993.
118. Kizu, R.; Nakanishi, T.; Miyazaki, M.; Tashiro, T.; Noji, M.; Matsuzawa, A.; Eriguchi, M.; Takeda, Y.; Akiyama, N.; Kidani, Y. *Anticancer Drugs* **1996,** *7,* 248–256.
119. Novakova, O.; Vrana, O.; Kiseleva, V. I.; Brabec, V. *Eur. J. Biochem.* **1995,** *228,* 616–624.
120. van Beusichem, M.; Farrell, N. *Inorg. Chem.* **1992,** *31,* 634–639.
121. Farrell, N.; Kelland, L. R.; Roberts, J. D.; Van Beusichem, M. *Cancer Res.* **1992,** *52,* 5065–5072.
122. Zou, Y.; Van Houten, B.; Farrell, N. *Biochemistry,* **1993,** *32,* 9632–9638.
123. Zakovska, A; Novakova, O; Balcarova, Z; Bierbach, U; Farrell, N; Brabec, V. *Eur. J. Biochem.* **1998,** *254,* 547–557.
124. Kelland, L. R.; Barnard, C. F. J.; Mellish, K. J.; Jones, M.; Goddard, P. M.; Valenti, M.; Bryant, A.; Murrer, B. A.; Harrap, K. R. *Cancer Res.* **1994,** *54,* 5618–5622.
125. Kelland, L. R.; Barnard, C. F. J.; Evans, I. G.; Murrer, B. A.; Theobald, B. R. C.; Wyer, S. B.; Goddard, P. M.; Jones, M.; Valenti, M.; Bryant, A.; Rogers, P. M.; Harrap, K. R. *J. Med. Chem.* **1995,** *38,* 3016–3024.
126. Mellish, K. J.; Barnard, C. F. J.; Murrer, B. A.; Kelland, L. R. *Int. J. Cancer* **1995,** *62,* 717–723.
127. Goddard, P. M.; Orr, R. M.; Valenti, M. R.; Barnard, C. F. J.; Murrer, B. A.; Kelland, L. R.; Harrap, K. R. *Anticancer Res.* **1996,** *16,* 33–38.

128. Coluccia, M.; Nassi, A.; Loseto, F.; Boccarelli, A.; Mariggio, M. A.; Gordano, D.; Intini, F. P.; Caputo, P.; Natile, G. *J. Med. Chem.* **1993,** *36,* 510–512.
129. Cini, R.; Caputo, P. A.; Intini, F. P.; Natile, G. *Inorg. Chem.* **1995,** *34,* 1130–1137.
130. Coluccia, M.; Boccarelli, A.; Mariggio, M. A.; Cardellicchio, N.; Caputo, P.; Intini, F. P.; Natile, G. *Chem. Biol. Inter.* **1995,** *98,* 251–266.
131. Coluccia, M.; Mariggio, M. A.; Boccarelli, A.; Loseto, F.; Cardellicchio, N.; Caputo, P.; Intini, F. P.; Pacifico, C.; Natile, G. "Platinum and Other Metal Coordination Compounds in Cancer Chemotherapy 2," Pinedo, H. M. and Schornagel, J. H., Eds.; pp. 27–36. Plenum: New York, 1993.
132. Brabec, V.; Vrana, O.; Novakova, O.; Kleinwachter, V.; Intini, F. P.; Coluccia, M.; Natile, G. *Nucleic Acids Res.* **1996,** *24,* 336–341.
133. Habtemariam, A.; Sadler, P. J. *Chem. Commun.* **1996,** 1785–1786.
134. Margiotta, N.; Habtemariam, A.; Sadler, P. J. *Angew. Chem. Int. Ed. Engl.* **1997,** *36,* 1185–1187.
135. Habtemariam, A.; Neplechova, K.; Brabec, V.; Margiotta, N.; Sadler, P. J. *J. Inorg. Biochem.* **1997,** *67,* 161.
136. Neplechova, K.; Kasparkova, J.; Vrana, O.; Novakova, O.; Habtemariam, A.; Watchman, B.; Sadler, P. J.; Brabec, V. *Mol. Pharm.* **1999,** *56,* 20–30.
137. Kratochwil, N. A.; Zabel, M.; Range, K. J.; Bednarski, P. J. *J. Med. Chem.* **1996,** *39,* 2499–2507.
138. Kratochwil, N. A.; Parkinson, J. A.; Bednarski, P. J.; Sadler, P. J. *Angew. Chem. Int. Ed. Engl.* **1999,** *38,* 1460–1463.
139. Kratochwil, N. A.; Guo, Z.; Murdoch, P. del S.; Parkinson, J. A.; Bednarski, P. J.; Sadler, P. J. *J. Am. Chem. Soc.* **1998,** *120,* 8253–8254.
140. Payet, D.; Leng, M. *Metal Based Drugs* **1995,** *2,* 137–141.
141. Kane, S. A.; Lippard, S. J. *Biochemistry* **1996,** *35,* 2180–2188.
142. Cleare, M. J.; Hoeschele, J. D. *Bioinorg. Chem.* **1973,** *2,* 187–195.
143. Inagaki, K.; Kidani, Y. *Inorg. Chem.* **1986,** *25,* 1–3.
144. Gust, R.; Schonenberger, H.; Kritzenberger, J.; Range, K.-J.; Klement, U.; Burgemeister, T. *Inorg. Chem.* **1993,** *32,* 5939–5950.
145. Vickery, K.; Bonin, A. M.; Fenton, R. R.; O'Mara, Russell, P. J.; Webster, L. K.; Hambley, T. W. *J. Med. Chem.* **1993,** *36,* 3663–3668.
146. Fenton, R. R.; Easdale, W. J.; Meng Er, H.; O'Mara, S. M.; McKeage, M. J.; Russell, P. J.; Hambley, T. W. *J. Med. Chem.* **1997,** *40,* 1090–1098.
147. Galeano, A.; Berger, M. R.; Keppler, B. K. *Cancer Chemother. Pharmacol.* **1992,** *30,* 131–138.
148. Bloemink, M. J.; Dorenbos, J. P.; Heetebrij, R. J.; Keppler, B. K.; Reedijk, J; Zahn, H. *Inorg. Chem.* **1994,** *33,* 1127–1132.
149. Einhauser, T. J.; Galanski, M.; Vogel, E.; Keppler, B. K. *Inorg. Chim. Acta,* **1997,** *257,* 265–268.
150. Köpf, H.; Köpf-Maier, P. *Angew. Chem.* **1979,** *91,* 509–512.
151. Yang, P.; Guo, M. L.; *Coord. Chem. Rev.* **1999,** *185–186,* 189–211.
152. Christodoulou, C.; Ferry, D.; Fyfe, D.; Young, A.; Doran, J.; Sass, G.; Eliopoulos, A.; Sheehan, T.; Kerr, D. J. "Proc. 88th Annual Meeting American Association for Cancer Research," April 12–16, 1997, San Diego, CA, Vol. 38, No. 1495, pp. 222.
153. Köpf-Maier, P. In "Metal Complexes in Cancer Chemotherapy," Keppler, B. K. Ed., pp. 259–296; VCH: Weinheim, 1993.
154. Dombrowski, K. E.; Baldwin, W.; Sheats, J. E.; *J. Organomet. Chem.* **1986,** *302,* 281–306.
155. Kuo, L. Y.; Liu, A. H.; Marks, T. J. *Met. Ions Biol. Syst.* **1996,** *33,* 53–85.

156. Murray, J. H.; Harding, M. M. *J. Med. Chem.* **1994,** *37,* 1936–1941.
157. Toney, J. H.; Brock, C. P.; Marks, T. J. *J. Am. Chem. Soc.* **1986,** *113,* 7263–7274.
158. Murray, J. H.; Harding, M. M. *J. Med. Chem.* **1994,** *37,* 1936–1941.
159. Harding, M. M.; Prodigalidad, M.; Lynch, M. J. *J. Med. Chem.* **1996,** *39,* 5012–5016.
160. Clarke, M. J. *Met. Ions Biol. Syst.* **1980,** *11,* 231–283.
161. Sava, G. In "Metal Compounds in Cancer Therapy," Fricker, S. P., Ed., pp. 65–91; Chapman & Hall: London, 1994.
162. Alessio, E.; Mestroni, G.; Nardin, G.; Attia, W. M.; Calligaris, M.; Sava, G.; Zorzet, S. *Inorg. Chem.* **1988,** *27,* 4099–4106.
163. Keppler, B. K.; Rupp, W.; Juhl, U. M.; Endres, H.; Niebl, R.; Balzer, W. *Inorg. Chem.* **1987,** *26,* 4366–4370.
164. Kratz, F.; Keppler, B. K.; Hartmann, M.; Messori, L.; Berger, M. R. *Metal-Based Drugs* **1996,** *3,* 15–23.
165. Keppler, B. K.; Lipponer, K.-G.; Stenzel, B.; Kratz, F. In "Metal Complexes in Cancer Chemotherapy," Keppler, B. K., Ed., pp. 187–220; VCH:Weinheim, 1993.
166. Alessio, E.; Balducci, G.; Lutman, A.; Mestroni, G.; Calligaris, M.; Attia, W. M. *Inorg. Chim. Acta* **1993,** *203,* 205–217.
167. Ni Dhubhghaill, O. M.; Hagen, W. R.; Keppler, B. K.; Lipponer, K.-G.; Sadler, P. J. *J. Chem. Soc. Dalton Trans.* **1994,** 3305–3310.
168. Hartmann, M.; Einhauser, T. J.; Keppler, B. K. *Chem. Commun.* **1996,** 1741–1742.
169. Vilaplana, S. R.; Basallote, M. G.; Ruiz-Valero, C.; Gutierrez, E.; González-Vílchez, F. *J. Chem. Soc., Chem. Commun.* **1991,** 100–101.
170. Vilaplana, R. A.; González-Vílchez, F.; Gutierrez-Puebla, E.; Ruiz-Valero, C. *Inorg. Chim. Acta* **1994,** *224,* 15–18.
171. Vilaplana, R. A.; Romero, M. A.; Quirós, M.; Salas, J. M.; González-Vílchez, F. *Metal-Based Drugs* **1995,** *2,* 211–219.
172. Vilchez, F. G.; Vilaplana, R.; Blasco, G.; Messori, L. *J. Inorg. Biochem.* **1998,** *71,* 45–51.
173. Novakova, O.; Kasparkova, J.; Vrana, O.; Vanvliet, P. M.; Reedijk, J.; Brabec, V. *Biochemistry* **1995,** *34,* 12369–12378.
174. van Vliet, P. M.; Toekimin, S. M. S.; Haasnoot, J. G.; Reedijk, J.; Novakova, O.; Vrana, O.; Brabec, V. *Inorg. Chim. Acta* **1995,** *231,* 57–64.
175. Frasca, D.; Ciampa, J.; Emerson, J.; Umans, R. S.; Clarke, M. J. *Metal-Based Drugs* **1996,** *3,* 197–209.
176. Smith, C. A.; Sunderlandsmith, A. J.; Keppler, B. K.; Kratz, F.; Baker, E. N. *J. Biol. Inorg. Chem.* **1996,** *1,* 424–431.
177. Gray, H. B.; Winkler, J. R. *Ann. Rev. Biochem.* **1996,** *65,* 537–561.
178. Kratz, F.; Hartmann, M.; Keppler, B.; Messori, L. *J. Biol. Chem.* **1994,** *269,* 2581–2588.
179. Messori, L.; Kratz, F.; Alessio, E. *Metal-Based Drugs* **1996,** *3,* 1–9.
180. Bastos, C. M.; OCain, T. D.; Gordon, K. A.; Sampo, T. M.; Clarke, M. J.; Daghalian, H. "Abstracts of the Papers 211th National Meeting of the American Chemical Society;" Washington DC., 1996.
181. Clarke, M. J.; Bailey, V. M.; Doan, P. E.; Jiller, C. D.; LaChance-Galang, K. J.; Daghalian, H.; Mandal, S.; Bastos, C. M.; Lang, D. *Inorg. Chem.* **1996,** *35,* 4896–4903.
182. van Vliet, T. M.; Haasnoot, J. G.; Reedijk, J. *Inorg. Chem.* **1994,** *33,* 1934–1939.
183. Clarke, M. J.; Stubbs, M. *Met. Ions Biol. Syst.* **1996,** *32,* 727–780.

184. Esposito, G.; Cauci, S.; Fogolari, F.; Alessio, E.; Scocchi, M.; Guadrifoglio, F.; Viglino P. *Biochemistry* **1992,** *31,* 7094–7103
185. Arkin, M. R.; Jenkins, Y.; Murphy, C. J.; Turro, N. J.; Barton, J. K. *Adv. Chem. Ser.* **1995,** *246,* 449–469.
186. Keppler, B. K.; Schmähl, D. *Arzneim.-Forsch / Drug Res.* **1986,** *36,* 1822–1828.
187. Köpf-Maier, P, Gerlach, S. *J. Cancer Res. Clin. Oncol.* **1986,** *111,* 243–247.
188. Keppler, B. K.; Friesen, C.; Vongerichten, H.; Vogel, E.; In "Metal Complexes in Cancer Chemotherapy," Keppler, B. K., Ed., pp. 297–323; VCH: Weinheim, 1993.
189. Ni Dhubhghaill, O. M.; Sadler, P. J. "Metal Complexes in Cancer Chemotherapy," Keppler, B. K., Ed., pp. 221–248; VCH: Weinheim, 1993.
190. Berners-Price, S. J.; Bowen, R. J.; Galettis, P.; Healy, P. C.; McKeage, M. J. *Coord. Chem. Rev.* **1999,** in press.
191. Berners-Price, S. J.; Sadler, P. J. *Struct. Bond.* **1988,** *70,* 27–102.
192. Berners-Price, S. J.; Collier, D. C.; Mazid, M. A.; Sadler, P. J.; Sue, R. E.; Wilkie, D. *Metal-Based Drugs* **1995,** *2,* 111.
193. Papathanasiou, P.; Salem, G.; Waring, P.; Willis, A. C. *J. Chem. Soc. Dalton Trans.* **1997,** 3435–3443.
194. Shi, J.-C.; Chen, L. J.; Huang, X. Y.; Wu, D.-X.; Kang, B.-S. *J. Organomet. Chem.* **1997,** *535,* 1–2.
195. Carotti, S.; Guerri, A.; Mazzei, T.; Messori, L.; Mini, E.; Orioli, P. *Inorg. Chim. Acta* **1998,** *281,* 90–94.
196. Calamai, P.; Carotti, S.; Guerri, A.; Messori, L.; Mini, E.; Orioli, P.; Speroni, G. P. *J. Inorg. Biochem.* **1997,** *66,* 103–109.
197. Calamai, P.; Carotti, S.; Guerri, A.; Mazzei, T.; Messori, L.; Mini, E.; Orioli, P.; Speroni, G. P. *Anti-Cancer Drug Design* **1998,** *13,* 67–80.
198. Parish, R. V.; Howe, B. P.; Wright, J. P.; Mack, J.; Pritchard, R. G.; Buckley, R. G.; Elsome, A. M.; Fricker, S. P. *Inorg. Chem.* **1996,** *35,* 1659–1666.
199. Keppler, B. K.; Vogel, E. A. "Platinum and Other Metal Coordination Compounds in Cancer Chemotherapy 2" Pinedo, H. M. and Schornagel, J. H., Eds., pp. 253–268; Plenum: New York, 1993.
200. Bernstein, L. R. US Pat. Appl. 5747482, 1998.
201. Collery, P.; Domingo, J. L.; Keppler, B. K. *Anticancer Res.* **1996,** *16,* 687–691.
202. Bernstein, L. R. *Pharmacol. Rev.* **1998,** *50,* 665–682.
203. Bernstein, L. R.; Reed, D. E. *Pub. Int. Appl.* PCT/US97/11220, 1998.
204. Ni Dhubhghaill, O. M.; Sadler, P. J. *Struct. Bond.* **1991,** *78,* 129–190.
205. Shen, Z. X.; Chen, G. Q.; Ni, J. H.; Li, X. S.; Xiong, S. M.; Qiu, Q. Y.; Zhu, J.; Tang, W.; Sun, G. L.; Yang, K. Q.; Chen, Y.; Zhou, L.; Fang, Z. W.; Wang, Y. T.; Ma, J.; Zhang, P.; Zhang, T. D.; Chen, S. J.; Chen, Z.; Wang, Z. Y. *Blood* **1997,** *89,* 3354–3360.
206. Chen, G. Q.; Shi, X. G.; Tang, W.; Xiong, S. M.; Zhu, J.; Cai, X.; Han, Z. G.; Ni, J. H.; Shi, G. Y.; Jia, P. M.; Liu, M. M.; He, K. L.; Niu, C.; Ma, J.; Zhang, P.; Zhang, T. D.; Paul, P.; Naoe, T.; Kitamura, K.; Miller, W.; Waxman, S.; Wang, Z. Y.; de Thé, H.; Chen, S. J.; Chen, Z. *Blood* **1997,** *89,* 3345–3353.
207. Soignet, S. J.; Maslak, P.; Wang, Z. G.; Jhanwar, S.; Calleja, E.; Dardashti, L. J.; Corso, D.; De Blasio, A.; Gabrilove, J.; Scheinberg, D. A.; Pandolfi, P. P.; Warrell, R. P. *N. Engl. J. Med.* **1998,** *339,* 1341–1348.
208. Warrell, R.; de Thé, H.; Wang, Z.; Degos, L. *N. Engl. J. Med.* **1993,** *329,* 177–189.
209. Zhu, J.; Kojen, M. H. M.; Quignon, F.; Chelbi-Alix, M. K.; Degos, L.; Wang, Z. Y.; Chen, Z.; de Thé, H. *Proc. Natl. Acad. Sci. USA,* **1997,** *94,* 3978–3983.

210. Narayanan, V. L.; Nasr, M.; Paull, K. D. In "Tin-Based Antitumor Drugs," Gielen, M., Ed., NATO ASI Series Vol. 7 pp. 201–217; Springer-Verlag: Berlin, 1990.
211. Gielen, M.; Bouhdid, A.; Kayser, F.; Biesemans, M.; Devos, D.; Mahieu, B.; Willem, R. *Appl. Organomet. Chem.* **1995,** *9,* 251–257.
212. Crowe, A. J. "Metal Compounds in Cancer Therapy," Fricker, S. P., Ed., pp. 147–179; Chapman & Hall: London, 1994.
213. Cleare, M. J. *Coord. Chem. Rev.* **1974,** *12,* 349–405.
214. Howard, R. A.; Sherwood, E.; Erck, A. *J. Med. Chem.* **1977,** *20,* 943–946.
215. Kadish, K. M.; Das, K.; Howard, R. A. *Bioelectrochem. Bioenergetics* **1978,** *5,* 741–753.
216. Pruchnik, F.; Dus, D. *J. Inorg. Biochem.* **1996,** *61,* 55–61.
217. Bear, J. L.; Gray, H. B.; Rainen, L. *et al. Cancer Chemother. Rep. Part 1,* **1975,** *59,* 611–620.
218. Tselepi-Kalouli, E.; Katsaros, N. *J. Inorg. Biochem.* **1990,** *40,* 95–102.
219. Dunbar, K. R.; Matonic, J. H.; Saharan, V. P.; Crawford, C. A.; Christou, G. *J. Am. Chem. Soc.* **1994,** *116,* 2201–2202.
220. Day, E. F.; Crawford, C. A.; Folting, K.; Dunbar, K. R.; Christou, G. *J. Am. Chem. Soc.* **1994,** *116,* 9339–9340.
221. Zassinovich, G.; Maestroni, G.; Camus, A. *J. Organometallic. Chem.* **1975,** *91,* 379–388.
222. Sava, G.; Zorzet, S.; Mestroni, G.; Zassinovich, G. *Anticancer Res.* **1985,** *5,* 249–252.
223. Sava, G.; Pacor, S.; Ceschia, V.; Zassinovich, G.; Mestroni, G. *Anticancer Res.* **1989,** *9,* 767–770.
224. Petering, H. G.; Buskirk, H. H.; Crim, J. A. *Cancer Res.* **1967,** *27,* 1115–1121.
225. West, D. X.; Liberta, A. E.; Padhye, S. B.; Chikate, R. C.; Sonawane, P. B.; Kumbhar, A. S.; Yerande, R. G. *Coord. Chem. Rev.* **1993,** *123,* 49–71.
226. Antholine, W. E.; Byrnes, R.; Petering, D. H. "Handbook of Metal-Ligand Interactions in Biological Fluids—Bioinorganic Chemistry," Berthon, G., Ed., pp. 1024–1038; Marcel Dekker: New York, 1995.
227. Byrnes, R. W.; Antholine, W. E.; Petering, D. H. *Free Rad. Biol. Med.,* **1992,** *12,* 457–469.
228. Byrnes, R. W.; Antholine, W. E.; Petering, D. H. *Free Rad. Biol. Med.,* **1992,** *13,* 469–478.
229. Singh, N. K.; Singh, N.; Prasad, G. C.; Sodhi, A.; Shrivastava, A. *Bioorg. Med. Chem.* **1997,** *5,* 245–251.
230. Ainscough, E. W.; Brodie, A. M.; Dobbs, A. J.; Ranford, J. D.; Waters, J. M. *Inorg. Chim. Acta.* **1998,** *267,* 27–38.
231. Ranford, J. D.; Sadler, P. J.; Tocher, D. A. *J. Chem. Soc. Dalton Trans.* **1993,** 3393–3399.
232. Lena Ruiz, A. USA Patent 5-107,005, 1992.
233. Pratviel, G.; Bernadou, J.; Meunier, B. *Angew. Chem. Int. Ed. Engl.* **1995,** *34,* 746–747.
234. Vol'pin, M.; Levitin, I.; Osinsky, S. *Angew. Chem. Int. Ed. Engl.* **1996,** *35,* 2395–2396.
235. For example, Bakac, A.; Espenson, J. H. *Inorg. Chem.* **1989,** *28,* 3901–3904.
236. Riordan, C. G.; Wei, P. *J. Am. Chem. Soc.* **1994,** *116,* 2189–2190.
237. Bales, J. R.; Sadler, P. J.; Coulson, C. J.; Laverick, M.; Nias, A. H. W. *Br. J. Cancer* **1982,** *46,* 701–705.

238. Chan, P. K. L.; Skov, K. A.; James, B. R.; Farrell, N. P. *Chem.-Biol. Inter.* **1986,** *59,* 247–254.
239. Roy, M. B.; Mandal, P. C.; Bhattacharyya, S. N. *Int. J. Radio. Biol.* **1996,** *69,* 471–480.
240. Youn, S. W.; Qing, F.; Harriman, A.; Sessler, J. L.; Dow, W. C.; Mody, T. D.; Hemmi, G. W.; Hao, Y. P.; Miller, R. A. *Proc. Natl. Acad. Sci. USA* **1996,** *93,* 6610–6615.
241. van de Vaart, P. J. M.; Klaren, H. M.; Hofland, I.; Begg, A. C. *Intl. J. Radio. Biol.* **1997,** *72,* 675–683.
242. Bonnett, R. *Chem. Soc. Rev.* **1995,** 19–33.
243. Dolphin, D. *Can. J. Chem.* **1994,** *72,* 1005–1013.
244. Crowe, A. J. "Metal Compounds in Cancer Therapy," Fricker, S. P., Ed., pp. 168–172; Chapman & Hall: London, 1994.
245. Sessler, J. L.; Hemmi, G.; Mody, T. D.; Murai, T.; Burrell, A.; Young, S. W. *Acc. Chem. Res.* **1994,** *27,* 43–50.
246. Maiya, B. G.; Harriman, A.; Sessler, J. L.; Hemmi, G.; Murai, T.; Mallouk, T. E. *J. Phys. Chem.* **1989,** *93,* 8111–8115.
247. Young, S. W.; Woodburn, K. W.; Wright, M.; Mody, T. D.; Fan, Q.; Sessler, J. L.; Dow, W. C.; Miller, R. A. *Photochem. Photobiol.* **1996,** *63,* 892–897.
248. Cannon, J. B. *J. Pharm. Sci.* **1993,** *82,* 435–446.
249. Vreman, H. J.; Cipkala, D. A.; Stevenson, D. K. *Can. J. Physio. Pharm.* **1996,** *74,* 278–285.
250. Vallier, H. A.; Rodgers, P. A.; Stevenson, D. K. *Life Sci.* **1993,** *52,* 79–84.
251. Morgan, A. R.; Garbo, G. M.; Keck, R. W.; Ericksen, L. D.; Selman, S. H. *Photochem. Photobiol.* **1990,** *51,* 589–592.
252. Polo, L.; Reddi, E.; Garbo, G. M.; Moregan, A. R.; Jori, G. *Cancer Lett.* **1992,** *66,* 217–223.
253. Kongshaug, M.; Moan, J.; Cheng, L. S.; Garbo, G. M.; Kolboe, S.; Morgan, A. R.; Rimington, C. *Int. J. Biochem.* **1993,** *25,* 739–760.
254. Emtestam, L.; Angelin, B.; Berglund, L.; Drummond, G. S.; Kappas, A. *Acta Dermato-Venereologica,* **1993,** *73,* 26–30.
255. Ando, T.; Irie, K.; Koshimizu, K.; Takemura, T.; Nishino, H.; Iwashima, A.; Takeda, N.; Nakajima, S.; Sakata, I. *Photochem. Photobiol.* **1993,** *57,* 629–633.
256. Keino, H.; Banno, T.; Mimura, S.; Kashiwamata, S. *Biol. Neonate* **1993,** *63,* 285–289.
257. Kappas, A.; Drummond, G. S.; Henschke, C.; Valaes, T. *Pediatrics,* **1995,** *95,* 468–474.
258. Wohrle, D.; Wendt, A.; Weitemeyer, A.; Stark, J.; Spiller, W.; Schneider, G.; Muller, S.; Michelsen, U.; Kliesch, H.; Heuermann, A.; Ardeschirpur, A. *Russ. Chem. Bull.* **1994,** *43,* 1953–1964.
259. Shopova, M.; Mantareva, V.; Krastev, K.; Hadjiolov, D.; Milev, A.; Spirov, K.; Jori, G.; Ricchelli, F. *J. Photochem. Photobiol. B. Biol.* **1992** *16,* 83–89.
260. Segalla, A.; Milanesi, C.; Jori, G.; Capraro, H.-G.; Isele, U.; Schieweck, K. *Br. J. Cancer* **1994,** *69,* 817–825.
261. Wohrle, D.; Shopova, M.; Moser, J. G.; Kliesch, H.; Michelsen, U.; Muller, S. *Macromol. Sym.* **1996,** *105,* 127–138.
262. Wohrle, D.; Shopova, M.; Muller, S.; Milev, A.; Mantareva, V.; Krastev, K. K. *J. Photochem. Photobiol. B* **1993,** *21,* 155–162.
263. Shopova, M.; Wohrle, D.; Stoichkova, N.; Milev, A.; Mantareva, V.; Muller, S.; Krastev, K. K.; Georgiev, K. *J. Photochem. Photobiol. B* **1994,** *23,* 35–42.

264. Miyoshi, N.; Misik, V.; Fukuda, M.; Riesz, P. *Radiat. Res.* **1995,** *143,* 194–202.
265. Yumita, N.; Sasaki, K.; Umemura, S.; Nishigaki, R. *Jpn. J. Cancer Res.* **1996,** *87,* 310–316.
266. Yumita, N.; Sasaki, K.; Umemura, S.; Yukawa, A.; Nishigaki, R. *Cancer Lett.* **1997,** *112,* 79–86.
267. Blower, P. J.; Lewis, J. S.; Zweit, J. *Nuc. Med. Biol.* **1996,** *23,* 957–980.
268. Walker, B.; Jarrit, P. "Nuclear Medicine in Clinical Diagnosis and Treatment," Murray, I. P. C.; Ell, P. J.; and William Strauss, H., Ed., pp. 1279–1290; Churchill-Livingstone: Edinburgh, 1994.
269. Jurisson, S.; Berning, D.; Jia, W.; Ma, D. *Chem. Rev.* **1993,** *93,* 1137–1156.
270. Dilworth, J. R.; Parott, S. J. *Chem. Soc. Rev.* **1998,** *27,* 43–55.
271. Friedlander, G.; Kennedy, J. W.; Miller, J. M. "Nuclear and Radiochemistry," 2nd ed., pp. 86–130; Wiley: New York, 1966.
272. Steigman, J.; Eckelman, W. C. "The Chemistry of Technetium in Medicine;" Nuclear Science Publication NAS-NS-3204, National Academy Press: Washington, DC, 1992.
273. Tisato, F.; Refosco, F.; Bandoli, G. *Coord. Chem. Rev.* **1994,** *135,* 325–397.
274. Jurisson, S.; Schlemper, E. O.; Troutner, D. E.; Canning, L. R.; Nowotnik, D. P.; Neirinckx, R. D. *Inorg. Chem.* **1986,** *25,* 543–549.
275. Sharp, P. F.; Smith, F. W.; Gemmell, H. G.; Lyall, D.; Evans, N. T. S.; Gvozdanovic, D.; Davidson, J.; Tyrrell, D. A.; Pickett, R. D.; Neirinckx, R. D. *J. Nucl. Med.* **1986,** *27,* 171–177.
276. Inoue, Y.; Momose, T.; Ohtake, T.; Nishikawa, J.; Sasaki, Y.; Waritani, T.; Inoue, M. *J. Nucl. Med.* **1997,** *38,* 1731–1737.
277. Vanbilloen, H. P.; Cleynhens, B. J.; Verbruggen, A. M. *Nucl. Med. Biol.* **1998,** *25,* 569–575.
278. Walovitch, R. C.; Hill, T. C.; Garrity, S. T.; Cheesman, E. H.; Burgess, B. A.; O'leary, D. H.; Watson, A. D.; Ganey, M. V.; Morgan, R. A.; Williams, S. J. *J. Nucl. Med.* **1989,** *30,* 1892–1901.
279. Kasina, S.; Fritzberg, A. R.; Johnson, D. L.; Eshima, D. *J. Med. Chem.* **1986,** *29,* 1933–1940.
280. Singh, J.; Powell, A. K.; Clarke, S. E. M.; Blower, P. J. *J. Chem. Soc. Chem. Commun.* **1991,** 1115–1116.
281. Deutsch, E.; Bushong, W.; Glavan, K. A.; Elder, R. C.; Sodd, V. J.; Scholz, K. L.; Fortman, D. L.; Lukes, S. J. *Science,* **1981,** *214,* 85–86.
282. Kronauge, J. F.; Leon, A. S.; Verdera, E. S.; Balter, H. S.; Leon, E. T.; Mut, F.; Oliveira, M. C.; Garcia, F. A.; Holman, B. L.; Davison, A.; Jones, A. G. *J. Nucl. Med.* **1992,** *33,* 1949–1957.
283. Deutsch, E.; Vanderheyden, J. L.; Gerundini, P.; Libson, K.; Hirth, W.; Colombo, F.; Zecca, L.; Savi, A.; Fazio, F. *J. Nucl. Med.* **1987,** *28,* 1870–1880.
284. Rossetti, C.; Vanoli, G.; Paganelli, G.; Kwiatkowski, M.; Zito, F.; Colombo, F.; Bonino, C.; Carpinelli, A.; Casati, R.; Deutsch, K.; Marmion, M.; Woulfe, S. R.; Lunghi, F.; Deutsch, E.; Fazio, F. *J. Nucl. Med.* **1994,** *35,* 1571–1580.
285. Gerson, M. C.; Millard, R. W.; Roszell, N. J.; McGordon, A. J.; Gabel, M.; Washburn, L. C.; Biniakiewicz, D.; Blankenship, D.; Mallin, W. H.; Elder, R. C.; Deutsch, E.; Walsh, R. A. *Circulation* **1994,** *89,* 1291–1300.
286. Kelly, J. D.; Forster, A. M.; Higley, B.; Archer, C. M.; Booker, F. S.; Canning, L. R.; Chiu, K. W.; Edwards, B.; Gill, H. K.; McPartlin, M.; Nagle, K. R.; Latham, I. A.; Pickett, R. D.; Storey, A. E.; Webbon, P. M. *J. Nucl. Med.* **1993,** *34,* 222–227.

287. Jain, D.; Wackers, F. J. T.; Mattera, J.; McMahon, M.; Sinusas, A. J.; Zaret, B. L. *J. Nucl. Med.* **1993,** *34,* 1254–1259.
288. Maecke, H. R.; Riesen, A.; Ritter, W. *J. Nucl. Med.* **1989,** *30,* 1235–1239.
289. Taliaferro, C. H.; Motekaitis, R. J.; Martell, A. E. *Inorg. Chem.* **1984,** *23,* 1188–1192.
290. Maguire, R. T.; Pascucci, V. L.; Maroli, A. N.; Gulfo, J. V. *Cancer* **1993,** *72,* 3453–3462.
291. Zuckier, L. S.; De Nardo, G. L. *Semin. Nucl. Med.* **1997,** *27,* 10–29.
292. Dillman, R. O. *Clin. Immunother.* **1994,** *2,* 206–219.
293. Blower, P. J.; Lewis, J. S.; Zweit, J. *Nucl. Med. Biol.* **1996,** *23,* 957–980.
294. Karam, L. R.; Mitch, M. G.; Coursey, B. M. *Appl. Radiat. Isotopes* **1997,** *48,* 771–776.
295. Cagle, D. W.; Thrash, T. P.; Alford, M.; Chibante, L. P. F.; Ehrhardt, G. J.; Wilson, L. J. *J. Am. Chem. Soc.* **1997,** *118,* 8043–8047.
296. Hom, R. Y.; Katzenellenbogen, J. A. *Nucl. Med. Biol.* **1997,** *24,* 485–498.
297. Baidoo, K. E.; Scheffe, U.; Lever, S. Z.; Stathis, M.; Wagner, H. N. *J. Nucl. Med.* **1995,** *36,* 28.
298. Meegalla, S. K.; Plössl, K.; Kung, M. P.; Stevenson, D. A.; Liable-Sands, L. M.; Rheingold, A. L.; Kung, H. F. *J. Am. Chem. Soc.* **1995,** *117,* 11037–11038.
299. Kung, H. F.; Kim, H. J.; Kung, M. P.; Meegalla, S. K.; Plössl, K.; Lee, H. K. *Eur. J. Nucl. Med.* **1996,** *23,* 1527–1530.
300. Liu, S.; Edwards, D. S.; Looby, R. J.; Harris, A. R.; Poirier, M. J. Barrett, J. A. *et al. Bioconjug. Chem.* **1996,** *7,* 63–71.
301. Redpath, T. W. *Br. J. Radiol.* **1997,** *70,* S70–S80.
302. Lauffer, R. B. *Chem. Rev.* **1987,** *87,* 901–927.
303. Rocklage, S. M.; Watson, A. D. *JMRI-J. Magn. Reson. Imaging* **1993,** *3(1),* 167–178.
304. Aime, S.; Botta, M.; Ermondi, G. *Magn. Reson. Imaging* **1992,** *10,* 849–854.
305. Peters, J. A.; Huskens, J.; Raber, D. J. *Prog. Nucl. Magn. Reson. Spec.* **1996,** *28,* 283–350.
306. Chang, C. A.; Francesconi, L. C.; Malley, M. F.; Kumar, K.; Gougoutas, J. Z.; Tweedle, M. F.; Lee, D. W.; Wilson, L. J. *Inorg. Chem.* **1993,** *32,* 3501–3508.
307. Aime, S.; Barge, A.; Botta, M.; De Sousa, A. S.; Parker, D. *Angew. Chem. Int. Ed. Engl.* **1998,** *37,* 2673–2675.
308. Wiener, E. C.; Brechbiel, M. W.; Brothers, H.; Magin, R. L.; Gansow, O. A.; Tomalia, D. A.; Lauterbur, P. C. *Magn. Reson. Med.* **1994,** *31,* 1–8.
309. Bligh, S. W. A.; Harding, C. T.; Sadler, P. J.; Bulman, R. A.; Bydder, G. M.; Pennock, J. M.; Kelly, J. D.; Latham, I. A.; Marriott, J. A. *Magn. Reson. Med.* **1991,** *17,* 516–532.
310. Aime, S.; Botta, M.; Crich, S. G.; Giovenzana, G. B.; Pagliarin, R.; Piccinini, M.; Sisti, M.; Terreno, E. *J. Biol. Inorg. Chem.* **1997,** *2,* 470–479.
311. Aime, S.; Botta, M.; Fasano, M.; Crich, S. G.; Terreno, E. *J. Biol. Inorg. Chem.* **1996,** *1,* 312–319.
312. Gallez, B.; Bacic, G.; Swartz, H. M. *Magn. Reson. Med.* **1996,** *35,* 14–19.
313. Michell, D. G.; Outwater, E. K.; Matteucci, T.; Rubin, D. L.; Chezmar, J. L.; Saini, S. *Radiol.* **1995,** *194,* 783–787.
314. Saini, S. K.; Jena, A.; Dey, J.; Sharma, A. K.; Singh, R. *Magn. Reson. Imaging* **1995,** *13,* 985–990.
315. Yu, O.; Namer, I. J.; Steibel, J.; Eclancher, B.; Poulet, P.; Chambron, J. *Magn. Reson. Mat. Phy. Biol. Med.* **1995,** *3,* 169–172.

316. Berry, I.; Benederbous, S.; Ranjeva, J. P.; Graciameavilla, D.; Manelfe, C.; Lebihan, D. *Magn. Reson. Med.* **1996,** *36,* 415–419.
317. Schaefer, M. *Metal-Based Drugs* **1997,** *4,* 159–171.
318. Rubin, D. L.; Falk, K. L.; Sperling, M. J.; Ross, M.; Saini, S; Rothman, B.; Shellock, F.; Zerhouni, E.; Stark, D.; Outwater, E. K.; Schmiedl, U.; Kirby, L. C.; Chezmar, J.; Coates, T.; Chang, M.; Silverman, J. M.; Rofsky, N.; Burnett, K.; Engel, J.; Young, S. W. *JMRI-J. Magn. Reson. Imaging* **1997,** *7,* 865–872.
319. Kayyem, J. F.; Kumar, R. M.; Fraser, S. E.; Meade, T. J. *Chem. Biol.* **1995,** *2,* 615–620.
320. Moats, R. A.; Fraser, S. E.; Meade, T. J. *Angew. Chem. Int. Ed. Engl.* **1997,** *36,* 726–728.
321. Uggeri, F.; Aime, S.; Anelli, P. L.; Botta, M.; Brocchetta, M.; De Haen, C.; Ermondi, G.; Grandi, M.; Paoli, P. *Inorg. Chem.* **1995,** *34,* 633–642.
322. Petre, C.; Ni, Y. C.; Marchal, G.; Yu, J.; Wevers, M.; Lauffer, R. B.; Baert, A. L. *Magn. Reson. Med.* **1996,** *35,* 532–539.
323. Franano, F. N.; Edwards, D. B.; Welch, M. J.; Brechbiel, M. W.; Gansow, O. A.; Duncan, J. R. *Magn. Reson. Imaging* **1995,** *13,* 201–214.
324. Lisowski, J.; Sessler, J. L.; Lynch, V.; Mody, T. D. *J. Am. Chem. Soc.* **1995,** *117,* 2273–2285.
325. Aime, S.; Ascenzi, P.; Comoglio, E.; Fasano, M.; Paoletti, S. *J. Chem. Soc. Dalton Trans.* **1995,** 2259–2266.
326. Aime, S.; Botta, M.; Parker, D.; Williams, J. A. G. *J. Chem. Soc. Dalton Trans.* **1996,** 17–23.
327. Bligh, S. W. A.; Harding, C. T.; McEwen, A. B.; Sadler, P. J.; Kelly, J. D.; Marriott, J. A. *Polyhedron,* **1994,** *13,* 1937–1943.
328. Hollinger, M. A. *Crit. Rev. Toxicol.* **1996,** *26,* 255–260.
329. Clement, J. L.; Jarrett, P. S. *Metal-Based Drugs* **1994,** *1,* 467–482.
330. Wells, T. N. C.; Scully, P.; Paravicini, G.; Proudfoot, A. E. I.; Payton, M. A. *Biochemistry,* **1995,** *34,* 7896–7903.
331. Hamilton-Miller, J. M. T., Shah, S. *Int. Antimicrob. Agent* **1996,** *7,* 97–99.
332. Berners Price, S. J.; Johnson, R. K.; Giovenella, A. J.; Faucette, L. F.; Mirabelli, C. K.; Sadler, P. J. *J. Inorg. Biochem.* **1988,** *33,* 285–295.
333. Nomiya, K.; Tsuda, K.; Sudoh, T.; Oda, M. *J. Inorg. Biochem.* **1997,** *68,* 39–44.
334. Lee, A. R.; Huang, W. H. *J. Pharm. Pharmacol.* **1995,** *47,* 503–509.
335. Fricker, S. P. *Toxicol. In Vitro* **1994,** *8,* 879–881.
336. Martin, C. *Chem. Br.* **1997,** *33,* 35–38.
337. Urbina, J. A.; Payares, G.; Molina, J.; Sanoja, C.; Liendo, A.; Lazardi, K.; Piras, M. M.; Piras, R.; Perez, N.; Wincker, P.; Ryley, J. F. *Science* **1996,** *273,* 969–971.
338. Sanchez-del Grado, R. A.; Lazardi, K.; Rincon, L.; Urbina, J. A.; Hubert, A. J.; Noels, A. N. *J. Med. Chem.* **1993,** *36,* 2041–2043.
339. Sanchez-del Grado, R. A.; Navarro, M.; Perez, H.; Urbina, J. A. *J. Med. Chem.* **1996,** *39,* 1095–1099.
340. Cantos, G.; Barbieri, C. L.; Iacomini, M.; Gorin, P. A. J.; Travassos, L. R. *Biochem. J.* **1993,** *289,* 155–160.
341. Roberts, W. L.; Berman, J. D.; Rainey, P. M. *Antimicrob. Agent Chemother.* **1995,** *39,* 1234–1239.
342. Goldberg, D. E.; Sharma, V.; Oksman, A.; Gluzman, I. Y.; Wellems, T. E.; Piwnica-Worms, D. *J. Biol. Chem.* **1997,** *272,* 6567–6572.
343. Sharma, V.; Beatty, A.; Goldberg, D. E.; Piwnica-Worms, D. *Chem. Commun.* **1997,** 2223–2224.

344. Golenser, J.; Tsafack, A.; Amichai, Y.; Libman, J.; Shanzer, A.; Cabantchik, Z. I. *Antimicrob. Agent Chemother.* **1995,** *39,* 61–65.
345. Albrechtgary, A. M.; Libman, J.; Shanzer, A. *Pure Appl. Chem.* **1996,** *68,* 1243–1247.
346. Behm, C. A.; Boreham, P. F. L.; Creaser, I. I.; Korybut-Daskiewicz, B.; Maddalena, D. J.; Sargeson, A. M.; Snowdon, G. M. *Aust. J. Chem.* **1995,** *48,* 1009–1030.
347. Behm, C. A.; Creaser, I. I.; Korybut-Daskiewicz, B.; Geue, R. J.; Sargeson, A. M.; Walker, G. W. *J. Chem. Soc. Chem. Commun.* **1993,** 1844–1845.
348. De Clercq, E. *J. Med. Chem.* **1995,** *38,* 2491–2517.
349. Raynaud, M.; Chermann, J. C.; Plata, F.; Jasmin, C.; Mathé, G. *C. R. Acd. Sci. Paris* **1971,** *272,* 347–348.
350. Rozenbaum, W.; Dormont, D.; Spire, B. Vilmer, E.; Gentilini, N.; Griscelli, C.; Montagnier, L.; Barre-Sinoussi, F.; Cherman, J. C. *Lancet* **1985,** *1,* 450–451.
351. Moskovitz, B. L. *Antimicrob. Agents Chemother.* **1988,** *32,* 1300–1303.
352. Rhule, J. T.; Hill, C. L.; Judd, D. A. *Chem. Rev.* **1998,** *98,* 327–357.
353. Hill, C. L.; Hartnup, M.; Faraj, M.; Weeks, M.; Prosser-McCartha, C. M.; Brown Jr., R. B.; Kadkhodayan, M.; Sommadossi, J.-P.; Schinazi, R. F. In "Advances in Chemotherapy of AIDS," Diasio, R. B. and Sommadossi, J.-P., Ed., pp. 33–41; 1990.
354. Inoye, Y.; Tokutake, Y.; Yoshida, T.; Yoshiko, S.; Hujita, H.; Dan, K.; Yamamoto, A.; Nishiya, S.; Yamase, T.; Nakamura, S. *Antiviral Res.* **1993,** *20,* 317–331.
355. Judd, D. A.; Hill, C. L., Schinazi, R. F. *Antiviral Chem. Chemother.* **1994,** *5,* 410–414.
356. Yamamoto, N.; Schols, D.; De Clercq, E.; Debyser, Z.; Pauwels, R.; Balzarini, J.; Nakashima, H.; Baba, M.; Hosoya, M.; Snoeck, R.; Neyts, J.; Andrei, G.; Murrer, B. A.; Theobald, B.; Bossard, G.; Henson, G.; Abrams, M.; Picker, D. *Mol. Pharmacol.* **1992,** *42,* 1109–1117.
357. Ikeda, S.; Neyts, J.; Yamamoto, N.; Murrer, B.; Theobald, B.; Bossard, G.; Henson, G.; Abrams, M.; Picker, D.; De Clercq, E. *Antiviral. Chem. Chemother.* **1993,** *4,* 253–262.
358. De Clercq, E. *Biomed. Pharmacother.* **1996,** *50,* 207–215.
359. Ni, L.; Boudinot, F. D.; Boudinot, F. D.; Henson, G. W.; Bossard, G. E.; Martellucci, S. A.; Ash, P.; Fricker, S. P.; Darkes, M. C.; Theobald, B. R. C.; Hill, C. L.; Schinazi, R. F. *Antimicrob. Agents Chemother.* **1994,** *38,* 504–510.
360. Ni, L.; Greenspan, P.; Gutman, R.; Kelloes, C.; Farmer, M. A.; Boudinot, F. D. *Antiviral Res.* **1996,** *32,* 141–148.
361. Cholewa, M.; Legge, G. J. F.; Weigold, H.; Holan, G.; Birch, C. J. *Life Sci.* **1994,** *54,* 1607–1612.
362. Kim, G.-S.; Judd, D. A.; Hill, C. L.; Schinazi, R. F. *J. Med. Chem.* **1994,** *37,* 816–820.
363. Sarafianos, S. G.; Kortz, U.; Pope, M. T.; Modak, M. J. *Biomed. J.* **1996,** *319,* 619–626.
364. Hill, C. J.; Weeks, M. S.; Schinazi, R. F. *J. Med. Chem.* **1990** *33,* 2767–2772.
365. De Clercq, E.; Yamamoto, N.; Pauwels, R.; Baba, M.; Schols, D.; Nakashima, H.; Balzarini, J.; Debyser, Z.; Murrer, B. A.; Schwartz, D.; Thornton, D.; Bridger, G.; Fricker, S.; Henson, G.; Abrams, M.; Picker, D. *Proc. Natl. Acad. Sci. USA.* **1992,** *89,* 5286–5290.
366. De Clercq, E.; Yamamoto, N.; Pauwels, R.; Balzarini, J.; Witvrouw, M.; Devreese, K.; Debyser, Z.; Rosenwirth, B.; Peichl, P.; Datema, R.; Thornton, D.; Skerlj, R.;

Gaul, F.; Padmanabhan, S.; Bridger, G.; Bridger, G.; Henson, G.; Abrams, M. *Antimicrob. Agents Chemother.* **1994,** *38,* 668–674.
367. Donzella, G. A.; Schols, D.; Lin, S. W.; Este, J. A.; Nagashima, K. A.; Maddon, P. J.; Allaway, G. P.; Sakmar, T. P.; Henson, G.; De Clercq, E.; Moore, J. P. *Nature Med.* **1998,** *4,* 72–77.
368. Bridger, G. J.; Skerlj, R. T.; Devreese, K.; Pauwels, R.; Declercq, E. *J. Med. Chem.* **1996,** *39,* 109–119.
369. Bridger, G. J.; Skerlj, R. T.; Thornton, D.; Padmanabhan, S.; Martellucci, S. A.; Henson, G. W.; Abrams, M. J.; Yamamoto, N.; Devreese, K.; Pauwels, R.; De Clercq, E. *J. Med. Chem.* **1995,** *38,* 366–378.
370. Devreese, K.; Reymen, D.; Griffin, P.; Steinkasserer, A.; Werner, G.; Bridger, G. J.; Este, J.; James, W.; Henson, G. W.; DesMyster, J.; Anne, J.; De Clercq, E. *Antiviral. Res.* **1996,** *29,* 209–219.
371. Devreese, K.; Koflermongold, V.; Leutgeb, C.; Weber, V.; Vermeire, K.; Schacht, S.; Anne, J.; De Clercq, E.; Datema, R.; Werner, G. *J. Virol.* **1996,** *70,* 689–696.
372. Inouye, Y.; Kanamor, T.; Yoshida, T.; Bu, X.; Shinoya, M.; Koike, T.; Kimura, E. *Biol. Pharmacol. Bull.* **1994,** *17,* 243–250.
373. Inouye, Y.; Kanamor, T.; Yoshida, T.; Koike, T.; Shinoya, M.; Fujioka, H.; Kimura, E. *Biol. Pharmacol. Bull.* **1996,** *19,* 456–458.
374. Inouye, Y.; Kanamori, T.; Sugiyama, M.; Yoshida, T.; Koike, T.; Shionoya, M.; Enomoto, K.; Suehiro, K.; Kimura, E. *Aniviral Chem. Chemother.* **1995,** *6,* 337–344.
375. Nation, D. A.; Reibenspies, J.; Martell, A. E. *Inorg. Chem.* **1996,** *35,* 4597–4603.
376. Koike, T.; Inoue, M.; Kimura, E.; Shiro, M. *J. Am. Chem. Soc.* **1996,** *118,* 3091–3099.
377. Green, L. M.; Berg, J. M. *Proc. Natl. Acad. Sci. USA* **1990,** *87,* 6403–6407.
378. Summers, M. F. *J. Cell Biochem.* **1991,** *45,* 41–48.
379. Otsuka, M.; Fujita, M.; Sugiura, Y.; Ishii, S.; Aoki, T.; Yamamoto, T.; Inoue, J. *J. Med. Chem.* **1994,** *37,* 4267–4269.
380. Otsuka, M.; Fujita, M.; Aoki, T.; Ishii, S.; Sugiura, Y.; Yamamoto, T.; Inoue, J. *J. Med. Chem.* **1995,** *38,* 3264–3270.
381. Fujita, M.; Otsuka, M.; Sugiura, Y. *J. Med. Chem.* **1996,** *39,* 503–507.
382. Rice, W. G.; Schaeffer, C. A.; Harten, B.; Villinger, F.; South, T. L.; Summers, M. F.; Henderson, L. E.; Bess, J. W.; Arthur, L. O.; McDougal, J. S.; Orloff, S. L.; Mendeleyev, J.; Kun, E. *Nature,* **1993,** *361,* 473–475.
383. Mathe, G.; Misset, J. L.; Gil-Delgrado, M.; Musset, M.; Reizenstein, P.; Canon, C. *Biomed. Pharmacother.* **1986,** *40,* 383–385.
384. Roveix, B.; Zayyo, J. F.; Rajagopalan, P.; Lavacher, M.; Girard, P. M.; Fusselier, M. *Int. J. Immunopharmacol.* **1988,** *10* (Suppl. 1), 36.
385. Zhang, Z.-Y.; Reardon, I. M.; Hui, J. O.; O'Connell, K. L.; Poorman, R. A.; Tomasselli, A. G.; Heinrikson, R. L. *Biochemistry,* **1991,** *30,* 8717–8721.
386. Ojwang, J. O.; Buckheit, R. W.; Pommier, Y.; Mazumder, A.; Devreese, K.; Este, J. A.; Reymen, D.; Pallansch, L. A.; Lackmansmith, C.; Wallace, T. L.; De Clercq, E.; McGrath, M. S.; Rando, R. F. *Antimicrob. Agents Chemother.* **1995,** *39,* 2426–2435.
387. Bishop, J. S.; Guycaffey, J. K.; Ojwang, J. O.; Smith, S. R.; Hogan, M. E.; Cossum, P. A.; Rando, R. F.; Chaudhary, N. *J. Biol. Chem.* **1996,** *271,* 5698–5703.
388. De Clercq, E. *Metal-Based Dugs* **1997,** *4,* 173–192.
389. Esté, J. A.; Schols, D.; De Vreese, K.; Cherepanov, P.; Witvrouw, M.; Panne-

couque, C.; Debyse, Z.; Rando, R. F.; Desmyter, J.; De Clercq, E. *Mol. Pharmacol.* **1997,** *52,* 98–104.
390. Pratviel, G.; Bernadou, J.; Meunier, B. *Adv. Inorg. Chem.* **1998,** *45,* 251–231.
391. Pitie, M.; Casas, C.; Lacey, C. J.; Prativiel, G.; Bernadou, J.; Meunier, B. *Angew. Chemie Int. Ed. Eng.* **1993,** *32,* 557–559.
392. Bigey, P.; Pratiel, G.; Meunier, B. *J. Chem. Soc. Chem. Commun.* **1995,** 181–182.
393. Bigey, P.; Pratiel, G.; Meunier, B. *Nucleic Acids Res.* **1995,** *23,* 3894–3900.
394. Pratviel, G.; Bernadou, J.; Meunier, B. *Met. Ions Biol. Sys.* **1996,** *33,* 399–426.
395. Pratviel, G.; Pitie, M.; Bernadou, J.; Meunier, B. *Nucleic Acids Res.* **1991,** *19,* 6283–6288.
396. Pitie, M.; Pratviel, G.; Bernadou, J.; Meunier, B. *Proc. Natl. Acad. Sci. USA* **1992,** *89,* 3967–3971.
397. Mestre, B.; Jakobs, A.; Pratviel, G.; Meunier, B. *Biochemistry* **1996,** *35,* 9140–9149.
398. Mestre, B.; Jakobs, A.; Pratviel, G.; Meunier, B. *Biochemistry* **1996,** *35,* 9140–9149.
399. Mestre, B.; Pitie, M.; Loup, C.; Claparols, C.; Pratviel, G.; Meunier, B. *Nucleic Acids Res.* **1997,** *25,* 1022–1027.
400. Duarte, V.; Pratviel, G.; Meunier, B.; Berton, M.; Sixou, S.; Favre, G. *N. J. Chem.* **1997,** *21,* 55–60.
401. Duarte, V.; Sixou, S.; Favre, G; Pratviel, G.; Meunier, B. *J. Chem. Soc. Dalton Trans.* **1997,** 4113–4118.
402. Karlstrom, A. R.; Levine, R. L. *Proc. Natl. Acad. Sci. USA* **1991,** *88,* 5552–5556.
403. Liu, J. K.; Shigenaga, M. K.; Yan, L. J.; Mori, A.; Ames, B. N. *Free Rad. Res.* **1996,** *24,* 461–472.
404. Davis, D. A.; Branca, A. A.; Pallenberg, A. J.; Marschner, T. M.; Patt, L. M.; Chatlynne, L. G.; Humphrey, R. W.; Yarchoan, R.; Levine, R. L. *Arch. Biochem. Biophy.* **1995,** *322,* 127–134.
405. Perrin, D. M.; Pearson, L.; Mazumder, A.; Sigman, D. S. *Gene* **1994,** *149,* 173–178.
406. Davies, II, J. F.; Hostomska, Z.; Hostomsky, Z.; Jordan, S. R.; Matthews, D. A. *Science* **1991,** *252,* 88–95.
407. Mahamood, N.; Burke, A.; Hussain, S.; Anner, R. M.; Anner, B. M. *Antiviral Chem. Chemother.* **1995,** *6,* 187–189.
408. Coluccia, M.; Boccarelli, A.; Cermelli, C.; Portolani, M.; Natile, G. *Metal-Based Drugs* **1995,** *2,* 271–292.
409. Balcarova, Z.; Kasparkova, J.; Zakovska, A.; Novakova, O.; Sivo, M. F.; Natile, G.; Brabec, V. *Mol. Pharmacol.* **1998,** *53,* 846–855.
410. Okada, T.; Patterson, B. K.; Ye, S. Q.; Gurney, M. E. *Virology* **1993,** *192,* 631–642.
411. Tepperman, K.; Zhang, Y.; Roy, P. W.; Floyd, R.; Zhao, Z.; Dorsey, J. G.; Elder, R. C. *Metal-Based Drugs* **1994,** *1,* 433–443.
412. Best, S. L.; Sadler, P. J. *Gold Bull.* **1996,** *29,* 87–93.
413. Shaw, III, C. F. *Comments Inorg. Chem.* **1989,** *8,* 233–267.
414. Fricker, S. P. *Gold Bull.* **1996,** *29,* 53–60.
415. Mazid, M. A.; Razi, M. T.; Sadler, P. J.; Greaves, G. N.; Hurman, S. J.; Koch, M. H. J.; Philips, J. C. *J. Chem. Soc. Chem. Commun.* **1980,** 1261–1262.
416. Elder, R.; Ludwig, K.; Cooper, J. N.; Eidsness, M. K. *J. Am. Chem. Soc.* **1985,** *107,* 5024–5025.
417. Isab, A. A.; Sadler, P. J. *J. Chem. Soc. Dalton Trans.* **1981,** 1657–1663.
418. Schröter, I.; Stráhle, J. *Chem. Ber.* **1991,** *124,* 2161–2164.
419. Bau, R. *J. Am. Chem. Soc.* **1998,** *120,* 9380–9381.

420. Graham, G. G.; Haavisto, T. M.; McNaught, P. J. *J. Rheumatol.* **1982,** *9,* 527–531.
421. Elder, R. C.; Jones, W. B.; Zhao, Z.; Dorsey, J. G.; Tepperman, K. *Metal-Based Drugs* **1994,** *1,* 363–374.
422. Ni Dhubhgaill, O. M.; Sadler, P. J.; Tucker, A. *J. Am. Chem. Soc.,* **1992,** *114,* 1118–1120.
423. Shaw, III, C. F.; Isab, A. A.; Hoeschele, J. D.; Starich, M.; Locke, J.; Schulteis, P.; Xiao, J. *J. Am. Chem. Soc.* **1994,** *116,* 2254–2260.
424. Christodoulou, J.; Sadler, P. L.; Tucker, A. *FEBS Lett.* **1995,** *376,* 1–5.
425. Mallya, S. K.; van Wart, H. E. *J. Biol. Chem.* **1989,** *264,* 1594–1601.
426. Snyder, R. M.; Mirabelli, C. K.; Crooke, S. T. *Semin. Arthritis Rheum.* **1987,** *17,* 71–80.
427. Handel, M. L.; Watts, C. K. W.; DeFazio, A.; Day, R. O.; Sutherland, R. L. *Proc. Natl. Acad. Sci. USA* **1995,** *92,* 4497–4501.
428. Griem, P.; Gleichmann, E. *Zeitsch. Rheumatol.* **1996,** *55,* 348–358.
429. Verwilghen, J.; Kingsley, G. H.; Gambling, L.; Panayi, G. S. *Arthritis Rheum.* **1992,** *35,* 1413–1418.
430. Romagnoli, P.; Spinas, G. A.; Sinigaglia, F. *J. Clin. Investig.* **1992,** *89,* 254–258.
431. Best, S. J.; Chattopadhyay, T. K.; Djuran, M. I.; Palmer, R. A.; Sadler, P. J.; Sovago, I.; Varnagy, K. *J. Chem. Soc. Dalton Trans.* **1997,** 2587–2596.
432. Hardy, M. M.; Flickinger, A. G.; Riley, D. P.; Weiss, R. H.; Ryan, U. A. *J. Biol. Chem.* **1994,** *269,* 18535–18540.
433. Faulkner, K. M.; Liochev, S. I.; Fridovich, I. *J. Biol. Chem.* **1994,** *269,* 23471.
434. Liochev, S. I.; Fridovich, I. *Arch. Biochem. Biophys.* **1995,** *321,* 271–275.
435. Szabo, C.; Day, B. J.; Salzman, A. L. *FEBS Lett.* **1996,** *381,* 82–86.
436. Gardner, P. R.; Nguyen, D.-D. H.; White, C. W. Arch. *Biochem. Biophys.* **1996,** *325,* 20–28.
437. Joester, K. E.; Jung, G.; Weber, U.; Weser, U. *FEBS Lett.* **1972,** *25,* 25–28.
438. deAlvare, L. R.; Goda, K.; Kimura, T. *Biochem. Biophy. Res. Commun.* **1976,** *69,* 687–695.
439. Nagano, T.; Hirano, T.; Hirobe, M. *J. Bio. Chem.* **1989,** *264,* 9243–9249.
440. Weiss, R. H.; Flickinger, A. G.; Rivers, W. J.; Hardy, M. M.; Aston, K. W.; Ryan, U. S.; Riley, D. P. *J. Biol. Chem.* **1993,** *268,* 23049–23054.
441. Riley, D. P.; Weiss, R. H. *J. Am. Chem. Soc.* **1994,** *116,* 387–388.
442. Black, S. C.; Schasteen, C. S.; Weiss, R. H.; Riley, D. P.; Driscoll, E. M.; Lucchesi, B. R. *J. Pharmacol. Exp. Ther.* **1994,** *270,* 1208–1215.
443. Riley, D. P.; Henke, S. L.; Lennon, P. J.; Weiss, R. H.; Neumann, W. L.; Rivers, W. J.; Aston, K. W.; Sample, K. R.; Rahman, H.; Ling, C. S.; Shieh, J. J.; Busch, D. H.; Szulbinski, W. *Inorg. Chem.* **1996,** *35,* 5213–5231.
444. Marla, S. S.; Lee, J.; Groves, J. T. *Proc. Natl. Acad. Sci. USA* **1997,** *94,* 14243–14246.
445. Groves, J. T.; Lee, J. B.; Marla, S. S. *J. Am. Chem. Soc.* **1997,** 119, 6269–6273.
446. Hunt, J. A.; Lee, J. B.; Groves, J. T. *Chem. Biol.* **1997,** *4,* 845–858.
447. Stern, M. K.; Jensen, M. P.; Kramer, K. *J. Am. Chem. Soc.* **1996,** *118,* 8735–8736.
448. Salvemini, D.; Wang, Z.-Q.; Stern, M. K.; Currie, M. G.; Misko, T. P. *Proc. Natl. Acad. Sci. USA* **1998,** *95,* 2659–2663.
449. Melov, S.; Schneider, J. A.; Day, B. J.; Hinderfeld, D.; Coskun, P.; Mirra, S. S.; Crapo, J. D.; Wallace, D. C. *Nature Gene* **1998,** *18,* 159–163.
450. Lee, J.; Hunt, J. A.; Groves, J. T. *Bioorg. Med. Chem. Lett.* **1997,** *7,* 2913–1918.
451. Baxter, G. F. *Chem. Br.* **1992,** *28,* 445–448.

452. Barrie, P. J.; Djuran, M. I.; Mazid, M. A.; McPartlin, M.; Sadler, P. J.; Scowen, I. J.; Sun, H. *J. Chem. Soc. Dalton Trans.* **1996,** 2417–2422.
453. Sun, H.; Li, H.; Sadler, P. J. *Coord. Chem. Rev.* **1999,** *185–186,* 689–709.
454. Asato, E.; Katsura, K.; Mikuriya, M.; Turpeinen, U.; Mutikainen, I.; Reedijk, J. *Inorg. Chem.* **1995,** *34,* 2447–2454.
455. Sadler, P. J.; Sun, H. *J. Chem. Soc. Dalton Trans.* **1995,** 1395–1401.
456. Clitherow, J. W. *UK Pat. Appl. GB2220937A,* 1990.
457. Lacey, L. F.; Frazer, N. M.; Keene, O. N.; Smith, J. T. L. *Eur. J. Clin. Pharmacol.* **1994,** *47,* 177–180.
458. Lee, S. P. *Res. Commun. Chem. Pathol.* **1981,** *34,* 359.
459. Diemer, R.; Keppler, B. K.; Dittes, U.; Nuber, B.; Seifried, V.; Opferkuch, W.; *Chem. Ber.* **1995,** *128,* 335–342.
460. Diemer, R.; Dittes, U.; Nuber, B.; Seifried, V.; Opferkuch, W.; Keppler, B. K. *Metal-Based Drugs.* **1995,** *2,* 271–292.
461. Sun, H.; Li, H.; Sadler, P. J. *Chem. Ber./Recueil* **1997,** *130,* 669–681.
462. Webb, M. In "Metallothionein II, Proceedings of the 2nd International Meeting on Metallothionein and Other Low Molecular Weight Metal-Binding Proteins," Kägi, J. H. R., and Kojima Y., Ed., pp. 109–134; Birkhäuser-Verlag: Basel, 1987.
463. Sun, H.; Li, H.; Harvey, I.; Sadler, P. J. submitted for publication.
464. Li, H.; Sadler, P. J.; Sun, H. *J. Biol. Chem.* **1996,** *271,* 9483–9489.
465. Sadler, P. J.; Sun, H.; Li, H. *Chem. Eur. J.* **1996,** *2,* 701–708.
466. Nenini, S.; Pypniewski, W. R.; Wilson, K. S.; Ciurli, S.; Mangani, S. *J. Biol. Inorg. Chem.* **1998,** *3,* 268–273.
467. Asato, E.; Kamamuta, K.; Akamine, Y.; Fukami, T.; Nukada, R.; Mikuriya, Deguchi, S.; Yokota, Y. *Bull. Chem. Soc. Jpn.* **1997,** *70,* 637–648.
468. Cade, J. F. J. *Med. J. Aust.* **1949,** *36,* 349–352.
469. "Lithium: Inorganic Pharmacology and Psychiatric Use," Birch N. J., Ed.; IRL Press: Oxford, 1988.
470. Atack, J. R.; Broughton, H. B.; Pollack, S. J. *Trends Neurosci.* **1995,** *18,* 343–349.
471. Emilien, G.; Maloteaux, J. M.; Seghers, A.; Charles, G. *Arch. Int. Pharmacodyn. Ther.* **1995,** *330,* 251–278.
472. Atack, J. R. *Med. Res. Rev.* **1997,** *17,* 215–224.
473. Dixon, J. F.; Georgyi, V. L.; Hokin, L. E. *Proc. Natl. Acad. Sci. USA* **1994,** *91,* 8358–8362.
474. Shute, J. K.; Baker, R.; Billington, D. C.; Gani, D. *J. Chem. Soc. Chem. Commun.* **1988,** 626–627.
475. Bone, R.; Springer, J. P.; Atack, J. R. *Proc. Natl. Acad. Sci. USA* **1992,** *89,* 10031–10035.
476. Bone, R.; Frank, L.; Springer, J. P.; Pollack, S. J.; Osborne, S.; Atack, J. R.; Knowles, M. R.; McAllister, G.; Ragan, C. I.; Broughton, H. B.; Baker, R.; Fletcher, S. R. *Biochemistry* **1994,** *33,* 9460–9467.
477. Bone, R.; Frank, L.; Springer, J. P. Atack; J. R. *Biochemistry* **1994,** *33,* 9468–9476.
478. Pollack, S. J.; Atack, J. R.; Knowles, M. R.; McAllister, G.; Ragan, C. I.; Baker, R.; Fletcher, S. R.; Iversen, L. L.; Broughton, H. B. *Proc. Natl. Acad. Sci. USA* **1994,** *91,* 5766–5770.
479. Wilkie, J.; Cole, A. G.; Gani, D. *J. Chem. Soc. Perkin Trans. I* **1995,** 2709–2727.
480. Klein, P. S.; Melton, D. A. *Proc. Natl. Acad. Sci. USA* **1996,** *93,* 8455–8459.
481. Margoshes, M.; Vallee, B. L. *J. Am. Chem. Soc.* **1957,** *79,* 4813–4814.
482. Kägi, J. H. R. In "Metallothionein," Suzuki, K. T., Imura, N., and N Kimura, I., Eds., pp. 29–55; Birkhauser-Verlag: Basel, 1993.

483. Kille, P.; Hemmings, A.; Lunney, E. A. *Biochim. Biophys. Acta* **1994,** *1205,* 151–161.
484. Uchida, Y.; Takio, K.; Titani, K.; Ihara, Y.; Tomonaga, M. *Neuron* **1991,** *7,* 337–347.
485. Sewell, A. K.; Jensen, L. T.; Erickson, J. C.; Palmiter, R. D.; Winge, D. R. *Biochemistry* **1995,** *34,* 4740–4747.
486. Bogumil, R.; Faller, P.; Pountney, D. L.; Vāsák, M. *Eur. J. Biochem.* **1996,** *238,* 698–705.
487. Assaf, S. Y.; Chung, S.-H. *Nature* **1984,** *308,* 734–736.
488. Howell, G. A.; Welch, M. G.; Frederickson, C. J. *Nature* **1984,** *308,* 736–738.
489. Koh, J. Y.; Choi, D. W. *Neurosci.* **1994,** *60,* 1049–1057.
490. Koh, J. Y.; Suh, S. W.; Gwag, B. J.; He, Y. Y.; Hsu, C. Y.; Choi, D. W. *Science* **1996,** *272,* 1013–1016.
491. Aschner, M.; Cherian, M. G.; Klaassen, C. D.; Palmiter, R. D.; Erickson, J. C.; Bush, A. I. *Toxicol. Appl. Pharmacol.* **1997,** *142,* 229–242.
492. Brown, D. R.; Qin, K. F.; Herms, J. W.; Madlung, A.; Manson, J.; Strome, R.; Fraser, P. E.; Kruck, T.; von Bohlen, A.; Schulz-Schaeffer, W.; Giese, A.; Westaway, D.; Kretzschmar, H. *Nature* **1997,** *390,* 684–687.
493. Stockel, J.; Safar, J.; Wallace, A. C.; Cohen, F. E.; Prusiner, S. B. *Biochemistry* **1998,** *37,* 7185–7193.
494. Goodwill, K. E.; Sabatier, C.; Marks, C.; Raag, R.; Fitzpatrick, P. F.; Stevens, R. C. *Nature Str. Biol.* **1997,** *4,* 578–585.
495. Haavik, J.; Toska, K. *Mol. Neurobiol.* **1998,** *16,* 285–309.
496. Segovia, G.; Mora, F. *Brain Res. Bull.* **1998,** *45,* 275–279.
497. Finch, C. E.; Cohen, D. M. *Exp. Neurol.* **1997,** *143,* 82–102.
498. Rootwelt, T.; Dunn, M.; Yudkoff, M.; Itoh, T.; Almaas, R.; Pleasure, D. *J. Neurochem.* **1998,** *71,* 1544–1553.
499. Clarke, M. J.; Gaul, J. B. *Struct. Bond.* **1993,** *81,* 147–181.
500. Kerwin, J. F.; Lancaster, J. R.; Feldman, P. L. *J. Med. Chem.* **1995,** *38,* 4343–4362.
501. Tuzel, I. H. *J. Clinic Pharmacol.* **1974,** *14,* 494–503.
502. Glidewell, C.; Johnson, I. L. *Inorg. Chim. Acta* **1987,** *132,* 145–147.
503. Campbell, J. M.; McCrae, F.; Reglinski, J.; Wilson, R.; Smith, W.E.; Sturrock, R. D. *Biochem. Biophys. Acta* **1993,** *1156,* 327–333.
504. Reglinski, J.; Butler, A. R.; Glidewell, C. *Appl. Organomet. Chem.* **1995,** *8,* 25–31.
505. Flitney, F. W.; Megson, I. L.; Thomson, J. L. M.; Kennovin, G. D.; Butler, A. R. *Br. J. Pharmacol.* **1996,** *117,* 1549–1557.
506. Zhou, J. H.; Xi, W.; Hurst, J. K. *Inorg. Chem.* **1990,** *29* 160–167.
507. Davies, N. A.; Wilson, M. T.; Slade, E.; Fricker, S. P.; Murrer, B. A.; Powell, N. A.; Henderson, G. R. *Chem. Commun.* **1997,** 47–48.
508. Fricker, B. A.; Slade, E.; Powell, N. A.; Vaughan, O. J.; Henderson, G. R.; Murrer, B. A.; Megson, I. L.; Bisland, S. K.; Flitney, F. W. *Br. J. Pharmacol.* **1997,** *122,* 1441–1449.
509. Kazimierski, W. M.; Wolberg, G.; Wilson, J. G.; Smith, S. R.; Williams, D. S.; Horp, H. H.; Molina, L. *Proc. Natl. Acad. Sci. USA* **1996,** *93,* 9138–9141.
510. Articles in *Mol. Cell. Biochem.* Vol. 153, 1995.
511. Orvig, C.; Thompson, K. H.; Battell, M.; McNeil, J. H. *Met. Ions Biol. Syst.* **1995,** *31,* 575–594.
512. Shechter, Y.; Karlish, S. J. D. *Nature,* **1980,** *286,* 556–558.
513. Dubyak, G. R.; Kleinzeller, A. *J. Biol. Chem.* **1980,** *255,* 5306–5312.
514. Heyliger, C. E.; Tahiliani, A. G.; McNeill, J. H. *Science,* **1985,** *227,* 1474–1477.

515. Sakurai, H.; Tsuchiya, K.; Nukatsuka, M.; Sofue, M.; Kawada, J.; Ishikawa, S.; Yoshida, H.; Komazawa, K. *J. Clin. Biochem. Nutr.* **1990,** *8,* 193–200.
516. Watanabe, H.; Nakai, M.; Komazawa, K.; Sakurai, H. *J. Med. Chem.* **1994,** *37,* 876–877.
517. Sakurai, H.; Fujii, K.; Watanabe, H.; Tamura, H. *Biochem. Biophys. Res. Commun.* **1995,** *214,* 1095–1101.
518. Fujimoto, S.; Fujii, K.; Yasui, H.; Matsushita, R.; Takada, J.; Sakurai, H. *J. Clin. Biochem. Nutr.* **1997,** *23,* 113–129.
519. Shaver, A.; Ng, J. B.; Hall, D. A.; Soo, Lum, B. ; Posner, B. I. *Inorg. Chem.* **1993,** *32,* 3109–3113.
520. Posner, B. I.; Faure, R.; Burgess, J. W.; Bevan, A. P.; Lachance, D.; Zhang-Sun, G.; Fantus, I. G.; Ng, J. B.; Hall, D. A.; Soo, Lum, B.; Shaver, A. *J. Biol. Chem.* **1994,** *269,* 4596–4604.
521. Cran, D. C.; Keramidas, A. D.; Hoover-Litty, H.; Anderson, O. P.; Miller, M. M.; Lemoine, L. M.; Pleasic-Williams, S.; Vandenberg, M.; Rossomando, A. J.; Sweet, L. J. *J. Am. Chem. Soc.* **1997,** *119,* 5447–5448.
522. McNeill, J. H.; Yuen, V. G.; Hoveyda, H. R.; Orvig, C. *J. Med. Chem.* **1992,** *35,* 1489–1491.
523. Yuen, V. G.; Orvig, C.; McNeill, J. H. *Can. J. Physiol. Pharmacol.* **1995,** *73,* 55–64.
524. Caravan, P.; Gelmini, L.; Glover, N.; Herring, F. G.; Li, H.; McNeil, J. H.; Rettig, S. J.; Setyawati, I. A.; Shuter, E.; Sun, Y.; Tracey, A. S.; Yuen, V. G.; Orvig, C. *J. Am. Chem. Soc.* **1995,** *117,* 12759–12770.
525. Sun, Y.; James, B. R.; Rettig, S. J.; Orvig, C. *Inorg. Chem.* **1996,** *35,* 1667–1673.
526. Tracey, A. S.; Gresser, M. J. *Proc. Natl. Acad. Sci. USA* **1986,** *83,* 609–613.
527. Toepfer, E. W.; Mertz, W.; Polansky, M. M.; Roginski, E. E.; Wolf, W. R. *J. Agr. Food Chem.* **1977,** *25,* 162–168.
528. Haylock, S. J.; Buckley, P. D.; Blackwell, L. F. *J. Inorg. Biochem.* **1983,** *19, 105–117.*
529. Evans, G. W.; Pouchnik, D. J. *J. Inorg. Biochem.* **1993,** *49,* 177–187.
530. Broadhurst, C. L.; Schmidt, W. F.; Reeves, III, F. B.; Polansky, M. M.; Gautschi, K.; Anderson, R. A. *J. Inorg. Biochem.* **1997,** *66,* 119–130.
531. Kingry, K. F.; Royer, A. C.; Vincent, J. B. *J. Inorg. Biochem.* **1998,** *72,* 79–88.
532. Stearns, D. M.; Wise, J. P.; Patierno, S. R.; Wetterhahn, K. E. *FASEB J.* **1995,** *9,* 1643–1649.
533. Stearns, D. M.; Belbruno, J. J.; Wetterhahn, K. E. *FASEB J.* **1995,** *9,* 1650–1657.
534. Stearns, D. M.; Belbruno, J. J.; Wetterhahn, K. E. *FASEB J.* **1995,** *9,* 142–153.
535. Goto, Y.; Kida, K. *Jpn. J. Pharmacol.* **1995,** *67,* 365–368.
536. Davis, C. M.; Vincent, J. B. *Biochemistry* **1997,** *36,* 4382–4385.
537. Antsyshkina, A. S.; Porai-Koshits, M. A.; Arkhangelskii, I. V.; Diallo, I. N. *Zh. Neorg. Khim.* **1987,** *32,* 2928–2932.
538. Davis, C. M.; Royer, A. C.; Vincent, J. B. *Inorg. Chem.* **1997,** *36,* 5316–5320.
539. Matsumoto, J. *Med. Hypotheses* **1994,** *43,* 177–182.
540. Goto, Y.; Kida, K.; Ikeuchi, M.; Kaino, Y.; Matsuda, H. *Biochem. Pharmacol.* **1992,** *44,* 174–177.
541. Li, J. P.; Elberg, G.; Gefel, D.; Shechter, Y. *Biochemistry* **1995,** *34,* 6218–6225.
542. Hossain, M. B.; Jalal, M. A. F.; van der Helm, D. *Acta Crystallogr. C* **1986,** *42,* 1305–1310.

543. Olivieri, N. F.; Brittenham, G. M.; McLaren, C. E.; Templeton, D. M.; Cameron, R. G.; McClelland, R. A.; Burt, A. D.; Fleming, K. A. *N. Engl. J. Med.* **1998,** *339,* 417–423.
544. Dobbin, P. S.; Hider, R. C.; Hall, A. D.; Taylor, P. D.; Sarpong, P.; Porter, J. B.; Xiao, G. Y.; van Derhelm, D. *J. Med. Chem.* **1993,** *36,* 2448–2458.
545. Rai, B. L.; Dekhordi, L. S.; Khodr, H.; Jin, Y.; Liu, Z. D.; Hider, R. C. *J. Med. Chem.* **1998,** *41,* 3347–3359.
546. Molenda, J. J.; Jones, M. M.; Basinger, M. A. *J. Med. Chem.* **1994,** *37,* 93–98.
547. Molenda, J. J.; Jones, M. M.; Johnston, D. S.; Walker, E. M.; Cannon, D. J. *J. Med. Chem.* **1994,** *37,* 4363–4370.
548. Baret, P.; Beguin, C. G.; Boukhalfa, H.; Caris, C.; Laulhere, J. P.; Pierre, J. L.; Serratrice, G. *J. Am. Chem. Soc.* **1995,** *117,* 9760–9761.
549. Serratrice, G.; Boukhalfa, H.; Beguin, C.; Baret, P.; Caris, C.; Pierre, J. L. *Inorg. Chem.* **1997,** *36,* 3898–3910.
550. Rakba, N.; Aouad, F.; Henry, C.; Caris, C.; Morel, I.; Baret, P.; Pierre, J. L.; Brissot, P.; Ward, R. J.; Lescoat, G.; Crichton, R. R. *Biochem. Pharmacol.* **1998** *55,* 1797–1806.
551. Durbin, P. W.; Kullgren, B.; Xu, J.; Raymond, K. N. *Radiat. Prot. Dosim.* **1998,** *79,* 433–443.
552. Whisenhunt, D. W.; Neu, M. P.; Hou, Z. G.; Xu, J.; Hoffman, D.C.; Raymond, K. N. *Inorg. Chem.* **1996,** *35,* 4128–4136.
553. Evertsson, B. *Acta Crystallogr. B* **1969,** *25,* 30–32.
554. Christodoulou, J.; Danks, D. M.; Sarkar, B.; Baerlocher, K. E.; Casey, R.; Horn, N.; Tumer, Z.; Clarke, J. T. R. *Am. J. Med. Gene.* **1998,** 76, 154–164.
555. Sikic, B. I.; Rosencweig, M.; Carter, S. K., Eds. "Bleomycin Chemotherapy"; Academic Press: Orlando, FL, 1985.
556. Sam, J. W.; Takahashi, S.; Lippai, I.; Peisach, J.; Rousseau, D. L. *J. Biol. Chem.* **1998,** *273,* 16090–16097.
557. Hecht, S. M. *Bioconjug. Chem.* **1994,** *5,* 513–526.
558. Takahashi, S.; Sam, J. W.; Peisach, J.; Rousseau, D. L. *J. Am. Chem. Soc.* **1994,** *116,* 4408–4413.
559. Loeb, K. E.; Zaleski, J. M.; Westre, T. E.; Guajardo, R. J.; Mascharak, P. K.; Hedman, B.; Hodgson, K.O.; Solomon, E. I. *J. Am. Chem. Soc.* **1995,** *117,* 4545–4561.
560. Stubbe, J.; Kozarich, J. W.; Wu, W.; Vanderwall, D. E. *Acc. Chem. Res.* **1996,** *29,* 322–330.
561. Husken, B. C. P.; De Jong, J.; Beekman, B.; Onderwater, R. C. A.; Vandervijgh, W. J. F.; Bast, A. *Cancer Chemother. Pharmacol.* **1995,** *37,* 35–62.
562. Duda, A. M.; Kowalik-Jankowska, T.; Kozlowski, H.; Kupka, T. *J. Chem. Soc. Dalton Trans.* **1995,** 2909–2913.
563. Kubiak, M.; Duda, A. M.; Ganadu, M. L.; Kozlowski, H. *J. Chem. Soc. Dalton Trans.* **1996,** 1905–1908.
564. Fan, J-Y.; Sun, D.; Yu, H.; Kerwin, S. M.; Hurley, L. H. *J. Med. Chem.* **1995,** *38,* 408–424.
565. Yu, H.; Hurtley, L. H.; Kerwin, S. M. *J. Am. Chem. Soc.* **1996,** *118,* 7040–7048.
566. Bal, W.; Dyba, M.; Kasprzykowski, F.; Kozlowski, H.; Latajka, R.; Lankiewicz, L.; Mackiewicz, Z.; Pettit, L. D. *Inorg. Chim. Acta* **1998,** *283,* 1–11.
567. Valensin, G.; Maccotta, A.; Gaggelli, E.; Grzonka, Z.; Kasprzykowski, F.; Kozlowski, H. *Eur. J. Biochem.* **1996,** *240,* 118–124.
568. Ohkawa, J.; Koguma, T.; Kohda, T.; Taira, K. *J. Biochem.* **1995,** *118,* 251–258.

569. Kiehntopf, M.; Esquivel, E. L.; Brach, M. A.; Herrmann, F. *J. Mol. Med.-JMM* **1995,** *73,* 65–71.
570. Kiehntopf, M.; Brach, M. A.; Herrmann, F. *Onkol.* **1995,** *18,* 180–187.
571. Pyle, A. M. *Met. Ions Biol. Sys.* **1996,** *32,* 479–520.
572. Shannon, R. D. *Acta Cryst.* **1976,** *A32,* 751–767.
573. Fletcher, J. I.; Smith, R.; O'Donghue, S. I.; Nilges, M.; Connor, M.; Howden, M. E. H.; Christie, M. J.; King, G. F. *Nature Str. Biol.* **1997,** *4,* 553–558.
574. Becket, R. P.; Davidson, A. H.; Drummond, A. H.; Huxley, P.; Whittaker, M. *Drug Discovery Today* **1996,** *1,* 16–26.
575. Wojtowiczpraga, S.; Low, J.; Marshall, J.; Ness, E.; Dickson, R.; Barter, J.; Sale, M.; McCann, P.; Moore, J.; Cole, A.; Hawkins, M. J. *Investig. New Drugs* **1996,** *14,* 193–202.
576. Grams, F.; Crimmin, M.; Hinnes, L.; Huxley, P.; Pieper, M.; Tschesche, H.; Bode, W. *Biochemistry* **1995,** *34,* 14012–14020.
577. Rockwell, A.; Melden, M.; Copeland, R. A.; Hardman, K.; Decicco, C. P.; DeGrado, W. F. *J. Am. Chem. Soc.* **1996,** *118,* 10337–10338.
578. Chapman, K. T.; Kopka, I. E.; Durrette, P. L.; Esser, C. K.; Lanza, T. J.; Izquierdo-Martin, M.; Niedzwieki, L. M.; Chang, B.; Harrison, R. K.; Kuo, D. W.; Lin, T.-Y.; Stein, R. L.; Hagmann, W. K. *J. Med. Chem.* **1993,** *36,* 4293–4301.
579. Brown, F. K.; Brown, P. J.; Bickett, D.; Chambers, C. L.; Davies, H. G.; Deaton, D. N.; Drewry, D.; Foley, M.; McElroy, A. B.; Gregson, M.; McGeehan, G. M.; Myers, P. L.; Norton, D.; Salovich, J. M.; Schoenen, F. J.; Ward, P. *J. Med. Chem.* **1994,** *37,* 674–688.
580. Gowravaram, M. R.; Tomczuk, B. E.; Johnson, J. S.; Delecki, D.; Cook, E. R.; Ghose, A. K.; Mathiowetz, A. M.; Spurlino, J. C.; Rubin, B.; Smith, D. L.; Pulvino, T.; Wahl, R. C. *J. Med. Chem.* **1995,** *38,* 2570–2581.
581. Tomczuk, B. E.; Gowavaram, M. R.; Johnson, J. S.; Delecki, D.; Cook, E. R.; Ghose, A. K.; Mathiowetz, A. M.; Spurlino, J. C.; Rubin, B.; Smith, D. L.; Pulvino, T.; Wahl, R. C. *Bioorgan. Med. Chem. Lett.* **1995,** *5,* 343–348.
582. Brenner, B. M.; Ballerman, B. J.; Gunning, M. E.; Zeidel, M. L. *Physiol. Rev.* **1990,** *70,* 665–700.
583. Kenny, A. J.; Stephenson, S. L. *FEBS Lett.* **1988,** *232,* 1–9.
584. Soubrier, F.; Alhenc-Gelas, F.; Huber, C.; Allegrini, J.; John, M.; Tregear, G.; Corvol, P. *Proc. Natl. Acad. Sci. USA* **1988,** *85,* 9386–9390.
585. Stanton, J. L.; Sperbeck, D. M.; Trapani, A. J.; Cote, D.; Sakane, Y.; Berry, C.; Ghai, R. D. *J. Med. Chem.* **1993,** *36,* 3829–3833.
586. Fournie-Zaluski, M. C.; Copic, P.; Turcaud, S.; Rousselet, N.; Gonzalez, W.; Barbe, B.; Pham I.; Jullian, N.; Michel, J. B.; Roques, B. P. *J. Med. Chem.* **1994,** *37,* 1070–1083.
587. Coric, P.; Turcaud, S.; Meudal, H.; Roques, B. P.; Fourine-Zaluski, M. C. *J. Med. Chem.* **1996,** *39,* 1210–1219.
588. Fink, C. A.; Qiao, Y.; Berry, C. J.; Sakane, Y.; Ghai, R. D.; Trapani, A. J. *J. Med. Chem.* **1995,** *38,* 5023–5030.
589. Fink, C. A.; Carlson, J. E.; McTaggart, P. A.; Qiao, Y.; Webb, R.; Chatelain, R.; Jeng, A. Y.; Trapani, A. J. *J. Med. Chem.* **1996,** *39,* 3158–3168.
590. Robl, J. A.; Cimarusti, M. P.; Simpkins, L. M.; Brown, B.; Ryono, D. E.; Bird, J. E.; Asaad, M. M.; Schaeffer, T. R.; Trippodo, N. C. *J. Med. Chem.* **1996,** *39,* 494–502.
591. Zhang, F. L.; Fu, H. W.; Casey, P. J.; Bishop, W. R. *Biochemistry,* **1996,** *35,* 8166–8171.

592. Nagasu, T.; Yoshimatsu, K.; Rowell, C.; Lewis, M. D.; Garcia, A. M. *Cancer Res.* **1995,** *55,* 5310–5314.
593. Vigushin, D. M.; Poon, G. K.; Boddy, A.; English, J.; Halbert, G. W.; Pagonis, C; Jarman, M.; Coombes, R. C. *Cancer Chemother. Pharmacol.* **1998,** *42,* 111–117.
594. Szekeres, T.; Fritzer-Szekeres, M.; Elford, H. L. *Critical Rev. Clin. Lab. Sci.* **1997,** *34,* 503–528.
595. Gandhi, V.; Plunkett, W.; Kantarjian, H.; Talpaz, M.; Robertson, L. E.; O'Brien, *S. J. Clin. Oncol.* **1998,** *16,* 2321–2331.
596. Beitler, J. J.; Smith, R. V.; Haynes, H.; Silver, C. E.; Quish, A.; Kotz, T.; Serrano, M.; Brook, A.; Wadler, S. *Investig. New Drugs* **1998,** *16,* 161–169.
597. Rutschmann, O. T.; Opravil, M.; Iten, M.; Malinverni, R.; Vernazza, P. L.; Bucher, H.; Bernasconi, E.; Perrin, L. H.; Yerly, S.; Hirschel, B. *Antiviral Ther.* **1998,** *3,* 65–67.
598. Liuzzi, M.; Déziel, R.; Moss, N.; Beaulleu, P.; Bonneau, A. M.; Bousquet, C.; Chafouleas, J. G.; Garneau, M.; Jaramillo, J.; Krogsrud, R. L.; Lagacé, L.; McCollum, R. S.; Nawoot, S.; Guindon, Y. *Nature,* **1994,** *372,* 695–698.
599. Newton, A. C. *J. Biol. Chem.* **1995,** *270,* 28495–28498.
600. Gong, C. X.; Singh, T. J.; Grundke-Iqbal, I.; Iqbal, K. *J. Neurochem.* **1994,** *62,* 803–806.
601. Gong, C. X.; Shaikh, S.; Grlundke-Iqbal, I.; Iqbal, K. *Brain Res.* **1996,** *741,* 95–102.
602. Kissinger, C. R.; Parge, H. E.; Knighton, D. R.; Lewis, C. T.; Pelletier, L. A; Tempczyk, A.; Kalish, V. J.; Tucker, K. D.; Showalter, R. E.; Moomaw, E. W.; Gastinel, L. N.; Habuka, N.; Chen, X. H.; Maldonado, F.; Barker, J. E.; Bacquet, R.; Villafranca, J. E. *Nature* **1995,** *378,* 641–644.
603. Cardenas, M. E.; Muir, R. S.; Breuder, T.; Heitman, J. *EMBO J.* **1995,** *14,* 2772–2783.
604. Onuma, H.; Lu, Y. F.; Tomizawa, K.; Moriwaki, A.; Tokuda, M.; Hatase, O.; Matsui, H. *Neurosci. Res.* **1998,** *30,* 313–319.
605. Tokime, T.; Nozaki, K.; Kikuchi, H. *Neurosci. Lett.* **1996,** *206,* 81–84.
606. Tatlock, J. H.; Linton, M. A.; Hou, X. J.; Kissinger, C. R.; Pelletier, L. A.; Showalter, R. E.; Tempczyk, A.; Villafranca, J. E. *Bioorg. Med. Chem. Lett.* **1997,** *7,* 1007–1012.
607. Barton, S. J.; Barnham, K. J.; Habtemariam, A.; Sadler, P. J.; Sue, R. E. *Inorg. Chim. Acta* **1998,** *273,* 8–13;
608. Gabriel, J. C. P.; Nagarajan, R.; Natarajan, S.; Cheetham, A. K.; Rao, C. N. R. *J. Solid State Chem.* **1997,** *129,* 257–262.
609. Barnham, K. J.; Berners-Price, S. J.; Frenkiel, T. A.; Frey, U.; Sadler, P. J. *Angew. Chem. Int. Ed. Engl.* **1995,** *34,* 1874–1877.
610. Bednarski, P. J. *J. Inorg. Biochem.* **1995,** *60,* 1–19.
611. Jestin, J. L.; Chottard, J. C.; Frey, U.; Laurenczy, G.; Merbach, A. E. *Inorg. Chem.* **1994,** *33,* 4277–4282.
612. Miller, S. E.; House, D. A. *Inorg. Chim. Acta,* **1991,** *187,* 125–132.
613. Bancroft, D. P.; Lepre, C. A.; Lippard, S. J. *J. Am. Chem. Soc.* **1990,** *112,* 6860–6871.
614. Berners-Price, S. J.; Frenkiel, T. A.; Frey, U.; Ranford, J. D.; Sadler, P. J. *J. Chem. Soc. Chem. Commun.* **1992,** 789–790.
615. Appleton, T. G.; Hall, J. R.; Ralph, S. F.; Thompson, C. S. M. *Inorg. Chem.* **1989,** *28,* 1989–1993.
616. Martin, R. B. *Am. Chem. Soc. Sym. Ser.* **1983,** *209,* 231–244.
617. Arpalahti, J.; Lehikoinen, P. *Inorg. Chem.* **1990,** *29,* 2564–2567.

618. Guo, Z.; Chen, Y.; Zang, E.; Sadler, P. J. *J. Chem. Soc. Dalton Trans.* **1997,** 4107–4111.
619. "CRC Handbook of Chemistry and Physics," Lide, D. R. and Frederikse, H. P. R., Eds.; CRC Press: Boca Raton, 1993.
620. Smith, P. H.; Brainard, J. R.; Morris, D. E.; Jarvinen, G. D.; Ryan, R. R. *J. Am. Chem. Soc.* **1989,** *111,* 7437–7443.
621. Cacheris, W. P.; Quay, S. C.; Rocklage, S. M. *Magn. Reson. Imaging* **1990,** *8,* 467–481.
622. Zhang, X.; Chang, C. A.; Brittain, H. G.; Garrison, J. M.; Telser, J.; Tweedle, M. F. *Inorg. Chem.* **1992,** *31,* 5597–5600.
623. Sessler, J. L.; Mody, T. D.; Hemmi, G.; Lynch, V.; Young, S.; Miller, R. A. *J. Am. Chem. Soc.* **1993,** *115,* 10368–10369.
624. Kang, S. I.; Ranganathan, R. S.; Emswiler, J. E.; Kumar, K.; Gougoutas, J. E.; Malley, M. F.; Tweedle, M. F. *Inorg. Chem.* **1993,** *32,* 2912–2918.
625. Uggeri, F.; Aime, S.; Anelli, P. L.; Botta, M.; Brocchetta, M.; Dehaen, C.; Ermondi, G.; Grandi, M.; Paoli, P. *Inorg. Chem.* **1995,** *34,* 633–642.
626. Lauffer, R. B.; Brady, T. J.; Brown, R. D.; Baglin, C.; Koenig, S. H. *Magn. Reson. Med.* **1986,** *3,* 541–548.
627. Rocklage, S. M.; Cacheris, W. P.; Quay, S. C.; Hahn, F. E.; Raymond, K. N. *Inorg. Chem.* **1989,** *28,* 477–485.
628. Powell, D. H.; Ni Dhubhghaill, O. M.; Pubanz, D.; Helm, L.; Lebedev, Y. S.; Schlaepfer, W.; Merbach, A. E. *J. Am. Chem. Soc.* **1996,** *118,* 9333–9346.
629. Tirkkonen, B.; Aukrust, A.; Couture, E.; Grace, D.; Haile, Y.; Holm, K. M.; Hope, H.; Larsen, A.; Lunde, H. S.; Sjogren, C. E. *Acta Radiol.* **1997,** *38,* 780–789.
630. De Clercq, E. *Metal-Based Drugs,* **1997,** *4,* 173–192.
631. Mazumder, A.; Neamati, N.; Ojwang, J. O.; Sunder, S.; Rando, R. F.; Pommier, Y. *Biochemistry* **1996,** *35,* 13762–13771.
632. Guo, Z; Sadler, P. J. *Angew. Chem. Int. Ed.* **1999,** *38,* 1512–1531.
633. "Uses of inorganic chemistry in medicine," Farrell, N. P., Ed.; Royal Society of Chemistry: Cambridge, **1999.**
634. "Medicinal inorganic chemistry" special issue of *Chem. Rev.* **1999,** in press.
635. "Cisplatin-chemistry and biochemistry of a leading anticancer drug," B. Lippert, Ed.; Wiley-VCH, Weinheim, **1999.**
636. Ohndorf, U.-M.; Rould, M. A.; He, Q.; Pabo, C.; Lippard, S. J. *Nature* **1999,** *399,* 708–712.
637. Gupta, A.; Matsui, K.; Lo, J. F.; Silver, S. *Nature Medicine* **1999,** *5,* 183–188.
638. Micskei, K.; Helm, L.; Brücher, E.; Merbach, A. E. *Inorg. Chem.* **1993,** *32,* 3844–3850.

ADVANCES IN INORGANIC CHEMISTRY, VOL. 49

THE COBALT(III)-PROMOTED SYNTHESIS OF SMALL PEPTIDES

REBECCA J. BROWNE, DAVID A. BUCKINGHAM, CHARLES R. CLARK, and PAUL A. SUTTON

The Department of Chemistry, University of Otago, Dunedin, New Zealand.

I. Introduction

This chapter comes about because of our long silence on criticisms leveled at the titled method since our first reports in 1981 (*1*, *2*). We were well aware, as early as 1967 (*3*, *4*), of some epimerization in the

Copyright © 2000 by Academic Press.
All rights of reproduction in any form reserved.
0898-8838/00 $30.00

Co(III)-chelated amino acid ester reactant and/or peptide product (Scheme 1). This basic difficulty was quickly pointed out (*5*), and has subsequently been examined and commented upon by others (*6*, *7*). Such criticisms are well-founded since epimerization (or racemization) is a common problem, at least to some degree, in all chemical methods of synthesis where acyl-activation is employed. As a result, metal-activation methods have received little attention. However, since 1981 we have refined the Co(III) method such that very fast, clean, couplings can now be carried out using Λ-[Co(en)$_2$((*S*)-AAOMe)]$^{3+}$ reagents, which involve minimal ($\leq$2%) epimerization/racemization provided experimental conditions are strictly adhered to.

We do not claim that the Co(III) method is superior to modern methods of chemical synthesis. However it does provide an alternative. The Co(III)-active ester, once made, can be stored for long periods of time, it provides both N-terminal protection and carbonyl-*O* activation in the one system, it is orange in color ($\varepsilon_{480} \simeq 100\ M^{-1}\ cm^{-1}$), generally quite water soluble (it is a "salt"), and the Co(III) metal plus ancillary ligands can easily be removed by chemical or electrochemical ($\sim$1.0 V vs SCE) reduction methods.

In this chapter we outline the historical development of the Co(III) method and give many of the details, especially those relating to epimerization, which have remained unpublished for so long.

II. Genealogy

The possibility of using a Co(III) metal center to promote the chemical synthesis of small peptides had its origins during the Australian summer of 1967, when one of us was attempting to prepare β-[Co(trien)(GlyOEt)$_2$]$^{3+}$ (containing two cis N-coordinated glycine residues) by adding excess freshly prepared GlyOEt to β_2-[Co(trien)Cl(GlyOEt)](ClO$_4$)$_2$ dissolved in DMF. A very rapid (seconds) color change from claret-red to orange-yellow took place, consistent with the anticipated product, but elemental analysis of the crystallized tris-ClO_4^- salt (and many recrystallized samples) was not in accord with expectation.

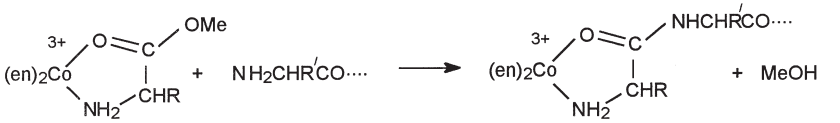

Scheme 1.

Also, an ^{1}H-NMR spectrum (obtained on a new 60-MHz spectrometer) did not give the correct ester: glycine-CH_2 peak area ratios. The following day the reaction was repeated, this time using β-[Co(trien)(TBP)$_2$]$^{3+}$, prepared by treating β-[Co(trien)(N$_3$)$_2$]ClO_4 with solid $NOClO_4$ in dry tri(*n*-butyl)phosphate (note that this reaction would not now be allowed since both reagents are potentially *very* explosive). However, the result was the same—the color was right, but the elemental analysis was not. Inspiration then arrived. It was already known from Searle's PhD work (*8*) that these β-trien complexes were very susceptible to losing monodentate acido ligands under mildly alkaline (aqueous) conditions. This suggested that in a nonaqueous medium the rapid amine-induced loss of Cl^- or TBP might lead to a carbonyl-*O*-bound ester intermediate and that this could undergo rapid aminolysis by a second GlyOEt residue (Scheme 2). It was already known from the study by Alexander and Busch (*9*) that such chelated esters hydrolyzed rapidly in aqueous solution (see Section III). Elemental analysis, ^{1}H-NMR, and a crystal structure of the $(ClO_4)_3 \cdot H_2O$ salt of **1** now agreed (*10*), and we were, of course, delighted. In order to establish that the reaction did indeed take place on the metal and that no scrambling of residues had taken place, a ^{14}C-label was introduced into the first glycine residue (**2**) and both the chelated dipeptide complex and unreacted GlyOEt as well as the subsequently hydrolyzed β_2-[Co(trien)(Gly)]$^{2+}$ product were examined for their ^{14}C content (*3*). The results confirmed both the stepwise nature of the reaction and the separate identities of the two amino acid residues. Subsequently, the carbonyl-*O*-bound ester complex (**3**)

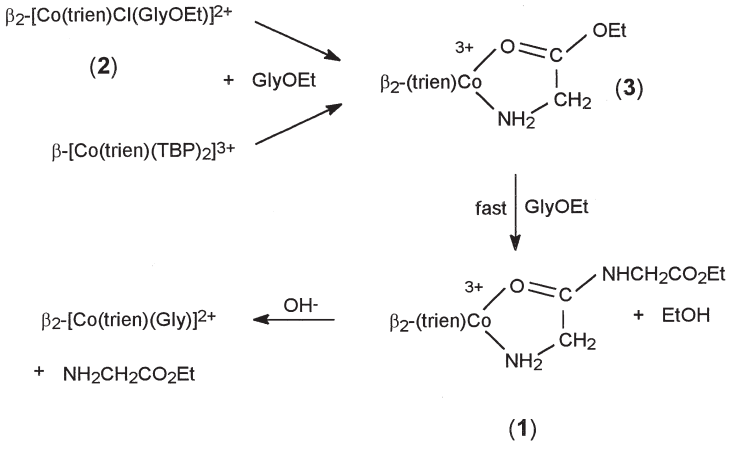

SCHEME 2.

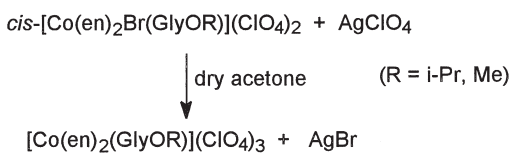

SCHEME 3.

was isolated in solid form by treating $[Co(en)_2Br(GlyOR)](ClO_4)_2$ with $AgClO_4$ in dry acetone (R = Me, i-Pr; Scheme 3) and its reactions with several amino acid and dipeptide esters as well as with Gly-GlyOEt and Gly-Gly-GlyOEt examined in anhydrous acetone, sulfolane, and Me_2SO (Scheme 4) (*4*, *11*). All reactions were fast, being complete within 1 min at 20°C, and the stability of the reactant chelated ester and dipeptide product was commented on in this publication. It was subsequently shown by using carbonyl-^{18}O-labeled GlyOMe that coordination to the metal was via this atom rather than via the alternative alcohol-O and that such attachment was maintained throughout the hydrolysis and aminolysis reactions, i.e., that carbonyl-*O* did not detach at any stage (*12*).

Then, during the early 1970s Dekkers, a PhD student from Sydney, found that the reaction of $[Co(en)_2(GlyOi\text{-}Pr)](ClO_4)_3$ with GlyOEt in Me_2SO occurred in two stages and determined the rate laws for both the addition of amine and loss of i-PrOH steps (cf. Section VI) as well as investigated the properties of the "tetrahedral" intermediate in alkaline and acidic aqueous solution (*13*). He also prepared a large number of $[Co(en)_2(AA\text{-}AA'OEt)]^{3+}$ dipeptide complexes (AA = Gly, Ala) and validated these by elemental analysis, ^1H-NMR, and optical rotational methods (*14*). He found that the Λ-Co(III) enantiomer (AA = Gly) or diastereomer (AA = (S)-Ala) was more reactive than its Δ-counterpart toward condensations with (*S*)-AlaOEt, (*S*)-ValOEt, and (*S*)-PheOEt. Substantial inversion of configuration occurred in the chelated S-Ala fragment when reactions were carried out in Me_2SO or MeOH in the absence of protonated amine. These stereose-

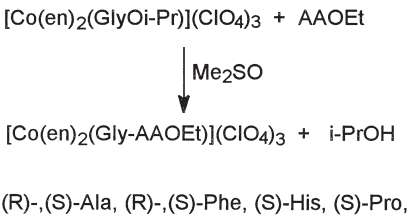

SCHEME 4.

lective and epimeric effects were shown to be of kinetic rather than thermodynamic origin. Dekkers was the first to uncover these factors, although his work in this area has remained largely unpublished. However, no attempt was made to quantify the effects at that time.

Because of the high level of acyl activation imparted by the Co(III) center doubts had been raised in our minds, and in the minds of others (*5*), as to the potential of the method for the synthesis of optically pure peptides. Epimerization is a problem common to all "chemical" methods of synthesis (*15*). In addition to direct activation of the carbonyl function the metal ion also enhances C–H acidity at the α-carbon atom through the additional binding of the amine nitrogen, and proton exchange at carbon will almost certainly result in some loss of chirality, if not to complete racemization. We were well aware of this possibility in 1967 (*4*) and this prompted a study of proton exchange and epimerization in Co(III)-chelated amino acid carboxylate systems (*16*); this work was extended once it was known that diastereomeric preferences for reprotonation of the resulting carbanion could be realized in some cases (*17*). However, it was found that moderately alkaline aqueous conditions were necessary for rapid proton loss in the carboxylate systems, and it was thought that the rate of amine addition to the ester under mild conditions in aprotic solvents would be fast enough to beat out epimerization. But we were wrong. Although we knew from Dekkers' work that epimerization had occurred in the nonbuffered reaction of $[Co(en)_2((S)\text{-AlaOMe})]^{3+}$ with AA′OEt (AA′ = Gly, (*S*)-Ala, (*S*)-Phe) and that this was more marked for the Δ-Co(III) isomer, we believed that this had occurred in the dipeptide product, since this retains both the carbonyl-O attachment to the metal and the 3+ charge and was present in the basic reaction medium for considerable periods of time.

Extension of this research was then delayed until two of us had returned to New Zealand. One of the first jobs of Tasker, a PhD student from Brisbane, was to use ^{3}H-labeling methods to examine epimerization. At that time we were under the impression that reprotonation of carbanion intermediates would be diffusion controlled, as was subsequently reported for phenylglycine in phosphate buffers (*18*), so that no isotopic discrimination against ^{3}H would be present. But then Wautier *et al.* reported (*6*) the complete loss of chirality in $[Co(tren)(AA\text{-}(S)\text{-}AA'OMe)]^{3+}$, prepared by treating $[Co(tren)((S)\text{-}AAOMe)]^{3+}$ (AA = Ala, Leu) generated *in situ* in MeOH with (*S*)-AA′OMe (AA′ = Leu, His, Ala, Val), although their reaction times and temperatures (1–15 h; sometimes 35–50°C) and other experimental conditions ([Co(III)] ~0.1 *M*; [*N*-ethylmorpholine salt of *p*-toluene sul-

fonate] ~1 *M*) seemed fairly harsh. However, these authors did show that deuterium incorporation into $[Co(en)_2(GlyOMe)]^{3+}$ in MeOD was very much faster than we had anticipated (25°C, $t_{1/2}$ = 19 s, pH 9.8), so that the necessity of examining this problem in more detail became critical. Tasker showed by using reversed phase-HPLC separations (*19*) that only small amounts of ^3H (0.1–0.3%) were incorporated into $[Co(en)_2((S)\text{-Thr(Bzl)-GlyOMe})]^{3+}$ and β_2-$[Co(trien)((S)\text{-Ala-Gly-Gly-OBzl})]^{3+}$ during their synthesis in an Et_3N-buffered Me_2SO solvent, so we thought we were still in good shape. We had (wrongly, as it turned out) assumed that these numbers represented maximum amounts of inversion, since reprotonation with retention of configuration would still involve ^3H incorporation, and it remained to be seen whether the numbers related only, or in major amount, to the slower reacting Δ-diastereomer. Further results on this saga are reported below. More recently Mensi and Isied have reported (*7*) some 18% inversion during the reaction of $[Co(en)_2((S)\text{-PheOMe})]^{3+}$ with (*S*)-PheOMe (Scheme 5) under conditions described by Tasker (*19*), but once again the reaction time (20 min) seemed too long, and the diastereomer property was not examined.

Tasker developed better methods of preparing the parent amino acid chelates, being successful with 19 of the 20 naturally occurring amino acids as well as with a few others (e.g., β-alanine, sarcosine). At about this time (1980) we also developed methods for synthesizing amino acid ester chelates for amino acids other than glycine. Many earlier attempts had been made to do this by preparing monodentate ester complexes similar to that with glycine, (cf. Scheme 2), but try as we might we were not successful via the Meisenheimer method (*20*) or variants on it (*21–23*). However, such experiments culminated in the use of CF_3SO_3Me. This was shown to be a most efficient alkylating agent of coordinated carboxyl groups and was found to be nondestructive of the complex and side-chain protecting groups. Sutton subsequently extended this work to include the esterification of the Met(O), Met(CH_3), and Cys(CH_2Ph) amino acid chelates (*24*) (cf. Section III,B). These developments opened the way to the synthesis of a wide range of di- and longer chain peptide units (*1*) and culminated in the synthesis of Leu[5]enkaphalin (*2*, *25*).

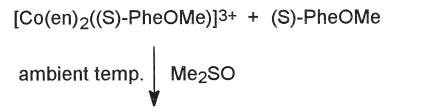

SCHEME 5.

A major contribution was the separation of the Δ- and Λ-isomers of many of the amino acid chelates and looking at changes in stereochemistry following methylation with CF_3SO_3Me and on subsequent reaction with various AA′OMe (*24*). Methods were developed for carrying out the coupling reactions with the minimum amount of epimerization, and studies began to determine reaction rates and rate laws for the aminolysis and epimerization pathways under the conditions of synthesis. This work is continuing (*26*). The most important results from these two investigations are reported in this chapter for the first time. During the 1980s several other Otago students investigated other ancillary Co(III) amino acid systems: Brown (1983) prepared a number of complexes in the Co(tren) system where both *p*- and *t*-isomers are possible; Fairbrother (1984) did likewise using the Co(trien) system, where β_1- and β_2-isomers were the easiest to prepare; Garnham (1982) and Binney (1984) both contributed toward an understanding of amide production on the reaction of $[Co(en)_2(AlaOMe)]^{3+}$ with ethylenediamine (*27*); Deva (1982) and Tasker developed reversed-phase liquid chromatographic methods for separating Δ- and Λ-isomers (*28*). Then, in the 1990s, Lorimer (1990) made a thorough study of ^3H incorporations into both the reactant esters and dipeptide product during the Δ- and Λ-$[Co(en)_2((S)\text{-AlaOMe})]^{3+}$ + (*S*)-AlaOMe couplings. More recently, Rogers has shown that $[Co(cyclen)(OH_2)OH]^{2+}$ and $[Co(N\text{-Mecyclen})(OH_2)OH]^{2+}$ readily react with amino acids to form chelates and has carried out exploratory condensations using their esterified derivatives. All these investigations have led to a better appreciation of some particular aspect of the Co(III)-promoted peptide synthesis method. In particular, it appears that the $Co(en)_2$ system is the most robust under the coupling conditions, with the tetra-ammine, trien, tren, cyclen, and *N*-Mecyclen systems all giving rise to particular problems, often related to reactant decomposition.

III. Synthetic Approaches

A. Amino Acid Chelates

Amino acids coordinated to $(en)_2Co(III)$ centers are the most useful in peptide synthesis, and general routes to the preparation of these important *N,O*-chelates are described below. Many of the corresponding trien complexes are also available, usually as β_2 isomers, but $[Co(NH_3)_4(AAO)]^{2+}$ species are less accessible. The $[Co(en)_2(AAO)]^{2+}$ complexes have been reported for 19 of the 20 naturally occurring

α-amino acids of L-configuration (note that these all have the *S*-stereochemistry by the Cahn-Ingold-Prelog convention, except for L-cysteine, which the sequence rules designate as *R*). Only *S*-histidine has failed to give a chelate.

The reaction of *trans*-$[Co(en)_2Br_2]Br$ with an (*S*)-amino acid in the presence of 1 mole equivalent of LiOH is the most useful method for preparing the complexes. The preparations involve reflux in aqueous methanol (20–60 min, *trans*-$[Co(en)_2Br_2]Br$ is insoluble in this medium) and the product often crystallizes from the resulting solution. It usually contains sparingly soluble $[Co(en)_3]Br_3$ as an impurity and this is best removed by ion-exchange chromotography on Dowex cation exchange resin using HCl as eluent. Evaporation of the orange fraction gives the very soluble Δ,Λ-$[Co(en)_2((S)\text{-AAO})]Cl_2$ complex and the diastereoisomeric mixture is readily crystallized as ClO_4^- or I^- salts. This procedure has been used to prepare the Gly, Ala, Val, Leu, Ileu, Phe, Thre, Ser, Lys, Asn, Met, Tyr, Trp, Pro, Glu, and Arg chelates (*14*). Variations on this approach include treating an aqueous solution of $[Co(en)_2(OH_2)OH]^{2+}$ with the (*S*)-amino acid for Gly (*29*, *30*), Ala (*29*, *30*), Val (*29*), Leu (*29*, *30*), Ile (*29*), Phe (*30*), Ser (*30*), and Orn (*31*); the modified Meisenheimer reaction of *trans*-$[Co(en)_2Cl_2]Cl$ with the amino acid for Gly, Ala, Leu, and Phe (*32*); and the reaction of either $[Co(en)_2(OClO_3)_2]ClO_4$ or $[Co(en)_2(OSO_2CF_3)_2]CF_3SO_3$ with the lithium salt of (*S*)-Ala or (*S*)-TyrBzl in sulfolane (*24*). The available evidence suggests that minimal racemization (<0.3%) occurs during these reactions (*24*).

Both Δ,Λ-$[Co(en)_2((S)\text{-Glu})]^{2+}$ and Δ,Λ-$[Co(en)_2((S)\text{-Asp})]^{2+}$ are formed in good yield (*ca.* 80%) on reacting the amino acid with $[Co(en)_2(O_2CO)]^+$ in the presence of activated charcoal (*33*). However, the reported preference for the Λ-*S*-isomer in these reactions has not been substantiated (*17*, *34*). Both protonated and deprotonated (dangling carboxylic acid group ionized) forms are available, with isolation being achieved using the ClO_4^- counterion (*33*). Sargeson and colleagues (*35, 36*) have prepared various Δ,Λ-$[Co(en)_2((S)\text{-AAO})]^{2+}$ complexes (Ala, Val, Tyr, Glu, Asp, Asn, Lys, Met) using *trans*-$[Co(en)_2(OH_2)OH](ClO_4)_2$ in Me_2SO at 80°C followed by ion exchange chromatography. Similarly, the side-chain-protected amino acid chelates Δ,Λ-$[Co(en)_2((S)\text{-SerBzl})]^{2+}$, Δ,Λ-$[Co(en)_2((S)\text{-ThrBzl})]^{2+}$, Δ,Λ-$[Co(en)_2((S)\text{-TyrBzl})]^{2+}$, Δ,Λ-$[Co(en)_2((S)\text{-AspBzl})]^{2+}$, Δ,Λ-$[Co(en)_2((S)\text{-GluBzl})]^{2+}$, Δ,Λ-$[Co(en)_2((S)\text{-LysZ})]^{2+}$ (Z = benzyloxycarbonyl), and Δ,Λ-$[Co(en)_2((S)\text{-ArgNO}_2)]^{2+}$ ions have been synthesized using $[Co(en)_2(Me_2SO)_2](ClO_4)_3$ and the appropriate side-chain-protected amino acid in Me_2SO solution and in the presence of Et_3N or LiOH at 40°C (*1*, *14*,

19). These complexes are readily isolated as their I^- salts. When cysteine acts as a bidentate it prefers *N,S*-attachment to Co(III) in most circumstances (*37*), but the *N,O*-chelate (**4**) is available via oxidation of *N,S*-[$Co(en)_2$(*R*)-Cys]$^{2+}$ in Me_2SO/Ac_2O to the sulfenamide (**5**) and subsequent borohydride reduction of this species (Scheme 6) (*38*). However, cysteine derivatives of the type (*R*)-Cys(*S*-*R′*) (*R′* = Me, CH_2Ph, $CHPh_2$, CPh_3) give *N,O*-[$Co(en)_2$((*R*)-Cys(*S*-*R′*))]$^{2+}$ species directly when reacted with *trans*-[$Co(en)_2Br_2$]Br using the general method described above (*24*), but only the R′ = $CHPh_2$ derivative is useful in peptide synthesis (Section VI).

Crystal structures are available for many $(N)_4Co$–amino acid complexes (Table I). Many of the diastereomers (Δ-*S,* Λ-*S*) in the bis-en series have been resolved using classic crystallization (usually via bromocamphor sulfonate, arsenyl-, or antimonyl-tartrate salts) or ion exchange methods (Table II). Reversed-phase ion-pair HPLC, using aryl phosphate or aryl/alkyl sulfonate ion pairing reagents in MeOH/H_2O eluent, has allowed diastereomer separations to be carried out on analytical amounts (*28*) (Table II).

B. Amino Acid Ester Chelates

1. Preparation

While the synthetic potential of amino acid ester chelates was made apparent by the isolation of [$Co(en)_2$(GlyOMe)]$(ClO_4)_3$ in 1967 (*4*), attempts to prepare the Co(III) complexes by direct acid-catalyzed esterification of [$Co(N)_4$(AAO)]$^{n+}$ species proved only partly successful. Equilibrium mixtures usually resulted for [$Co(en)_2$(AAO)]$^{n+}$ in dry MeOH or EtOH on treatment with HCl_g, $SOCl_2$, PCl_3, PBr_3, BF_3, or MeCOCl (*14*). Prolonged treatment, or heating, usually resulted in extensive decomposition. Similarly, treatment of the amino acid complexes with Et_3OBF_4, $CH(OEt)_3$, or $Me_2C(OMe)_2$ in CH_2Cl_2/Me_2SO so-

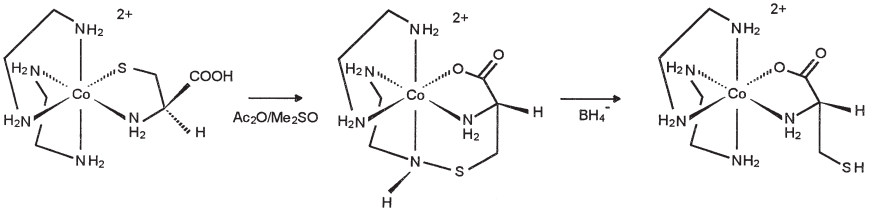

(**5**) (**4**)

Scheme 6.

TABLE I

CRYSTAL STRUCTURES OF $[Co(N)_4(AA)]X_n$ COMPLEXES

Compound	Reference	Compound	Reference
$(+)_{436}$-$[Co(NH_3)_4(N\text{-MeGly})](NO_3)_2$	a	Δ,Λ-α-(RR,RS)-$[Co(trien)(Gly)]I_2 \cdot 3H_2O$	k
Δ-$[Co(en)_2(N\text{-MeGly})]Cl_2$	b	Δ,Λ-β_2-(SR,RS)-$[Co(trien)(Gly)]Cl_2 \cdot H_2O$	l
Δ- and Λ-$[Co(en)_2((S)\text{-Met})](ClO_4)_2 \cdot H_2O$	c	$t(N)$-$[Co(tren)((S)\text{-}NH_2CH(CH_2SO_2)COO)]ClO_4$	m
Λ-$[Co(en)_2((S)\text{-Ala})]S_2O_6$	d	$t(N)$-$[Co(tren)((S)\text{-}NH_2CH(COOH)CH_2SO_2)]Br_2$	m
Λ-$[Co(en)_2((S)\text{-Met})]Br_2$	d	$t(O)$-$[Co(tren)(Gly)](ClO_4)_2$	n
Λ-$[Co(en)_2((S)\text{-MetO})]Cl_2 \cdot CH_3OH$	d	$t(N)$-$[Co(tren)(Gly)]Cl(ClO_4)$	n
Δ-$[Co(en)_2((S)\text{-MetO}_2)](ClO_4)_2$	d	$t(N)$-$[Co(tren)((R,S)\text{-Val})](ClO_4)_2$	o
Δ- and Λ-$[Co(en)_2(Gly)](Sb_2(+)tart)_2 \cdot 4H_2O$	e	$t(N)$-$[Co(tren)((R,S)\text{-Met})]I_2$	p
Λ-$[Co(en)_2((S)\text{-Glu})](ClO_4)_2$	f	$t(N)$-$[Co(tren)((R,S)\text{-norLeu})]X_2$	o, p
Λ-$[Co(en)_2((R)\text{-N-BzGly})]Cl_2$	g	$t(N)$-$[Co(tren)((R,S)\text{-Leu})]I_2$	o
β_2-(R,R,S)-$[Co(trien)((S)\text{-Pro})]I_2$	h	$[Co(N\text{-Mecyclen})((S)\text{-Ala})]X_2$ (five isomers)	q
β_2-(S,S,S)-$[Co(trien)((S)\text{-Pro})]ZnCl_4$	i	$[Co(cyclen)((S)\text{-Ala})]X_2$ (three isomers)	r
Δ-β_1-(R,R + R,S)-$[Co(trien)(Gly)]I_2$	j		

References: (**a**) Larsen, S.; Watson, K. J.; Sargeson, A. M.; Turnbull, K. R. *J. Chem. Soc. Chem. Commun.* **1968,** 847; (**b**) Blount, J. F.; Freeman, H. C.; Sargeson, A. M.; Turnbull, K. R. *J. Chem. Soc. Chem. Commun.* **1967,** 324; (**c**) Saunaullah, G.; Wilson, S.; Glass, R. S. *J. Inorg. Biochem.* **1994,** *68,* 2543; (**d**) ref. *24*; (**e**) Gajhede, M.; Larsen, S. *Acta Cryst.* **1986,** *B42,* 172; (**f**) Gillard, R. D.; Payne, N. C.; Robertson, G. B. *J. Chem. Soc. A* **1970,** 2579; (**g**) Golding, B. T.; Gainsford, G. J.; Herlt, A. J.; Sargeson, A. M. *Angew. Chemie. Int. Ed.* **1975,** *14,* 495; (**h**) Freeman, H. C.; Maxwell, I. E. *Inorg. Chem.* **1970,** *9,* 649; (**i**) Freeman, H. C.; Marzilli, L. G.; Maxwell, I. E. *Inorg. Chem.* **1970,** *9,* 2408; (**j**) Buckingham, D. A.; Cresswell, P. J.; Dellaca, R. J.; Dwyer, M.; Gainsford, G. J.; Marzilli, L. G.; Maxwell, I. E.; Robinson, W. T.; Sargeson, A. M.; Turnbull, K. R. *J. Am. Chem. Soc.* **1974,** *96,* 1713; (**k**) Anderson, B. F.; Bell, J. D.; Buckingham, D. A.; Cresswell, P. J.; Gainsford, G. J.; Marzilli, L. G.; Robertson, G. B.; Sargeson, A. M. *Inorg. Chem.* **1977,** *16,* 3233; (**l**) Buckingham, D. A.; Dwyer, M.; Gainsford, G. J.; Janson Ho, V.; Marzilli, L. G.; Robinson, W. T.; Sargeson, A. M.; Turnbull, K. R. *Inorg. Chem.* **1975,** *14,* 1739; (**m**) Akhter, F. M. D.; Hirotsu, M.; Sugimoto, I.; Kojima, M.; Kashino, S.; Yoshikawa, Y. *Bull. Chem. Soc. Jpn.* **1996,** *69,* 643; (**n**) Mitsui, Y.; Watanabe, J.; Harada, Y.; Sakamaki, T.; Iitaca, Y.; Kushi, Y.; Kimura, E. *J. Chem. Soc. Dalton Trans.* **1976,** 2095; (**o**) Yamanari, K.; Fuyuhiro, A. *Bull. Chem. Soc. Jpn.* **1996,** *69,* 1289; (**p**) Yamanari, K.; Fuyuhiro, A. *Bull. Chem. Soc. Jpn.* **1995,** *68,* 2543; (**q**) Buckingham, D. A.; Clark, C. R.; Rogers, A. J.; Simpson, J. *Aust. J. Chem.* **1998,** *51,* 461; (**r**) Buckingham, D. A.; Clark, C. R.; Rogers, A. J.; Simpson, J. *Inorg. Chem.* **1995,** *34,* 3646.

lution also failed to give the desired product. However, alkylation, using either FSO_3Me or CF_3SO_3Me, provides an efficient general route to methyl ester complexes. Trimethylphosphate solvent is favored for these reactions, with equilibrium methyl group transfer to phosphate oxygen (*39*) providing facile-room temperature alkylation of coordinated carboxylate

$$OP(OMe)_3 + CF_3SO_3Me \rightleftharpoons P(OMe)_4^+ + CF_3SO_3^- . \quad (1)$$

In practice iodide salts of the amino acid complexes are used, as I^- is lost as MeI under conditions of excess alkylating agent.

$$[Co(en)_2((S)\text{-AAO})]I_2 + 3CF_3SO_3Me \rightarrow [Co(en)_2((S)\text{-AAOMe})](CF_3SO_3)_3 + 2MeI. \quad (2)$$

The $[Co(en)_2((S)\text{-AAO})]I_2$ reactants are insoluble in $(MeO)_3PO$, but pass into solution as the reaction proceeds allowing the resulting amino acid ester chelates to be isolated in pure form as triflate salts following MeOH/Et_2O precipitation. The $[HgI_4]^{2-}$, TFA^-, and $CF_3SO_3^-$ salts have also been used successfully. Such reactions are quantitative. Many Δ- and Λ-$[Co(en)_2(AAOMe)](CF_3SO_3)_3$ complexes (AA = (*S*)-SerBzl, (*S*)-ThrBzl, (*S*)-AspBzl, (*S*)-GluBzl, (*S*)-LysZ, (*S*)-$ArgNO_2$ (unresolved Δ,Λ-forms) and Gly, (*S*)-Ala, (*S*)-Val, (*S*)-Leu, (*S*)-Ile, (*S*)-Phe, (*S*)-Trp, (*S*)-Pro, (*S*)-Met(O), (*R*)-Cys(S-$CHPh_2$) (unresolved Δ,Λ- and resolved Δ,Λ-forms)) have been prepared using this approach (*19*, *24*). Likewise for other $[Co(N)_4(AAOMe)](CF_3SO_3)_3$ complexes ($(N)_4$ = trien, AA = Gly, (*S*)-Ala, (*S*)-Leu, (*S*)-Phe; $(N)_4$ = $(NH_3)_4$, AA = Gly, (*S*)-Phe; $(N)_4$, = cyclen, AA = (*S*)-Ala) (*19*).

Protection of sensitive side-chain groups is important; e.g., $[Co(en)_2((S)\text{-Met})]I_2$ is alkylated at sulfur as well as at oxygen under the conditions, whereas the sulfoxide complex $[Co(en)_2((S)\text{-Met}(O))](CF_3SO_3)_2$ is converted cleanly to the corresponding methyl ester complex. Similarly for coordinated cysteine, but with $[Co(en)_2((R)\text{-Cys}(S\text{-}R'))](CF_3CO_2)_2$ complexes (R′ = CH_2Ph, $CHPh_2$, CPh_3), only diphenylmethane substitution fully protects against sulfonium ion formation during the alkylation reaction (*24*). The steric bulk afforded by the $CH(Ph)_2$ group appears to be the reason why thioether in this situation is not attacked, whereas it is in the Met complex. Benzylation offers full protection to side-chain OH and COOH groups. The indole nitrogen in $[Co(en)_2((S)\text{-Trp})]I_2$ is not alkylated on treatment with CF_3SO_3Me but the corresponding Lys complex requires Z-protection. Wautier *et al.* have reported the alkylation of $[Co(tren)(Gly)]Cl_2$ *in situ* using either $(MeO)_2SO_2$ in sulfolane or methyl-*p*-toluenesulfonate in MeOH (*40*); but the $[Co(tren)(AAOMe)]^{3+}$ complexes are more easily prepared using CF_3SO_3Me, as described above. Alkylation is thus far limited to production of amino acid methyl ester complexes, and we comment on this in the "Concluding Remarks" section (Section IX). None of the amino acid ester chelates have been characterized by X-ray crystallography.

2. *Hydrolysis*

It is now almost 50 years since Kroll (*41*) first reported that hydrolysis rates of amino acid esters were accelerated by the addition of certain divalent transition metal ions. His observations prompted numerous studies in this area, but even today exact descriptions of these

TABLE II

RESOLUTION OF Δ,Λ-[Co(en)$_2$((*S*)-AA)]$^{2+}$ IONS

AA	Resolution by crystallization	Resolution by IE chromatography[a]	Resolution by HPLC[a]
Gly	SbO-(*R*)-tart$^-$ salt, Δ-form least sol[b]	—	—
Ala	SbO-(*R*)-tart$^-$ salt, Δ-form least sol[b,c] (+)-BCS$^-$ salt, Λ-form least soluble. Λ-form isolated as SbO-(*S*)-tart$^-$ and I$^-$ salts; I$^-$ salt, Δ-form least sol[e,d]	Dowex 50W-X8, NaCl[e]	RP-C$_{18}$, *p*-toluene phosphate, Δ-form elutes first[f]
Pro	ClO_4^-, AsO-(*R*)-tart$^-$ and I$^-$ salts, Δ-form least sol[c,g,h]	Dowex 50W-X8, NaCl eluent, pH 6.2 phosphate[e,g]	RP-C$_{18}$ *p*-toluene sulfonate, Δ-form elutes first[f]
Leu	(*R*)-tart$^-$ salt.[c,h,i,j] (+)-BCS$^-$ salt, Δ-form least soluble. SbO-(*R*)-tart$^-$ salt, Λ-form least soluble[b]	Dowex 50W-X8, NaCl eluent, Δ-form elutes first[e]	RP-C$_{18}$ *p*-toluene sulfonate, Δ-form elutes first[f]
Ileu	—	—	RP-C$_{18}$, *p*-toluene sulfonate[f]
Val	SbO-(*R*)-tart$^-$ salt, Δ-form least sol,[d,j] Λ-form isolated using SbO-(*S*)-tart$^-$[d,j,k]	Dowex 50W-X2, pH 7 phosphate buffer[l]	RP-C$_{18}$ *p*-toluene sulfonate[f]
Phe	(+)-BCS$^-$ salt, Λ-form least soluble[b]	Sephadex SP C25, pH 7 phosphate buffer; Dowex 50W-X2, SbO-(*R*)-tart$^-$[l,m]	RP-C$_{18}$ *p*-toluene sulfonate[f]
Cys	—	Sephadex SP C25, SbO-(*R*)-tart$^-$; Dowex 50W-X2, NaCl for Cys(Me) deriv[n,e] Sephadex SP C25 with pH 7 phosphate for the Cys(CH(Ph)$_2$) deriv[p]	—
Met	Resolved using SbO-(*R*)-tart$^-$[h,p]	—	Not resolved
Glu	ClO_4^- salt, Λ-form least soluble[p,q]	Dowex 50W or Sephadex with NaCl, HCl or $NaClO_4$[q,r]	RP-C$_{18}$ *p*-toluene sulfonate, *O*-Bzl derivative unresolved[f]
GluNH$_2$	—	Dowex 50W-X8, NaCl, Δ-form elutes first[r]	—
Asp	—	Dowex 50W-X8, NaCl[r]	Not resolved
AspNH$_2$	—	Dowex 50W-X8, NaCl[r]	—
Ser	Resolved using SbO-(*R*)-tart$^-$, I$^-$ salt, Λ-form least soluble[h]	Dowex 50W-X2, phosphate buffer pH 7[s]	RP-C$_{18}$ *p*-toluene sulfonate, OBzl deriv[f]

TABLE II (*Continued*)

AA	Resolution by crystallization	Resolution by IE chromatography[a]	Resolution by HPLC[a]
Thr	Resolved using SbO-(*R*)-tart$^-$, I^- salt, Λ-form least soluble[h]	Dowex 50W-X2, pH 6.8 phosphate buffer; Dowex 50W-X2 HCl[l,t]	RP-C_{18} *p*-toluene sulfonate, OBzl deriv also[f]
Tyr	—	—	RP-C_{18} *p*-toluene sulfonate, OBzl derivative also[f]

[a] Λ-Form eluted first unless otherwise stated.
[b] Ref. (*32*).
[c] Ref. (*14*).
[d] Ref. (*16*).
[e] Keyes, W. E.; Legg, J. I. *J. Am. Chem. Soc.* **1976,** *98,* 4970.
[f] Ref. (*28*) and Buckingham, D. A. *J. Chrom.* **1984,** *313,* 93.
[g] Buckingham, D. A.; Dekkers, J.; Sargeson, A. M.; Wein, M. *Inorg. Chem.* **1973,** *12,* 2019.
[h] Hall, S. K.; Douglas, B. E. *Inorg. Chem.* **1969,** *8,* 372.
[i] Ref. (*21*).
[j] Ref. (*29*).
[k] Shimura, Y. *Bull. Chem. Soc. Jpn.* **1958,** *31,* 315.
[l] Buckingham, D. A.; Clark, C. R.; Wein, M., unpublished data.
[m] Taura, T.; Tamada, H.; Yoneda, H. *Inorg. Chem.* **1978,** *17,* 3127.
[n] Nakazawa, H.; Yamazaki, S.; Yoneda, H. "*36th Annual Meeting of the Chemical Society of Japan,*" Osaka, 1975.
[o] Dunlop, J. H.; Gillard, R. D.; Payne, N. C. *J. Chem. Soc. A* **1967,** 1469.
[p] Ref. (*24*).
[q] Ref. (*34*).
[r] Keyes, W. E.; Caputo, R. E.; Willett, R. D.; Legg, J. I. *J. Am. Chem. Soc.* **1976,** *98,* 6939.
[s] Chong, E. K.; Harrowfield, J. M.; Jackson, W. G.; Sargeson, A. M.; Springborg, J. *J. Am. Chem. Soc.* **1985,** *107,* 2015.
[t] Dabrowiak, J. C.; Cooke, D. W. *Inorg. Chem.* **1975,** *14,* 1305.

exchange-labile systems are lacking. It is known that complexation to Cu^{2+} generally leads to the greatest reactivity, while Zn^{2+}, Ni^{2+}, Co^{2+}, and Mn^{2+}, for example, are considerably less effective. However, precise mechanistic information is hard to come by. It is often difficult to obtain exact formation constant data or to unequivocally identify the reactive species. The problems are compounded by kinetically ambiguous reaction pathways, since observed rate laws and spectroscopic data rarely allow distinction between an intramolecular reaction, involving attack by coordinated OH on a monodentate N-bound ester (**6**) and one involving direct OH^- attack on the chelated ester (**7**) (Scheme 7). An early review (*42*) gives data on these systems and discusses such difficulties.

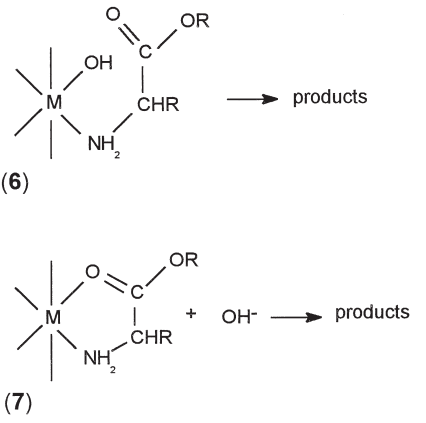

SCHEME 7.

Many of these problems have been removed through studies using exchange-inert complexes, particularly those incorporating Co(III) centers. In the 20-year period following 1967 studies with preformed complexes of the type *cis*-$[Co(N)_4(OH/H)(AAOR)]^{2+/3+}$ and $[Co((N)_4(AAOR)]^{3+}$ $(N)_4 = (en)_2$, AA = Gly, β-Ala, R = Me, Et, i-Pr) have allowed precise information to be acquired (*43*) and Table III lists rate data for the latter *N* carbonyl-*O*-chelated esters. What has been established for these systems may be summarized as follows.

1. The Co(III) center is generally regarded as lacking the polarizing power of a proton but its attachment to the N-terminus of an amino acid ester, as in $[Co(NH_3)_5(GlyOEt)]^{3-}$, accelerates OH^--catalyzed hydrolysis by *ca*. 100-fold. This is similar to the effect observed for N-protonation.

2. Attachment of carbonyl-*O* to the metal center leads to much greater rate enhancements, but this requires N,O-chelation of the amino acid ester (no examples of monodentate O-bound amino acid esters are known). Such coordination results in substantial electron withdrawal from the carbonyl group and this is reflected both in accelerated rates observed for OH^--catalyzed and spontaneous hydrolyses (by *ca.* 10^6) and in the carbonyl stretch frequencies; $[Co(en)_2(GlyOR)]^{3+}$ chelates have $\nu_{C=O}$ ~1640 cm^{-1} (R = Me, Et, i-Pr) (*9*), while the corresponding (N-bound) ester monodentates, $[Co(en)_2(GlyOR)Cl]^{2+}$, have $\nu_{C=O}$ ~1745 cm^{-1} (*23*). Oxygen-18 tracer studies (*12*, *45*) have established that C–OR bond cleavage is normally involved in the hydrolytic processes (Scheme 8), although for R = *t*-Bu O-R cleavage occurs (*46*). However, in this case the rate acceleration is only ~300-fold (*47*).

TABLE III

RATE CONSTANTS (k_{H2O}, k_{OH}) FOR INTERMOLECULAR HYDROLYSIS OF SOME FREE AND Co(III)-CHELATED AMINO ACID ESTERS AT 25°C, I = 1.0 M

Compound	k_{H2O}/s^{-1}	$k_{OH}/M^{-1}\ s^{-1}$
$[Co(NH_3)_5(GlyOEt)]^{3+}$ [a]	—	50
GlyOEt [b]	5×10^{-9}	0.58, 0.63 [c]
$HGlyOEt^{+}$ [b]	1.0×10^{-8}	23
$[Co(en)_2(GlyOi\text{-}Pr)]^{3+}$ [d]	1.1×10^{-3}	1.5×10^{6}
GlyOi-Pr [b]	—	0.11
$[Co(en)_2(GlyOMe)]^{3+}$ [e,f]	3.86×10^{-2} (Δ), 3.81×10^{-2} (Λ)	—
$[Co(en)_2((S)\text{-}AlaOMe)]^{3+}$ [e]	9.10×10^{-3} (Δ), 1.21×10^{-2} (Λ)	—
$[Co(en)_2((S)\text{-}LeuOMe)]^{3+}$ [e]	3.83×10^{-3} (Δ), 7.38×10^{-3} (Λ)	—
$[Co(en)_2((S)\text{-}ProOMe)]^{3+}$ [e]	4.26×10^{-3} (Δ), 5.34×10^{-3} (Λ)	—
$[Co(en)_2((S)\text{-}ValOMe)]^{3+}$ [e,g]	1.29×10^{-3} (Δ), 5.32×10^{-3} (Λ)	1.3×10^{6} (Δ), 2.9×10^{6} (Λ)
$[Co(en)_2((S)\text{-}PheOMe)]^{3+}$ [e]	1.20×10^{-2} (Δ), 1.12×10^{-2} (Λ)	—
$[Co(en)_2(\beta\text{-}AlaOi\text{-}Pr)]^{3+}$ [h]	4.6×10^{-5}	4×10^{4}
$[Co(en)_2(\beta\text{-}AlaOMe)]^{3+}$ [h]	5.5×10^{-4}	—
β-AlaOi-Pr [h]	—	0.02

[a] Ref. (*44*).

[b] Conley, H. L.; Martin, R. B. *J. Phys. Chem.* **1965,** *69,* 2914, I = 0.16 M; estimated as 5 times slower than the Et ester.

[c] Hay, R. W.; Porter, L. J.; Morris, P. J.; *Aust. J. Chem.* **1960,** *19,* 1197, I = 0.10 M.

[d] Ref. (*11*).

[e] Clark, C. R.; unpublished data.

[f] A rate constant of 0.027 s^{-1} has been reported (Δ,Λ-reactant) for the I = 0.66 M condition; Ref. (*9*).

[g] The rate constants for the pyridine and α-picoline catalyzed hydrolysis of this complex have been reported: $k(\Delta)$ = 0.18 and 0.12 $M^{-1}\ s^{-1}$ respectively; $k(\Lambda)$ = 0.51 $M^{-1}\ s^{-1}$ (catalysis by α-picoline not measured); Ref. (*24*).

[h] Ref. (*46*).

3. Hydrolysis of the ester chelate occurs with little or no stereochemical change ($S \leftrightarrow R$) at the α-carbon atom. The spontaneous reactions of Δ- and Λ-$[Co(en)_2((S)\text{-}AlaOMe)]^{3+}$ (in 0.1 M H^+) result in Δ- and Λ-$[Co(en)_2((S)\text{-}Ala)]^{2+}$ exclusively, while the corresponding OH^--catalyzed process gives only 2–4% Δ-$[Co(en)_2((R)\text{-}Ala)]^{2+}$ (pH 7.8, 10.9,

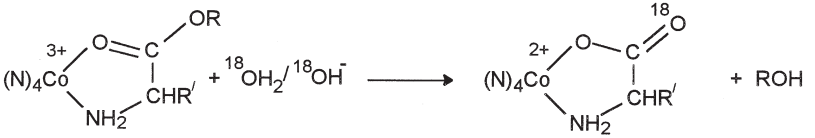

SCHEME 8.

0.1 *M* OH^-). Under these latter conditions Λ-$[Co(en)_2((S)\text{-AlaOMe})]^{3+}$ again gives Λ-$[Co(en)_2((S)\text{-Ala})]^{2+}$ exclusively (indeed no H-exchange was found on hydrolysis in 0.1 *M* $NaOD/D_2O$ for this isomer). Similar observations have been made for hydrolysis of a number of other Δ- and Λ-$[Co(en)_2((S)\text{-AAOMe})]^{3+}$ complexes (*24*).

4. Moderate kinetic discriminations are found on hydrolysis of the Δ- and Λ-$[Co(en)_2((S)\text{-AAOMe})]^{3+}$ diastereomers (AA = Gly, Ala, Leu, Pro, Val, Phe). The spontaneous reactions of these complexes are rapid at 25°C, with $t_{1/2}$ ranging from 18s (Gly) to 9 min (Val, Δ-diastereomer) and with $k_\Delta/k_\Lambda = 0.75$ (Ala), 0.52 (Leu), 0.80 (Pro), 0.24 (Val), 1.07 (Phe). Similar distinctions are observed in the OH^--catalyzed reactions (cf. Table III), but there is no obvious reason why the Λ-*S* diastereomers are usually the more reactive.

5. In aqueous solution $[Co(en)_2(\beta\text{-AlaOi-Pr})]^{3+}$ is hydrolyzed to $[Co(en)_2(\beta\text{-AlaO})]^{2+}$ without opening of the six-membered ring (*45*). The rate law for this reaction is

$$k_{obs} = (k[OH^-] + k'[OH^-]^2)/(1 + K[OH^-]), \qquad (3)$$

which is consistent with loss of i-Pro^- from the protonated tetrahedral intermediate (**IH**, Scheme 9) being rate-determining below pH 8.5,

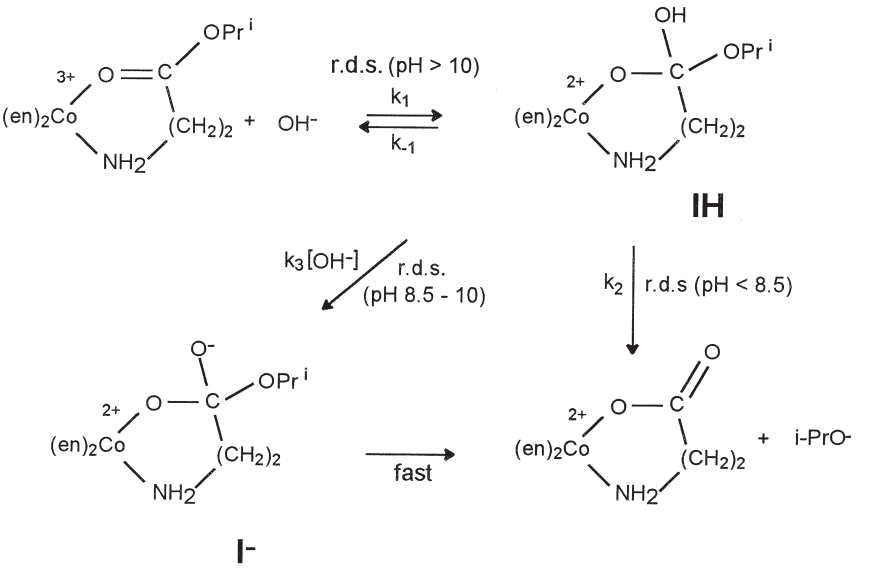

SCHEME 9.

whereas between pHs 8.5 and 10 the second-order in OH^- kinetics are interpreted in terms of rate-determining deprotonation of **IH** (pK_a ~14, est.). Above pH 10 the rate of this pathway ($k_3[OH^-]$) exceeds that for the formation of **IH** (k_1) so that the addition of OH^- to the chelated ester becomes rate determining. Similar pathways probably operate for hydrolysis of the five-membered amino acid ester chelates $[Co(en)_2(AAOR)]^{3+}$. Certainly, OH^- addition will be faster in these systems since activation by the electron-withdrawing Co(III) moiety will be greater in the five-membered chelate and this is borne out by experiment; hydrolysis of $[Co(en)_2(GlyOi\text{-}Pr)]^{3+}$ is *ca.* 375-fold faster than OH^- addition to $[Co(en)_2(\beta\text{-}AlaOi\text{-}Pr)]^{3+}$ (Table III). The significantly higher reactivity of the five-membered chelates has limited studies to pH values <6 (*11*, *24*).

6. Other bases also catalyze hydrolysis although their contribution to the rate, shown below,

$$k_{obs} = k_{H2O} + k_{OH}[OH^-] + k_B[B], \tag{4}$$

in most cases, is slight. It was originally proposed (*11*) that all N-bases act as nucleophiles, and amines, NH_2R, were indeed shown to result in (stable) amide products: O-bases were suggested to have a general base capability, promoting the addition of H_2O. However, the $k_{OAc}[OAc^-]$ term seen in the rate law for hydrolysis of $[Co(en)_2(GlyOi\text{-}Pr)]^{3+}$ in the presence of acetate ion must arise, at least in part, from a nucleophilic pathway (*48*). This part of the rate law leads to additional $[Co(en)_2(Gly\text{-}GlyOEt)]^{3+}$ when the reaction is carried out in the presence of GlyOEt competitor and to $[Co(en)_2(Gly)]^{2+}$ when the amine is absent. Such a result is only consistent with aminolysis of a first-formed anhydride intermediate (Scheme 10). It was then proposed (*48*) that all N- and O-bases acted directly as nucleophiles, but it is now known that this is not so; they do have a general-base capability (Eq. (4)). Thus pyridine and α-picoline catalyze the hydrolyses of Δ- and Λ-$[Co(en)_2((S)\text{-}ValOEt]^{3+}$ (see footnote to Table III), and these (tertiary) bases cannot give rise to an amide product. Likewise, imidazole, N-Meimidazole, and GlyOEt contribute to hydrolysis of $[Co(en)_2(\beta\text{-}AlaOi\text{-}Pr)]^{3+}$ according to Eq. (4) (*45*) under conditions where addition of OH^- is not rate determining (pH 7.3–8.5; $k_B/M^{-1}\ s^{-1} = 8 \times 10^{-3}$ (Im); 6×10^{-3} (N-MeIm); 3×10^{-3} (GlyOEt); $k_{OH}/M^{-1}\ s^{-1} = 5 \times 10^3$) so that they must be involved in promoting the addition of H_2O rather than in assisting the deprotonation of IH (Scheme 9).

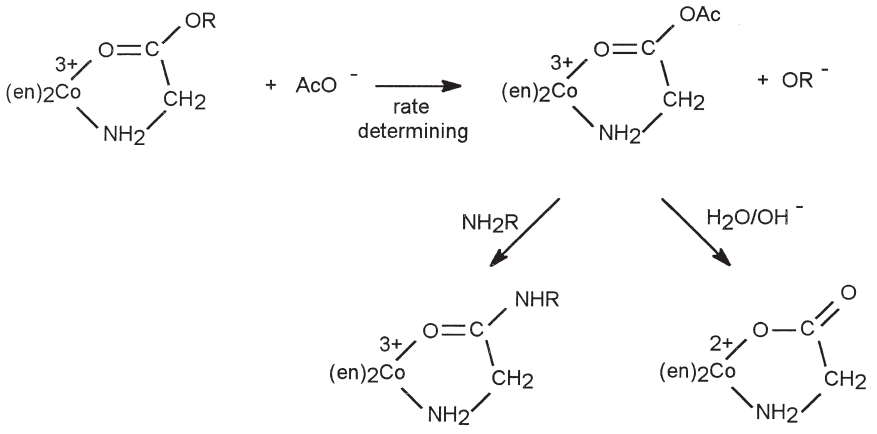

SCHEME 10.

7. Some bases, such as HPO_4^{2-} and HCO_3^-, play a marked role in the hydrolysis of $[Co(en)_2(\beta\text{-AlaOi-Pr})]^{3+}$ ($k_B/M^{-1}\ s^{-1} = 30$ (HPO_4^{2-}), 40 (HCO_3^-), under conditions where addition of OH^- is not rate determining (PO_4^{3-} and CO_3^{2-} are ineffective). It has been suggested (*45*) that these bases act by assisting the addition of H_2O, thus avoiding the high-energy **IH** addition intermediate by transferring the proton directly to the leaving group (Scheme 11). In the case of HCO_3^- some ring-opened $[Co(en)_2(OH)(\beta\text{-AlaOi-Pr})]^{2+}$ is also formed (34% at $HCO_3^- = 0.25\ M$) and this extraordinary reaction, involving ring cleavage, is considered to result from proton transfer to the ring O-atom as well as to the leaving i-PrOH moiety.

The second-order terms in [B] (B = Me_2NH, NH_3, GlyOEt, GlyOi-Pr, aminoacetonitrile) seen in the rate law for reaction of $[Co(en)_2(GlyOi\text{-}Pr)]^{3+}$ in aqueous solution lead to the corresponding amide products rather than to hydrolysis (*11*). Similarly for lysis of $[Co(en)_2(\beta\text{-AlaOi-Pr})]^{3+}$ by GlyOEt in the presence of imidazole (*49*), where the second-order terms (k[GlyOEt]^2 or k'[GlyOEt][B], B = OH^-, Im) lead to formation of $[Co(en)_2(\beta\text{-Ala-GlyOEt})]^{3+}$. Such results underscore the importance of a second base molecule in this process and point to deprotonation of an amine–alcohol intermediate as being rate-determining. This aspect is discussed in detail in Section VI.

C. Peptide Ester Complexes and Peptides

The N,O-$[Co(en)_2(AA\text{-}AA'OR)]^{3+}$ dipeptide ester complexes are formed rapidly (seconds to minutes) at room temperature on treating

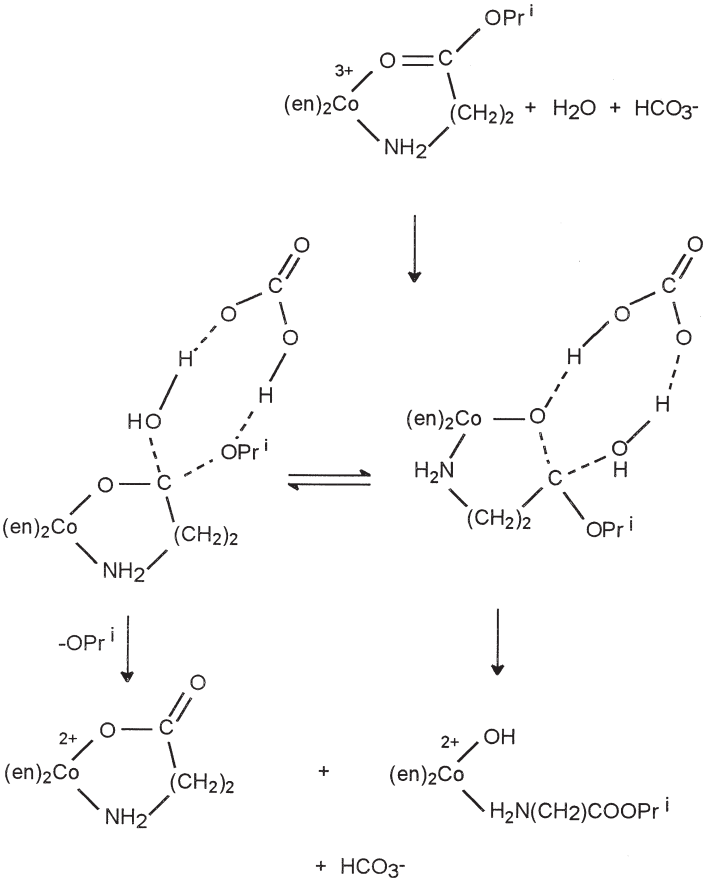

SCHEME 11.

$[Co(en)_2(AAOMe)](CF_3SO_3)_3$ with a "buffered" solution of AA′OR/AA′OR · HCl in anhydrous Me_2SO; this is the preferred solvent although rigorously dried MeOH, CH_3CN, and sulfolane may also serve. The conditions used in the preparations are dictated in part by the stability of the tetrahedral intermediate formed on addition of AA′OR to the carbonyl carbon of the reactant ester complex and in part by the need to achieve peptide bond formation while minimizing epimerization. If the reactions are carried out in the absence of protonated amine (AA′OR · HCl) decomposition of the tetrahedral intermediate may compete with its conversion to product. This problem is particularly marked for condensations involving $[Co(en)_2((S)\text{-ProOMe})]^{3+}$ and to a lesser extent for other amino acid ester chelates, but is not a

factor for $[Co(en)_2(GlyOMe)]^{3+}$. Decomposition involves reduction at the metal (Co(III) → Co(II)), with the liberated ethylenediamine ligand (en) then available to attack any ester complex remaining. This has been shown to be the case for $[Co(en)_2((S)\text{-AlaOMe})]^{3+}$ with various AA′OR, where it leads to the formation of $[Co(en)_2((S)\text{-Ala-en})]^{3+}$ (**8**) and the dimer $[(en)_2Co((S)\text{-Ala-en-}(S)\text{-Ala})Co(en)_2]^{6+}$ (**9**) as side-products (*25*). Both **8** and **9** have been prepared via direct syntheses

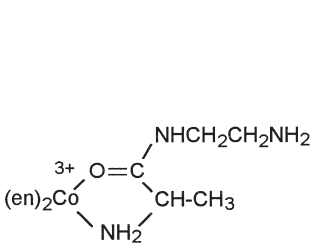

(**8**)

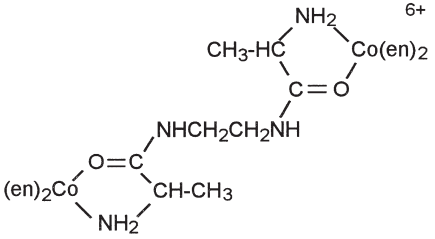

(**9**)

and a crystal structure of $\Delta\text{-}[Co(en)_2((S)\text{-Ala-enH})](NO_3)_2(ClO_4)_2$ is available (*27*). The problem is avoided if the protonated amine AA′OR · HCl (the $CF_3SO_3^-$ salt is preferred, but is less readily available) is present in the reaction mixture since it catalyzes the conversion of the addition intermediate to coordinated dipeptide ester (general acid catalysis, see Section VI,C) and so limits the opportunity for reduction.

Epimerization results from amine (AA′OR)-catalyzed H-exchange at the α-carbon in the $[Co(en)_2((S)\text{-AAOMe})]^{3+}$ reactant; such exchange is orders of magnitude slower for the product dipeptide complex (see Section V,D) so that it is exchange in the reactant ester, which is important in determining product stereochemical integrity. The identities of the chiral centers in the $Co(en)_2$ (Δ or Λ) and amine nucleophile (usually *S*) fragments are not affected during, or subsequent to, the coupling reaction.

Despite the rapidity of the coupling reactions epimerization may be extensive. It may be substantially reduced if the condensations are carried out using high concentrations of AA′OR. This is a consequence of the differing dependencies of epimerization (first-order) versus coupling (second-order) on AA′OR concentration. Both processes are sensitive to the stereochemistry of the reactants, and the balance of factors is such that coupling of (*S*)-AA′OMe with Λ-

$[Co(en)_2((S)\text{-AAOMe})]^{3+}$ always leads to very much lower levels of racemic product than does reaction with Δ-$[Co(en)_2((S)\text{-AAOMe})]^{3+}$ (see Section V,D). Table IV lists final optical yields for a number of condensations (*24*) using conditions which were, in some cases, subsequently found not to be optimum. The following comments apply to the table and to our present understanding of the conditions necessary to reduce epimerization to a minimum. (1) Epimerization in the Λ-ester reagent (0–6%) is considerably less than in the Δ-ester reagent (20–77%). The coupling reactions of the former are also faster. The Λ-ester should therefore be used for all preparative work where optical integrity is important. (2) Comparisons suggest that epimerization depends more on the amino acid ester in the Co(III)-chelate than on the amino acid ester nucleophile. Thus for Λ-$[Co(en)_2((S)\text{-AAOMe})]^{3+}$ couplings (AA = Ala, Leu, Phe) with (*S*)-AlaOMe 2.4, <1, 1.4% Λ-*R*-*S* products result; for Λ-$[Co(en)_2((S)\text{-AlaOMe})]^{3+}$ with (*S*)-AA′OMe (AA′ = Ala, Leu, Phe) a common 2–3% Λ-*R*-*S* impurity is found. (3) Other results (*24*, *26*) show, and the aminolysis and epimerization rate laws

TABLE IV

EPIMERIZATION DATA FOR $[Co(en)_2((S,R)\text{-AA-}(S)\text{-AA′OMe})]^{3+}$ PRODUCTS PREPARED IN Me_2SO SOLUTION (~18°C)

$[Co(en)_2(AAOMe)]^{3+}$ Reactant	(*S*)-AA′OMe	Ratio [Co(III)] : [(*S*)AA′OMe] : [(*S*)-AA′OMe · HCl]	Reaction time (min)	% *R*-*S* product
Λ-(*S*)-AlaOMe	AlaOMe	1 : 3 : 2	0.33	6[a]
Δ-(*S*)-AlaOMe	AlaOMe	1 : 3 : 2	0.33	53[a]
Λ-(*S*)-AlaOMe	PheOMe	1 : 3 : 2	2	5[a]
Δ-(*S*)-AlaOMe	PheOMe	1 : 3 : 2	2	40[a]
Λ-(*S*)Met(CH_3)	AlaOMe	1 : 3 : 2	2	4[a]
Δ-(*S*)Met(CH_3)	AlaOMe	1 : 3 : 2	2	50[a]
Λ-(*S*)Pro	AlaOMe	1 : 3 : 2	2	0[a]
Δ-(*S*)MetO	AlaOMe	1 : 3 : 2	2	34[a]
Δ-(*R*)Cys($CHPh_2$)	AlaOMe	1 : 3 : 2	2	20[a]
Λ-(*S*)AlaOMe	LeuOMe	1 : 1.2 : 1	1	3[b]
Δ-(*S*)AlaOMe	LeuOMe	1 : 1.2 : 1	1	70[b]
Λ-(*S*)AlaOMe	PheOMe	1 : 2.4 : 1	1	2[b]
Δ-(*S*)AlaOMe	PheOMe	1 : 2.4 : 1	2	77[b]
Λ-(*S*)LeuOMe	AlaOMe	1 : 1.2 : 1	1	<1[b]
Δ-(*S*)-LeuOMe	AlaOMe	1 : 1.2 : 1	1	26[b]
Λ-(*S*)-PheOMe	AlaOMe	1 : 1.2 : 1	1	4[b]
Δ-(*S*)-PheOMe	AlaOMe	1 : 1.2 : 1	1	49[b]

[a] Estimated by ^{1}H-NMR (300 MHz).

[b] Reversed-phase HPLC result on recovered dipeptides.

(Section V,D) require, that increasing the AA′OMe nucleophile concentration reduces epimerization. The 1:3:2 reactant concentration ratios given in Table IV provide a good starting point, but clearly it is important not to waste AA′OMe reagent. Somewhat lower levels of epimerization have been obtained using a 1:1.2:1 ratio (Table V) and this suggests that titration of the AA′OMe reagent into the reaction mixture may offer a better procedure. (4) It is important to have the "acid" buffer AA′OMe · HCl present, but some recent results suggest this could be replaced with (soluble) $Et_3N \cdot HTFA$ to conserve the amino acid. (5) Significantly greater amounts of epimerization were found to occur in the otherwise alternative MeOH, sulfolane, solvents.

Table VI lists a number of dipeptide ester complexes prepared via aminolysis in Me_2SO and isolated using ion-exchange chromatography; many others have been obtained from similar syntheses. Crystal structures are available for Λ-[Co(en)$_2$((*S*)-Ala-(*R*)-Phe)]$Br_3 \cdot H_2O$ (*26*), obtained from reaction of Λ-[Co(en)$_2$((*S*)-AlaOMe]$^{3+}$ with (*R*)-PheOMe and acid hydrolysis (Fig. 1), and for Λ-[Co(en)$_2$((*S*)-Leu-(*S*)-Leu OMe)]$Cl_3 \cdot 4H_2O$ (*24*), Λ-[Co(en)$_2$((*S,R*)-Ala-(*S*)-ValOMe)]$(ClO_4)_3$ (*24*), and β-[Co(trien)(Gly-GlyOEt)]$(ClO_4)_3 \cdot H_2O$ (*10*). These show considerable variation in chelate O–C_1–C_2–N dihedral angles (0–35°) (**10**) and it remains to be seen whether this property is important to epimerization (at C_2) in these species.

TABLE V

EPIMERIZATION IMPURITY FOLLOWING COUPLINGS OF Λ-[Co(en)$_2$((*S*)-AAOMe)]$(CF_3SO_3)_3$ WITH (*S*)-AA′OMe IN Me_2SO[a]

AA	AA′	Time/min	Yield	% Λ–*R*–S
Ala	Ala	0.33	95	2.4
Ala	Leu	1	80	3.0
Ala	Phe	2	90	3
Leu	Ala	1	80	<1
Leu	Leu	2	90	<1
Phe	Ala	1	90	4.0
Phe	Phe	2	95	4.0
Pro	Ala	2	95	0
Met(CH_3)	Ala	2	95	0

[a] ([Co-ester] = 5.8×10^{-2} *M*; [Co]:[AA′OMe]:[AA′OMe · HCl] = 1:1.2:1; *ca.* 18°C)

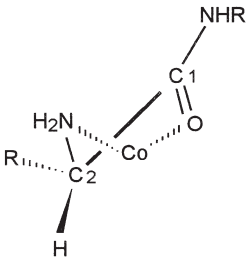

(**10**)

Removal of the dipeptide ester from the $Co(N)_4$ center is best achieved (*1*) by electrolytic reduction of aqueous solutions at an Hg electrode (−1.0 V vs S.C.E., pH ~5, NaCl/HCl electrolyte) and with recovery by ion-exchange (*1*, *2*, *25*) or reversed-phase HPLC separation (*24*). In the latter cases the Co(III)–dipeptide ester was first converted to the Co(III)–dipeptide acid by overnight hydrolysis in 6 *M*

TABLE VI

COUPLINGS OF AA′OMe TO $[Co(en)_2(AAOMe)](CF_3SO_3)_3$ IN Me_2SO AND RECOVERED YIELDS[a]

Co(III)–AAOMe reactant	AA′OMe nucleophile	Co(III)–AAAA′OMe product	Yield
Phe	His	Phe–His	90
Trp	Ala	Trp–Ala	91
Arg(NO_2)	Gly	Arg(NO_2)–Gly	85
Ala	Cys(Bzl)	Ala–Cys(Bzl)	85
Phe	Phe	Phe–Phe	73
Ala	Phe	Ala–Phe	83
Ser(Bzl)	His	Ser(Bzl)–His	83
Phe	Cys(Bzl)	Phe–Cys(Bzl)	72
Phe	Leu	Phe–Leu	88
Glu(Bzl)	His	Glu(Bzl)–His	76
Thr(Bzl)	Gly	Thr(Bzl)–Gly	89
Ala	Gly	Ala–Gly	89
Cys($CHPh_2$)[b]	Ala	Cys($CHPh_2$)–Ala	90
Met(O)[b]	Ala	Met(O)–Ala + Met–Ala	95
Met(CH_3)[b]	Ala	Met(CH_3)–Ala	95

[a] Ref. (*1*) unless stated otherwise.
[b] Ref. (*24*).

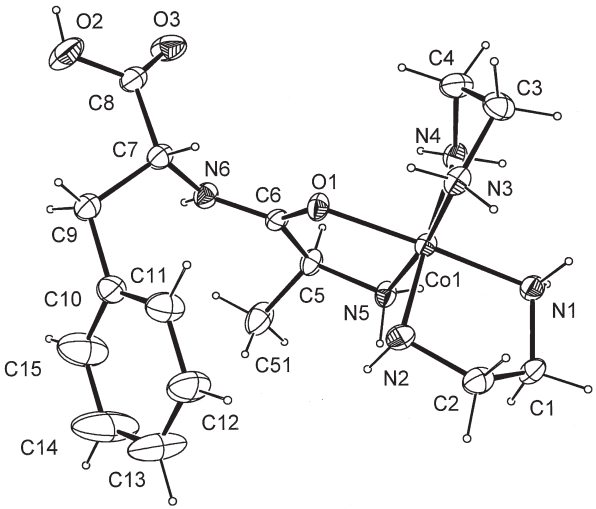

FIG. 1. Crystal structure of the Co(III) cation in Λ-[Co(en)$_2$((*S*)-Ala-(*R*)-PheOH)]-$Br_3 \cdot H_2O$ prepared by reacting Λ-[Co(en)$_2$((*S*)-AlaOMe)]$(CF_3SO_3)_3$ with (*R*)-PheOMe in Me_2SO. R(conventional) = 2.7% (H atoms not found; thermal ellipsoids drawn at the 50% level).

HCl (18°C), recovery by rotary evaporation, and electrolytic reduction. Once isolated, the free dipetide ester (or acid) is available for chain lengthening (cf. Scheme 1) and Table VII gives examples of peptides prepared using this approach.

IV. Cobalt(III) as a Protecting Group

The use of the $Co(NH_3)_5$ center as a protecting group in solution-phase peptide synthesis was first proposed in 1978 by Isied and Kuehn (*50*). No activation of the peptide-forming step is involved. They demonstrated that carboxyl-protected amino acids in $[H_2NCH(R)COOCo(NH_3)_5]^{2+}$ species may be coupled to activated Boc-amino acids (BocHNCH(R′)COOX (Boc = *t*-butoxycarbonyl)) to generate dipeptide complexes ($[BocHNCH(R')CONHCH(R)COOCo(NH_3)_5]^{2+}$). The necessary carbonyl activation is achieved either via symmetric anhydride formation or hydroxybenzotriazole (HOBt) derivatization. Following Boc deprotection the N-terminus of the coordinated peptide becomes available for further chain elongation. Coupling times for such processes are of the order of 1–6 h, depending on the number of

TABLE VII

TRI-, TETRA- AND PENTAPEPTIDES PREPARED BY THE Co(III) METHOD

Gly-Gly-Gly[a,b]	Gly-Gly-Gly-Gly[a]
Ala-Gly-Gly[a]	Ala-Gly-Phe-Phe[d]
Ala-Gly-Phe[a]	Leu-Ala-Gly-Gly[b]
Gly-Phe-Phe[b]	
Lys-Gly-Phe[a]	Tyr(Bzl)-Gly-Gly-Phe-Leu[c]
Pro-Gly-Gly[b]	
Pro-Phe-Phe[b]	
GlyPheLeuOAz[d]	

[a] Ref. (*14*).
[b] Ref. (*25*).
[c] Ref. (*19*).
[d] Ref. (*2*), Az = 4-(4-dimethylamino)phenylazo)benzyl.

residues. Complexes isolated include $[(Phe\text{-}Leu)Co(NH_3)_5]X_3$ (X = BF_4, TFA) (*51*), $[(Ala\text{-}Thre)Co(NH_3)_5]^{3+}$ (*52*), $[(Gly\text{-}Gly\text{-}Phe\text{-}Leu)Co(NH_3)_5](TFA)_3$ (*51*), $[(Gly\text{-}Phe\text{-}Leu)Co(NH_3)_5](TFA)_3$ (*51*), and $[(Tyr\text{-}Gly\text{-}Gly\text{-}Phe\text{-}Leu)Co(NH_3)_5](TFA)_3$ (Tyr-Gly-Gly-Phe-Leu = Leu[5]-enkephalin) (*51*).

Deprotection is facile, with ready reduction to labile Co(II) on treatment of $[peptideCo(NH_3)_5]^{n+}$ with either NaHS or $NaBH_4$. A number of dipeptides, and also penta and hexapeptides (e.g., Leu[5]enkephalin, Met[5]enkephalin, His-Gly-His-Gly-His-Gly), have been produced using this method (*51*). The $(NH_3)_5Co^{3+}$ center affords certain benefits when compared to other forms of carboxylate protection: The orange-red color of the CoN_5O chromophore allows ready visualization of both reactant and product species and, since these are positively charged, solubility and liquid chromatographic behavior can be manipulated to advantage during purification processes. The general strategy developed by Isied (*50*, *51*, *53*) is shown in Scheme 12. More recently, a variation of this technique has been used in the solid-phase synthesis of peptides (*54*, *55*). The approach here involves the attachment of a Co(III)–Boc–amino acid spacer to a polystyrene-based resin (**11**) and the subsequent construction of the peptide chain from the N-terminus (following Boc removal from **11**) using conventional solid-phase methods. The advantage of the method lies in the ease with which the Co(III) spacer can be removed, allowing ready recovery of the synthesized peptide (e.g., Leu[5]enkephalin) (*54*).

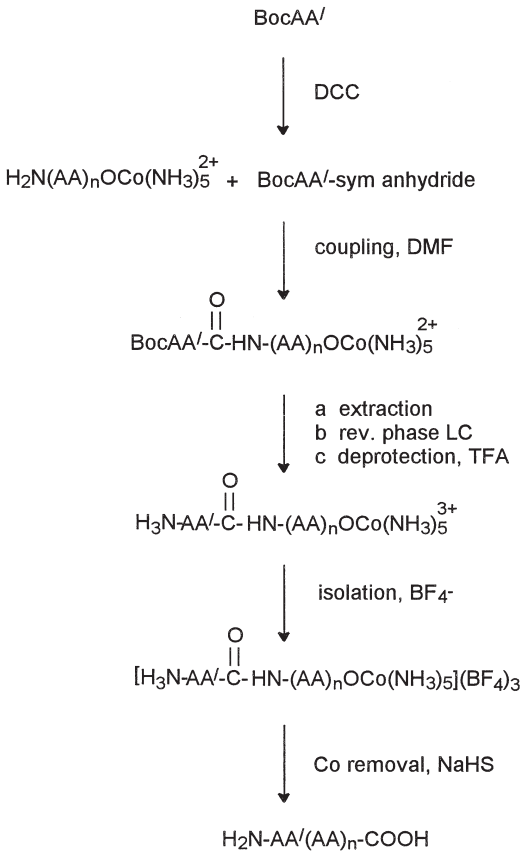
BocAA/
DCC
H2N(AA)nOCo(NH3)5 2+ + BocAA/-sym anhydride
coupling, DMF
BocAA/-C-HN-(AA)nOCo(NH3)5 2+
a extraction
b rev. phase LC
c deprotection, TFA
H3N-AA/-C-HN-(AA)nOCo(NH3)5 3+
isolation, BF4-
[H3N-AA/-C-HN-(AA)nOCo(NH3)5](BF4)3
Co removal, NaHS
H2N-AA/(AA)n-COOH

SCHEME 12.

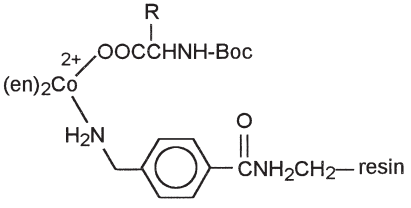
R
OOCCHNH-Boc
2+
(en)2Co
H2N
O
CNH2CH2— resin

(**11**)

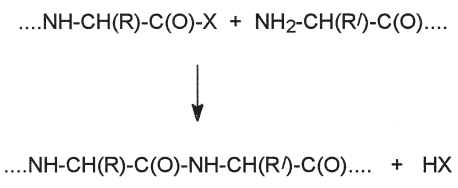

SCHEME 13.

V. Optical Purity and Epimerization

A. BACKGROUND

The chemical synthesis of peptides is not a rapid process in the absence of peptide-forming enzymes (*56*). But the synthetic utility of the method does allow wide variation, with the inclusion of nonnaturally occurring amino acids and other "spacer" reagents producing new reagents of biochemical and pharmacological usefulness. To speed up the process and to improve yields, some form of activation is required, and this is usually achieved by activating the carbonyl function of one amine acid residue toward nucleophilic attack by the amino group of another (cf. Scheme 13).

Table VIII lists some commonly used activating groups. That most widely in use is dicyclohexylcarbodiimide (DCC), often in conjunction with additives such as *N*-hydroxysuccinimide (HONSu) or HOBt. These convert the *O*-acyl isourea intermediate **12** into the *N*-acyl derivative **13** (Scheme 14), which is less prone to racemization under the experimental conditions. But it must be emphasized that all such chemical methods involve some racemization of asymmetric centers, and the trick is to reduce this to an absolute minimum.

TABLE VIII

COMMONLY USED CARBONYL ACTIVATING REAGENTS IN PEPTIDE SYNTHESIS (. . .NHCH(*R*)C(O)-X)

X =		
	$-OArNO_2$	Active ester
	$-OC(O)OCH_2CH_3$	Mixed anhydride
	$-OC(O)OCH_2CH(CH_3)_2$	Mixed anhydride
	$-N_3$	Acid azide
	$(C_6H_{11})N{=}C(O-)NH(C_6H_{11})$	DCC

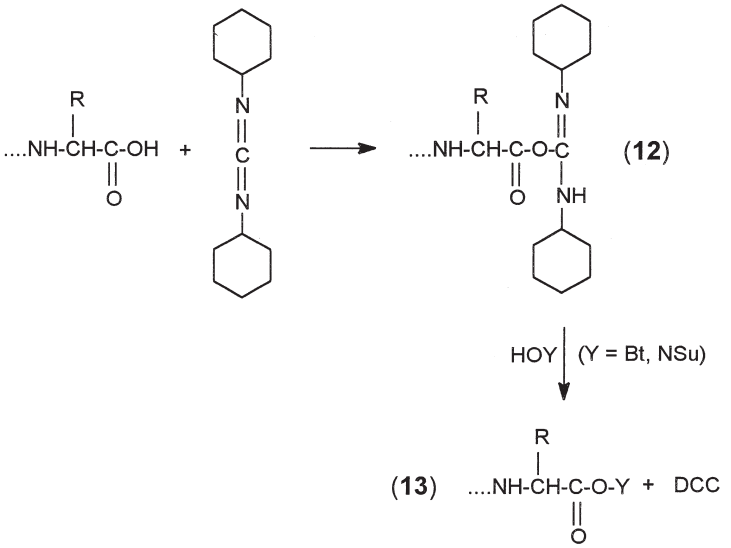

Scheme 14.

B. Cobalt(III) Activation and Epimerization

Electrophilic metals are known to enhance the carbon acidity of amino acids, and Co(III) complexes provide possibly the best examples of this. Electron withdrawal occurs through both the carbonyl-*O* and amino-*N* atoms of the five-membered chelate, making the asymmetric C–H proton at least 10^6 times more acidic. Hydrogen-exchange and epimerization studies (*16*, *17*) have shown that both processes occur via a common carbanion intermediate (**15**) (Scheme 15) (there is no additional barrier to inversion following proton loss), and kinetic and thermodynamic preferences for reprotonation of the prochiral C atom of **15** (structures **14** and **16** are diastereotopic) have been fully investigated; significant differences between k_{-1} and k_{-2} have been found (*17*). This suggested to us that such differences, if also present for the less conjugated ester carbanion **18** (Scheme 16) might prove useful in peptide synthesis if enhanced C–H acidity in the chelated ester was a problem. It was therefore of some interest to compare k_{-2}/k_{-1} ratios for **18** with those already known for **15**.

To do this we knew that ^{3}H-incorporation experiments would measure these ratios directly, with the ^{3}H label once inserted into **17** or **19**, remaining essentially inert to subsequent exchange. We had already shown for **15** (AA = Val, Asp) that the k_{-2}/k_{-1} ratio was isotope

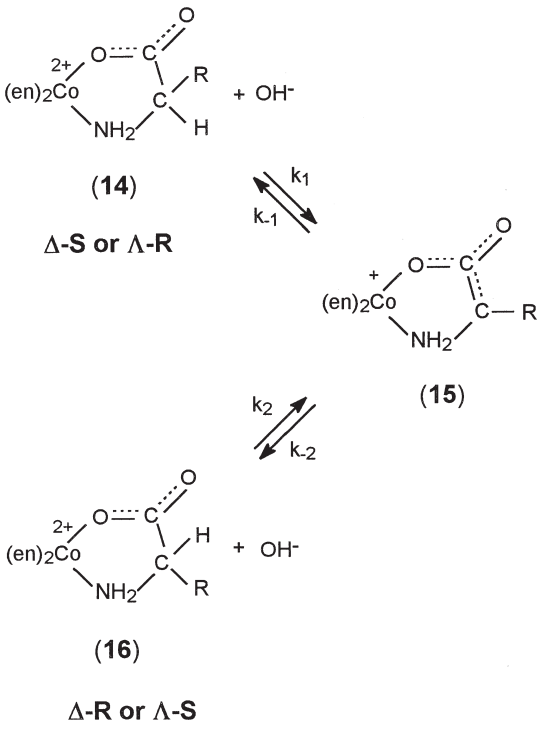

SCHEME 15.

independent (^{3}H, ^{2}H) so that the same ratio would hold for ^{1}H. Also, we initially thought that the less conjugated carbanion **18** might now be sufficiently unstable to show little kinetic isotope preference for reprotonation (i.e., the absolute magnitudes of k_{-1}, k_{-2} would be similar for ^{3}H, ^{1}H) so that ^{3}H incorporations would provide a sensitive measure and possibly upper limit for epimerization, since retention with ^{3}H incorporation would also occur. This latter idea received some support from the studies of Smith *et al.* (*18*, *57*), who reported no ^{1}H/^{3}H preference for reprotonating the carbanion produced from phenylglycine in phosphate buffer at elevated temperatures (80–110°C). However, Denkewalter and co-workers (*58*) had shown a ^{1}H/^{3}H preference of 4.6 in the synthesis of Tyr-(*S*)-Ser when using the *N*-carboxyanhydride coupling method in aqueous solution.

Initial experiments by Tasker (*19*) were encouraging. He used ^{3}H incorporations and RP-HPLC separations of diastereomers to show very small, and similar, ^{3}H-incorporations and inversions (0.2–0.4%) in the synthesis of $[Co(en)_2((S)\text{-Thr(Bzl)-GlyOMe})]^{3+}$ (*1*) and β-[Co

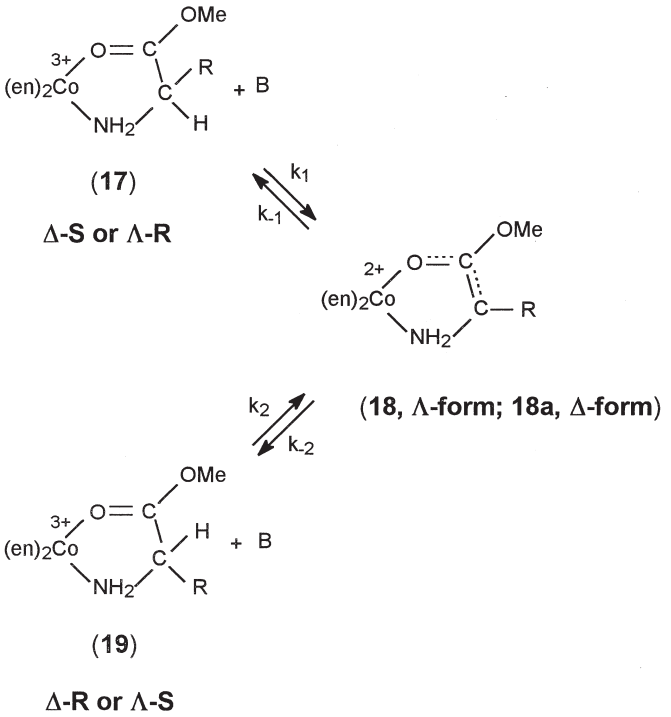

SCHEME 16.

(trien)((*S*)-Ala-Gly-GlyOCH$_3$)]$^{3+}$ in Me$_2$SO. In retrospect these results now appear suspect. Wautier *et al.* (*6*) then reported complete loss of optical integrity in the chelated amino acid when coupling several [Co(tren)(AAOMe)]$^{3+}$ complexes (AA = (*S*)-Ala, (*R*)-Ala, (*S*)-Leu) with (*S*)-AA′OMe (AA′ = Leu, His, Ala, Val) in MeOH, using a "one-pot" esterification method prior to adding AA′OMe · HCl and *N*-ethylmorpholine (as deprotonating base). However, long reaction times, high ionic strengths, and sometimes elevated temperatures were used for coupling (Table IX), and such conditions can lead to substantial epimerization in the [Co(tren)((*S*)-AA-AA′OMe)]$^{3+}$ product, as we show below. Likewise, Mensi and Isied have more recently reported (*7*) using the Tasker method ([Co-ester] = 0.021 *M,* [AA′OR] = 0.063 *M*; [AA′OR.HCI] = 0.042 *M*), 18% inversion of configuration in the chelated amino acid of [Co(en)$_2$(Phe-(*S*)-PheOR)]$^{3+}$ (R = Me, *t*-Bu) following a 20-min reaction time at room temperature. Couplings of [Co(en)$_2$((*S*)-PheOMe)]$^{3+}$ show more epimerization than most, but the amount can be substantially reduced by using the Λ-[Co(en)$_2$((*S*)-

TABLE IX

REACTION CONDITIONS AND EPIMERIZATION FOR COUPLINGS IN MeOH[a]

[Co(tren)(AAO)]$^{2+}$ starting complex	Amine AA′OMe	Reaction time	Temp (°C)	[Co(tren)(AA-AA′OMe)] product	% Epimerization
Gly	Gly	10	r.t.	Gly-Gly	—
Gly	(*S*)-Ala	60	r.t.	Gly-(*S*)-AlaOMe	—
Gly	(*S*)-Asp	90	r.t.	Gly-(*S*)-AspOMe	—
(*S*)-Ala	(*S*)-Leu	60	r.t.	(*S*,*R*)-Ala-(*S*)-Leu	53(2)
(*R*)-Ala	(*S*)-Leu	60	r.t.	(*R*,*S*)-Ala-(*S*)-Leu	55(2)
(*S*)-Ala	(*S*)-His	90	35	(*S*,*R*)-Ala-(*S*)-His	54(2)
(*S*)-Leu	(*S*)-Ala	75	45	(*S*,*R*)-Leu-(*S*)-Ala	54
(*S*)-Leu	(*S*)Val	900	50	(*S*,*R*)-Leu-(*S*)-Val	58(2)

[a] See Ref. (*6*).

PheOMe)]$^{3+}$ reagent (rather than Δ), a higher AA′OMe concentration, and a shorter reaction time. It is likely that the Mensi and Isied result arises largely from using the racemic Δ,Λ-Co(III) reagent.

C. TRITIUM INCORPORATION EXPERIMENTS

Even though these experiments subsequently proved of little value in determining the optical purity of the resulting dipeptides, they did provide useful fundamental information. Results given here (*59*, *24*) have not been published previously. Experiments were carried out using facilities previously used by Tasker (*19,* see also Section VIII).

Figure 2A gives results for [Co(en)$_2$(GlyOMe)]$^{3+}$ couplings with GlyOMe and (*S*)-LeuOMe. The similar $t = 0$ intercepts of ~1.0% ^{3}H incorporation means that exchange into [Co(en)$_2$(GlyOMe)]$^{3+}$ catalyzed by (*S*)-LeuOMe is slower than that catalyzed by GlyOMe since the coupling reaction is also slower (cf. Section VI,C). Subsequent exchange into [Co(en)$_2$(Gly-(*S*)-LeuOMe)]$^{3+}$ is so slow as to be unmeasurable over 30 min, whereas exchange into [Co(en)$_2$(Gly-GlyOMe)]$^{3+}$ is quite fast (it was the fastest of all the dipeptide complexes). Which of the two prochiral H atoms in the chelated Gly residue undergoes exchange remains unknown, but for [Co(en)$_2$(Gly)]$^{2+}$ the Δ-*R* (Λ-*S*) proton is some 25% more labile than Δ-*S* (Λ-*R*) proton (*17*). Figure 2B gives results for [Co(en)$_2$((*S*)-AlaOMe)]$^{3+}$ couplings with GlyOMe. The $t = 0$ results of 0.9% (Λ) and 0.5% (Δ) ^{3}H incorporation means that exchange into the Λ-ester is faster than into the Δ-ester since the former couples faster with GlyOMe (cf. Section VI,C). This interesting result could come about from significant chiral recognition in the

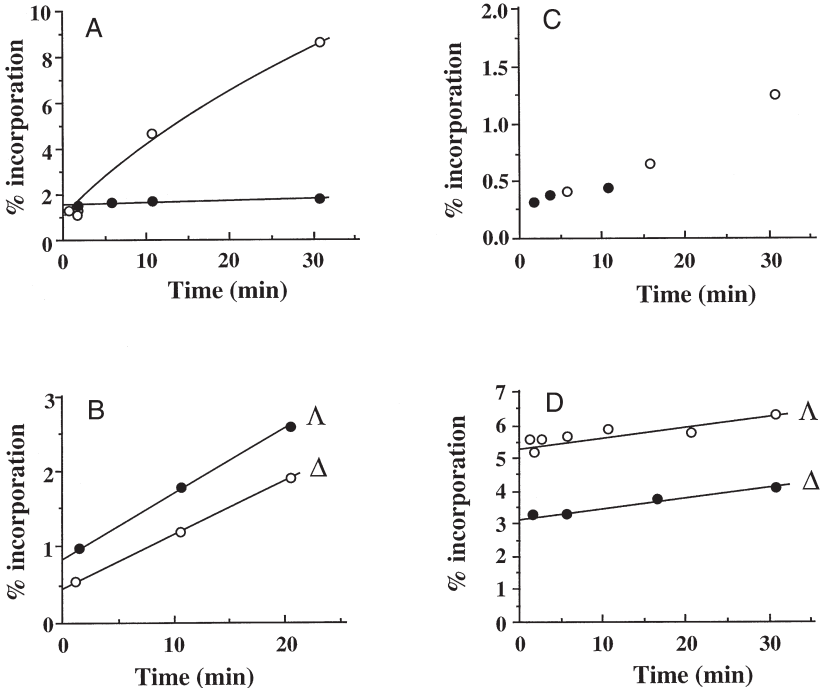

FIG. 2. Percentage of ^3H incorporation vs time data in Me_2SO. The following experimental conditions applied: [Co-ester] = 0.058 *M*; [AA′OMe] = 0.174 *M*; [AA′OMe · HCl] = 0.116 *M*; volume = 6 ml containing 1 μl of ^3H-labeled H_2O (5 Ci/ml). (A) $[Co(en)_2(GlyOMe)](CF_3SO_3)_3$ + GlyOMe (O); + LeuOMe (●); (B) Δ- and Λ-$[Co(en)_2((S)$-AlaOMe$)](CF_3SO_3)_3$ + GlyOMe; (C) Λ-$[Co(en)_2((S)$-LeuOMe$)](CF_3SO_3)_3$ + GlyOMe (O) + (*S*)-LeuOMe (●); (D) Δ- and Λ-$[Co(en)_2((S)$-AlaOMe$)](CF_3SO_3)_3$ + (*S*)-AlaOMe.

k_{-2}/k_{-1} reprotonation ratio favoring the Λ-*S* and Δ-*R* isomers (see below). However, subsequent exchange into the Λ- and Δ-$[Co(en)_2$(Ala-GlyOMe$)]^{3+}$ products occurs at similar rates (note here that the Δ-product contains appreciable quantities of the Δ-*R*-*S* epimer (cf. Table IV). Figure 2C gives results for Λ-$[Co(en)_2((S)$-LeuOMe$)]^{3+}$ couplings with GlyOMe and (*S*)-LeuOMe (5 min quench). Very little (~0.3%) ^3H incorporation occurs in the Λ-ester, and subsequent exchange into the dipeptide product is also slow. The former result suggests that the coupling reaction, although itself very slow, is somewhat faster than H-exchange. Figure 2D gives results for Δ- and Λ-$[Co(en)_2((S)$Ala-OMe$)]^{3+}$ couplings with (*S*)-AlaOMe. This has been the most studied exchange reaction. The slower reacting Δ-isomer gives a $t = 0$ result of 5.4 ± 0.4% ^3H, whereas the Λ-isomer gives 3.1 ± 0.3% ^3H; subse-

quent exchanges in the two dipeptide products occur at similar rates. The immediate products from two further experiments under the same conditions (after 1 min both reactions were complete) were then subjected to detailed study. The ^{1}H-NMR analysis of the Co(III) dipeptides and RP-HPLC separations of the recovered dipeptides gave the following epimer ratios: 44% Δ-*S*-*S,* 56% Δ-*R*-*S* from the Δ-reactant and 94.4% Λ-*S*-*S,* 5.6% Λ-*R*-*S* from the Λ-reactant. Representative data from which this information was obtained are given in Figures 3A–3D. Following removal of all ^{3}H from other exchange labile sites (amine/amide, washing on IE resin) incorporations into the Co(III) dipeptides were found to be 5.3 ± 0.3% (Δ) and 2.7 ± 0.3% (Λ). Total measured incorporations into the RP-HPLC separated dipeptides were (cpm ± σ) 119 ± 9 (*S*-*S*) and 300 ± 13 (*R*-*S*) for the Δ-system and 138 ± 7 (*S*-*S*) and 63 ± 5 (*R*-*S*) for the Λ-system (*24*). These data correspond to 2.9% (Δ) and 2.8% (Λ) ^{3}H incorporations into the stereoretentive *S*-*S* dipeptides and to 7.2% (Δ) and 1.3% (Λ) incorporations into the epimerized *R*-*S* dipeptides. The latter values give an apparent ^{1}H/^{3}H isotope ratio for inversion of 6.8 (Δ) and 3.3 (Λ), although these must represent minimum values since ^{1}H-incorporations into the carbanion with inversion continue to give further ^{3}H labeling with inversion (Scheme 17). More certain k_{-2}/k_{-1} ratios for reprotonation of the chiral carbanions **18** and **18a** can be obtained from the measured activities in the dipeptide products, giving 2.5 ± 0.3 (300/119) for the Δ-system and 2.2 ± 0.3 (138/63) for Λ. Perhaps these experiments should be repeated using higher enrichments, and possibly the alternative Δ- and Λ-reactants $[Co(en)_2((S)\text{-AlaOMe})]^{3+}$ and $[Co(en)_2((R)\text{-AlaOMe})]^{3+}$ should be examined before any appreciable coupling has taken place. However the present results do show that **18** has a larger discrimination ratio for reprotonation ($k_{-2}/k_{-1} = k^*_{-2}/k^*_{-1}$ (*17*)) than does the more conjugated amino acid carbanion **15** (cf. Scheme 15). For **15** $k_{-2}/k_{-1} = 1.15$ (reprotonation by H_2O in aqueous solution), whereas for **18** (Λ) $k_{-2}/k_{-1} = 2.2$ for reprotonation by chiral (*S*)-AlaOMeH$^+$. For **18a** (Δ) k_{-2}/k_{-1} takes on the value 2.5 for reprotonation by the same chiral acid. Apparently the achiral α-C atom of the anion (**18**, **18a**) favors reprotonation by (*S*)-AlaOMeH$^+$ to give the Λ-*S* and Δ-*R* diastereomers and by roughly the same amount. This same result was suggested above for reprotonation of **18** by achiral GlyOMeH$^+$. It may not be a coincidence that addition of the (*S*)-AlaOMe and GlyOMe bases to the adjacent carbonyl center also favors in a rate sense the Λ-*S* and Δ-*R* diastereomers. But the above results do show that the Δ- and Λ-Co(III) stereochemistries play a vital, possibly dominant, role in the epimerization process.

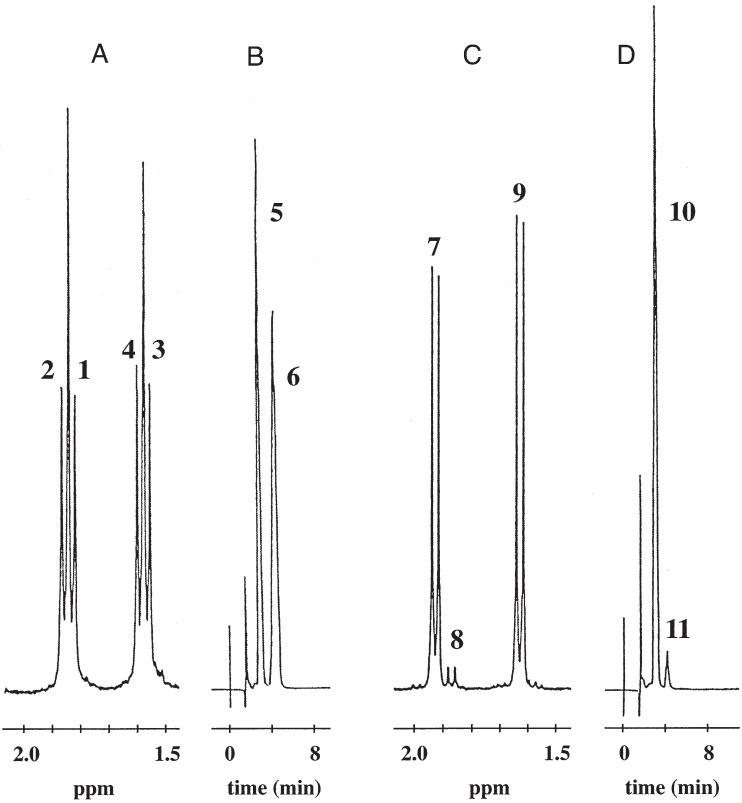

FIG. 3. The 300 MHz ^{1}H-NMR spectra (A and C) and RP-HPLC chromatograms (B and D) for the Co(III) complexes and recovered dipeptides from the reactions of Δ-[Co(en)$_2$((*S*)-AlaOMe)](CF$_3$SO$_3$)$_3$ and Λ-[Co(en)$_2$((*S*)-AlaOMe)](CF$_3$SO$_3$)$_3$ with (*S*)-AlaOMe in Me$_2$SO ([Co-ester] = 0.058 *M*; [(*S*)-AlaOMe] = 0.176 *M*; [(*S*)-AlaOMe · HCl] = 0.116 *M*; acid quench after 1 min). For Δ-[Co(en)$_2$((*S*+*R*)-Ala-(*S*)AlaOMe)]Cl$_3$ (A) overlapping doublets for the chelated and terminal alanine-Me resonances are designated (**1, 4**) for the Δ-*R*-*S* isomer and (**2**, **3**) for the Δ-*S*-*S* isomer, for Λ-[Co(en)$_2$((*S*+*R*)-Ala-(*S*)-AlaOMe)]Cl$_3$ (C) the chelated and terminal doublets are (**7**, **9**) for Λ-*S*-*S* and (**8**, **9**) for Λ-*R*-*S*. The corresponding chromatograms for the isolated dipeptides are assigned (**5**, **10**) for (*S*)-Ala-(*S*)-Ala and (**6**, **11**) for (*R*)-Ala-(*S*)-Ala. The NMR spectra were run in ^{2}H$_2$O referenced to CH$_3$OH (3.50 ppm). Elution conditions for HPLC: 100% aqueous 35 m*M* NaMe$_2$PO$_4$, pH 3.25; flow rate 2 ml min^{-1}; λ = 207 nm.

Other experiments showed that varying the temperature (18–45°C) in the Λ-[Co(en)$_2$((*S*)-AlaOMe)]$^{3+}$ + (*S*)-AlaOMe reaction in Me$_2$SO (15-sec to 2-min reaction times) increases slightly ^{3}H incorporation into the chelated ester (from 3.0 to 4.3%), suggesting a slightly greater temperature dependence for H-exchange compared to cou-

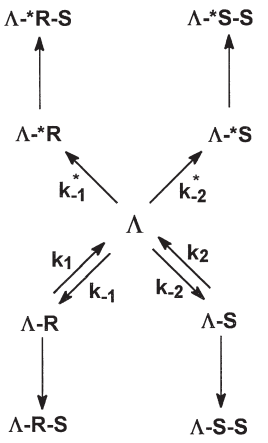

Λ ≡ 18 (cf. Scheme 16)

k^*_{-1}, k^*_{-2} represent rate constants for ^3H incorporation which, once bound, remain with the reactant ester, and product peptide

SCHEME 17.

pling. Also, seven experiments (at 25°C) where the (*S*)-AlaOMe concentration ratio was increased from N = 1.2 to 4.7 ([Co]:[(*S*)-AlaOMe]:[(*S*)-AlaOMe · HCl] = 1.0 : N : 2.0) showed ^3H incorporations to decrease from 12.2 to 0.7% in roughly a $1/N^2$ dependence; this was independent of whether the (*S*)-AlaOMe was added directly or was prepared by titration of (*S*)-AlaOMe · HCl with NEt_3. *N*-Methylmorpholine was shown to be not as effective a deprotonating base, even though in this case all the reagents remained in solution.

D. Epimerization and Rate Laws for Epimerization and Aminolysis

The above ^3H experiments do not give a direct measure of inversion in the $[Co(en)_2((S)\text{-AAOMe})]^{3+}$ reactant, although they do establish that it is fast under the coupling conditions (seconds), while in the dipeptide product $[Co(en)_2((S)\text{-AA-}(S)\text{AA}'\text{OMe})]^{3+}$ it is slow (hours). But this much was already known, in a qualitative way, from the published literature (*6*, *7*). To minimize the problem it was essential to determine the rate laws and rate constants for both epimerization and aminolysis and to investigate differences between the Δ- and Λ-reactants. The following experiments established the rate laws for these two processes and outline the difficulties associated with using

the Δ reagents. Figure 4 gives rate data for epimerization in Δ-$[Co(en)_2((S)\text{-AlaOMe})]^{3+}$ during its reaction with both (*S*)- and (*R*)-AlaOMe in Me_2SO. Each data point was obtained by injecting 150 μl of a 0.211 *M* solution of Δ-$[Co(en)_2((S)\text{-AlaOMe})](CF_3SO_3)_3$ into 5.0 ml of a rapidly stirred solution of the amine reagent (0.03 and 0.06 *M*) buffered with 0.16 *M* amine · HCl, quenching after a short time (seconds) by adding 200 μl of 6 *M* HCl and then H_2O, hydrolyzing, and then separating the reactant (as Δ-$[Co(en)_2(Ala)]^{2+}$) from Δ-$[Co(en)_2$ (Ala-(*S*)-AlaOMe)$]^{3+}$ by ion exchange chromatography and examining both for inversion by reversed-phase HPLC. The data clearly follow first-order kinetics, with that using 0.03 *M* (*S*)-AlaOMe (Fig. 4A) coming to an equilibrium value of 27% Δ-*R* after 50 s ($1 \times t_{1/2}$ for aminolysis) with $k_{obs} = 0.090\ s^{-1}$ ($t_{1/2} = 7.75$ s); with 0.06 *M* amine (Fig. 4B) an equilibrium value of 25.5% Δ-*R* after 24 s ($2 \times t_{1/2}$ for aminolysis)

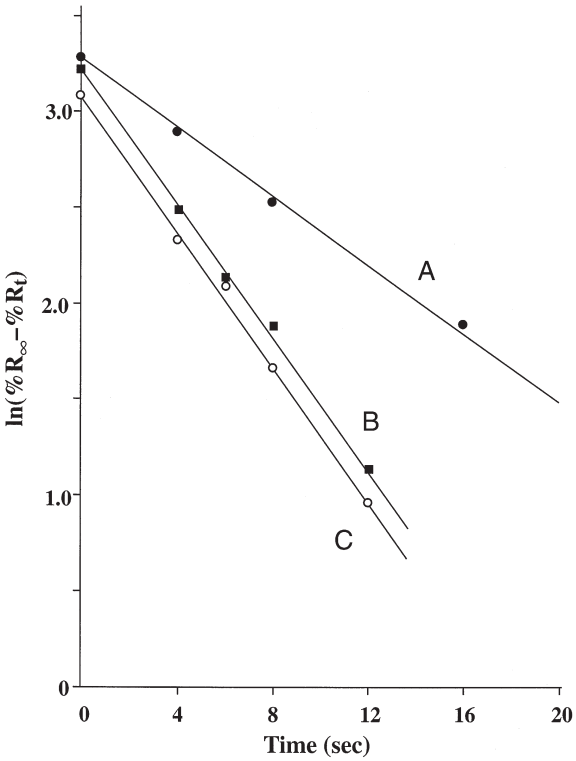

FIG. 4. Epimerization rate data for Δ-$[Co(en)_2((S)\text{-AlaOMe})]^{3+}$ in its reactions with (*S*)-AlaOMe (A, 0.03 *M*; B, 0.06 *M*) and (*R*)-AlaOMe (C, 0.06 *M*) in Me_2SO (0.16 *M* (*S*)- or (*R*)-AlaOMe · HCl buffer).

was found, with k_{obs} = 0.18 s^{-1} ($t_{1/2}$ = 3.9 s). Clearly under these low amine concentrations epimerization is considerably faster than aminolysis. When 0.06 *M* (*R*)-AlaOMe was used as the amine reagent (Fig. 4C) 22% Δ-*R* ester was present at equilibrium, but the rate was the same, k_{obs} = 0.18 s^{-1} ($t_{1/2}$ = 3.9 s). The rate law for epimerization is clearly first-order in amine, $k_{obs} = k$[amine] with k = 3.0 M^{-1} s^{-1}, and apparently independent of the chirality of the amine. The slightly different observed equilibrium positions suggest that either the true equilibrium position for epimerization (k_1/k_2, Scheme 18) or the aminolysis rate constants (k_3, k_4) are slightly affected by the amine chirality. This problem is addressed below. It is important to recognize in this context that the above observed "equilibrium" positions and rate constants differ from the true values ($K_E = k_1/k_2$, $k_E = k_1 + k_2$; Scheme 18) because the Δ-*R* reactant is undergoing aminolysis with (*S*)-AlaOMe at the same time and much more rapidly (k_4) than is the Δ-*S* reactant (k_3).

Now let us turn to an examination of the Δ-[$Co(en)_2$(Ala-(*S*)-AlaOMe)]$^{3+}$ products. When 0.03 *M* (*S*)-AlaOMe was used RP-HPLC gave 50% Δ-*R*-*S* and 50% Δ-*S*-*S* after 8 s, building to 76% Δ-*R*-*S* and 24% Δ-*S*-*S* at the conclusion of the reaction (500 s). With 0.06 *M* (*S*)-AlaOMe the result was 32% Δ-*R*-*S* and 68% Δ-*S*-*S* (4 s) building to 58% Δ-*R*-*S* and 42% Δ-*S*-*S* (24 s); with 0.06 *M* (*R*)-AlaOMe the comparison were 34% Δ-*R*-*S* (4 s) building to 55% (24 s), i.e., nearly the same distributions. These results require the Δ-*R* ester to react with (*S*)- or (*R*)-AlaOMe to give the Δ-*R*-*S* (or Δ-*R*-*R*) product at a considerably faster rate (via k_4) than does the Δ-S ester to give Δ-*S*-*S* (or Δ-*S*-*R*). Also, either differences between the rate constants for epimerization and aminolysis cancel the effect of chirality of the amine base or the rate constants themselves are little affected by the amine chirality. Subsequent analysis on other systems found the latter explanation to hold.

We then set about establishing the rate law for aminolysis under the same conditions. It was clear that the Λ-*S* ester was far more reactive than the Δ-*S* ester, and the above results showed that little

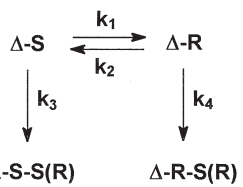

SCHEME 18.

epimerization to give a Λ-*R*-*S* product took place. Stopped flow spectrophotometric traces using Λ-[Co(en)$_2$((S)-AlaOMe)]$^{3+}$ and (*S*)-AlaOMe in Me_2SO gave excellent first-order fits (480 nm), and plots of log k_{obs} vs log [amine] for reaction in Me_2SO and MeOH are given in Fig. 5. The slope of 2.0 in Me_2SO clearly establishes the $k_{obs} = k_4$[amine]^2 rate law, with $k_4 = 55\ M^{-2}\ s^{-1}$. In MeOH the shallower slope of 1.6 suggests a less than second-order dependence, but we interpret this as resulting from increasing amounts of the unreactive addition intermediate (**20**, cf. Scheme 19) being formed as the amine concentration is raised. Such a species represents the intermediate for alcohol exchange, and in the absence of amine it is very obvious (as a red color) in alkaline MeOH (*60*).

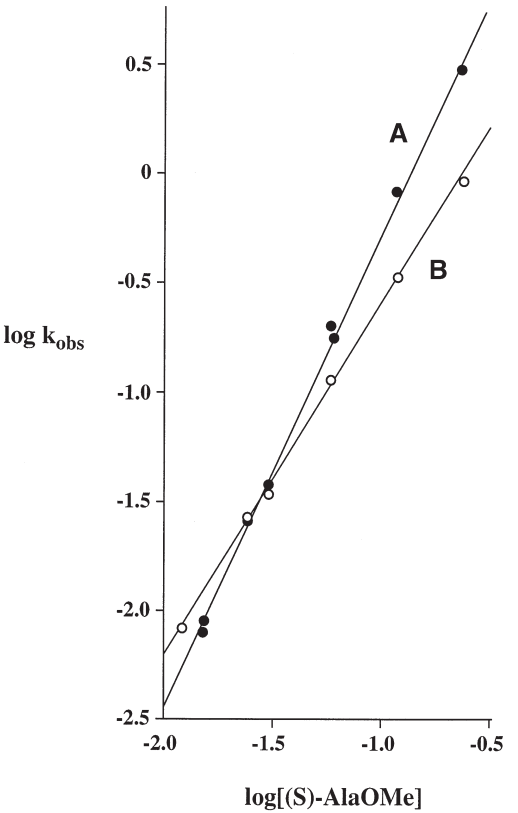

FIG. 5. Plots of log k_{obs} vs log [(*S*)-AlaOMe] for the reaction of Λ-[Co(en)$_2$((*S*)-AlaOMe)](CF$_3$SO$_3$)$_3$ with (*S*)-AlaOMe in (A) Me_2SO (slope = 2.0) and (B) MeOH (slope = 1.6).

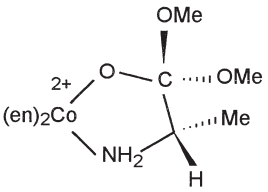

(**20**)

SCHEME 19.

Using the diastereotopic information for the Δ- and Λ-esters at pseudoequilibrium and similar data for the final Co(III) dipeptide products it was possible (*61*) to find ratios of rate constants (k_3/k_1, k_4/k_2, k_1/k_2; Scheme 18), assuming the chirality of the amine reagent was unimportant (viz. k(Λ-*S*) ≡ k(Δ-*R*)). From the measured k_4 value of 55 M^{-2} s^{-1} for the Λ-*S* ester the remaining rate constants could then be obtained; k_1 = 0.67 M^{-1} s^{-1}, k_2 = 0.58 M^{-1} s^{-1}, k_3 = 4.9 M^{-2} s^{-1}. Thus the Λ-*S* ester undergoes aminolysis by (S)-AlaOMe some 11 times faster than the Λ-*R* ester, and in 0.12 *M* amine aminolysis of the Λ-*S* ester is some 11 times faster than its epimerization to give the Λ-*R* ester. These factors combine to give a theoretical product (at the completion of the reaction) containing 2.4% Λ-*R*-*S*; using higher amine concentrations further reduces the Λ-*R*-*S* impurity. Also, from the above true equilibrium ratio K_E = 0.67/0.58 = 1.16 together with the ^{3}H results given earlier (cf. Section V,C), it is possible to conclude that just as the Λ-*S* (Δ-*R*) ester reacts more rapidly with amine at the activated carbonyl center than does the Λ-*R* (Δ-*S*) ester (k_4/k_3), so too does it lose a proton more rapidly from the adjacent asymmetric C atom to the same base, although the discriminating factor is not as great ($k_2/k_1 = k_{-2}/k_{-1} \cdot K_E$ = 2.2/1.16 = 1.9). Such results clearly demonstrate that the stereochemistry about the Co(III) center markedly influences reprotonation of the carbanion **18** (cf. Schemes 16, 17) and plays a major role in determining the stereochemical outcome in the final dipeptide product. Finally, the kinetic preferences for aminolysis (k_3, k_4) are not mirrored in a thermodynamic sense. When the final dipeptide product of 76% Δ-*R*-*S* and 24% Δ-*S*-*S*, formed from Δ-*S* ester reacting with 0.03 M (*S*)-AlaOMe, was left to equilibrate for 2 days in the reaction mixture the system mutarotated to the final values of 49% Δ-*R*-*S* and 51% Δ-*S*-*S* (K_p = 1.0).

$$\Delta\text{-}[Co(en)_2((S)\text{-Ala-}(S)\text{-AlaOMe})]^{3+} + (S)\text{-AlaOMe} \rightleftharpoons \Delta\text{-}[Co(en)_2((R)\text{-Ala-}(S)\text{-AlaOMe})]^{3+} + (S)\text{-AlaOMe}. \quad (5)$$

This equilibrium value is the same as that found for the chelated acid (K_A = 1.0) (*17*) so it is likely that the dipeptide carbanion, like **15** (Scheme 15), shows less kinetic discrimination for reprotonation (k_{-1}/k_{-2}) than does the ester carbanion **18**. In D_2O H-exchange and epimerization occur at the same rate, $k_{obs} = 6.4 \times 10^{-4}$ s^{-1} (pD = 8.4, 34°C), to give the same equilibrium distribution of Λ-*S*-*S* and Λ-*R*-*S* products (*24*).

Let us now look briefly at some other epimerization results. When working with the Δ-*S* ester the amount of inversion was always sufficient, irrespective of amine nucleophile concentration, to examine the Co(III) dipeptide product directly by ^{1}H-NMR (300 MHz), sometimes following overnight hydrolysis in 6 *M* HCl to remove the terminal methyl ester function. For couplings using the Λ-ester the small amount of inversion usually meant using the more sensitive (~0.05% detection limit) RP-HPLC separation of the recovered dipeptide (rather than dipeptide ester) diastereomers. Removal of Co(III) was best achieved by reduction (potentiostat) and the rotary-evaporated residue examined without further purification. Figure 6 shows the effectiveness of the HPLC method for two dipeptide products. Table V gives epimerization results under optimum conditions found by Sutton (*24*).

By quenching the aminolysis reaction at various times and examining the diastereomer ratios in the unreacted Co(III)–ester and Co(III)–dipeptide products it has been possible to build up complete concentration–stereochemistry–time profiles for several couplings. One such example is given in Fig. 7, and kinetic analysis of these data allows the rate constants for epimerization (k_1, k_2) and aminolysis (k_3, k_4) to be found. Some results obtained in this way are listed in Table X.

These data show that while the Λ-*S* (Δ-*R*) diastereomer undergoes aminolysis some 10–20 times faster than Δ-*S* (Λ-*R*), the final optical outcome in the dipeptide product also depends on the relative rates of epimerization. Thus, to take two extreme examples, the reaction of Λ-[Co(en)$_2$((*S*)-AlaOMe)]$^{3+}$ with 0.12 *M* (*S*)-PheOMe has k_4(obs)/k_2(obs) = 1.7, whereas that for the Λ-[Co(en)$_2$((*S*)-LeuOMe)]$^{3+}$ with 0.12 *M* (*S*)-AlaOMe has k_4(obs)/k_2(obs) = 1550. The former results in ~3% Λ-*R*-*S* impurity, while the latter coupling gives an optically pure product.

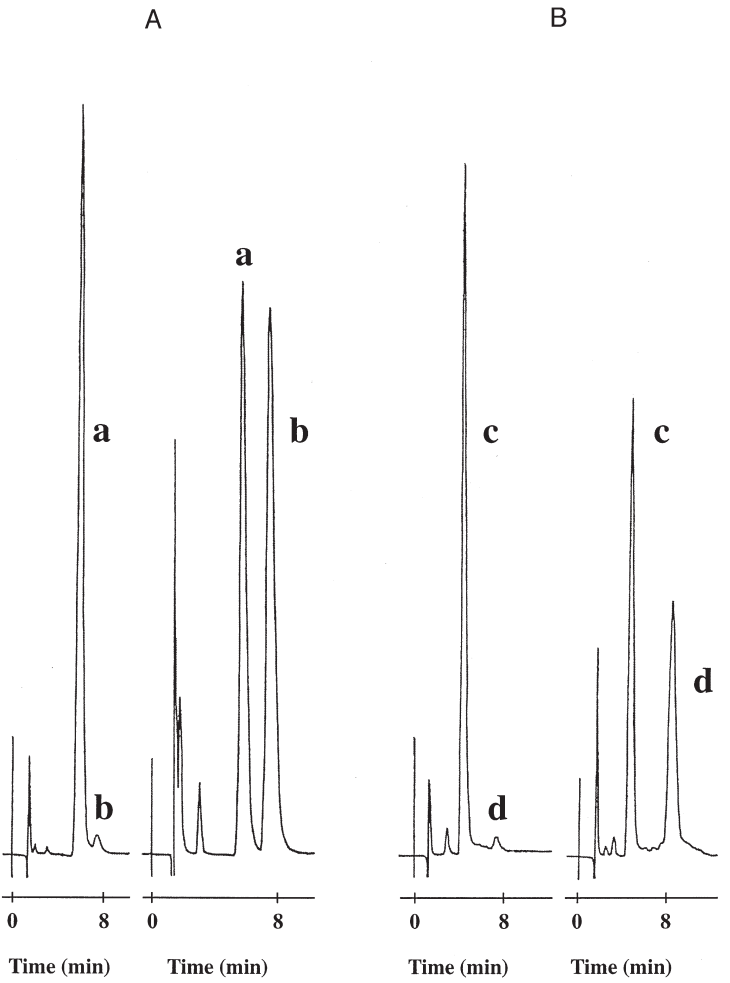

FIG. 6. The RP-HPLC chromatograms of the dipeptides recovered from (A) Λ-(left) and Δ-(right) $[Co(en)_2((S+R)\text{-Ala-}(S)\text{-PheOMe})]Cl_3$; (a) (*S*)-Ala-(*S*)-Phe, (b) (*R*)-Ala-(*S*)-Phe; and (B) from Λ-(left) and Δ-(right) $[Co(en)_2((S+R)\text{-Phe-}(S)\text{-AlaOMe})]Cl_3$; (c) (*S*)-Phe-(*S*)-Ala, (d) (*R*)-Phe-(*S*)-Ala (25% MeOH, aqueous; 35 m*M* $NaMe_2PO_4$, pH 3.25; flow rate 2 ml min^{-1}; λ = 207 nm).

VI. Mechanisms of Ester Aminolysis

Before outlining our studies in this area it is useful to have some understanding of what is to know about organic ester aminolysis.

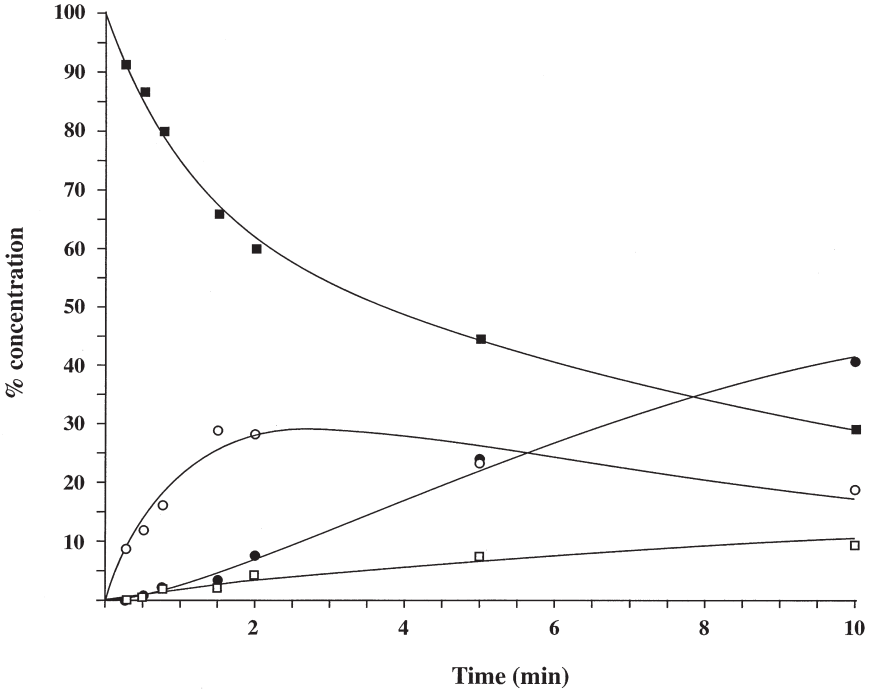

FIG. 7. Concentration–time plots for the condensation of Δ-[Co(en)$_2$((*S*)-AlaOMe)] (CF_3SO_3)$_3$ with 0.03 *M* (*S*)-PheOMe in Me_2SO, (*S*)-PheOMe · HCl = 0.06 *M*; LiCl = 0.18 *M*; 18°C. (■) Δ-*S* reactant (O) Δ-*R* reactant; (□) Δ-*S*-*S* product; (●) Δ-*R*-*S* product.

TABLE X

OBSERVED RATE CONSTANTS FOR EPIMERIZATION AND AMINOLYSIS FOR SEVERAL COUPLINGS IN Me_2SO[a]

		Epimerization rate constants (M^{-1} s^{-1})		Aminolysis rate constants (M^{-2} s^{-1})	
Co(III) complex	AA′OMe	k_1	k_2	k_3	k_4
Δ-(*S*)-AlaOMe	(*S*)-PheOMe	0.17	0.24	0.35	3.4
Δ-(*S*)-AlaOMe	(*S*)-AlaOMe	0.67	0.58	4.9	55
Δ-(*S*)-LeuOMe	(*S*)-AlaOMe	0.028	0.0017	1	22
Δ-(*S*)-ValOMe	(*S*)-AlaOMe	0.20	0.12	0.24	2.8

[a] [AA′OMe · HCl] = 0.06, 0.16 *M*; *I* = 0.27 (LiCl); T = 25°C.

A. Background

The most significant term in the rate law for the aminolysis of organic esters RC(O)OR′ is that second-order in amine (k_2, Eq. (6)). Only for reactive esters possessing excellent leaving groups (e.g., nitrophenylacetates) does the k_1 pathway make a useful contribution (*62–65*). However, under most conditions, and especially in nonaqueous solvents, the k_3 term can also make a useful contribution.

$$k_{obs} = k_1[\text{amine}] + k_2[\text{amine}]^2 + k_3[\text{amine}][\text{B}]. \quad (6)$$

In Eq. (6) B represents any base capable of removing a proton; R_3N or imidazole will do, and for aqueous solution at high pH B = OH^- is common. Variations in the contributions of the k_2 and k_3 terms as a function of pH at constant free amine concentration have required the overall reaction to be multistep, involving the formation of "tetrahedral" intermediates. The compositions and stabilities of these were investigated by a number of research groups in the 1960s and early 1970s, and were put on a firm foundation by Jencks and co-workers, as shown in two important papers which appeared at that time (*66*, *67*).

The various protonic forms $T^{\pm}$, T^+, T^o, and T^- of these intermediates (cf. Scheme 20) were shown to not necessarily be in equilibrium under a particular experimental condition, with $T^{\pm}$ and T^- normally being the most important with regard to product formation. For a not-too-reactive ester with a poor leaving group (e.g., R′ = Me, Et) in reaction with a moderately nucleophilic amine containing an ionizable proton, the general base (B = amine, buffer), or specific OH^- catalyzed formation of T^- from $T^{\pm}$ is considered to be overall rate-determining at high pH. At lower pH the slower-than-expected, and OH^- dependent, reaction is interpreted as rate-determining loss of OR^- from T^-; i.e., $T^{\pm}$ and T^- are in equilibrium under such a condition (Fig. 8). Sometimes, and at still lower pH, specific H^+ or general acid HA-catalyzed loss of HOR from $T^{\pm}$ is observed (this path is not included in Eq. (5), which relates to the higher pH condition). Whether $T^{\pm}$ exists as a true intermediate depends on the ester and amine involved and on the solvent employed ($T^{\pm}$ is more likely to exist in aprotic media). Recent ^{13}C, ^{18}O, and ^{15}N studies (*68*) have suggested that when transfer of the ionizable proton to B is thermodynamically favored the direct formation of T^- from reactants, via a termolecular process with a late transition state, may be possible. But under most conditions, and for most esters and amines, k_2 and k_3 (Eq. (5)) are the most impor-

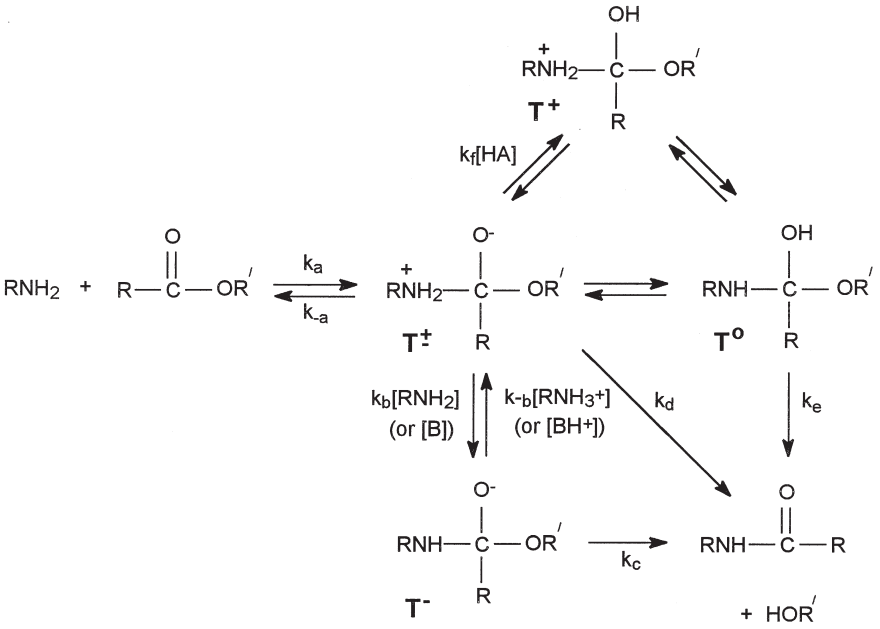

SCHEME 20.

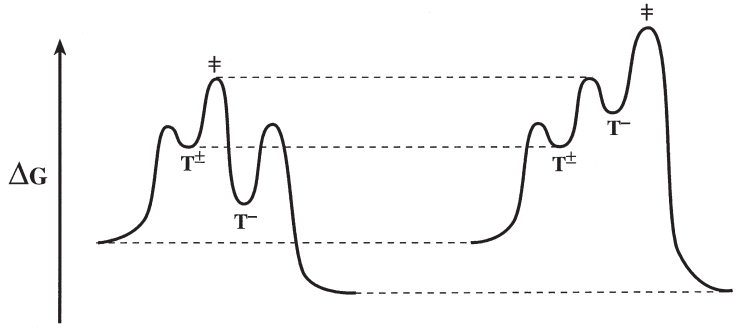

FIG. 8. Reaction coordinate profiles for aminolysis of an organic ester. For esters with moderately poor leaving groups (i.e., R = alkyl) reacting with a moderately good nucleophilic amine (i.e., NH_2R), deprotonation of the first-formed addition intermediate, $T^{\pm}$, by NH_2R is considered to be rate determining at high pH, while at lower pH loss of RO^- from T^- is considered rate determining (specific OH^- catalysis).

tant terms in the rate law and result from rate-determining proton abstraction from $T^{\pm}$ to form T^{-} (k_b in Scheme 20). In the following section we discuss how metal ion catalysis influences this process.

B. Activation by Metals

Electrophilic metals or metal complexes, when incorporated into either the acyl or alcohol functions of the ester, might be expected to increase the rate of addition of amine . This might occur through direct carbonyl-O or alcohol-O coordination (**21** or **22**, Scheme 21) or by being positioned at a discrete distance from these (cf. **23** and **24**). When the metal is attached to the alcohol function loss of this group might also be accelerated (in a stepwise addition–elimination reaction), but with acyl activation loss of alcohol might be expected to be retarded.

In the latter bonding situation the overall rate enhancement over that for the noncoordinated ester will depend on the relative stabilities, and acidities, of tetrahedral intermediates, provided these are formed. There have been no detailed mechanistic studies on systems incorporating metals "at a distance" (**23**, **24**; Scheme 21) but $[(NH_3)_5Co(GlyOEt)]^{3+}$ undergoes hydrolysis some 10^2 times faster than free GlyOEt (*44*), and the effectiveness of the Co(III) center in this case is similar to that of protonation (see Table III). In other situations Co(III) centers are somewhat less effective than H^+, but the sig-

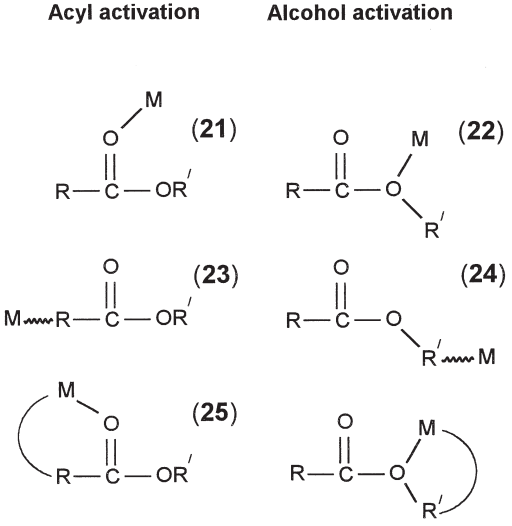

Scheme 21.

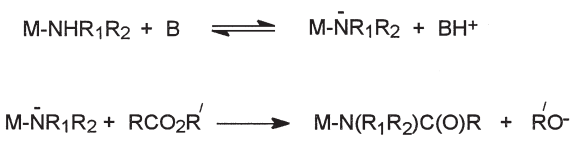

Scheme 22.

nificance here is that such attachment is pH independent so that the full capability of the metal can be realized. However, the general effectiveness of a metal coordinated "at a distance" will always be slight, probably less than 10-fold in a biomolecular kinetic sense. Direct acyl activation by Co(III), on the other hand, such as in **21** or **25**, results in 10^4- to 10^6-fold accelerations in aminolysis. In this case well-defined tetrahedral intermediates are formed, and subsequent deprotonation is rate determining (Section VI,C). Other metals might be expected to behave similarly although, since Co(III) is an especially "hard" acid, the effectiveness of softer metals might well be less in a kinetic sense. Alternatively, the amine nucleophile may be coordinated to the metal and become activated by ionization. The coordinated amine ion then attacks the ester (Scheme 22). Demonstrated cases of this are rare and have been restricted to intramolecular situations where the ester is also part of the complex. In such cases the ester is not directly activated and rate accelerations are not usually large, since prior ionization of a proton from a neutral coordinated amine is usually not substantial. Although a detailed mechanistic study on the intramolecular aminolysis of $[Co(NH_3)_5(GlyOEt)]^{3+}$ has not been carried out the observed rate law for this part of the reaction, $k_{obs} = k[OH^-]^2$ (*44*), requires initial deprotonation of a *cis*-ammine residue ($pK \geq 14$) and subsequent ring closure to be nonrate determining (Scheme 23). In line with the mechanism proposed for the intermolecular aminolysis of $[Co(en)_2(\beta\text{-AlaOi-Pr})]^{3+}$, it is likely that deprotonation of the tetrahedral intermediate (**26**) is rate limiting, rather than loss of E + O^-. It is also likely that general base catalysis will be observed, with terms $k[OH^-][B]$ in the rate law, when other bases are present.

C. Direct Carbonyl-*O* Activation

There have been only two detailed mechanistic studies on metal-activated ester aminolysis where the coordination situation remains certain. The first involves the addition of GlyOEt to $[Co(en)_2(GlyOi\text{-}Pr)](ClO_4)_3$ in Me_2SO (*13*) and the second the reaction of GlyOEt with

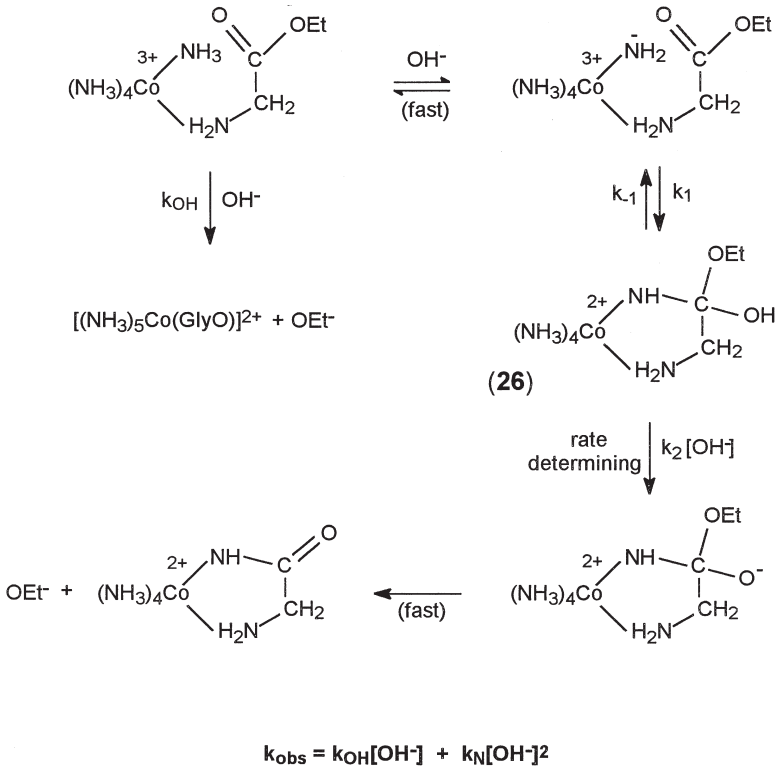

$$k_{obs} = k_{OH}[OH^-] + k_N[OH^-]^2$$

SCHEME 23.

$[Co(en)_2(\beta\text{-AlaOi-Pr})](ClO_4)_3$ in aqueous solution (*49*). We add some further information on these two studies here. Both esters are bound via terminal amino-*N* as well as carbonyl-*O*. Such chelation stabilizes carbonyl-*O* coordination and the O-donor is not displaced from the metal at any stage. The other amine ligands surrounding Co(III) provide the necessary octahedral ligand field (**27**), and we have found the

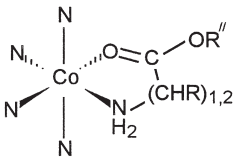

(**27**)

$(N)_4$ = $(en)_2$ system the most stable under the basic conditions of reaction with amines.

We pointed out in 1970 (*11*) that a "hard" metal ion might be expected to act like an acyl-activating organic group, assisting addition of an amine nucleophile and retarding loss of the alcohol leaving group. The overall rate enhancement, if any, would depend on the relative bond strengths and/or stabilities of tetrahedral intermediates. For such systems the possibility of a stable, even isolable, tetrahedral intermediate was also entertained.

The first detailed study in Me_2SO (*13*) used conditions where protonated amine was absent; i.e., the reaction was unbuffered. The final product (Scheme 24) contained the carbonyl-O-chelated Gly–GlyOEt dipeptide. Two distinct reactions were seen; the first involved the rapid formation of a deep-red solution, from orange (the color change was not instantaneous as might be expected for a simple deprotonation) and followed the straightforward rate law $k_{obs}(1) = k_1$[amine]. The second, much slower, reaction resulted in the return of the original color (the overall OD change was small at all wavelengths) and followed the amine-limiting rate law $k_{obs}(2) = k_2K$[amine]/(1 + K[amine]). The two reaction were interpreted as, first, addition of amine to form the rather stable tetrahedral intermediate T^+ (cf. Scheme 25; k_1 = 14 M^{-1} s^{-1} for this reaction with R′ = H; R″ = i-Pr, R = CH_2CO_2Et), followed by the loss of HOR″ from T^o (k_2 = 1.4 × 10^{-2} s^{-1}) catalyzed, probably, by the small amount of NH_3R^+ generated in the first reaction. Consistent with this interpretation was the loss and then gain of the IR absorption at 1630 cm^{-1}. Figure 9 gives a reaction coordinate diagram. The equilibrium constant governing the second reaction (K = 16 M^{-1}) represents the acidity of T^+ in Me_2SO, and we estimate that this corresponds to a pK_a of ~7 for this species in H_2O. Also, changing the ester to R″ = Me does not affect the rate constant for the addition step (k_1 = 11 M^{-1} s^{-1}, 25°C), but markedly improves the rate of loss of alcohol (fourfold for k_2, Table XI). Subsequent data obtained by Dekkers (*14*) (Table XI) show that the addition step is slower for the more bulky (*S*)-AlaOEt and (*S*)-ValOEt amines (5–10 times for k_1), but loss of i-PrOH (k_2) is not affected.

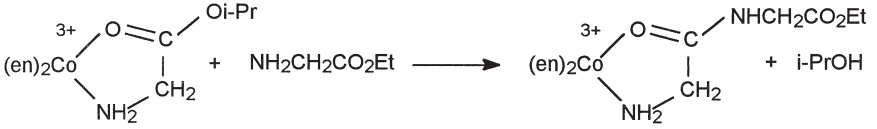

SCHEME 24.

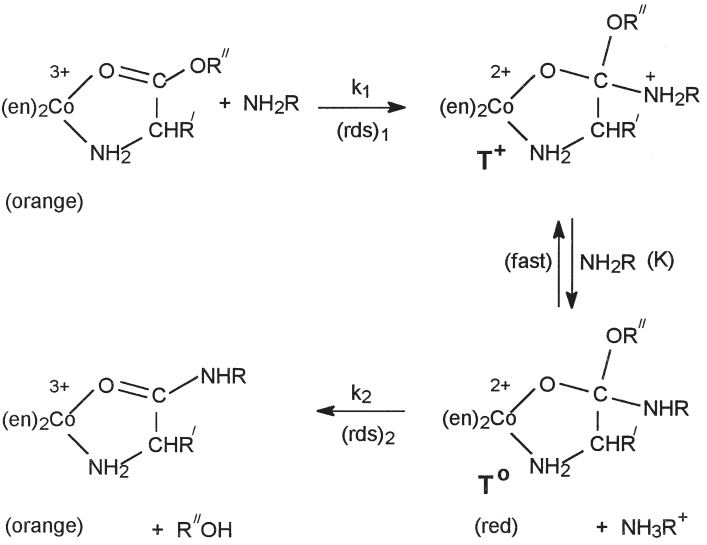

SCHEME 25.

In acetonitrile only the addition step was found to give useful kinetic data (480 nm; protonated amine absent) (*69*) and the more bulky amines were again slower to react (Table XII). The two sets of data (Tables XI, XII) confirm the order Gly > (S)-Ala > (S)-Phe > (*S*)-Val for both the chelated active ester (R) and amine nucleophile (R′), although differences (apart from the Gly-GlyOMe couplings) are not large. It can be seen that half-lives at the 0.1 *M* amine level are <10 s

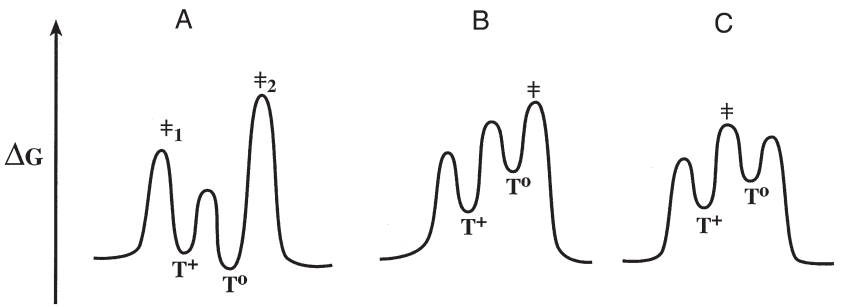

FIG. 9. Reaction coordinate profile for (A) a two-stage reaction for the addition of NH_2R to a Co(III)-active ester ($\ddagger_1$), followed by the loss of ROH from T^o ($\ddagger_2$), observed in the absence of protonated amine. (B and C) One-stage reaction observed in the presence of protonated amine: (B) rate-determining general acid (NH_3R^+, BH^+) catalyzed loss of ROH from T^o; (C) rate-determining deprotonation of T^+.

TABLE XI

RATE CONSTANTS FOR ADDITION OF AMINE (k_1) AND LOSS OF ALCOHOL (k_2) FOR THE AMINOLYSIS OF $[Co(en)_2(GlyOi\text{-}Pr)](ClO_4)_3$ IN Me_2SO AT 25°C (450 NM DATA, I = 0.015 [Co] = 2–5 mM

Co(III) chirality	AAOEt (0.02 M)	k_1/M^{-1} s^{-1}	10^3 k_2/s^{-1} ([AAOEt] = 0.02 M)
Δ, Λ	GlyOEt	14	3.7
Δ, Λ[a]	GlyOEt	11	15.2[b]
Λ	(*S*)-AlaOEt	2.9	2.0
Δ	(*S*)-AlaOEt	1.3	1.9
Λ	(*S*)-ValOEt	2.6	2.0
Δ	(*S*)-ValOEt	1.0	2.0

[a] Δ,Λ-$[Co(en)_2(GlyOMe)](ClO_4)_3$ reactant.
[b] [AAOEt] = 0.025 M.

in every case, so that reaction times of 1 min are sufficient for all couplings.

The presence of protonated amine (AAOMe · HX; X^- = Cl^-; TFA^-; $CF_3SO_3^-$) in the reaction mixtures results in loss of the red intermediate color and eliminates the small amount of side-product produced in its absence (cf. Section III,C). Only one kinetic process is now seen, but the rate of dipeptide production is little changed from that ob-

TABLE XII

RATE CONSTANTS FOR ADDITION OF AMINES (k_1) IN THE AMINOLYSIS OF $[Co(en)_2(AAOMe)](CF_3SO_3)_3$ IN ACETONITRILE (T = 25°C, I = 0.1 M (LiCl); [AA′OEt] = 0.04–0.30 M)

Co(III) complex AAOMe	(*S*)-AA′OEt	k_1/M^{-1} s^{-1}	$k_1(\Lambda/\Delta)$
Λ-Gly	Phe	4.75 (9 M^{-2} s^{-1})[a]	0(0.6)
Δ-Gly	Phe	4.75 (16 M^{-2} s^{-1})[a]	
Λ-Ala	Phe	11.3	2.7
Δ-Ala	Phe	4.1	
Λ-Val	Phe	1.0	0.55
Δ-Val	Phe	1.8	
Λ-Phe	Phe	4.2	1.05
Δ-Phe	Phe	4.0	
Λ-Ala	Val	3.5	1.5
Δ-Ala	Val	2.3	

[a] Estimated second-order rate constant for general-base catalyzed addition.

served for the addition step alone (k_1). Clearly, loss of alcohol (k_2) has been catalyzed, and T^+ and T^o have become steady-state intermediates rather than intermediate products (Figure 9). But the energies of T^+ and T^o may not be much higher than those of the reactants since little epimerization is found when only small amounts of AAOMe are present (see Table V). This suggests that some is taken up by T^+ and T^o and is therefore unavailable to catalyze epimerization (cf. Figs. 9B and 9C). The observed rate law is $k_{obs} = k[\text{amine}]^2$ or $k_{obs} = k[\text{amine}]^2 + k'[\text{amine}][B]$ when another proton-abstracting base is present, and this implies that addition (k_1) is still not rate determining. The possibility of general base-catalyzed addition, with k_1 representing a termolecular process to form T^o directly, is unlikely in view of the distinct separation of the two amine dependencies in the absence of NH_3R^+; but some general base catalysis is observed for addition in acetonitrile (cf. Table XII). The absence of a term in $[NH_3R^+]$, or $[BH^+]$, in the observed rate law (this has been tested over a concentration range of 0.06–0.24 *M* in recent studies (*26*)) allows two possible interpretations. Either deprotonation of T^+ to form T^o is rate determining (Mechanism A) or general acid-catalyzed loss of ROH from T^o is rate determining (Mechanism B). Both lead to similar rate laws

(Mechanism A)

$$k_{obs} = \frac{k_1k_2[NH_2R]\cdot[B]}{k_{-1} + k_2[B]} \rightarrow \frac{k_1k_2[NH_2R]\cdot[B]}{k_{-1}} \tag{7}$$

since $k_{-1} > k_2[B]$, whence:

$$k_{obs} = K_1k_2[NH_2R][B] \tag{8}$$

or (Mechanism B)

$$k_{obs} = \frac{k_1k_2k_3[NH_2R]\cdot[B]}{k_{-1}(k_3 + k_{-2}) + k_2k_3[B]} \rightarrow \frac{k_1k_2k_3[NH_2R]\cdot[B]}{k_{-1}k_{-2} + k_2k_3[B]} \tag{9}$$

since $k_{-2} > k_3$. Also, since we could not discover a limiting rate for [B] up to 0.5 *M* (AAOMe, or Im), then $k_{-1}k_{-2} > k_2k_3[B]$ under these conditions, whence

$$k_{obs} = \frac{k_1k_2k_3[NH_2R]\cdot[B]}{k_{-1}k_{-2}} \rightarrow K_1K_2k_3[NH_2R]\cdot[B]. \tag{10}$$

The similarity in the rate laws does not allow a clear choice to be made between mechanisms, but Mechanism A is required in H_2O by the observation of general base catalysis. However, the relative stability of the (red) T^o intermediate in Me_2SO (this is dependent on the nature of the AA side chain, cf. Section III,C) in the absence of protonated amine makes us prefer Mechanism B for reaction in this solvent, since the solvent is unable to assist the departure of MeOH. The similar catalytic rate constants found for B = imidazole, *N*-methylimidazole (*26*) suggest that transfer of the proton from T^+ to the alcohol function remains stepwise (i.e., via T^o) since *N*-methylimidazole cannot carry out a concerted transfer. Such general acid-catalyzed loss of MeOH from T^o supports a suggestion made many years ago by Burnett and Davies relating to purely organic esters (*62*).

Similar color changes occur when MeOH is used as solvent. In the absence of protonated amine the red T^o intermediate is very obvious and the reaction is two stage. But in its presence the red color is absent and only one reaction is observed. Under the latter condition a new term k_3 [NH_2R][OMe^-] appears in the rate law making the overall reaction somewhat faster in this solvent at very low amine concentrations (see Fig. 5). The appearance of this term implies that OMe^- is a particularly good base at abstracting the proton from T^+ and, as we shall see, this is also true of OH^- in H_2O.

The second published mechanistic study involves the reaction of [$Co(en)_2$(β-AlaOi-Pr)](ClO_4)$_3$ with GlyOEt in H_2O (*49*). The six-membered β-alanine system reacts more slowly than the five-membered glycine ester (~10 times), allowing more accurate kinetic data to be collected in the pH 7–8 range. Only one kinetic process was observed although two products are formed, the hydrolysed ester complex [$Co(en)_2$(β-AlaO)]$^{2+}$ (for which the kinetic term k[OH^-] is the major contributor) and the chelated dipeptide (Scheme 26) for which the rate law $k_{obs} = k$[GlyOEt][B] applies (B = GlyOEt, OH^-, and Im when present). General base catalysis in H_2O requires removal of the proton from T^+ to be rate determining, so that loss of alcohol is a faster subsequent step. Other base species were also found to be effective pro-

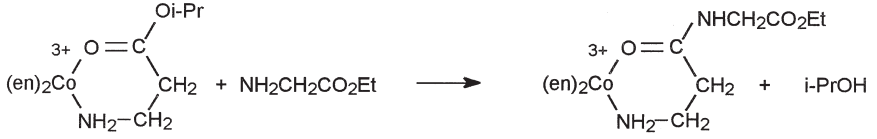

SCHEME 26.

vided they were sufficiently basic, the estimated pK_a of T^+ being ~7 in the aqueous environment (AcO^- was ineffective). Mechanism A now operates with the solvent (possibly) assisting in the departure of ROH and making this process non-rate determining. Proton removal by B = OH^- will be diffusion controlled ($k_2 \sim 10^{10} M^{-1}$ s^{-1}), giving $K_1 = 10^{-6}-10^{-7} M^{-1}$ for the addition of amine; this agrees with our inability to detect T^+ or T^o at the highest amine concentrations (1.0 M).

Table XIII lists third-order rate constants for the aminolysis of both the β-alanine and glycine ester chelates in aqueous solution and it is clear that the more electrophilic five-membered glycine system is some $10-10^2$ more reactive (this is also true of the hydrolysis reaction where loss of i-PrOH is also rate determining in the pH < 10 region (*45*)). Steric bulk in the amine nucleophile plays a role, with more basic Me_2NH being some 10^2 times less effective than NH_3 in the B = OH^--catalyzed reaction. But steric bulk seems less important in the proton abstraction process since Me_2NH is better than NH_3 in this respect, its poorer nucleophilicity being cancelled by its stronger basicity (B = Me_2NH, NH_3). Similar conclusions apply to the reactions in Me_2SO. The data of Table XI, which concerns the two-step reaction in the absence of protonated amine, show that addition (k_1) is faster for GlyOEt than for (*S*)-AlaOEt or (*S*)-ValOEt, whereas k_2 is little affected. It also appears that k_{-1} (the reverse loss of amine from T^+) is also affected since the overall rate constant for the GlyOMe system

TABLE XIII

AMINOLYSIS RATE CONSTANTS (k/M^{-2} s^{-1} = k_{obs}/[NHR_1R_2][B]) FOR REACTIONS OF [$Co(en)_2$($AAOi$-Pr)](ClO_4)$_3$ WITH VARIOUS AMINES IN AQUEOUS SOLUTION

Chelated ester ($AAOi$-Pr)	NHR_1R_2	B	k/M^{-2} s^{-1}
β-AlaOi-Pr[a]	GlyOEt	GlyOEt	3.5×10^{-2}
β-AlaOi-Pr[a]	GlyOEt	Im	2.9×10^{-2}
β-AlaOi-Pr[a]	GlyOEt	OH^-	3.9×10^{3}
GlyOi-Pr[b]	NH_3	NH_3	31
GlyOi-Pr[b]	NH_3	OH^-	9×10^{5}
	Me_2NH	Me_2NH	29
	Me_2NH	OH^-	9×10^{3}
	GlyOEt	GlyOEt	3.9×10^{-1}
	GlyOEt	OH^-	6×10^{5}

[a] Ref (*9*).
[b] Ref (*10*)

(in the presence of protonated amine) is some 20–100 times that for (*S*)-AlaOMe or (*S*)-PheOMe (see Table XIV).

D. Chiral Sensitivity

The preparative and kinetic aspects of having three asymmetric centers present in most coupling reactions are discussed in Sections III,C and V,D respectively (see also Tables IV and V). Here we only point out their effect on mechanism. The data of Table XI show that changing the Co(III) chirality from Λ to Δ results in a small decrease in the rate constant for addition (k_1) of (*S*)-AlaOEt and (*S*)-ValOEt to $[Co(en)_2(GlyOi\text{-}Pr)]^{3+}$ in Me_2SO, but no change in the rate constant for loss of i-PrOH (k_2). Small differences are also apparent (Table XII) for reactions in acetonitrile where the addition step is the observed reaction. This idea that addition of amine rather than elimination of alco-

TABLE XIV

Third-Order Rate Constants (k/M^{-2} s^{-1} = $k_{obs}/[AA'OMe]^2$) for Aminolysis of Δ- and Λ-$[Co(en)_2(AAOMe)](CF_3SO_3)_3$ in Me_2SO ($[AA'OMeH^+]$ = 0.16, 0.06 *M*; *I* = 0.27 (LiCl); *T* = 25°C)

Co(III) chelate	AA′OMe	k/M^{-2} s^{-1}
Δ,Λ-GlyOMe	GlyOMe	2500
Λ-GlyOMe	(*S*)-AlaOMe	95
Δ-GlyOMe	(*S*)-AlaOMe	52
Λ-GlyOMe	(*S*)-PheOMe	23
Δ-GlyOMe	(*S*)-PheOMe	35
Λ-GlyOMe	(R)-PheOMe	37
Δ-GlyOMe	(*R*)-PheOMe	23
Λ-(*S*)-AlaOMe	(*S*)-AlaOMe	55
Λ-(*R*)-AlaOMe	(*S*)-AlaOMe	4.9
Λ-(*S*)-AlaOMe	(*S*)-PheOMe	4.5
Λ-(*S*)-AlaOMe	(*R*)-PheOMe	5.8
Δ-(*R*)-AlaOMe	(*S*)-PheOMe	3.4
Δ-(*S*)-AlaOMe	(*S*)-PheOMe	0.35
Λ-(*S*)-ValOMe	(*S*)-AlaOMe	2.8
Λ-(*R*)-ValOMe	(*S*)-AlaOMe	0.24
Λ-(*S*)-LeuOMe	(*S*)-AlaOMe	22
Δ-(*R*)-LeuOMe	(*S*)-AlaOMe	22
Δ-(*S*)-LeuOMe	(*S*)-AlaOMe	1
Λ-(*S*)-PheOMe	(*S*)-AlaOMe	45[a]

[a] MeOH solvent.

hol is chirally sensitive is supported by recent experiments in buffered Me_2SO where only one rate process is observed. Thus the relative contributions of (*S*)-PheOMe and imidazole as a proton-abstracting base to the reactions of Δ-$[Co(en)_2((S)\text{-AlaOMe})]^{3+}$ and Δ-$[Co(en)_2((R)\text{-AlaOMe})]^{3+}$ with (*S*)-PheOMe are given by the rate law

$$k_{obs} = k'[(S)\text{-PheOMe}]^2 + k''[(S)\text{-PheOMe}][\text{Im}]. \quad (10)$$

For the Δ-R diastereomer k' and k'' take on values 3.4 and 6.3 M^{-2} s^{-1} (25°C, 0.06 *M* (*S*)-PheOMe · HCl), while for the Δ-*S* diastereomer these are 0.35 and 0.67 M^{-2} s^{-1} respectively (Table XIV). Thus while the Δ-*R* isomer is some 10 times more reactive than the Δ-*S*-isomer for both pathways, imidazole is some 2 times more effective than *S*-PheOMe for both complexes. This implies that while proton removal from T^+ to form T^o is sensitive to the nature of the proton abstracting base, it is insensitive to whether it is chiral.

VII. Peptide Synthesis at Metal Centers Other Than Cobalt(III)

In the early 1970s Yamada *et al.* (*70–72*) showed that simple dipeptide esters (AA-AAOR′; R′ = Me, Et) could be produced in low to moderate yield (7–35%) by reacting (*S*)-amino acid esters (AA = Ala, Leu, Trp, Phe, Ser, Met, Asp(OEt), Glu(OMe)) with salts of labile first-row transition metal ions ($CuCl_2$ was the most effective) in dry solvent (EtOH, MeOH) and in the presence of Et_3N. Diastereomer distributions in the dipeptide esters products (these were isolated as their Z-derivatives) were not examined directly, but optical rotations were consistent with substantial retention of configuration at the chiral centers. On the basis of i.r. measurements (*72*) it was concluded that the reactions were unlikely to involve direct M^{2+}–carbonyl-*O* activation, and it was proposed that amide bond formation occurred within the coordination sphere of the metal via intramolecular nucleophilic attack of a deprotonated amine center in one N-bound amino acid ester on the carbonyl carbon of another (cf. **28**). This type of reaction has subsequently been exploited by Beck and Krämer (*72*) and used to produce sequence-specific peptides at Ir(Cp*) and Rh(Cp*) centers (Cp* = η^5-C_5Me_5). These reactions involve the formation of bidentate diglycine ester complexes [M(Cp*)(Gly-GlyOR′)Cl] (**29**, M = Rh, R′ = Me, Et; M = Ir, R′ = Et), which are then coupled with (*S*)-AA′OR in the presence of Et_3N to give tripeptide ester complexes [M(Cp*)(AA′-

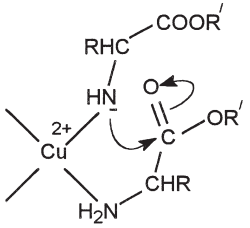

(**28**)

Gly-GlyOR′)Cl] (M = Rh, R′ = Et, AA′ = Gly, Ala, Asp(β-OMe), Ser; Leu (R′ = Me); M = Ir, R′ = Et, AA′ = Gly, Ser) (Scheme 27). Coupling conditions (15 h, 20°C, MeOH solvent) are relatively mild and lead to high yields (70 to 90%) and low epimerization, at least for the AlaOEt and LeuOMe couplings (~ 1%). The free peptides are recovered on treating the complexes with methanolic HCl. Extension of the peptide chain is possible; treating a basic MeOH solution of **29** (M = Rh, R′ = Me) successively with GlyOEt, then SerOMe results in the formation of **30**, containing the complexed Ser-Gly-Gly-GlyOMe tetra-

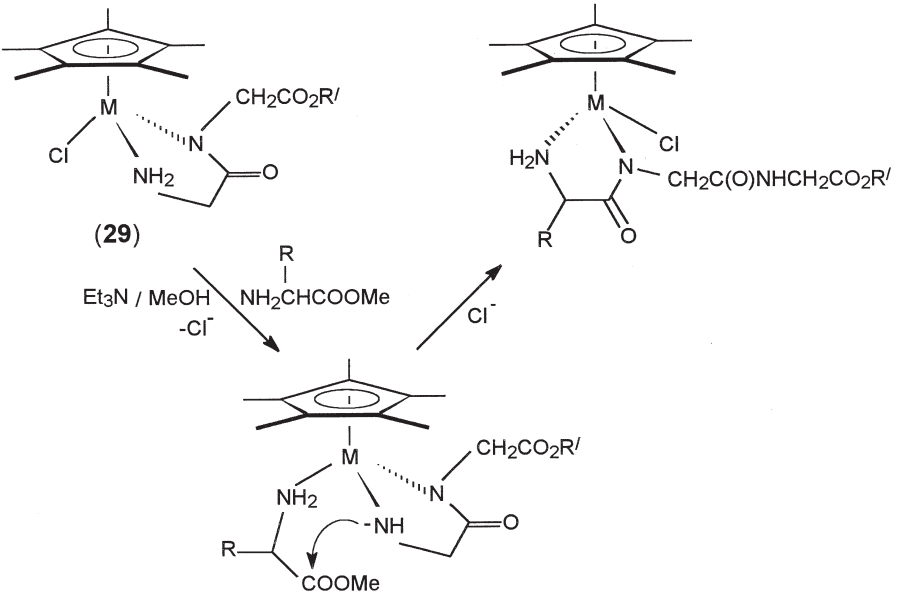

SCHEME 27.

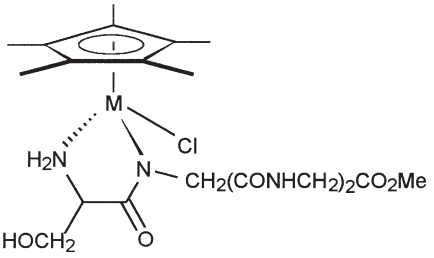

(**30**)

peptide ester (*73*). Peptide bond formation in this system has so far been limited solely to production of AA′-Gly fragments and it remains to be seen whether the method will have wider utility. However, addition of AlaOMe to [Ru(η^6-4-cymene)(Gly-Gly-GlyOMe)Cl] (4-cymene = 4-isopropyl toluene) affords both the Ala-Ala-Gly-Gly-Gly and Ala-Gly-Gly-Gly complexes (*74*).

The reaction of aromatic amino acids, dipeptides, or protected amino acids with [Ru(Cp*)($CH_3CN)_3$]PF_6 in THF (THF = tetrahydrofuran) leads to the formation of robust Ru(Cp*) sandwich complexes in which side-chain phenyl (e.g., Phe, Tyr) or indole groups (Trp) are bound η^6 to a Ru(Cp*) center (cf. **31**; AA = Phe) (*75*, *76*). The similar

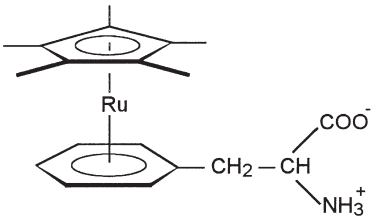

(**31**)

reaction of $[Ru(Cp^*)Cl_2]_2$ with alanine or phenylalanine in MeOH/NaOMe gives *N,O*-[Ru(Cp*)(AAO)Cl] complexes at low temperatures (0–20°C) and, for the latter, [Ru(Cp*)(η^6-Phe)Cl] under reflux conditions (*77*). The corresponding ester complex [Ru(Cp*)(η^6-PheOMe)]Cl in basic dichloromethane gives [(Z-Phe-η^6-Phe(OMe))Ru(Cp*)]$^+$ (**32**) on diimide coupling (12 h, −50°C) with Z-Phe (*76*). The Ru(Cp*) attachment in **32** survives N-deprotection conditions (98% HOAc) and

the resulting product is readily cyclized to the diketopiperazine (**33**) (cf. the intermolecular cyclization of free amino acid esters).

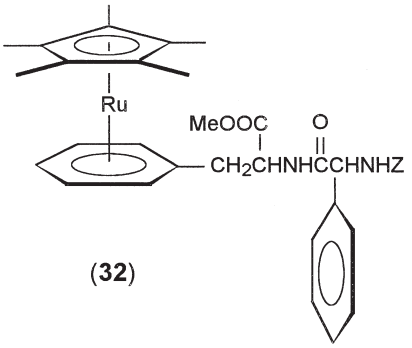

(**32**)

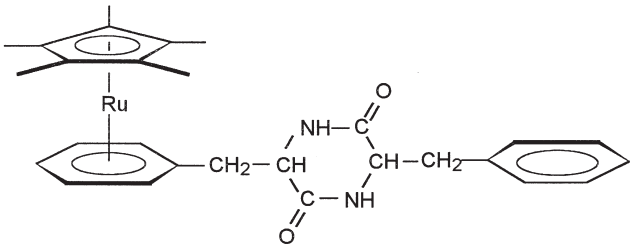

(**33**)

Janetka and Rich (*78*) have utilized the considerable stability of ruthenium-π-arene systems in the synthesis of cyclic tripeptides as analogs of the protease inhibitor K-13 (cf. **34**, Scheme 28). Their approach involves the construction of linear tripeptide complexes (**35**) using diimide/HOBt coupling of [Ru(Cp)(Boc-*p*-Cl-PheOH)]PF_6 (Cp = η^5-C_5H_5) with the appropriate dipeptide ester. Cyclization of **35** affords the biphenyl ether **36**, which on photolysis (350 nm) gives **34**.

Metal-bound carboxylate can be directly acylated without M–O bond breaking. In Co(III) chemistry this is evidenced by the slow OH-induced $^{18}O/^{16}O$ isotopic exchange observed for Co(III)-chelated glycinate and oxalate (*79*, *80*); however, the carbonyl centers of carboxylate ligands bound to Co(III) are not sufficiently electrophilic to undergo aminolysis. This is not so for Ti(IV), Zr(IV), and Ta(V) carboxylates (cf. **37**, **38**, and **39** respectively), which exhibit significantly higher degrees of acyl activation (*81, 82*). Thus, aminolysis of the bis-amino acid complex **37** (R = *Z*-NHCH(CH_3)-) in THF solution, using stoichio-

metric quantities of AlaOMeHCl and Et_3N (2 equiv.), gives Z-Ala-AlaOMe in 45% yield following hydrolysis and removal of the metal. However, the conditions required for aminolysis of both **37** (R = *Z*-NHCH(CH_3)-, $(CH_3)_2$CH-), and **38** (R = $(CH_3)_2$CH-) are relatively harsh, involving extended reaction times (24 h), basic media, and ele-

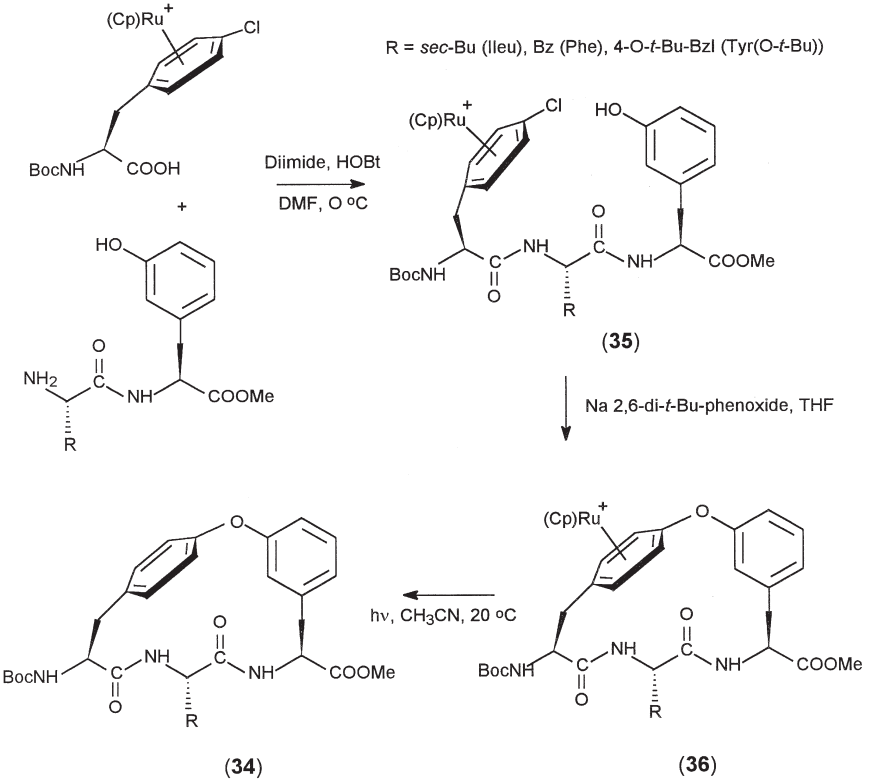

SCHEME 28.

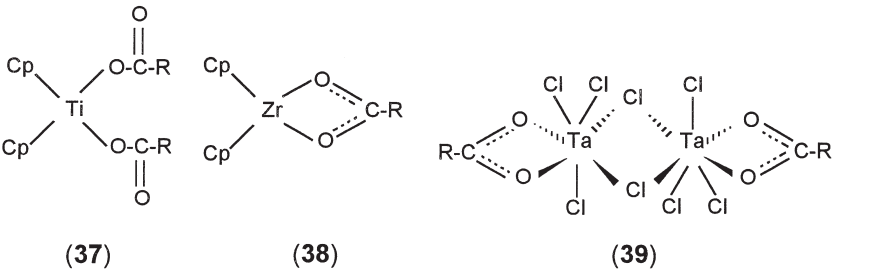

vated temperatures (67°C). Much less forcing conditions are needed for aminolysis of **39** (R = $(CH_3)_2CH$-) (*81*).

As part of a study of Ta(V)-carboxylates Joshi *et al.* (*82*) prepared monodentate amino acid complexes, [$CpTaCl_3$(*Z*-(*S*)-Ala)] and [$CpTaCl_3$(*N*-Ac-(*S*)-Ala)], and reacted these directly with AAOMe species (generated from AAOMe · HCl by addition of Et_3N or *N*-methylmorpholine, AA = (*S*)-Ala, (*S*)-Phe, (*S*)-Leu). Such couplings were able to be carried out under mild conditions (toluene solution, −14°C, 1 h) and gave, following hydrolysis, the corresponding N-protected (*S*)-Ala-(*S*)-AAOMe dipeptide esters in yields of between 70 and 80%. These reactions appear to have considerable potential since recemization in the products (determined by ^1H and ^{13}C NMR spectroscopy, HPLC) was found to be <0.2% for *Z*-Ala-AlaOMe and *Z*-Ala-PheOMe, 0.4% for *N*-Ac-Ala-PheOMe, and 1.1% for *N*-Ac-Ala-LeuOMe when *N*-methylmorpholine was the deprotonating base. Use of Et_3N gave somewhat higher levels of racemization. The similar coupling of [$(Cp)_2TiCl$(*Z*-(*S*)-Ala)] with (*S*)-PheOMe · HCl, under more forcing conditions and using Et_3N as the base, leads to significant amounts of *Z*-(*R*)-Ala-(*S*)-PheOMe product (*82*).

VIII. Experimental Methods

Typical syntheses of Co(III)-amino acid, amino acid ester, and dipeptide ester chelates are described below. The NMR spectra of the isolated products were in accord with expectation. The procedures given here are generally applicable, except for that given for [$Co(en)_2$((*S*)-GluOBzl)]I_2. If this method is used to coordinate amino acids that are only partially soluble in Me_2SO, more forcing conditions (extended reaction times, 1–5 h, 50–60°C) may be required. Dipeptide ester complexes are not always as amenable as [$Co(en)_2$(Val-GlyOEt)]I_3 to crystallization from water.

A. [$Co(en)_2$((*S*)-Ala)]I_2 (*trans*-[$Co(en)_2Br_2$]Br Method)

To finely powdered *trans*-[$Co(en)_2Br_2$]Br (41.9 g, 0.10 mol) in 50% methanol-water (400 ml) was added a solution of lithium hydroxide (monohydrate, 4.1 g, 0.10 mol) in 50% methanol–water (200 ml). The mixture was stirred and heated under reflux for 30 min. Water (1 liter) and conc. HCl (25 ml) were added and the solution was sorbed onto a column of Dowex 50W-X2 ion-exchange resin (H^+ form, 10 × 35 cm). The column was washed with HCl (0.20 *M* 1 liter) and the

major orange product recovered on elution with 1 *M* HCl. This fraction was reduced to dryness (rotary evaporator) and the solid residue dissolved in hot water. The solution was then neutralized (Et_3N, dropwise addition) and treated with excess NaI. On cooling in ice orange crystals deposited. These were recovered by filtration, washed thoroughly with a small amount of ice water, then with EtOH, and air dried. Calc. for $CoC_7H_{22}N_5O_2I_2$: C, 16.14; H, 4.26; N, 13.44. Found: C, 16.21; H, 4.32; N, 13.55%.

B. $[Co(en)_2((S)\text{-GluOBzl})]I_2$ (Me_2SO METHOD)

To (*S*)-glutamic acid γ-benzyl ester (3.57 g, 1.50×10^{-2} mol) and $[Co(en)_2(Me_2SO)_2](ClO_4)_3$ (9.50 g, 1.50×10^{-2} mol) in dry Me_2SO (75 ml) was added Et_3N (1.50 g, 1.50×10^{-2} mol) and the mixture stirred at 50°C until all the amino acid ester had dissolved (15 min). The solution was cooled and stirred for a further 2 h at room temperature before being poured into weakly acidified water (750 ml, 3 ml HOAc). The reaction products were sorbed onto Sephadex SP C-25 ion exchange resin and the column (5 × 35 cm) was washed with water (2 liters). The products were eluted with aqueous pyridinium acetate (pyH^+OAc^-, 0.5 *M,* pH 5) and the major orange band was collected and taken to dryness (rotary evaporator, 40°C). Crystallization from warm water on addition of NaI gave the desired complex, which was filtered off, washed with EtOH and then Et_2O, and air dried (6.0 g, 60%). Calc. for $CoC_{16}H_{30}N_5O_4I_2 \cdot H_2O$: C, 27.96; H, 4.69; N, 10.19. Found: C, 28.02; H, 4.81; N, 10.10%.

C. $[Co(en)_2((S)\text{-Glu(OBzl)OMe})](CF_3SO_3)_3$

To $[Co(en)_2((S)\text{-GluOBzl})]I_2$ (5.0 g, 7.3×10^{-3} mol) in dry trimethylphosphate (18 ml, 4A sieves) contained in a conical flask equipped with a drying tube was added methyl trifluoromethane sulfonate (8.0 g, 4.9×10^{-2} mol) and the mixture was stirred at room temperature for 30 min (*Caution:* The alkylating agent is believed to be extremely toxic. Use a hood and avoid skin and vapor contact). The deep orange solution was then slowly poured into rapidly stirred dry ether (600 ml) and the precipitated semisolid recovered by decantation. The residue was dissolved in the minimum volume of dry methanol (10–20 ml), the product reprecipitated using further dry ether (400 ml), and the solid recovered as before. A further precipitation using methanol (10–20 ml) and dry ether (800 ml) produced the complex as a finely divided solid. This was recovered by filtration (porosity 4 sin-

ter) with precautions being taken to avoid exposure to air. The product was washed thoroughly with dry Et_2O, transferred to a vacuum dessicator while still damp, and carefully dried at room temperature (*ca.* 20 mm Hg, then 0.5 mm Hg, 6.1 g, 95%). Calc. for $CoC_{20}H_{33}N_5O_{13}S_3F_9$; C, 27.37; H, 3.79; N, 7.98. Found: C, 27.31; H, 3.99; N, 8.19%.

D. $[Co(en)_2(Val\text{-}GlyOEt)]I_3$

To $[Co(en)_2((S)\text{-}ValOMe)](CF_3SO_3)_3$ (2.0 g, 2.64×10^{-3} mol) in dry Me_2SO (10 ml) was added a solution of $GlyOEt \cdot HCl$ (3.66 g, 2.64×10^{-3} mol) and Et_3N (0.53 g, 5.2×10^{-3} mol) in Me_2SO (10 ml). After 10 min the reaction was quenched by the addition of acidified water (300 ml, 1 ml HOAc) and the products sorbed onto a Sephadex SP C-25 ion exchange column (2×20 cm). The column was washed with water (500 ml) and eluted with pyridinium acetate (pyH^+OAc^-, 0.5–1.5 *M,* pH 5). This gave two orange bands, the second of which (major, >85%) was collected and rotary evaporated to dyness. The resulting oil in warm water (7 ml) was treated with excess NaI, giving the crystalline dipeptide ester complex on cooling. This was filtered off, washed with acetone and then Et_2O, and air dried (0.85 g, 42%, $\nu_{C=O}$ = 1730, 1625 cm^{-1} (nujol)). Calc. for $CoC_{13}H_{34}N_6O_3I_3 \cdot H_2O$: C, 20.01; H, 4.65; N, 10.77. Found: C, 20.07; H, 4.55; N, 10.62%.

E. Tritium Incorporation Experiments

The two reactants Δ- (or Λ-) $[Co(en)_2((S)\text{-}AAOMe)](CF_3SO_3)_3$ and AA′OMe were mixed following separate solution in dry Me_2SO (6.0 ml final volume). The latter reagent was either a freshly prepared sample (GlyOMe, (*S*)-AlaOMe) or was prepared *in situ* by partial titration of $AA'OMe \cdot HCl$ with NEt_3 ($NEt_3 \cdot HCl$ precipitated); ^3H-labeled H_2O (1 μl; 5Ci ml^{-1}) was included in this solution. Generally the following concentration ratios applied; $Co : AA'OMe : AA'OMe \cdot HCl = 0.058 : 0.174 : 0.116$ *M;* such conditions are close to those found to produce the least amount of epimerization in the final dipeptide product (see Section IIIC). Tritium incorporation was quenched by addition of HOAc after 1 min (coupling reaction complete) or at longer times (to allow for exchange into the Co(III)–dipeptide product). Ancillary experiments established that (1) ^3H incorporated into the complex could be related to both the total activity of the solution and to the total number of exchangeable protons present, the latter included all amine protons, coordinated and noncoordinated; (2) no additional un-

accounted source of protons was present (i.e., residual H_2O); and (3) subsequent washing of Co(III) species on the ion-exchange column (H_2O followed by 0.05 *M* phosphate buffer pH 6.8, 1–5 days), although resulting in some epimerization in the Co(III)–dipeptide product (particularly for Λ-*S*-*S*), only removed ^3H label from amine residues—it did not affect ^3H attached to α-C. The dipeptide ester complex was recovered from the column, hydrolyzed (6 *M* HCl, 16 h), reduced to dryness, and reduced (potentiostat). The liberated dipeptide diastereomers were separated by HPLC and their ^3H content estimated using standard methods (*24*).

IX. Concluding Remarks

Features exhibited by the Co(III) method can be summarized as follows.

1. It combines amine protection with considerable carbonyl activation.
2. Couplings are fast, and high yields are obtained when H_2O (moisture) is rigorously excluded.
3. The reagents, once prepared, can be stored for long periods.
4. The method can be applied to the majority of amino acids and to other amines (or nucleophiles) as required.
5. The orange color of the Co(III) chromophore ($\varepsilon \sim 100\ M^{-1}\ cm^{-1}$, 485 nm) allows ready visual detection.
6. The Co(III) reagent can be readily removed by chemical or electrochemical (preferred) methods.
7. Low levels of epimerization (racemization) can be achieved, provided the Λ-*S* reagent is used and the reaction medium is appropriately buffered.

Some comment concerning the last point is appropriate, since stereochemically exclusive methods of chemical synthesis are eagerly sought. It appears from our studies that the Λ-*S* combination is useful in this regard, without yet being as optically rewarding as conventional methods. Table XV clearly shows that DCC-mediated couplings are superior to the Co(III)-promoted reactions. However, it is also clear that the stereochemistry of the amine nucleophile plays only a minor role in the Co(III) method. Thus couplings involving Λ-S reactants are some 10–20 times faster than those of their Δ-*S* counterparts, irrespective of the nature of the amine nucleophile or its stereochemistry, whereas the epimerization rates are more similar (these differ by a factor of ~2). Such effects need to be researched for other

TABLE XV

EPIMERIZATIONS OBSERVED IN DCC-MEDIATED PEPTIDE COUPLING

Coupling	Activation method	Solvent	Reaction time	% Epimerisation in product
Boc-(*S*)-Phe + Gly-OCH_2P	DCC	CH_2Cl_2		0.0 (Isotopic dilution)[a]
Boc-(*S*)-Phe + Gly-(*S*)-Val-OCH_2P	DCC	CH_2Cl_2	150 min	0.02 (HPLC)[b]
Boc-(*S*)-Leu + (*S*)-Ala-Gly-(*S*)-Val-OCH_2P	DCC	CH_2Cl_2	150 min	0.03 (HPLC)[b]
Bzl-(*S*)-X + (*S*)-Lys(Z)-OMe (X = (*S*)-Leu,Ala,Val,Phe,Ile)	DCC, HOBt	CH_2Cl_2	Overnight	<1.5 (^{1}-H-NMR)[c]
Z-Gly-(*S*)-X + (*S*)-Lys(Z)-Obzl (X = (*S*)-Ala,Leu,Phe,Val,Ile)	DCC, HOBt	CH_2Cl_2	Overnight	<0.05 (HPLC)[d]
Z-Gly-(*S*)-Val + (*S*)-Val-OMe	DCC, HOBt, DCC, $CuCl_2$	DMF DMF	24 h 24 h	0.4 (HPLC)[e] <0.1[e]

[a] Rebek, J.; Feither, D. *Int. J. Pept. Prot. Res.* **1975,** *7,* 167.
[b] Kent, S.; Mitchell, A.; Barany, G.; Merrifield, R. *Anal. Chem.* **1978,** *50,* 155.
[c] Benoiton, N.; Kuroda, K.; Chen, F. *Int. J. Pept. Prot. Res.* **1979,** *13,* 403.
[d] Benoiton, N.; Kuroda, K. *Int. J. Pept. Prot. Res.* **1981,** *17,* 197.
[e] Miyazawa, T.; Otomatsu, T.; Yamada, T.; Kuwata, S., *Tetrahedr. Lett.* **1984,** *25,* 771.

asymmetric systems, with the aim being to discover, and then exploit, a metal (or other) system which is stereospecific in this regard rather than being just stereoselective. It is possible to imagine an activating group such that, even if removal of the asymmetric H atom of the amino acid occurs, reprotonation of the resulting carbanion results in full retention for a Λ-*S* reactant. Likewise, it is possible to imagine the same stereochemistry as resulting in exclusive attack of the amine nucleophile on one face of the carbonyl center to give an optically pure product. Surely this is how the ribosome works. Let us duplicate it in the laboratory. The Co(III) system described here goes only partway to achieving this goal.

A better leaving group should also be sought. Our studies show that the rate-determining step is even further moved toward loss of the alcohol function (from the ester). The reaction is also clearly two step. The choice of methyl ester is perhaps the worst in this regard, and an anhydridelike system would be better. An alternative, where the carbonyl–OX bond is weaker without being electron attracting would move the rate-determining step toward amine addition without further activating the carbonyl and adjacent asymmetric C centers; Co(III) is good enough in this regard. Also, it would be advantageous to provide a spacer "X," as in **40**, such that activation of the

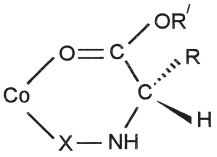

(**40**)

asymmetric C center via the amine function is reduced without altering its effectiveness on the carbonyl group. But the implementation of such suggestions will have to await another place and time.

References

1. Clark, C. R.; Tasker, R. F.; Buckingham, D. A.; Knighton, D. R.; Harding, D. R. K.; Hancock, W. S. *J. Am. Chem. Soc.* **1981,** *103,* 7023.
2. Knighton, D. R.; Harding, D. R. K.; Friar, M. J.; Hancock, W. S.; Reynolds, G. D.; Clark, C. R.; Tasker, R. F.; Buckingham, D. A. *J. Am. Chem. Soc.* **1981,** *103,* 7025.
3. Buckingham, D. A.; Marzilli, L. G.; Sargeson, A. M. *J. Am. Chem. Soc.* **1967,** *89,* 2772.
4. Buckingham, D. A.; Marzilli, L. G.; Sargeson, A. M. *J. Am. Chem. Soc.* **1967,** *89,* 4539.
5. Collman, J. P.; Kimura, E. *J. Am. Chem. Soc.* **1967,** *89,* 6096.
6. Wautier, H.; Marchal, D.; Fastrez, J. *J. Chem. Soc. Dalton Trans.* **1981,** 2484.
7. Mensi, N.; Isied, S. S. *Inorg. Chem.* **1986,** *25,* 147.
8. Sargeson, A. M.; Searle, G. H. *Nature* **1963,** *200,* 356; *Inorg. Chem.,* **1965,** *4,* 45; *Inorg. Chem.,* **1967,** *6,* 787; *Inorg. Chem.* **1967,** *6,* 2172.
9. Alexander, M. D.; Busch, D. H. *J. Am. Chem. Soc.* **1966,** *88,* 1130.
10. Buckingham, D. A.; Marzilli, P. A.; Maxwell, I. E.; Sargeson, A. M.; Fehlmann, M; Freeman, H. C. *J. Chem. Soc. Chem. Commun.* **1968,** 488.
11. Buckingham, D. A.; Foster, D. M.; Sargeson, A. M. *J. Am. Chem. Soc.* **1970,** *92,* 5701.
12. Buckingham, D. A.; Foster, D. M.; Sargeson, A. M. *J. Am. Chem. Soc.* **1968,** *90,* 6032.
13. Buckingham, D. A.; Dekkers, J.; Sargeson, A. M. *J. Am. Chem. Soc.* **1973,** *95,* 4173.
14. Dekkers, J.; PhD Thesis, Aust. Natl. Univ., 1972.
15. Jones, J. In "Amino Acid and Peptide Synthesis," Chapt. 5; Oxford Chemistry Primer Series, 1992.
16. Buckingham, D. A.; Marzilli, L. G.; Sargeson, A. M. *J. Am. Chem. Soc.* **1967,** *89,* 5133.
17. Buckingham, D. A.; Stewart, I.; Sutton, P. A. *J. Am. Chem. Soc.* **1990,** *112,* 845.
18. Straud, E. D.; Fife, D. J.; Smith, G. G. *J. Org. Chem.* **1983,** *48,* 4368.
19. Tasker, R. F.; PhD Thesis, Univ. Otago, 1982.
20. Meisenheimer, J.; Angermann, C.; Holsten, H.; Kinderlen, E. *Annalen* **1924,** *438,* 217.
21. Liftschitz, I. *Rec. Trav. Chim* **1939,** *58,* 785; *Proc. Acad. Sci. Amsterdam* **1939,** *42,* 173.

22. Werner, A. *Annnalen* **1912,** *386,* 1. Werner, A.; Schoke, E. *Berichte* **1911,** *44,* 1896.
23. Alexander, M. D.; Busch, D. H. *Inorg. Chem.,* **1966,** *5,* 602.
24. Sutton, P. A.; PhD Thesis, Univ. Otago, 1988.
25. Knighton, R. F.; MSc Thesis, Massey Univ., 1979.
26. Browne, R.; unpublished work.
27. Buckingham, D. A.; Binney, G. S.; Clark, C. R.; Garnham, B.; Simpson, J. *Inorg. Chem.* **1985,** *24,* 135.
28. Buckingham, D. A.; Clark, C. R.; Deva, M. M.; Tasker, R. F. *Inorg. Chem.* **1983,** *22,* 2754.
29. Mathieu, J. P. *Bull. Soc. Chim. France* **1939,** *6,* 873.
30. Buckingham, D. A.; Collman, J. P. *Inorg. Chem.* **1967,** *6,* 1803.
31. Clark, C. R.; Sargeson, A. M.; unpublished results.
32. Liu, C. T.; Douglas, B. E. *Inorg. Chem.* **1964,** *3,* 1356.
33. Legg, J. I.; Steele, J. *Inorg. Chem.* **1971,** *10,* 2177.
34. Buckingham, D. A.; Dekkers, J.; Sargeson, A. M.; Marzilli, L. G. *Inorg. Chem.* **1973,** *12,* 1207.
35. Hammershøi, A.; Hartshorn, R. M.; Sargeson, A. M. *Inorg. Chem.* **1990,** *29,* 4525.
36. Chong, E. K., Harrowfield, J. M. Jackson, W. G., Sargeson, A. M., Springborg, J., *J. Am. Chem. Soc.* **1985,** *107,* 2015.
37. Kothari, V. M.; Busch, D. H. *Inorg. Chem.* **1969,** *8,* 2276.
38. Jackson, W. G.; Sargeson, A. M.; Tucker, P. A. *J. Chem. Soc. Chem. Commun.* **1977,** 199.
39. Wong, C. P.; Jackman, L. M.; Portman, R. G. *Tet. Letts.* **1974,** 921.
40. Wautier, H.; Daffe, V.; Smets, M-N.; Fastrez, J. *J. Chem. Soc. Dalton Trans.* **1981,** 247.
41. Kroll, H. *J. Am. Chem. Soc.* **1952,** *74,* 2036.
42. Hay, R. W.; Morris, P. J. In *"Metal Ions in Biological Systems"* (H. Sigel, Ed.), p. 173; Marcel Dekker: New York, 1976.
43. Sutton, P. A.; Buckingham, D. A. *Accts. Chem. Res.* **1987,** *20,* 357.
44. Buckingham, D. A.; Foster, D. M.; Sargeson, A. M. *J. Amer. Chem. Soc.* **1969,** *91,* 3451.
45. Baraniak, E.; Buckingham, D. A.; Clark, C. R.; Moynihan, B. H.; Sargeson, A. M. *Inorg. Chem.,* **1986,** *25,* 3466.
46. Buckingham, D. A.; Foster, D. M.; Sargeson, A. M. *Aust. J. Chem.* **1969,** *22,* 2479.
47. Wu, Y.; Busch, D. H. *J. Am. Chem. Soc.* **1970,** *92,* 3326.
48. Buckingham, D. A.; Dekkers, J.; Sargeson, A. M.; Wein, M. *J. Am. Chem. Soc.* **1972,** *94,* 4032.
49. Buckingham, D. A.; Clark, C. R. *Inorg. Chem.* **1986,** *25,* 3478.
50. Isied, S. S.; Kuehn, C. G. *J. Am. Chem. Soc.* **1978,** *100,* 6752.
51. Isied, S. S.; Vassilian, A.; Lyon, J. M. *J. Am. Chem. Soc.* **1982,** *104,* 3910.
52. Bagger, S.; Kriistjansson, I.; Soetofte, I.; Thorlacius, A. *Acta. Chem. Scand.* **1985,** *A39,* 125.
53. Isied, S. S.; Lyon, J. M.; Vassilian, A. *Int. J. Peptide Res.* **1982,** *19,* 354.
54. Mensi, N.; Isied, S. S. *J. Am Chem. Soc.* **1987,** *109,* 7882.
55. Arbo, B. E.; Isied, S. S. *Int. J. Pept. Prot. Res.* **1993,** *42,* 138.
56. Schellenberger, V.; Jakubke, H-D. Angew. *Chem. Int. Ed Engl.* **1991,** *30,* 1437.
57. Smith, G. G.; Sivakua, T. *J. Org. Chem.* **1983,** *48,* 627.
58. Denkewalter, R. G.; Schwan, H.; Strachan, R-G.; Beesley, T. E.; Veber, D. F.; Schoenewaldt, E. F.; Barkemeyer, H.; Paleveda, W. J.; Jacob, T. A.; Hirschmann, R. *J. Am. Chem. Soc.* **1966,** *88,* 3168.

59. Clark, C. R.; Lorimer, A.; unpublished results.
60. Buckingham, D. A.; Clark, C. R.; unpublished results.
61. Liddell, G. F.; Evans, A. B.; Buckingham, D. A. *Int. J. Chem. Kinet.* **1990,** *22,* 951.
62. Burnett, J. F.; Davies, G. T. *J. Am. Chem. Soc.* **1960,** *82,* 665.
63. Jencks, W. P.; Carriulo, J. *J. Am. Chem. Soc.,* **1960,** *82,* 675.
64. Bruice, T. C.; Mayahi, M. F. *J. Am. Chem. Soc.* **1960,** *82,* 3067.
65. Holmquist, B.; Bruice, T. C. *J. Am. Chem. Soc.* **1969,** *91,* 2985.
66. Blackburn, G. M.; Jencks, W. P. *J. Am. Chem. Soc.* **1968,** *90,* 2638.
67. Satterthwaite, A. C.; Jencks, W. P. *J. Am. Chem. Soc.* **1974,** *96,* 7018, 7031.
68. Marlier, J. F.; Haptonstall, B. A.; Johnson, A. J.; Sacksteder, K. A. *J. Am. Chem. Soc.* **1997,** *96,* 119, 8838.
69. Clark, C. R.; unpublished data.
70. Yamada, S.; Wagatsuma, M.; Takeuchi, Y.; Terashima, S. *Chem. Pharm. Bull.* **1971,** *19,* 2380.
71. Terashima, S.; Wagatsuma, M.; Yamada, S. *Tetrahedron* **1973,** *29,* 1487.
72. Wagatsuma, M.; Terashima, S.; Yamada, S. *Tetrahedron* **1973,** *29,* 1497.
73. Beck, W.; Krämer, R. *Angew. Chem. Int. Ed. Engl.* **1991,** *30,* 1467.
74. Hoffmueller, W.; Maurus, M.; Severin, K.; Beck, W. *Eur. J. Inorg Chem.* **1998,** *6,* 729.
75. Moriarty, R. M.; Ku, Y.-Y.; Gill. U. S. *J. Chem. Soc. Chem. Commun.* **1987,** 1837.
76. Gleichmann, A. J.; Wolff, J. M.; Sheldrick, W. S. *J. Chem. Soc. Dalton Trans.* **1995,** 1549.
77. Sheldrick, W. S.; Gleichmann, A. J. *J. Organomet. Chem.* **1994,** *470,* 183.
78. Janetka, J. W.; Rich, D. H. *J. Am. Chem. Soc.* **1995,** *117,* 10585.
79. Miskelly, G. M.; Clark, C. R.; Buckingham, D. A. *J. Am. Chem. Soc.* **1986,** *108,* 5202.
80. Boreham, C. J.; Buckingham, D. A. *Aust. J. Chem.* **1980,** *37,* 27.
81. Recht, J.; Cohen, B. I.; Goldman, A. S.; Kohn, J. *Tetrahed. Lett.* **1990,** *31,* 7284.
82. Joshi, K.; Bao, J.; Goldman, A. S.; Kohn, J. *J. Am. Chem. Soc.* **1992,** *114,* 6649.

This Page Intentionally Left Blank

STRUCTURES AND REACTIVITIES OF PLATINUM-BLUES AND THE RELATED AMIDATE-BRIDGED PLATINUM^{III} COMPOUNDS

KAZUKO MATSUMOTO* and KEN SAKAI†

*Department of Chemistry, School of Science and Engineering, Waseda University, Japan Science and Technology Corporation, Tokyo 169-8555, Japan
and †Department of Applied Chemistry, Science University of Tokyo, Tokyo 162, Japan

Copyright □ 2000 by Academic Press.
All rights of reproduction in any form reserved.
0898-8838/00 $30.00

I. Introduction

In contrast to the numerous synthetic and reaction chemistry studies of Pt^0, Pt^{II}, and Pt^{IV}, only a few Pt^{III} complexes are known and their reactivities are yet to be explored. Platinum^{III} is usually unstable and can be isolated only in complexes with certain special ligands. Monomeric Pt^{III} complex is very rare and so far only one well-characterized complex is known, in contrast to the now increasing knowledge of Pt^{III} dinuclear complexes. Thus, $(NBu_4)[Pt(C_6Cl_5)_4]$ appears to be the only well-characterized monomeric Pt^{III} complex (*1*). Dinuclear Pt^{III} complexes usually have bridging ligands of suitable bite distances such as deprotonated amidate (*2*) pyrimidine nucleobases (*3*) and their analogs (*4*, *5*), acetates (*6–10*) and thioacetates (*11*), sulfates (*12*), phosphates (*13*), and diphosphites (*14*, *15*). In most of these complexes, the two metal centers are bridged by either four or two bridging ligands, with bridging fragments being NCO, NCS, or OXO (X = C, S, P). There are, however, also a few examples in which a single atom of a ligand (e.g., a C atom (*16*)) functions as a bridge between the metals or where the dinuclear structure is retained only with a Pt–Pt bond without any bridging ligand (*17*, *18*).

In this chapter, amidate-bridged dinuclear Pt^{III} complexes and multinuclear $Pt^{II,III}$ mixed-valent complexes, generally called "platinum-blues," are reviewed. The novel zigzag chain structures of the platinum blues having Pt–Pt bonds, redox chemistry between Pt^{II} and Pt^{III} in these complexes, ESR spectra of Pt^{III}, ^{195}Pt-NMR of Pt^{III}, and various stoichiometric and catalytic reactions with organic molecules mostly involving $Pt^{II/III}$ redox reactions are summarized. Through these physiocochemical properties and reactivities, the novel nature of Pt^{III}, compared to those of Pt^{II} and Pt^{IV}, is clarified.

II. Syntheses and Structures of Platinum-Blues and Related Amidate-Bridge Platinum^{III} Complexes

A. Original Platinblau Compounds Prepared from *Cis*-$PtCl_2(RCN)_2$ or K_2PtCl_4

In contrast to the usual yellow, orange, red, or colorless platinum complexes, platinum-blues are unusual for their intense blue or purple colors. The first blue platinum compound was prepared by German chemists at the beginning of this century (*19*). This unusual material was prepared by the reaction of Ag_2SO_4 with yellow *cis*-

$Pt^{II}Cl_2(CH_3CN)_2$ and was first proposed to have a mononuclear composition of $Pt^{II}(CH_3CONH)_2 \cdot H_2O$. However, the compound was later proposed to be polymeric with bridging acetamidate linkages (*20*). This idea, although speculative, does not seem unreasonable considering the fact that various square-planar platinum complexes tend to stack at close distances to form favorable metal–metal interactions or bounds (21–23). A later study using trimethylacetamidate instead of acetamidate suggested that this material is formulated as $Pt^{IV}(CH_3CONH)_2 \cdot (OH)_2$ (*24*, *25*). In order to account for the origin of the blue chromophore, various platinum blue compunds were further prepared with a variety of amide ligands (see Fig. 1), mostly using K_2PtCl_4 as the starting material (*26–36*). However, none of these studies afforded a clear conclusion about the structure and formula, due to the failure of obtaining single crystals suitable for determing the structure using X-rays.

Owing to later studies made by using *cis*-$Pt(NH_3)_2Cl_2$ instead of $PtCl_4^{2-}$, it is thought that the original "platinblau" may have the structural framework illustrated in Fig. 2 or one having slightly modified bridging modes. Important examples demonstrating the possibilities of such polymeric frameworks were very recently provided by the structural determinations of the polymeric mixed-metal (Pt–Ag) complexes *cis*-$[(H_3N)_2Pt(\mu\text{-}CH_3CONH)_2Ag](NO_3) \cdot 4H_2O$ and *trans*-$[(H_3N)_2Pt(\mu\text{-}CH_3CONH)_2Ag](NO_3) \cdot 1.5H_2O$ (*37*). In addition, we cannot exclude the possibility that carboxylate bridges may take part in coordination in the case of amidate ligands having a carboxyl group (oxamate, acid amidates, and orotinate), since it is reported that carboxylate ligands also afford blue platinum compounds (*38, 39, 40*).

B. *Cis*-Diammineplatinum-Blues and Related Complexes

Several decades later, progress was made in determining the chemistry of platinum-blues by employing the "*cis*-$Pt(NH_3)_2$" moiety of *cis*-$Pt(NH_3)_2Cl_2$. Since Rosenberg discovered the antitumor activity of *cis*-$Pt(NH_3)_2Cl_2$ (*cis*-DDP, cisplatin) (*41–44*), the chemistry of *cis*-DDP and its analogs have received considerable attention because of their potential application as anticancer drugs. Moreover, special attention was paid to the platinum-blues produced from the reactions between the hydrolysis product of *cis*-DDP (i.e., *cis*-$[Pt(NH_3)_2(OH_2)_2]^{2+}$) and pyrimidine bases such as uracil, since these so-called "platinum–pyrimidine-blues" were found to have a high index of antitumor activity with a lower associated nephrotoxicity than *cis*-DDP (*45*, *46*). The medical interest thus required chemists to unveil the structure of

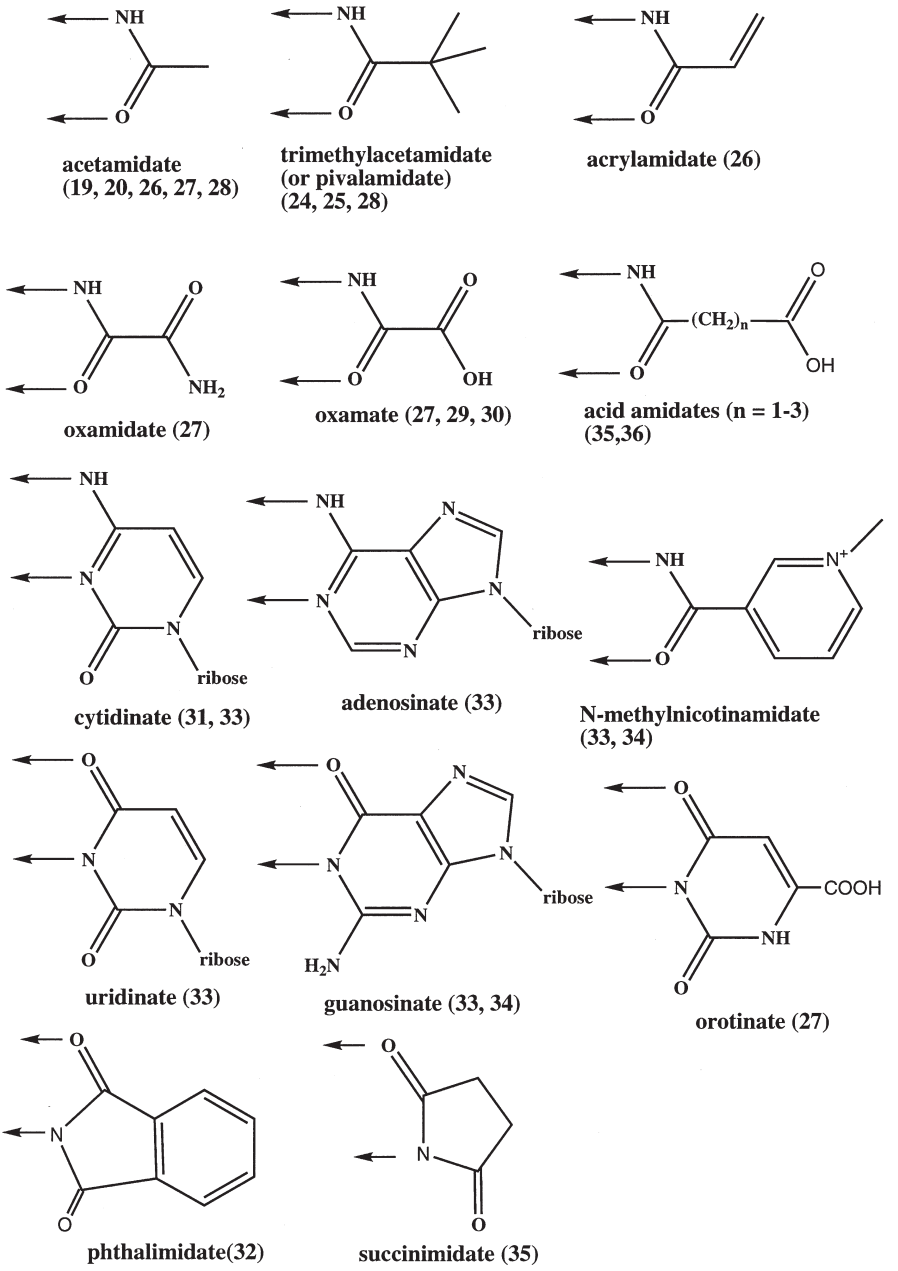

FIG. 1. Bridging ligands employed in the original "platinblau" compounds prepared from the reaction of *cis*-$PtCl_2(RCN)_2$ or K_2PtCl_4 with these ligands. Arrows show the most likely coordination atoms bridging two platinum atoms. The bridging modes of both cytidine and adenosine are assumed to have the same bridging mode as cytosine in Fig. 3. Numbers in parentheses correspond to the references.

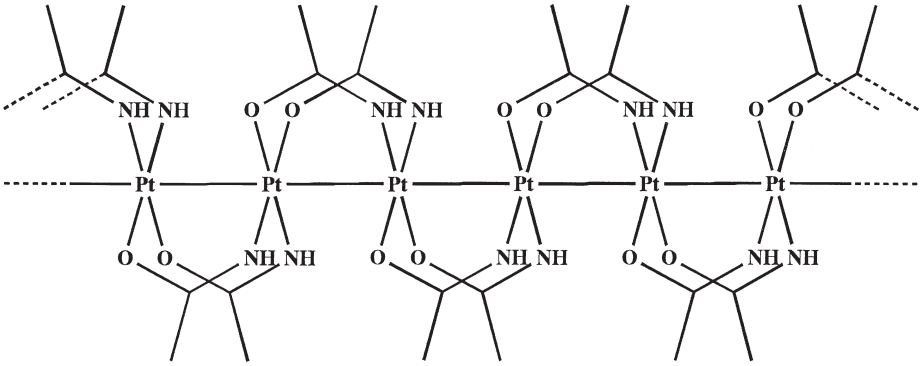

FIG. 2. A possible polymeric structure of the original $Pt(CH_3CONH)_2$ system.

platinum-blues. However, no structural evidence for the platinum–pyrimidine-blues (*27*, *47*) was obtained until the first structural analysis of α-pyridonate-blue (Section I,B,1) was reported.

1. The First Determination of the Structure of Platinum-Blues

The first direct evidence for the structure of platinum-blues was provided by the single-crystal X-ray studies of *cis*-diammineplatinum α-pyridonate-blue, $[Pt(2.25+)_4(NH_3)_8(\mu\text{-}\alpha\text{-pyridonato-N,O})_4]\ (NO_3)_5 \cdot H_2O$ (*48*, *49*). In the study, Barton and Lippard selected α-pyridone as a simplified model of pyrimidine bases (see Fig. 3), which must be the primary reason of their success in obtaining the first crystalline-blue material.

Figure 4 shows an ORTEP view of the α-pyridonate-blue cation. The chemical formula and the structure reveal that the complex cation is mixed valent, comprised of three Pt(II) and a Pt(III) atoms. This Pt(III) atom has one unpaired electron and causes paramagnetism to the compound. The complex is a tetraplatinum zigzag chain structure made up of two platinum dimeric units doubly bridged with deprotonated amidate ligands. Both the intra- and interdimer Pt–Pt distances (2.7745(4) and 2.8770(5) Å, respectively, (see also Table I) revealed that the platinum centers are metal–metal bonded to each other (*48*). These distances are comparable to the Pt–Pt bond lengths observed in the partially oxidized one-dimensional metal chain complexes, such as the tetracyanoplatinate compounds (e.g., 2.89 Å for $K_2[Pt(2.3+)(CN)_4]Br_{0.3} \cdot 3H_2O$) (*21*). Another important feature is that the dimer–dimer interaction is also stabilized by four hydrogen bonds formed between the ammine ligands and the oxygen atoms of the amidate ligand (see Fig. 4). On the other hand, the spin density measure-

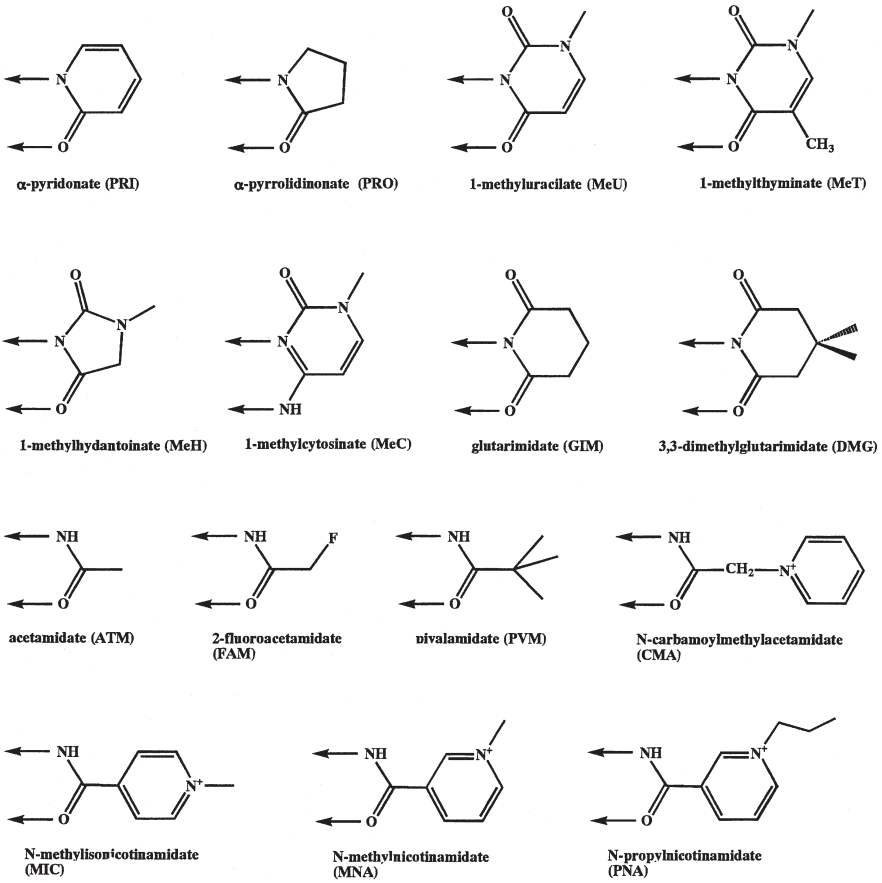

FIG. 3. Bridging amidate and imidate ligands used for the *cis*-diammineplatinum-blues and the related complexes. Arrows for each ligand show the bridging mode observed crystallographically.

ment by ESR (*48*) as well as the magnetic susceptibility measurement (*49*) indicated that the one unpaired electron is delocalized over the four platinum atoms (three Pt(II) (d^8) and one Pt(III) (d^7)) (see Section II,A). The mixed-valence state of the tetranuclear platinum blues is formally expressed in this chapter as $Pt(2.25+)_4$ (or $Pt(II)_3Pt(III)$).

2. Syntheses of Platinum-Blue and the Related Compounds

Followed by the X-ray studies on α-pyridonate-blue, various platinum-blues and the related complexes of exocyclic amidate and imidate ligands (see Fig. 3) have been prepared and structurally ana-

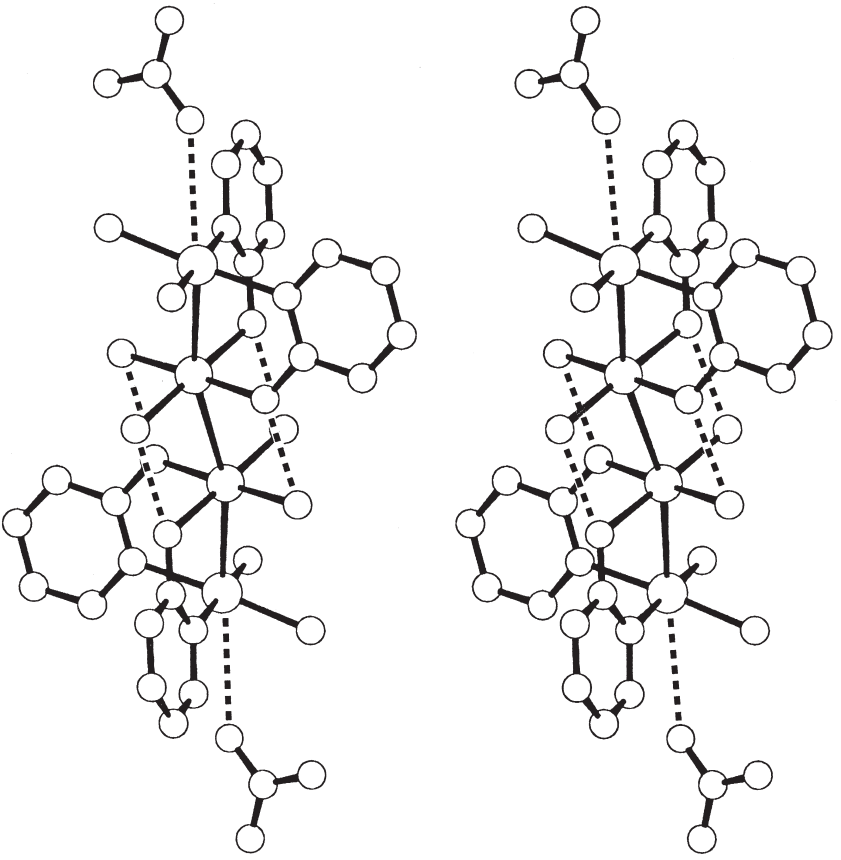

FIG. 4. Stereo diagram for the $[Pt(2.25+)_4(NH_3)_8(\mu\text{-}\alpha\text{-pyridonato})_4]^{5+}$ cation, together with the loosely associated nitrate ions (Pt $\cdots$ O(nitrate) = 3.321(9)Å).

lyzed by X-ray diffraction. The structurally characterized compounds are summarized in Table I, together with their geometrical parameters. As a result of the extensive synthetic and crystallographic works, several other Pt(II) and Pt(III) compounds structurally related to platinum-blues were found. These include yellow $[Pt(II)_2(NH_3)_4(L)_2]^{2+}$ (*50–59*, *62*, *69*, *70*, *75*, *77–85*, *94*), blue $[Pt(II)_3Pt(III)(NH_3)_8(L)_4]^{5+}$ (*56*, *57*, *61–63*, *70*, *71*, *84*, *86*, *96*, *97*), dark red $[Pt(II)_2Pt(III)_2(NH_3)_8(L)_4]^{6+}$ (*64*, *65*), and yellow $[Pt(III)_2(NH_3)_4(L)_2L'L'']^{n+}$ (*23*, *54*, *58*, *66*, *67*, *72–74*, *94*, *98*) (L = amidate bridging ligand, L′, L″ = neutral or anionic axial ligand) compounds, and therefore the platinum-blue family can now be classified into four groups on the basis of the average platinum oxidation state, Pt(2.0+), Pt(2.25+),

TABLE I

Comparison of Geometric Features of Platinum-Blues and Related Complexes

No.	Type	Chemical formula	Color	Oxidation state[a]	Pt–Pt distance (Å)		Pt–Pt–Pt angle (deg.)	τ (deg.)[e]	ω (deg.)[f]	Reference[c]
					Intradimer[b]	Interdimer[d]				
cis-Pt(NH_3)$_2$, α-pyridonate (PRI = μ-C_5H_4NO-N,O)										
1	A 2	HT-[Pt(2.0+)$_2$(NH_3)$_4$(PRI)$_2$](NO_3)$_2$ · 2H_2O	Pale yellow	Pt(2.0+)$_2$	2.8981(5)		28.8	13.0		*50*, *51*
2	A 3	HH-[Pt(2.0+)$_2$(NH_3)$_4$(PRI)$_2$]$_2$(NO_3)$_4$	Yellow	Pt(2.0+)$_4$	2.8767(7)	3.1294(9)	158.40(3)	30.0	20.3	*50*, *51*
3	B 1	HH-[Pt(2.25+)$_2$(NH_3)$_4$(PRI)$_2$]$_2$(NO_3)$_5$ · H_2O	Blue	Pt(2.25+)$_4$	2.7745(4)	2.8770(5)	164.60(2)	27.4	22.8	*48*, *49*
4	D 1	HH-[Pt(3.0+)$_2$(NH_3)$_4$(PRI)$_2$(H_2O)(NO_3)](NO_3)$_3$ · 2H_2O	Red-orange	Pt(3.0+)$_2$	2.5401(5)		20.0	23.2		*2*, *52*
5	D 2	HT-[Pt(3.0+)$_2$(NH_3)$_4$(PRI)$_2$(NO_3)$_2$](NO_3)$_2$ · 0.5H_2O	Red	Pt(3.0+)$_2$	2.5468(8)		20.3	26.3		*52*, *53*
6	D 2	HT-[Pt(3.0+)$_2$(NH_3)$_4$(PRI)$_2$(NO_2)$_2$](NO_3)$_2$ · 0.5H_2O	Yellow	Pt(3.0+)$_2$	2.5759(7)		20(1)	27.1		*53*, *54*
7	D 2	HT-[Pt(3.0+)$_2$(NH_3)$_4$(PRI)$_2$(Cl)$_2$](NO_3)$_2$	Orange	Pt(3.0+)$_2$	2.5684(5)		20(1)	27.4		*54*
8	D 2	HT-[Pt(3.0+)$_2$(NH_3)$_4$(PRI)$_2$(Br)$_2$](NO_3)$_2$ · 0.5H_2O	Orange	Pt(3.0+)$_2$	2.5820(7)		20(1)	29.4		*54*
cis-Pt(en), α-pyridonate (PRI = μ-C_5H_4NO-N,O)										
9	A 3	HH-[Pt(2.0+)$_2$(en)$_2$(PRI)$_2$]$_2$(NO_3)$_4$	Yellow	Pt(2.0+)$_4$	2.9915(4)	3.2355(5)	160.58(2)	39.6	24.9	*55*
10	B 1	HH-[Pt(2.25+)$_2$(en)$_2$(PRI)$_2$]$_2$(NO_3)$_5$ · H_2O	Blue	Pt(2.25+)$_4$	2.8296(5)	2.9158(6)	164.33(3)	32.1	24.3	*56*, *57*
11	D 1	HH-[Pt(3.0+)$_2$(en)$_2$(PRI)$_2$(NO_3)(NO_2)](NO_3)$_2$ · 0.5H_2O	Red	Pt(3.0+)$_2$	2.6382(6)		30.7	36.2		*58*
cis-Pt(NH_3)$_2$, α-pyrrolidinonate (PRO = μ-C_4H_6NO-N,O)										
12	A 3	HH-[Pt(2.0+)$_2$(NH_3)$_4$(PRO)$_2$]$_2$(PF_6)$_3$(NO_3) · H_2O	Yellow	Pt(2.0+)$_4$	3.029(2)	3.185(2)	157.94(5)	35.9	1.0	*59*
13	A 2	HT-[Pt(2.0+)$_2$(NH_3)$_4$(PRO)$_2$](ClO_4)$_2$	Yellow	Pt(2.0+)$_2$	3.085(1)	5.8515(7)	—[b]	37.6	2.3	*60*
14		HH-[Pt(2.14+)$_2$(NH_3)$_4$(PRO)$_2$]$_2$(PF_6)$_2$(NO_3)$_{2.56}$ · 5H_2O (random mixture of A3 and B1)	Violet	Pt(2.14+)$_4$	2.848(2)	2.875(2)	166.53(6)	26.2	0.5[i] 2.0[i,j]	*61*, *62*
				Pt(2.14+)$_4$	2.839(2)	2.875(2)	168.31(6)	23.5[i]	6.3[i] 0[i,j]	
15	B 1	HH-[Pt(2.25+)$_2$(NH_3)$_4$(PRO)$_2$]$_2$(ClO_4)$_5$	Blue	Pt(2.25+)$_4$	2.8782(8)	2.894(1)	165.58(3)	29.2	6.0 0.8[j]	*60*
16	B 1	HH-[Pt(2.25+)$_2$(NH_3)$_4$(PRO)$_2$]$_2$(PF_6)$_3$(NO_3)$_2$	Blue	Pt(2.25+)$_4$	2.840(2)	2.868(3)	167.3(1)	28.0	4.3 1.5[j]	*60*
17		HH-[Pt(2.37+)$_2$(NH_3)$_4$(PRO)$_2$]$_2$(NO_3)$_{5.48}$ · 3H_2O (random mixture of B1 and C1)	Green	Pt(2.37+)$_4$	2.764(8) 2.740(8)	2.739(8)	166.6(3) 167.2(3)	24.5 17.4[i] 3.56[i,j]	3.8[i] 6.3[i] 30.5[i,j]	*63*
				Pt(2.37+)$_4$	2.761(8) 2.753(9)	2.724(8)	168.5(3) 170.9(3)	26.9 17.1[i] 10.0[i,j]	2.3[i] 5.0[i] 33.3[i,j]	

18	B 1	HH-{[Pt(2.25+)$_2$(NH$_3$)$_4$(PRO)$_2$]$_2$}{[Pt(2.5+)$_2$-(NH$_3$)$_4$(PRO)$_2$(NO$_3$)$_2$]$_2$}(NO$_3$)$_9$(PF$_6$)$_2\cdot$6H$_2$O	Green	Pt(2.25+)$_4$	2.862(1)	2.864(2)	166.50(4)	28.1	1.7 0[i]	*60*
18	C 1	(1 : 1 mixture of B1 and C1)		Pt(2.5+)$_4$	2.719(1)	2.818(2)	169.78(5)	21.4	2.1 1[i]	
19	C 1	HH-[Pt(2.5+)$_2$(NH$_3$)$_4$(PRO)$_2$]$_2$(NO$_3$)$_6\cdot$2H$_2$O	Tan (dark red)	Pt(2.5+)$_4$	2.702(6) 2.706(6)	2.710(5)	170.4(1) 168.8(1)	17.9[h] 20.6[h] 1.6[h,i]	1.3[h] 1.3[h] 29.5[h,i]	*64*, *65*
20	C 2	HH-[Pt(2.5+)$_4$(NH$_3$)$_8$(PRO)4(Cl)](ClO$_4$)$_5$Cl$_2$	Red	Pt(2.5+)$_4$	2.701(4) 2.793(4)	2.724(4)	171.6(1) 168.3(1)	21.8 24.2 3.6[i]	3.0 4.0 35.8[i]	*60*
21	D 1	HH-[Pt(3.0+)$_2$(NH$_3$)$_4$(PRO)$_2$(NO$_2$)(NO$_3$)](NO$_3$)$_2\cdot$H$_2$O	Orange	Pt(3.0+)$_2$	2.644(1)	—[g]	—[g]	19.6	0.0	*66*, *67*
22	D 1	HH-[Pt(3.0+)$_2$(NH$_3$)$_4$(PRO)$_2$(Cl)$_2$](NO$_3$)$_2$	Yellow	Pt(3.0+)$_2$	2.6366(7)	—[g]	—[g]	18.9	1.5	*60*
23	D 1	HH-[Pt(3.0+)$_2$(NH$_3$)$_4$(PRO)$_2$(Cl)(NO$_3$)](NO$_3$)$_2\cdot$H$_2$O	Orange	Pt(3.0+)$_2$	2.6239(9)	—[g]	—[g]	19.6	0.7	*60*
24	E 1	HH-[(NO$_3$)(NH$_3$)$_2$Pt(3.0+)(PRO)$_2$Pt(3.0+)(NH$_3$)(μ-NH$_2$)]$_2$(NO$_3$)$_4$	Yellow	Pt(3.0+)$_2$]$_2$	2.608(1)	3.160[1]	—[g]	17.7	0.4	*68*
25	E 2	HT-[(H$_2$O)(NH$_3$)$_2$Pt(3.0+)(PRO)$_2$Pt(3.0+)(NH$_3$(μ-OH)]$_2$(NO$_3$)$_6\cdot$4H$_2$O	Yellow	Pt(3.0+)$_2$]$_2$	2.5527(7)	3.1578(6)	—[g]	16.9	10.7	*60*
Pt(bpy), α-pyrrolidinonate (PRO = μ-C$_4$H$_6$NO-N,O)										
26	A 2	HT-[Pt(2.0+)$_2$(bpy)$_2$(PRO)$_2$](ClO$_4$)$_2$	Reddish-brown	Pt(2.0+)$_2$	2.899(2)	3.765(2)		21.1	7.5	*69*
cis-Pt(NH$_3$)$_2$, 1-methyluracilate (MeU = μ-C$_5$H$_5$N$_2$O$_2$-N,N)										
27	A 1	HH-[Pt(2.0+)$_2$(NH$_3$)$_4$(MeU)$_2$](NO$_3$)$_2\cdot$H$_2$O	Yellow	Pt(2.0+)$_2$	2.937(1)	4.798(1)	—[g]	34.1	25.2	*70*
28	B 1	HH-[Pt(2.25+)$_2$(NH$_3$)$_4$(MeU)$_2$]$_2$(NO$_3$)$_5\cdot$5H$_2$O	Blue	Pt(2.25+)$_4$	2.810(2) 2.793(2)	2.866(2)	165.02(5) 164.81(5)	27.3 26.4 0.05[i]	6.1 8.4 21.1[i]	*70*, *71*
29	A 2	HT-[Pt(2.0+)$_2$(NH$_3$)$_4$(MeU)$_2$](NO$_3$)$_2\cdot$3H$_2$O	Yellow	Pt(2.0+)$_2$	2.954(2)			35.8	20.5	*57*
30	D 2	HT-[Pt(3.0+)$_2$(NH$_3$)$_4$(MeU)$_2$(NO$_2$)(OH$_2$)]-(NO$_3$)$_3\cdot$5H$_2$O	Orange	Pt(3.0+)$_2$	2.574(1)			21.5	31.5	*3*
31	D 2	HT-[Pt(3.0+)$_2$(NH$_3$)$_4$(MeU)$_2$(NO$_3$)(OH$_2$)]-(NO$_3$)$_3\cdot$3H$_2$O	Orange	Pt(3.0+)$_2$	2.556(1)			22.6		*72*
32	D 2	HT-[Pt(3.0+)$_2$(NH$_3$)$_4$(MeU)$_2$(NO$_3$)(OH$_2$)]-(NO$_3$)$_3\cdot$2H$_2$O	Orange	Pt(3.0+)$_2$	2.560(1)			22.7		*72*
33	D 3	HH-[Pt(3.0+)$_2$(NH$_3$)$_4$(MeU)$_2$(NO$_3$)$_3\cdot$H$_2$O	Orange	Pt(3.0+)$_2$	2.607(1)			19	3.6	*73*
34	D 1	HH-[Pt(3.0+)$_2$(NH$_3$)$_4$(MeU)$_2$(Cl)$_2$](Cl)$_2\cdot$3.5H$_2$O	Orange	Pt(3.0+)$_2$	2.573(1)			21.1		*74*
cis-Pt(NH$_3$)$_2$ and *cis*-PtCl$_2$, 1-methyluracilate (MeU = μ-C$_5$H$_5$N$_2$O$_2$-N,O)										
35	D 1	HH-[(Cl)(H$_3$N)$_2$Pt(3.0+)(MeU)$_2$Pt(3.0+)(Cl)$_3$]$\cdot$2H$_2$O	Dark red	Pt(3.0+)$_2$	2.543(1)			16		*74*
cis-Pt(NH$_3$)$_2$ and Pt(bpy), 1-methyluracilate (MeU = μ-C$_5$H$_5$N$_2$O$_2$-N,O)										
36	A 1	HH-[(H$_3$N)$_2$Pt(2.0+)$_2$(MeU)$_2$Pt(2.0+)(bpy)]-(NO$_3$)$_2\cdot$3H$_2$O (*pseudo tetramer*)	Red	Pt(2.0+)$_2$	2.929(1)	3.849	165.7	30.4	10.2	*75*

(*continued*)

TABLE I (*Continued*)

No.	Type	Chemical formula	Color	Oxidation state[a]	Pt–Pt distance (Å)[b,c]		Pt–Pt–Pt angle (deg.)[e]	τ (deg.)[f]	ω (deg.)[g]	Reference
					Intradimer	Interdimer[d]				
cis-Pt(NH_3)$_2$ and Pd(en), 1-methyluracilate (MeU = μ-$C_5H_5N_2O_2$-N,O)										
37	A 3	HH-[$(H_3N)_2$Pt(2.0+)(MeU)$_2$Pd(2.0+)(en)]$_2$(NO_3)$_4\cdot 4H_2O$	Orange-brown	$Pt^{II}Pd^{II}$	2.927(1)	Pd···Pd = 3.255(1) Pt···Pt = 4.553(1)		34.2	17.3	*76*
cis-Pt(NH_3)$_2$, 1-methylthyminate (MeT = μ-$C_6H_7N_2O_2$-N,O)										
38	A 1	HH-[Pt(2.0+)$_2$(NH_3)$_4$(MeT)$_2$](NO_3)$_2$	Yellow	Pt(2.0+)$_2$	2.927(1)	5.66		31.4	1.9	*77*, *78*
39	A 2	HT-[Pt(2.0+)$_2$(NH_3)$_4$(MeT)$_2$](NO_3)$_2\cdot H_2O$	Yellow	Pt(2.0+)$_2$	2.974(1)			36.1	13.8	
40	A 2	HT-[Pt(2.0+)$_2$(NH_3)$_4$(MeT)$_2$](NO_3)$_2\cdot 4.5H_2O$	Yellow	Pt(2.0+)$_2$	2.920(1) 2.915(1)			35.2.1 30.7	25.7 17.9	*79*
cis-Pt(NH_3)$_2$ and *cis*-Pt(NH_3)Cl, 1-methylthyminate (MeT = μ-$C_6H_7N_2O_2$-N,O)										
41	A 1	HH-[$(H_3N)_2$Pt(2.0+)(MeT)$_2$Pt(2.0+)(NH_3)Cl]-[Pt(NH_3)Cl_3]$\cdot H_2O$	Yellow-green	Pt(2.0+)$_2$	2.939(1)	4.28		31.5	0.8	*80*
cis-Pt(NH_3)$_2$ and *cis*-$PtCl_2$, 1-methylthyminate (MeT = μ-$C_6H_7N_2O_2$-N,O)										
42	A 1	HH-[$(H_3N)_2$Pt(2.0+)(MeT)$_2$Pt(2.0+)Cl_2]$\cdot 3H_2O$	Reddish-black	Pt(2.0+)$_2$	2.861(1)	4.49		22.5	3.0	*80*
cis-Pt(NH_3)$_2$, 1-methylhydantoinate (MeH = μ-$C_4H_5N_2O_2$-N,O)										
43	A 3	HH-[Pt(2.0+)$_2$(NH_3)$_4$(MeH)$_2$]$_2$(NO_3)$_4\cdot H_2O$	Yellow	Pt(2.0+)$_4$	3.131	3.204	160.5	38.6	7.5[h]	*81*
cis-Pt(NH_3)$_2$, 1-methylcytosinate (MeC = μ-$C_5H_6N_3O$-N,N)										
44	A 2	HT-[Pt(2.0+)$_2$(NH_3)$_4$(MeC)$_2$](NO_3)$_2\cdot 2H_2O$	Yellow	Pt(2.0+)$_2$	2.981(2)			34	16	*82*
45	D 2	HT-[Pt(3.0+)$_2$(NH_3)$_4$(MeC)$_2$(NO_2)$_2$](NO_3)$_2\cdot 2H_2O$***	Yellow	Pt(3.0+)$_2$	2.584(2)			21	25	*82*
cis-Pt(NH_3)$_2$, 3,3-dimethylglutarimidate (DMG = μ-$C_7H_{10}NO_2$-N,O)										
46	A 2	HT-[Pt(2.0+)$_2$(NH_3)$_4$(DMG)$_2$](NO_3)$_2\cdot H_2O$	Yellow	Pt(2.0+)$_2$	2.939(1)			35.2	21.3	*83*
47	B 1	HH-[Pt(2.25+)$_2$(NH_3)$_4$(DMG)$_2$]$_2$(NO_3)$_5\cdot 2H_2O$	Blue	Pt(2.25+)$_4$	2.860(2)	3.020(2)	161.74(5)	27.1	0.5	*84*
Pt(bpy) and/or Pd(bpy), 3,3-dimethylglutarimidate (DMG = μ-$C_7H_{10}NO_2$-N,O)										
48	A 1	HH-[Pt(2.0+)$_2$(bpy)$_2$(DMG)$_2$](NO_3)$_2\cdot 2H_2O$ (pseudo tetramer)	Deep violet	Pt(2.0+)$_2$	2.833(3) 2.845(3)	3.201(3)				*85*
49	A 1	HH-[$Pt^{II}Pd^{II}$(bpy)$_2$(DMG)$_2$](NO_3)$_2\cdot 2H_2O$	Red	$Pt^{II}Pd^{II}$	2.854(2)	3.829(2)	(Pd···Pd)			*85*
50	A 1	HH-[Pd(2.0+)$_2$(bpy)$_2$(DMG)$_2$](NO_3)$_2\cdot 2H_2O$	Orange	Pt(2.0+)$_2$	2.844(2)	3.849(3)	(Pd···Pd)			*85*

Pt(bpy), glutarimidate (GIM = μ-$C_5H_6NO_2$-N,O)										
51	A 1	HH-[Pt(2.0+)$_2$(bpy)$_2$(GIM)$_2$]$_2$(NO$_3$)$_2$ · 3.5H$_2$O	Violet	Pt(2.0+)$_2$	X-ray data not available					*86*
52	B 1	HH-[Pt(2.25+)$_2$(bpy)$_2$(GIM)$_2$]$_2$(NO$_3$)$_5$ · 2H$_2$O	Deep violet	Pt(2.25+)$_4$	X-ray data not available					*86*
cis-Pt(NH$_3$)$_2$, acetamidate (ATM = μ-CH_3CONH-N,O)										
53	F 1	HH-[Pt(2.25+)$_2$(NH$_3$)$_4$(ATM)$_2$]$_4$(NO$_3$)$_{10}$ · 4H$_2$O	Red-purple	Pt(2.25+)$_8$	2.778(1)	2.934(1)	168.78(5)	25.6	5.6	*87*, *88*
							165.51(4)	10.7	37.9	
					2.880(2)	2.900(1)	163.77(5)	28.4	3.7	
						4.905(2)	161.21(4)			
cis-Pt(NH$_3$)$_2$, 2-fluoroacetamidate (FAM = μ-CH_2FCONH-N,O)										
54	F 1	HH-[Pt(2.08+)$_2$(NH$_3$)$_4$(FAM)$_2$]$_4$(NO$_3$)$_{8.66}$ · 4H$_2$O	Bluish-purple	Pt(2.08+)$_8$	2.835(5)	2.979(5)	169.5(1)		4	*88*, *89*
							166.4(2)	8.3	37	
					2.938(6)	2.962(5)	161.8(1)	32.3	4	
						7.128(7)				
cis-Pt(NH$_3$)$_2$, pivalamidate (PVM = μ-$C_5H_{10}NO$-N,O)										
55	D 1	HH-[Pt(3.0+)$_2$(NH$_3$)$_4$(PVM)$_2$(CH$_2$COCH$_3$)(NO$_3$)]-(NO$_3$)$_2$ · H$_2$O	Yellow	Pt(3.0+)$_2$	2.6892(6)			23.6	1.5	*90*
56	D 1	HH-[Pt(3.0+)$_2$(NH$_3$)$_4$(PVM)$_2$(NO$_2$)(NO$_3$)](NO$_3$)$_2$ · H$_2$O	Orange	Pt(3.0+)$_2$	2.6091(4)			22.3	4.8	*90*
57	B 2	HH-[Pt(2.25+)$_2$(NH$_3$)$_4$(PVM)$_2$]$_2$(NO$_3$)$_5$	Blue	Pt(2.25+)$_4$	2.723(1)	2.843(1)	173.05(4)	23.7	4.3	*91*
					2.851(1)		165.65(3)	30.0	10.1	
cis-Pd(en), α-pyridonate (PRI = μ-C_5H_4NO-N,O)										
58	A 3	HT-[Pt(2.0+)$_2$(en)$_2$(PRI)$_2$]$_2$(NO$_3$)$_2$ · 2H$_2$O	Orange-yellow	Pt(2.0+)$_2$	2.981(1)			39.7	25.5	*92*, *93*

[a] Average Pt oxidation state.
[b] Bridged Pt–Pt distances.
[c] Reference codes for the Cambridge Structural Database.
[d] Interdimer Pt–Pt distances.
[e] Dihedral cant between the two adjacent platinum coordination planes.
[f] Twist angle of the two platinum coordination planes about the Pt–Pt vector.
[g] No interdimer Pt–Pt interaction is achieved.
[h] Calculated by us, where ESDs were not estimated.
[i] Twist angle for the interdimer association, while the nonlabeled values correspond to the bridged Pt–Pt associations.

Pt(2.5+), and Pt(3.0+). These oxidation states correspond to their formal oxidation states of $Pt(II)_2$, $Pt(II)_3Pt(III)$, $Pt(II)_2Pt(III)_2$, and $Pt(III)_2$, respectively. To date the Pt(2.75+) state corresponding to $Pt(II)Pt(III)_3$ has never been found. In addition to this classification, the structures can also be grouped according to the orientation of the two bridging amidate ligands within a dimeric unit; head-to-head (HH) and head-to-tail (HT) are known to $Pt(II)_2$ and $Pt(III)_2$ compounds (*52*, *53*, *94*, *95*) (see A-1, A-2, D-1, and D-3 in Fig. 5). However, only the HH isomers afford a dimer of dimers, leading to the tetraplatinum chain structure of platinum-blues. On the other hand, the HT

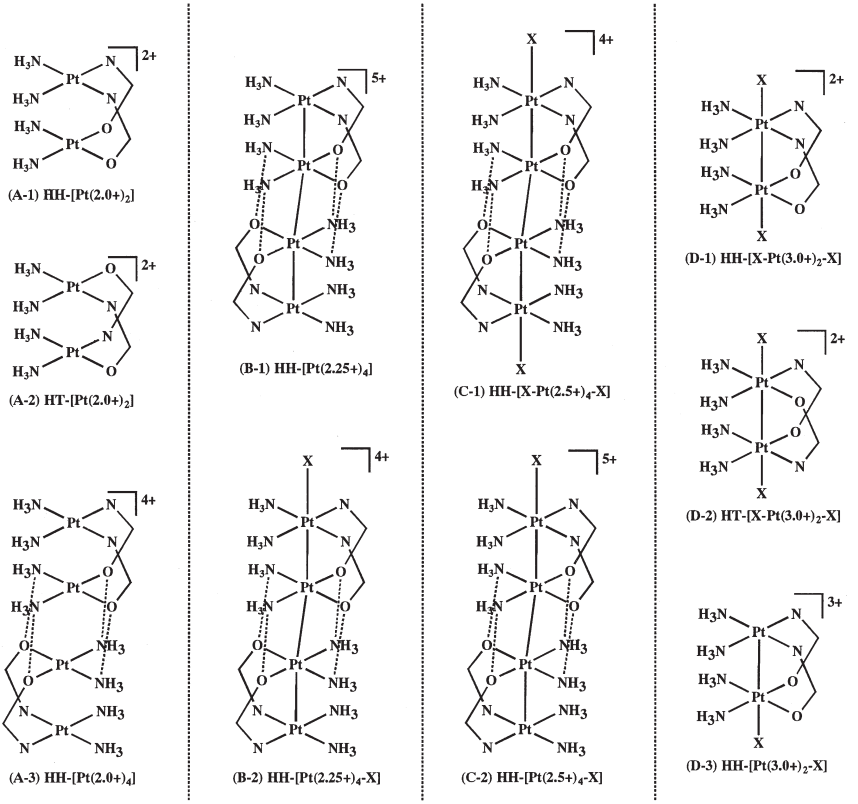

FIG. 5. Ten types of different structures identified by X-ray diffraction, where the abbreviated N–O is used to express each bridging amidate ligand and X denotes axial donors such as OH_2, NO_3^-, NO_2^- (nitro), Cl^-, and Br^-. For the compounds involving axial ligands (X), the total complex charge is given assuming that X is a monoanion. Note that, in some cases, amine ligand in *cis*-$Pt(NH_3)_2$ will be replaced with other ligands, such as in Pt(en), *cis*-$Pt(NH_3)Cl$, *cis*-$PtCl_2$, and Pt(bpy).

isomers do not dimerize to give the tetramer due to the steric bulk of the exocyclic amidate rings at the ends of the dimetric unit. But this is not the case for amidate-bridged dimer compounds with chain (or acyclic) amidates such as acetamidate, as described below. The third classification is related to the nuclearity of the complex; two major groups exist, dimer and tetramer. In addition, the chain structures are classified based on whether they have axial ligands. All these classified structures are shown in Fig. 5. Several Pd analogs are also listed in Table I. In addition to these dimeric and tetrameric structures, two other groups, illustrated in Fig. 6, are known. Compounds E1 (*68*) and E2 are produced as a result of deprotonation at one of the four equatorial ammine ligands of the dinuclear α-pyrrolidinonate Pt(3.0+) species. Two octanuclear platinum-blues (F1) are known when acyclic amidate (acetamidate and 2-fluoroacetamidate) is employed instead of cyclic ones (*87–89*).

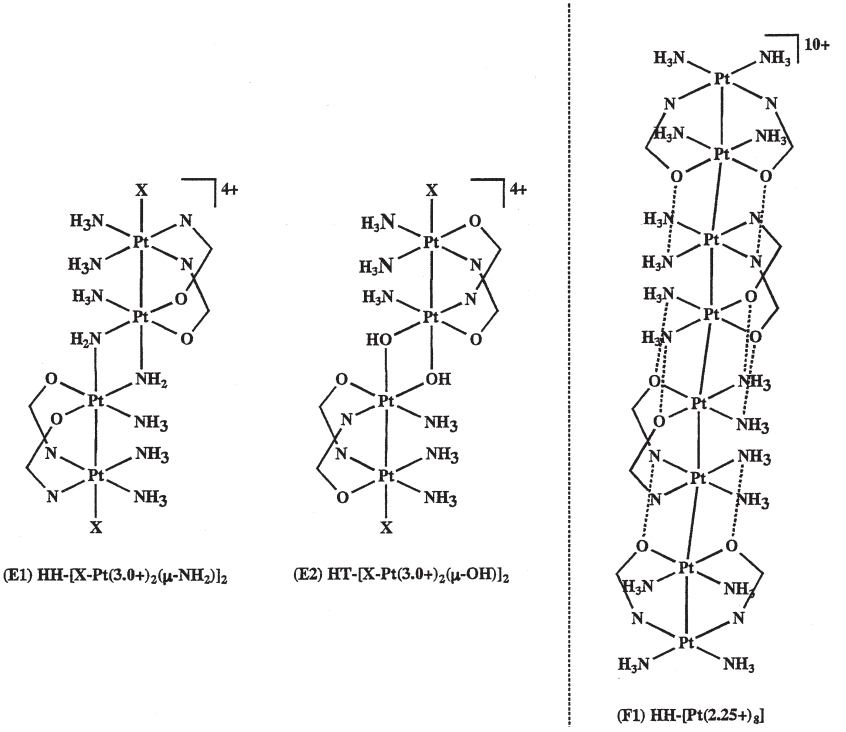

FIG. 6. Two novel structures observed for Pt(3.0+)$_2$, and an octaplatinum chain structure observed in the acyclic amidate systems.

In general, the Pt–Pt distance tends to decrease as the average platinum oxidation state increases (see Table I), but this is also dependent on the bridging mode: doubly bridged dimer units listed in Table I show slightly longer Pt–Pt distances than the corresponding quadruply bridged lantern dimers (*99*).

III. Basic Spectroscopic Properties of Platinum-Blues and Related Platinum (3.0+) Complexes

A. Magnetic Properties and ESR

As mentioned above, the $Pt(2.25+)_4$ species (B1 and B2) possesses one unpaired electron of Pt(III) ($S = 1/2$) and is the only species which exhibits paramagnetism among the four oxidation states. The ESR spectrum of the α-pyridonate-blue species shown in Fig. 7 exhibits an axial signal characteristic of the platinum-blues ($g_\perp = \sim 2.4$ and $g_\parallel = \sim 2.0$) (*48*, *49*, *70*, *96*). Similar signal patterns are also observed for several other blue compounds (*34*, *47*, *57*, *86*, *88*, *89*), and these common features show that the unpaired electron resides on the dz^2 orbital located along the Pt chain. The g values observed for the para-

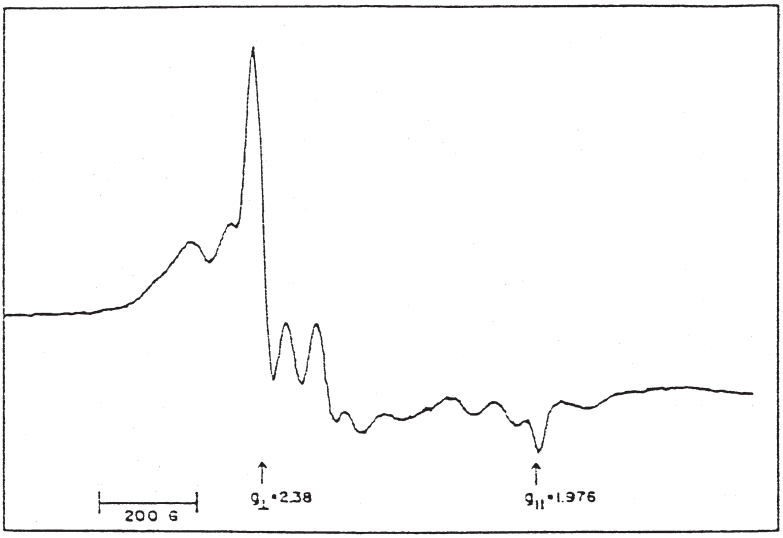

Fig. 7. The ESR spectrum of *cis*-diammineplatinum α-pyridonate-blue (5 mM Pt) in 0.05 M HNO_3.

magnetic blues are listed in Table II. The axial patterns observed for the platinum-blues resemble those observed for the partially oxidized one-dimensional platinum chain materials (see also Table II). Moreover, the detailed investigations of the hyperfine structure revealed that the unpaired electron has interactions with all four ^{195}Pt nuclei (I = 1/2, 33.7% of natural abundance) within the tetraplatinum chain (*96*, *100*), indicating that the unpaired electron is delocalized over the four platinum atoms. This was further supported by the results of SCF-Xα calculation (*97*) (Section II,D). It is also noteworthy that the unpaired electron densities within the tetraplatinum chain are different between the inner two and the outer two platinum atoms, since two different hyperfine coupling constants (a_{inner} and a_{outer}) were required for the spectral simulation of the hyperfine pattern (*96*). The relative ratio, $a_{\text{outer}} \sim 2a_{\text{inner}}$, shows that the unpaired electron resides longer at the two terminal Pt atoms.

The temperature dependence of the magnetic susceptibility of the Pt(2.25+)$_4$-blues generally obeys the Curie–Weiss law, indicating that the intertetramer magnetic interaction in the solid state is negligible (*49*, *57*, *60*, *63*, *89*, *88*). Therefore, the effective magnetic moments observed for the blue complexes are usually close to the value of μ_{eff} = 1.73 B.M., corresponding to S = 1/2 (see Table II). Based on this value, the relative abundance of the paramagnetic-blue species mixed in the diamagnetic isostructural species were estimated for "nonstoichiometric mixtures," **17** and **54** in Table I, from the apparent effective magnetic moments. As for **54**, it is supposed that a diamagnetic Pt(2.25+)$_8$ and a paramagnetic Pt(2.125+)$_8$ species are mixed in the lattice to give the average Pt oxidation state of 2.08+. In the octanuclear species, however, whether the unpaired electron is indeed delocalized over the eight atoms remains unclear, since no well-resolved hyperfine structure is observed in the solid-state ESR spectrum and in solution part of the octanuclear structure seems to be disrupted, as described in Section III,B. Considering the disruption behavior in solution, it is possible that Pt(2.125+)$_8$ should actually be expressed as Pt(2.0+)$_2\cdots$Pt(2.25+)$_4\cdots$Pt(2.0+)$_2$, and the unpaired electron is delocarized only over the central four Pt atoms.

B. X-Ray Photoelectron Spectroscopy

X-ray photoelectron spectroscopy (XPS) is a good means to probe the real oxidation state of the metal centers by observing the Pt $4f_{7/2}$ and $4f_{5/2}$ binding energies. As summarized in Table III, the Pt 4f binding energies for the common Pt(IV) compounds are 2–3 eV higher

TABLE II

COMPARISON OF GEOMETRIC FEATURES OF PLATINUM-BLUES AND RELATED COMPLEXES

No.	Compound	*g* values (ESR) $g\perp$	*g* values (ESR) $g\parallel$	μ_{eff} (B.M.)	Reference
Platinum-blues with known structures					
3	HH-[Pt(2.25+)$_2$(NH$_3$)$_4$(PRI)$_2$(NO$_3$)$_5$ · H$_2$O	2.38	1.976	1.81	*48*, *49*, *70*, *96*
10	HH-[Pt(2.25+)$_2$(en)$_2$(PRI)$_2$]$_2$(NO$_3$)$_5$ · H2O	2.355	1.970	1.939	*57*
14	HH-[Pt(2.14+)$_2$(NH$_3$)$_4$(PRO)$_2$]$_2$(PF$_6$)$_2$(NO$_3$)$_{2.56}$ · 5H$_2$O	—[a]	—[a]	—[a]	
15	HH-[Pt(2.37+)$_2$(NH$_3$)$_4$(PRO)$_2$]$_2$(ClO$_4$)$_5$	—[a]	—[a]	2.06	*60*
16	HH-[Pt(2.25+)$_2$(NH$_3$)$_4$(PRO)$_2$]$_2$(PF$_6$)$_3$(NO$_3$)$_2$	2.40	1.985	—[a]	*100*
17	HH-[Pt(2.37+)$_2$(NH$_3$)$_4$(PRO)$_2$]$_2$(NO$_3$)$_{5.48}$ · 3H$_2$O	—[a]	—[a]	1.30	*63*
18	HH-{[Pt(2.25+)$_2$(NH$_3$)$_4$(PRO)$_2$]$_2$}{[Pt(2.5+)$_2$-(NH$_3$)$_4$(PRO)$_2$(NO$_3$)$_2$]$_2$}(NO$_3$)$_9$(PF$_6$)$_2$ · 6H$_2$O	—[a]	—[a]	1.79	*60*
28	HH-[Pt(2.25+)$_2$(NH$_3$)$_4$(MeU)$_2$]$_2$(NO$_3$)$_5$ · 5H$_2$O	2.363	1.995	1.891	*57*
47	HH-[Pt(2.25+)$_2$(NH$_3$)$_4$(DMG)$_2$]$_2$(NO$_3$)$_5$ · 2H$_2$O	—[a]	—[a]	—[a]	*84*
52	HH-[Pt(2.25+)$_2$(bpy)$_2$(DMG)$_2$]$_2$(NO$_3$)$_5$ · 2H$_2$O	2.40	2.000	—[a]	*86*
54	HH-[Pt(2.08+)$_2$(NH$_3$)$_4$(FAM)$_2$]$_4$(NO$_3$)$_{8.66}$ · 4H$_2$O	2.40	2.000	1.41	*88*, *89*
Platinum-blues with unknown structures					
	HH-[Pt(2.25+)$_2$(NH$_3$)$_4$(ATM)$_2$]$_2^{5+}$	2.45	1.988	—[a]	—[a]
	Blue from *cis*-DDP and uracil	2.3–2.5	—[a]	—[a]	*47*
	Blue from *cis*-DDP and thymine	2.3	—[a]	—[a]	*47*
	Blue from *cis*-DDP and cytosine	2.4	—[a]	—[a]	*47*
	Blue from K$_2$PtCl$_4$[b]	2.41	1.979	—[a]	*34*
	Oxamate-blue	2.5	2.0	0.72	*36*
	Malonic-acid-blue	2.39	1.99	—[a]	*36*
	Succinamic-acid-blue	2.42	1.99	1.97	*35*, *36*
	Glutaramic-acid-blue	2.39	1.98	0.32	*36*
	3-Methylglutaramic acid blue	2.43	1.97	—[a]	*36*
	3,3-Dimethylglutaramic acid blue	2.45	1.98	0.94	*36*
	3,3-Diphenylglutaramic acid blue	2.37	1.98	1.10	*36*
	3,3-Tetramethyleneglutaramic acid blue	2.44	1.97	1.42	*36*
	1-Carboxy-2-(aminocarboxyl)cyclobutane blue	2.44	1.98	—[a]	*36*
	Cis-1-carboxy-2-(aminocarboxyl)-2-cyclohexane blue	2.36	1.98	1.15	*36*
	Trans-1-carboxy-2-(aminocarboxyl)cyclohexane blue	2.36	1.98	1.01	*36*
	1,2,3,6-Tetrahydrophthalamic acid blue	2.37	1.97	—[a]	*36*
	Phthalamic-acid-blue	2.43	1.98	—[a]	*36*
	2-Carboxy-2′-(aminocarboxyl)-1,1′-biphenyl blue	2.41	1.99	—[a]	*36*
	3-Oxaglutaramic acid blue	2.33	2.03	—[a]	*36*
	Orotic acid blue	2.47	1.97	0.87	*36*
	K$_2$Pt(2.33+)(CN)$_4$Br$_{1/3}$ · 3H$_2$O	2.336	1.946	—[a]	*101*
	[Pt(NH$_3$)$_4$][PtCl$_4$](Pt(IV) doped) (Magnus' green salt)	2.504	1.939	—[a]	*102*

[a] Not reported.

[b] The blue compound prepared by reacting K$_2$PtCl$_4$ with both *N*-methylnicotinamide and guanosine.

TABLE III

PLATINUM $4f_{7/2}$ AND $4f_{5/2}$ BINDING ENERGIES OF PLATINUM-BLUES AND RELATED COMPLEXES

No.	Chemical formula	Binding energy (eV)[a] Pt $4f_{5/2}$	Pt $4f_{7/2}$	Reference
Common Pt complexes				
	Cis-$PtCl_2(NH_3)_2$ (Pt(II))	75.4 (1.9)	72.0 (1.8)	*30*
		76.1 (1.3)	72.8 (1.3)	*70*
		76.9 (1.7)	73.6 (2.0)	*103*
	K_2PtCl_4 (Pt(II))	77.9 (1.8)	74.6 (1.7)	*30*
	Wolfram's red salt (Pt(II) and Pt(IV))	77.4[b]	74.1[b]	*104*
		79.8[b]	76.4[b]	*105*
	Cis-$PtCl_4(NH_3)_2$ (Pt(IV))	78.7 (1.3)	75.4 (1.3)	*70*
Amidate-bridged compounds				
3	HH-$[Pt(2.25+)_2(NH_3)_4(PRI)_2]_2(NO_3)_5 \cdot H_2O$	76.2 (1.5)	72.8 (1.4)	*70*
9	HH-$[Pt(2.0+)_2(en)_2(PRI)_2]_2(NO_3)_4$	76.4 (1.7)	73.1 (1.6)	*88*
14	HH-$[Pt(2.14+)_2(NH_3)_4(PRO)_2]_2(PF_6)_2(NO_3)_{2.56} \cdot 5H_2O$	76.4[b]	73.2[b]	*88*
	HH-$[Pt(2.25+)_2(NH_3)_4(PRO)_2]_2(ClO_4)_2(NO_3)_3 \cdot 5H_2O$	76.7 (2.6)	73.3 (2.2)	*88*
15	HH-$[Pt(2.25+)_2(NH_3)_4(PRO)_2]_2(ClO_4)_5$	76.1 (2.0)	72.8 (2.0)	*40*
19	HH-$[Pt(2.5+)_2(NH_3)_4(PRO)_2]_2(NO_3)_6 \cdot 2H_2O$	76.7[b]	73.5[b]	*88*
		76.4 (2.2)	72.9 (2.1)	*40*
21	HH-$[Pt(3.0+)_2(NH_3)_4(PRO)_2(NO_2)(NO_3)](NO_3)_2 \cdot H_2O$	77.9[b]	74.6[b]	*88*
28	HH-$[Pt(2.25+)_2(NH_3)_4(MeU)_2]_2(NO_3)_5 \cdot 5H_2O$	76.1 (1.6)	72.7 (1.5)	*70*
53	HH-$[Pt(2.25+)_2(NH_3)_4(ATM)_2]_4(NO_3)_{10} \cdot 4H_2O$	76.5[b]	73.3[b]	*88*
54	HH-$[Pt(2.08+)_2(NH_3)_4(FAM)_2]_4(NO_3)_{8.66} \cdot 4H_2O$	76.4[b]	73.4[b]	*88*
Carboxylate-bridged compounds				
	$[Pt(2.0+)_2(NH_3)_4(\mu\text{-acetato})_2](ClO_4)_2 \cdot 2H_2O$	76.1 (2.2)	72.8 (2.2)	*40*
	$[Pt(2.0+)_2(NH_3)_4(\mu\text{-acetato})_2](NO_3)_2 \cdot 2H_2O$	75.7 (2.2)	72.7 (2.2)	*40*
	$[Pt(2.0+)_2(NH_3)_4(\mu\text{-acetato})_2(SiF_6) \cdot 4H_2O$	76.2 (2.1)	73.1 (2.0)	*40*
	$[Pt(2.0+)_2(NH_3)_4(\mu\text{-benzoato})_2]_2(SiF_6)(BF_4)_2$-[*cis*-$Pt(2.0+)(NH_3)_2(benzoato)_2 \cdot 3H_2O$	76.4 (1.9)	73.1 (1.9)	*40*
	$[Pt(2.25+)_2(NH_3)_4(\mu\text{-phbz})_2]_2(SO_4)_{2.25}(phbz)_{0.5} \cdot 5H_2O$[c]	76.1 (2.0)	72.9 (2.0)	*40*
Some blues obtained from K_2PtCl_4				
	Acetamide blue	76.1 (1.6)	72.9 (1.6)	*70*
	Oxamidate blue	75.7 (1.8)	72.3 (1.7)	*30*
		77.3 (2.2)	74.1 (2.2)	
	Succinamidate blue	77.9[b]	74.5[b]	*35*
		79.7[b]	76.3[b]	

[a] Values in parentheses correspond to the full width at half maximum (Fwhm) for each peak.
[b] Fwhm values not reported.
[c] phbz = *p*-hydroxybenzoate.

than those for the common Pt(II) complexes. Therefore, intermediate shifts are expected when the metal centers are oxidized from Pt(II) to Pt(III). However, it must always be borne in mind that substitution of the donor ligands can also lead to a shift of 1–2 eV at each peak (e.g., compare the shifts of *cis*-$PtCl_2(NH_3)_2$ and K_2PtCl_4). As for the XPS of the platinum-blue family, the assignment of the oxidation state is not difficult when the compound is homovalent, such as $Pt(2.0+)_2$ and $Pt(3.0+)_2$; the difference in shift between **9** and **21** clearly demonstrates the capability of the method for the detection of Pt(II) and Pt(III). However, in case of the mixed-valence compounds, deconvolution of the spectra does not always result in successful resolution of the Pt(II) and Pt(III) components. For instance, the α-pyridonate $Pt(2.25+)_4$-blue is reported to show only a single peak at both $4f_{7/2}$ and $4f_{5/2}$ energy regions, respectively, with fwhm (full width at half maximum) values comparable to that of *cis*-DDP (*70*) (see also Table III). The fact reveals that the four Pt atoms are equivalent within the XPS time scale due to the rapid delocalization of Pt(III). Although in certain compounds it is reported that peaks attributable to Pt(III) are observable as higher energy shoulders on the main peaks of the Pt(II) (*88*), deconvolution of the peaks to Pt(II) and Pt(III) components is in many cases difficult due to the broad peak profiles (*40*). Therefore, the apparent binding energies observed for the mixed-valence compounds are not much different from those of the $Pt(2.0+)_2$ compounds, since peaks arising from Pt(II) generally dominate the overall spectral profiles. In some acid amide-blues (oxamidate- and succinamidate-blues in Table III), deconvolution was possible, and it was reported that the peaks at the higher energy region were ascribed to Pt(IV) centers. However, at that time, the presence of Pt(III) was not shown, and reconsideration of all the data in Table III now suggests that there is no need to postulate the presence of Pt(IV), since the first structural study by Barton and Lippard clarified the presence of Pt(III) (*70*). For instance, the lower energy set of the double peaks observed for the oxamidate-blue can closely be related to those of the $Pt(2.0+)_2$ compounds, and the higher energy set can be assigned to the $Pt(3.0+)_2$ dimer (*30*). In the case of the succinamidate-blue, the peak-to-peak separation between the two sets of double peaks is quite similar to that observed for the oxamidate-blue, implying that these peaks may also correspond to the presence of Pt(II) and Pt(III) (*35*).

C. ^{195}Pt- and Other NMR Spectroscopies

Platinum-195-NMR spectroscopy is an effective means to probe the electronic state of the Pt atoms in the compounds. The ^{195}Pt nucleus,

having $I = 1/2$ with the natural abundance of 33.7%, is NMR active, while all other Pt nuclei do not have nuclear spin. The ^{195}Pt-NMR signal can be obtained with relatively high sensitivity (sensitivity relative to $^{13}C = 19.9$) if the measurement conditions are suitably selected. The chemical shift of ^{195}Pt is usually reported as referenced to $Na_2Pt(IV)Cl_6$ set at 0 ppm and appears in a very wide range from -6000 to 12000 ppm, depending on the Pt oxidation state, donor or accepter characteristics of the coordinating ligand, and the nature of the metal–ligand interaction (*107–109*). The large ^{195}Pt chemical shift range and the predictable chemical shifts depending on the ligand provide a powerful means for identifying the reaction product. Since Pt(III) is a very rare oxidation state, its NMR data is worthy of particular attention. Table IV summarizes the Pt(III) chemical shifts and the ^1J(Pt–Pt) for HH and HT dinuclear Pt(III) and Pt(II) complexes. Several relevant Pt(II) and Pt(IV) monomeric compounds are also included in the table. No ^{195}Pt NMR data is observed for tetranuclear Pt-blue species having the formal oxidation state of $Pt(III)Pt(II)_3$, since they are paramagnetic. The diamagnetic Pt-tan species of $Pt(III)_2Pt(II)_2$ oxidation state shows paramagnetism when disolved in water, since the compound is partly reduced by water to the corresponding Pt-blue species (*vide infra*) and therefore does not show any ^{195}Pt-NMR signal. In Table IV, each of the two Pt atoms in the HH dinuclear complexes are distinguished by the four coordinating atoms: One of the Pt atoms has two ammine ligands and two nitrogen donors of amidate and is thus expressed as N_4 Pt in Table IV, while the other is coordinated by two ammine ligands and two oxygen donors of amidate (N_2O_2 Pt) (see Fig. 5, A-1). So far chemical shifts of Pt(III) are known only for two Pt(III) dinuclear compounds, and it seems from Table IV that the Pt(III) chemical shift depends, among several factors, strongly on the type of the bridging ligand. Inorganic ligands such as HPO_4^{2-} and SO_4^{2-} give positive lower field chemical shifts, whereas those of amidate ligands are in a higher field negative region ($-2253 \sim +541$ ppm). In HH dinuclear Pt(III) complexes, the N_2O_2-coordinated Pt(III) always shows lower chemical shifts than the other N_4-coordinated Pt(III). The Pt(III) chemical shifts for compounds of $P_2O_5H_2^{2-}$ bridging ligands are by far high field, in the range of -4236 to -5103 ppm. For comparison, typical simple compounds of Pt(II) and Pt(IV) are also included in Table IV. Although Pt(II) and Pt(IV) compounds show their chemical shifts in totally different ranges according to the oxidation state (*107–109*), such definite classification is not possible for Pt(III), since the Pt(III) chemical shift is strongly dependent on the bridging ligand and covers all the ranges of both Pt(II) and Pt(IV). Although a detailed explanation for such large

TABLE IV

^{195}Pt-NMR Chemical Shifts for HH and HT Dimers of Pt(II) and Pt(III) and Several Related Monomers[a]

Chemical formula	Coord. atoms	$\delta(^{195}Pt)$ (ppm)	$^1J(^{195}Pt-^{195}Pt)$ (Hz)	Reference
$Na_2Pt(4.0+)Cl_6$	C_{16}	0		
$K_2Pt(2.0+)Cl_4$	C_{14}	−1623		
Cis-$[Pt(2.0+)(NH_3)_2(OH_2)_2](NO_3)_2$	N_2O_2	−1588		*51*
$[Pt(2.0+)(NH_3)_2(OH)]_2(NO_3)_2$	N_2O_2	−1153		*51*
$[Pt(2.0+)(NH_3)_2(OH)]_3(NO_3)_3$	N_2O_2	−1505		*51*
Cis-$[Pt(2.0+)(NH_3)_2(PRIH)(OH_2)](NO_3)_2$	N_3O	−2015		*51*
Cis-$[Pt(2.0+)(NH_3)_2(PRIH)_2](NO_3)_2$	N_4	−2495		*51*
$[Pt(2.0+)(en)(OH_2)_2]^{2+}$	N_2O_2	−1835		*53*
$[Pt(2.0+)(en)(PRIH)(OH_2)]^{2+}$	N_3O	−2316		*53*
$[Pt(2.0+)(en)(PRIH)_2]^{2+}$	N_4	−2685		*53*
HH-$[Pt(2.0+)_2(NH_3)_4(PRI)_2]_2(NO_3)_4$ (**2**)	N_2O_2	−1308		*51*
	N_4	−2261		
HT-$[Pt(2.0+)_2(NH_3)_4(PRI)_2](NO_3)_2$ (**1**)	N_3O	−1810		*51*
HH-$[Pt(2.0+)_2(en)_2(PRI)_2]_2(NO_3)_4$ (**9**)	N_2O_2	−1611	<800	*53*
	N_4	−2480		
HT-$[Pt(2.0+)_2(en)_2(PRI)_2](NO_3)_2$	N_3O	−2056	6850	*53*
HT-$[Pt(2.0+)_2(en)_2(6\text{-Me-PRI})_2][(NO_3)_2$[b]	N_3O	−2031		*53*
HH-$[Pt(3.0+)_2(en)_2(PRI)_2(NO_2)(NO_3)](NO_3)_2\cdot 0.5H_2O$ (**11**)	N_2O_2	541		*58*
	N_4	−1141		
HH-$[Pt(2.0+)_2(NH_3)_4(PRO)_2]_2(PF_6)_3(NO_3)\cdot H_2O$ (**12**)	N_2O_2	−1396		*59*
	N_4	−2446		
HT-$[Pt(2.0+)_2(NH_3)_4(PRO)_2]^{2+}$ (**13**)	N_3O	−1940		*59*
HH-$[Pt(3.0+)_2(NH_3)_4(PRO)_2X_2]^{2+}$ (X = unknown)	N_2O_2	196 ~ 205		*67*
	N_4	−843 ~ 845		
HH-$[Pt(2.0+)_2(NH_3)_4(DMG)_2]^{2+}$	N_2O_2	−1259		*84*, *106*
	N_4	−2233		
Cis-$[Pt(2.0+)(NH_3)_2(DMG)_2]$	N_4	−2423		*84*, *106*
HT-$[Pt(2.0+)_2(NH_3)_4(DMG)_2](NO_3)_2$ (**46**)	N_3O	−1770		*83*
Cis-$[Pt(2.0+)(NH_3)_2(DMG)(OH_2)]^+$	N_3O	−2008		*83*
Cis-$[Pt(2.0+)(NH_3)_2(GIM)(OH_2)]^+$	N_3O	−1988		*84*, *106*
Cis-$[Pt(2.0+)(NH_3)_2(DMG)(DMSO)]^{2+}$	N_3S	−3133		*83*
HH-$[Pt(3.0+)_2(NH_3)_4(PVM)_2(NO_2)(NO_3)]^{2+}$	N_2O_2	134		*91*
HH-$[Pt(3.0+)_2(NH_3)_4(PVM)_2(CH_2COCH_3)(NO_3)]^{2+}$ (**55**)	N_2O_2C	−100	3477	*90*
	N_4O	−1892		
HT-$[Pt(3.0+)_2(NH_3)_4(PVM)_2(CH_2COCH_3)(NO_3)]^{2+}$	N_3OC	−623	3625	*90*
	N_3O_2	−1368		
HH-$[Pt(3.0+)_2(NH_3)_4(PVM)_2(CH_2\overline{CH(CH_2)_3O}]^{3+}$	N_2O_2	−272	2560	*91*
	N_4	−905		
HH-$[Pt(2.0+)(bpy)_2(GIM)_2](NO_3)_2\cdot 3.5H_2O$	N_2O_2	−1429		*86*
	N_4	−2224		
HT-$[Pt(2.0+)_2(bpy)_2(GIM)_2]^{2+}$	N_3O	−1860		*86*
$[Pt(2.0+)(bpy)(GIM)(OH_2)]^+$	N_3O	−2120		*86*
HT-$[Pt(2.0+)(bpy)_2(PRO)_2](ClO_4)_2$ (**26**)	N_3O	−1710		*69*
$[Pt(3.0+)(CN_5)_2^{4-}$	N_5	116	1800	*111*
$[Pt(3.0+)_2(HPO_4)_4(Cl)(H_2O)]^{3-}$	O_5	1889	5342	*110*
	O_4Cl	1713		
$[Pt(3.0+)_2(SO_4)_4(Cl)(H_2O)]^{3-}$	O_5	1808	3464	*110*
	O_4Cl	1638		
$[Pt(3.0+)_2(P_2O_5H_2)_4Cl_2]^{4-}$	P_4Cl	−4236		*112*
$[Pt(3.0+)_2(P_2O_5H_2)_4Br_2]^{4-}$	P_4Br	−4544		*112*
$[Pt(3.0+)_2(P_2O_5H_2)_4I_2]^{4-}$	P_4I	−5103		*112*

[a] See Table I for the ligand abbreviations.

[b] 6-Me-PRI = 6-methyl-α-pyridonate.

chemical-shift deviation depends on theoretical calculation, in the three distinct groups of Pt(III) compounds mentioned above, i.e., those with either HPO_2^{2-} or SO_4^{2-}, amidate, and $P_2O_5H_2^{2-}$, the ligands apparently coordinate to Pt(III) using distinctly different ligand orbitals. The ligands HPO_4^{2-} and SO_4^{2-} coordinate to Pt(III) by acting as σ-donors, whereas deprotonated amidate ligands make both σ- and π-coordiantion to Pt(III) and act as strong donor ligands. The $P_2O_5H_2^{2-}$ ligand coordinates with its phosphorus atoms, which act as both σ-donors and π-acceptors. The extensive interaction of the d orbitals of Pt and P would move the chemical shift into such a surprisingly high-field region.

The Pt(III) chemical shift is also affected by the axial ligands. Especially noteworthy in this respect are **55**, its HT isomer, and HH-$[Pt(3.0+)_2(NH_3)_4(PVM)_2(CH_2\overline{CH(CH_2)_3O}]^{3+}$ in Table IV, all having alkyl axial ligands. These compounds have outstandingly high-field chemical shifts compared to those of the corresponding Pt(III) compounds with nonalkyl axial ligands, reflecting the strong donor effect of the alkyl ligands. It should also be emphasized here that despite the fact that the alkyl ligands are always coordinated to N_2O_2-Pt(III), such high-field chemical shifts specific to alkyl compounds are observed for the other Pt(III), i.e., N_4–Pt(III). This is explained by the strong trans influence of the alkyl ligands, which extends even to the other Pt atom through the metal–metal bond. The strong trans influence is also in accordance with the longer Pt–Pt distances (see Section II,B,1) and the absence of the axial ligand opposite to the alkyl ligand (see also Section V,B).

The $^1J(^{195}Pt–^{195}Pt)$ coupling constant is observed only for Pt(III) dinuclear compounds and not for Pt(II) ones. The value for the latter would be smaller than for the former and hidden in the broad peak profiles of Pt(II), which is the actual meaning of the $^1J(^{195}Pt–^{195}Pt)$ value for **9** in Table IV (*53*). The platinum satellite is observed also in ^{13}C- and ^1H-NMR spectra and can be used as evidence for coordination of the ligand atoms to the Pt center. Figure 8 is the ^{195}Pt-NMR spectra of **11**, which clearly shows the satellites of ^{195}Pt due to a $^{195}Pt(III)–^{195}Pt(III)$ coupling (*58*). The broad line shape of ^{195}Pt usually observed in this class of compounds is partly due to the coordinated ^{14}N atoms, which has nuclear quadrupole. By substituting ^{15}N for all the ^{14}N atoms in the ligand and employing suitable measurement conditions, such broad peaks become more fine structured, and multiplets due to $J(^{195}Pt–^{15}N)$ couplings can be observed in the ^{195}Pt spectra (*90*). In some cases, where solubility of the compound is high, the J(Pt–N) can be obtained in the ^{195}Pt spectra even without ^{15}N enrichment (see Fig. 9).

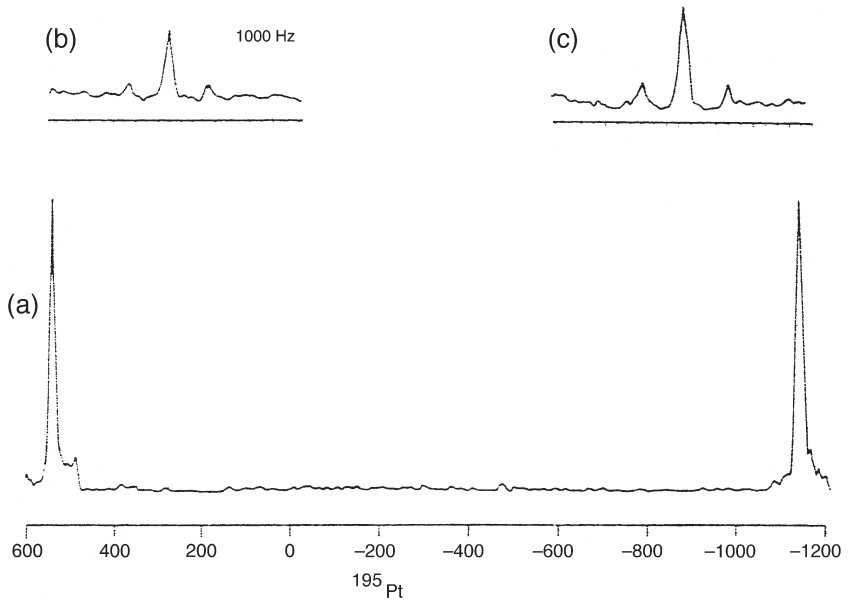

FIG. 8. The ^{195}Pt-NMR spectra of a DMF solution of $[Pt_2(en)_3(PRI)_2(NO_2)(NO_3)](NO_3)_2 \cdot 0.5\ H_2O$ (**11**) at 5°C, acquired on a Bruker WM-250 spectrometer operating at 53.6 MHz. (a) Power spectrum of the Fourier transform of a 1 K FID accumulated with a 5-μs pulse width, 100-kHz spectral width, and 2000 K transients. (b and c) Normal Fourier transforms of 1 K FIDs accumulated with 10-μs pulsewidths, 42-kHz spectral width, and 64 K transients per spectrum. All FIDs were treated with 400-Hz line broadening functions to suppress noise (**58**).

Platinum-195-NMR spectroscopy can also be used to monitor the HH to HT isomerization of a Pt(II) dimer complex, which is described in Section III,A.

D. Molecular Orbital Calculations

A qualitative view for the molecular orbitals of the basic $Pt(2.0+)_2$ dimer is given in Fig. 10, in which the filled d orbitals for the starting monomer are also shown for comparison. An important feature is the strong filled–filled interaction between the d_z2 orbitals, leading to a large energy splitting between the Pt–Pt bonding and antibonding orbitals. On the other hand, the first quantum mechanical approach to the mixed-valence tetramer was made by use of the EHMO method (*28*), in which a half-structure of α-pyridonate-blue was employed to understand the origin of the blue chromophore. Although the study concluded that the blue chromophore is based on the LMCT from α-

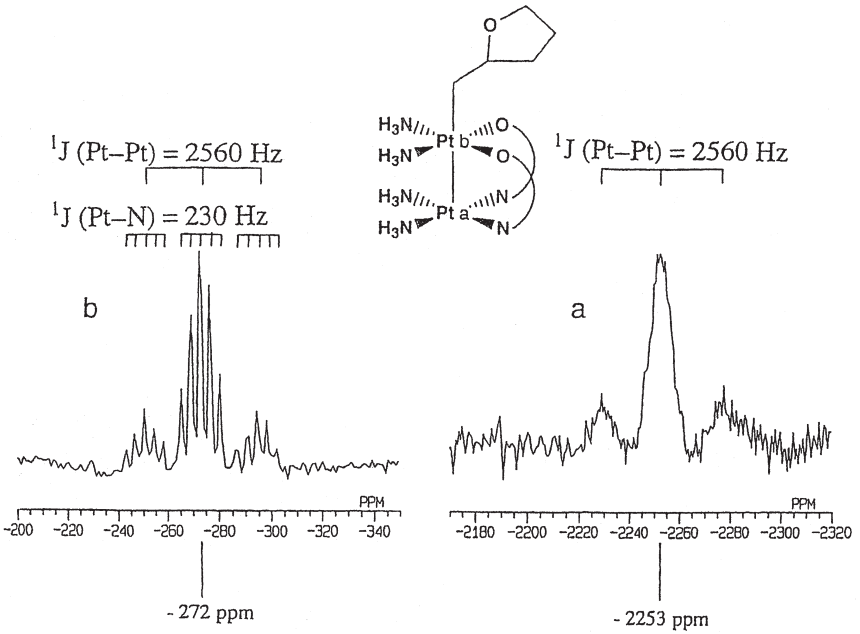

FIG. 9. The ^{195}Pt–NMR spectrum of HH-[Pt(3.0+)$_2$(NH_3)$_4$(PVM)$_2$($CH_2CH(CH_2)_3O$)(NO_3)$_3 \cdot H_2O$ in D_2O. The spectrum was obtained without ^{15}N enrichment.

pyridonate to the Pt–Pt σ^* orbital, this was later found to be wrong as a result of SCF-Xα-SW calculation (*97*). The Xα calculation revealed that the visible transitions of α-pyridonate-blue are based on the intense z-polarized transitions at 1.82 eV (680 nm) and 2.58 eV (480 nm). These transitions were qualitatively assigned as inner Pt–Pt $\sigma \rightarrow$ inner Pt–Pt σ^* and inner Pt–Pt $\pi \rightarrow$ inner Pt–Pt σ^*, therefore the main character of the blue band was deemed metal-to-metal charge transfer. The metal–metal bonds in this system were characterized as due to σ-overlap between Pt d_z2 orbitals with some contribution of $d\pi$–$d\pi$ bondings. The study also showed that 92% of the unpaired spin density is distributed over the four Pt atoms (41% in the terminal Pt atoms and 51% in the two inner atoms). As a result, the platinum-blues were designated Robin–Day class III-A mixed-valence compounds. It was also reported that the electron within the four d_z2-derived orbitals may be described as a free electron moving in a one-dimensional box having a length of L, where L is the length of the Pt zigzag chain. Therefore the energy levels (E_n) may be estimated by the equation $E_n = n^2h^2/8mL^2$ (n = 1–4) (*57*).

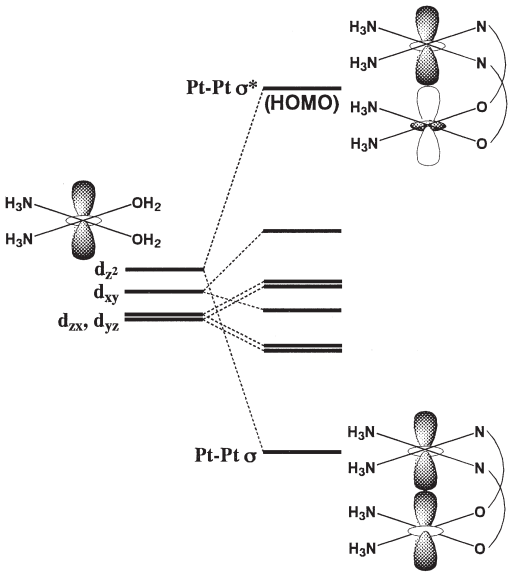

FIG. 10. Molecular orbital diagrams of *cis*-$[Pt(NH_3)_2(OH_2)_2]^{2+}$ (left) and $[Pt(2.0+)_2(NH_3)_4$ (μ-amidato$)_2]^{2+}$ (right).

IV. Basic Reactions in Solution

A solution of the isolated platinum blue compound usually contains several chemical species described in the previous section. Such complicated behaviors had long been unexplored, but were gradually unveiled as a result of the detailed equilibrium and kinetic studies in recent years. The basic reactions can be classified into four categories: (1) HH–HT isomerization; (2) redox disproportionation reactions; (3) ligand substitution reactions, especially at the axial coordination sites of both $Pt(3.0+)_2$ and $Pt(2.5+)_4$; and (4) redox reactions with coexisting solvents and atmosphere, such as water and O_2. In this chapter, reactions 1–4 are summarized.

A. Isomerization and Formation of HH and HT Pt(II) Dimer Complexes Studied by NMR Spectroscopy

Platinum-195-NMR spectroscopy is a useful means to prove isomerization of the HH and HT isomers of $Pt(2.0+)_2$. Both ^{1}H- and ^{13}C-NMR spectroscopies may also be used to examine isomerization (*59*, *67*); however, quite often these are not useful enough because of the overlap of peaks for both isomers and difficulty in assignment. The large

chemical shift and the limited number of peaks in ^{195}Pt-NMR spectroscopy are advantageous in such cases to assign peaks and follow the isomerization reaction.

The HH Pt(2.0+)$_2$ dimers possess two magnetically nonequivalent Pt nuclei, one being coordinated by two ammine ligands and two nitrogen atoms of the amidate ligand (N_4–Pt), the other Pt by two ammine ligands and two oxygen atoms of the amidate ligand (N_2O_2–Pt). On the other hand, the two Pt atoms in the HT dimers are magnetically equivalent, both having an N_3O-coordinated geometry (Fig. 5, A-2). Since the electronegativity of oxygen and nitrogen atoms is significantly different, N_2O_2- and N_4-coordinated Pt nuclei give their peaks in totally different regions, which enables the HH → HT isomerization reaction to be monitored. As shown in Fig. 11, the two peaks corresponding to the N_2O_2– and N_4–Pt atoms of the α-pyridonate-bridged ethylenediamineplatinum(II) HH dimer (**9**) gradually decreases, while a new peak corresponding to the N_3O–Pt atoms of the HT dimer increases at around the midpoint of the HH signals (*52*, *53*).

Detailed kinetic study on the reaction further revealed that the isomerization reaction occurs intramolecularly and proceeds via the initial dissociative bond cleavage of either Pt–N(amidate) or Pt–O(amidate) (*53*) (see Fig 12). In addition, it was suggested that the

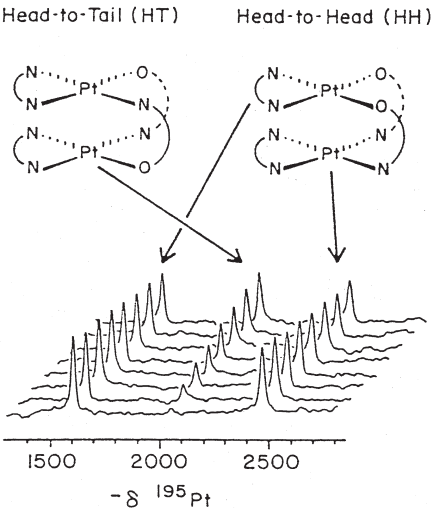

FIG. 11. The time course (0.43–23.6 h) of ^{195}Pt-NMR spectra observed for the HH–HT isomerization after dissolution of HH-[Pt(2.0+)$_2$(en)$_2$(PRI)$_2$](NO$_3$)$_2$ (**9**). The spectrum closest to the abscissa corresponds to the first run.

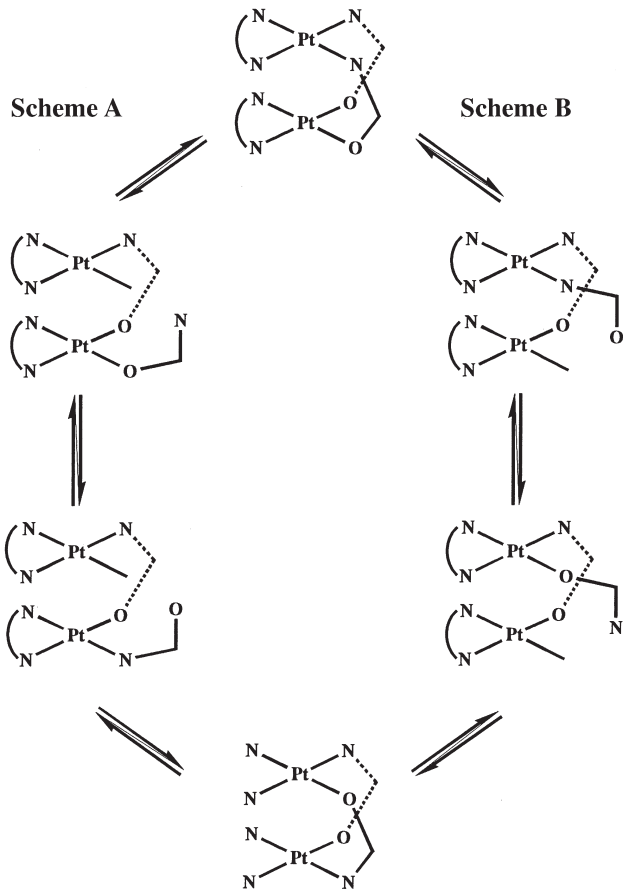

FIG. 12. Two proposed intramolecular mechanisms for the HH–HT isomerization.

dissociation is enhanced by the steric repulsion between the two ethylenediamine moieties within the dimeric unit, since the HH → HT isomerization is extremely slowed in the *cis*-diammineplatinum analog, which has the same bridging ligand (**2**) (*53*). However, the isomerization reaction of the *cis*-diammine α-pyrrolidinonate-bridged $Pt(2.0+)_2$ dimer was reported to be very rapid. Even the solution just after dissolution of the HH compound contains both HH and HT isomers, and therefore the isomerization process cannot be observed (*59*). The HH → HT conversion process is also reported for the 3,3-dimethylglutarimidate-bridged *cis*-diammineplatinum(II) and (2,2′-

bipyridine)platinum(II) complexes, which have the same bridging ligand (*85*, *86*). The HH–HT isomerization process is not observed for the $Pt(3.0+)_2$ dimers. This is presumably because the high rigidity of the dinuclear core, which has a single Pt–Pt bond and higher positive charge of the Pt atoms, does not allow dissociation of the bridging amidate.

The formation process of 1-methyluracilate-bridged HH/HT $Pt(2.0+)_2$ dimers and other side products in the reactions of *cis*-$Pt(NH_3)_2(H_2O)_2$ and 1-methyluracile was revealed by means of ^{1}H-NMR spectroscopy (*70*). The α-pyrrolidinonate-bridged $Pt(2.0+)_2$ and $Pt(3.0+)_2$ dimers in the HH forms were characterized by ^{13}C-NMR spectroscopy, which clearly showed two sets of peaks for HH and HT $Pt(2.0+)_2$ dimers (*59*, *67*). The ^{195}Pt satellites were weakly detected in the ^{1}H-NMR spectra of some 1-methyluracilate-bridged $Pt(3.0+)_2$ dimers (*72*). The reduction process from the paramagnetic $Pt(2.25+)_4$ complex $[(H_3N)_2Pt(2.25+)(\mu\text{-MeU})_2Pt(2.25+)(bpy)]_2^{5+}$ to the corresponding dinuclear $Pt(2.0+)_2$ complex $[(H_3N)_2Pt(2.0+)(\mu\text{-MeU})_2(bpy)]^{2+}$ was examined by means of ^{1}H-NMR spectroscopy (*75*). A redox disproportionation cleavage process of the α-pyrrolidinonate-bridged $Pt(2.5+)_4$ tetramer into the $Pt(2.0+)_2$ and $Pt(3.0+)_2$ dimers was also monitored using ^{1}H-NMR (*113*) (Section III,B). The cleavage of the Pt–Pt bonds in the acetamidate-bridged $Pt(2.25+)_8$ octamer was also examined using ^{1}H-NMR spectroscopy (*114*) (Section III,B).

B. Redox Disproportionation of Mixed-Valence Tetranuclear and Octanuclear Compounds

Dissolution of the mixed-valence tetranuclear or octanuclear compounds into water partially disrupts the high-nuclearity structure of the amidate-bridged dinuclear compounds. This can be observed through the decay of the visible absorption bands of the high-nuclearity structure and the growth of new UV bands of the dinuclear structure. The spectral features and the rate of the decay or growth are generally sensitive to the pH, the coexisting anion, and the complex concentration. The visible absorption decay was first reported for the α-pyridonate-blue (**3**) as a mere decomposition (*96*), but was later suggested to be due to a disproportionation reaction into the corresponding $Pt(2.0+)_2$ and $Pt(3.0+)_2$ dimers (*97*), without any direct experimental evidence. The first experimental attempt to clarify such phenomena was carried out on the disproportionation reaction of the

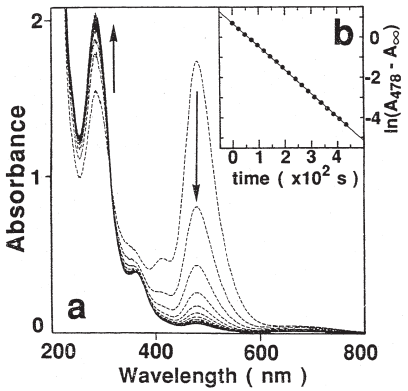

FIG. 13. (a) The time course of the UV–Vis spectra after dissolution of **19** into 2 *M* H_2SO_4 at 25°C in air (every 2 min). (b) The first-order decay at 478 nm in 0.254 *M* H_2SO_4 at 23°C in air. Reproduced with permission from Ref. (*114*). Copyright 1993 Elsevier Sequoia.

α-pyrrolidonate Pt(2.5+)$_4$ compound (**19**), expressed as Eq. (1) (*113*, *115*). The observed spectral changes are shown in Fig. 13.

$$\underset{\mathbf{19}}{\mathbf{Pt(2.5+)_4}} \rightleftharpoons \mathbf{Pt(2.0+)_2 + Pt(3.0+)_2}. \qquad (1)$$

The reaction rate was found to obey the rate expression $k_{obs} = k_1 + k_2/[H^+]$ (*113*) for compounds **18** and **20.** The acetamidate-bridged Pt(2.25+)$_8$ octamer $[Pt_8(NH_3)_{16}(acetamidato)_8]^{10+}$ (**53**) was also reported to exhibit similar behavior after dissolution in aqueous media (Eq. (2)) (*114*).

$$\underset{\mathbf{53}}{\mathbf{Pt(2.25+)_8}} \xrightarrow[\text{rapid}]{\text{extremely}} \begin{cases} \underset{\mathbf{19}}{\mathbf{Pt(2.5+)_4}} \rightleftharpoons \mathbf{Pt(2.0+)_2 + Pt(3.0+)_2} \\ + \\ \mathbf{2Pt(2.0+)_2} \end{cases} \qquad (2)$$

It was proposed that Pt(2.25+)$_8$ rapidly releases the outer two dimeric units upon dissolution, and the Pt(2.5+)$_4$ species formed further undergoes a disproportionation reaction similar to Eq. (1) (*114*).

As for the disproportionation pathway of Pt(2.25+)$_4$, recent studies

on the α-pyrrolidonate Pt(2.25+)$_4$ (**15**) revealed that a reaction such as that in Eq. (3) completes very quickly on dissolution (*60*).

$$\mathbf{2Pt(2.25+)_4} \xrightarrow[\text{rapid}]{\text{very}} \mathbf{Pt(2.5+)_4 + Pt(2.0+)_4} \xrightarrow[\text{rapid}]{\text{very}} \mathbf{Pt(2.5+)_4 + 2Pt(2.0+)_2}. \quad (3)$$

15 **19** **19**

C. Axial Ligand Substitution Reactions of Dinuclear Pt(3.0+)$_2$ Compounds

Spectral features in the UV region of the platinum-blue solutions are generally dramatically affected by anions, such as halides, sulfate, and acetate, and these anions also cause bleaching of the blue color. Recent spectroscopic studies on the α-pyrrolidonate-bridged HH–Pt(3.0+)$_2$ suggest that the intense UV absorption bands are mostly attributable to the dinuclear Pt(3.0+)$_2$ species, and the band profile is affected by axial ligand substitution (*114*, *117*, *118*). A good example demonstrating the effect of the ligand substitution in Pt(3.0+)$_2$ is shown in Fig. 14. Figure 14a shows that dissolution of HH-O_2NO-Pt(3.0+)$_2$-NO_2 (**21**) leads to gradual release of the axial NO_2^- (nitro) ligand according to Eq. (4). Since addition of NO_3^- to the solution of Pt(3.0+)$_2$ never affects the spectral feature, the stability constant of the nitrate coordination must be extremely low. Therefore, it is assumed that the axial nitrate undergoes rapid displacement by other ligands such as solvent water, as illustrated in Eq. (4). The reversibil-

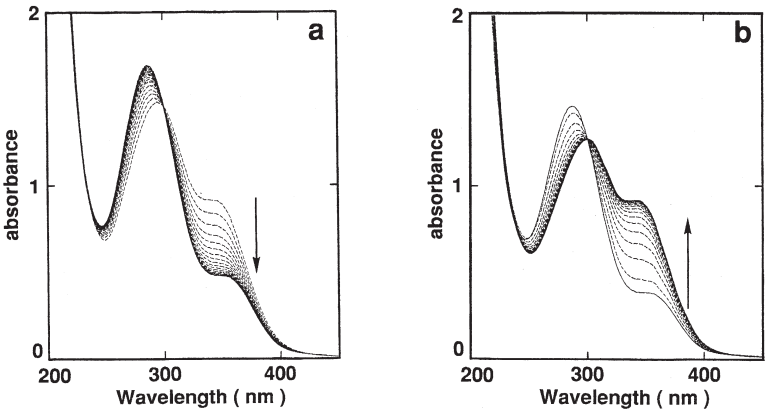

Fig. 14. (a) Spectral changes after dissolution of **21** into 0.5 *M* H_2SO_4 (0.1 m*M*, 25°C, in air) recorded every 1 min. (b) A small amount of $NaNO_2$ was added to the resulting solution in (a). Unpublished results of Sakai and Matsumoto.

ity of this process was also confirmed by adding $NaNO_2$ to the resulting solution (see Fig. 14b).

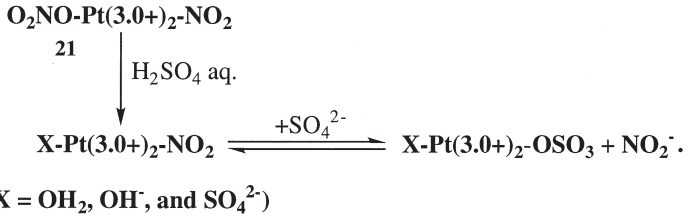

(4)

Similar spectroscopic studies were also carried out for the ligand substitution reactions with SO_4^{2-} (*113*, *116*) and Cl^- (*116*, *118*). However, the reaction rates were so fast that only the equilibrated spectra were observed. The gradual displacement of NO_2^- discussed above is possible merely because most of the NO_2^- exists in its protonated form in the strongly acidic solution. Hydrolysis of the axial aqua ligand was also examined spectroscopically (*116*, *117*), and the stepwise formation constants (Eq. (5)) and hydrolysis constants (Eq. (6)) were determined as follows: $K_{1,SO_4} = 3.4 \times 10^2\ M^{-1}$, $K_{2,SO_4} = 2.6 \times 10\ M^{-1}$ (*115*, *116*); $K_{1,Cl} = 1.7 \times 10^5\ M^{-1}$, $K_{2,Cl} = 4.0 \times 10^3\ M^{-1}$ (*116*, *118*); $K_{1,NO_2} = 3.7 \times 10^7\ M^{-1}$, $K_{2,NO_2} = 7.8 \times 10^4\ M^{-1}$ (*116*); $K_{h1,OH_2} = 9.6 \times 10^{-4}\ M$ (*117*); $K_{h1,SO_4} = 4.6 \times 10^{-4}\ M$ (*117*).

$$\begin{aligned} H_2O\text{-}Pt(3.0+)_2\text{-}OH_2 + X &\overset{K_{1,X}}{\rightleftharpoons} H_2O\text{-}Pt(3.0+)_2\text{-}X \\ H_2O\text{-}Pt(3.0+)_2\text{-}X + X &\overset{K_{2,X}}{\rightleftharpoons} X\text{-}Pt(3.0+)_2\text{-}X, \end{aligned} \tag{5}$$

$$\begin{aligned} X\text{-}Pt(3.0+)_2\text{-}OH_2 &\overset{K_{h1,X}}{\rightleftharpoons} X\text{-}Pt(3.0+)_2\text{-}OH + H^+ \\ H_2O\text{-}Pt(3.0+)_2\text{-}OH &\overset{K_{h2,OH2}}{\rightleftharpoons} HO\text{-}Pt(3.0+)_2\text{-}OH + H^+. \end{aligned} \tag{6}$$

As for the hydrolysis of the axial aqua ligand, pK_a values were determined for the 1-methyluracilate-bridged HT-O_2NO-Pt(3.0+)$_2$-OH_2 by means of potentiometric titration ($K_{h1,OH_2} = 3.2 \times 10^{-4}\ M$; $K_{h2,OH_2} = 2.0 \times 10^{-7}\ M$) (*72*). In addition, it was also suggested that the first ligation in Eq. (5) selectively occurs at one of the two chemically nonequivalent Pt atoms of HH–Pt(3.0+)$_2$, for a clear isosbestic point was observed when the first ligation was predominant (*113*, *116*, *118*).

On the other hand, ligand substitution reactions on the equatorial

ammines were also reported (*74*). The study revealed that 1-methyluracilate-bridged HH-Pt(3.0+)$_2$-Cl (*34*) dissolved in 1 *M* HCl gradually undergoes ligand substitution reaction at the equatorial ammines trans to the O(MeU) atoms to give **35**.

D. Redox Reactions Involving Pt(II) and Pt(III)

1. Redox Reactions with Molecular Oxygen and Water

One of the most important redox reactions of this class of compounds is the oxidation of Pt(2.0+)$_2$ by O_2, for this is the main cause of the appearance of the blue, purple, or dark red colors of the mixed-valence species. Although no detailed examination has been performed, the kinetics of the O_2 oxidation of $[Pt^{II}_2(NH_3)_4(\alpha\text{-pyrrolidonato})_2]^{2+}$ into $[Pt^{III}_2(NH_3)_4(\alpha\text{-pyrrolidonato})_2(H_2O)_2]^{4+}$ (Eq. (7)) was spectrophotometrically examined (*117*). The study showed that the reaction proceeds over several days at room temperature. The first-order rate constants in acidic media were in the range of $k_{obs} = 4.2 \times 10^{-5}$ s^{-1} (pH = 0.23) − 1.13×10^{-5} s^{-1} (pH = 2.1) (at 25°C, in air, I = 1.5 *M*) (*117*).

$$2Pt(2.0+)_2 + O_2 + 4H^+ \rightarrow 2Pt(3.0+)_2 + 2H_2O. \quad (7)$$

On the other hand, O_2-evolving reactions (Eqs. (8) and (9)), corresponding to the reverse reaction of Eq. (7), were reported for the α-pyrrolidonate family (*120*, *121*). In these studies, dissolution of the Pt(3.0+)$_2$ or Pt(2.5+)$_4$ compounds resulted in O_2 production from water. As expected from Eqs. (8) and (9), addition of NaOH to an aqueous solution of Pt(2.5+)$_4$ (**19**) affords the Pt(2.0+)$_2$ dimer (**12**) (*59*, *98*).

$$2Pt(2.5+)_4 + 2H_2O \rightarrow 4Pt(2.0+)_2 + O_2 + 4H^+, \quad (8)$$

$$2Pt(3.0+)_2 + 2H_2O \rightarrow 2Pt(2.0+)_2 + O_2 + 4H^+. \quad (9)$$

The amount of O_2 evolved upon dissolution of Pt(2.5+)$_4$ (**19**) into water was examined in detail as a function of pH and the anion concentration. The results given in Fig. 15 reveal that this not a quantitative reaction. Some undesirable reactions seem to be promoted at the same time, and it remains unclear whether the compound indeed evolves considerable amounts of O_2 even in the presence of O_2, i.e., the reaction might be reversible. Further experiments are needed to better understand the nature of these reactions.

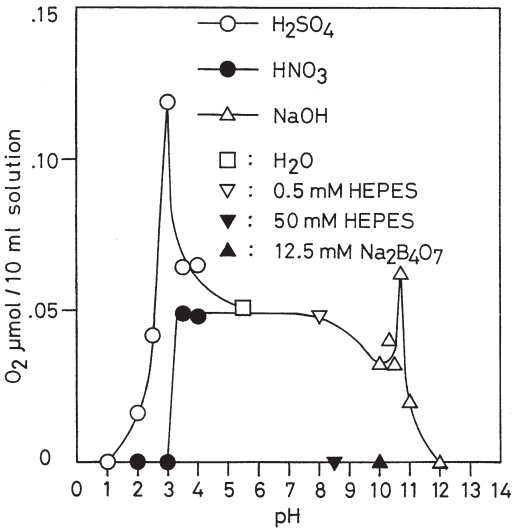

FIG. 15. Evolution of molecular oxygen, detected right after dissolution of 1 μmol of **19** into 10 ml of various solutions at various pHs at room temperature under a helium atmosphere (HEPES = *N*′-2-hydroxyethylpiperazine-*N*-2-ethanesulfonic acid). All the measurements were performed under a helium atmosphere in glove box equipped with a gas chromatograph. Reproduce under permission from Ref. (*115*).

2. *Electrochemistry*

Electrochemistry of $Pt(II)_2$ and $Pt(III)_2$ compounds can be represented by a two-electron one-step oxidation or reduction of the dinuclear compounds, i.e. the redox of the $Pt(III)_2/Pt(II)_2$ couple. Generally, a quasireversible metal-based wave is observed in the range of 0.4–1.2 V vs SCE. The redox potentials reported so far are summarized in Table V. The α-pyridonate-bridged $Pt(II)_2$ and $Pt(III)_2$ compounds **1**, **4**, and **5** are most thoroughly examined by cyclic voltammentry and differential voltammetry, and their novel one-step 2e process has been established. The redox potential is quite sensitive to the donor/acceptor properties of both equatorial and bridging ligands. For instance, replacement of the equatorial ammines into bpy causes an anodic shift of about 0.5 V. On the other hand, compounds of aromatic amides, such as α-pyridonate, have a higher potential in comparison with those of aliphatic amides. This difference is due to the stronger donating property of the aliphatic group, which results in a net increase of electron density at the metal centers.

On the other hand, the electrochemistry of the mixed-valence species cannot be exactly explained. The difficulty lies in that a pure

TABLE V

REDOX POTENTIALS OF PLATINUM-BLUES AND RELATED COMPLEXES

Chemical formula	$E_{1/2}$ (V vs SCE)	ΔE_p (mV)	Solution	Reference
HH-[Pt(3.0+)$_2$(NH$_3$)$_4$(PRI)$_2$(H$_2$O)(NO$_3$)](NO$_3$)$_3\cdot$2H$_2$O (**4**)	0.63	80	1 *M* KNO$_3$/H$_2$O	*2*, *94*
HT-[Pt(3.0+)$_2$(NH$_3$)$_4$(PRI)$_2$(NO$_3$)$_2$](NO$_3$)$_2\cdot$0.5H$_2$O (**5**)	0.61	48	1 *M* KNO$_3$/H$_2$O	*94*
HT-[Pt(2.0+)$_2$(NH$_3$)$_4$(PRI)$_2$](NO$_3$)$_2\cdot$2H$_2$O (**1**)	0.61	45	1 *M* KNO$_3$/H$_2$O	*2*, *94*
HH-[Pt(2.5+)$_2$(NH$_3$)$_4$(PRO)$_2$]$_2$(NO$_3$)$_6\cdot$2H$_2$O (**19**)	0.53	70	4.5 *M* H$_2$SO$_4$/H$_2$O	*98*
HT-[Pt(2.0+)$_2$(bpy)$_2$(PRO)$_2$](ClO$_4$)$_2$ (**26**)	1.01	360	0.1 *M* TBAP/AN[a]	*69*
HH-[Pt(2.25+)$_2$(NH$_3$)$_4$(ATM)$_2$]$_4$(NO$_3$)$_{10}\cdot$4H$_2$O (**53**)	0.42	120	0.1 *M* H$_2$SO$_4$/H$_2$O	*114*
HH-[Pt(2.08+)$_2$(NH$_3$)$_4$(FAM)$_2$]$_4$(NO$_3$)$_{8.66}\cdot$4H$_2$O (**54**)	0.52	270	0.1 *M* H$_2$SO$_4$/H$_2$O	*114*

[a] TBAP = tetra(*n*-butyl)ammonium perchlorate; AN = acetonitrile.

solution of the mixed-valence compound contains several related species because of the disproportionation reactions described above (Section III,B). Nevertheless, measurements carried out for solutions containing the mixed-valence species in detectable amounts revealed no peaks other than those of the Pt(II)$_2$ and Pt(III)$_2$ species. This fact indicates that all the possible redox waves included for the mixed-valence species are overlapped on the Pt(II)$_2$/Pt(III)$_2$ wave in a narrow range (**98**).

V. Catalysis of Amidate-Bridged Platinum(III) Complexes

A. ELECTROCATALYTIC OXIDATION OF WATER INTO MOLECULAR OXYGEN

Cyclic voltammetric experiments carried out in the aqueous solution of **21** or with **21**-adsorbed electrodes achieved catalytic formation of molecular oxygen when the electrode potential was at 0.8 V vs SCE (*119*). It was proposed that the electrocatalytic generation of molecular oxygen occurs according to Eq. (10).

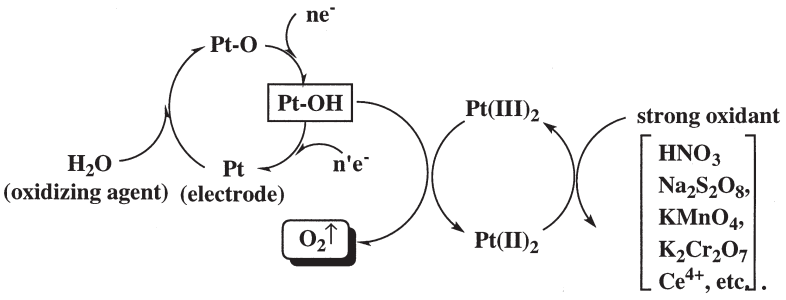

(10)

At 0.8 V, the Pt electrode surface is oxidized to the oxide and hydroxide, which in turn is oxidized to O_2 by the $Pt(III)_2$ complex. The resulting $Pt(II)_2$ is reoxidized to $Pt(III)_2$ by the oxidizing agent.

B. Photochemical Reduction of Water into Molecular Hydrogen

The platinum-blue family exhibits high activity as an H_2-evolving catalyst in the water-reduction process. The activities of a large variety of compounds have been evaluated by using a well-known photosystem consisting of EDTA (sacrifical electron donor), tris(2,2′-bipyridyl)ruthenium(II)(photosensitizer), and methyl viologen (electron relay) (*114*, *115*, *120*). Although the early reports (*115*, *120*) failed to clarify the active species during the catalysis, it was later confirmed that all the Pt species are converted to the dinuclear $Pt(2.0+)_2$ species in the presence of EDTA, serving as a reducing agent (*114*). As a result, the catalysis is now understood as Eq. (11), regardless of the oxidation level of the complex initially dissolved in the solution.

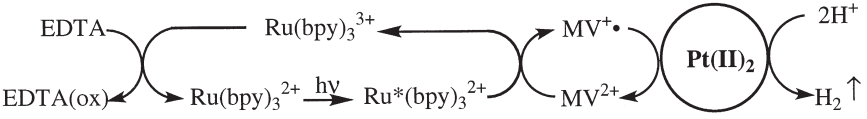

(11)

C. Oxidation of Organic Substances Catalyzed by Amidate-Bridged Platinum(III) Complexes

1. *Catalytic Oxidation of Hydroquinone to Quinone* via *O_2 Activation*

The O_2-oxidation of hydroquinone into quinone, which is very slow in the absence of a catalyst, was found to be accelerated by the addition of the α-pyrrolinonate-bridged $Pt(2.5+)_4$ (**19**) (*117*). The detailed kinetic investigation revealed that the $Pt(2.0+)_2$ species formed according to Eq. (1) plays a major role as the catalyst. The reaction rate of the quinone formation is higher than that of O_2 oxidation of $Pt(2.0+)_2$ into $Pt(3.0+)_2$ and was found to be rather linear to the hydroquinone concentration. Therefore, it was suggested that the quinone formation proceeds via a certain intermediate formed between the $Pt(2.0+)_2$ species and molecular oxygen (e.g., peroxo species). The possible schematic mechanism is illustrated in Eq. (12).

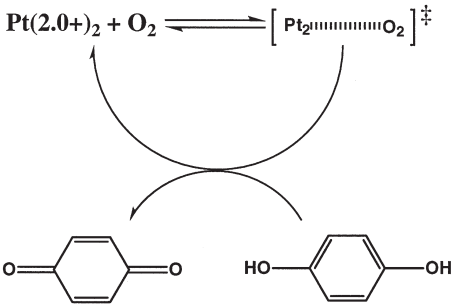

(12)

2. Oxidation of Benzene to Phenol by H_2O_2

The α-pyrrolidonate Pt(2.5+)$_4$ (**19**) was also found to catalyze the oxidation of benzene to phenol by hydrogen peroxide (*121*). By HPLC, ESR, and UV–Vis absorption spectroscopy, the main reaction pathway was confirmed to be Eq. (13).

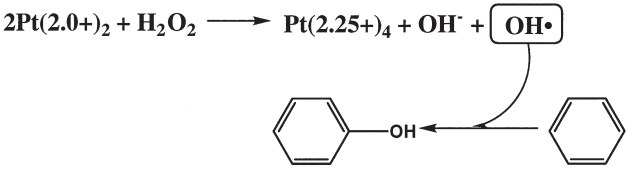

(13)

As shown above, addition of H_2O_2 into a solution of the complex caused a prompt color change into blue to give hydroxyl radical, which was detected with a spin-trapping method. The reaction was found therefore to be a "Fenton-like" reaction.

VI. Organometallic Chemistry of Dinuclear Pt(III) Complexes

A. Catalytic Ketonation and Epoxidation of Olefins

Since tetranuclear platinum-blues are oxidized by O_2 to Pt(III) dinuclear complexes and are reversively reduced to the platinum-blues and further to the Pt(II) dinuclear complexes, an attempt was made to use these complexes as catalysts for olefin oxidation to ketones and epoxides. The catalysts used were α-pyrrolidonato-bridged Pt-tan $[Pt_4(NH_3)_8(C_4H_6NO)_4](NO_3)_6 \cdot 2H_2O$ (**19**), pivalamidato-bridged Pt-blue $[Pt_4(NH_3)_8(C_5H_{10}NO)_4](NO_3)_5$ (**57**), α-pyrrolidonato-tan $[Pt_4(NH_3)_8$

$(C_4H_6NO)_4](n\text{-}C_{12}H_{25}SO_3)_6$ (**59**), pivalamidato-blue $[Pt_4(NH_3)_8(C_4H_6NO)_4](n\text{-}C_{12}H_{25}SO_3)_5$ (**60**), 3-methyl-2-pyrrolidonato-tan $[Pt_4(NH_3)_8(C_5H_8NO)_4](NO)_3)_6 \cdot 3H_2O$ (**61**), and 5-methyl-2-pyrrolidonato-blue $[Pt_4(NH_3)_8(C_5H_8NO)_4](ClO_3)_5$ (**62**). Since most of the platinum complexes are insoluble in dichloroethane, the reaction was carried out in a H_2O/CH_2ClCH_2Cl biphasic solution. In a typical experiment, 10 μmol of the platinum complex and 5-fold (**57**, **60**, **62**) or 6-fold (**19**, **59**, **61**) equivalent amounts of a phase transfer agent, $C_{12}H_{25}SO_3Na$, were dissolved in a mixture of 1 ml of 0.05 $M H_2SO_4$ and 1 ml of CH_2ClCH_2Cl containing a 400-fold equivalent amount of olefin. The solution was stirred vigorously in a closed O_2-filled Teflon vial (5 ml), which was placed in an O_2-filled glass bottle with a screwstopper to avoid O_2 leakage from the Teflon vial. The reaction was carried out at 50°C for 5 days, and an aliquot of the solution was analyzed with gas chromatography.

The results of the olefin oxidation catalyzed by **19**, **57**, and **59**–**62** are summarized in Tables VI–VIII. Table VI shows that linear terminal olefins are selectively oxidized to 2-ketones, whereas cyclic olefins (cyclohexene and norbornene) are selectively oxidized to epoxides. Cyclopentene shows exceptional behavior, it is oxidized exclusively to cyclopentanone without any production of epoxypentane. This exception would be brought about by the more restrained and planar pentene ring, compared with other larger cyclic nonplanar olefins in Table VI, but the exact reason is not yet known. Linear inner olefin, 2-octene, is oxidized to both 2- and 3-octanones. 2-Methyl-2-butene is oxidized to 3-methyl-2-butanone, while ethyl vinyl ether is oxidized to acetaldehyde and ethyl alcohol. These products were identified by NMR, but could not be quantitatively determined because of the existence of overlapping small peaks in the GC chart. The last reaction corresponds to oxidative hydrolysis of ethyl vinyl ether. Those olefins having bulky (α-methylstyrene, β-methylstyrene, and allylbenzene) or electon-withdrawing substituents (1-bromo-1-propene, 1-chloro-1-propene, fumalonitrile, acrylonitrile, and methylacrylate) are not oxidized.

Since it is known that the tetranuclear mixed-valent platinum-blue complexes such as **19** and **57** undergo disproportionation and reduction by water as Eqs. (1)–(3) and (7)–(9) show (*106*, *113*), all the species appearing in Eqs. (1)–(3) and (7)–(9) are present in the solution. However, only one or several of the four species in the solution may in fact be resposible for the catalytic olefin oxidation. To clarify this point, the effect of the Pt oxidation state in the platinum complexes was compared. The results are summarized in Table VII, which

TABLE VI

OLEFIN OXIDATION CATALYZED BY PLATINUM-BLUE COMPOUNDS

Substrate	Product	Turnover number[a] for catalyst **19**	**57**
1-Hexene	2-Hexanone	11.9	3.8
	1,2-Epoxyhexane	8.6	8.8
1-Heptene	2-Heptanone[b]	13.3	4.5
1-Octene	2-Octanone[b]	15.8	12.4
1-Decene	2-Decanone	10.9	4.1
2-Octene	2-Octanone	1.7	1.6
	3-Octanone	2.2	1.6
Cyclohexene	Cyclohexane	22.8	15.0
	Cyclohexanone[c]	1.9	1.4
Cyclopentene	Cyclopentanone	2.0	2.5
Norbornrnr	Epoxynorbprnane	7.2	5.2
	Norbornanone[d]	2.3	0.6
2-Methyl-2-butene	3-Methyl-2-butanone		
Ethyl vinyl ether	Acetaldehyde		
	Ethylalcohol		
1-Chloro-1-propene		No reaction	
1-Bromo-1-propene		No reaction	
α-Methylstyrene		No reaction	
β-Methylstyrene		No reaction	
Allylbenzene		No reaction	

[a] Turnover number = [product]/[complex].
[b] Minor products (less than 1%): 1,2-epoxide.
[c] Minor product (less than 1%): cyclopentanecarboxyaldehyde.
[d] Minor product (less than 1%): norborneol.

TABLE VII

EFFECT OF PLATINUM OXIDATION STATE IN THE CATALYTIC OXIDATION OF CYCLOHEXENE

Catalyst	Turnover number for product: Epoxycylohexane	Cyclohexanone
$[Pt_2^{III}(NH_3)_4(C_4H_6NO)_2(H_2O)_2](NO_3)_4$[a]	24.7	1.4
$[Pt_2^{II}Pt_2^{III}(NH_3)_8(C_4H_6NO)_4](NO_3)_6$ (**19**)	22.8	1.9
$[Pt_2^{II}(NH_3)_4(C_4H_6NO)_2(NO_3)_2$[b]	0.5	1.8

[a] The complex was prepared *in situ* by electrochemical oxidation at 0.60 V vs SCE[8].
[b] The complex was prepared *in situ* by electrochemical oxidation at 0.35 V vs SCE[8].

TABLE VIII

EFFECT OF SURFACTANT, SOLVENT, AND ATMOSPHERE ON THE CATALYTIC OXIDATION OF CYCLOHEXENE

Run	Catalyst	Surfactant[a]	Solvent	Atmosphere	Turnover number for product	
					Epoxycylohexane	Cyclohexanone
1	None	+	0.05 *M* H_2SO_4/CH_2ClCH_2Cl	O_2	0	0.4
2	**19**	+	0.05 *M* H_2SO_4/CH_2ClCH_2Cl	O_2	22.8	1.9
3	**19**	+	0.05 *M* H_2SO_4/CH_2ClCH_2Cl	Air	18.6	1.2
4	**19**	+	0.05 *M* H_2SO_4/CH_2ClCH_2Cl	N_2	4.7	0.8
5	**19**	−	0.05 *M* H_2SO_4/CH_2ClCH_2Cl	O_2	0	0.8
6	**19**	+	CH_2ClCH_2Cl	O_2	0	0
7	**19**	+	0.05 *M* H_2SO_4	O_2	0	0.3
8	**19**	+	H_2O/CH_2ClCH_2Cl	O_2	2.3	0.1
9	**19**	+	CF_3SO_3H[b]$/CH_2ClCH_2Cl$	O_2	0	0
10	**59**	+	0.05 *M* H_2SO_4/CH_2ClCH_2Cl	O_2	20.3	1.5
11	**59**	−	0.05 *M* $H_2SO_4/SO_4/CH_2ClCH_2Cl$	O_2	17.3	1.2
12	**57**	+	0.05 *M* H_2SO_4/CH_2ClCH_2Cl	O_2	15.0	1.4
13	**60**	+	0.05 *M* H_2SO_4/CH_2ClCH_2Cl	O_2	14.5	1.0
14	**60**	−	0.05 *M* H_2SO_4/CH_2ClCH_2Cl	O_2	12.2	0.7
15	**61**	+	0.05 *M* H_2SO_4/CH_2ClCH_2Cl	O_2	21.7	1.3
16	**62**	+	0.05 *M* H_2SO_4/CH_2ClCH_2Cl	O_2	4.2	0.3

[a] (+) Added; (−) not added.
[b] Two drops of CF_3SO_3H added to CH_2ClCH_2Cl.

clearly shows that the Pt^{III} dinuclear complex is most effective and would be the real catalyst. Compound **19** also exhibits high activity, whereas the Pt^{II} dinuclear complex is ineffective. All other factors expected to affect the catalysis efficiency, including the presence of O_2 and surfactant, and selection of the solvent have been examined, and the results are summarized in Table VIII. It is clear from runs 2, 3, and 4 in Table VIII that O_2 is indispensable to the oxidation reaction. Addition of surfactant or the presence of surfactant as the counter ion is necessary (runs 2, 5, 10, 11, 13, and 14), and the reaction must be carried out in a biphasic solution, i.e., a mixture of CH_2ClCH_2Cl and 0.05 *M* H_2SO_4. Neither 0.05 *M* H_2SO_4 nor CH_2ClCH_2Cl alone gave appreciable products, even with addition of surfactant (runs 6 and 7). It is also clear that water is essential to the reaction (runs 6 and 9). Acid is also necessary to the reaction; the oxidation does not proceed in a biphasic solution of H_2O/CH_2ClCH_2Cl (run 8). The effect of various acids was also examined, and the result showed that $HClO_4$ was as effective as H_2SO_4, while other coordinating acids, such as HNO_3 and HCl, were much less effective. The effect of a substituent on the α-pyrrolidone ring is compared in runs 2, 15, and 16, and it is evident that a substituent near the amidate group of the α-pyrrolidonate ring suppresses the reaction (run 16).

Although the olefins seem to be oxidized by O_2 from the experiments described above, GC-MS analysis of the oxidation products showed that all of the oxygen atoms in the products are from H_2O and not from O_2, as the following experiment shows. The oxidation reactions were carried out in both $^{16}O_2$ and $^{18}O_2$, and the products were analyzed with GC-MS. Contrary to our expectation, all of the oxygen atoms in the products, i.e., ketones and opoxides, were ^{16}O irrespective of whether the reaction had been carried out in $^{16}O_2$ or $^{18}O_2$. In the next step, the reactions were carried out in $^{16}O_2$ with either $H_2{}^{18}O$ or $H_2{}^{16}O$. The GC-MS analysis of the products revealed that oxygen from water is exclusively introduced into the oxidation products. The reactions were also carried out under $^{16}O_2$ in $D_2{}^{16}O$, and it was confirmed that deuterium does not exist in the products. From these facts, the mechanism of the catalytic oxidation of olefins to ketones and epoxides seems to be similar to that of the Wacker reaction using Pd(II) (*122*, *123*), as shown in Fig. 16 for ketones and epoxides. There exist, however, several differences in this reaction and the Wacker process: (1) epoxide is not produced as a main product in the Wacker process and (2) inner olefins are not oxidized in the Wacker process, whereas

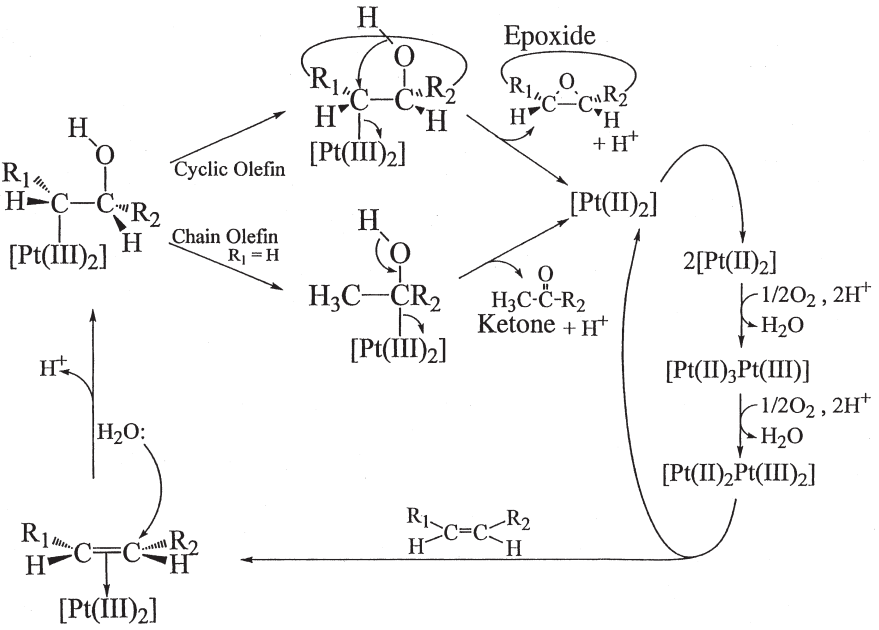

FIG. 16. Proposed reaction mechanism for the olefin ketonation and epoxidation catalyzed by platinum-blues.

they are oxidized in the present reaction. For linear olefins, the 1–2 shift of the coordinated Pt takes place giving selectively ketones or aldehydes, while for sterically more restrained cyclic olefins, the 1–2 shift does not take place and epoxides are formed as major products. Similar ketone vs epoxide selectivity based on the ease of the 1–2 shift has been proposed for olefin oxidation catalyzed by [Pt(diphoe)(CF_3)(OH)] (*124*) (diphoe = *cis*-1, 2-bis(diphenylphosphino) ethane), where peroxide is used as the oxidizing agent.

During the reaction, most of the platinum complex is transferred to the organic phase, as observed with the dark blue or tan color of the tetranuclear complexes in the organic phase. After the catalytic reaction ceases, both phases are pale yellow. The tan color and the catalytic reaction can be recovered at this stage by adding sodium persulfate to the solution. This indicates that the Pt^{III} catalyst is gradually reduced to the Pt^{II} dinuclear complex as the catalytic reaction proceeds, and therefore the reaction finally stops. Acid and O_2 are necessary in the catalysis to reoxidize the Pt^{II} dinuclear complex to the Pt^{III} dinuclear complex (*91*, *125*). The oxidation reaction is, however, not fast enough, and the reduced Pt^{II} dinuclear species gradually accumulates in the solution. Addition of $Na_2S_2O_8$ from the beginning of the reaction in order to increse the lifetime of the catalyst, however, decreases the turnover number (*91*, *125*).

B. Synthesis of Alkyl–Pt(III) Dinuclear Complexes from Olefins and Its Implication on Olefin Oxidation

According to the reaction mechanism in Fig. 16, olefins coordinate axially to the dinuclear Pt(III) complexes. Whether olefins really coordinate to Pt(III) is particularly a target of research, since Pt(II) is known to coordinates various olefins, whereas Pt(IV) does not coordinate any of them. Therefore an attempt was made to isolate the olefin π-complex of the Pt^{III} dimer in order to prove the proposed mechanisms in Fig. 16. While no olefin π-complex was obtained, despite our intensive efforts, 4-pentene-1-ol and ethylene glycol vinyl ether were found to give alkyl complexes. The alkyl complexes isolated in the present study are 2-methyl-tetrahydrofurfuryl Pt^{III} complex, $[Pt_2(NH_3)_4((CH_3)_3CCONH)_2(\overline{O(CH_2)_3CH}CH_2](NO_3)_3 \cdot H_2O$ (**63**) and oxyethyl complex, $[Pt_2(NH_3)_4((CH_3)_3CCONH)_2((CH_2CHO)](NO_3)_3 \cdot H_2O$ (**64**), which were obtained from the reaction of $[Pt_2(NH_3)_4((CH_3)_3CCONH)_2(H_2O)_2)]^{4+}$ with 4-pentene-1-ol and ethylene glycol vinyl ether, respectively. The reactions support π-coordination of the olefins to the Pt^{III} axial position in the first step of the reaction, although that π-

coordination is very unstable and the π-complex cannot be isolated. The reactions are also very important in the sense that they give a general route for synthesizing alkyl–Pt^{III} dinuclear complexes (**91**).

The crystal structures of **63** and **64** are shown in Figs. 17 and 18,

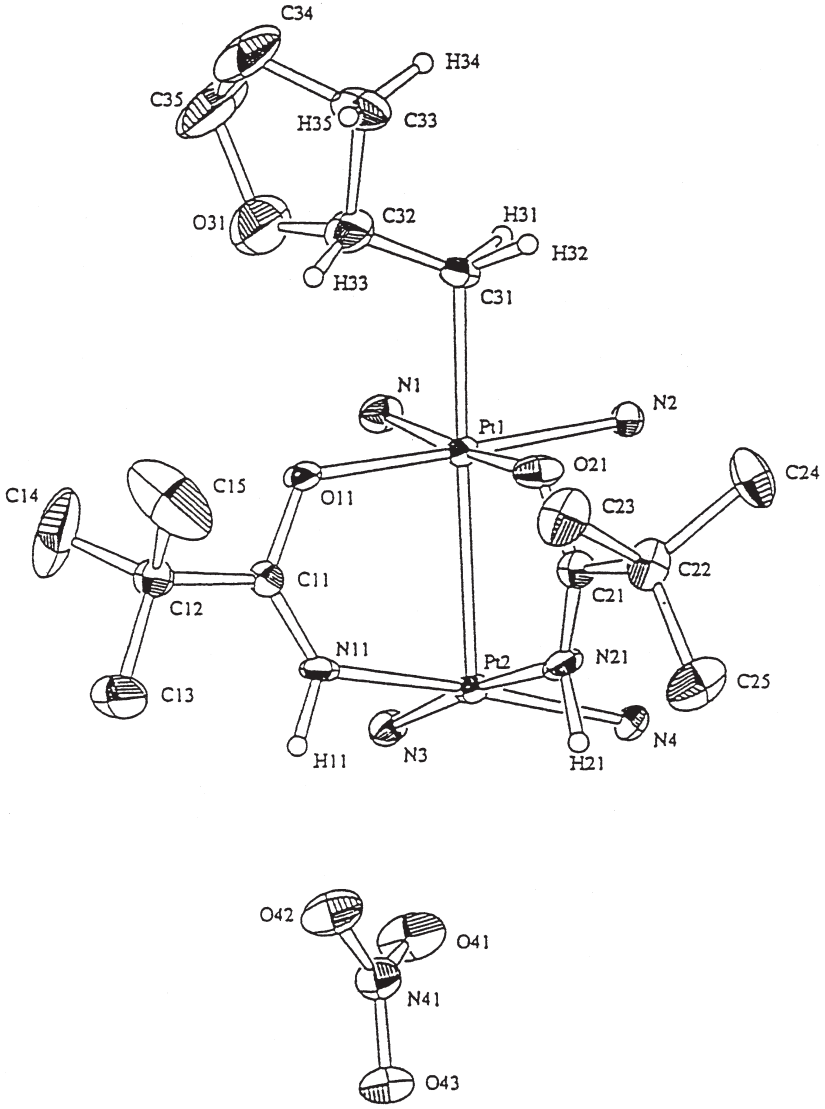

FIG. 17. An ORTEP drawing of $[Pt^{III}_2(NH_3)_4(CCH_3)_3CCONH)_3(CH_2CH(CH_2)_3O)](NO_3)_3 \cdot H_2O$ (**63**).

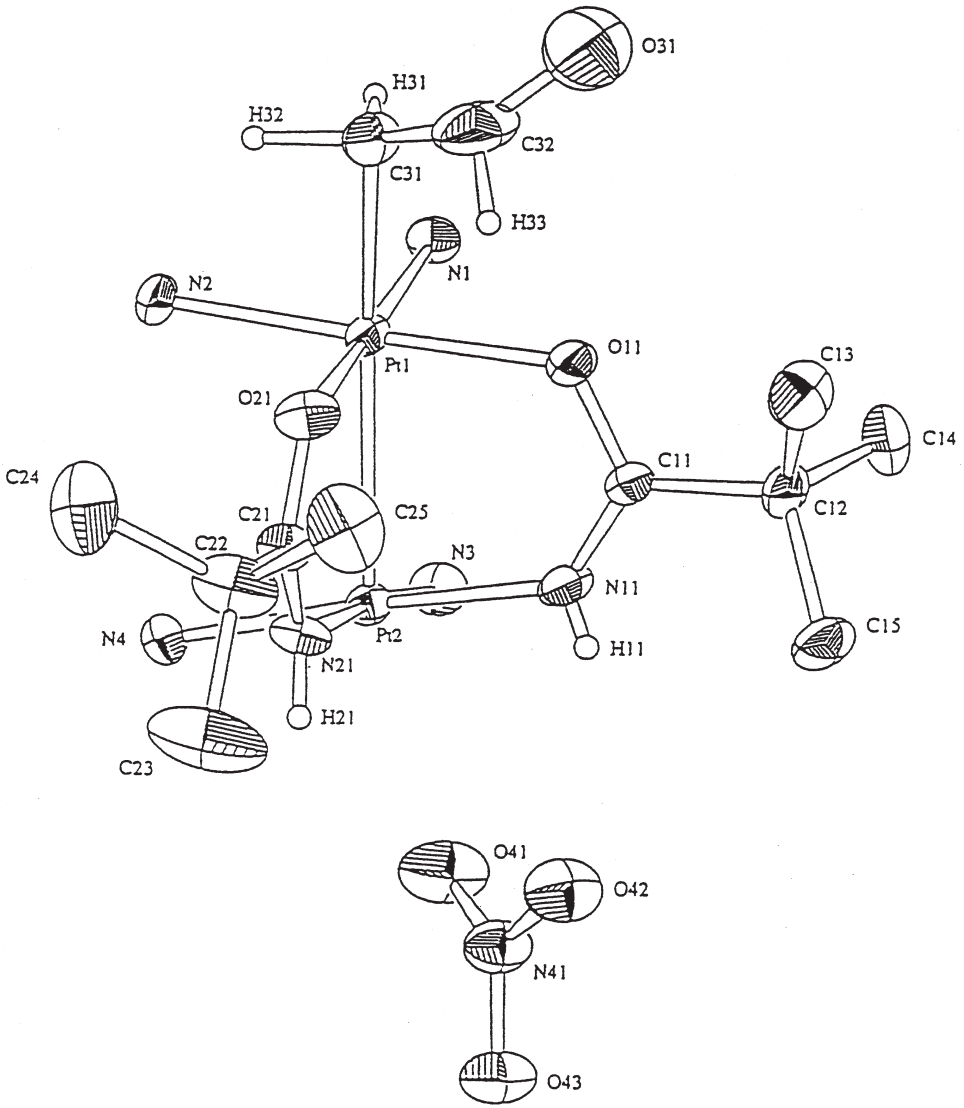

FIG. 18. An ORTEP drawing of $[Pt^{III}_2(NH_3)_4(CCH_3)_3CCONH)_2(CH_2CHO)](NO_3)_3\ H_2O$ (**64**).

respectively. The reactions of 4-pentene-1-ol and ethylene glycol vinyl ether with the amidate-bridged Pt^{III} dinuclear complex are expressed as Eqs. (14) and (15), respectively. Both **63** and **64** are not very stable in air and must be kept in a desiccator.

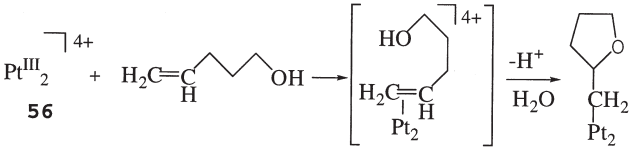

(14)

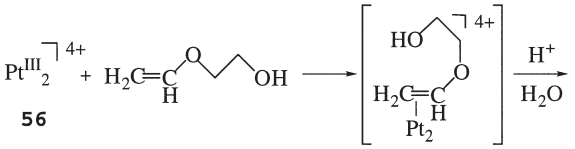

(15)

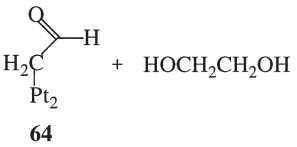

Selected bond distances (Å) and angles for **63** and **64** are listed in Ref. (*91*). Both of the Pt–Pt distances (2.7687(8) Å in **63** and 2.7106(7) Å in **64**) are significantly longer than those in previously reported amidate-bridged dinuclear Pt^{III} complexes with nonalkyl axial ligands such as halide, H_2O, NO_2^-, or NO_3^- (2.165(10) to 2.644(1) Å) (*50–53*). The present long Pt–Pt distances are caused by the strong trans influence of the alkyl ligand, and this strong trans influence extends further to the other axial end, i.e. the Pt–O (axial nitrate) distances of **63** (2.92(1) Å) and **64** (2.7498(8) Å) are significantly longer than the usual nitrate coordination distances to Pt^{III} (2.36(3) to 2.71(1) Å) (*2*, *50–54*, *58*, *66*, *67*, *94*, *95*). The Pt–O(axial nitrate) is so long that it is not even considered coordination. Such remote trans influence via a Pt–Pt bond would be caused by a strong dipole-inducing effect of the alkyl ligand, and a dipole along the Pt–Pt axis, $R–Pt^{\delta+}–Pt^{\delta-}–L$, is induced. Judging from the fact that one terminal of the Pt–Pt axis is bonded to an alkyl group, while the other end does not have any axial ligand, the Pt atom bonded to the alkyl (R) is close to Pt^{IV}, whereas the other Pt atom is close to Pt^{II}. This valence localization is also observed in the ^{195}Pt-NMR spectra (*91*).

The bond distances of the alkyl group in **64** are shown in Fig. 19, together with the related C=C, C–C, C–O, and C=O distances. The C–C distance in **64** is intermediate between the typical C–C and C=C distances, and the C–O distance of **64** is also between the typi-

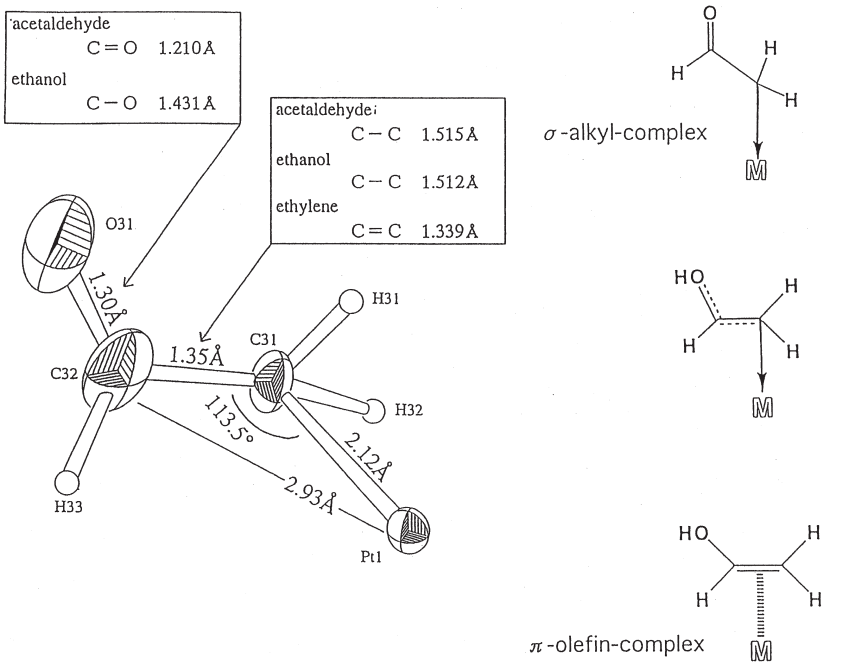

FIG. 19. Bond distances and angles of the β-oxyethyl group in **64**.

cal C–O and C=O distances. This fact means that the actual electronic state of the alkyl group is an intermediate of the σ- and π-complexes, as shown in Fig. 19. The Pt–C–C angle of 113.5° in **64** is close to that of the σ-complex. Although complexes **63** and **64** do not prove directly the existence of olefin π-complexes, the present reactions strongly support the mechanism in Fig. 16, indicating that an alkyl complex is produced by nucleophilic attack of H_2O on the olefinic carbon of the π-complex.

Complex **63** is stable in acidic to weakly basic aqueous solution. However, on addition of 0.1 *M* NaOH, nucleophilic attack on the β-carbon atom takes place as shown in Eq. (16). This reaction, may also be considered to proceed via the initial α-hydroxylation, followed by dehydration to give the product.

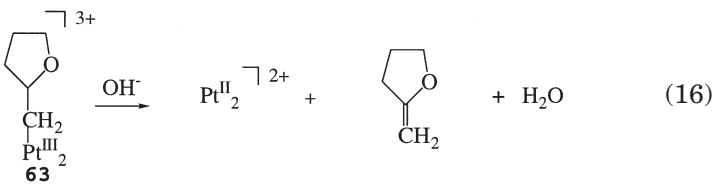

Complex **64** is unstable at room temperature even as a solid and is easily hydrolyzed in neutral water to produce glycol aldehyde (Eq. (17)). In 0.1 *M* $HClO_4$, **64** produces glycol aldehyde and acetic acid in a *ca.* 9 : 1 ratio.

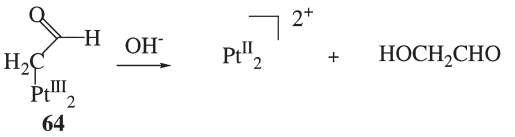

64 (17)

The reason that OH^- does not attack the α-carbon in **63,** in contrast to the reaction in Eq. (17), would be due to the stronger electron donation by the β-carbon in **63,** which increases the electron density at the α-carbon atom. Addition of ethylene glycol vinyl ether to the *p*-toluenesulfonate salt of **64** in $CDCl_3$ catalytically yields 2-methyl-1,3-dioxolane (Eq. (18)). The reaction proceeds almost instantaneously, and a 50-fold equivalent of the substrate is completely converted to 2-methyl-1,3-dioxolane, which was confirmed by ^{1}H-NMR. After the reaction, the Pt(III) dimer complex without alkyl ligand is left in the solution, which is still capable of catalysis. The reaction is shown as Eq. (18).

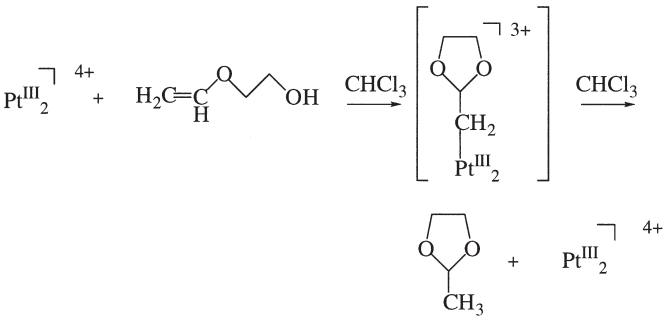

(18)

A similar reaction was not observed for 4-pentene-1-ol. It should be noted that a Pt(III) dimer complex is released after the reaction in Eq. (18), which is in contrast to the release of olefin and a Pt(II) dimer complex in aqueous solution by reductive elimination (Eq. (16)). The difference of such reactivity depending on the alkyl and the solvent would be caused by the difference of the electron density of the α-carbon atom and the dipole structure along the Pt–Pt bond in the solvents of different polarities. In aprotic organic solvent, the electron distribution along the Pt–Pt bond would be less polar, i.e., close to

R–Pt^{III}–Pt^{III}, whereas in aqueous solution, it would be more polar, being close to R–Pt^{IV}–Pt^{II}, as indicated in the X-ray structure of **63**. Recent work of Labinger and Bercaw's group on C–H activation of alkane by a mixture of Pt(II) and Pt(IV) shows that R–Pt^{IV} receives nucleophilic attack by Nu: to release NuR and Pt(II); no such behavior is observed for R–Pt^{II} (*126, 127*). It is therefore reasonable that R–Pt^{IV}–Pt^{II} undergoes nucleophilic attack by OH^- to release ROH or olefin and a Pt(II) dinuclear complex in aqueous solution. Although it is essential to compare the reactivity of an identical compound in organic and aqueous solusions, **63** and **64** are not soluble in organic solvents and exhibit complicated decomposition if dissolved forcedly with the aid of surfactant.

Similar to the above reactions, we found that acetone easily reacts with Pt(III) dimer complexes as follows.

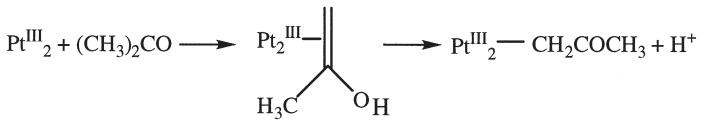

(19)

In this reaction, the enol form of acetone reacts with the Pt(III) dimer complex, and therefore the reaction mechanism seems to be the same with those of the olefin reactions (*90*).

Synthesis of **63** and **64** supports the olefin oxidation mechanisms in Fig. 16. These mechanisms have several important and noteworthy points about Pt^{III} chemistry: (1) olefins coordinate to Pt^{III} at the axial position, which is contrasted to the π-coordination of olefins perpendicular to the square-planar coordination plane of Pt^{II}. Olefin coordination to Pt(III) should also be contrasted to the fact that olefins do not coordinate to Pt(IV). (2) Platinum^{III} is strongly electron-withdrawing, and the coordinated olefins receive nucleophilic attack. (3) The alkyl α-carbon on the Pt^{III} undergoes nucleophilic attack in aqueous solution, whereas in aprotic solvent, aldhyde (and possibly also ketone in other cases) is produced by reductive elimination.

The Pt^{III}–Pt^{III} bond in the alkyl complexes exhibits a unique character in that the Pt atom acts both as Pt^{II} and Pt^{IV} or the intermediate through electron localization and delocalization along the Pt–Pt axis: (1) coordination of olefin is a Pt^{II} character, since no olefin–Pt^{IV} complex is known; and (2) the very easy and rapid nucleophilic attack on the coordinated alkyl α-carbon atoms is a Pt^{IV} character. Alkyl–Pt^{II} complexes do not easily undergo nucleophilic attack unless the com-

plex is cationic, and only a few nucleophilic attacks are reported for neutral Pt^{II} complexes (*131–134*).

VII. Antitumor Active Platinum-Blue Complexes

In the process of identifying the reaction products of the anticancer drug *cis*-DDP with DNA bases, unusually dark blue compounds were found, which were called "platinum-pyrimidine-blues." Interestingly,

TABLE IX

ANTITUMOR ACTIVITIES OF PLATINUM COMPOUNDS AGAINST *L1210 in Vivo*

Complex	Dose (mg/kg)	%T/C
Glutarimide-blue,	50	102
$[Pt_4(NH_3)_8(GI)_4](NO_3)_5 \cdot 2H_2O$	26	164
	12.5	139
3,3-Dimethylglutarimide-blue,	50	131
$[Pt_4(NH_3)_8(DMGI)_4](NO_3)_5 \cdot 2H_2O$ **47**	25	156
	12.5	200
	6.25	132
	3.12	114
3,3-Dimethylglutarimide HH dimer,	50	0[a]
$[Pt_2(NH_3)_4(DMGI)_2](NO_3)_2 \cdot H_2O$	25	133
	12.5	140
	6.25	162
	3.12	125
	1.56	111
3,3-Dimethylglutarimide HT dimer,	50	98
$[Pt_2(NH_3)_4(C_4H_6NO)_2](NO_3)_2 \cdot H_2O$ **46**	25	93
	12.5	90
α-Pyrrolidone-tan,	50	111
$[Pt_4(NH_3)_8(C_4H_6NO_4](NO_3)_6 \cdot 2H_2O$ **19**	25	102
	12.5	102
Acetamide-blue,	50	107
$[Pt_8(NH_3)_{16}(C_2H_4NO)_8](NO_3)_{10} \cdot 4H_2O$ **53**	25	110
	12.5	102
Cis-DDP[b]	25	202
$[PtCL_2(NH_3)_2]$	12.5	278
	6.25	220
	3.12	200

[a] %T/C value of 0 means that more than three mice died "before day 5."

[b] %T/C values for *cis*-DDP were taken from ref. (*136*).

these blue compounds also exhibit antitumor activity against S180 (*45*). This activity was, however, not fully pursued at that time because the synthesis of the blue compounds lacked reproducibility and presumably also because the high optimal dose level of the compounds made them seem less promising as practical chemotherapeutic reagents. Although several groups again, after about a decade, reported antitumor activities and preparative procedures for other platinum-blue compounds (*135*, *136*), the mechanistic study of the antitumor activities did not progress, since they still lacked reliable formulas (they may be mixtures) and the structuers were not known. We have recently isolated the antitumor active compounds whose structures have been solved by X-ray diffraction analysis (*84*). The detailed NMR study of these compounds revealed the solution behavior, which is closely related to the mechanism of the antitumor activity. Table IX summarizes the results of the antitumor screening test for platinum-blue and related complexes. Complexe **47**, its HH Pt(II) dimer, and glutarimide-blue have activity almost comparable to that of *cis*-DDP, while another tetranuclear complex **19** is inactive. Di-

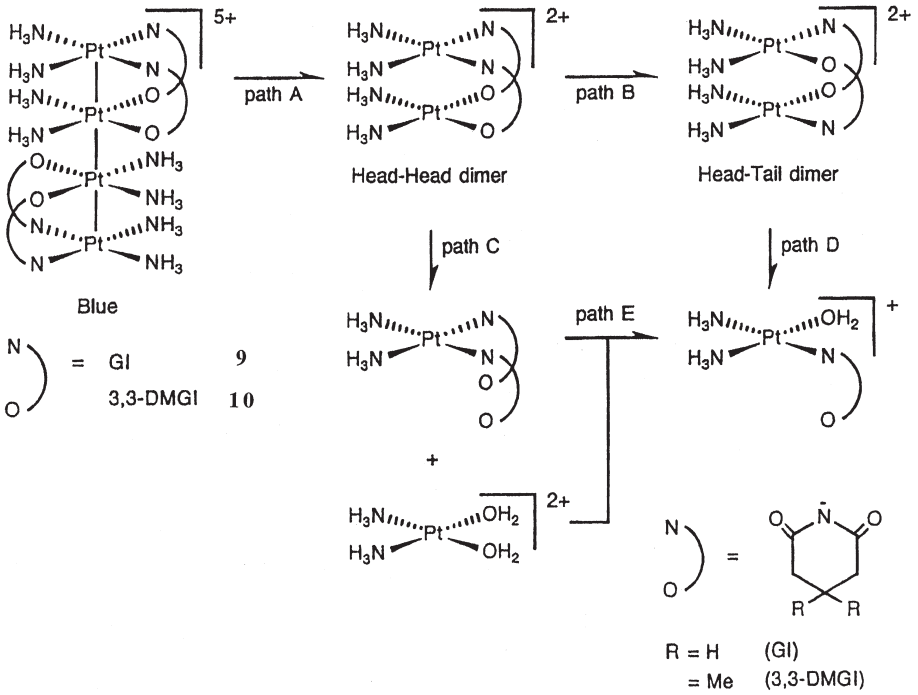

FIG. 20. Solution behavior of **47** and its glutarimidate analog in H_2O.

nuclear HH isomer with DMGI ligand is also active, whereas its HT isomer **46** is inactive. Octanuclear acetamidate-bridged complex **53** is also inactive. These results show that the antitumor activities are different even among complexes with an identical bridging ligand but with different structures or different Pt oxidation states (*106*).

The advantage of these complexes is that each Pt complex is isolated in pure form, and the crystal structure is known. Based on ^{1}H- and ^{195}Pt-NMR spectroscopy, the antitumor active compounds were found to be disrupted as shown in Fig. 20, giving finally $[Pt(NH_3)_2(H_2O)_2]^{2+}$, which is the same hydrolysis product as *cis*-DDP and is responsible for the activity. Therefore, the subsequent reaction with DNA bases and the mechanism would be the same with those of *cis*-DDP. The antitumor inactive compounds are relatively stable and are disrupted only to dinuclear amidate-bridged compounds. No further decomposition to $[Pt(NH_3)_2(H_2O)_2]^{2+}$ occurs.

References

1. Usón, R.; Forniés, J.; Tomás, M.; Menjön, B.; Sünkel, K.; Bau, R. J. *Chem. Soc. Chem. Commun.* **1984,** *751.*
2. Hollis, L. S.; Lippard, S. J. *J. Am. Chem. Soc.* **1981,** *103,* 6761.
3. Lippert, B.; Schöllhorn, H.; Thewalt, U. Z. *Naturforschung,* **1983,** *38,* 1441.
4. Goodgame, D. M. L.; Rollins, R. W.; Slawin, A. M. Z.; Williams, D. I.; Zard, P. W. *Inorg. Chim. Acta* **1986,** *120,* 91.
5. Umakoshi, K.; Kinoshita, I.; Ichimura, A.; Ooi, S. *Inorg. Chem.* **1987,** *26,* 3551.
6. Kuyper, J.; Vrieze, K. *Trans. Met. Chem.* **1976,** *1,* 208.
7. Steel, B. R.; Vieze, K. *Trans. Met. Chem.* **1977,** *2,* 169.
8. Schagen, J. D.; Overbeck, A. R.; Schenk. H. *Inorg. Chem.* **1978,** *17,* 1938.
9. Appleton, T. G.; Byriel, K. A.; Hall, J. R.; Kennard, C. H. L.; Mathieson, M. T. *J. Am. Chem. Soc.* **1992,** *114,* 7305.
10. Appleton, T. G.; Byriel. K. A.; Garrett, J. M.; Hall, J. R.; Kennard, C. H. L.; Mathieson, M. T.; Stranger, R. *Inorg. Chem.* **1995,** *34,* 5646.
11. Bellito, C.; Flamini, A.; Gastaldi, L.; Scaramuzza, L. *Inorg. Chem.* **1983,** *22,* 444.
12. Cotton, F. A.; Falvello, L. R.; Han, S. *Inorg. Chem.* **1982,** *21,* 2889.
13. El-Mehdawi, R.; Fronczek, F. R.; Roundhill, D. M. *Inorg. Chem.* **1986,** *25,* 1155.
14. Che, C.-M.; Lee, W.-M.; Mak, T. C. W.; Gray, H. B. *J. Am. Chem. Soc.* **1986,** *108,* 4446.
15. Zipp, A. P. *Coord. Chem. Rev.* **1988,** *84,* 47.
16. Usón, R.; Forniés, J.; Falvello, L. R.; Tomás, M.; Casas, J. M.; Martin, A.; Cotton, F. A. *J. Am. Chem. Soc.* **1994,** *116,* 7160.
17. Cini, R.; Fanizzi, F. P.; Intini, F. P.; Natile, G. *J. Am. Chem. Soc.* **1991,** *113,* 7805.
18. Baxter, L. A. M.; Heath, G. A.; Raptis, R. G.; Willis, A. C. *J. Am. Chem. Soc.* **1992,** *114,* 6944.
19. Hofmann, K. A.; Bugge, G. *Berichte* **1908,** *41,* 312.
20. Gillard, R. D.; Wilkinson, G. *J. Chem. Soc.* **1964,** 2835.

21. Keller, H. J. In "Extended Linear Chain Complexes"; Miller, J. S., Ed.; Plenum: New York, **1982,** Vol. 1–3.
22. Keller, H. J., Ed. "Chemistry and Physics of One Dimensional Metals"; Plenum: New York, **1977**.
23. Day, P. In "Low Dimensional Cooperative Phenomena"; Keller, H. J., Ed.; Plenum: New York, **1974,** 191.
24. Brown, D. B.; Burbank, R. D.; Robin, M. B. *J. Am. Chem. Soc.* **1968,** *90,* 5621.
25. Brown, D. B.; Burbank, R. D.; Robin, M. B. *J. Am. Chem. Soc.* **1969,** *91,* 2895.
26. Schmuckler, G.; Limoni, B. *J. Inorg. Nucl. Chem.* **1977,** *39,* 137.
27. Flynn, C. M., Jr.; Viswanthan, T. S.; Martin, R. B. *J. Inorg. Nucl. Chem.* **1977,** *39,* 437.
28. Laurent, M. P.; Tewksbury, J. C.; Krogh-Jespersen, M.-B.; Patterson, H. *Inorg. Chem.* **1980,** *19,* 1656.
29. Arrizabalaga, P.; Castan, P.; Laurent, J.-P. *Trans. Met. Chem.* **1980,** *5,* 204.
30. Burness, J. H. *Inorg. Chim. Acta* **1980,** *44,* L49.
31. Ettorre, R. *Inorg. Chim. Acta* **1980,** *46,* L27.
32. Allen Chan, C.; Marcotte, R. B.; Patterson, H. H. *Inorg. Chem.* **1981,** *20,* 1632.
33. Laurent, J.-P.; Lepage, P. *Can. J. Chem.* **1981,** *59,* 1083.
34. Laurent, J.-P.; Lepage, P.; Castan, P.; Arrizabalaga, P. *Inorg. Chim. Acta* **1982,** *67,* 31.
35. Arrizabalaga, P.; Castan, P.; Laurent, J.-P. *J. Am. Chem. Soc.* **1984,** *106,* 1300.
36. Arrizabalaga, P.; Castan, P.; Laurent, J.-P. *J. Am. Chem. Soc.,* **1984,** *106,* 4814.
37. Erxleben, A.; Lippert, B. *J. Chem. Soc. Dalton Trans.* **1996,** 2329.
38. Appleton, T. G.; Berry, R. D.; Davis, C. A.; Hall, J. R.; Kimlin, H. A. *Inorg. Chem.* **1984,** *23,* 3514.
39. Appleton, T. G.; Hall, J. R.; Ralph, S. F.; Thompson, C. M. *Inorg. Chem.* **1984,** *23,* 3521.
40. Sakai, K.; Takeshita, M.; Tanaka, Y.; Ue, T.; Yanagisawa, M.; Kosaka, M.; Tsubomura, T.; Ato, M.; Nakano, T. *J. Am. Chem. Soc.* **1998,** *120,* 11353.
41. Rosenberg, B.; Van Camp, L.; Krigas, T. *Nature* (*London*) **1965,** *205,* 698.
42. Rosenberg, B.; Van Camp, L.; Trosko, J. E.; Mansour, V. H. *Nature* (*London*) **1969,** *222,* 385.
43. Rosenberg, B.; Van Camp, L. *Cancer Res.* **1970,** *30,* 1799.
44. For a review: Hill, J. M.; Loeb, E.; McLellan, A.; Hill, N. O.; Khan, A.; King, J. J. *Cancer Chemother. Rep.* **1975,** *59,* 647.
45. Davidson, J. P.; Faber, P. J.; Fisher, R. G., Jr.; Mansy, S.; Peresie, H. J.; Rosenberg, B.; Van Camp, L. *Cancer Chemother. Rep.* **1975,** *59,* 287.
46. Rosenberg, B. *Cancer Chemother. Rep.* **1975,** *59,* 589.
47. Zaki, A. A.; McAuliffe, C. A.; Friedman, M. E.; Hill, W. E.; Kohl, H. H. *Inorg. Chim. Acta* **1983,** *69,* 93.
48. Barton, J. K.; Rabinowitz, H. N.; Szalda, D. J.; Lippard, S. J. *J. Am. Chem. Soc.* **1977,** *99,* 2827.
49. Barton, J. K.; Szalda, D. J.; Rabinowitz, H. N.; Waszczak, J. V.; Lippard, S. J. *J. Am. Chem. Soc.* **1979,** *101,* 1434.
50. Hollis, L. S.; Lippard, S. J. *J. Am. Chem. Soc.* **1981,** *103,* 1230.
51. Hollis, L. S.; Lippard, S. J. *J. Am. Chem. Soc.* **1983,** *105,* 3494.
52. O'Halloran, T. V.; Lippard, S. J. *J. Am. Chem. Soc.* **1983,** *105,* 3341.
53. O'Halloran, T. V.; Lippard, S. J. *Inorg. Chem.* **1989,** *28,* 1289.
54. Hollis, L. S.; Roberts, M. M.; Lippard, S. J. *Inorg. Chem.* **1983,** *22,* 3637.
55. Hollis, L. S.; Lippard, S. J. *Inorg. Chem.* **1983,** *22,* 2600.

56. O'Halloran, T. V.; Roberts, M. M.; Lippard, S. J. *J. Am. Chem. Soc.* **1984,** *106,* 6427.
57. (a) O'Halloran, T. V.; Mascharak, P. K.; Williams, I. D.; Roberts, M. M.; Lippard, S. J. *Inorg. Chem.* **1987,** *26,* 1261. (b) Faggiani, R.; Lock, C. J. L.; Pollock, R. J.; Rosenberg, B.; Turner, G. *Inorg. Chem.* **1981,** *20,* 804.
58. O'Halloran, T. V.; Roberts, M. M.; Lippard, S. J. *Inorg. Chem.* **1986,** *25,* 957.
59. Matsumoto, K.; Miyamae, H.; Moriyama, H. *Inorg. Chem.* **1989,** *28,* 2959.
60. Sakai, K.; Tanaka, Y.; Tsuchiya, Y.; Hirata, K.; Tsubomura, T.; Iijima, S.; Bhattacharjee, A. *J. Am. Chem. Soc.* **1998,** *120,* 8366.
61. Matsumoto, K.; Fuwa, K. *Chem. Lett.* **1984,** 569.
62. Matsumoto, K. *Bull. Chem. Soc. Jpn.* **1985,** *58,* 651.
62a. Lock, C. J. L.; Peresie, H. J.; Rosenberg, B.; Turner, G. *J. Am. Chem. Soc.* **1978,** *100,* 3371.
63. Matsumoto, K.; Takahashi, H.; Fuwa, K. *J. Am. Chem. Soc.* **1984,** *106,* 2049.
64. Matsumoto, K.; Fuwa, K. *J. Am. Chem. Soc.* **1982,** *104,* 897.
65. Matsumoto, K.; Takahashi, H.; Fuwa, K. *Inorg. Chem.* **1983,** *22,* 4086.
66. Abe, T.; Moriyama, H.; Matsumoto, K. *Chem. Lett.* **1989,** 1857.
67. Abe, T.; Moriyama, H.; Matsumoto, K. *Inorg. Chem.* **1991,** *30,* 4198.
68. Matsumoto, K.; Harashima, K. *Inorg. Chem.* **1991,** *30,* 3032.
69. Matsumoto, K.; Harashima, K.; Moriyama, H.; Sato, T. *Inorg. Chim. Acta* **1992,** *197,* 21.
70. Lippert, B.; Neugebauer, D.; Raudaschl, G. *Inorg. Chim. Acta* **1983,** *78,* 161.
71. Mascharak, P. K.; Williams, I. D.; Lippard, S. J. *J. Am. Chem. Soc.* **1984,** *106,* 6428.
72. Schöllhorn, H.; Eisenmann, P.; Thewalt, U.; Lippert, B. *Inorg. Chem.* **1986,** *25,* 3384.
73. Lippert, B.; Schöllhorn, H.; Thewalt, U. *J. Am. Chem. Soc.* **1986,** *108,* 525.
74. Lippert, B.; Schöllhorn, H.; Thewalt, U. *Inorg. Chem.* **1986,** *25,* 407.
75. Trötscher, G.; Micklitz, W.; Schöllhorn, H.; Thewalt, U.; Lippert, B. *Inorg. Chem.* **1990,** *29,* 2541.
76. Micklitz, W.; Riede, J.; Huber, B.; Müller, G.; Lippert, B. *Inorg. Chem.* **1988,** *27,* 1979.
77. Lippert, B.; Neugebauer, D.; Schubert, U. *Inorg. Chim. Acta* **1980,** *46,* L11.
78. Schöllhorn, H.; Thewalt, U.; Lippert, B. *Inorg. Chim. Acta* **1984,** *93,* 19.
79. Neugebauer, D.; Lippert, B. *Inorg. Chim. Acta* **1982,** *67,* 151.
80. Micklitz, W.; Renn, O.; Schöllhorn, H.; Thewalt, U.; Lippert, B. *Inorg. Chem.* **1990,** *29,* 1836.
81. Laurent, J.-P.; Lepage, P.; Dahan, F. *J. Am. Chem. Soc.* **1982,** *104,* 7335.
82. Faggiani, R.; Lippert, B.; Lock, C. J. L.; Speranzini, R. A. *J. Am. Chem. Soc.* **1981,** *103,* 1111.
83. Urata, H.; Moriyama, H.; Matsumoto, K. *Inorg. Chem.* **1991,** *30,* 3914.
84. Matsumoto, K.; Matsunami, J.; Urata, H. *Chem. Lett.* **1993,** 597.
85. Matsumoto, K.; Urata, H. *Chem. Lett.* **1993,** 2061.
86. Matsumoto, K.; Urata, H. *Chem. Lett.* **1994,** 307.
87. Sakai, K.; Matsumoto, K. *J. Am. Chem. Soc.* **1989,** *111,* 3074.
88. Matsumoto, K.; Sakai, K.; Nishio, K.; Tokisue, Y.; Ito, R.; Nishide, T.; Shichi, Y. *J. Am. Chem. Soc.* **1992,** *114,* 8110.
89. Sakai, K.; Matsumoto, K.; Nishio, K. *Chem. Lett.* **1991,** 1081.
90. Matsumoto, K.; Matsunami, J.; Mizuno, K.; Uemura, H. *J. Am. Chem. Soc.* **1996,** *118,* 8959.
91. Matsumoto, K.; Nagai, Y.; Matsunami, J.; Mizuno, K.; Abe, T.; Somazawa, R.; Kinoshita, J.; Shimura, H. *J. Am. Chem. Soc.* **1998,** *120,* 2900.

92. Suzuki, K.; Matsumoto, K. *Chem. Lett.* **1989,** 317.
93. Matsumoto, K.; Moriyama, H.; Suzuki, K. *Inorg. Chem.* **1990,** *29,* 2096.
94. Hollis, L. S.; Lippard, S. J. *Inorg. Chem.* **1983,** *22,* 2605.
95. Hollis, L. S.; Lippard, S. J. *Inorg. Chem.* **1982,** *21,* 2116.
96. Barton, J. K.; Caravana, C.; Lippard, S. J. *J. Am. Chem. Soc.* **1979,** *101,* 7269.
97. Ginsberg, A. P.; O'Halloran, T. V.; Fanwick, P. E.; Hollis, L. S.; Lippard, S. J. *J. Am. Chem. Soc.* **1984,** *106,* 5430.
98. Matsumoto, K.; Matoba, N. *Inorg. Chim. Acta* **1986,** *120,* L1.
99. Stranger, R.; Medley, G. A.; McGrady, J. E.; Garrett, J. M.; Appleton, T. G. *Inorg. Chem.* **1996,** *35,* 2268, and references therein.
100. Matsumoto, K.; Watanabe, T. *J. Am. Chem. Soc.* **1986,** *108,* 1308.
101. Mehran, F.; Scott, B. A. *Phys. Rev. Lett.* **1973,** *31,* 1347.
102. Mehran, F.; Scott, B. A. *Phys. Rev. Lett.* **1973,** *31,* 99.
103. Palmans, R.; MacQueen, D. B.; Pierpont, C. G.; Frank, A. J. *J. Am. Chem. Soc.* **1996,** *118,* 12647.
104. Burroughs, P.; Hamnet, A.; McGilp, J. F.; Orchard, A. F. *J. Chem. Soc. Farad. Trans. 2* **1975,** *71,* 177.
105. Cahen, D.; Lester, J. E. *Chem. Phys. Lett.* **1978,** *18,* 108.
106. Matsunami, J.; Urata, H.; Matsumoto, K. *Inorg. Chem.* **1995,** *34,* 202.
107. Pregosin, P. S. *Ann. Rep. NMR Spectrosc.* **1986,** *17,* 285.
108. Pregosin, P. S. *Coord. Chem. Rev.* **1982,** *44,* 247.
109. Pregosin, P. S. In "Transition Metal Nuclear Magnetic Resonance"; Elsevier: Amsterdam, **1991,** 216.
110. Appleton, T. G.; Hall, J. R.; Neale, D. W.; Ralph, S. F. *Inorg. Chim. Acta* **1983,** *77,* L149.
111. Maliarik, M.; Glaser, J.; Tóth, I. *Inorg. Chem.* **1998,** *37,* 5452.
112. Che, C.-M.; Schaefer, W. P.; Gray, H. B.; Dickson, M. K.; Stein, P. B.; Roundhill, D. M. *J. Am. Chem. Soc.* **1982,** *104,* 4253.
113. Sakai, K.; Tsubomura, T.; Matsumoto, K. *Inorg. Chim. Acta* **1993,** *213,* 11.
114. Sakai, K.; Kizaki, Y.; Tsubomura, T.; Matsumoto, K. *J. Mol. Catal.* **1993,** *79,* 141.
115. Sakai, K.; Matsumoto, K. *J. Mol. Catal.* **1990,** *62,* 1.
116. Sakai, K., Ph.D. Dissertation, Waseda University, **1993**.
117. Sakai, K.; Tsubomura, T.; Matsumoto, K. *Inorg. Chim. Acta* **1995,** *234,* 157.
118. Sakai, K.; Tsuchiya, Y.; Tsubomura, T. *Technol. Rep. Seikei Univ.* **1992,** *54,* 77.
119. Matsuomoto, K.; Matoba, N. *Inorg. Chim. Acta.* **1988,** *142,* 59.
120. Sakai, K.; Matsumoto, K. *J. Coord. Chem.* **1988,** *18,* 169.
121. Sakai, K.; Matsumoto, K. *J. Mol. Catal.* **1991,** *67,* 7.
122. Bäckvall, J. E.; Ålkermark, B.; Ljunggren, S. O. *J. Am. Chem. Soc.* **1979,** *101,* 241.
123. Stille, J. K.; Divakaruni, R. *J. Organomet. Chem.* **1979,** *169,* 239.
124. Strucul, G.; Sinigalia, R.; Zanardo, A.; Pinna, F.; Michelin, R. A. *Inorg. Chem.* **1989,** *28,* 554.
125. Matsumoto, K.; Mizuno, K.; Abe, T.; Kinoshita, J.; Shimura, H. *Chem. Lett.* **1994,** 1325.
126. Stahl, S.; Labinger, J. A.; Bercaw, J. E. *J. Am. Chem. Soc.* **1996,** *118,* 5961.
127. Labinger, J. A.; Herring, A. M.; Lyon, D. K.; Luinstra, G. A.; Bercaw, J. E. *Organotetallics* **1993,** *12,* 895.
128. Luinstra, G. A.; Wang, L.; Stahl, S. S.; Labinger, J. A.; Bercaw, J. E. *J. Organomet. Chem.* **1995,** *504,* 75.
129. Sen, A.; Lin, M.; Kao, L. C.; Hutson, A. C. *J. Am. Chem. Soc.* **1992,** *114,* 6385.

130. Arrizabalaga, P.; Castan, P.; Laurent, J.-P.; Cros, S.; Francois, G. *Eur. J. Med. Chem.* **1984,** *19,* 501.
131. Fanizzi, F. P.; Intini, F. P.; Maresca, L.; Natile, G.; Gasparrini, F. *J. Chem. Soc. Dalton Trans.* **1990,** 1019.
132. Fanizzi, F. P.; Intini, F. P.; Maresca, L.; Natile, G.; Gasparrini, F. *J. Chem. Soc. Dalton Trans.* **1992,** 309.
133. Maresca, L.; Natile, G.; Gasparrini, F. *J. Am. Chem. Soc.* **1982,** *104,* 7661.
134. Panunzi, A.; De Renzi, A.; Palumbo, R.; Paiaro, G. *J. Am. Chem. Soc.* **1969,** *91,* 3879.
135. Okuno, Y.; Tonosaki, K.; Inoue, T.; Yonemitsu, O.; Sasaki, T. *Chem. Lett.* **1986,** 1947.
136. Conners, T. A.; Roberts, J. J. In "Platinum Coordination Complexes in Cancer Chemotherapy: Recent Results in Cancer Research", Springer-Verlag, New York, **1974,** 48.

This Page Intentionally Left Blank

SUBJECT INDEX

D

N

O

P

W

X

Z

CONTENTS OF PREVIOUS VOLUMES